

Institut für Erdöl- und Erdgastechnik (ITE)

Technische Universität Clausthal

Machbarkeitsstudie über das CO₂-Speicherungspotenzial und die Erhöhung des Ausbeutegrades in maturen Erdgaslagerstätten



TU Clausthal
Clausthal University of Technology

VATTENFALL

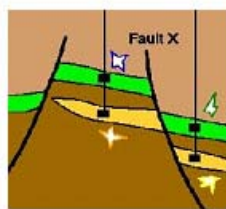
BGR
Bundesanstalt für
Geowissenschaften
und Rohstoffe

CSEGR

wintershall
D-BASF Gruppe

e-on | Ruhrgas

GDF SUEZ



Abschlussbericht zum BMBF-Forschungsvorhaben
Mit dem Förderkennzeichen 03G0627A
Zeitraum 01.04.2005 – 31.10.2008

Univ. Prof. Dr. mont. Günter Pusch- Lehrstuhl für Erdöl-/
Erdgaslagerstättentechnik

Agricolastraße 10- 38678 Clausthal Zellerfeld – Tel.: 05323/72-2618 – Fax: 05323/72-3146

Abschlussbericht

zum BMBF- Forschungsvorhaben

**Machbarkeitsstudie über das
CO₂ -Speicherungspotenzial
und die Erhöhung des Ausbeutegrades
in maturen Erdgaslagerstätten**

**Feasibility Study on the
Potential of CO₂ Storage
For Enhanced Gas Recovery in
Mature German Gas Reservoirs**

Förderkennzeichen 03G0627A

Zeitraum 01.04.2005 – 31.10.2008

Clausthal, im April 2009

Univ. Prof. Dr. mont. Günter Pusch

Danksagung

Das diesem Forschungsbericht zugrunde liegende Vorhaben wurde vom Bundesministerium für Bildung und Forschung gefördert.

Für die Finanzierung dieses Projektes möchten wir dem BMBF herzlichen Dank sagen.

Wir bedanken uns auch bei den Firmen: Vattenfall AB, E.ON Ruhrgas AG, Wintershall AG und GDF SUEZ E&P Deutschland für die zusätzliche finanzielle Unterstützung und für die Überlassung von Proben- und Datenmaterial.

Die Verantwortung für den Inhalt der Veröffentlichung liegt bei den Autoren.

Content

| | |
|---|-----|
| Introduction | 1 |
| WP1: Surface equipment for CO ₂ separation and injection..... | 15 |
| WP2: CO ₂ Compression, Injection/Production, Well Integrity..... | 41 |
| WP3: Reservoir Modelling..... | 103 |
| WP4: Process Modelling..... | 135 |
| WP5: Geochemical Risk Assessment..... | 175 |
| WP6: Simulation of CO ₂ Sequestration and Natural Gas Production Enhancement.... | 209 |
| WP7: Technical, Economical and Environmental Analyses-Feasibility Report..... | 251 |

Introduction – Scope of the Project

The German government aims at a 20% reduction of greenhouse gases until 2020. Even though Germany has achieved a remarkable reduction of CO₂ emissions since 1990, annual reduction increments are declining. Globally, CO₂ emissions are even increasing. Thus additional measures are needed to achieve the long-term reduction targets (Ziesing 2004). According to the scientific advisory council of the federal government for global change (WBGU), underground storage of CO₂ will be necessary to keep the effects of climate change within acceptable limits in the current century (Edenhofer 2003).

The Bundesanstalt für Geowissenschaften und Rohstoffe (BGR) has compared different options for the underground storage of CO₂ in Germany (May et al. 2003); accordingly gas fields would be the prime choice for CO₂ storage. More than 50% of the gas reservoirs are already in a mature status and they are potential candidates for future CO₂ storage. Injection of CO₂ into depleted natural gas reservoirs could increase the reservoir pressure and enhance the recovery of the residual gas. This combination of CO₂ storage and recovery enhancement (CO₂-EGR or CSEGR = CO₂ storage and enhanced gas recovery) is a theoretical concept still, that has not been practiced yet anywhere in the world.

This study shall investigate the feasibility of CSEGR for likely separation and storage systems (source–transport–sink) representing typical industrial sources and reservoir types in Germany. The proposed study will consider two systems for the technical evaluation of CO₂-EGR feasibility:

- A large lignite fired power plant in East Germany emitting about 10 Mt of CO₂ annually shall be the source of CO₂ for EGR operations in heterogeneous, fine-scale structured, and anisotropic layered gas carrier rocks of the Rotliegend reservoirs in the Altmark. The Altmark would provide sufficient storage capacity for the CO₂ emitted during the life-time of a large lignite fired power station.
- A homogeneous, large-scale structured, isotropic Buntsandstein gas reservoir in Northwestern Germany shall be used for EGR using CO₂ separated at a planned industrial natural gas treatment facility emitting a few hundred thousand tons of CO₂ annually. Data of the mature field Barrien will be used as an example, because this reservoir has been used previously already for enhanced recovery tests.

Within this feasibility study the geological, technical, and economical key parameters that will influence the optimisation of CSEGR will be investigated.

Consortium

The research consortium submitting this proposal includes two competent geo-scientific engineering research institutes and four industry partners that supply relevant information and participate actively in the work programme.

The project management will be taken by the Technical University Clausthal represented by the chairs Petroleum Geology (Prof. Wolfgang Blendinger), Reservoir Engineering & Simulation (ELT, Prof. Guenter Pusch), Oil/Gas Recovery and Gas Supply (EGV, Prof. Kurt M. Reinicke). The activities of the Institute of Petroleum Engineering (ITE) cover: reservoir engi-

neering, drilling, production, natural gas storage and transportation. ITE has more than 20 years of experience in the simulation of complex problems of reservoir processes, using commercial software like ECLIPSE. It has unique experimental database on enhanced recovery methods, including CO₂ flooding in oil reservoirs and special core analysis. It participated in and co-ordinated 7 EU research and demonstration projects. Research at the chair of Petroleum Geology in the Institute of Geology and Palaeontology (IfGP) is mainly focused on reservoir sedimentology, characterization and modelling.

BGR will support the project management and co-ordination of the project work. BGR participates in major EU funded CO₂ storage R&D projects. Within these projects storage capacities of gas fields in North Germany have been determined (Schupperts et al. 2003). The injection of CO₂ into the Altmark gas field Salzwedel-Peckensen, the Rotliegend field Alfeld-Elze, and the Buntsandstein aquifer near Lubmin have been simulated with TOUGHII (Obdam et al. 2003, Rebscher et al. 2004), and geochemical reactions have been studied with PHREEQC (May 2004a, 2004b).

Industrial partners are:

- the operator of the large Altmark gas field GDF SUEZ E&P Deutschland GmbH in Lingen,
- the exploration and production enterprise Wintershall AG in Kassel, owner of one of the largest natural gas storage in Rheden and operator of the gas field Barrien.
- Vattenfall AB in Stockholm, considering the emission free power generation in one of its East German lignite fuelled power stations near Cottbus,
- E.ON-Ruhrgas GmbH AG in Essen, an international gas company, considering the CO₂ separation of North Sea gas near the pipeline terminal Dornum.

The industrial parties will work within the consortium by providing source data, geologic models from their assets and advice to the project. They will use own resources but without applying for funds of the Geotechnologien Programme.

The project results should facilitate a first evaluation of the CO₂-EGR option by the industrial partners. Even if this evaluation should be positive, it will still be a long way to a large-scale commercial application, which would require additional research, development, and testing. Thus, there is no direct commercial benefit from this project, but it is of value for the companies' strategic planning.

Present State of Knowledge

No commercial projects or field test of CSEGR do exist. Generic numerical simulations or core flooding experiments have been performed in order to study distinct aspects of CO₂ injection. In the EU integrated project CASTOR CSEGR shall be studied in a small gas field in the Austrian Molasse basin. In a government supported pilot project offshore The Netherlands Injection of CO₂ into a Natural Gas Field has begun in May 2004. However EGR presently is not considered to be economical in small onshore fields (van Luijk 2003).

Conceptual (generic) numerical simulation studies have been performed in order to determine the potential of the CSEGR concept. The first numerical modelling results of CSEGR in Dutch gas fields were published by van der Burgt et.al. (1992). The Lawrence Berkeley National Laboratory performed a simulation study on the basis of the Californian Rio Vista gas

field and concluded that CO₂ can be injected to produce significant quantities of additional natural gas (Oldenburg et al. 2001). The simulations indicated little mixing of CO₂ and methane because of the large density and viscosity differences between the two gas components. However, permeability heterogeneity is a critical parameter, because it accelerates the CO₂ break-through. Oldenburg and Benson (2002) stated that the injection of CO₂ at relatively deep levels in a reservoir, while producing from higher levels, will allow the operator to decrease the rise of CO₂ and mixing with natural gas. Additional calculations of the economics of the proposed CSEGR project in the Rio Vista field have been published by Oldenburg et al. (2003). In another conceptual study, the researchers from the United States Department of Energy and from National Energy Technology Laboratory, studied the effect of methane displacement by CO₂ in a thin rim reservoir with low permeability, congruent to tight gas formations in North Germany (SPE84813). Jikich et. al. (2003) investigated the optimal time for starting the enhanced gas recovery process and they have shown that maximum recovery is possible, if the reservoir has been depleted to minimum reservoir pressure, whereas the injection of CO₂ at higher pressures has only the effect of production acceleration. Rebscher et al. (2004) have calculated CO₂ break-through times for CO₂ injection into a generic Altmark Rotliegend reservoir. A comparable study has been performed by Clemens und Wit (2001) based on models of typical Rotliegend reservoirs in The Netherlands.

In an international benchmark tests the ability to predict the phase behaviour and physical phase properties of CO₂–CH₄–brine–rock systems, chemical reactions of CO₂ with host rock minerals, combined diffusion and advection flow processes, and miscible displacement of oil by CO₂ of eight different codes has been examined (Pruess et al. 2003). Most of the process simulators yielded reasonable results in the particular areas of the complex, integrated process chain. However, no particular numerical simulator was able to address all problems with sufficient accuracy and reliability. Two of the tested codes ECLIPSE and TOUGH II are in use at the ITE and BGR respectively.

The impact of possible geochemical reactions in the reservoir and cap rocks of underground CO₂ storage is a major concern that is being recognised and addressed by geochemical experiments and numerical simulations. Usually batch reaction, reaction kinetic, reactive transport, or mass transfer approaches are used for predictive geochemical simulations. Reactive transport simulations require a range of necessary input information from existing geologic structures. Thus, the prediction of likely reactions will be very much site-specific, and it has to take into account actual reservoir mineralogy and fluid composition for the selected real, geologically complex reservoirs and hence the industrial data will be important to determine the most appropriate simulation strategy.

Transport codes that have been used for CO₂ injection simulations are e.g. CHEMTOUGH (Industrial Research Ltd.), TOUGHREACT (Lawrence Berkeley National Lab), or SHEMAT (RWTH-Aachen). More powerful geochemical modelling codes like PHREEQC (US Geological Survey) have limited fluid transport simulation capabilities. All of the above codes are under current development. TOUGHREACT will be available to the public in October 2004 and shall be used in the proposed project. In addition to experiments and simulation, studies of natural rocks that have been altered by CO₂ rich fluids will yield valuable information especially about slow geochemical reactions involving silicates (May 2004).

Vattenfalls experience concerning transport and separation costs, e. g. Odenberger and Svenson (2003) and the GESTCO-DSS, developed by Egberts et al. (2003), has been used

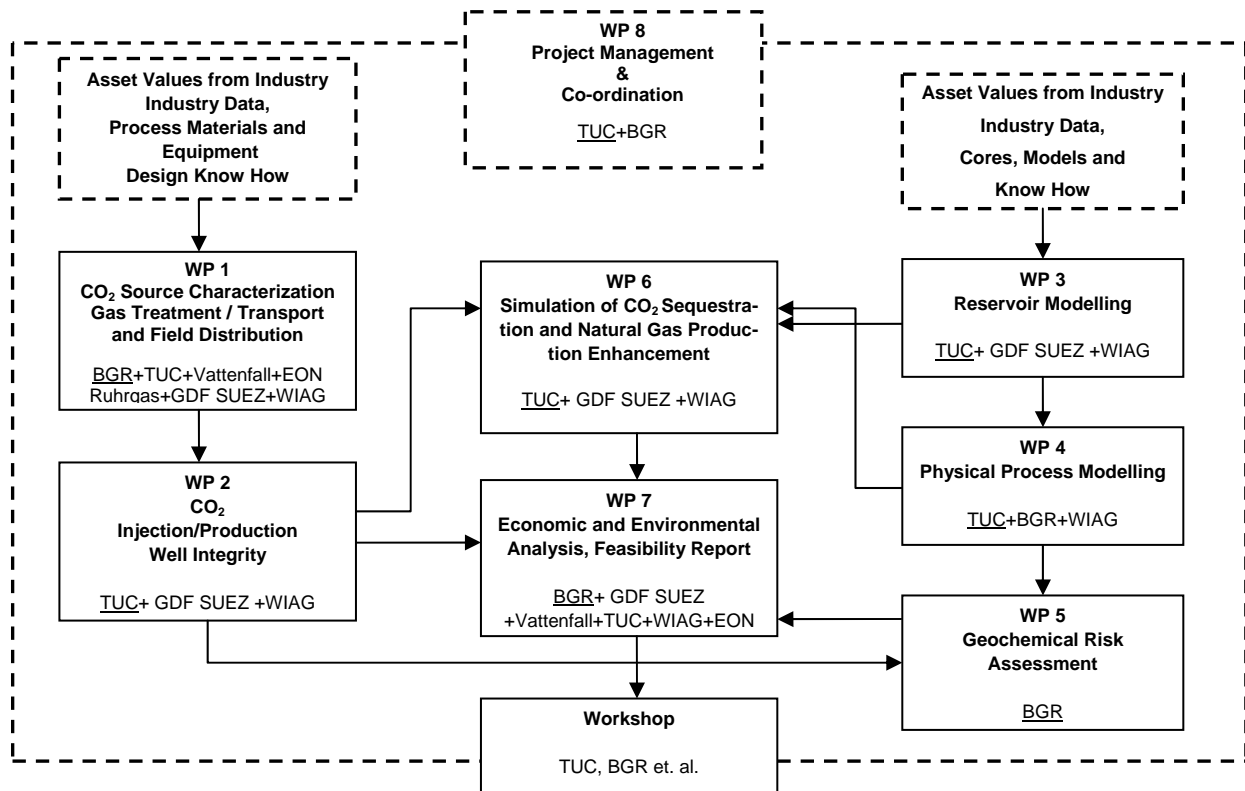
by BGR and Vattenfall to calculate CO₂ separation, transport and storage costs for case studies in Germany.

Work Plan

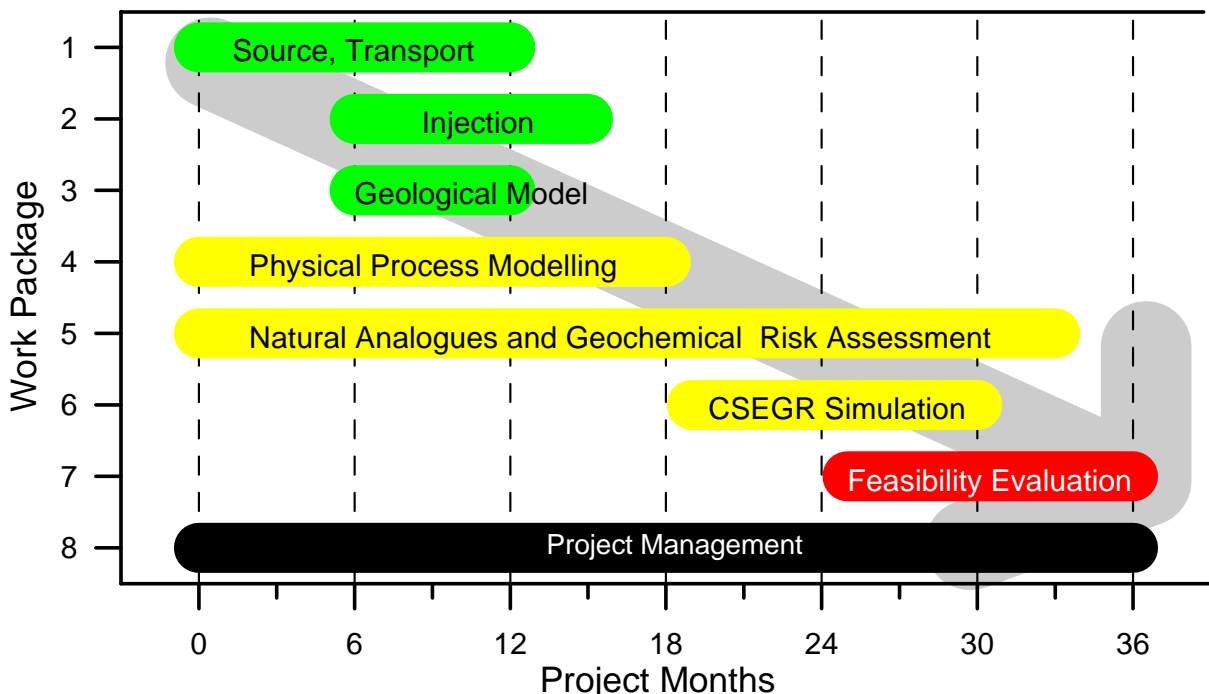
The following diagram gives an overview of the project structure, the work packages, the information flow, and the partners involved in each package. The project contains three basic work packages (1-3) using industrial data to provide input to the central work packages.

The CO₂ sources are characterised and the requirements for CO₂ transport and field distribution are defined in work package 1.

In work package 2 the suitability of existing well technology for CO₂-EGR will be investigated. Geological reservoir models will be built or updated in work package 3. In the main work packages (4-6) physical and chemical reactions induced by CO₂ injection in the reservoir and the overburden will be investigated. Work package 4 focuses on CO₂ induced hydrodynamic processes and on physical properties of CO₂ and their incorporation into reservoir simulation modules. Information from natural analogues and reservoir rocks and fluids shall be used in work package 5 to identify geochemical reactions in reservoir and caprocks that are likely to occur during CO₂-EGR. Predictive geochemical modelling shall be used to assess the potential impact of the identified reactions. It is internally structured in a way that much of the necessary input for simulation will be generated during the first year within the work package and additional information provided by work packages 1 and 2 on p-T conditions and impurities shall be available prior to the start of the reactive transport process simulations. While the process simulations in work packages 4 and 5 are more generic, reservoir simulations of CO₂ injection and natural gas production from the two representative case studies will be performed in work package 6. In work package 7 all of the information will be compiled and serve as a base for the technical, economical and environmental feasibility study of the entire CCS-system.



This interdisciplinary research project was scheduled to last 36 months. The anticipated time of Individual work packages and the general project progress and information exchange between work packages is indicated in the time planning overview following below.



The acquisition and recruiting of personal for the execution of the proposed work plan was unfortunately delayed, caused by the fact that experienced researchers especially for WP 5

were not available. Therefore the project partners BGR and TUC asked for a project extension for 6 months without additional finances.

The project management of the “Geotechnologien Programm” agreed on the request. The project was extended and ended officially on October 31st 2008.

The objectives of the integrated work program contain formal deliverables which are necessary elements to assess the closed chain of CCS from the source to the sink.

Deliverables:

WP 1:

- Specification of storage system I: East German lignite fired power plant – Altmark Rotliegend reservoir (month 12)
- Specification of storage system II: Natural gas terminal – Barrien Buntsandstein reservoir
- definition of infrastructure acceptability for CSEGR
- analysis for pilot area infrastructure
- front end design (modifications and facility additions) and costing for injection and production in pilot area using state-of-the-art technology
- list of required step changes in the production scheme upon CO2 break through

WP 2:

- definition of well integrity acceptable for CSEGR
- integrity analysis for pilot area
- front end design (modification/repair of existing wells and new wells) and costing for injection and production in pilot area using state-of-the-art technology
- further work to develop technology able to provide optimum completions and a long term CO₂ resistant seal for CO₂ injection and production wells

WP 3:

- Fine-tuned reservoir sector models for process simulation

WP 4:

- PVT-Package for Hydrocarbon/CO₂
 - Hydrodynamic Dispersion Parameters CO₂/HC and CO₂/water
-
- Modelling of a system of two gases separated by high density differences
 - Rock alteration by CO₂
 - Porosity-permeability versus pore pressure functions
 - Pore pressure dependent capillary pressure curves and relative permeabilities

WP 5:

- Geochemical characterisation of representative reservoir and cap rocks
- Identification of possible reactions
- Numerical simulation of possible reactions
- Evaluation of possible impact

WP 6:

- Best Practice of CO₂-Storage and Enhancing Gas Recovery for two Candidate Reservoirs
- Definition of Limiting Geological and Technical Parameter Ranges

WP 7:

- The main delivery of this project will be a feasibility study report, including generic results, a discussion of the uncertainties in simulation results, identified gaps in knowledge, and recommendations for further actions. Results for the two representative storage systems will include an analysis of CO₂ storage capacity, EGR potential, economic considerations, and a discussion of potential storage risks.

WP 8:

- Interim Technical and Finance Report
- Final Technical and Finance Report
- International Workshop on Study Results

Synopse zur Einleitung

Die Bundesregierung strebt eine Reduktion der Treibhausgasemissionen um 40 % bis zum Jahr 2020 an. Trotz der beachtlichen Reduktion der CO₂-Emissionen seit 1990 in Deutschland, ist die Tendenz der jährlichen Emissionsminderung abnehmend und weltweit sogar steigend, so dass zusätzliche Maßnahmen zum Erreichen der langfristigen Klimaschutzziele unerlässlich sind (Ziesing 2004). Der Wissenschaftliche Beirat der Bundesregierung Globale Umweltveränderungen (WBGU) ist daher der Auffassung, dass die Untertagespeicherung von CO₂ zusätzlich zu anderen Maßnahmen der Emissionsminderung erforderlich ist, um die Auswirkungen der vorhergesagten Klimaänderungen in akzeptablen Grenzen zu halten (Edenhofer 2003).

Die Bundesanstalt für Geowissenschaften und Rohstoffe (BGR) hat eine erste vergleichende Bewertung der verschiedenen Möglichkeiten der Untertagespeicherung in Deutschland durchgeführt (May et al. 2003). Dementsprechend stellen Gasfelder die erste Wahl für die CO₂-Speicherung dar. Mehr als die Hälfte der Deutschen Erdgaslagerstätten befinden sich in einem fortgeschrittenen Abbaustadium und sind potenziell geeignete Kandidaten für zukünftige Untergrundspeicher. Die Injektion von CO₂ in mature Erdgaslagerstätten könnte zur Steigerung des Lagerstättendruckes und damit zur Steigerung der Erdgasausbeute der Felder genutzt werden. Diese Kombination von CO₂-Speicherung und Ausbeutesteigerung – als CO₂-EGR oder CSEGR = (CO₂ storage and enhanced gas recovery) bezeichnet – ist bisher noch nur ein theoretisches Konzept, dass bislang noch nicht in der industriellen Praxis erprobt wurde.

In dieser Studie soll die Machbarkeit des CSEGR-Konzeptes anhand für Deutschland repräsentativer Beispiele untersucht werden. Dabei soll das ganze System der CO₂-Abscheidung und Speicherung einschließlich typischer CO₂-Quellen, Transportmöglichkeiten und Lagerstättentypen betrachtet und zwei Fallstudien untersucht werden:

1. Ein großes Ostdeutsches Braunkohlekraftwerk, welches jährlich etwa 10 Mt CO₂ emittiert, wird als CO₂-Quelle für EGR-Maßnahmen in Erdgasfeldern der Altmark angesehen. Die kleinräumig heterogenen und anisotropen Kluftspeicher der Rotliegendsandsteine der Altmark besitzen eine ausreichende Kapazität zur Speicherung des während der Betriebsdauer eines Kraftwerkes emittierten CO₂.
2. Im Gegensatz zum Rotliegend sind die Buntsandsteinlagerstätten in Nordwestdeutschland großräumiger strukturiert, homogen und lateral isotrop. Exemplarisch wird für die mature Gaslagerstätte Barrien die Speicherung von CO₂ aus einer geplanten Erdgasaufbereitungsanlage untersucht, die einige hunderttausend Tonnen pro Jahr emittieren könnte. In der Lagerstätte Barrien wurden bereits früher Versuche zur Ausbeutesteigerung durchgeführt.

In dieser Machbarkeitsstudie sollen die wesentlichen technischen, geologischen und wirtschaftlichen Parameter untersucht werden, welche für die Optimierung von CSEGR Vorhaben von Bedeutung sind.

Konsortium

Dieses Vorhaben wird von zwei geowissenschaftlichen Forschungseinrichtungen und vier Industrieunternehmen getragen, welche relevante Daten ihrer Anlagen und Lagerstätten bereitstellen, sich aber auch aktiv an der Durchführung des Projektes beteiligen.

Die Projektleitung übernimmt die Technische Universität Clausthal. Beteiligt sind der Lehrstuhl Erdölgeologie (Prof. Blendinger) des Instituts für Geologie und Paläontologie sowie die Abteilungen Erdöl-/Erdgasgewinnung und Erdgasversorgung (Dr. Reinicke) und Erdöl-Erd-gaslagerstättentechnik (Prof. Pusch) des Instituts für Erdöl- und Erdgastechnik (ITE). Schwerpunkte der Forschung und Entwicklung des ITE sind Lagerstätten- und Bohrtechnik, Kohlenwasserstoffförderung, Erdgasspeicherung und -Transport. Das ITE besitzt mehr als 20 Jahre Erfahrung auf dem Gebiet der Simulation komplexer Lagerstättenprozesse mittels des Programms ECLIPSE. Es besitzt eine einmalige Datenbasis über Methoden zur Ausbeutesteigerung von Lagerstätten, einschließlich CO₂-Fluten von Öllagerstätten. Das ITE beteiligte sich an und koordinierte 7 EU Forschungs- und Entwicklungsprojekte. Der Lehrstuhl Erdölgeologie beschäftigt sich vor allem mit der Erfassung und Modellierung sedimentologischer Strukturen von Erdöllagerstätten.

Die BGR unterstützt die TU-Clausthal in der Koordination des Projektes. Aufgrund ihrer Beteiligung an mehreren EU-geförderten Forschungs- und Entwicklungsprojekten zur CO₂-Speicherung pflegt sie die projektbezogenen Kontakte zu internationalen Forschergruppen. Im Rahmen von europäischen Projekten bestimmte die BGR Speicherkapazitäten von Erdgaslagerstätten in Norddeutschland (Schuppers et al. 2003). Numerische Modelle zur CO₂-Injektion in die Altmark Lagerstätte Salzwedel-Peckensen, das Rotliegend Gasfeld Alfeld-Elze und eine Buntsandstein-Struktur bei Lubmin wurden mit einer eigens modifizierten Version des TOUGH II Programms erstellt (Obdam et al. 2003, Rebscher et al. 2004). Geochemische Reaktionen wurden mit dem vom U.S. Geological Survey entwickelten Programm PHREEQC berechnet (May 2004a, 2004b).

Die Industriepartner des Projektes sind:

- GDF SUEZ E&P Deutschland GmbH, Berlin, als Betreiber der Erdgaslagerstätten in der Altmark,
- Das Explorations- und Produktionsunternehmen Wintershall Aktiengesellschaft, Kassel, Eigentümer des größten Deutschen Erdgasspeichers in Rheden und Betreiber des Feldes Barrien,
- Vattenfall AB, Stockholm, als Betreiber Ostdeutscher Braunkohlekraftwerke,
- E.On-Ruhrgas GmbH AG, Essen, als internationales Gasunternehmen und möglicher Lieferant von CO₂ aus einer geplanten Gasaufbereitungsanlage bei Dornum.

Die Industriepartner stellen Informationen zu Anlagen, und geologische Modelle der Lagerstätten bereit. Sie beteiligen sich mit eigenen Ressourcen an den entsprechenden Arbeitspaketen, ohne Fördermittel aus dem Geotechnologien-Programm zu beantragen. Die Zusammenarbeit der Forschungsinstitute mit den Industriepartnern, z. B. Vertraulichkeit der

Daten, Verwertung von Ergebnissen, finanzielle Beteiligung, etc. ist in einem Konsortialvertrag vor Projektbeginn zu regeln.

Die Projektergebnisse sollen eine erste Bewertung des CO₂-EGR Konzeptes ermöglichen. Auch wenn die Bewertung positiv ausfällt, wird noch ein erheblicher Forschungs-, Entwicklungs- und Erprobungsaufwand erforderlich sein, bevor das Konzept kommerziell im industriellen Maßstab angewandt werden kann. Es bestehen keine direkt finanziellen Umsetzungsmöglichkeiten der Projektergebnisse. Jene sind lediglich für strategische, mittel- und langfristige Unternehmensplanungen verwertbar. Dementsprechend wird zusätzlich zu den Eigenleistungen eine angemessene finanzielle Beteiligung der Unternehmen in Höhe von 10% der beantragten Fördersumme angestrebt.

Stand der Forschung

Bisher existieren keine kommerziellen CSEGR-Projekte oder Feldversuche. Zur Untersuchung spezieller Aspekte der CO₂-Injektion wurden numerische Simulationen und Flutungsexperimente an Bohrkernen durchgeführt. Im EU-Projekt CASTOR soll CSEGR in einem Erdgasfeld in der Österreichischen Molasse untersucht werden. Die Niederländische Regierung unterstützt seit Mai 2004 die CO₂-Speicherung in einem Erdgasfeld in der Nordsee. Jedoch wird CO₂-EGR in kleinen Feldern bisher als unwirtschaftlich betrachtet (van Luijk 2003).

Zur Abschätzung des Speicherpotenzials und der Ausbeutesteigerung, wurden konzeptionelle numerische Simulationen für CSEGR-Fallstudien durchgeführt. Die Ersten Ergebnisse numerischer Modellierungen wurden von van der Burgt et. al. (1992) veröffentlicht. Am Lawrence Berkeley National Laboratory wurde eine Simulationsstudie auf der Basis des Kalifornischen Rio Vista Gasfeldes erstellt, der zufolge eine signifikante Steigerung der Erdgasausbeute des Feldes durch die Injektion von CO₂ erreicht werden kann (Oldenburg et al. 2001). Die Vermischung von CO₂ und Methan erfolgt aufgrund der Dichte- und Viskositätsunterschiede der beiden Gaskomponenten nur langsam, jedoch beschleunigen Heterogenitäten des Speichergesteins den Durchbruch von CO₂ zu den Fördersonden. Durch Injektion des spezifisch schweren CO₂ in tiefe Lagerstättenteile und Erdgasförderung aus dem Top der Lagerstätte lässt sich die Vermischung der Gase reduzieren (Oldenburg und Benson (2002). Wirtschaftlichkeitsberechnungen für ein mögliches Rio Vista CSEGR-Projekt stammen von Oldenburg et al. (2003). Eine weitere konzeptionelle Studie stammt vom U.S. Department of Energy und vom National Energy Technology Laboratory in der Lagerstätten ähnlich der „tight gas formations“ in Norddeutschland untersucht wurden. (SPE84813). Jikich et. al. (2003) versuchten anhand von Modellrechnungen den optimalen Zeitpunkt zum Beginn von CSEGR-Maßnahmen bei reifen Lagerstätten zu bestimmen. Rebscher et al. (2004) berechneten CO₂-Durchbruchszeiten für die Injektion in ein idealisiertes Altmark Rotliegendreservoir. Sie erhielten ähnliche Ergebnisse wie Clemens und Wit (2001) für ein Modell typischer Rotliegend-Lagerstätten der Niederlande.

In einem internationalen Programmvergleich wurden 8 verschiedene Lagerstätten- und Fluidtransportprogramme u. a. bezüglich ihrer Eignung zu Simulation des Phasenverhaltens im H₂O–CO₂–CH₄–NaCl-System sowie chemischer Reaktionen zwischen CO₂ und Nebengesteinsmineralen verglichen (Pruess et al. 2003). Obwohl die meisten Simulatoren vielfach vergleichbare Ergebnisse lieferten, war kein Programm in der Lage alle Problemstellungen der Testaufgaben mit ausreichender Genauigkeit zu lösen. Zwei der

getesteten Programme ECLIPSE und TOUGH II sind am ITE bzw. in der BGR im Einsatz und sollen zur Simulation der Fallbeispiele modifiziert und genutzt werden.

Die Auswirkung möglicher geochemischer Reaktionen auf CO₂-Speichergesteine und Deckschichten ist eines der Besorgnisse die mit Hilfe geochemischer Experimente und Simulationen untersucht werden. Verschiedene Simulationskonzepte kommen je nach Problemstellung zur geochemischen Prognose in Frage: Reaktionsgleichgewichte, reaktions-kinetische Ansätze, reaktive Transportsimulationen oder Reaktionsfortschrittberechnungen. Zur Berechnung reaktiver Transportmodelle ist die detaillierte Kenntnis der geologischen und chemischen Eigenschaften der Speicherstrukturen erforderlich. Daher muss die Prognose geochemischer Reaktionen auf standortspezifischen Informationen der Speicherbetreiber zur Mineralogie, Fluidzusammensetzung und zur komplexen Architektur der Lagerstätten aufbauen, welche durch spezielle Fluid- und Mineralanalysen und die Untersuchung natürlicher Vorkommen analoger, CO₂-beeinflußter Gesteine, entsprechend der ausgewählten Simulationskonzepte, in geeigneter Weise zu ergänzen sind. CO₂-beeinflußte Gesteine, wie z.B. aus den Thüringischen CO₂-Lagerstätten im Rotliegenden, oder des Buntsandsteins können Informationen zu langsam verlaufenden Reaktionen der Silikatumwandlung liefern, die in Laborexperimenten schlecht quantifiziert werden können.

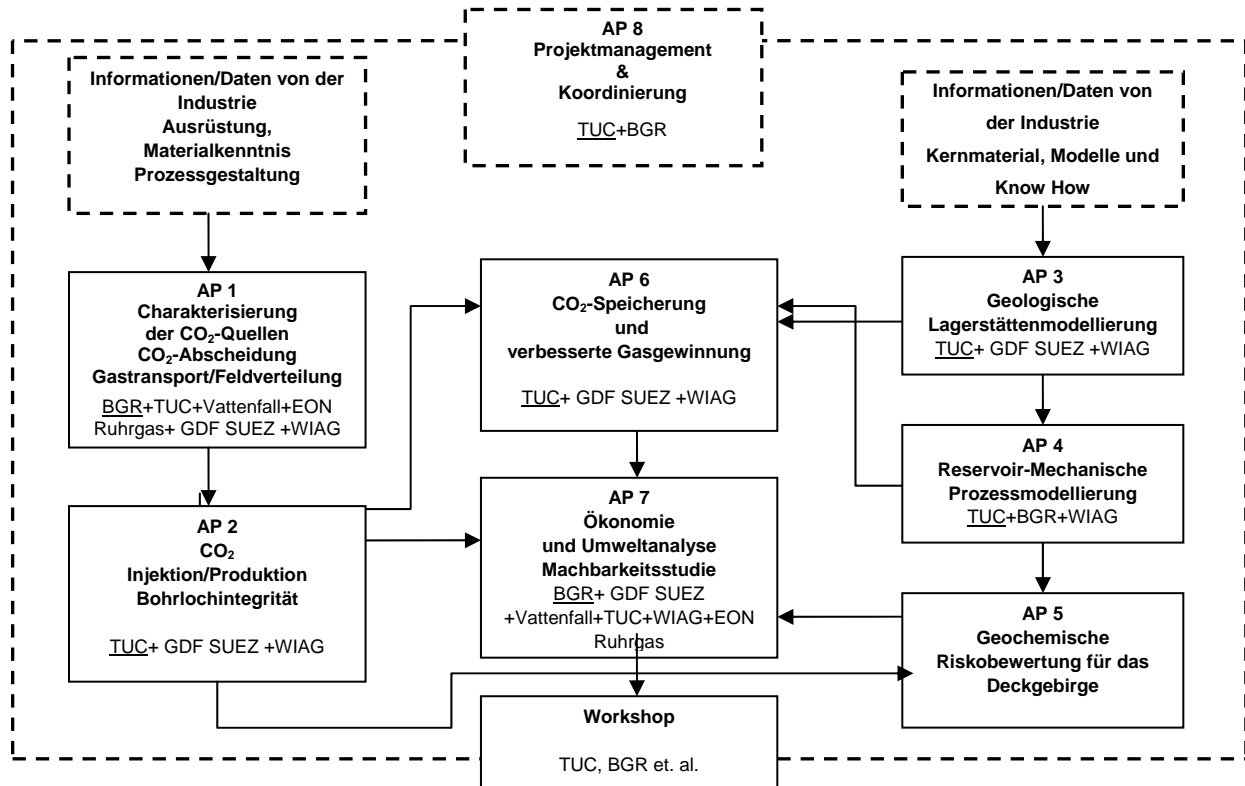
Für die reaktiven Transportsimulationen in Frage kommende Programme sind z. B. CHEMTOUGH (Industrial Research Ltd.), TOUGHREACT (Lawrence Berkeley National Lab), oder SHEMAT (RWTH-Aachen). Leistungsfähigere geochemische Simulationsprogramme, wie PHREEQC haben nur begrenzte Möglichkeiten zur Fluidtransportsimulation. Die genannten Programme werden auf der Basis langjährig erprobter Versionen weiterentwickelt. TOUGHREACT wird im Oktober dieses Jahres öffentlich erhältlich sein und im vorgeschlagenen Projekt zum Einsatz kommen (May 2004).

Zur Berechnung der Investitions- und Betriebsausgaben bei Abtrennung, Transport und Speicherung von CO₂ kann auf Erfahrungen von Vattenfall AB (Odenberger und Svenson 2003) zurückgegriffen und das von Egberts et al. (2003) entwickelte und bereits von BGR zur Untersuchung möglicher Speicherszenarien genutzte GESTCO-DSS eingesetzt werden.

Arbeits- und Zeitplanung

Das folgende Diagramm gibt einen Überblick über die Projektstruktur, die Arbeitspakete und die daran mitwirkenden Partner, sowie den Informationsfluss innerhalb des Projektes. Die ersten drei Arbeitspakete stellen aufgrund der aufbereiteten Industriedaten Informationen für die Kernarbeitspakete (4-6) bereit. Die Charakterisierung der CO₂-Quellen, sowie die Definition der Anforderungen an CO₂-Transport und Feldverteilung sind Gegenstand des Arbeitspaketes 1. Die Eignung bestehender Untertageinstalltionen und die technischen Anforderungen an Injektions- und Fördersonden werden im Arbeitspaket 2 untersucht. Die Erstellung neuer, sowie die Verbesserung bestehender geologischer Lagerstättenmodelle sind im 3. Arbeitspaket vorgesehen. Durch CO₂-Injektion verursachte physikalische und chemische Reaktionen des Speichers und der Deckschichten werden in den Kernarbeitspaketen (4-6) untersucht. Im Arbeitspaket 4 werden die physikalischen Eigenschaften des CO₂-reichen Gases und die durch CO₂ induzierten hydrodynamischen Prozesse untersucht. Das 5. Arbeitspaket widmet sich der Simulation geochemischer Reaktionen und der Abschätzung deren Auswirkungen auf Speicher und überlagernde Schichten. Die Zeitplanung für Arbeitspaket 5 sieht vor, dass die für die numerischen

Modelle benötigten Informationen im ersten Projektjahr erarbeitet werden, so dass zusätzliche Informationen aus den Arbeitspaketen 1 und 2 über die Gaszusammensetzung und dessen Eigenschaften bei den reaktiven Transportsimulationen mit berücksichtigt werden können.



Die Simulationen in den Arbeitspaketen 4 und 5 sind mehr grundsätzlicher Natur, während im 6. Arbeitspaket Lagerstättensimulationen zur CO₂-Injektion und Ausbeutesteigerung anhand der repräsentativen Fallbeispiele durchgeführt werden. Die Informationen aller vorhergehenden Arbeitspakete gehen in die technische, ökonomische und ökologische Gesamtbewertung der CSEGR-Option, einschließlich Abscheidung und Transport, im 7. Arbeitspaket ein.

Für die Durchführung des interdisziplinären Forschungsvorhabens waren 36 Monate vorgesehen. Die Dauer einzelner Arbeitspakete und der generelle Informationsfluss zwischen den Arbeitspaketen sind im voranstehenden Diagramm dargestellt. Bedingt durch Personalakquisitionsprobleme wurde das Projekt mit einer 6-monatigen Verspätung gestartet. Der Projektträger Geotechnologien gewährte jedoch eine kostenneutrale Verlängerung, so dass die Projektlaufzeit am 31.10. 2008 endete.

References

- Clauser, C. (ed., 2003): Numerical Simulation of Reactive Flow in Hot Aquifers SHEMAT and Processing SHEMAT. Springer.
- Clemens, T., Wit, K. (2001): Zero Emission Power Generation. Power plant concepts and CO₂ injection into gas fields. Report EP 2001-5403, Shell Technology EP, Rijswijk.

- Edenhofer, O. (2003): Wege zur nachhaltigen Klima- und Energiepolitik. Aus Politik und Zeitgeschichte B27, 2003:18-26.
- Egberts, P., Keppel, J. F., Wildenborg, T., Hendriks, C., van der Waart, A. S. (2003): GESTCO-DSS; A decision support system for underground carbon dioxide sequestration. GESTCO project final report (unpublished).
- Gauss, I., M. Azaroual, I. Czernichowski-Lauriol (2003): Long term geochemical modelling of CO₂-caprock interactions. in: Gas-Water-Rock Interactions Induced by Reservoir Exploitation, CO₂ Sequestration, and other Geological Storage. Les Recontres Scientifiques de l'IFP. Abstract Volume: S. 34.
- Jikich, S.A., Smith, D.H., Sams, W.N., Bromhal, G.S.: Enhanced Gas Recovery (GR) with Carbon Dioxide Sequestration: A Simulation Study of Effects of Injection Strategy and Operational Parameters, SPE 84813, SPE Eastern Regional/AAPG Eastern Section Joint Meeting, Pittsburgh, Pennsylvania, 6-10 Sept. 2003
- Johnson, J. W., J. J. Nitao (2003): Reactive transport modelling of geologic CO₂ sequestration at Sleipner. In: Gale, J., Y. Kaya Greenhouse Gas Control Technologies (Pergamon).
- Mamora, D.D.; Seo, J.G. (2002): Enhanced Gas Recovery by Carbon Dioxide Sequestration in Depleted Gas Reservoirs, SPE 77347, Annual Techn. Conference and Exhibition, San Antonio, Texas, 29.Sept.-02.Oct. 2002
- May, F., S. Brune, P. Gerling, P. Krull (2003): Möglichkeiten zur untertägigen Speicherung von CO₂ in Deutschland – eine Bestandsaufnahme. Geotechnik 26,3: 162–172.
- Odenberger, M., Svenson, R. (2003): Transportation Systems for CO₂. – Application to Carbon Sequestration. Chalmers University of Technology, Department of Energy Conversion, Technical Report No. T2003-273.
- Oldenburg, C.M., S. M. Benson (2002): CO₂ injection for enhanced gas production and carbon sequestration. SPE 74367, International Petroleum Conference and Exhibition, Mexico, 10-12. Febr. 2002
- Oldenburg, C.M., K. Pruess, S. M. Benson (2001): Process modelling of CO₂ injection into natural gas reservoirs for carbon sequestration and enhanced gas production. Energy and Fuels 15:293–298.
- Oldenburg, C. M., S.H. Stevens, S.M. Benson (2003): Economic feasibility of carbon sequestration with enhanced gas recovery (CSEGR). In: Gale, J., Y. Kaya Greenhouse Gas Control Technologies (Pergamon).
- Pearce, J.M., Baker, I. Czernichowski-Lauriol, C. A. Rochelle, N. Springer, E. Brosse, B. Sanjun, K. Bateman, S. Lanini (2001): How will reservoir and caprock react with injected CO₂ at Sleipner? Preliminary evidence from experimental investigations. — In: D. Williams et al. (eds.) Greenhouse Gas Control Technologies. (Cisro Publishing) Collinwood, p. 355-359.

Pruess, K. (2003): Numerical simulation of leakage from a geologic disposal reservoir for CO₂, with transitions between super- and sub-critical conditions. Proceedings, TOUGH Symposium 2003, <http://esd.lbl.gov/TOUGHsymposium/>

Pruess K., A. Bielinski, J. Ennis-King, Y. Le Gallo, J. Garcíá, K. Jessen, T. Kovcek, D. H.-S. Law, P. Lichtner, C. Oldenburgh, R. Pawar., J. Rutqvist, C. Steefel, B. Travis, C.-F. Tsang, S. White, T. Xu. (2003): Code intercomparison builds confidence on numerical models for geologic disposal of CO₂. In: Gale, J., Y. Kaya Greenhouse Gas Control Technologies (Pergamon).

Van der Burgt, M.J., J. Candle, V. K. Boutkan (1992): „Carbon dioxide disposal from coal-based IGCC's in depleted gas fields“, Energy Conversions Management, 33 (1992, 5-8), 603.

van Luijk (2003): CO₂ reduction by subsurface storage in a depleted gas field. <http://www.crust.nl>

WBGU (2003): Energiewende zur Nachhaltigkeit. (Springer), Berlin, Heidelberg, New York.

Xu, T, J. A. Apps, and K. Pruess, Reactive geochemical transport simulation to study mineral trapping for CO₂ disposal in deep arenaceous formations. Journal of Geophysical Research 108, No. B2.

Ziesing, H.-J. (2003): Treibhausgas-Emissionen nehmen weltweit zu - Keine Umkehr in Sicht. DIW-Wochenbericht 39/03.

Ziesing, H.-J. (2004): CO₂-Emissionen in Deutschland im Jahre 2003: Witterungsbedingt leichte Steigerung. DIW-Wochenbericht 10/04.

Work Package 1: Surface equipment for CO₂ separation and injection

Issues:

- Main Characteristics for the Source of CO₂
- Transport Network and Conditions for 2 cases
- Cost Estimation for CO₂ Transport
- Field Distribution of the CO₂

Authors:

Christian Bernstone, Vattenfall R&D AB, Stockholm

Stefan Liljemark, Vattenfall Power Consultant AB, Gothenburg

Josef Höllwart, Reservoir/Storage Facilities, Competence Centre, E.ON Ruhrgas AG, Essen

| | |
|---|----|
| 1.1 Case Study Schwarze Pumpe – Altmark | 18 |
| Kurzfassung | 18 |
| Summary..... | 19 |
| 1.1.1 Introduction | 21 |
| Background | 21 |
| Purpose of report..... | 21 |
| 1.1.2 Characterization of industrial source | 22 |
| Schwarze Pumpe power plant..... | 22 |
| Capture based on O ₂ /CO ₂ recycle (oxyfuel) combustion | 22 |
| Estimation of CO ₂ quantities versus time | 23 |
| 1.1.3 Pipeline route | 24 |
| Pipeline evaluation criteria..... | 24 |
| Suggested route Schwarze Pumpe – Altmark | 24 |
| Transportation scenarios (different pipeline dimensions) | 26 |
| 1.1.4 Boundary conditions for the CO ₂ transportation | 27 |
| CO ₂ quality | 27 |
| Determination of gas mixture components | 28 |
| Gas-conditioning for transport | 29 |
| 1.1.5 Cost of CO ₂ transportation | 30 |
| Introduction..... | 30 |
| Capital cost calculation models | 30 |
| Total cost economical model | 31 |
| Resulting scenario-based investment costs | 32 |
| Conclusions | 33 |
| References..... | 34 |
| 1.2 Case Study CO ₂ Transport Dornum – Barrien | 35 |
| Kurzfassung | 35 |
| Summary..... | 35 |

| | |
|--|----|
| 1.2.1 Characterization of industrial source, Dornum Gas Separation Plant | 36 |
| 1.2.2 Estimation of CO ₂ quantities vs. time | 37 |
| 1.2.3 Pipeline route, suggested route Dornum – Barrien Gasfield | 38 |
| Diameter determination | 38 |
| 1.2.4 CO ₂ Quality | 39 |
| 1.2.5 Cost of CO ₂ transportation | 39 |
| Conclusions | 40 |
| References..... | 40 |

1.1 Case Study Schwarze Pumpe – Altmark

Authors: Christian Bernstone, Vattenfall Research and Development AB, Stockholm

Stefan Liljemark, Vattenfall Power Consultant AB, Gothenburg

Kurzfassung

Um wirtschaftliche Vorteile für den Einsatz der Kohlendioxidabscheidung und -speicherung (CCS) in fossil gefeuerten Kraftwerken zu erreichen, sind die Anlagen und Verfahrensweisen für Abscheidung, Transport und Speicherung auf die größten fossil gefeuerten Kraftwerke auszulegen. Das Braunkohlekraftwerk Schwarze Pumpe, das ca. 10 Mt CO₂ pro Jahr ausstößt, ist eine solche Großanlage.

Unter Berücksichtigung der verfügbaren Speicherkapazität, der vorhandenen Infrastruktur sowie der gesammelten Erfahrungen in den Bereichen Technik und Sicherheit bieten sich die Erdgaslagerstätten im Norden Deutschlands zur CO₂-Speicherung an. Sie sind gut erkundet und bieten ein geeignetes Deckgebirge zur langfristigen Speicherung von Flüssigkeiten bzw. Gasen. Ihre Speicherkapazität lässt sich relativ zuverlässig anhand vorhandener Daten aus der Erdgasförderung abschätzen.

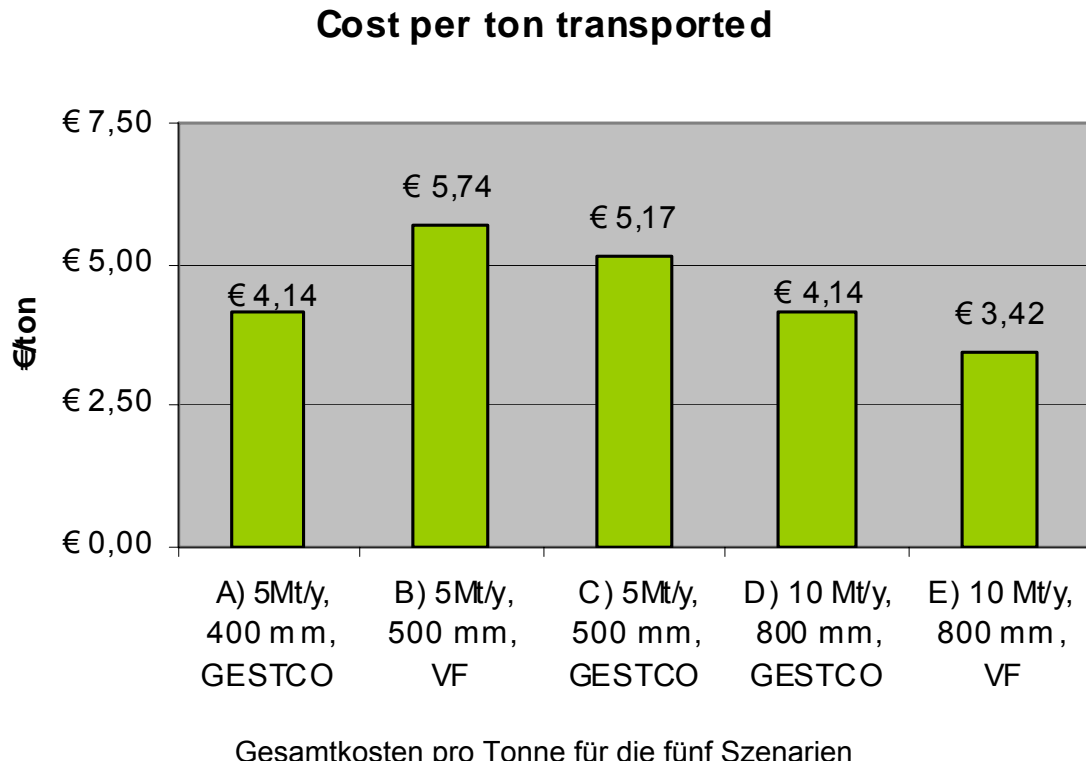
Im F&E-Projekt CSEGR wird die Machbarkeit der Kohlendioxidspeicherung in ausgebeuteten Erdgaslagerstätten mittels der so genannten „Enhanced Gas Recovery“ Technik, d.h. Nutzung der Injektion von Gasen zur Steigerung der Gasausbeute, untersucht. Der vorliegende Bericht bezieht sich auf Maßnahmen im Arbeitspaket 1, das sich mit der technischen und materiellen Grundlage der Behandlung des einzuspeisenden CO₂-haltigen Gases und dem Transport des CO₂ in die Erdgaslagerstätte Altmark befasst.

Die Erdgaslagerstätten in der Altmark bilden einen großen zusammenhängenden Speicher, der Schätzungen zufolge die Gesamtmenge des im Kraftwerk Schwarze Pumpe abgeschiedenen CO₂ aufnehmen kann. Bei voller Kapazitätsauslastung könnten im Speicher jährlich 10 Mt CO₂ eingelagert werden (entspricht zwei Blöcken mit einer Produktion von jeweils 5 Mt). Unter Ansatz einer voraussichtlichen Lebensdauer von ca. 40 Jahren beläuft sich die Gesamtproduktion auf etwa 400 Mt CO₂, wobei der Transport des CO₂ mittels Pipeline erfolgt. Im vorliegenden Bericht werden zwei Fälle analysiert, nämlich die Abscheidung von CO₂ in nur einem oder in zwei Blöcken, d.h. 5 Mt bzw. 10 Mt CO₂-Produktion pro Jahr.

Die im Bericht dargelegten Erkenntnisse lassen sich kurz wie folgt zusammenfassen:

- Ein anzunehmendes definiertes CO₂-Gasgemisch aus der CO₂-Abscheidung basierend auf einem Verbrennungsprozess in O₂/CO₂-Atmosphäre (Oxyfuel).
- Eine 330 km lange in Frage kommende Pipelinetrasse vom Kraftwerk Schwarze Pumpe in die Altmark. Die Trasse folgt zwar bestehenden Pipelinetrassen, eine neue Pipeline ist dennoch zu errichten (d.h. es gibt keine bestehende Pipeline, die genutzt werden könnte).

- CO₂ muss im überkritischen Zustand transportiert werden. Die Verflüssigung und Komprimierung ist in die Abscheideanlage integriert und so konfiguriert, dass entlang der Trasse keine Verdichterstationen erforderlich sind. Aus transporttechnischer Sicht ist ein Mindestdruck von 85 bar aufrechtzuerhalten, um das CO₂ konstant im überkritischen Zustand zu halten. Unter Berücksichtigung eines Druckabfalls um 25 bar über die Gesamtlänge der Pipeline sollte der Eintrittsdruck am Kraftwerk 110 bar betragen.
- Die Gesamtkosten für den CO₂-Transport vom Kraftwerk Schwarze Pumpe in die Altmark wurden ausgehend von einer Abschreibung über 25 Jahre und einem Zinssatz von 7 % berechnet. Für die untersuchten Fälle auf der Grundlage von 5 Mt/a liegen die Investitionen zwischen 187 Mio. € und 320 Mio. €. Die Investitionskosten für den Fall 10 Mt schwanken zwischen 373 Mio € und 384 Mio €. Die spezifischen Kosten liegen bei allen Szenarien zwischen 3,4 €/t und 5,7 €/t, d.h. für den Pipelinetransport ergeben sich klare wirtschaftliche Vorteile für den Transport von großen CO₂ Volumen.



Summary

To achieve economies of scale for CCS, the capture, transportation and storage system needs to be designed for the largest fossil-fuelled power plants. The large-scale lignite-fired power plant Schwarze Pumpe, which emits around 10 Mt of CO₂ per year, represents such a plant.

Considering the available storage capacity, surface infrastructure, security and technical experience, the gas fields in northern Germany provide good opportunities for CO₂ storage. These are well explored and have suitable overburden for the long-term

storage of fluids and their storage capacities can be estimated quite well from existing gas-field production data.

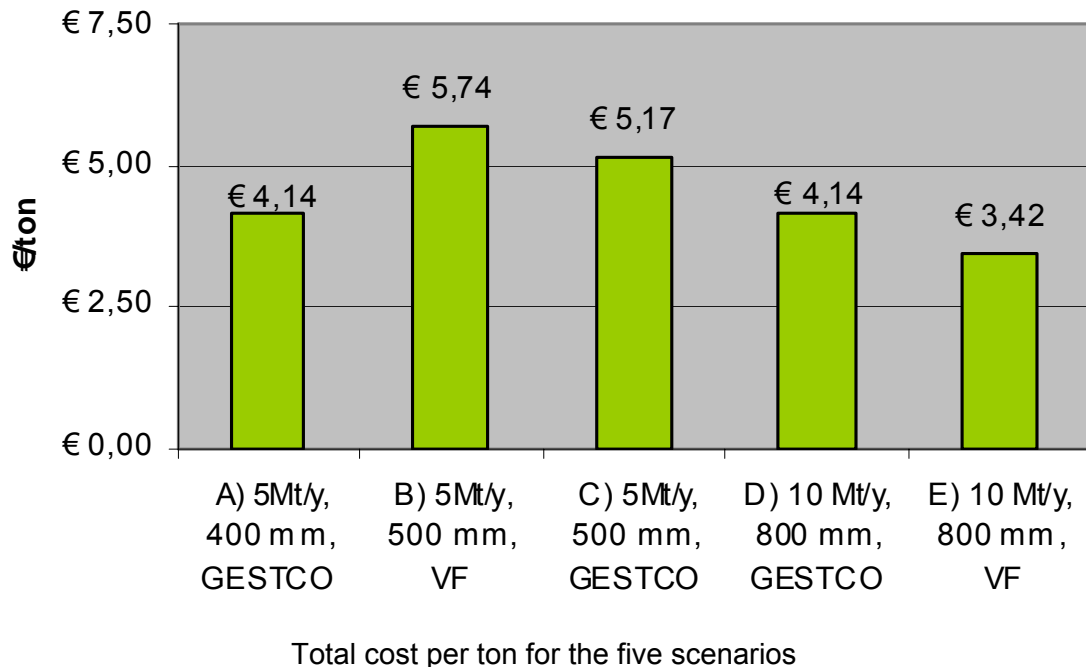
The R&D project CSEGR investigates the feasibility of Carbon dioxide Storage in depleted gas reservoirs by Enhancing natural Gas Recovery. This report concerns work contained in work package 1, investigating the technical and material basis to process the CO₂-carrying feed gas and transport the CO₂ to the Altmark natural gas reservoirs.

The Altmark natural gas reservoirs represent a large single-storage site, likely capable to take in the total amount of CO₂ produced by Schwarze Pumpe power plant. At full capacity, the storage would imply 10 Mt CO₂ to be stored annually (two blocks producing 5 Mt respectively). Considering an expected operation lifetime of about 40 years, the total output becomes about 400 Mt CO₂, with CO₂ transport by pipeline. Both cases of having one or two blocks with CO₂ capture will be analysed in this report, i.e. 10 Mt and 5 Mt CO₂ per year respectively.

In brief, the findings presented in this report are:

- A defined likely CO₂ gas mixture to be delivered from CO₂ capture based on O₂/ CO₂ recycle (oxyfuel) combustion
- A 330 km candidate pipeline route from the Schwarze Pumpe power plant to Altmark. The route follows existing pipeline corridors, though a new pipeline needs to be built (i.e., no existing pipelines can be utilised).
- CO₂ need to be transported in the dense phase. The liquefaction and pressurisation is integrated to the capture plant in such a way that no booster stations are required along the route. From the transport perspective, the minimum acceptable pressure of 85 bars should be maintained, securing that the CO₂ always stay as dense phase. Considering a pressure drop in that range of 25 bars over the length of the pipeline, the inlet pressure at the power plant should be 110 bars.
- The total cost for CO₂ transportation from Schwarze Pumpe power plant to Altmark was calculated using a fixed yearly instalment calculation method with 25 years and depreciation at 7% interest rate. For the 5Mt/y cases studied, the investment varies between M€ 187 to M€ 320. The investment cost for 10 Mt case varies between M€ 373 and M€ 384. The cost per tonne for all scenarios varies from € 3.4 to € 5.7, i.e., there is a clear economics of scale for pipeline transportation.

Cost per ton transported



1.1.1 Introduction

Background

To achieve economies of scale for CCS, the capture, transportation and storage system needs to be designed for the largest fossil-fuelled power plants. The large-scale lignite-fired power plant Schwarze Pumpe, which emits around 10 Mt of CO₂ per year, represents such a plant.

Considering the available storage capacity, surface infrastructure, security and technical experience, the gas fields in northern Germany provide good opportunities for CO₂ storage. These are well explored and have suitable overburden for the long-term storage of fluids and their storage capacities can be estimated quite well from existing gas-field production data.

Purpose of report

The purpose of the report is to contribute with results of WP1, CO₂ source-transport and field distributions (CO₂ supply and logistics), regarding:

- Characterization of power plant and fuel gas separation technology
- Identification of likely transport route and pipeline design
- Calculation of source to wellhead cost

The results are used in WP2, CO₂ compression, injection and production (completion of CO₂-injectors, well integrity, and surface & subsurface equipment).

1.1.2 Characterization of industrial source

Schwarze Pumpe power plant

The modern, 1600 MW lignite-fired power plant Schwarze Pumpe is a good representative of the power plants operated by Vattenfall Europe in NE Germany, both from its size and location (Figure 1.1). Assuming an utilisation of 7500 h per year, each block will produce 5.2 Mt CO₂ per year. Over an operational lifetime of 40 years, both blocks of the Schwarze Pumpe power plant would emit about 400 Mt CO₂.

The CO₂ storage potential of the hydrocarbon fields was covered by the European FP5 project GESTCO. The total capacity of the larger German gas deposits is around 2.5 Gt CO₂. The natural gas reservoirs of Altmark are located approximately 150 km west of Berlin. There are nine sub-reservoirs, of which the main sub-reservoir is the Salzwedel-Peckensen. Altogether the reservoirs since 1969 have produced more than 200 billion m³ of gas, a volume equivalent to more than 500 Mt of CO₂ under reservoir conditions. This capacity is sufficient for storing all of the CO₂ emitted during the lifetime of a large lignite-fired power station, like the Schwarze Pumpe power plant.

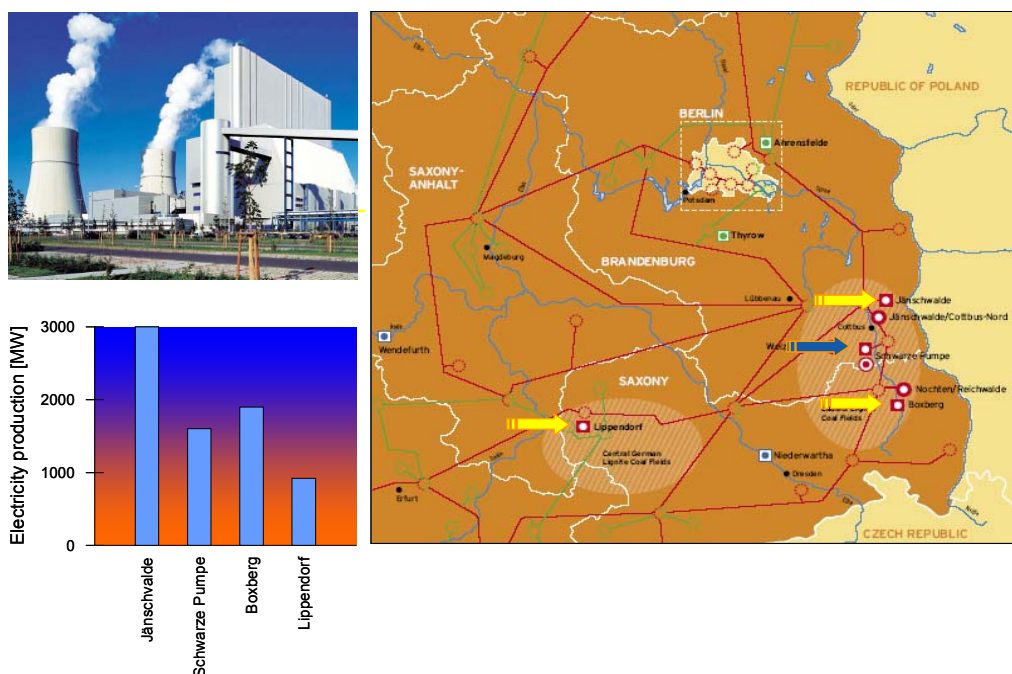


Figure 1.1: Schwarze Pumpe power plant is a good representative of the lignite-fuelled power plants operated by Vattenfall in the Lausitz area.

Capture based on O₂/CO₂ recycle (oxyfuel) combustion

Numerous concepts for CO₂ capture from power processes have been proposed. These concepts are in various stages of development and are therefore associated with a range of time frames for possible commercial application in power plants. Many of these concepts also require a considerable research and development effort prior to commercialisation. Of the three major approaches for CO₂ removal (post-

combustion capture, pre-combustion capture and oxyfuel combustion) this case study focuses on the oxyfuel combustion technology.

In oxyfuel combustion, the fuel is combusted in an atmosphere of oxygen and recycled CO₂, instead of air (Figure 1.2). This results in a flue gas consisting mainly of CO₂ and water vapour. Cleaning of the flue gases, i.e. removing the conventional pollutants and condensing the water vapour, produces an almost pure CO₂ stream. Combustion in oxygen is a widespread technology in the steel and glass manufacturing industry. Cryogenic air separation for production of oxygen is also commercially well established, although at a somewhat smaller scale than required for the largest power plants. Coal fired steam boilers would require slight modification.

To capture CO₂ always requires energy, which results in a higher fuel-consumption and consequently a lower electric efficiency than the baseline plant without CO₂ capture. This, together with the need for additional equipment, increases the specific investment. The combination of these two factors increases the electricity generation costs.

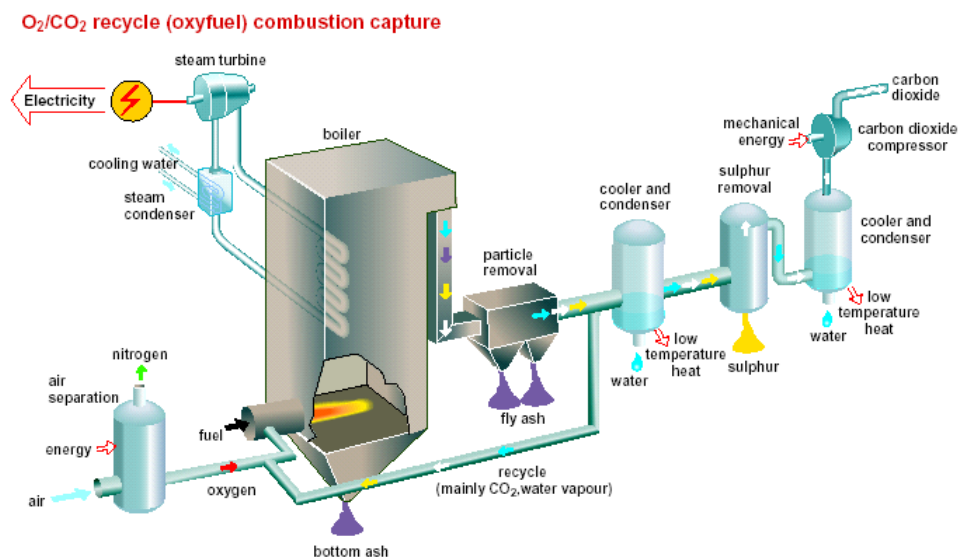


Figure 1.2: Coal-fired power plant with O₂/CO₂ recycle (oxyfuel) combustion capture.

Estimation of CO₂ quantities versus time

A CCS system requires transportation of the captured CO₂ from the power plant to the storage site in an economical and technologically feasible way. For large quantities onshore (> 1 Mt/y), pipeline is the transportation alternative that provides this (SVENSSON et al, 2004). Common for all CO₂ pipelines are that they are designed for dense phase/supercritical conditions

The Altmark natural gas reservoirs represent a large single-storage site, likely capable to take in the total amount of CO₂ produced by Schwarze Pumpe power plant. At full capacity, the storage would imply 10 Mt CO₂ to be stored annually (two blocks producing 5 Mt respectively). Considering an expected operation lifetime of about 40 years, the total output becomes about 400 Mt CO₂, with CO₂ transport by pipeline.

Both cases of having one or two blocks with CO₂ capture will be analysed in this report, i.e. 10 Mt and 5 Mt CO₂ per year respectively.

The volumes that need to be handled from high-range point sources, such as the Schwarze Pumpe power plant, are significant, with a project of scale much larger than any of the current CO₂-storage projects that are in operation today. For example, the annual storage volumes of Sleipner are 1 Mt, In Salah ~1.1 Mt, and Weyburn 1.7 Mt respectively.

1.1.3 Pipeline route

Pipeline evaluation criteria

The route is the main factor that decides the feasibility of a pipeline project. A number of criteria were set up for the Schwarze Pumpe – Altmark pipeline route (see Table 1.1). Gate valves are installed to shut down the pipeline flow in case of a rupture. The location and the distance between valves depend on site-specific factors such as population density and topography. The gate valves are controlled by the measurement system that controls the flow and detects if there are any rapid pressure drops. However, no characterization of suitable intervals of gas discharge safety valves has been done as part of this work. A standard 20 km interval distance is used in the cost calculations.

Table 1.1: Criteria for assessing a suitable pipeline corridor

| No. | Criteria | Description |
|-----|---|---|
| 1 | Minimisation of overall length and number of crossings (bodies of water, streets, railways) | This minimisation is relevant for the costs of realisation as well as the costs for operation as pressure loss depends on the length of the pipeline. |
| 2 | Extensive use of existing routes | The joint use of existing routes is common practice. This minimise the interference with other interests and results in an integration in the existing regional development and consequently in a route layout with a good chance of success. |
| 3 | Avoidance of residential structures as well as topographic depressions | The properties of the medium as well as the assumed throughput in case of damage suggest that the pipeline should be constructed with a minimum distance to gatherings of any type as a function of topographical and other conditions. |
| 4 | Avoidance of higher ground | When crossing high elevations, a loss in pipeline pressure may result in a drop below the minimum system pressure. This may require an additional station suitable for increasing the pressure |
| 5 | Avoidance of nature reserves, closed woodlands etc | Crossing nature reserves is generally a problem (exemptions with conditions under nature protection laws). Woodlands are a problem if the construction requires clearings and replacement of plantations. |

Suggested route Schwarze Pumpe – Altmark

Based on the criteria list, and a map with existing pipeline corridors in Germany, a suggestion for a route southwest of Berlin has been constructed, see Figure 1.3 and Figure 1.4. As can be seen in Figure 1.4, the whole route follows existing pipeline

corridors. The approximate elevation profile for the route is shown in Figure 1.5. The highest point is 150 meter (above sea level), the lowest 20 meters and the greatest single elevation is approximately 60 meters. The approximate length is 330 km.

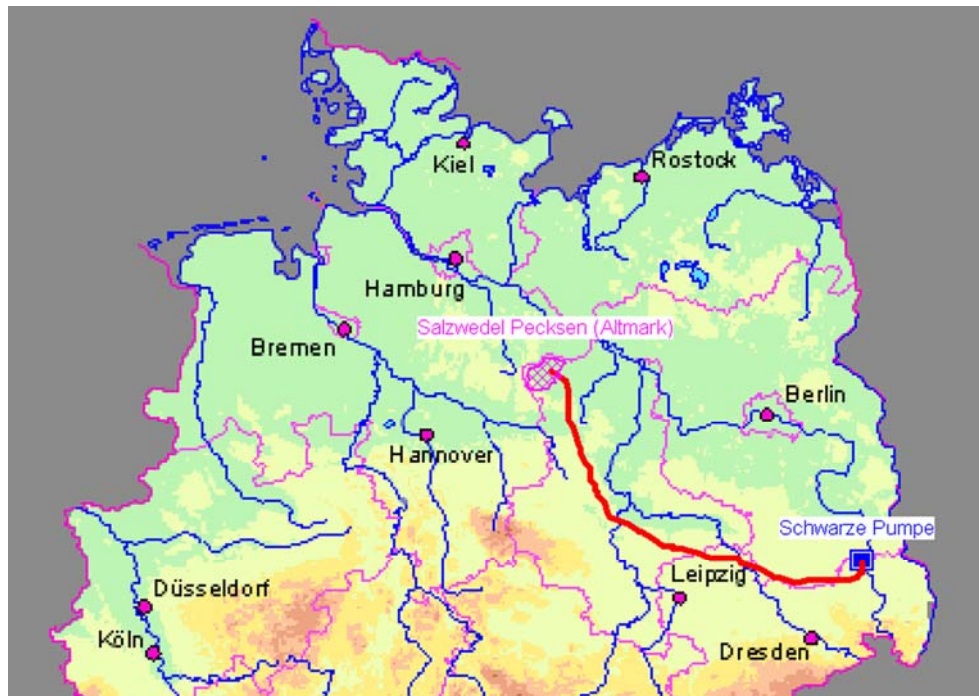


Figure 1.3: Overview of the route from Schwarze Pumpe to Altmark.

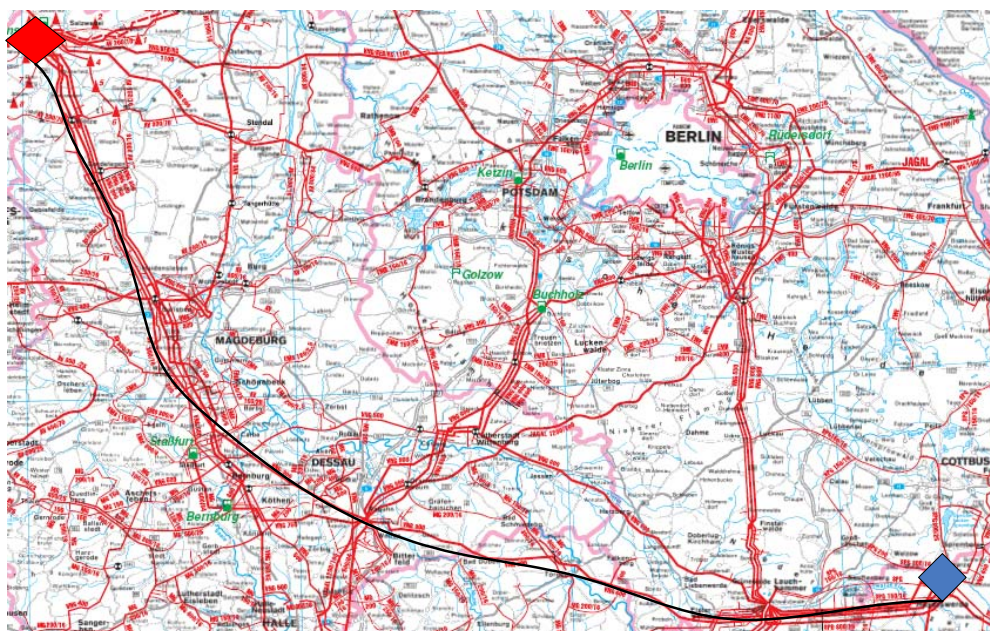


Figure 1.4: The route follows existing pipelines corridors. (Map from Verlag Glückauf Essen GmbH, 2003).

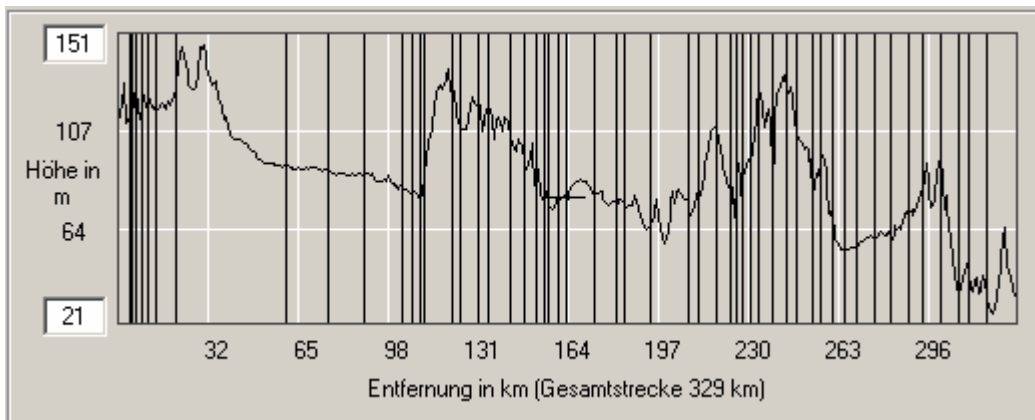


Figure 1.5: Approximate elevation profile for the suggested route

Transportation scenarios (different pipeline dimensions)

It is assumed that new pipelines are required for CO₂ transport, i.e., no existing pipelines can be reused. Five scenarios using different cost-calculation tools and different amounts of CO₂ transported have been evaluated. The scenarios are:

Scenario A: 5Mt/y 400-GESTCO: Total amount transported is 5 Mt/y. The pipeline diameter was determined by an equation (Equation 1) published in the report “Building the cost curves for CO₂ storage” (IEA Greenhouse gas R&D programme, 2005) resulting in a diameter of 400 mm. The costs were calculated using the GESTCO DSS cost equation (Egberts, 2003).

Scenario B: 5Mt/y 500-VF: Total amount transported is 5 Mt/y. The pipeline diameter was determined using the GESTCO DSS tool (Egberts et al, 2003) resulting in a diameter of 500 mm. The costs were calculated using a modified cost-calculation tool.

Scenario C: 5Mt/y 500-GESTCO: Total amount transported is 5 Mt/y. The pipeline diameter was determined using the GESTCO DSS tool, i.e. 500 mm (Egberts et al, 2003). The costs were calculated using the GESTCO DSS cost equation (Egberts, 2003).

Scenario D: 10Mt/y 800-GESTCO: Total amount transported is 10 Mt/y. The pipeline diameter was determined on basis of results from the European FP5 project CO2STORE, which showed that an 800 mm pipeline would be sufficient for a 10 Mt/y scenario in eastern Germany. The costs were calculated using the GESTCO cost equation (Egberts, 2003)

Scenario E: 10Mt/y 800-VF: Total amount transported is 10 Mt/y. The pipeline diameter was determined on basis of the same study as case D, i.e. 800 mm. The costs were calculated using the same model as in Scenario B.

IEA-GHG diameter equation

The outside diameter for the Scenario A pipeline was calculated using Equation 1. It is an approximation that calculates the diameter (D) based on the maximal mass flow (F), velocity (v) and density (ρ) of the transported CO₂.

$$D = \frac{\left(\frac{F}{v \times \pi \times 0.25 \times \rho} \right)^{0.5}}{0.001}$$

The input data is listed in Table 1.2. The resulting pipeline diameter for scenario is 383 mm. Round-off value used in the cost calculations was 400 mm.

Table 1.2: Data used in the calculation of pipeline diameter of Scenario A.

| Symbol | Description | Unit | Comment |
|--------|-------------------|-------------------|---|
| D | Pipeline diameter | mm | Outer diameter |
| F | Flow | kg/s | 185 kg/s (assuming 7500 operating hours per year) |
| v | Velocity | m/s | Set to 2 m/s |
| ρ | Density | kg/m ³ | Set to 800 kg/m ³ |

Diameter determination by GESTCO DSS

The GESTCO DSS tool uses a look-up table to determine optimal diameter. It matches the mass flow of CO₂ with different diameters to identify the optimal one (Egberts et al, 2003). For the mass flow 5 Mt/y, the GESTCO DSS tool gave a diameter of 500 mm. This figure was used in Scenario B and C.

Diameter determination by Flow Simulator

Because pipelines suffer from temperature and pressure loss due to factors such as surrounding temperature, frictional loss and elevation, the flow properties may be simulated in order to determine the optimum pipeline diameter. Such flow simulations can be done using, for example, the process simulator ASPEN Plus® 11.1. The scenario D and E is based on the results from such a simulation, though using a slightly different elevation profile. The differences between the two profiles are small, and are not believed to have impact on the result.

1.1.4 Boundary conditions for the CO₂ transportation

CO₂ quality

Small amounts of other components will always be present in the captured CO₂ stream, and may affect the properties of the captured CO₂, e.g. the density. The amount of impurities in the captured stream technically depends on the fuel and

process technology, the approach used for the capture process and to what extent additional combustion gas cleaning technologies are applied. Thus, all capture technologies can supply an almost clean CO₂ stream. Still, CO₂ quality requirement is an important issue for the CO₂ captured from fossil fuel power generation because it has a significant influence on the capture cost. Principally the CO₂ quality requirement should be defined by CO₂ processing, transport, storage, and environmental and/or legal regulations. However, a balance must be made between the CO₂ quality requirement and the capture cost in order to achieve a cost-effective CO₂ avoidance.

Comparing with post-combustion and pre-combustion CO₂ capture technologies, a relatively simplified flue gas cleaning system is preferable for the oxyfuel combustion CO₂ capture technology. In addition, the CO₂ stream captured from post-combustion and oxyfuel combustion represent the characteristics of CO₂ impurities under an oxidation condition, and the CO₂ stream captured from the hydrogen/syngas approach shows the impurity characteristics under semi-reducing condition especially for sulphur components. As a part of optimisation, the implications of CO₂ qualities from various capture and cleaning approaches have to be investigated for CO₂ transport and storage. The starting point should be to investigate the CO₂ quality from a cost-efficient capture concept, which for oxidising conditions is represented by oxyfuel combustion with co-capture of SO₂ and corresponding flue gas cleaning technologies available today.

Determination of gas mixture components

The CO₂ quality is estimated based on the impurity removal efficiency of corresponding flue gas cleaning and CO₂ processing steps including necessary information on the trace components. The result is presented in Table 1.3.

Table 1.3: Estimated quality of CO₂ stream captured from coal-fired power plant (under oxidising conditions) for CO₂ transport and storage based on the oxyfuel co-capture concepts (without flue gas desulphurisation).

| Component | mass% | mol% | mg/Nm ³ |
|------------------|--------|--------|--------------------|
| CO ₂ | 96.898 | 96.423 | 1894409 |
| H ₂ O | 0.003 | 0.006 | 50 |
| O ₂ | 0.508 | 0.696 | 9937 |
| Ar | 0.944 | 1.035 | 18462 |
| N ₂ | 0.756 | 1.182 | 14783 |
| SO ₂ | 0.841 | 0.575 | 16453 |
| SO ₃ | 0.001 | 0.001 | 20 |
| NO | 0.048 | 0.070 | 937 |
| NO ₂ | 0.005 | 0.005 | 106 |
| CO | 0.003 | 0.005 | 58 |
| Cl | 0.001 | 0.002 | 25 |
| F | 0.0003 | 0.001 | 6 |
| Particulates | | | <5 |

There are some uncertainties on the behaviours of trace impurities in the CO₂ processing/liquefaction processes because the engineering data are currently not avail-

able for the type of industrial systems. With respect to this CO₂ quality presented in Table 1.3 is a conservative estimate.

It is possible to have a deep cleaning for the flue gas to provide a high quality of CO₂ stream, but the costs of flue gas cleaning may be increased significantly. A relatively lower quality of CO₂ stream captured from oxyfuel coal-fired combustion could be used to check how sensitive of the impurities impacting on the CO₂ transport and storage, and how large the cost saving margin could be for the flue gas cleaning.

Gas-conditioning for transport

After the CO₂ has been captured, it needs to be conditioned to meet the requirements for transportation and storage, i.e., compression of CO₂, purification, liquefaction/non-condensable gas separation, and further raising the pressure depending on the requirements for CO₂ transport and injection. For pipeline transportation, the CO₂ stream pressure needs to be raised above the critical pressure, i.e. a CO₂ pressure above 73.8 bar (HOLTZ et al, 1999).

Booster/regulator stations may be installed along the route to adjust the pressure to desired level. Considering the total economy of a CCS project, it is better to raise the pressure to sufficient level at the power plant than to have booster stations along the route. The Altmark case study has a similar transportation outline to the CO2STORE case study that investigated CO₂ capture at the Schwarze Pumpe power plant with storage at the saline reservoir Schweinrich. The distance is similar, though with a slightly different elevation profile. The pressure loss along the pipeline was 25 bars. Due to the similarities between the two pipelines routes it is assumed that the pressure loss for the Altmark pipeline is of the same size, i.e. 25 bars.

Determining the operating pressure at the top of the well requires consideration of the pressure required at the bottom of the well to force CO₂ into the injection zone, the pressure increase in the pipe due to the height of the CO₂ column, and the pressure loss due to flow in the pipe. To displace the resident fluid in the formation, the pressure of the injected CO₂ must be somewhat higher than the formation pressure. On the other hand, increasing formation pressure may induce fractures in the formation.

The depth to the top of gas bearing layers considered for CO₂ storage at Altmark is 3135 meters. At present, the pressure in the undisturbed reservoir compartments amounts to 42.5MPa. During the production, the pressure evolved differently due to inhomogeneity between the layers and varies now between 4.5MPa and 22MPa. The formation temperature ranges from 115 °C to 130 °C. Water infiltrates from the edges, but mainly from the bottom into the initially gas-saturated layers.

Injection into low-pressure reservoirs bears the transient risk of two-phase conditions in the wells or in the reservoir. Therefore, the pressure requirement to keep the CO₂ as dense phase while transported will result in a pressure that needs to be reduced from the injection standpoint, at least in the early stages of injection. As the reservoir

pressure is raised to the same level as the adjacent undisturbed reservoir compartments, the risk of two-phase conditions is reduced.

Due to the above-mentioned reasons, the design inlet pressure from capture at Schwarze Pumpe power plant is set to 110 bar, with a well head delivery pressure of 85 bar. No additional booster station is required.

1.1.5 Cost of CO₂ transportation

Introduction

A realistic economical target for a complete large-scale CCS chain, including capture, transport and storage, is a total cost of 20 €/tonne CO₂. The largest item is the CO₂ capture cost. Capture is also the technical part that has the largest potential for improvement, while transportation and storage of CO₂ often is referred to as known technology. The cost for transportation and storage is still a critical factor for the commercialisation of CCS.

The purpose is to evaluate the economics for a CO₂ transportation of scenarios based on the case study Schwarze Pumpe to Altmark.

The following is not included in the cost evaluation:

- CO₂ Capture. Note that included in the capture stage is the CO₂ conditioning, i.e. compression, cooling and separation of non-wanted components prior to entering the pipeline.
- CO₂ Storage. The cost for storage, including CO₂ injection will be covered in other parts of the CSEGR project

Capital cost calculation models

The GESTCO DSS model

The capital costs can be calculated using generic cost equations. Such an equation was developed for the GESTCO-DSS software (Egberts et. al. 2003). The investment in pipeline (C) is based on the specific investment (S), a terrain factor (T), an assurance factor (A), the outside diameter (D) and the pipe length (L). This equation has been used for the cost calculations for the Scenario A, C and D. The input data is listed in Table 1.4.

$$C = S \times A \times D \times \sum_i^n L_i \times T_i$$

The terrain cost is an important cost factor that varies with the type of terrain. Egberts with others (2003) have quantified relative cost-factors for different terrain types. The relative cost is considered to be 0.9 while utilising existing routes, 1.0 in normal terrain, 1.4 in the case of road and river crossings, and 10 for urban areas. Based on the findings in the scenario description, the eastern route has been divided in four different terrain types of various lengths (L):

- Existing routes – the use of existing infrastructure corridors, distance 295 km
- Normal terrain – typical countryside terrain, distance 10 km
- Crossings – crossings of rivers/roads/railways, distance 20 km.
- Urban area, distance 5 km

Table 1.4: Data used in the calculation of specific pipeline investment of Scenario A, C and D.

| Symbol | Description | Unit | Comment |
|----------------|------------------------------------|------------------|--|
| S | Specific investment pipeline | €/m ² | Factor for material costs. Set to 1100 [†] |
| T _i | Terrain factor | - | Impact from different terrain types, as describe in text |
| A | Assurance factor | | Factor for miscellaneous costs. Set to 1.2 [†] |
| D | Outside diameter | m | Result from diameter determination |
| L _i | Pipe length for different terrains | m | Result from route identification |

[†] Egberts et al, 2003

Modified model

Based on other studies a modified cost-calculation tool has been set up and tested for the Scenario B and E. The following input is required for the Schwarze Pumpe-Altmark route:

- Diameter of pipeline
- Total length using existing pipeline corridors: 330 km
- Estimation of the number of highway crossings: 5 crossings
- Estimation of the number of great water passages: 5 crossings
- Distance between gate valves: used value 20 km + 2 stations in the ends
- Steel price: 16400 €/m³ (~2050 €/ton)
- Electricity consumption gate valves: used value 30000 kWh/y per station
- Electricity price: used value 0.08 €/kWh

Total cost economical model

The economical model used for calculating the total costs is an annuity model divided by the amount of CO₂ transported (I), as described by Equation 3:

$$Cost = \frac{C \cdot \frac{r}{1 - (1+r)^{-n}} + O}{I}$$

The operation and maintenance costs (O) include costs for routine operation as well as costs for maintenance and repair. If booster stations are needed, energy costs are also included. In the GESTCO DSS, the operation and maintenance costs are calculated as a factor to the investment (Egberts et. al. 2003). The default value in the GESTCO DSS program (2.5%) has also been used for this case.

Table 1.5. Description of the parameters used in calculation of the total transportation cost

| Symbol | Description |
|--------|--|
| C | Capital investment costs |
| O | Operation and maintenance |
| r | Discount rate. In this study a general rate of 7% is used. |
| n | Depreciation time. In this study a general time of 25 years is used. |
| I | Transported amount of CO ₂ . |

Resulting scenario-based investment costs

The total investment costs for the five scenarios are illustrated in Figure 1.6. For the three 5Mt/y cases, the investment varies between M€ 187 to M€ 320. The investment cost for 10 Mt case varies between M€ 373 and M€ 384. The cost per tonne for all scenarios varies from € 3.4 to € 5.7 (see Figure 1.7). The Figure shows the economics of scale for pipeline transportation.

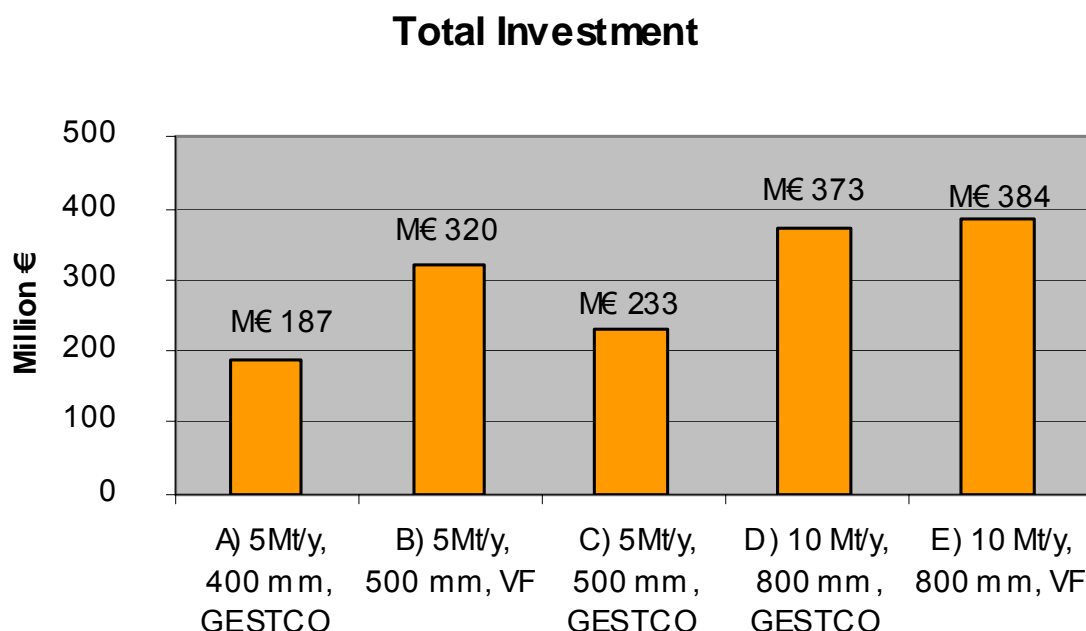


Figure 1.6: Total investment cost for the five scenarios

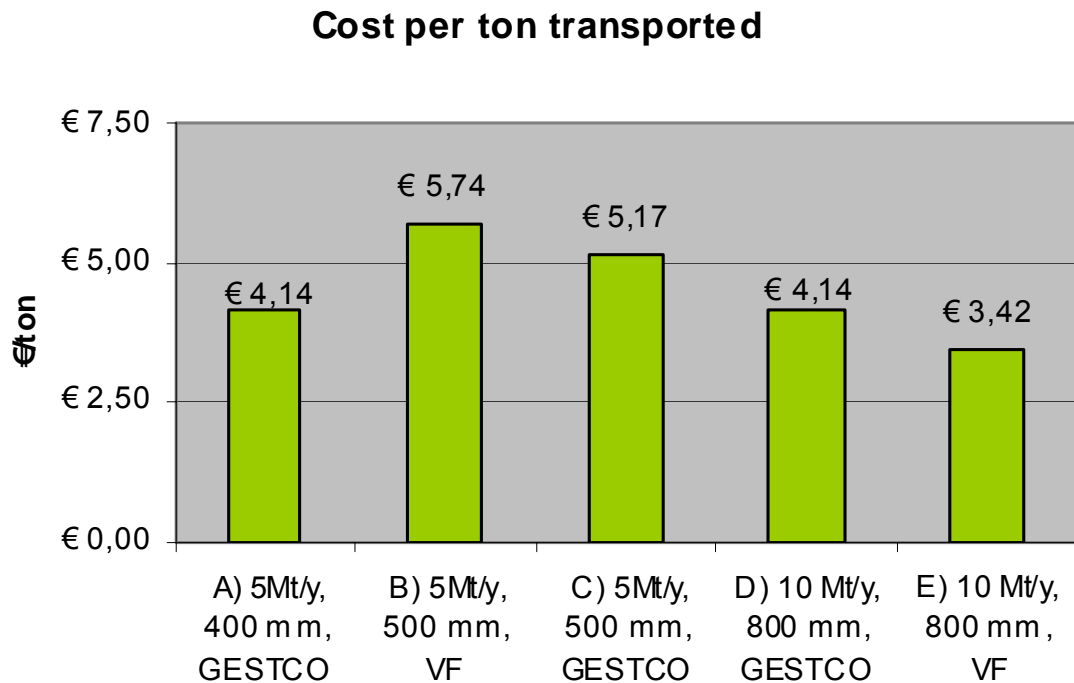


Figure 1.7: Total cost per ton for the five scenarios

Conclusions

- A defined likely CO₂ gas mixture to be delivered from CO₂ capture based on O₂/ CO₂ recycle (oxyfuel) combustion
- A 330 km candidate pipeline route from the Schwarze Pumpe power plant to Altmark. The route follows existing pipeline corridors, though a new pipeline need to be built (i.e., no existing pipelines can be utilised).
- CO₂ need to be transported as dense phase. The liquefaction and pressurisation is integrated to the capture plant in such a way that no booster stations are required along the route. The depth of the natural gas reservoir is about 3100 meters. The required injection pressure at surface is 85 bars, which is equivalent to the required pipeline outlet pressure. Considering a pressure drop in that range of 25 bars over the length of the pipeline, the inlet pressure at the power plant is 110 bars.
- The total cost for CO₂ transportation from Schwarze Pumpe power plant to Altmark was calculated using a fixed yearly instalment calculation method with 25 years and depreciation at 7% interest rate. For the 5Mt/y cases studied, the investment varies between M€ 187 to M€ 320. The investment cost for 10 Mt case varies between M€ 373 and M€ 384. The cost per tonne for all scenarios varies from € 3.4 to € 5.7, i.e., there is a clear economics of scale for pipeline transportation.

References

Egberts, P, et al, 2003, GESTCO-DSS; A Decision Support System for Underground Carbon Dioxide Sequestration, Report included in the GESTCO project.

IEA Greenhouse gas R&D programme, 2005. Building the cost curves for CO₂ storage: European sector, Report nr 2005/2

Verlag Glückauf Essen GmbH, 2003, Gasversorgungsnetze in Deutschland

1.2 Case Study CO₂ Transport Dornum – Barrien

Author: Josef Höllwart, Reservoir / Storage Facilities, Competence Centre, E.ON Ruhrgas AG, Essen

Kurzfassung

In der zweiten Fallstudie des Arbeitspakets 1 wird als CO₂-Quelle eine geplante Gasaufbereitungsanlage bei Dornum betrachtet. Dort erreicht Norwegisches Erdgas, welches per Pipeline geliefert wird das deutsche Festland. Bei der Gasaufbereitung werden jährlich unter anderem 300.000 Tonnen CO₂ aus dem Rohgas entfernt. In dieser Fallstudie wird die Möglichkeit des Pipeline-Transports des abgeschiedenen CO₂ und dessen Speicherung in der Erdgaslagerstätte Barrien, südlich von Bremen betrachtet.

Die Lagerstätte Barrien ist ein matures Erdgasfeld, in welches das CO₂ zur Steigerung der Erdgasausbeute injiziert werden könnte. Die wesentlichen Ergebnisse der Betrachtung dieser Studie sind:

- Eine mögliche Pipelinetrasse von Dornum nach Barrien wurde ausgearbeitet. Existierende Pipelines können nicht für den Transport von CO₂ genutzt werden. Eine neue Rohrleitung von 160 km Länge müsste parallel zu den bestehenden Rohrleitungen verlegt werden.
- Aufgrund der vergleichsweise geringen Gasmenge kann das CO₂ gasförmig transportiert werden. Ein Gasdruck von 30 bar, der am Ausgang der Gasreinigungsanlage zur Verfügung steht, ist ausreichend für den Transport nach Barrien durch eine Rohrleitung von 300 mm Durchmesser.
- Die Kosten für den CO₂ Transport von der Gasaufbereitungsanlage Dornum zur Lagerstätte Barrien wurden für eine Abschreibungsduer von 25 Jahren berechnet. Die gesamten Investitionskosten für die Errichtung einer 160 km langen Rohrleitung wurden bei einer Zugrundelegung der Preise von 2006 auf 82 Millionen € geschätzt. Daraus ergeben sich spezifische Transportkosten 30 € pro Tonne.

Summary

The R&D project CSEGR investigates the feasibility of Carbon Dioxide Storage in depleted gas reservoirs by Enhancing Natural Gas Recovery. This report concerns work contained in work package 1, investigating the transport of CO₂ which is generated as a by-product at a potential Gas Separation Plant (GSP) near Dornum, where the landfall of major gaslines from Norway is located. The yearly output of CO₂ is about 300,000 tons. In the study it is assumed that the CO₂ is transported via pipeline to the Barrien Gas Field, south of Bremen.

The Barrien field is a mature gas reservoir, where the CO₂ would be injected and used to enhance the ultimate gas recovery. In brief, the findings presented in this report are:

- A 160 km pipeline route from the Dornum GSP to Barrien has been defined. Existing pipelines in this area cannot be used. But the route of the new line to be built follows existing pipeline corridors.
- Because of the relatively small volumes, the CO₂ can be transported in the gaseous state. The pressure of 30 bars which is available at the exit of the GSP is sufficient to transport the CO₂ through a 300 mm line to Barrien.
- The cost for CO₂ transportation from Dornum GSP to the Barrien gas field was calculated using a fixed yearly instalment calculation method with 25 years and depreciation at 7% interest rate. The total investment for the 160 km pipeline was estimated with 82 Mio. € (2006 prices). With these figures the specific transport cost amounts to 30 €/ton.

Purpose of report

The purpose of this report is to document the results of Work Package 1, “CO₂ source evaluation treatment, gas transport and field distribution”.

- Description of CO₂-source, gas composition
- Identification of likely transport route and pipeline design
- Calculation of the transport cost

The results are used as input for WP2, “CO₂ compression, injection and production, well integrity”.

1.2.1 Characterization of industrial source, Dornum Gas Separation Plant

The planned gas separation plant is located at the landfall of the major gas pipelines from the North Sea, near Dornum in Lower Saxony (Figure 1.8). The facility is part of a project to separate ethane from the natural gas stream from Norway and to use it as a feedstock for the chemical industry. This first step of gas separation is accomplished by a low-temperature-process, which yields a mixture of ethane and carbon dioxide. In the 2nd step the CO₂ is removed from the ethane with a methyl-diethanolamine (MDEA) process. The schematic of this process is shown in figure 1.9.

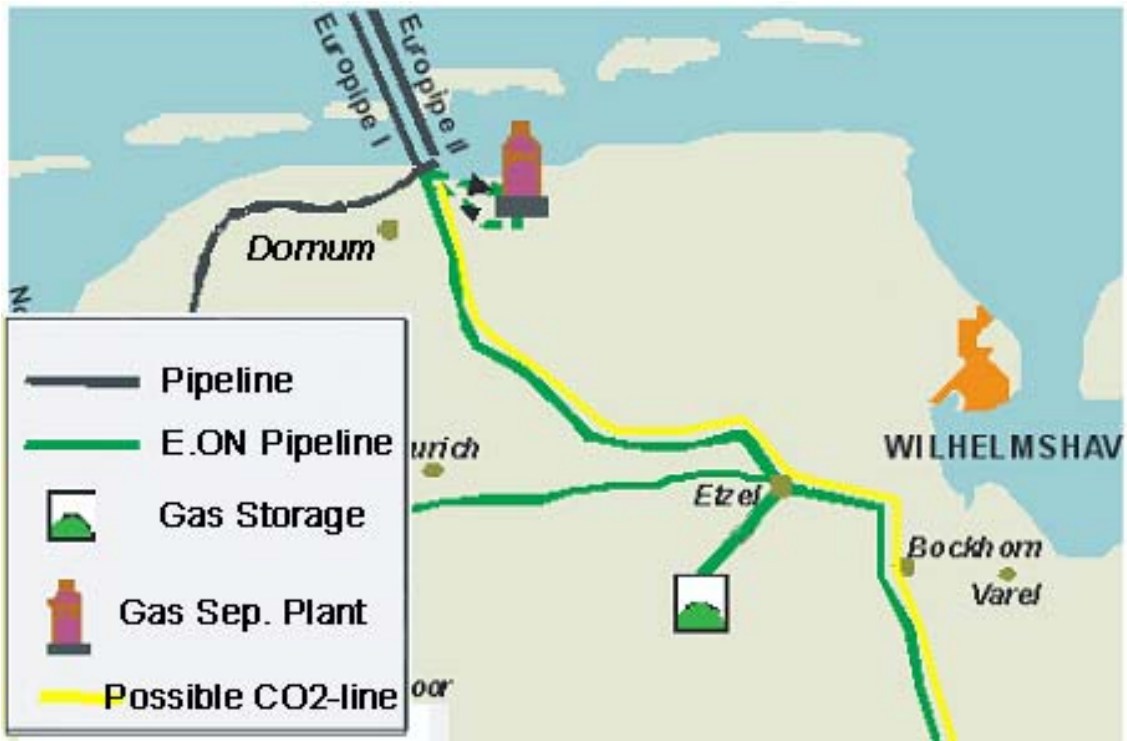


Figure 1.8: Location of the Gas Separation Plant.

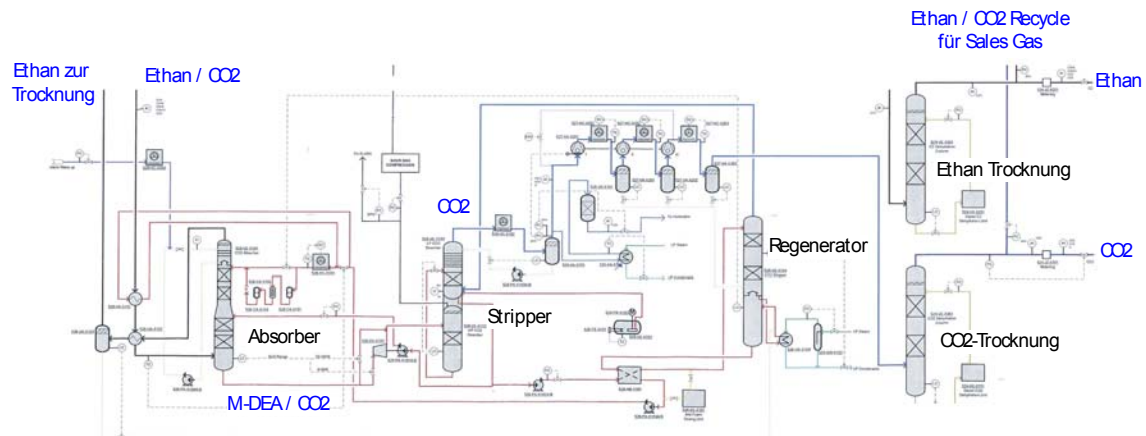


Figure 1.9: Schematic of MDEA-Process to remove CO₂ from the ethane.

1.2.2 Estimation of CO₂ quantities vs. time

The CO₂-discharge of the GSP will be about 300.000 tons/year. Considering an expected operation lifetime of about 40 years, the total output becomes about 12 Mt CO₂.

Assuming 8000 h operation per year, the discharge rate will be 37,5 t/h which is equivalent to a volumetric rate of 19.000 Nm³/h.

1.2.3 Pipeline route, suggested route Dornum – Barrien Gasfield

Along the envisaged transport route no idle gas lines are available. Therefore a new pipeline for CO₂-transport is required.

One major objective for designing the new route was to follow existing traces where possible. The selected route from Dornum via Etzel and Wardenburg to Barrien uses almost entirely E.ON pipelines (Figure 1.10). The total length of the line is 158 km.

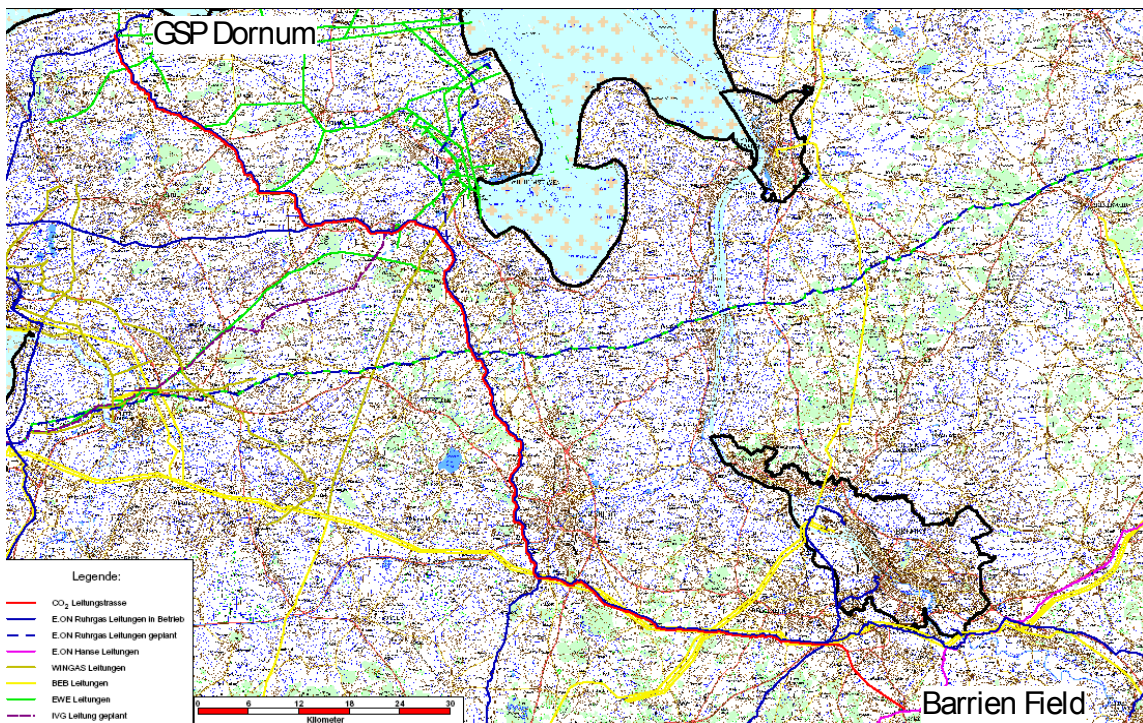


Figure 1.10: Overview of the route from Dornum to Barrien.

Diameter determination

The input parameters for designing the appropriate diameter of the pipeline were:

- length: 158 km
- inlet pressure: 30 bar
- outlet pressure: 20 bar
- max. operating pressure: 30 bar
- pipe roughness: 0,01 mm,
- max. transport capacity: 20.000 Nm³/h

The calculation was performed with the E.ON Ruhrgas proprietary software "Pipeline". The determined diameter for the line is 300 mm (DN 300).

Because of the relative small volumes it was decided to transport the CO₂ in gaseous state and to compress it at Barrien to the required injection-pressure.

1.2.4 CO₂ Quality

The Gas Separation Plant delivers rather pure CO₂ together with traces of hydrocarbons. The expected gas stream consists of the following components:

Table 1.6: Estimated quality of CO₂ stream from gas separation plant

| Component | mol % |
|--------------------------------|---------|
| CO ₂ | 99.345 |
| CH ₄ | 0.279 |
| C ₂ H ₆ | 0.142 |
| C ₃ H ₈ | 0.070 |
| C ₄ H ₁₀ | 0.005 |
| H ₂ O | 0.006 |
| H ₂ S | 200 ppm |

The relative high H₂S-content is a matter of concern, as the reservoir gas in Barrien does contain no H₂S. Therefore provisions at the Gas Separation Plant to remove this impurity might be necessary. The applicable process and the related cost have not been investigated in the present study.

1.2.5 Cost of CO₂ transportation

The purpose is to determine the costs for CO₂ transportation from Dornum GASP to Barrien as part of the evaluation of the overall-economics of the entire project.

Limitations:

The following is not included in the cost evaluation

- CO₂-conditioning, i.e. removing the H₂S
- CO₂-compression at Barrien

Capital investment calculation:

Based on the above-mentioned layout parameters, the necessary investment was calculated, using the E.ON Ruhrgas proprietary software "Picasso". The CAPEX was estimated to be 82 Mio.€ (accuracy ± 30%).

Total cost economical model:

The economical model used for calculating the total costs is an annuity model divided by the amount of CO₂ transported (I), as described by Equation 3:

$$Cost = \frac{C \cdot \frac{r}{1-(1+r)^n} + O}{I}$$

The operation and maintenance costs (O) include costs for routine operation as well as costs for maintenance and repair. In the GESTCO DSS, the operation and maintenance costs are calculated as a factor to the investment (Egberts et. al. 2003). The default value in the GESTCO DSS program (2.5%) has also been used for this case.

Table 1.7: Description of the parameters used in calculation of the total transportation cost

| Symbol | Description | Value |
|--------|---------------------------------------|----------------|
| C | Capital investment costs | 82 Mio.€ |
| O | Operation and maintenance | 2.5 % of CAPEX |
| r | Discount rate | 7.0 % |
| n | Depreciation time | 25 years |
| I | Transported amount of CO ₂ | 0.3 Mio.t/a |

The combination of relative small CO₂-volumes with a long transport distance leads to very high specific transport costs of 30 €/ton. This value seriously challenges the commercial viability of the project.

Conclusions

In brief, the findings presented in this report are:

- A 158 km candidate pipeline route from the Dornum GSP to Barrien. The route follows existing pipeline corridors, though a new pipeline need to be built (i.e., no existing pipelines can be utilised).
- The CO₂ can be transported in gaseous state through a 300 mm pipeline.
- The total CAPEX for the pipeline was estimated to be 82 Mio. €.
- The relative small CO₂-volume leads to high specific transport costs of 30 €/ton.

References

Egberts, P, et al, 2003, GESTCO-DSS; A Decision Support System for Underground Carbon Dioxide Sequestration, Report included in the GESTCO project.

Work Package 2

CO₂ Compression,

Injection/Production,

Well Integrity

Issues:

- Compression of the CO₂
- Production and Injection aspects
- Well integrity
- Well abandonment

Authors:

K. M. Reinicke, O. Franz, C. Fichter ITE TU-Clausthal

| | |
|---|----|
| Kurzfassung..... | 44 |
| Summary | 45 |
| 2.1 Description of Scope..... | 46 |
| 2.2 Review of Literature on CO ₂ Corrosion and Projects and Analysis of Information..... | 49 |
| 2.2.1 State of the Art of CO ₂ (Metallic) Corrosion and Control | 49 |
| 2.2.2 State of the Art of CO ₂ Cement Corrosion and Control | 51 |
| 2.3 Technical Integrity Issues of Wellbore Completion and Cementation..... | 54 |
| 2.3.1 Operations Phase | 56 |
| 2.3.1.1 Technical Integrity of Wellbore Completion and Completion Integrity Management | 56 |
| 2.3.1.2 Completion Integrity Monitoring | 60 |
| 2.3.1.3 Technical Integrity of Wellbore Cementation and Cementation Integrity Management | 61 |
| 2.3.1.4 Cementation Integrity Monitoring..... | 65 |
| 2.3.1.5 Re-establishing Wellbore Integrity | 66 |
| 2.3.1.6 Facilities Integrity | 67 |
| 2.3.2 Storage Phase | 69 |
| 2.3.2.1 Plugging and Abandonment | 69 |
| 2.3.2.2 Abandoned Well Integrity | 72 |
| 2.4 Well Integrity Acceptable for CSEGR and Identification of Problem Areas..... | 73 |
| 2.4.1 New Wells | 74 |
| 2.4.2 Existing Wells..... | 78 |
| 2.4.3 Monitoring | 80 |
| 2.4.4 Well Abandonment..... | 81 |
| 2.4.5 Abandoned Well Integrity | 82 |
| 2.5 Analysis of Integrity of Pilot Area Wells | 84 |
| 2.5.1 Pilot Project Area Data..... | 84 |
| 2.5.2 Accessible Well Analysis..... | 86 |

| | |
|---|----|
| 2.5.2.1 Production Well with CBL Information (P-Well 1) | 86 |
| 2.5.2.2 Production Well with no CBL Information | 87 |
| 2.5.3 Abandoned Well Analysis | 88 |
| 2.5.3.1 Abandoned Well with Standard Abandonment Procedure..... | 88 |
| 2.5.3.2 Abandoned Well with Non-Standard Abandonment Procedure..... | 90 |
| References | 94 |

Kurzfassung

Für die Lagerung von CO₂ im Geogrund kommen Erdöllagerstätten, Erdgaslagerstätten, Aquifere (salzhaltige Grundwasserleiter) und Kohleflöze in Frage. Die sichere Ausführung solcher CO₂ Sequestrierungsprojekte erfordert den

- Erhalt der technischen Integrität der Produktions- und Injektionssysteme, um einen sicheren Betrieb während der Betriebsphase von typischerweise 10 bis 50 Jahren zu gewährleisten,
- Erhalt der technischen Integrität der Bohrungen über den Zeitraum der Einlagerung von 100 bis 5.000 Jahren, um ein Zutage treten des CO₂ über die Wegsamkeit der Bohrungen nach ihrer Verfüllung auszuschließen.

Im Umgang mit CO₂ liegen in der Industrie langjährige Erfahrungen vor für die Injektion von CO₂ in Erdöllagerstätten im Rahmen von CO₂ Enhanced Oil Recovery (EOR) Maßnahmen, für die Produktion von Hochdrucksauergas aus Erdgaslagerstätten sowie für die für die Injektion der aus der Sauergasproduktion abgetrennten sauren Bestandteile H₂S und CO₂. Durch Untersuchungen an Bohrungskomplettierungen und Einrichtungen von CO₂ EOR und Sauergas Projekten wurden umfängliche Informationen über auftretende Versagensprozesse und Konsequenzen erarbeitet und für die Entwicklung der heute bekannten Sauergastechnologie genutzt. Bei Einsatz dieser Technologie sind keine grundsätzlichen Probleme zu erwarten, um während der Betriebsphase eine sichere Injektion und Produktion zu gewährleisten. Der Nachweis der technischen Integrität über Lagerzeiträume von 1.000 Jahren und mehr stellt eine Herausforderung dar, denn die Erfahrungswerte der Industrie sind auf Zeiträume von wenigen Dekaden beschränkt. Hier liegt der Schwerpunkt der weltweit laufenden Forschungsarbeiten.

Im ersten Abschnitt dieser Arbeit wird der derzeitige Stand der Technik zusammengestellt und zeigt Möglichkeiten für eine sichere CO₂ Verwahrung auf.

Der zweite Abschnitt umfasst Empfehlungen für Gewährleistung und Nachweis der mechanischen Integrität werden für Neubohrungen, Altbohrungen, verfüllte Bohrungen und Monitoring gegeben.

Die dargestellten Ergebnisse sind ein kleiner Teil der Arbeiten, die im Rahmen des Verbundvorhabens CSEGR (Carbon Sequestration with Enhanced Gas Recovery) durchgeführt wurden. Am Projekt sind neben der Universität Clausthal beteiligt: Bundesanstalt für Geowissenschaften und Rohstoffe Hannover, EEG - Erdgas Erdöl GmbH Berlin, Wintershall AG Kassel, Vattenfall AB und E.ON Ruhrgas GmbH Essen. Das Vorhaben erfährt Förderung unter dem BMBF Sonderprogramm GEOTECHNOLOGIEN.

Summary

Implementation of carbon dioxide (CO_2) storage in geological media, i.e. depleted oil and gas reservoirs, (saline) aquifers and coal beds, requires the construction of wells and systems, which allow safe operations during the injection phase and abandonment practices ensuring a long term safe CO_2 retention in the subsurface.

CO_2 - injection schemes have been in operation since as early as the 1970s for tertiary oil recovery as miscible floods. In other injection schemes, CO_2 and H_2S are injected into the subsurface for disposal. Approximately 80 acid gas (CO_2 and H_2S) injection plants are in operation throughout the world. Studies of well completions and facilities from CO_2 EOR and acid gas operations offer significant data on real failure processes and consequences. They provide a good basis for the design of CO_2 sequestration projects although areas for research remain because of the high concentration of CO_2 , the permanent re-charging of oil and gas reservoirs or charging of saline aquifers, the volumes and time spans involved for CO_2 sequestration.

This work summarizes the state-of-the-art relevant for CO_2 injection and production. In this context far more than 100 publications up to mid 2007 have been reviewed. Based on the experience documented in the sighted literature recommendations are made with respect to the design of new wells, the conversion of old wells, the abandonment of wells and the integrity assessment of open and abandoned wells.

The work has been carried out within the context of the research project CSEGR (Carbon Sequestration with Enhanced Gas Recovery) under the sponsorship of the GEOTECHNOLOGIEN research program of the German Federal Ministry of Education and Research.

2.1 Description of Scope

Carbon dioxide (CO_2) injection into oil reservoirs for enhanced oil recovery (EOR) is successfully in use for several decades. Likewise, high pressure sour gas reservoirs containing natural gases with both H_2S and CO_2 are in production and acid gas injection projects in operation since many years, (Bliss 2005).

Although the technology of injecting CO_2 into mature gas reservoirs for CO_2 sequestration with enhanced gas recovery (CSEGR) appears promising, it has not yet advanced beyond pilot testing it in the field, Van der Meer et al. (2005), Bennaceur et al. (2004), Oldenburg et al (2004), Mamora and Seo (2002).

Also, ensuring well integrity over long timescales has not been attempted before and represents a new challenge to the oil and gas industry. The integrity of well bores still is a significant potential risk for the long-term security of geological storage facilities, because CO_2 is known to cause severe corrosion in oil and gas production and transportation facilities, in particular if not designed for CO_2 service. CO_2 is also known to disintegrate the traditional types of cement.

The timeline for CO_2 sequestration projects is typically 10 to 50 years for the operations phase and 100 to 10,000 years for the post-injection phase, WBGU (2006), Gérard et al. (2006), Duval (2004) with a most likely value of 1,000 years, recommended by IPCC (2005), Bouc et al. (2007). Thus, executing CO_2 sequestration projects safely, requires

- maintaining technical integrity of production and injection systems to ensure safe operations during the operation phase and
- maintaining technical integrity of well bores over the storage period to ensure a long term, safe CO_2 retention in the subsurface.

Based on current industry experience, no fundamental problems are expected in maintaining technical integrity during the operations phase. Studies of well completions and facilities from CO_2 EOR and acid gas operations offer significant data on real failure processes and consequences. Although these offer the longest “experiments” to date, timescales are still limited to a few decades. International research therefore focuses on

- laboratory investigations that attempt to simulate long term geochemical and mechanical processes that may affect well completion materials – mainly cement
- field studies of well completions that have been exposed to CO_2
- modelling studies both of local and upscaled simulations.

Against this background the integrity of wells and subsurface equipment and surface equipment for a CSEGR pilot project in a pilot area was investigated based on state-of-the-art technology, schematically shown in Figure 2.1. This study builds on the

published experience gained in applications of CO₂ rich (sour) gas production, acid gas injection, or CO₂ injection schemes for EOR. The project is outlined in May et al. (2006). First results on wellbore integrity are documented in Reinicke et al. (2007).

The work on **wells and subsurface equipment** assumes that on the injection side the CO₂ is received at the wellhead. The work addresses all injection issues up to the perforations. On the production side it is assumed that the gas recovered is received at the perforated interval. All production issues up to the well head, where the gas is feed into the surface system are addressed.

In the area of well integrity and subsurface equipment the following areas of concern exist:

- potential material corrosion problems in the injection and production wells
- durability of wellbore cements during the injection phase and the long CO₂ confinement
- integrity problems in existing wells and the options for their repair.

The work includes

- review of literature on CO₂ corrosion and projects and analysis of information
- technical integrity issues of the hardware of the in- and outflow system according to Figure 2.1 and the cementation in open and abandoned wells
- definition of well integrity acceptability for CSEGR and identification of problem areas
- data gathering for pilot project area in Figure 2.2
- analysis of the integrity of the pilot project area wells, both open and abandoned, based on description of well completions, logs, tests, etc.
- definition of state-of-the-art solutions to modify and repair the completion and cementation of existing wells
- proposal for optimum new well design and materials including cements/sealing materials based on state-of-the-art technology
- identification of further, in particular testing work, to develop technology able to provide a long term CO₂ resistant seal for wells in CO₂ service.

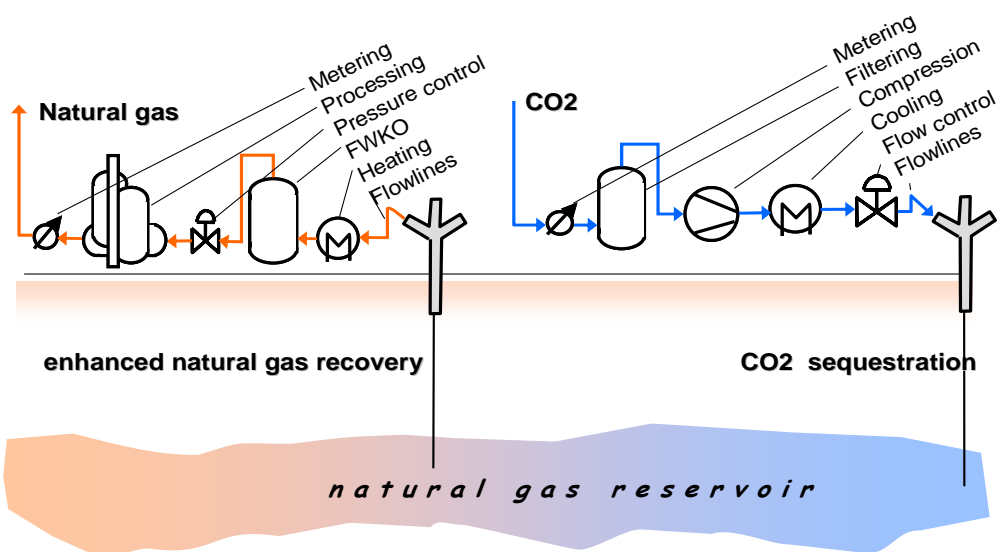


Figure 2.1: CO₂ Inflow and Outflow System

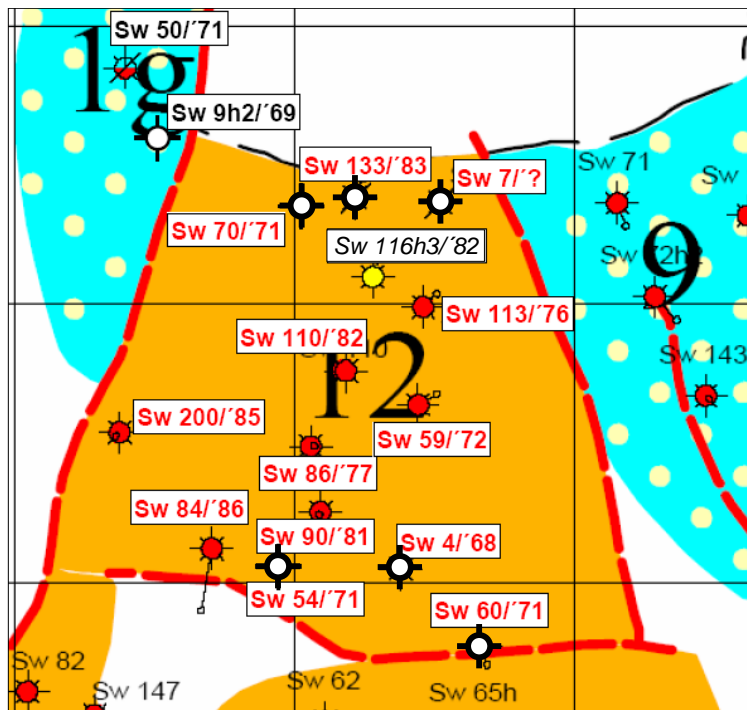


Figure 2.2: Pilot Project Area

Deliverables of the work on well integrity and subsurface equipment are

- definition of well integrity acceptable for CSEGR
- integrity analysis for pilot area
- recommendations for front end design (modification/repair of existing wells and new wells) for injection and production in the pilot area using state-of-the-art technology

- further work to develop technology able to provide optimum completions and a long term CO₂ resistant seal for CO₂ injection and production wells.

The work on **surface equipment** on the injection side assumes that the CO₂ is received from a pipeline at the border of the injection station and deals with issues up to the well head with the exception of compression, which is dealt with in work package 1. On the production side the work assumes that the recovered enhanced gas is received at the production wellhead and deals with issues up to a feed point into the gas transmission network where the produced gas is delivered according to the DVGW G 260 specification.

In the surface area mainly the following areas of concern exist:

- potential material and corrosion problems in the injection and production equipment
- processing challenges (in particular during compression) due to CO₂ physical behaviour
- produced gas processing or blending requirements after breakthrough and CO₂ increase above tolerated values.

The work for surface equipment includes

- literature review and analysis of information
- definition of infrastructure acceptability for CSEGR
- data gathering for pilot project area
- analysis of the pilot project area infrastructure
- front end design for both injection and production

Deliverables on the work for surface equipment are

- definition of infrastructure acceptability for CSEGR
- analysis for pilot area infrastructure
- recommendation for front end design (modifications and facility additions) for injection and production in the pilot area using state-of-the-art technology

2.2 Review of Literature on CO₂ Corrosion and Projects and Analysis of Information

2.2.1 State of the Art of CO₂ (Metallic) Corrosion and Control

Corrosion of steel due to acid gas containing brines is well documented in the literature, and to a lesser extent, data about the degradation by wet CO₂ or wet H₂S can be found, Schlumberger (1994). One such documentation on CO₂ corrosion and control is that by Kerney and Smith (1997) acting as editors for the documentation of

findings of the CO₂ Corrosion Work Group of the European Federation of Corrosion Working Party on Corrosion in Oil and Gas Production.

For CO₂ corrosion to occur there must be water present and it must wet the steel surface. CO₂ corrosion results from the reaction of a steel surface with carbonic acid arising from the solution of CO₂ in an aqueous phase – i.e. it is not a direct reaction with gaseous CO₂. Dry gaseous or supercritical CO₂ is not corrosive, Neubert (2005).

The principle factors determining the rate of corrosion are the temperature and CO₂ partial pressure. Other factors are, Farshad (2000), Kermany and Smith (1997), Cui et al. (2004)

- gas/water ratio
- flow rate and regime
- surface conditions (roughness, cleanliness)
- water drop out (low spots)
- water shedding due to change in flow profile (bends, welds)
- 3rd part entries (mixing effects)

CO₂ corrosion may manifest itself as

- general corrosion, i.e., a uniform dissolution or general thinning
- localized attack in the form of pits under stagnant to moderate flow conditions
- mesa attack under medium flow conditions or
- flow induced slits/grooves above critical flow intensities.



Figure 2.3: CO₂ Corrosion Caused by Wet CO₂

Case histories show that in oil and gas wells maximum corrosion takes place where the temperature is between 60 and 100°C, which may coincide with dew point tem-

perature in gas wells. Under these conditions CO₂ corrosion rates on carbon steel can reach very high levels: 25 mm/a at 65 °C and 1 MPa CO₂ pressure and 250 mm/a at 82 °C and 16 MPa CO₂ pressure, Cailly et al. (2005), Hesjekvik et al. (2003). Nugent (2005) reports significant corrosion in wells of the CO₂ producing Sheep Mountain Unit with tubing replacements in 18 out of 28 wells. Well head repairs included 8 master valve replacements and wing valve replacements in 15 wells.

CO₂ corrosion prediction models for carbon steel exist in various degree of complexity, relating corrosion rate to the partial pressure of CO₂, temperature, pH, scale, fluid velocity, steel composition, and other factors of influence.

CO₂ corrosion damage can be mitigated by

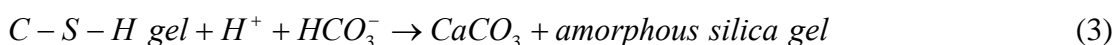
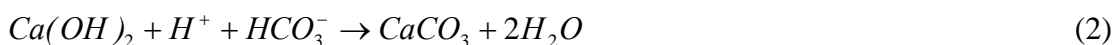
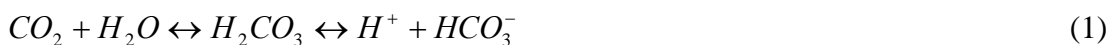
- design over-thickness
- changing from carbon and low alloy steels (LAS) to corrosion resistant steels (CRA)
- alteration of the environment to render it less corrosive by introducing glycol or methanol to dilute free water and
- reducing the corrosivity of the resulting water phase or corrosion inhibitors,

Cailly et al. (2005), Neubert (2005). Kermany and Smith (1997).

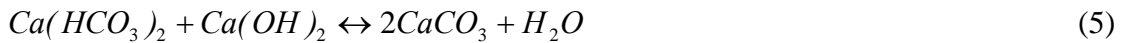
2.2.2 State of the Art of CO₂ Cement Corrosion and Control

For cementitious materials, one can find abundant literature dealing with the deterioration of cement pastes in acid gas (CO₂ and/or H₂S) environment, Barlet-Gouédard et al. (2006), Lecolier et al. (2006), Strazisar and Kutchko (2006). According to this, Portland-based cement systems conventionally used for well isolation in oil and gas production, tend to degrade, once exposed to acid rich gases. Despite all the information Barlet-Gouédard et al. (2006) conclude in their recent publication that “long-term isolation and integrity of CO₂ injection wells clearly must be improved to ensure long-term environmental safety”.

The basic chemistry describing the process of CO₂ corrosion is as follows, Krilov et al. (2000), Bruckdorfer (1986), Kuennen W.H. (1966), Verbeek G.J. (1958):



In equation 1, approximately 1% of the dissolved carbon reacts with water to form carbonic acid. As the carbon dioxide-laden water diffuses into the cement matrix, the dissolved acid is free to react with the free calcium hydroxide (equation 2) and calcium silicate gel, C-S-H (equation 3). As carbon dioxide-laden water continues to invade the matrix, other equilibria are established:



In the presence of excess carbon dioxide (equation 4), calcium carbonate is converted to water soluble calcium bicarbonate, which can migrate out of the cement matrix. In equation 5, the dissolved calcium bicarbonate can react with calcium hydroxide, forming calcium carbonate and “fresh water”. The liberated water can then dissolve more calcium bicarbonate. The net result is a

- leaching of cementitious material from the cement matrix
- increase in porosity and permeability
- loss of density
- decrease in strength and finally
- a loss of casing protection and zonal isolation.



Figure 2.4: Cement Corrosion by super-critical CO₂

The principle factors influencing the rate of cement degradation include

- type and amount of hydrated phases (corrosion rate increases with increasing content of Portlandite)
- type and amount of cement additives (corrosion rate increases with increasing content of Bentonite), Strazisar and Kutchko (2006), Duguid et al. (2004)
- cement preparation (corrosion rate increases with increasing water/cement ratio), Bruckdorfer (1986)

- pH (corrosion rate increases with decreasing pH), Lecolier et al. (2006), Scherer (2005)
- acid phase (wet super-critical CO₂ versus CO₂ dissolved water fluid), Barlet-Gouédard et al. (2006), Strazisar and Kutchko (2006), Duguid et al. (2005)
- contacting conditions (corrosion rate under dynamic conditions is significantly larger than under static conditions) Scherer (2005), Van Gerven et al. (2004)
- temperature and pressure, Strazisar and Kutchko (2006), Scherer (2005), Duguid et al. (2004)
- exposure time (corrosion rate decreases with time), Barlet-Gouédard et al. (2006)

Recently published results of various investigators are shown in Table 2.1. From the information there is an obvious lack of an industry standard for experiments to investigate the long term wellbore isolation behaviour and the durability of hydrated cements. This makes a comparison of results difficult. Older publications on laboratory investigations report a “corrosion rate” ranging from approx. 0.2 to 1.3 mm/d under static conditions. Rates reported for dynamic conditions are two orders of magnitude higher.

More recent publications report the corrosion rate as a function of time suggesting a decrease. Assuming that the results by Barlet-Gouédard et al. (2006), see Figure 2.5, are representative to describe the long term alteration behaviour, one obtains

- alteration depth of 0.11 m after 20 years of CO₂ attack
- alteration depth of 1.74 m after 5,000 years of CO₂ attack

Caution is advisable to extrapolations of the Barlet-Gouédard et al. results over times larger than two orders the testing times, considered the allowable maximum in construction engineering research, Wittke (1991-6). Nevertheless, the results are of the same order of magnitude as the rate of 0.2 m/100 years, reported for use in the CRUST Project, Van Luijk (2003).

Whilst there is room for debate about the mechanisms of CO₂ corrosion in terms of the extent by which above listed factors influence cement degradation, published information warrants the conclusions that

- static conditions are considered to best simulate the CO₂-exposure conditions at the formation/cement sheath interface, except around the perforations, where the exposure is under a dynamic state during CO₂ injection
- under static conditions the CO₂ alteration process follows a diffusion law with the alteration rate decreasing with time

Table 2.1: Experimental Result for Cement Carbonation Rate

| | Cement | Carbonating Fluid | Temperature, °C | Pressure, bar | Rate, mm/d |
|----------------------------------|---|--|-----------------|---------------|--|
| V.Gerven et al. (2004) | | 5% CO ₂ | 37 | | 0.4 |
| | | 20% CO ₂ | 37 | | 1.3 |
| | | scCO ₂ , dynamic | 80 | 400 | 150 |
| Short et al. (2001) | | scCO ₂ static | 59 | 97 | scCO ₂ accel. |
| Duguid et al. (2005) | Class H, w/c 0.38, matured for 28d in brine bath | CO ₂ leaching fluid pH 3.7 / 2.4 (after HCl add.) dynamic | 20 / 50 | | 0.24 (31 d) |
| Barlet-Gouédard et al. (2006) | Class G, 1.89 g/cm ³ , w/c 0.44 | wet scCO ₂ , static | 90 | 280 | 0.14 (av. 3 mon); $e=0.26 \cdot \text{sq.root of time}$ |
| | | CO ₂ sat.water, static | 90 | 280 | 0.1 (av. 3 mon); $e=0.22 \cdot \text{sq.root of time}$ |
| Lubena (2006) | Portland Cement | | 40 | 100 | 0.2 (55 d) |
| Strazisar, Kutchko (2006) | Class H, hydrated for 28 days in 1% NaCl solution | wet scCO ₂ , static | 22 / 50 | 1 / 300 | degradation in "headspace" less than in aqueous phase |
| | | CO ₂ saturated water, static | | | 0.03 (av. 9 d), decreasing with time; lowest for HPHT |
| | Class H with 6% Bentonite | wet scCO ₂ / CO ₂ saturated water, static | 22 / 50 | 1 / 300 | additive bentonite resulted in complete degradation |

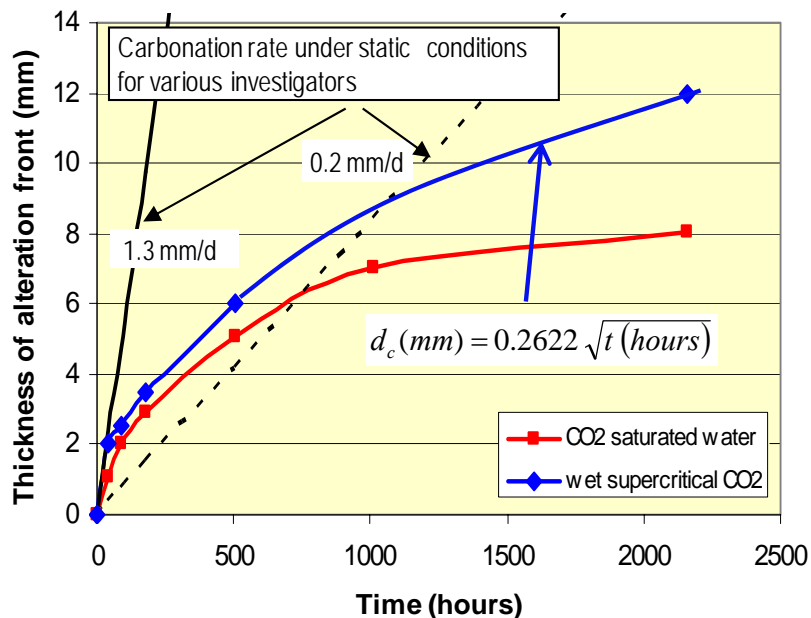


Figure 2.5: Evolution of alteration for Portland cement, Barlet-Gouédard et al., 2006

2.3 Technical Integrity Issues of Wellbore Completion and Cementation

Storing carbon dioxide underground requires long-term wellbore integrity. A leaking wellbore, may it be open or plugged and abandoned, can be a pathway for CO₂ migration into unplanned zones potentially leading to the unwanted escape of CO₂ into the atmosphere. The chance of this happening was estimated in IEA (2006) to be perhaps 1 in 100,000. The possibility of such leaks raises considerable concern about the long-term wellbore isolation and the durability of the hydrated cement that is used to isolate the annulus across the production/injection intervals in CO₂ related wells or to seal the formations used for CO₂ storage after well abandonment, Figure

2.6, Celia et al. (2004). Of all risks, leakage up abandoned wells is of most concern according to W. Heidug (Shell), Bennaceur K. (2004).

Large scale geologic sequestration requires the demonstration of long term mechanical well integrity (MI). Significant national and international efforts are currently undertaken to extend the rules and guidelines developed for underground injection, e.g. EPAs Underground Injection Control Program, EPA (1998), to account for the peculiarities of CO₂.

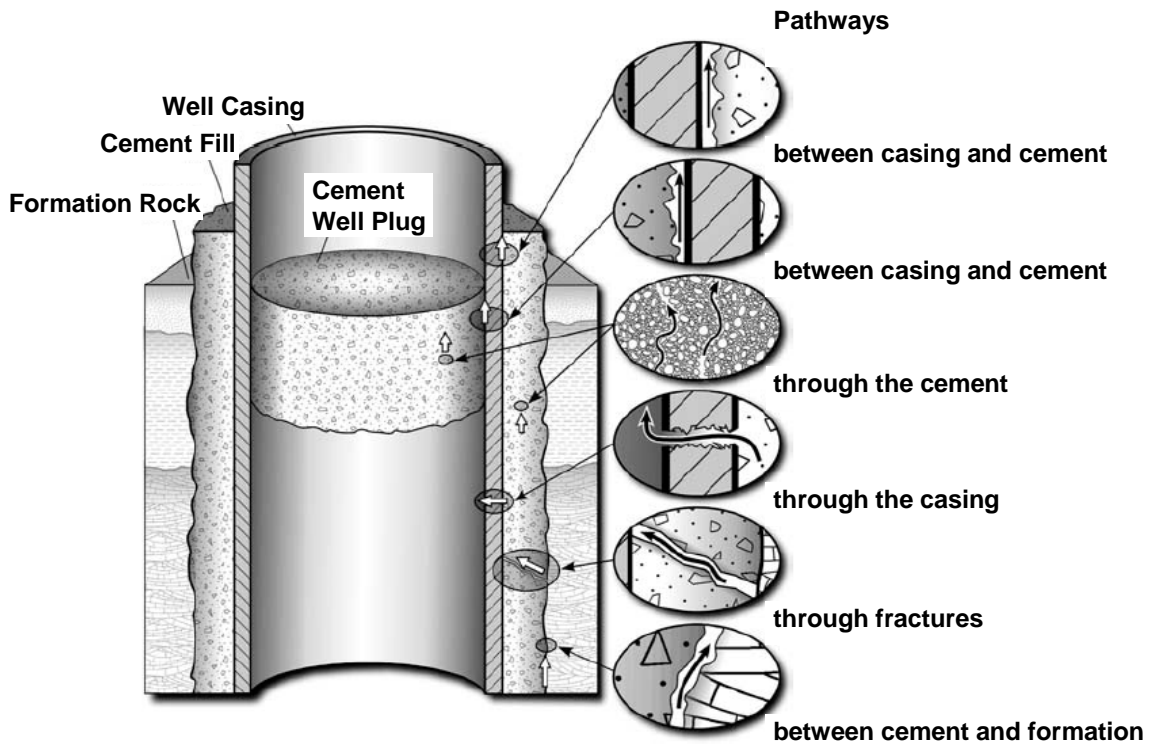


Figure 2.6: Potential Leakage Pathways along an Existing Well (after Celia et al. (2004))

In the context of demonstrating long term mechanical well integrity, risk based approaches have been proposed by many investigators IEA (2005), Gérard et al. (2006), Duguid and Celia (2006), Jammes (2007). A good overview of the risks associated with CO₂ sequestration is provided by Damen et al. (2003). A good field case is provided with the summary report on the Weyburn project, edited by Wilson and Monea (2004).

In consideration of the requirements for the design of CO₂ sequestration with enhanced gas recovery (CSEGR) systems, this section is divided into the subsection operations phase and storage phase. Operations and storage phase are different in mechanical loading and downhole environment, Lecolier et al. (2006). These differences are:

Mechanical loading:

- production/injection operations cause thermal and/or pressure changes in the well inducing stress variations within the cement sheath

- after well plugging, mechanical loading – if any – will occur more slowly and last over a very long period of time, e.g. continuing reservoir compaction, which can apply high axial loads on casing strings.

Downhole environment:

- downhole pressure and temperature, as well as the nature of the fluids in contact with the cementations sheath, are generally varying with time and well location.

The operations phase is further divided into well completion or injection wells, well completions for production wells, and facilities.

2.3.1 Operations Phase

The challenge to maintain wellbore integrity during the operations phase must be met against the following background

- Rapid changes in mechanical loading
- Rapid changes in downhole pressure and temperature
- Intimate (dynamic) contact between CO₂ and completion and cement in the perforation area
- Possibility to monitor
- Possibility to intervene
- Relatively short time frame of several tens of years

Both completion and cementation together with corrosion control measures must enable safe operations of injection and production. Well completion is assumed to mean all hardware up to the Xmas tree outlet. This includes the well bore liner, the production tubing including subsurface safety valves, expansion joint, nipples, hangers etc. and the Xmas tree itself. Cement in this section is assumed to mean the cement sheath of liner – if any – and casings.

2.3.1.1 Technical Integrity of Wellbore Completion and Completion Integrity Management

The U.S. Environmental Protection Agency, EPA (1998), defines a well to have technical or mechanical integrity if: “(1) there is no significant leak in the casing, tubing, or packer; and (2) there is no significant fluid movement into an underground source of drinking water”. As to what constitutes a “significant leak”, Crotogino (1996) suggested 50 kg/day as a minimum detectable leak rate and 150 kg/day as a maximum admissible leak rate.

Maintaining technical integrity of the completion requires first and foremost control over the corrosion. CO₂ corrosion of the completion may cause localized or general weight loss and consequent failure. (i.e. loss of pressure integrity). Penetration of the

tubing string by localized or general corrosion is the most common mode of failure, but functional failure of liners, seals, sub-surface safety valves (SSSV), or Xmas tree valves may also occur.

Conventionally, the equipment required is specified in carbon and low alloy steels (CLAS) with the aim of achieving the required function at minimum cost. Completions designs are dominated by:

- Tubing size required to provide necessary flow performance
- Mechanical integrity requirements (principally tension, burst and collapse)
- Life expectancy

Material should be selected to eliminate an unexpected workover due to corrosion failure. Depending on the severity of the environment specific alternative design approaches may be taken to incorporate some protection against CO₂ corrosion, Kermani and Smith (1997), e.g.

- Provision of a corrosion allowance by increasing the wall thickness of the tubing and/ or the liner over the minimum mechanical requirement – this option is not normally used, Kermani and Smith (1997)
- Control of fluid velocities to reduce corrosion/erosion by increasing tubing size or restricting flow rate
- Use of “flow couplings” (i.e. extra thick tubing) either side of flow restrictions to reduce local flow disturbance
- Use of internal “flush” tubular connections (without upsets or collars) to minimize local flow disturbance
- Improve “jewellery” life by selective use of corrosion resistant alloys
- Improve completion integrity by use of corrosion resistant materials, internally coated/ lined pipe and internal cladding
- Selective protection of critical Xmas tree components by use of corrosion resistant components and/ or overlays.

For design overthickness by provision of a corrosion allowance, a minimum required wall thickness is calculated based on the appropriate standards when designing piping and piping components, pressure vessels, etc. This minimum calculated wall thickness includes two parts; the “pressure containment” part, d_{min} , of the wall thickness plus a part called corrosion allowance. This declared design corrosion allowance, d_c , is normally regarded as that part of the pipe wall thickness required by design because of corrosion, in addition to that required for pressure containment, i.e.,

$$d_{req} = d_c + d_{min}$$

where d_{req} is the thickness of the pipe, required to ensure pressure containment over the design life time. The corrosion allowance is either determined from the predicted corrosion rate and the design life time t_d of the pipe, or, conversely, it is chosen from experience. For a more detailed approach see Kermany and Smith (1997).

Production and injections systems are typically designed and operated on the basis of critical erosion velocity calculations, Cameron et al. (1992) or internal standards, Van Grinsven et al. (2005). A very common standard for the maximum velocity is 20 m/s, Van Grinsven et al. (2005).

For the design of two high rate acid gas injection wells, the use of “flow couplings” (i.e. extra thick tubing) above and below the subsurface safety valve is reported by Duncan and Hartford (1998) either side of flow restrictions to reduce local flow disturbance. In preference to corrosion resistant alloys or coated tubing, water removal from the injected gas, corrosion monitoring at the tree and corrosion inhibition were chosen.

For the design of two other high rate (ca. 75,000 m³/h) acid gas (65% H₂S and 35% CO₂) injection wells Benge and Dew (2005) used “flush” connections without upsets and collars to minimize local flow disturbance.

Conventionally, the equipment required is specified in carbon and low alloy steels with the aim of achieving the required function at minimum cost. As more and more wells were drilled into severe corrosive environments, corrosive resistant alloys were developed (CRA). Chromium is the most commonly used alloying element added to steel to improve the corrosion resistance in wet CO₂ environments. Against the background of diminished cost differences between carbon and low alloy steels and some CRAs, protection under highly corrosive conditions is often accomplished by use of CRAs, IEA-Mulders (2006), van Grinsven et al. (2005), GdF (2003), Ikeda et al. (1985). Besides CRAs fibre reinforced plastics may also be considered for some service conditions, Kenneth (2001).

The selective use of corrosion resistant alloys to improve “jewellery” life is reported by

- Bowser (1989), who document the development of CRA use in CO₂ EOR injection wells, i.e. packers coupled with on off tools, packer mandrels, and profile nipples from 9Cr-1 to 13Cr, 17.4 pH stainless steel in H-1150 heat treat condition and Inconel 71 stainless steel
- Baklid et al. (1996), who document use of Inconel 718 and Incoloy 925 for the machined components of the completion
- Duncan and Hartford (1998), who documented the use of Incoloy in wells for acid gas injection for sub-surface safety valves, safety valve landing nipple, selective lock mandrels, packer bodies below the sealing element, and electrolyses nickel coated perforated tubing pup for acid gas injection wells.

In addition to CRA use, to improve “jewellery” life, CRAs are also used for sections of or complete liners and tubing to accomplish improved integrity:

- Baklid et al. (1996) report use of annealed 25Cr duplex stainless steel for the tubular and the exposed part of the casing for the injection wells of the Sleipner Vest CO₂ storage project
- Benge and Dew (2005) report a mixed completion for their high rate acid injection wells consisting of SM-2550, high Nickel, chrome and molybdenum alloy used as material for the liner portion across the potential injection zone with P-110 and L-80 grade above it
- Duncan and Hartford (1998) report setting a casing section with an internal electrolyses nickel coating as a place to set the packer
- Hanssen (2005) reports the use of 13Cr steel for the total tubing in the Snøhvit CO₂ injection wells
- IEA-Mulders (2006), Van der Meer (2005), GdF (2003) report use of 13Cr stainless steel in their K-12B CO₂ injection well
- Van Grinsven et al. (2005) report 13Cr to be used routinely as tubing material for service in H₂O-CO₂-Cl systems

In addition to steel, fibreglass may be used as material for well tubulars. Their use is reported by Bowser et al. (1989) to convert old water flood injectors to CO₂ injectors.

Selective protection of critical Xmas tree components by use of corrosion resistant components and/or overlays is also reported by:

- Baklid et al. (1996) report the christmas tree of the Sleipner Vest CO₂ injection well to be fully cladded with Inconel 625
- Duncan and Hartford (1998) report surfaces in primary wellhead components, directly exposed to injected acid gases, to be made up of corrosion resistant metals or clad with corrosion resistant Inconel overlays

For many applications, carbon and low alloy steels remain the preferred materials despite their poor resistance to corrosion. To achieve cost effective corrosion control, there is a strong reliance on inhibitor deployment. Treatments are carried out by periodic tubing displacement treatment, periodic squeeze treatments in which the inhibitor is forced into the reservoir or by continuous inhibitor injection. The corrosion inhibitors are generally nitrogenous (amines, amides, etc.) or organophosphates. Introduced into the production system, they will be absorbed onto the metal surface to generate a film depressing the electrochemical reaction taking place during the corrosion process. Successful absorption depends on the environment (pH, temperature, and liquid shear stress) the state of the metal surface (roughness, scales, etc.) and competition from other surface active species, Kermany and Smith (1997).

The use of CRA completion equipment versus corrosion inhibition for sour gas production wells is discussed in Cox (1990). A field case for the inhibition of deep, hot sour gas wells with high H₂S and CO₂ content is contained in Cameron et al. (1992).

Local flow disturbances in high velocity flows will increase corrosion and decrease inhibitor effectiveness. When relying on inhibition for corrosion protection, inhibitors should therefore be deployed from the very beginning. The necessity to do so and the limits of inhibition to provide corrosion protection in the presence of pitting corrosion are discussed by Van Grinsven (2005) for a high capacity gas well with a carbon steel completion.

Kinzel et al. (1996, 2006) report improved corrosion performance in H₂S and CO₂ by using a novel gripping system to handle and run CRA tubulars in order to prevent marks on the surface of the tubulars.

2.3.1.2 Completion Integrity Monitoring

Monitoring the mechanical integrity of wells is integral to proper operation in CO₂ injection. The techniques that are available to monitor the mechanical integrity of the completion (i.e. absence of leaks in tubing, casing, or packer or their condition) may be divided according to whether they provide direct measures of tubing conditions or are indicators of corrosion risk. They may further be divided according to the need for well intervention for their application, Kermani and Smith L.B. (1997), IEA (1998), PTTC (2006):

Direct measures of tubing conditions:

Without well intervention

- Annulus pressure monitoring
- Annulus pressure test
- Downhole corrosion probes (under development)

With well intervention

- Annulus pressure and leak test
- Closed circuit television visual inspection
- Mechanical calliper multi finger analysis
- Ultrasonic internal diameter calliper
- Ultrasonic wall thickness calliper
- Electromagnetic thickness survey
- Inspection of recovered tubing (pipe analysis survey)
- Radioactive tracer survey

- Noise logging
- Temperature logging

Indirect measures of tubing conditions:

Without well intervention

- Fluid samples for analysis which may include iron count and other corrosion products as well as inhibitor returns
- Corrosion and erosion monitoring in surface flowlines With well intervention
- Downhole corrosion coupon
- Inspection of recovered tubing incl. that from other wells with similar conditions

The techniques may also be divided according to whether they provide a measure of leakage or a measure of fluid movement, a differentiation pursuant to the US Code of Federal Regulations 40 CFR § 146.6(a), EPA (1998).

A good definition of many of the above mentioned mechanical integrity tests can be found at EPA (1998): 40 CFR 146.8(a), Shinde (2006).

A well integrity program is described by Anders et al., see Bybee (2007-1).

2.3.1.3 Technical Integrity of Wellbore Cementation and Cementation Integrity Management

To fulfil the EPA (1998) requirement of “no significant fluid movement”, technical integrity of the cementation requires achieving and maintaining a hydraulic seal between casing and formation and isolation of formations in the long term. Maintaining pressure integrity in the long term requires control over cement properties and the processes threatening its integrity.

As discussed in IEA (2006), failure of pressure integrity leading to sustained casing pressure is not that uncommon, even for non acid environments. A preliminary analysis of information of the Alberta Energy and Utilities Board on 315,000 oil and gas wells, and injection wells in the province of Alberta, Canada indicates that approx. 4.6% of these wells have recorded surface casing vent flow or gas migration through wellbore annuli or outside casing, Bachu and Watson, Watson and Bachu (2007). By assessing the available information combining it with field studies and research, factors and their level of affect on well integrity were determined by Bachu and Watson (2007). Their study suggests that geographic area, well deviation, well type, abandonment method, and economic activity have a major affect with minimal or none observed for well age, operational mode and completion interval. All other factors considered like licensee, depth, etc. had minor affect.

According to a recent study undertaken by Louisiana State University for the Mineral Management Service in Louisiana, 60-70% of the 8,100 natural gas production wells in the Gulf of Mexico are affected by sustained casing pressure (SCP), IEA-Crow

(2006). Benge in IEA-Benge (2005) reports 5,000 Gulf of Mexico wells to have sustained casing pressure, indicating some leakage up the annular intervals, out of a total number of wells of up to 100,000 (i.e. 5%). Gas flow through the cement is believed to be the main cause of SCP.

The typical problems causing sustained casing pressure, i.e., micro annuli, channels, lost circulation, flow after cementing, mud cake leaks, are attributed in particular to poor hole cleaning and improper cement slurry placement during well construction (e.g. poor centralization), Creel (2006), IEA-Ravi-Sweatman (2006), Bybee (2005). Tensile cracking is typically the result of pressure and temperature cycling during the wells productive life or excessive pressuring during fracturing operations or pressure testing, for example. To reduce incidents of SCP API has produced a set of standards incorporating best practice and lessons learned, IEA-Sweatman (2006).

In acid CO₂ environment, two additional types of deterioration can be distinguished:

- Mechanical deterioration for instance caused by geochemical deposits in the cement pores which can generate stresses which in turn can induce cracks, Cailly et al. (2005)
- Chemical deterioration at the interface between cement and casing and cement and formation, caused by the carbonic acid leaching described in section 2.2.

Traditionally, Portland based cements have been used for wellbore cementation with the aim of achieving the required function at minimum cost. Portland based cements, however, show relatively high rates of deterioration, in particular under dynamic conditions. Dynamic conditions are the likely conditions around the perforations, while static conditions are considered to best simulate the CO₂-exposure conditions at the formation/cement sheath interface at large. Under static conditions the CO₂ alteration process follows a diffusion law with the alteration rate decreasing with time, Figure 2.5.

As more and more wells are drilled for acid gas and CO₂ injection, new designs are applied. Depending on the severity of the environment, the following approaches can be distinguished, to incorporate some protection against CO₂ degradation:

- Use of Engineered Young's Modulus and Expandable Cement Systems for higher flexibility cements, Krusche et al. (2006)
- Use of cement systems with special additives and/or smaller amounts of Portland cement for higher CO₂ corrosion resistance
- Use of cement systems like high alumina systems with no calcium at all that can be converted to a carbonate by CO₂
- Use of newly developed cement systems with higher CO₂ corrosion resistance
- Carefully planned engineering solution for centralizer selection and placement, running casing, efficient preflush for mud displacement, cementing materials and equipment to ensure optimum conditions for cementation and setting.

Duncan and Hartford (1998) report use of acid resistant latex cement. Ackervoll et al. (2005) and Lubenau (2005) reported cement corrosion rates reduced by 50 and 70%, respectively, by adding Pozzolin.

Calcium phosphate cements, which contain mainly aluminate hydrates, calcium phosphate hydrates and calcium aluminosilicates have been used for a CO₂ injector in Oklahoma and in an 18.000 ft sour gas injector in Wyoming, Lance Brothers (2005).

In the context of their design of two high rate acid gas injection wells (65% H₂S, 35% CO₂) Benge and Dew (2005) and IEA-Benge (2005) increased resistance of a Portland cement to chemical degradation by adding a latex diluent of a specific particle size and adding a high alumina cement with newly developed fluid loss additives to reduce the amount of Portland cement.

Experimental investigations on newly developed materials with smaller amounts of Portland cement or no Portland cement at all, are reported to demonstrate comparably inert material behaviour in both wet supercritical CO₂ and CO₂-saturated water, suggesting that significantly lower alternation rates are achievable, Barlet-Gouédard (2006).

For a wellbore cementation to provide a hydraulic isolation a minimum interval of quality cementation is required. Cement quality is usually derived from a cement bond log, a representation of the integrity of the cement job, especially whether the cement is adhering solidly to the outside of the casing. The log is typically obtained from one of a variety of sonic-type tools. These tools measure the loss of acoustic energy as it propagates through casing. This loss of energy is related to the fraction of the casing perimeter covered by cement.

Two classes of sonic logging tools exist: sonic and ultrasonic. Ultrasonic tools provide a high resolution, 360° scan of the condition of the casing-to-cement bond, while the sonic tools CBL/VDL gives an average volumetric assessment of the cement in the casing-to-formation annular space., Bybee (2007-7), Frisch et al. (2006), Schlumberger (1989).

In its simplest form as Cement Bond Log (CBL) the transit time and attenuation of acoustic waves are recorded after their propagation through the borehole fluid and the casing wall. For a properly centralized and calibrated tool, low amplitudes mean a good bond, while high amplitudes indicate ambiguously problems like microannuli, channels, contaminated cement and fast formations. To mitigate the ambiguity, a Variable Density Log (VDL) is measured to display the waveform of the acoustic signal and indicate cement the formation bond, Bybee (2007-7).

From the CBL/VDL, compressive strength and bond index are derived, the latter by use of a CBL log interpretation nomogram. The nomograms differ from tool to tool and borehole fluid. A bond index of 0.8 or greater over a minimum interval, which varies with casing diameter, has been found to be a good indicator of hydraulic isolation.

Directional cement quality is determined by cement mapping tools (CET, CMT). The CMT works on the principle of the CBL but has 6, 8, or 10 receivers, which record the acoustic signal dependent on direction. The signal is transmitted by one transmitter or a number of transmitters equal to the number of receivers. The CET uses ultrasonic pulses (300-600 kHz) and measures radially and not axially. Eight transducers, positioned 45 degrees from each other operate as transmitters and receivers at the same time. Ultrasonic pulses are also used by USI tools, which use rotating transmitters. The signal is used to derive the acoustic impedance depending on direction as a measure of cement quality. The tools allow the prediction of channels with greater accuracy than the other tools.

To declare probable behind casing annular isolation between two points, the required minimum lengths, found in a publication by the U.S. Environmental Protection Agency, are 33 ft for 7 in. casing and 45 ft for 9 5/8 in. casing. Oil-industry service companies recommendation before declaring the interval isolated are 10 to 11 ft for 7 in. casing and 15 ft for 9 5/8 in. casing, which is supported by drilling experts, Bybee (2007-7), Schlumberger (1989). The criterion for hydraulic isolation documented in Laws et al. (2006) for South Oman wells is 10m.

Adoption of a “corrosion allowance” approach as for metal corrosion, section 3.1, would lead to a minimum required interval of good cement bond, d_{req} , to ensure hydraulic isolation over the design life of

$$d_{req} = d_c + d_{min}$$

where d_c , is the cemented interval required because of corrosion and d_{min} minimum interval to ensure hydraulic isolation.

Thus, after 20 years of CO₂ attack on neat Portland cement, the corrosion allowance would be approx. 1.5 to 10 m for static contacting conditions and constant corrosion rates of 0.2 to 1.3 mm/d, respectively. According to results published in the last two years, the alteration rate of Portland cement should – under static conditions – follow a diffusion law and hence decrease with time. The newly reported rates lead to significantly lower alteration depths, in particular for longer exposure times. Using the findings of Barlet-Gouédard et al (2006), Brunet et al. (2007) for scCO₂, the corrosion allowance for Portland cement for a design life of 20 years would be

$$\begin{aligned} d_c (\text{mm}) &= 0.2622 \cdot \sqrt{t(\text{hours})} \\ &= 0.2622 \cdot \sqrt{20 \cdot 365 \cdot 24} = 110 \text{ mm} \end{aligned}$$

(see Figure 2.5). Besides the bulk alteration of neat cement described above, alterations may take place along the interfaces between cement and casing on one hand and between cement and formation on the other. It is suspected that degradation along these interfaces due to chemical alterations and to mechanical stresses during the life cycle of the well (injection/production, reservoir compression, abandonment, ...) can lead to gas migration pathways. In that case, risks of leakage through these

mechanisms could be much higher than those expected through bulk alteration of cement or even steel.

2.3.1.4 Cementation Integrity Monitoring

The various techniques to confirm the cement bond between casing and formation have differing applicabilities and limitations, whether in interpretation or detection capacity. As for completion integrity monitoring, the techniques, IEA (1998), OGP (2000), Rusch and Slezak (2005), PTTC (2006) may be divided into direct and indirect measures of cementing conditions

Direct measures of cement conditions:

Without well intervention

- Annulus pressure monitoring and testing

With well intervention

- Annulus pressure and leak test
- Physical-communication test
- Cement bond or evaluation logging
- Radioactive tracer survey
- Temperature survey
- Noise logging
- Oxygen activation logging
- Flowmeter survey

Indirect measures of cement conditions:

Without well intervention

- Cementing records (theoretical length of the cemented interval based on calliper log derived annular volumes and actual length; casing shoe strength test)
- Fluid samples for analysis

While cement bond log interpretation is fairly reliable, it is no guarantee for an annular cementation to provide a hydraulic seal between formations. This is the conclusion of Boyd et al. (see Bybee, 2007-7) based on a comparison of physical inter-zonal communication tests with interpretations of cement bond logs. Boyd et al.'s conclusion is that communication tests, while jeopardizing casing integrity and costly, are the most definitive means to test behind-casing isolation.

A good definition of many of the above mentioned mechanical integrity tests can be found at EPA (1998): 40 CFR 146.8(a), Shinde (2006). A good overview is provided with Schlumberger (2001).

2.3.1.5 Re-establishing Wellbore Integrity

The loss of well bore integrity, indicated for example by sustained casing pressure (SCP), requires the repair of the well. The options are, PTTC (2006), Schlumberger (1999)

- squeeze operations
- expandables technology
- well workover
- and other technologies

There are a number of materials that can be used in squeeze operations to remediate SCP including fine cements and low density sealants (polymers, gels and resins), IEA-Sabins (2006). Materials need to be injected or squeezed into the well. Successful remedial operations have been reported by using

- foamed cements for squeeze cementing low-pressure reservoirs by Chmilowski (1992)
- ultra fine cements by Harris and Johnson (1992)
- thixotropic coiled tubing cementing by Welch et al. (1990)
- coiled tubing contaminated squeeze by Wilson et al. (2003) in an 18,600 ft sour gas well containing 15 ppm H₂S and 5% CO₂
- polymers to reduce SCP, IEA-Sabins (2006)
- gels to remediate cement bond failure, tubing and casing leaks, IEA-Sabins (2006)
- resins to seal casing leaks and shut off gas for abandonment, IEA-Sabins (2006)

Expandable tubulars technology are reported to have proven effective for isolation of production perforations and worn, weakened, corroded or eroded production casing, Storaune et al. (2005), Jabs et al. (2004). When applying this technology a smaller ID pipe is run into the well over the section to be repaired and expanded against the existing pipe. Thus the material used for the expandable tubular is required to have sufficient ductility to be safely expanded by 20-25%. The CRA of choice for mild H₂S and hot chloride environments, 13Cr steel, lacks the necessary ductility. For use in these environments the austenitic stainless steel S31603 is proposed by Chitwood and Skogsberg (2006).

Well workover operations for remediating casing deformations by milling the deformed casing and cementing a liner extending across the milled is described in Allen and Philippacopoulos and Philippacopoulos and Berndt (2000).

To repair severely corroded casing strings use of cements with fibres added is reported by Simbala et al. (2005).

2.3.1.6 Facilities Integrity

The principal integrity issues for injection and production facilities, flowlines, processing equipment (piping, valves, vessels, etc.) and export lines, are similar to the considerations for wells whilst there are specific aspects which are of particular significance to each, Kermani and Smith (1997).

On the injection side the CO₂ gas stream is received at low pressure. For injection it is compressed in one or several steps. At each compression step, the gas heats up. Before the next step, the gas is cooled to moderate temperatures (usually approx. 40 °C). During this cooling step, most of the water vapour present is condensed. The condensed water is immediately separated in a scrubber in order to prevent liquid carry over to the inlet of the next compression step. In the presence of acid gases (CO₂ and /or H₂S), the freshly condensed water is inevitably corrosive to carbon steel. Due to the negligible amount of dissolved iron in the water phase, there is no mechanism for building up protective corrosion layers.

For onshore projects, where the last compression stage is followed by the same cooling and scrubbing steps as the previous stages, the dew point of the gas stream is the temperature at the inlet of the gas injection line leading to the injection well. It will be close to ambient temperature, which results in favourable conditions regarding CO₂ corrosion, i.e. low temperature, low condensation rate, and very low water content. Under normal conditions, corrosion cannot occur on carbon steel. Intermittent batching is considered to manage corrosion risk, Kermani and Smith (1997).

Recent publications on facility design of acid gas injection facilities are Baklid et al. (1996), Cailly et al. (2005), GdF (2003), Van der Meer et al. (2005), reporting on CO₂ injection projects. Duncan and Hartford (1998) and Wall and Kenefake (2005), report on the design of the acid gas injection projects. The Shute Creek acid gas injection (AGI) facility described by Wall and Kenefake, is currently one of about 80 AGI plants in operation throughout the world.

The publications stress the importance of the provision of compression to inject the acid gas into the reservoir. The question is related to the injection concept chosen, i.e. whether to inject in liquid phase, two phase or gaseous phase at the well head.

The publications also stress the importance of water removal and temperature control for acid gas injection. As described before, free water can significantly increase rates of weight loss corrosion and sulphide stress cracking. Free water can also cause hydrates. Both corrosion and hydrates are significant reliability and safety concerns. Therefore proper water removal is essential to the operation as is the control

of temperature. Establishing the hydrate line and the water holding capacity in the gas as compared to the liquid and dense the phase are essential tasks.

Because of the strong dependence of the density of supercritical CO₂ on temperature, temperature control is reported by Baklid et al. (1996) to be used to achieve a constant wellhead pressure independent of rate.

To take advantage of the flexibility and energy savings for pumping liquids instead of achieving the full injection pressure with compressors, a combination of multistage centrifugal compressors and multistage centrifugal pumps are used for the Shute Creek AGI project Wall and Kenefake (2005). The scenarios injection as a liquid, injection as gas and liquid two-phase or injection as a dense (supercritical) fluid are discussed in Baklid et al. (1996). They report preference for injection of CO₂ as supercritical fluid, because of the difficulties to prevent the formation of hydrates under the other injection scenarios. For the Sleipner Vest project, described by Baklid et al., compression is achieved by a three stage compressor with water being knocked out after each stage at 30 °C. Injection as supercritical fluid is also reported by Duncan and Hartford (1998) and Van der Meer for the K12-B Offshore Re-injection (test) of CO₂ (ORC), the Gaz de France project subsidized by Crust, Van Luijk (2003). Van der Meer et al. report use of multistage reciprocating compressors to inject the CO₂ as a supercritical fluid is reported in Van der Meer et al (2005).

Insulation of the gas injection line from the last stage of compression to the injection wells is reported by Duncan and Hartford (1998).

To prevent dangerous high pressure buildup on surface equipment, CO₂ injection must be stopped as soon as leaks occur. Rupture disks and pop-off valves can be used to relieve build-up pressure, Cailly et al. (2005).

For the typical way of processing the acid gas stream for injection, the acid gas cannot be regarded as dry under all circumstances. Because of the nature of the injected CO₂ fluid, any leak with a resulting pressure drop can potentially cause localized freezing and the formation of ice. This can reduce the temperature of a component locally to approx. -60 °C, which could potentially produce a brittle fracture problem. Processing facilities are normally regarded as experiencing turbulent flow conditions which often results in potentially higher corrosion rates.

Material selection for the CO₂ containing equipment have to account for the corrosivity of the contained medium and the corrosion conditions in terms of CO₂ corrosion resistance and resistance to sulphide stress cracking, if H₂S is present. In cases where there is a desire to minimize weight or ensure long service life, selection of corrosion resistant alloys may be favoured instead of adding corrosion allowances to carbon steel and use corrosion inhibitor injection. For The Sleipner Vest project, Baklid et al. (1996) report selection of CRA materials to satisfy the requirement of a 25 year service life.

The production side, where the occurrence of water cannot be avoided, requires more stringent material selection and design at least up to the water separators.

Equipment downstream of the separator(s) will often have minimal water content and slower fluid velocities, resulting in less aggressive corrosion conditions which can be handled with carbon steel, with, or in some cases without any corrosion allowance or corrosion inhibitor injection.

Design information on a CO₂ pipeline system may be found in Barry (1985)

2.3.2 Storage Phase

2.3.2.1 Plugging and Abandonment

The timeline for the storage phase of CO₂ sequestration projects is 100 to 5,000 years according to Gérard et al. (2006) and Duval (2004) with a most likely value of 1,000 years, recommended by IPCC (2005), Bouc et al. (2007). For this phase wells must be plugged and abandoned (p&a) using procedures, which ensure a long term safe CO₂ retention in the subsurface. The challenge of maintaining integrity must be met against the following background

- slow but lasting well loading
- inaccessibility for direct monitoring
- inaccessibility to intervene
- long time frames of thousand of years

The standard plugging procedure of wells in Germany is to cement or squeeze the perforations, to pull the un-cemented parts of the casings, to set cement plugs at various depth intervals, to fill the volume in between with heavy weight mud, to cut and weld-shut the surface casing several meters below the surface, and cover it with a cement plate. The procedure is carried out to achieve a hydraulic seal between the utilized formation and any overlying formations able to store and flow fluids. For cementation typically Portland or Pozzolin based cement systems are used. Typical cements plug thicknesses range from several meters (in general 5 m minimum) to several hundred meters. Typical muds are suspensions of bentonite in fresh water with densities ranging from approx. 1.1 to 1.4 g/cm³. The well sketch for an abandoned well in the pilot project area is shown Figure 2.7.

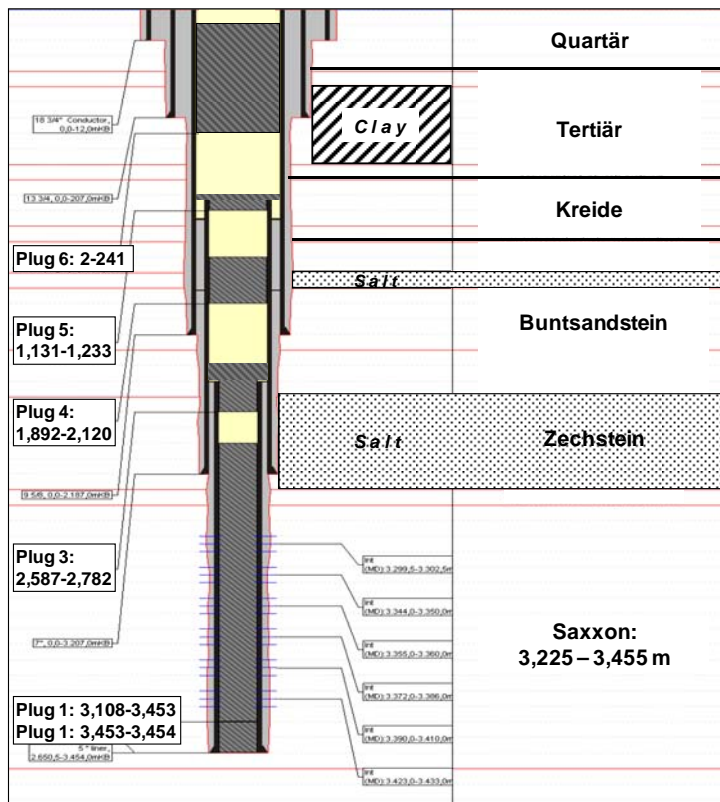


Figure 2.7: Well Sketch for Abandoned Well in Pilot Project Area

Minimum requirements for the decommissioning of wells within the jurisdiction of the German “Tiefbohrverordnung - BVOT” are specified in “Richtlinie über das Verfüllen auflässiger Bohrungen”, LBEG (1998). They have to be observed by all operators within Lower Saxony. The guideline contains among others:

- wellbores have to be plugged completely. Plugging materials should not react with ground water, geologic materials, casing and the materials used for sections of special plugging
- special seals are necessary for sections opposite reservoirs (i.e. oil gas and salt reservoirs, storages and usable water horizons, and any other pressurized formations able to flow fluids), liner hangers, cut casings, open annuli as well as the shoe of the deepest tubular in a partially open hole
- for the special seals suitable cements or other solid materials should be used (e.g. compacted shales, Lecolier et al. (2006)) in combination with mechanical plugs if appropriate
- special seals should range from 50m below to 50m above reservoirs
- perforated intervals should be pressure squeezed or – if a squeeze is not possible – sealed off with a mechanical plug immediately above the perforations and covered with a special seal of at least 50m
- liner hangers and cut piping has to be sealed off by special seal sections of at least 100m

- specials seals are required for the wellbore section from the surface down to the base of potential underground sources of drinking water or 100m whatever is deeper
- all casings have to be cut at a depth sufficiently below the surface to not interfere with a subsequent use of land
- The wellbore has to be secured with a concrete slab
- The tops of the special seal sections has to be determined, the seal as to be verified

In well sections, where problems were encountered during drilling and/or production (damaged casing, sustained annular pressure) or in long sections of salt (more than 1,000 m) the plugging guideline requires additional special seal sections. A typical abandonment procedure is also described in Cailly et al. (2005) and Gérard et al. (2006).

The well condition after completing p&a operations can not be considered representative for the conditions for very long times, in particular for the storage times of CO₂ sequestration projects. Changes of this condition will or are likely to take place because of

- sedimentation of the heavy weight mud
- decomposition of the cement plugs
- corrosion of the casing sections left in the subsurface
- development of an excavation-damaged zone
- self healing effects

Quantitative descriptions of these changes have been carried out in the context of investigations on the Schacht Konrad repository for radioactive waste, Wittke (1991-6).

The heavy weight mud systems filling the volume between the cement plugs are suspension of solids made up primarily of bentonite with small amounts of sand. Over time the solids settle to the bottom to form a relatively low permeable deposit. The relative heights of the solids deposits for mud with a density of 1.25 g/cm³, as determined by Buß und Schmidt (1991) after 750 hours, ranges from 49 to 68%. Measured hydraulic conductivities of the sediments averaged $2 \cdot 10^{-8}$ m/s with a value of $1 \cdot 10^{-8}$ m/s considered to represent the conductivities in the longer term.

Over geologic times the cement disintegrates. The rate at which the process takes place depends on the nature of the hardened cement paste, the type of fluid, and the contact conditions between cement paste and fluid. Based on theoretical considerations, Schorn (1990), see Wittke (1991-6) concludes that over times of more than 10,000 years cement plugs are likely to disintegrate, while plugs of neat cement

paste should survive time intervals of far more than 1,000 years also under corrosive environments. Experiments were not carried out, because extrapolations of experimental results over times, two orders of magnitude larger than test times, are considered the allowable maximum in construction engineering research.

The casing sections left in the hole prevent the hole from caving in. The casing loses its supporting property when it is corroded to the point that collapse occurs as a result of the formation pressure. According to Heusler (1988), see Wittke (1991-6) casing collapse of J-55 or K-55 grade carbon steel pipe with wall thicknesses of 7 to 9 mm is likely to occur after approximately 14,000 to 18,000 years. Heuslers results suggest that the wellbore stabilizing function of casing sections left in the hole remains intact over typical CO₂ storage times.

According to experience the generation of an excavation leads to the formation of a damaged zone around it. In this zone permeability may be higher than original. Extent and permeability change in this excavation-damaged zone depend on stress conditions, formation properties, geometry and original permeability. In the case of wells, the zone is also influenced by drilling conditions. A method to quantify the parameters for the damaged zone has been developed by Wittke (1991-3). For the particular conditions considered, increases in hydraulic conductivities less than $1 \cdot 10^{-8}$ m/s were obtained.

Well sections not supported by casings or plugging material show caving behaviour in formations, which tend to collapse contingent to either tectonic or mineralogical conditions. This leads to a back filling of the wellbore with the breakout material. Borehole breakout for shaly formations and its effect on vertical permeability in the wellbore has been investigated by Wittke (1991-6). For the particular conditions considered hydraulic conductivities less than $1 \cdot 10^{-8}$ m/s were obtained.

Borehole closure can also be expected in formations of plastic salt, which under the influence of the pressure caused by the weight of the overburden will move in to close the hole.

2.3.2.2 Abandoned Well Integrity

Plugging practices have dramatically improved over the last century. Worldwide the development has progressed similar to that described by Ide et al. (2006) for the USA. Ide et al. distinguish three groups of abandoned wells: wells without cement plugs (typically pre 1930 shallow wells), wells plugged before 1952 and wells plugged after 1952. Despite this improvement, the risk of CO₂ leakage from wells remains a substantial risk in CO₂ sequestration projects.

The task of evaluating abandoned well integrity is a difficult one. The older the well is, the less demanding the abandonment standard but also the less likely the availability of information sufficient for a conclusive assessment of the integrity at the time of abandonment. Also, the older the well, the less likely it is, that the well status at abandonment is an adequate representation of its current state.

The question of abandoned well integrity has been addressed in the context of the safety case for the Schacht Konrad [repository](#) for radioactive waste, Wittke (1991-6). For the conditions present in the Schacht Konrad project, it was concluded on the basis of simulations, that wells are of sufficient integrity, if hydraulic wellbore conductivities are in the order of $k_f = 10^{-8}$ m/s over the “plugged” wellbore sections (“*versetzt angenommene Bohrloch Abschnitte*”), in particular the sections extending through the sealing formations. The required conductivities were shown to be achieved by the cement plugs placed, or by the self healing effects taking place in form of the sedimentation of heavy weight mud and caving of shaly formation. Conditions in the considered project were an initially under-hydrostatic pressure in the formations below the seal, equalizing over a period of approx. 1,000 years and water as the carrier during the migration of the radio nuclides. For full scale CO₂ sequestration project, these conditions are not necessarily given. So while the processes investigated by Wittke are relevant also for CO₂ sequestration projects, his results cannot be simply transferred.

The options which are available to demonstrate wellbore integrity range from a “do nothing in old fields with no evidence of leakage approach” to a “re-completion of all historically abandoned wells” as required by the new regulation in force in Alberta, Canada. This regulation demands a “re-completing of old wells using a cement squeeze process”. Discussions of these options at the 3rd IEA-GHG Workshop on Wellbore Integrity in March 2007 lead to the “compromise” option of performing a “ranked” risk assessment of all wells within the storage area, and remediating the wells at a higher risk of leaking, and installing monitoring equipment around the lower risk wells, IEA (2007).

According to Mulders (2007), the analysis of abandoned well integrity requires a thorough understanding of the wells present condition, well geometry, construction materials, and construction methods.

In the case study, presented by Mulders, abandoned wells were examined for signs of corrosion and the primary cement sheath and bridge plug were analysed to determine the presence and extent of corrosion. From the study it was concluded that corrosion of the primary cement sheath and the well casing are the areas to hold the greatest potential leakage opportunity. From the study it was also concluded that stress and deformations in the surrounding reservoirs – while insufficient to seriously damage the wells – “may enhance and promote the corrosion rates encountered by the primary cement sheath and well casing”.

2.4 Well Integrity Acceptable for CSEGR and Identification of Problem Areas

The issue of well integrity acceptable for CSEGR is divided into (1) mechanical integrity of new wells, (2) mechanical integrity of old wells, (3) mechanical integrity of abandoned wells, and (4) Monitoring. For the sake of this paper,

- Mechanical integrity of wells for CO₂ service means that there is no significant leak in the casing, tubing, or packer; and there is neither significant fluid movement into an underground source of drinking water nor to the surface.

- Mechanical well integrity of wells during the storage phase means that there is neither significant fluid movement into an underground source of drinking water nor to the surface

The above definition of well integrity is in line with that of the Landesamt für Bergbau, Energie und Geologie, LBEG (1998) and U.S. Environmental Protection Agency, EPA (1998). Significant national and international efforts are currently undertaken to extend the rules and guidelines developed for underground injection to account for the peculiarities of CO₂.

To ensure well integrity, design, construction, operation, and abandonment of wells within the storage site are key factors. System requirements are greatly influenced by composition and water content of the injection gas. System design should aim to minimize future well intervention.

Recommendation: Water in the injection fluid should be eliminated to prevent wasting corrosion, Duncan and Hartford (1998).

Recommendation: As far as possible injection gas should be free of H₂S.

Recommendation: Injection gas should be free of oxygen.

Recommendation: Temperatures of the injection stream should be modelled to ensure that injected fluids remain above hydrate temperatures, Duncan and Hartford (1998).

2.4.1 New Wells

New well design and construction should account for operating conditions (volumes, pressures, temperatures, fluid composition and acidity, duration, etc.) and address identified potential well failure scenarios, Karman and Wildenborg (2006). The OGP guidelines for injection of produced water list many of the elements that need to be considered, OGP (2000). The specific costs for new wells are listed in the annex.

In injection wells, where CO₂ is injected in a dry supercritical state, there is no significant risk of (metallic) corrosion, because the corrosion rate of metals in the presence of dry supercritical CO₂ is very low. In this case, carbon steel is sufficient, sometimes with the help of corrosion inhibitors and corrosion monitoring at the tree, Duncan and Hartford (1998).

Recommendation: Materials for well head, valves, tubing, and the exposed part of the casing, etc. should be selected, which are compatible with the acidity of the contacting fluids, e.g. the acidity of carbonic acid which may be formed at the point of injection, Baklid et al. (1996).

Recommendation: For fluids containing H₂S, sulphide stress cracking should be considered in material design.

Use of the following materials has been reported in the literature:

Tubing

- 19.5 and 15.6 ppf L-80, Benge and Dew (2005)
- Seamless 9.2 ppf L-80 with Hydrill CS premium connections, Duncan and Hartford (1998)

Casing/ Liner

- Seamless MN-80, Duncan and Hartford (1998)
- P110, L80, Benge and Dew (2005)
- Annealed 25% Cr duplex stainless steel, Baklid et al. (1996)
- SM-2550 (high nickel, chrome and molybdenum alloy), Benge and Dew (2005)
- Electroless Nickel coated casing at packer setting depth, Duncan and Hartford (1998)

Subsurface components

- 9Cr-1Mo, Bowser et al. (1989)
- 13Cr, Bowser et al. (1989),
- 17.4 pH stainless steel in H-1150 heat treated condition, Bowser et al. (1989),
- Inconel 71, Bowser et al. (1989),
- Inconel 718, Baklid et al. (1996)
- Incoloy 925, Baklid et al. (1996)
- Incoloy (Packer inner mandrels and packer body below sealing element), Duncan and Hartford (1998)

Christmas tree

- ASTM A182 Grade F22 fully cladded with Inconel 625, Baklid et al. (1996)
- PSL-3 materials for primary components, with exposed surfaces clad with Inconel overlays or of corrosion resistant metals, Duncan and Hartford (1998)
- PSL-2 Materials for non primary components, Duncan and Hartford (1998)

Elastomers, Seals

- NITRILE elastomers, Baklid et al. (1996)
- TEFLON, Jarrel et al. (2002), Cox (1990)
- AFLAS, Cox (1990) (packer elements), Duncan and Hartford (1998) (packer seal assemblies, safety valve)

- RYTON, KALREZ, TEFLON (packer locator seal) Cox (1990)
- METAL-TO-METAL (primary wellhead seals), Cox (1990)

Topside equipment

- 22% Cr duplex steel, Baklid et al. (1996)

Recommendation: If protection against the acidity of carbonic acid is by corrosion inhibition, inhibition should be initiated with the start of operation, preferably by continuous inhibition allowing 99% inhibitor availability. Inhibitors should be selected, which have been proven effective and compatible with the other fluids in the system, Van Grinsven et al. (2005).

Recommendation: For completion a monobore design should be selected, to minimize flow disturbances and provide good access for remedial actions, Baklid et al. (1996)

Recommendation: The optimal tubing type and size should be determined based on injection and production requirements and conditions. When sizing, consideration should be given to erosion-corrosion observed for high velocities (20 m/s and more), Van Grinsven et al. (2005).

Recommendation: Injection and production wells should be equipped with a packer to isolate the pressure of the injection interval, minimize contact with the corrosive fluids and allow annular pressure monitoring, Cailly et al. (2005).

Recommendation: At packer setting depth, special materials should be considered for the casing to ensure proper setting, Duncan and Hartford (1998).

Recommendation: The completion for CO₂ wells should include a downhole safety valve in the tubing to ensure that in case of surface equipment failure, the well is automatically shut down. The valves should be made of a special type of stainless steel, e.g. Incoloy, Cailly et al. (2005), Duncan and Hartford (1998).

Recommendation: Besides a packer and a subsurface safety valve, a typical down-hole configuration for an injection well should include an on-off tool with a profile nipple, and a downhole shutoff valve made from CRA, to ensure that no CO₂ release occurs and to prevent CO₂ from inadvertently flowing back into the injection system, Jarrell et al. (2002).

Recommendation: An expansion joint, to allow for travel due to temperature, should be considered for inclusion in the completion.

Recommendation: The use of flow couplings on either side of safety valve should be considered to minimize local flow disturbances, Duncan and Hartford (1998).

Recommendation: The use of flush connections should be considered to minimize local flow disturbances, Benge and Dew (2005).

Recommendation: Further components which warrant consideration are a chemical injection line for continuous inhibitor injection in production wells, Cameron et al. (1992), Van Grinsven (2005), and side pocket mandrels for corrosion coupons, Cox (1990), Cameron et al. (1992).

At prolonged shut in periods, the temperature at the top part of a well may drop to temperatures and pressures which are within the hydrate formation area, Baklid et al, (1996)

Recommendation: Installation of an injection sub for methanol injection in the top part of well completions should be considered, Baklid (1996).

Recommendation: Considerations in cementing design and implementation include, OGP (2000),

- Appropriate design of the compressive strength of the cement
- Determining the theoretical and actual length of the cemented interval
- Casing shoe strength testing
- Conforming the cement bond between casing and formation

Recommendation: To ensure optimum conditions for cementation and setting, cementations should be carried out using carefully planned engineering solutions for centralizer selection and placement, running casing, efficient preflush for mud displacement, and equipment, Benge and Dew (2005).

Recommendation: Cement systems should be selected with a view of their resistance to CO₂ degradation, see 3.2.1.

Use of the following materials has been reported in the literature:

- Pozzolin-Portland blends densified by deleting the bentonite additive, Acker-voll et al. (2005), Lubbenau (2005)
- Acid resistant latex cement, Duncan and Hartford (1998),
- Portland-Alumina cement blends with a particle size controlled, latex diluent, Benge and Dew (2005)
- Calcium phosphate cements with aluminate and calcium phosphate hydrates, and calcium aluminosilicates, Lance Brothers (2005)
- Low-Portland or Non-Portland cements, Barlet-Gouédard (2006).

Recommendation: Casing/liner across the CO₂ target formation should be rotated (or reciprocated) throughout the cement job, Benge and Dew (2005), Duncan and Hartford (1998).

Each string of casing along with the cement, that seals its annulus against the CO₂ injectate, represents a layer of protection which confines the injected fluid to its design pathway direct to the injection zone.

Recommendation: In cementation design, consideration should be given to overlapping cementation in successive annuli.

Recommendation: Cement integrity should be verified with segmented cement evaluation tools, Duncan and Hartford (1998).

Recommendation: The well head should be equipped with two valves (gate or ball valves) for well control: an outside valve for regular use and an inside valve for safety, Cailly et al. (2005).

2.4.2 Existing Wells

Old wells should be selected for CSEGR service on the basis of the following key factors:

- well integrity performance
- mechanical state of the well
- quality of the primary cementation
- well maintenance

Recommendation: Well file information should be synthesized and integrated into a data base for use in performance assessments, Moreno et al. (2004).

Recommendation: Wells with casing pressure problems in the past or present should not be used.

Recommendation: Wells with casing pressure problems in the past or present should be plugged and abandoned.

Where an existing production well is to be converted to injection, casing and cement may not be designed to provide isolation of injected fluids.

Recommendation: Prior to converting production wells to CO₂ injection, wells should be checked for meeting the new requirements of a CO₂ injection.

Recommendation: Open hole completions should be converted into cased hole completion in a process, which allows the running and cementing of a liner across a completion interval, Bowser et al. (1989), Duncan and Hartford (1998).

Recommendation: A conversion to CO₂ injection wells should be carried out only after mechanical integrity has been demonstrated.

Duncan and Hartford (1998), in the process of the re-configuration of a 37 year old producer as a backup injector, used inspections with (1) a casing inspection log, (2) a

segmented bond tool, and (3) a casing pressure test to demonstrate mechanical integrity of the well.

Recommendation: Mechanical Integrity should be demonstrated on the basis of standard annulus pressure testing and a detailed logging program.

Recommendation: The logging program should allow an unambiguous assessment of the integrity of tubing, casing, and cement and provide a baseline against which changes during the CO₂ project can be measured.

Recommendation: Tubing and casing integrity should be assessed over the full length.

Recommendation: Wells with significant corrosion should be recompleted, casing sections with significant corrosion should be repaired. For recompletions the recommendation in section 4.1 should be taken into account.

The use of old cement bond logs is not appropriate for the assessment of actual cement bond integrity.

Recommendation: Cement integrity should be verified with segmented cement evaluation tools, Duncan and Hartford (1998).

Recommendation: To assess the integrity of existing well, use of a workflow as proposed by Jammes (2007), allowing a structured evaluation of mitigation options versus assessed risks, should be considered, Figure 2.8.

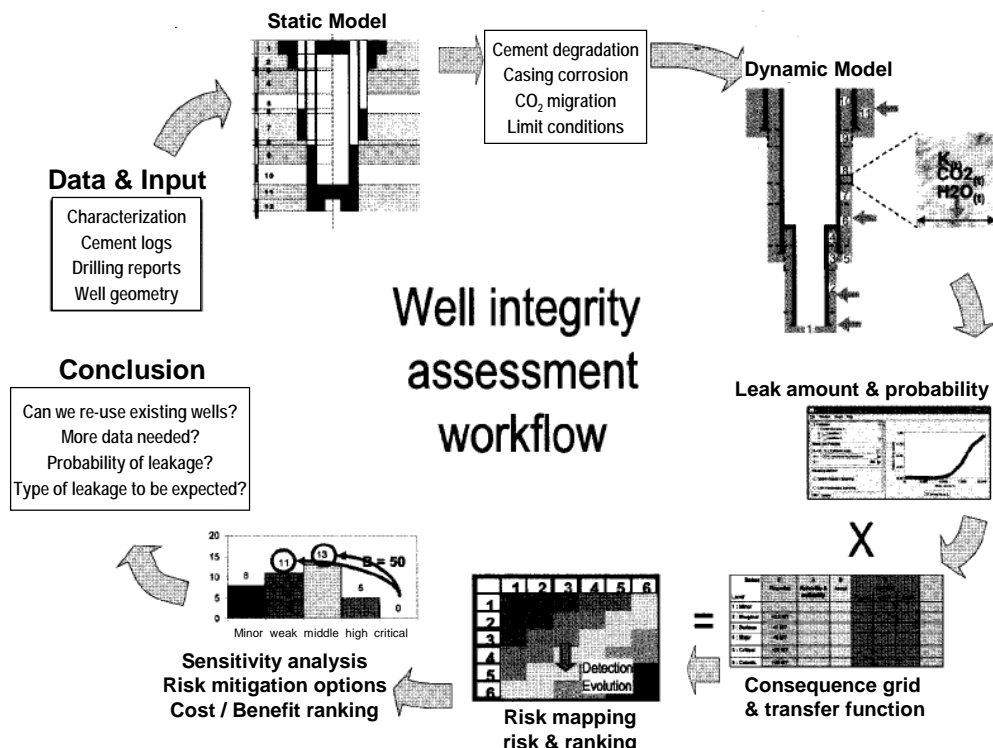


Figure 2.8: Well Integrity Assessment Workflow (after Jammes, 2007)

2.4.3 Monitoring

Monitoring may be divided into injection (/production) operation monitoring, verification monitoring, and environment monitoring, Jammes L. (2007). In the context of well integrity only operations and environment monitoring are relevant and only operations monitoring will be addressed. The monitoring of well head pressures and rates, as well as annular pressures can provide indications of the status of mechanical integrity of the well without interrupting injection operations. The additional monitoring of injected and produced fluid composition, temperatures, cumulative volumes, and subsurface geomechanics and petrophysics ensures performance objectives are achieved. For a meaningful monitoring, baseline measurements on the mechanical condition of the completion and petrophysical conditions (fluid content) in the target formation should be available.

Recommendation: Well monitoring should include well head pressure, rate, temperature, cumulative volume, and fluid composition and analysis at injection and production wells.

A detailed continuous downhole injection system monitoring program for deep, hot, sour gas wells under continuous inhibition is described in Cameron et al. (1992)

Recommendation: The monitoring program should include measurements of annular pressures and fluid levels to detect leaks in packers and tubing, which is important for taking quick corrective actions.

The well head, casing, and tubing can also be monitored for signs of erosion or corrosions, but this may require suspending injection operations while the survey is run.

Recommendation: For wellhead inspections involvement of video cameras and ultrasonic test (UT) on the valve bodies should be considered.

Recommendation: Regular calliper runs should be carried out to record changes in the condition of the tubing, in particular if corrosion prevention relies on down hole corrosion inhibition.

Recommendation: To monitor the corrosivity of the environment in the wells the placement of corrosion coupons may be considered, Cameron et al. (1992).

Recommendation: For monitoring of cement integrity the repetition of directional cement evaluation measurements may be considered.

If a leak is suspected, shutting in the injection and performing a simple pressure integrity test on the annulus may confirm the problem. Then running the logs and survey listed above may be considered. Of these techniques, the noise and temperature logs and radioactive tracer survey have the capability to detect leaks in tubing, casing, or packer as well as fluid movement behind casing, OGP (2000).

Recommendation: To test casing integrity, consideration should be given to carrying out hydrotests during workovers, Nugent (2005)

2.4.4 Well Abandonment

Because of the long time frames and the inaccessibility for monitoring and intervention abandonment of wells in (potential) CO₂ injection areas must be done right the first time. Careful review of well information should be conducted prior to abandoning wells. This may include, Ohio EPA (2005)

- review of records pertaining to well construction and repair or modifications
- review of analytical chemical data for formation and fluids
- current condition of well

Based on the analysis, specific designs should be considered for

- well preparation
- plugging material selection
- Barrier placement
- monitoring

in particular after a long period of production/injection and implemented with care.

In addition to the requirements imposed by the German mining authorities the following recommendations are made:

Recommendation: Well file information should be synthesized and integrated to assess well integrity.

Recommendation: To allow a fit for purpose design, the running of logs should be considered, e.g. calliper and cement bond logs, to survey the status of casing and cementation.

Recommendation: In well sections with questionable cement integrity, under reaming and plug placement between the formation walls may the barrier placement of choice as shown in Figure 2.9, taken from Gérard et al. (2006).

Recommendation: Plugging material should be selected with a view of their resistance to CO₂ degradation.

Recommendation: When filling the volume between the plugs with mud, consideration should be given to heavy weight muds resulting in a high sedimentation height.

Recommendation: For the design, use of a risk based approach as documented by Jammes (2007) should be considered.

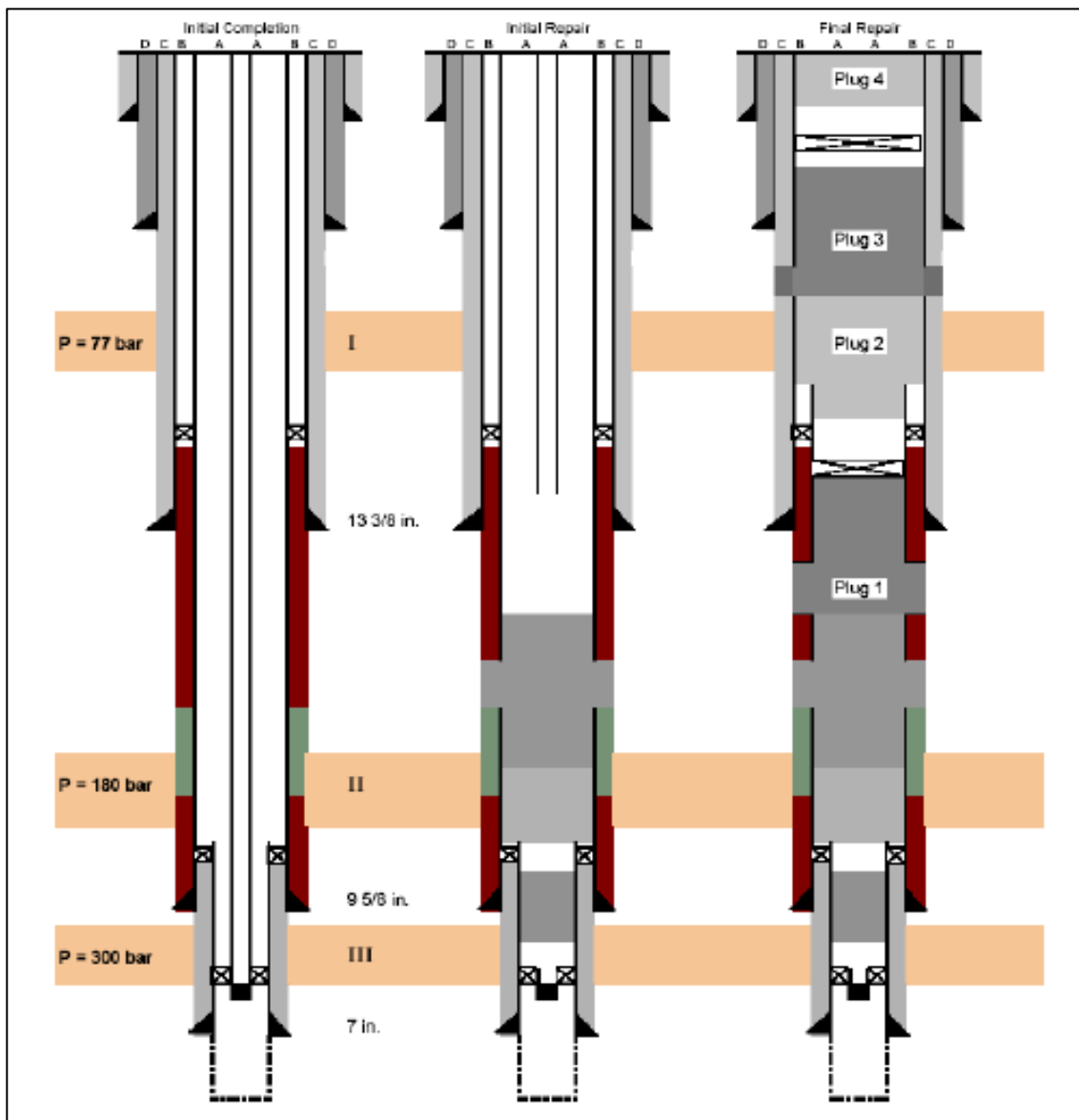


Figure 2.9: Well Repair and Abandonment. Gérard et al. (2006)

In wells where layers of plastic salt and/or clays have been encountered, consideration should be given to the activation of natural barriers, e.g., by underreaming the well in the sections where plastic salt (clay) is present and allowing the salt (clay) to move in to form a natural barrier. Variations of such an abandonment procedure are being investigated at Clausthal University of Technology.

Recommendation: Abandonment design and implementation should be properly documented and stored for easy access.

2.4.5 Abandoned Well Integrity

The task of evaluating well integrity of abandoned wells is a difficult one. The desired information for a straightforward integrity assessment may not be available, but the wells are inaccessible for direct monitoring and intervention. If the information is available, in the case of old wells, the status they reflect may not be representative of the current status. It is easy to demand that all historical wells are re-drilled and re-

plugged as required under Alberta law, but one must realize, that a general requirement of this nature would have a significant adverse effect on the economy of sequestration projects. On the other hand the affect on project economics cannot be a license to do nothing.

Recommendation: The compromise option proposed in IEA (2007) of performing a ranked risk assessment of all wells within a CO₂ storage area should be followed. According to this proposal wells at a higher risk of leaking should be remediated while monitoring equipment should be installed around lower risk wells.

Recommendation: For the risk assessment, well file information should be synthesized and integrated.

Recommendation: The risk assessment should be carried out on the basis of a thorough understanding of, Mulders (2007),

- present well condition
- well geometry
- construction materials
- construction methods
- geology

giving particular consideration to corrosion of the primary cement sheath and the well casing.

Recommendation: In assessing the risks, considerations should be given to the findings of Bachu and Watson (2007) with respect to well conditions and factors and the level, to which they affect well integrity.

Recommendation: Risks assessments should take into account the conditions under which the abandonment was carried out. In doing so one should distinguish

- standard abandonment procedure and wells without well related problems (e.g. sustained casing pressure)
- “standard” abandonment procedure and wells without well related problems but with deposition of production wastes
- abandoned wells with sustained casing pressure during well life
- abandoned wells with non-standard abandonment because of well related problems (e.g. casing collapse, fish in hole, etc.)

Recommendation: For the assessment a structured approach as proposed by Jammes (2007) should be considered.

2.5 Analysis of Integrity of Pilot Area Wells

The pilot project area is a fault block of a large gas field. The gas field is located at the southern edge of the North East German Basin. It is part of the Central European natural gas province, extending from the Southern North Sea passing Groningen to the Eastern Polish border. The gas bearing horizons belong to the subsalt sequence of the Rotliegendes. The siliciclastic reservoir rocks are part of a stacked and complex sequence of sandstones, siltstones, and claystones. In total some 420 wells have penetrated the Rotliegendes reservoir at an average depth of 3,350 m. Of the 420 wells, ca. 250 wells served as gas producers. Recovery of the gas in place has reached 78% during the 37 years of production, Florette et al. (2007).

The natural gas accumulation in the Rotliegendes is sealed by thick layers of Zechstein salt which represents an effective barrier. For all practical purposes, this configuration of salt as sealing element reduces the risk of leakage to wells only. Along the wells, the effect of moving salt can only be towards reducing any leakage which may exist. Also, it provides for a unique abandonment methods by using the movable salt as a natural barrier. Variations of such an abandonment procedure are being investigated at Clausthal University of Technology.

2.5.1 Pilot Project Area Data

The pilot area contains 13 wells, Figure 2.10, plus a service well. Of the 13 wells, 6 wells were plugged and abandoned between 1991 and 2005.

The information which was available consists of

- Well bore diagram with casing scheme and primary cementation intervals
- Cement analysis and cementation protocols for primary cementation
- Cement analysis and cementation protocols for well plugging for plugged wells
- Well situation after abandonment for plugged and abandoned (p&a) wells
- Hole condition with materials left in the hole, casing collapse etc.

For some wells, additional information was available in form of CBL logs (cement bond logs), VDL logs, CBL interpretations, open hole calliper logs, and well stratigraphy.

For the wells in the pilot area, wellbore diagrams were prepared with software Well-View, Shinde (2006). The diagrams depict the casing scheme, tops of cement, and the geology over the full length of the well. For wells with CBL information additional wellbore diagrams were prepared highlighting the depth below 2,000 m to indicate the areas of good to moderate and bad cement bond. For the p&a wells, the diagrams include information on the well situation after abandonment. Wellbore diagrams for the sample wells offered here are shown in Figures 2.11-2.14. The diagrams show at least two thick layers of salt to be present above the target formation, the Zechstein and the Röt Salt.

As described before, cement quality in its simplest form is usually derived from a cement bond log and represented by a bond index. Bond index determination requires the use of a CBL log interpretation nomogram. The nomograms differ from tool to tool and calibration fluid, information which was not available. Therefore the cement quality, indicated in the wellbore diagrams in Figures 2.11-2.14, is qualitative only, unless it stems from an interpretation provided by the operator of the field. The limited information, which was available for this study, prevented the determination of the compressive strength of the cement. The terms good cementing zones and bad cementing zones in the wellbore diagrams refer to zones characterized by nature of CBL amplitude and not to zones characterized by actual Bond Index. The highest value of amplitude are considered as free pipe value and zones with less than 20% of its value are referred as good cement bond, Shinde (2006).

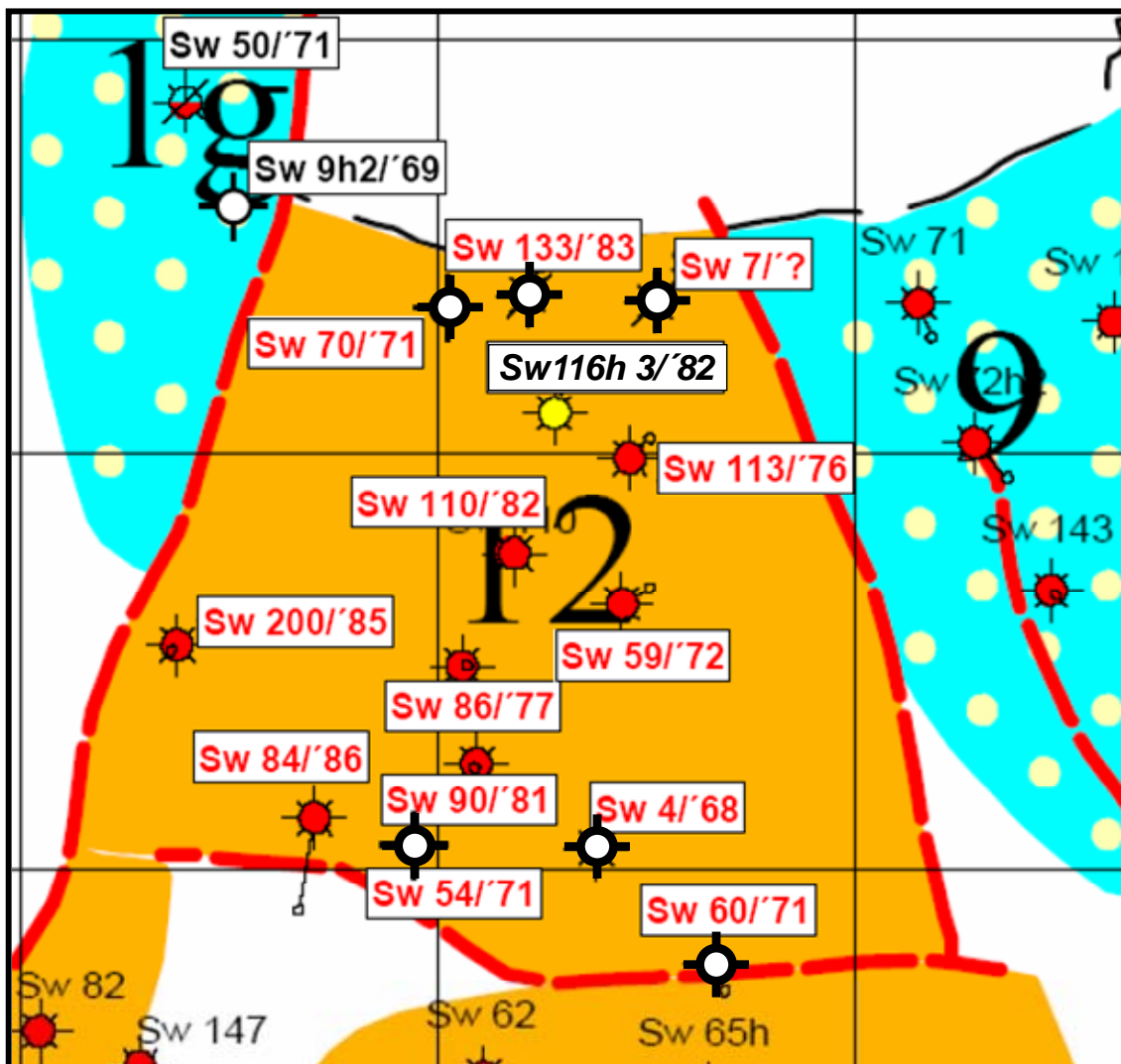


Figure 2.10: Pilot Project Area

The cement bond logs which are available, are logs taken after primary cementation, typically some 30 years ago. If at all, they represent the quality of the cementation 30 years ago. In the 30 years of wells service, cement quality may have suffered as described in section 3.1.3. Therefore integrity conclusions drawn on the basis of 30 year old cement bond data must be taken with a grain of salt.

In the following the available well information is described and evaluated to assess well suitability for CSEGR use and recommendations are made for further work on the wells.

2.5.2 Accessible Well Analysis

Key to the assessment of wellbore integrity is the assessment of the quality of the primary cementation of casing and liner. Relying only on cement analysis and cementation protocols would be inadequate to make any integrity conclusions. To draw meaningful conclusions, cement bond logs are necessary.

For many of the wells in the pilot area CBLs were not provided. When CBLs were made available, this was typically done without the information necessary for a proper interpretation. Therefore a conclusive assessment of cement quality was not possible.

The interpretation of the data available is described in the following for two sample wells. Cement quality for the well with CBL information / CBL interpretation results is shown in the wellbore diagram in Figures 2.11-2.14 in blue colour and yellow colour to indicate good to moderate and bad cement bond, respectively.

2.5.2.1 Production Well with CBL Information (P-Well 1)

Salt Layer No information was made available on the salt layers encountered in the well

Perforated Intervals: 3,365-3,368m (B14), 3,385-3,387.5m (C),
 3,412.5-3,414.5m (Cu)

Wellbore Diagram: Figure 2.11

CBL interpretation for the primary cementing made available by EEG is shown in tabular form below and in graphical form in Figure 2.11.

Analysis:

Cementing protocols indicate no problems during primary cementing.

Top of cement (TOC) for 7" casing is indicated at 1,640m by gamma ray. According to the CBL for the primary cementing cement bond should be of good quality.

The well was re-completed 06/1995. The table describing well status, dated 31/01/1999, contains information about components lost in the well.

Table 2.2: Cement Quality for P-Well 1

| Cas-ing/ Liner | For-mation | Good Bonding | | Moderate Bonding | | Bad or No Bond-ing | |
|-----------------------|----------------------|---------------|--------|------------------|--------|--------------------|--------|
| | | Interval | Height | Interval | Height | Interval | Height |
| 7" to 3224 | P2: 3124- 3235 | 15-2330 | 2315 | | | | |
| | | | | 2330- 2400 | 70 | | |
| | | 2400- 2640 | 240 | 2640- 2685 | 45 | | |
| | | 2685- 2930 | 245 | 2930- 3095 | 165 | | |
| | | 3095- 3130 | 35 | | | 3130- 3180 | 50 |
| 5" be- low 3147 | P2: 3124- 3235 | | | 3180- 3210 | 30 | 3210- 3235 | 25 |
| | | | | 3235- 3255 | 20 | | |
| | P1: 3235- 3454 | 3255- 3425 | 170 | | | | |
| | | 3225- 3455 | 30 | | | | |

Recommendations:

A casing inspection log should be carried out to assess the integrity of the casing.

A variable density log (VDL), or better a segmented cement evaluation log should be taken to assess the current condition of the cementation and/or detect and characterize cementing defects like channelling, micro annulus which are not detectable by CBL alone.

The well seems to be suitable for use in CSEGR.

2.5.2.2 Production Well with no CBL Information

Salt Layers: No information was made available on the salt layers encountered in the well

Perforated Intervals: 3,212.5-3,223m (Ca1/ROF), 3,229-3,234m (ROF+10), 3,253-3,256.5m (B17), 3,344.5-3,346.5m (B14)

Wellbore Diagram: Figure 2.12

Analysis:

Cementing protocols indicate no problems during primary cementing.

Top of cement indications are contained in the wellbore diagram supplied by EEG at 160m and 2,180m for 9 5/8" casing and 7" casing cementation, respectively.

The well was re-completed 09/2001.

Recommendations:

A casing inspection log should be carried out to assess the integrity of the casing.

A segmented cement evaluation tools should be taken to assess the current condition of the cementation.

Without further surveying the well should not be used for CSEGR

2.5.3 Abandoned Well Analysis

Key to the assessment is the integrity of cement sheath and the casing, the cement plugs or any other material used for plugging the well and plug placement. No information was available on well performance during the life of the wells such as sustained casing pressure. Also, the condition of the casing at the time of abandonment is not known. The assessment therefore had to rely on whatever information had been made available on cement, casing scheme, placement of abandonment material, cementation protocols, and geology.

In the pilot project area, six wells have been abandoned. Based on the information available, three of the wells have seen standard abandonment procedure, while three wells had to be abandoned with non-standard procedures because of well related problems.

2.5.3.1 Abandoned Well with Standard Abandonment Procedure

Abandonment Type/Date: Standard, 09/1992

Salt Layers: 2,031-2,124m (Röt), 2,738.5-3,158m (Zechstein)

Perforated Intervals: 3,215-3,221m, 3,227-3,230m, 3,241-3,243.5m, 3,337-3,339m, 3,345-3,349m, 3,361-3,379m, 3,382-3,400m, 3,415-3,423m

Wellbore Diagram: Figure 2.13

Fish in hole: below 3,475m: Packer 5" (approx. 1.5m), approx. 0.5 m tubing

below 3,493m: Packer PD-2 5" (approx. 1.5m)

| Cement Plug Positions: | Depth Interval (m) | Length (m) |
|------------------------|--------------------|------------|
| 1 | 3,519 – 3,506 | 13 |
| 2 | 3,475 – 2,987.9 | 487.1 |
| 3 | 2,840 – 2,643 | 197 |
| 4 | 2,180 – 1,558 | 622 |

| | | |
|---|-----------------|-------|
| 5 | 1,201 – 1,060.8 | 140.2 |
| 6 | 600 - 21.6 | 578.4 |

The Borehole volume between the plugs is filled with Tixoton mud of density=1.04 g/cm³

CBL interpretation for the primary cementing of 9 5/8" casing is shown in tabular form in Table 2.3 and in graphical form in Figure 2.13.

Analysis:

For the upper part of the 9 5/8" casing from 150-650m, the CBL indicates no cement. Overall, cementation is bad up to depth of 1,590m except zone from 788-1,000m which has moderate to good cement bond.

According to the CBL, the zone from 2,000-2,650m has a moderate to very good cement bond.

The cased depth for the well is 3,519m, but CBL are given only up to 2,650m. CBL for the 7" casing and the 5" liner were not available.

The complex casing scheme suggests that problems were encountered when drilling this well.

Table 2.3: Cement Quality for A-Well 1

| Cas-ing/ Liner | Formation | Good Bonding | | Moderate Bond-ing | | Bad or No Bond-ing | |
|------------------------|-----------|---------------|--------|-------------------|--------|--------------------|--------|
| | | Interval | Height | Interval | Height | Interval | Height |
| 9 5/8" to 2657.5 | | | | | | 150-769 | 619 |
| | | | | | | 788-1800 | 1012 |
| | | | | 1800- 1892 | 92 | | |
| | | 1892- 1913 | 21 | 1913- 1993 | 80 | | |
| | T1.3 | 1955- 2128 | 44 | 2037- 2200 | 163 | | |
| | | 2200- 2224 | 24 | 2200- 2325 | 125 | | |
| | P2: | 2722- 3212 | 325 | | | | |

Recommendations:

Further analysis is required for this well. The quality of the cement bond below 2,650m should be re-assessed. If CBL are not available consideration should be given to re-drilling the well. This is also suggested by the poor quality of the cementation in the upper 1,800m warranting remediation of these zones.

Candidate for further analysis and/or remediation measures.

2.5.3.2 Abandoned Well with Non-Standard Abandonment Procedure

Abandonment Type/Date: Non-Standard-Fish in Hole, 12/2000

Salt layers: 2,234-2,255m (Muschelkalk), 2,462-2,609m (Röt), 3,123-3,258m (Zechstein)

Perforated Intervals: 3,260-3,267m (ROF), 3,368.5-3,372m (A), 3,381-3,387.5m (B14), 3,391.5-3,401m (B13), 3409-3,425m (C12/11), 3,428-3,434m (C10)

Wellbore Diagram: Figure 2.14

Fish in hole: below 2,547-3,364m approx. 817m Tubings

| Cement Plug Positions: | Depth Interval (m) | Length (m) |
|------------------------|--------------------|------------|
| 1 | 3,470 - 3,4911 | 21 |
| 2 | 2,155 - 2,535 | 335 |
| 3 | 2 - 250 | 202 |

The Borehole volume between the plugs is filled with mud of density = 1.04 g/cm³

CBL interpretation for the primary cementing of the 11 3/4" casing and the 8 5/8" are shown in tabular form in Tables 2.4 and 2.5, respectively. A graphical representation is provided with Figure 2.14.

Analysis:

The 11 3/4" casing appears to be of adequate cement bond above approximately 800m and below approx. 2,000m.

The poorly and only moderately bonded 8 5/8" liner sections between 3,141m and 3,248m are opposite Zechstein salt such that self healing is likely.

No information is available for the 6 5/8" x 5 3/4" casing extending to the wells final depth of 3,486m which is shown to be fully cemented over the total length of the well.

A casing collapse is reported for the section opposite Zechstein salt at depth 2,547m. Below it, an 817m fish is reported. Since no plug could be set across the formation a thick 380m cement plug is shown to have been set above a cement retainer at 2,535m (plug depths according to the cementation protocol are 2,168-2,535m). The volume between the lower plug and the surface plug from 2-250m is filled by mud of density = 1.04 g/cm³.

Table 2.4: Cement Quality for A-Well 1 – 11 3/4" Casing

| Cas-ing/ Liner | Formation | Good Bonding | | Moderate Bond-ing | | Bad or No Bonding | |
|----------------------------|---------------------|---------------|--------|-------------------|--------|-------------------|--------|
| | | Interval | Height | Interval | Height | Interval | Height |
| 11 ¾ Casing: 0- 3050 | T1.3: 2373- 2607 | | | -813 | 813 | 813-1999 | 1186 |
| | | | | 2211- 2296 | 85 | 2296- 2383 | 87 |
| | | | | 2383- 2398 | 15 | 2398- 2494 | 96 |
| | | 2494- 2499 | 5 | 2499- 2507 | 8 | | |
| | | 2507- 2523 | 16 | | | 2523- 2532 | 9 |
| | | 2532- 2598 | 66 | | | 2598- 2697 | 99 |
| | | | | 2697- 2918 | 221 | 2918-- 3037 | 119 |
| | | 3037- 3044 | 7 | 3044- 3050 | 6 | | |

Table 2.5: Cement Quality for A-Well 1 – 8 5/8" Liner

| Cas-ing/ Liner | Formation | Good Bonding | | Moderate Bond-ing | | Bad or No Bonding | |
|--|---------------------|---------------|--------|-------------------|--------|-------------------|--------|
| | | Interval | Height | Interval | Height | Interval | Height |
| 11 ¾ Casing to 3050 | T1.3: 2373- 2607 | | | | | 2685- 2705 | 20 |
| | | 2705- 2715 | 10 | | | 2715- 2752 | 37 |
| | | 2752- 2758 | | 2758- 2772 | | | |
| 8 5/8 Liner: 2796,5 - 3249,5 | P2: 3123- 3261 | 2772- 2804 | 32 | | | 2804- 2849 | |
| | | | | 2849- 2869 | 20 | 2869- 3132 | 263 |
| | | 3132- 3141 | 9 | | | 3141- 3196 | 55 |
| | | | | 3196- 3248 | 52 | | |

Recommendations:

If available the logs for the 6 5/8" x 5 ¾" casing should be reinterpreted.

Despite all well problems "Well K" seems to fulfil the requirements of well integrity for CSEGR.

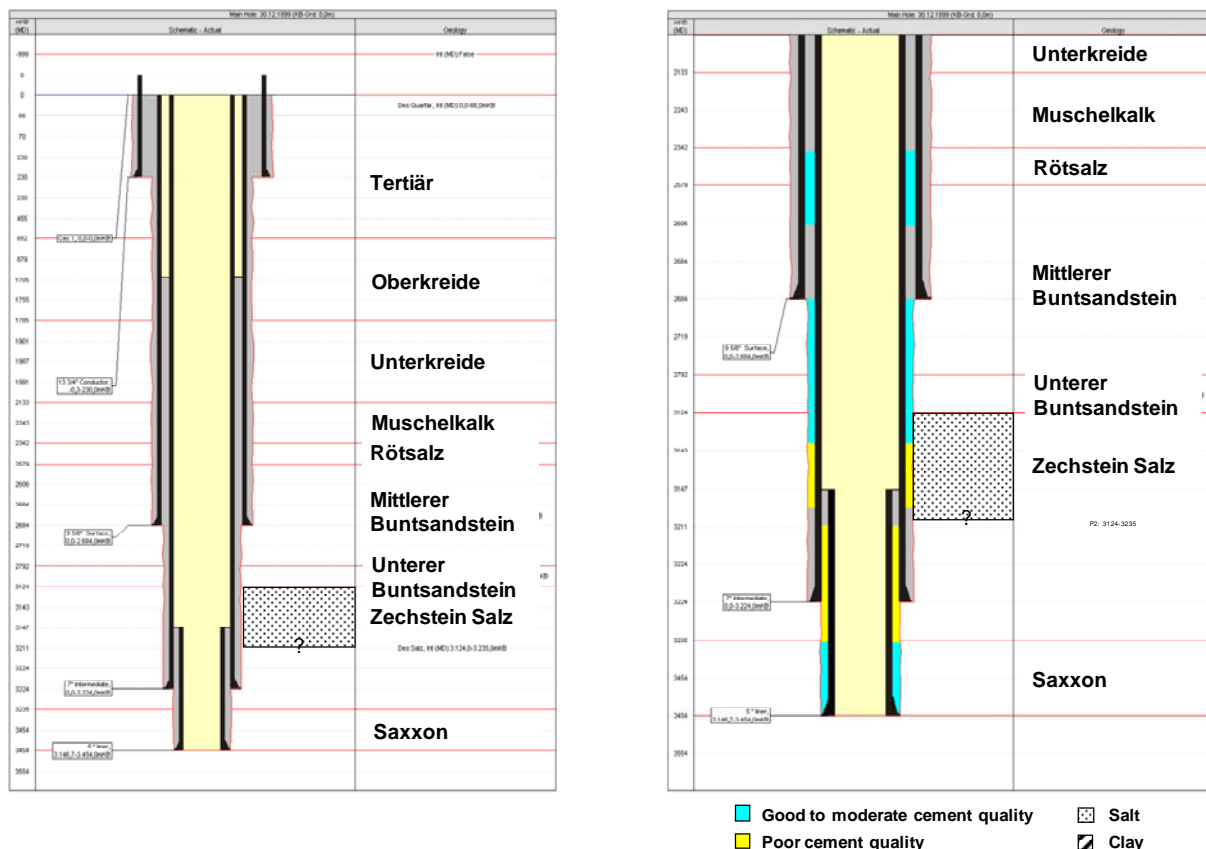


Figure 2.11: Wellbore Diagram for Production Well with CBL Information (P-Well 1)

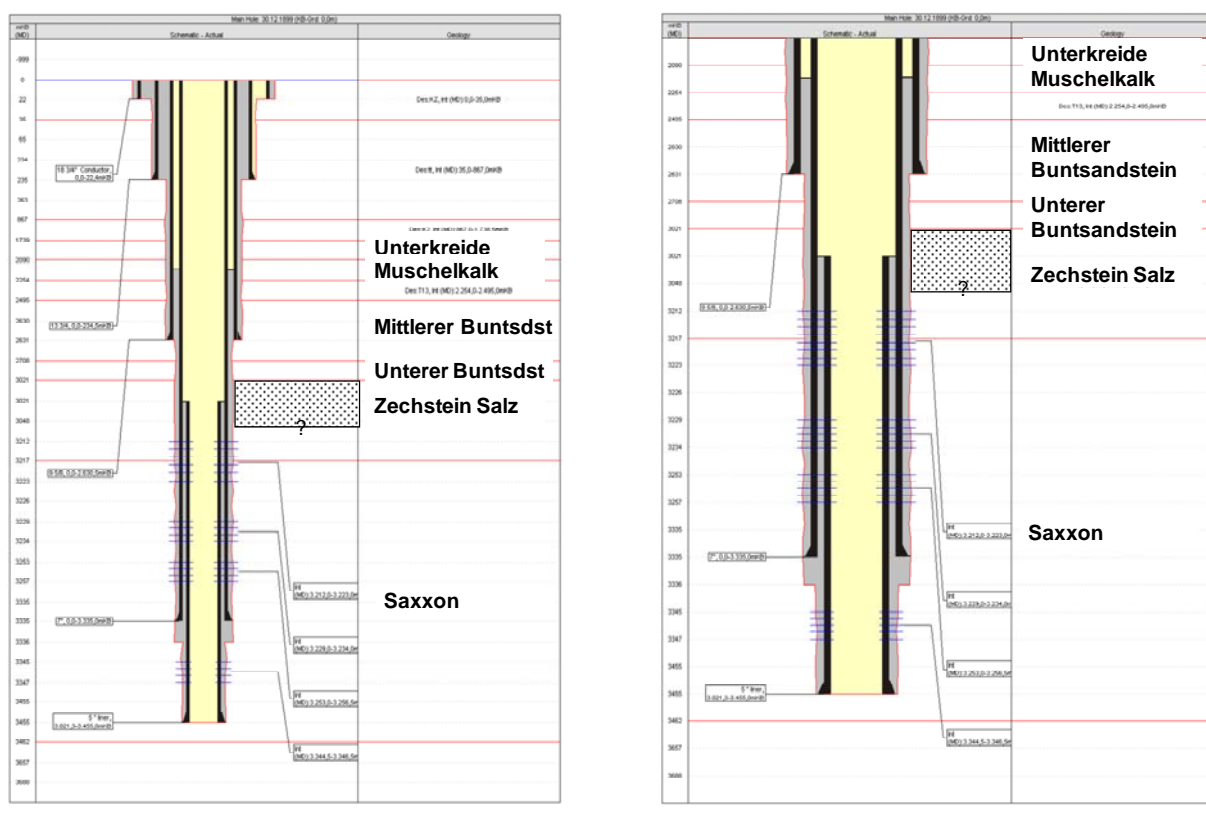


Figure 2.12: Wellbore Diagram for Production Well with no CBI Information

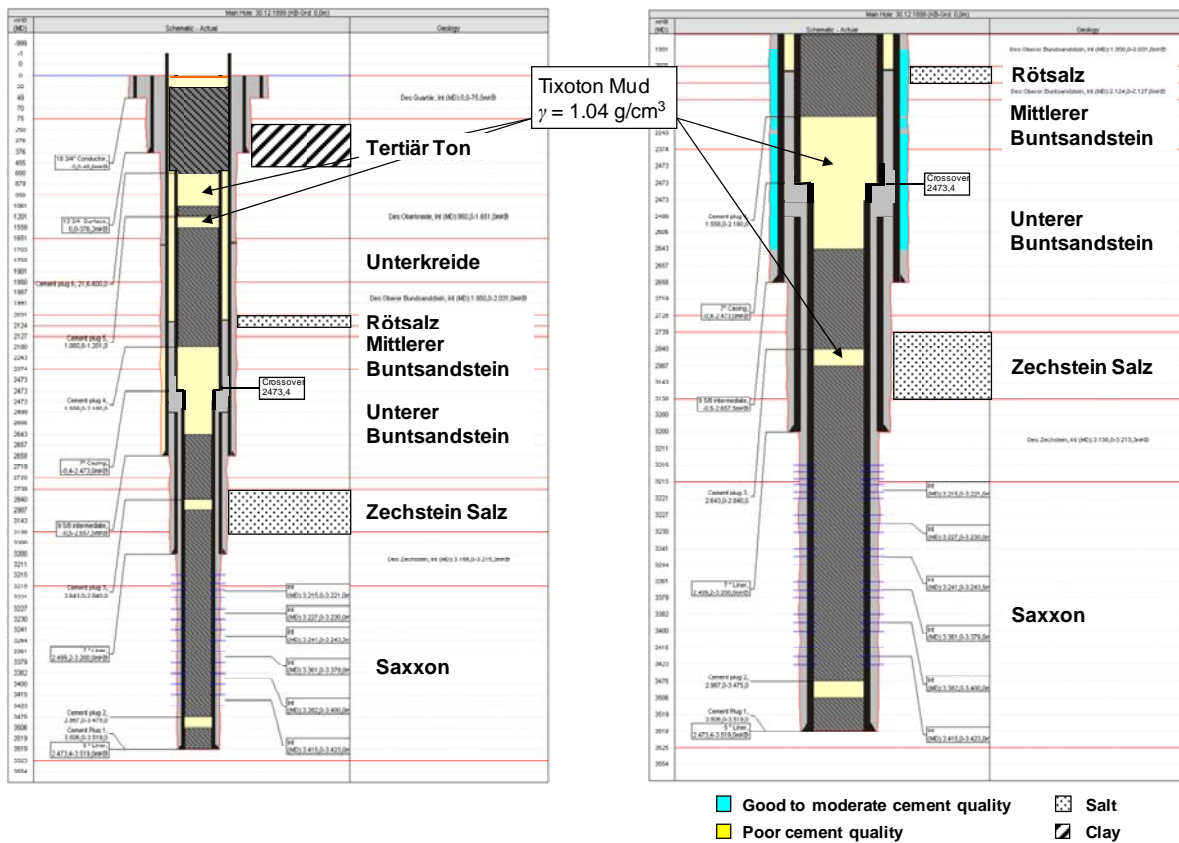


Figure 2.13: Wellbore Diagram for Abandoned Well with Standard Abandonment Procedure (A-Well 1)

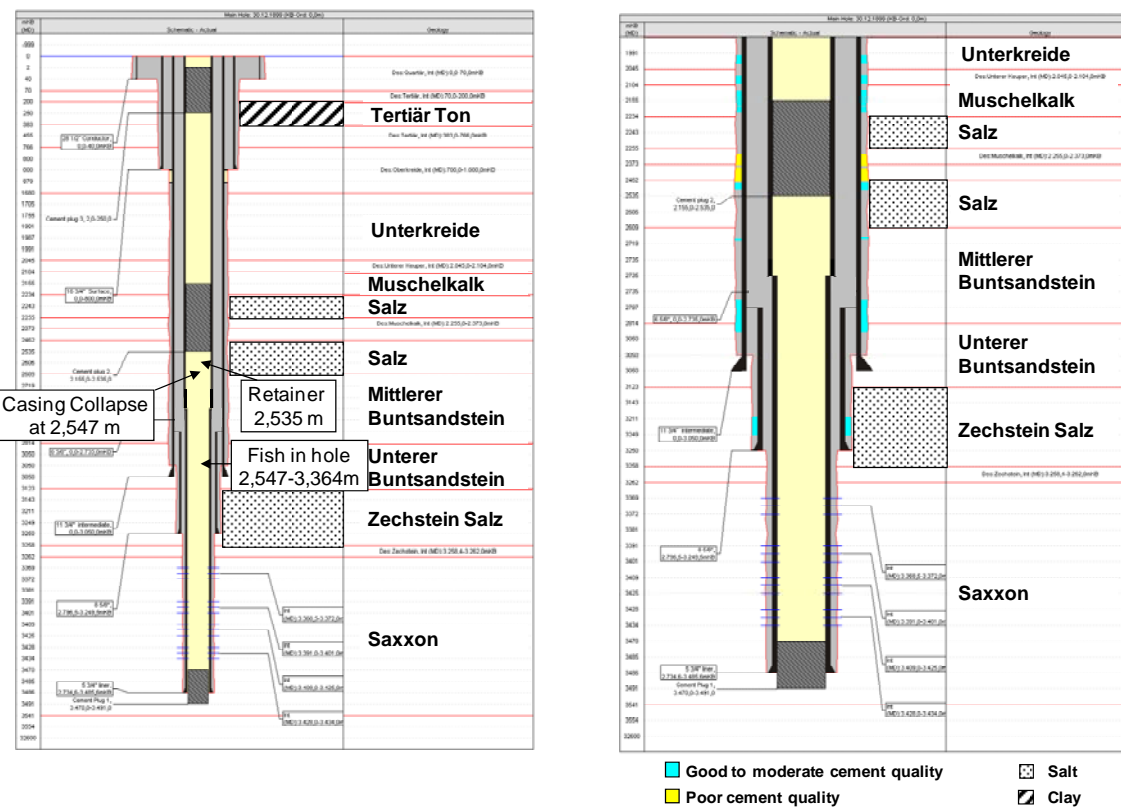


Figure 2.14: Wellbore Diagram for Abandoned Well with Non-Standard Abandonment Procedure (A-Well 2)

References

- Akervoll I., Mo S., Boe R., Pillitteri A., Larsen I. **(2005)**: "Leaking Well Modelling & CO₂ interaction with cured well cement." Report on Well Bore Integrity Workshop. Meeting organized by IEA Greenhouse Gas R&D Programme and BP, held at Marriott Woodlands Waterway Hotel and Convention Center, Houston, TX, U.S.A, 4-5 April, 2005.
- Allan M.L., Philippacopoulos A.J.: « Literature Survey on Cements for Remediation of Deformed Casing in Geothermal Wells". BNL-66071 Informal Report.
- Bachu S., Watson T.L. **(2007)**: "Factors Affecting or Indicating Potential Wellbore Leakage". July 2007, see IEA 3rd Well Bore Integrity Workshop (2007).
- Bachu S., Watson T.L.: "Possible Indicators for CO₂ Leakage along Wells". Alberta Energy and Utilities Board, Edmonton, TL Watson & Assocs., Calgary, Canada.
- Baklid A., Korbol R. Owren G. **(1996)**: "Sleipner Vest CO₂ Disposal, CO₂ Injection into a Shallow Underground Aquifer". Society of Petroleum Engineers SPE 36600.
- Barlet-Gouedard V., Rimmele G., Goffe B., Porcherie O. **(2006)**: "Mitigation Strategies for the Risk of CO₂ Migration through Wellbores". Society of Petroleum Engineers 98924. IADC/SPE Drilling Conference held in Miami, Florida, U.S.A, February 21-23, 2006.
- Barry D.W. **(1985)**: "Design of Cortez CO₂ System detailed". Oil & Gas Journal, July 22, 1985 pp 96-104.
- Benge G., Dew E.G. **(2005)**: "Meeting the Challenges in Design and Execution of Two High Rate Acid Gas Injection Wells". Society of Petroleum Engineers SPE 91861, 2005.
- Bennaceur K., Gupta N., Monea M., Ramakrishnan T.S., Trygve R., Sakurai S., Whittaker S. **(2004)**: "CO₂ Capture and Storage – A Solution Within". Schlumberger Oilfield Review, Autumn 2004.
- Bennaceur, K. **(2004)**: "CO₂ Sub-Surface Risk Management & Mitigation". Schlumberger Contribution to the IEA / CSLF Workshop on Legal Aspects of Storing CO₂, Paris 12-13 July 2004.
- Bliss K. **(2005)**: IOGCC CO₂ Geological Sequestration Task Force. Report by Interstate Oil and Gas Compact Commission, DOE Award No. DE-FC26-03NT41994, Amendment No. A000, 24 January 2005.
- Bouc O., Quisel N., Le Gouevec J. **(2007)**: "Risk and Safety Evaluation for CO₂ Geological Storage". Geotechnologien Science Report on 1. French-German Symposium on Geological Storage of CO₂, June 21./22., 2007 Geoforschungszentrum Potsdam.
- Bowser P.D., Corey J.D., Darr C.D.K., Caro D.A. **(1989)**: „Innovative Techniques for Converting Old Waterflood Injectors to State-of-the-Art CO₂ Injectors. Society of Petroleum Engineers SPE 18976, 1989.
- Bruckdorfer R.A. **(1986)**: "Carbon Dioxide Corrosion in Oilwell Cements". Society of Petroleum Engineers SPE-15176, presented at Rocky Mountain Regional Meeting of SPE in Billings, MT, May 19-21, 1986.

Brunet F., Corvisier J., Barlet-Gouédard V., Rimmelé G., Fabbri A., Schubnel A., Porcherie O., Goffé B. (**2007**): "Well-Bore Integrity : Cement – Fluid Interaction under Supercritical CO₂ Conditions (Model and Experiment)". Geotechnologien Science Report on 1. French-German Symposium on Geological Storage of CO₂, June 21./22., 2007 Geoforschungszentrum Potsdam.

Buß J., Schmidt J (**1991**): "Schachtanlage Konrad, Sedimentationsverhalten und Durchlässigkeit von Bohrspülungen". Bericht des Leichtweiß Instituts der TU Braunschweig, Januar 1991.

Bybee K. (Editor) (**2005**): "Cementing Technology: SPE 88016, SPE 90829, 94039". Oil & Gas Journal, August 2005.

Bybee K. (Editor) (**2007-1**): "Well Integrity Operatons at Orudhoe Bay, Alaska: Summary of SPE 102524 by Anders J., Rossberg S., Dube A., Engel H., Andrews D. (2006).

Bybee K. (Editor) (**2007-7**): "Evaluation of the Potential for Gas and CO₂ Leakage Along Wellbores: Summary of SPE 106817 by Watson T.L., Bachu S.". JPT, July 2007

Cailly B., Le Thiez P., Egermann P., Audibert A., Vidal-Gilbert S., Longaygue X. (**2005**): "Geological Storage of CO₂: A State of the Art of Injection Processes and Technologies". Oil & Gas Science and Technology-Rev. IFP, Vol. 60 (2005), No.3, pp. 517-525.

Cameron G.R., Katz D.C., Hull, J.E., Barker D.E., Elser M.W. (**1992**): "Successful Inhibition of Deep, Hot Sour-Gas Wells", Society of Petroleum Engineers SPE 20766, 1992.

Celia M.A., Bachu S., Nordbotten J.M., Gasda S.E., Dahle H.K. (**2004**): "Quantitative Estimation of CO₂ Leakage from Geological Storage: Analytical Models, Numerical Models, and Data Needs, *Proc. GHGT-7 Meeting*, Vancouver, September 2004.

Chitwood G., and Skogsberg L. (**2006**): "Cost-Effective Solutions for Corrosion-Resistant Expandable Screen Base Pipe in Sour/Brine Service". Journal of Canadian Petroleum Technology, December 2006, Volume 45, Nr. 12, pp. 18-22.

Chmilowski W. (**1992**): "Foamed Cement for Squeeze Cementing Low-Pressure, Highly Permeable Reservoirs: Design and Evaluation". Society of Petroleum Engineers 20425, 1992.

Cox J.B., c/o Babitzke E.H. (**1990**): "Completion design for Wells with high H₂S and CO₂ Content". USMS 019513, Society of Petroleum Engineers, submitted for publication March 10, 1989..

Creel P. (**2006**): "Geothermal Prospects – Well Integrity Considerations". Halliburton Presentation 28 March 2006.

Crotogino F. (**1996**): "SMRI Reference for External Well Mechanical Integrity Testing/Performance, Data Evaluation and Assessment; SMRI Spring Meeting, Short Class, Houston.

Cui Z.D., Wu S.L., Li C.F., Zhu S.L., Yang X.J. (**2004**): Corrosion behaviour of oil tube steels under conditions of multiphase flow saturated with super-critical carbon dioxide. Materials Letters, 58, 1035-1040.

Damen K., Faaij A., Turkenburg W. (2003): "Health, Safety and Environmental Risks of Underground CO₂ Sequestration – Overview of Mechanisms and Current Knowledge" Copernicus Institute for Sustainable Development and Innovation, 2003.

Duguid A., Celia M.A., (2006): "Geologic CO₂ Sequestration in Abandoned Oil and Gas Fields and Human Health Risk Assessment". Fifth Annual Conference on Carbon Capture and Sequestration DOE/NETL, May 8-11, 2006.

Duguid A., Scherer G., Radonjić M. (2005): "Degradation of Well Cements Exposed to Carbonated Brine". Fourth Annual Conference on Carbon Capture and Sequestration DOE/NETL held at Hilton Alexandria Mark Center, Alexandria, Virginia, U.S.A, May 2-5, 2005.

Duguid A., Scherer G., Radonjić M., Bruant R., Mandecki T. (2004): "The Effect of CO₂ Sequestration on Oil Well Cements". 7th international conference on greenhouse gas control technologies, September 5-9, 2004, Vancouver, Ca.

Duncan G.J., Hartford C.A. (1998): "Design, Operation of Acid Gas Injection/Disposal Wells". World Oil Magazine, October 1998.

Duval P.-P. (2004): "Sustainable Future for Hydrocarbons". IfP Contribution to TOG 2004 Tarablos, Libya

Environmental Protection Agency, EPA (1998): "Determination of the Mechanical Integrity of Injection Wells". United States Environmental Protection Agency Region 5 – Underground Injection Control (UIC) Branch – June 11, 1998.

URL:http://www.epa.gov/R5water/uic/r5guid/r5_05.htm

Farshad F.F., Garber J.D., Polaki V. (2000): "Comprehensive Model for Predicting Corrosion Rates in Gas Wells Containing CO₂". SPE Prod. & Facilities, Vol. 15, No. 3, August 2000.

Florette M., Rückheim J., Voigtländer G., Wendel H. (2007): "Gaz de France's Current and Future Involvement in CCS Projects – A commitment to Sustainable Development". Geotechnologien Science Report on 1. French-German Symposium on Geological Storage of CO₂, June 21./22., 2007 Geoforschungszentrum Potsdam.

Frisch G., Fox P., Hunt D., Kaspereit D. (2006): "Advances in Cement Evaluation Tools and Processing Methods Allow Improved Interpretation of Complex Cements". Society of Petroleum Engineers 97186, 2005

GdF (2003): "ORC project – Offshore re-injection of CO₂ at the K12-B platform – Phase 1: Feasibility study – Final report". Gaz de France Production Nederland B.V., February 2003.

Gérard B., Frenette, R., Augé L., Desroches J., Barlet V., Jammes L. (2006): "Well Integrity in CO₂ Environments Performance & Risk – Technologies". Schlumberger Presentation at Berkeley, 21 March, 2006.

Hansen T. (2005): "Permanent CO₂ Storage". Report on Well Bore Integrity Workshop. See IEA GHG R&D Programme, BP

Harris K.L., Johnson B.J. (1992): "Successful Remedial Operations using Ultrafine Cement". Society of Petroleum Engineers 24294, presented at SPE Mid-Continent Gas Symposium held in Amarillo, Texas, U.S.A, 1992.

Heusler E. (1988): „Korrosion von im Bohrloch verbliebener Verrohrung“. Bericht der Abteilung Korrosion und Korrosionsschutz der Instituts für Metallkunde und Metallphysik der TU Clausthal., November 1988.

Ide S.T., Friedmann S.J., Herzog H.J. (2006): “CO₂ Leakage through Existing Wells: Current Technology and Regulations”. 8th International Conference on Green House Gas Control Technologies, Trondheim, June 19-22, 2006.

IEA Greenhouse Gas R&D Programme (2007): “Summary Report (No 2007/6 July 2007) of 3rd Well Bore Integrity Workshop”. Meeting held March 12-13, 2007 in Santa Fe, New Mexico, U.S.A.

IEA Greenhouse Gas R&D Programme (2006): “Summary Report of 2nd Well Bore Integrity Workshop”. Meeting held March 28-29, 2006 at Princeton University, New Jersey, U.S.A.

IEA Greenhouse Gas R&D Programme (2005): “Report on Well Bore Integrity Workshop”. Meeting held April 4-5, 2005 in Houston, TX, U.S.A.

Ikeda A., Mukai S., Ueda M. (1985): Corrosion Behavior of 9 to 25% Cr Steels in Wet CO₂ Environments”. National Association of Corrosion Engineers, Vol. 41, No. 4, April 1985, pp. 185-192.

IPCC (2005): “IPCC Special Report on Carbon Dioxide Capture and Storage”. Cambridge University Press, Cambridge, UK and New York, USA, 442 p.

Jabs M., Harmon C.E., Harmon S.C., Harmon R.E. (2004): “New Expandable Cladding Technique Enables Extended Length Casing Repair”. Society of Petroleum Engineers 87212, presented at SPE/IADC conference held in Dallas, Texas, U.S.A, 2004.

Jammes L. (2007): “Schlumberger Involvement in CO₂ Geological Storage – R&D and On-Going Projects”. Geotechnologien Science Report on 1. French-German Symposium on Geological Storage of CO₂, June 21./22., 2007 Geoforschungszentrum Potsdam.

Jarrel P.M., Fox C.E., Stein M.H., Webb S.L. (2002): “CO₂ Flood Environmental, Health, and Safety Planning”. Chapter 9 of Practical Aspects of CO₂ Flooding. Monograph 22, Society of Petroleum Engineers, Richardson Texas, 2004.

Karman C.C., Wildenborg A.F.B. (Editors) (2006): “Draft Framework for Risk Assessment and Management of storage of CO₂ in sub-seabed geological formations (version 1.0)”. Results of Experts Workshop on Technical and Environmental Issues of storage of CO₂ in sub-seabed geological formations, October 25-27, London, UK.

Kenneth R. (2001): “GRE Composite-Lined Tubular Products in Corrosive Service: A Study in Workover Economics”. Society of Petroleum Engineers SPE 94129, SPE Permian Basin Oil and Gas Recovery Conference held in Midland, Texas, 15-16 May 2001.

Kermani M.B., Smith L.B. (Editors) (1997): “CO₂ Corrosion Control in Oil and Gas Production-Design Considerations”. European Federation of Corrosion Publications Number 23, 1997.

Kinzel H., Tai P.T., Büttner K. (**1996**): "Evaluation of the Corrosion caused by Elevator and Spider Marks on C.R.A.-Pipe comparing Conventional Inserts and a New Gripping System". Society of Petroleum Engineers 36386, 1989.

Kinzel H., Kiess C., Wachs T.P., Badrak R.P. (**2006**): "New Ways of Handling and Running C.R.A. Tubulars prevent Corrosion in H₂S and CO₂ Environments. 2006 SPE Int'l Oilfield Corrosion Symposium Aberdeen, U.K., 30 May 2006.

Krilov Z, Loncaric B, Miksa Z. (**2000**): Investigation of a Long-Term Cement Deterioration under a High Temperature Sour Gas Downhole Environment". Society of Petroleum Engineers 58771, 2000.

Krusche K., Johnson C.R., Braud N.Y., Ghazi H.B (**2006**): Application of Engineered Cementing Solution to Solve Long-Term Cement Integrity Issues in Tunisia". Society of Petroleum Engineers, SPE100390, September 2006.

Kuenning W.H. (**1966**): Resistance of Portland Mortar to Chemical Attack – A Progress Report". R&D Laboratories of the Portland Cement Association, Research Bulletin 204, 1966.

Lance Brothers (**2005**): "Corrosion Resistant Cements for Carbonic Acid Environments". Report on Wellbore Integrity Workshop by IEA Greenhouse Gas R&D Programme and BP, Marriott Woodlands Waterway Hotel and Convention Center, Houston, TX, U.S.A, 4-5 April, 2005.

Laws M., Riyami A., Soek H., Edwards J., Elmarsafawi S., Abdenour S., Valstar D., Misran M., Hassan A. (**2006**): "Special Cement System and Cementing Techniques Improve Zonal Isolation in South Oman Fields". Society of Petroleum Engineers 102414, 2006

LBEG, Landesamt für Bergbau, Energie und Geologie (**1998**): „Richtlinien über das Verfüllen auflässiger Bohrungen. Rundverfügung des Oberbergamtes Clausthal Zellerfeld vom 29.07.1998 20.1 - 3/98 - B III d 1.2 - IV

Lecolier E., Rivereau A., Ferrer N., Audibert A., Longaygue X. (**2006**): "Durability of Oilwell Cement Formulations Aged in H₂S-containing Fluids". IADC/SPE 99105 presented at IADC/SPE Drilling Conference held in Miami, Florida, U.S.A, 21-23 February 2006.

Lubenau U. (**2006**): "Well Bore Integrity". Presented at Investigation, Utilization and Protection of the Underground CO₂ Storage in Geological Formations; Technologies for an Underground Survey in Urban Areas - Status Seminar, R&D Programme GEOTECHNOLOGIEN held at Technische Universität Bergakademie Freiberg, Germany, September 21-22, 2006.

Mamora D.D., Seo J.G. (**2002**): "Enhanced Gas Recovery by Carbon Dioxide Sequestration in Depleted Gas Reservoirs". Society of Petroleum Engineers SPE-77347, SPE Annual Technical Conference and Exhibition in San Antonio, Texas, 29 Sept.-2 Oct. 2002.

May F., Berg C., Henke C., Pusch G., Rebscher D., Reinicke K.M. (2006): "Storage of CO₂, a future option for the mature Altmark gas field?" 8th International Conference on Greenhouse Gas Technologies, Trondheim, June 2006.

Moreno F.J., Chalaturnyk R., Jimenez J. (2004): Methodology for Assessing Integrity of Bonding Seals (Wells and Caprock) For Geologic Storage of CO₂: 7th Int'l Conference on Greenhouse Gas Technology 2004.

Mulders F. (2007): “Analysis of Abandoned Well Integrity at a Potential CO₂ Storage Site”, July 2007, see IEA 3rd Well Bore Integrity Workshop (2007).

Neubert V. (2005): “Corrosion Aspects for Subsurface Equipment and Well Integrity for CSEGR”. 25CSEGR-01, 12.02.1005.

Nugent L. (2005): “Sheep Mountain Unit, Colorado Presentation - Report on Well Bore Integrity Workshop”. Organized by IEA Greenhouse Gas R&D and BP, held at Marriott Woodlands Waterway Hotel and Convention Center, Houston, TX, U.S.A, 4-5 April, 2005.

OGP, International Association of Oil & Gas Producers (2000): "Guidelines for Produced Water Injection". Report No. 2.80/302, January 2000.

Ohio Environmental Protection Agency (2005): “Sealing Abandoned Monitoring Wel2s and Boreholes”. Technical Guidance for Groundwater Investigations, Chapter 9, February 2005 (Revision 1), <http://www.epa.state.oh.us/ddagw/>

Oldenburg C.M., Pruess K., Benson S.M. (2001): “Process Modelling of CO₂ Injection into Natural Gas Reservoirs for Carbon Sequestration and Enhanced Gas Recovery,” Energy and Fuels, 15, 293–298, 2001.

Oldenburg C.M. (2003): “Carbon Sequestration in Natural Gas Reservoirs: Enhanced gas Recovery and Natural Gas Storage”. Proceedings TOUGH Symposium 2003 Lawrence Berkeley National Laboratory, Berkeley, California, May 12 -14, 2003.

Oldenburg C.M., Stevens S.H., Benson S.M (2004): “Economic Feasibility of Carbon Sequestration with Enhanced Gas Recovery (CSEGR)”. Energy 29, pp 1413-1422, 2004 LBNL-49762.

Philippacopoulos A.J, Berndt M.L. (2000): “Characterization and Modelling of Cements for Geothermal Well Casing Remediation”. Geothermal Resources Council Trans., Vol. 24, 81-86, San Francisco, 2000.

PTTC (2006): “Maintaining and Repairing Casing Integrity”. Workshop by PTTC North Mid Continent Region and SPE Wichita Section in Wichita, Kansas, April 11, 2006.

Reinicke K.M., Nangue Donfack R., Shinde S., Franz, O.: „CO₂ Lagerung im Geogrund: Integrität von Tiefbohrungen unter Einfluss von CO₂“. DGMK/ÖGEW-Frühjahrstagung 2007, Fachbereich Aufsuchung und Gewinnung, Celle

Rusch D., Slezak M. (2005): “Annulus Communications Eliminated using Pressure-Activated Sealant”. Solution Mining Research Institute Spring Conference – April 17-20, 2005. www.solutionmining.org, smri@solutionmining.org

Scheerer G. (2005): Evaluating Risk of Leakage. Report on Well Bore Integrity Workshop, see IEA Greenhouse Gas R&D Programme, BP.

Schlumberger (1989): “Schlumberger Cased Hole Log Interpretation Principles/ Applications”. Schlumberger Educational Services, 1989.

Schlumberger (**1994**): "Corrosion in the Oil Industry". Oilfield Review, April 1994, pp4-18.

Schlumberger (**1999**): "Concrete Developments in Cementing Technology". Oilfield Review, Spring 1999, pp16-29.

Schlumberger (**2001**): "Diagnostics – Water Management – From Production to Disposal". Schlumberger Presentation at West Coast PTTC Workshop Santa Clarita, 18 October, 2001.

Schorn H. (**1990**): "Korrosion von Zementbrücken, Gutachterliche Stellungnahme und baustoffliche Bewertung zur Dauer der Funktionsfähigkeit von Zementbrücken im Bereich der Schachtanlage Konrad". Arbeitsgruppe für Materialtechnologie der Ruhr Universität Bochum, November 1990.

Shinde S.S. (**2006**): "CO₂ Sequestration and Enhanced Gas Recovery – Well Integrity for Safe Operations and Storage". Master Thesis, Institute of Petroleum Engineering at Clausthal University of Technology, October 2006.

Short N.R., Purnell P., Page C.L. (**2004**): "Preliminary investigations into the super-critical carbonation of cement pastes". Journal of Material Science, Vol. 36, Nr. 1, January 2001.

Simbala V., Palomeque M., Evers R., Ordonez E. (**2005**): "An Effective Solution to Repair severely Corroded Casing strings: Application in the Oriente Basin of Ecuador". Society of Petroleum Engineers, SPE 93950, 2005.

Storaune A., Warren J., Winters (**2005**): "Versatile Expandables Technology for Casing Repair". Society of Petroleum Engineers, SPE 92330, 2005.

Strazisar B., Kutchko B. (**2006**): "Degradation of Wellbore Cement Due to CO₂ Injection – Effects of Pressure and Temperature". Int'l Symposium on Site Characterization for CO₂ Geological Storage

Van der Meer L.G.H., Kreft E., Geel C., Hartman J. (**2005**): "K12-B A Test Site for CO₂ Storage and Enhanced Gas Recovery". Society of Petroleum Engineers SPE-94128, SPE / EAGE Annual Conference held in Madrid, Spain, 13-16 June 2005.

Van Gerven T., Van Bealen F., Dutré V., Vandecasteele C. (**2004**): "Influence of Carbonation and carbonation methods on Leaching of Metals from Mortars". Cement and Concrete Research 34 (2004) 149-156.

Van Grinsven R., Jackson L., Suarez I., Bouts M. (**2005**): "Corrosion of High Rate Gas Wells - A Case History". Society of Petroleum Engineers 94795, SPE International Symposium on Oilfield Corrosion, Aberdeen, United Kingdom, 13 May 2005.

Van Luijk (Teamleader) (**2003**): "CRUST – CO₂ reuse through underground storage - CO₂ reduction by subsurface storage in a depleted gas field; a feasibility study conducted by Shell and NAM". CO₂ Reduction Plan Project Office, P.O. Box 10073, 8000 GB Zwolle, The Netherlands.

Verbeek G.J. (**1958**): Carbonation of Hydrated Cement". R&D Laboratories of the Portland Cement Association, Research Bulletin 87, 1958.

Wall R., Kenefake D. (2005): "Acid gas Injection Facilities for Gas Disposal at the Shute Creek Treating Facility". Society of Petroleum Engineers SPE 10944, International Petroleum Technology Conference, Doha, Qatar, 21-23 November 2005.

Watson T.L., Bachu S. (2007): "Evaluation of the Potential for Gas and CO₂ Leakage Along Wellbores". 2007 SPE E&P Environmental and Safety Conference, Galveston Texas March 5-7, 2007, Society of Petroleum Engineers, SPE 106817.

WBGU – Wissenschaftlicher Beirat der Bundesregierung Globale Umweltveränderungen (2006): Sondergutachten 2006, Kapitel 5.
http://www.wbgu.de/wbgu_sn2006/wbgu_sn2006_voll_5.html

Welch J.L., Mason C.M, Pavlich J.P. (1990): "Tixotropic Cementing With Coiled Tubing at Prudhoe Bay". Society of Petroleum Engineers-20906, presented at Europe 90, The Hague, Netherlands 1990.

Wilson M., Monea M., (Editors) (2004): IEA GHG Weyburn CO₂ Monitoring & Storage Project Summary Report 2000-2004". Proceedings 7th International Conference on Greenhouse Gas Control Technologies, September 5-9, 2004, Vancouver, Canada.

Wilson K.J., Morrison D., Sackash M.J. Jr., Poole D. (2003): "New Boundaries for Cementing with Coiled Tubing", Society of Petroleum Engineers-81711, presented at SPE/ICoTa coiled tubing conference held in Houston, Texas, U.S.A, 2003.

Wittke W. (1991-3): „Endlager Konrad, Schachtverfüllung/ Alte Bohrungen, Bericht Teil A1, Ergebnisse des Untersuchungsprogramms im Bereich der Unterkreide 343 m – Sohle“. Bundesamt für Strahlenschutz, EU 424, 22.03.1991.

Wittke W. (1991-6): Endlager Konrad, Schachtverfüllung/ Alte Bohrungen, Bericht Teil E, Nachweis der Dichtigkeit alter Bohrungen. Bundesamt für Strahlenschutz, EU 437, 28.06.1991.

List of Figures

Figure 2.1: CO₂ Inflow and Outflow System

Figure 2.2: Pilot Project Area

Figure 2.3: CO₂ Corrosion Caused by Wet CO₂

Figure 2.4: Cement Corrosion by Super-Critical CO₂

Figure 2.5: Evolution of Alteration for Portland Cement, Barlet-Gouedard et al., 2006

Figure 2.6: Potential Leakage Pathways along an Existing Well (after Celia et al. (2004))

Figure 2.7: Well Sketch for Abandoned Well in Pilot Project Area

Figure 2.8: Well Integrity Assessment Workflow

Figure 2.9: Well Repair and Abandonment, Gérard et al. (2006)

Figure 2.10: Pilot Project Area

Figure 2.11: Wellbore Diagram for Production Well with CBL Information (P-Well 1)

Figure 2.12: Wellbore Diagram for Production Well with no CBL Information

Figure 2.13: Wellbore Diagram for Abandoned Well with Standard Abandonment Procedure (A-Well 1)

Figure 2.14: Wellbore Diagram for Abandoned Well with Non-Standard Abandonment Procedure (A-Well 2)

List of Tables

Table 2.1: Experimental Result for Cement Carbonation Rate

Table 2.2: Cement Quality for P-Well 1

Table 2.3: Cement Quality for A-Well 1

Table 2.4: Cement Quality for A-Well 1 – 11 3/4" Casing

Table 5: Cement Quality for A-Well 1 – 8 5/8" Liner

Work Package 3

Reservoir Modelling

Issues:

- Data screening: log, core, seismic, well data
- Data loading
- Model construction: 3D grid, petrophysical, facies & fault modelling, well correlations

Authors:

G. Voigtlander, L. Stecken GDF SUEZ E&P Deutschland

G.F. Ionescu ITE TU-Clausthal

| | |
|--|-----|
| 3.1 Geology Review of Barrien Gas Field..... | 105 |
| 3.2 Altmark Reservoir Modeling..... | 109 |
| Kurzfassung | 109 |
| 3.2.1 Introduction and Project Summary | 110 |
| 3.2.2 Setting of Tasks | 110 |
| 3.2.3 Sphere of Activity: Altmark Gas Field..... | 111 |
| 3.2.4 Work Steps (General Workflow)..... | 113 |
| 3.2.5 Input Data | 113 |
| 3.2.5.1 Used Data / Data Quality | 114 |
| 3.2.5.2 Data Preparations..... | 114 |
| 3.2.5.3 Data Types and Sources | 115 |
| 3.2.6 Modeling in PETREL..... | 124 |
| 3.2.6.1 Defining Boundaries | 124 |
| 3.2.6.2 Cultural Data..... | 124 |
| 3.2.6.3 Data Import..... | 125 |
| 3.2.6.4 Generating Surfaces from Seismic Grids (<i>Make Surface</i>) | 125 |
| 3.2.6.5 Stratigraphic Modeling..... | 126 |
| 3.2.6.6 Fault Modeling (<i>Fault Modeling</i>) | 127 |
| 3.2.6.7 Building the 3D Grid (<i>Pillar Gridding</i>)..... | 128 |
| 3.2.6.8 Defining Horizons (<i>Make Horizons</i>) | 129 |
| 3.2.6.9 Defining Zones (<i>Make Zones</i>) | 129 |
| 3.2.6.10 Defining the Number of Vertical Cells (<i>Layering</i>)..... | 129 |
| 3.2.6.11 QC of the 3D Grids..... | 130 |
| 3.2.6.12 Upscaling of the Logs (<i>Upscaling</i>) | 130 |
| 3.2.6.13 Petrophysical Modeling | 132 |
| 3.2.6.14 Exporting Data and Results..... | 133 |

3.1 Geology Review of Barrien Gas Field.

The Barrien natural gas field is situated in the Federal State Lower Saxony in North Germany. The Barrien gas field belongs to Thüringen Trias age (Figure 3.1). The sediment deposits of the Trias cover the entire North German basin. From the geological chronology of the Trias, sandstone in the Buntsandstein and sandstone in the Rhät-Keuper are of important to natural gas and petroleum respectively.

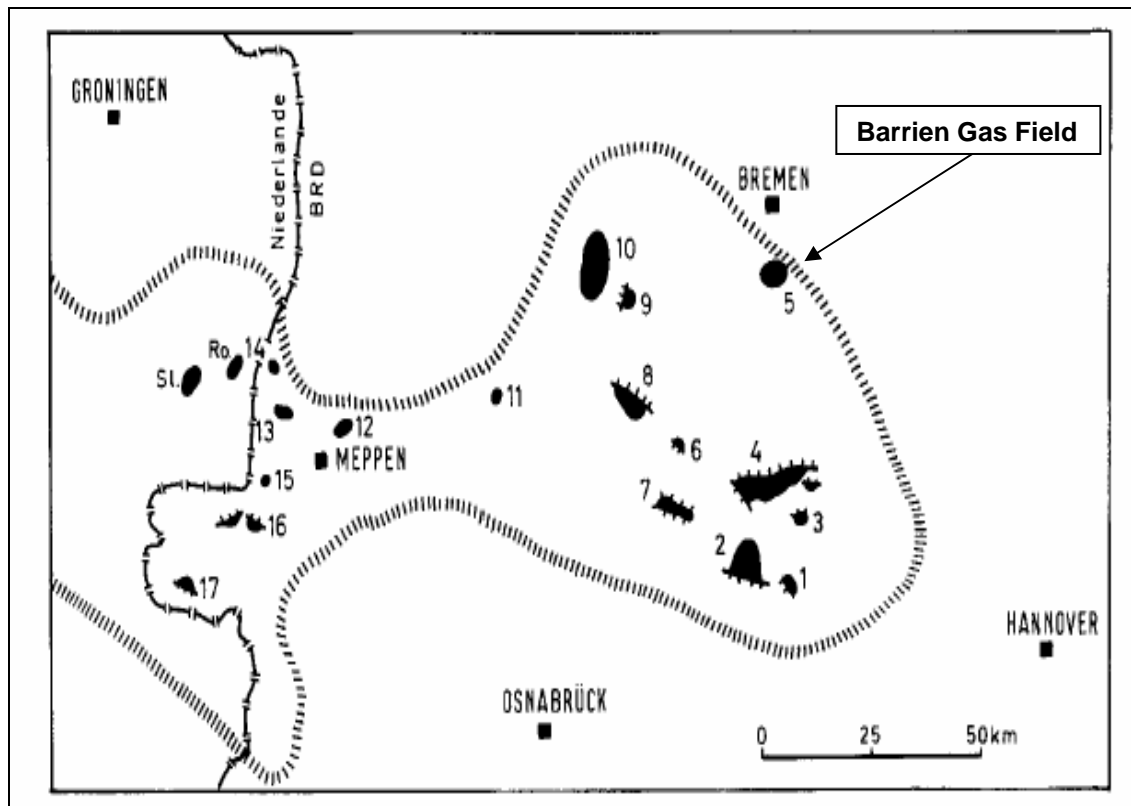


Fig. 3.1: Gas field locations in the Buntsandstein of Emsland area and between the rivers Weser and Erns.

The Structural map in Figure 3.2 represents the top of the Detfurth formation in Barrien gas field. Barrien reservoir is a faulted and compartmentalized anticlinal structure, divided by numerous faults of different sizes and covered by Keuper rock. Red lines indicate the faults. The reservoir itself is composed of alternating red sandstone in the middle and lower part, sandstone with shelly limestone in the upper part of the reservoir.

The Barrien reservoir extent laterally 7000 m in X direction and 4700 m in Y direction, with vertical extent of 200 m. Barrien reservoir is mainly sandstone and consists of 18 layers

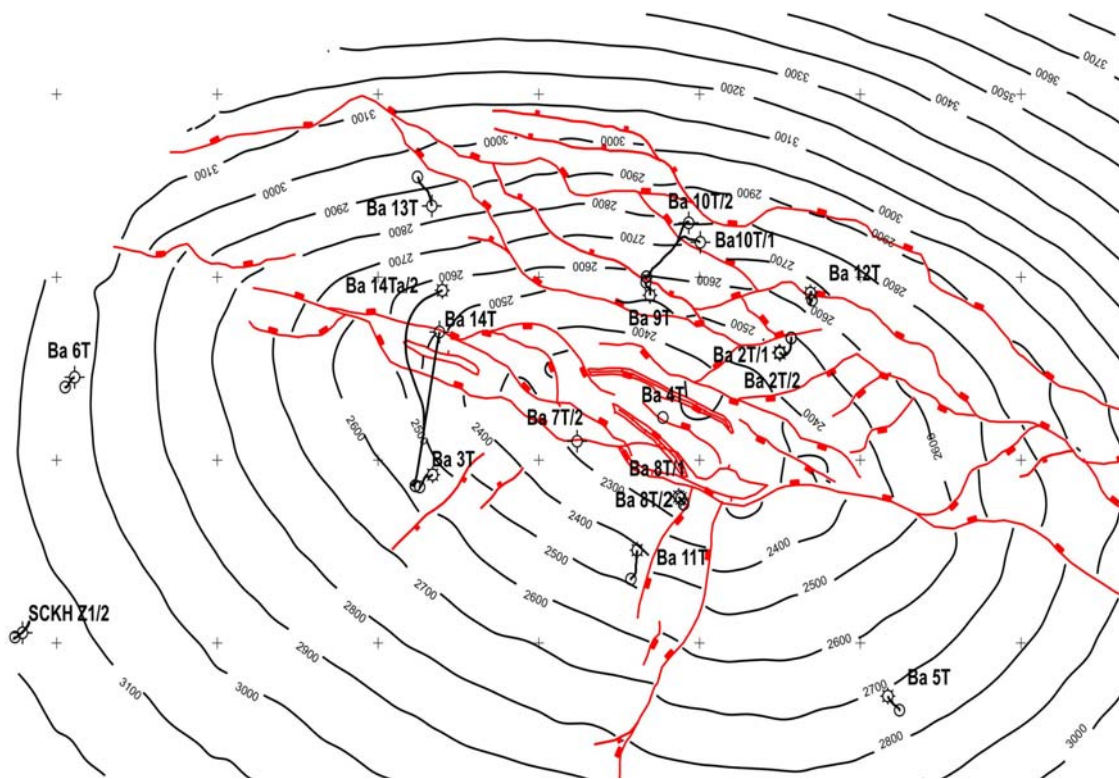


Fig. 3.2: Structural map of Barrien anticline reservoir

Barrien gas field consists of four formations from top of the reservoir to bottom, Solling, Hardegsen, Detfurth, and Volpriehausen. The gas bearing were generated in the middle to the lower Triassic 195-230 million years at an average depth of approximately 2500 m (Figure 3.3).

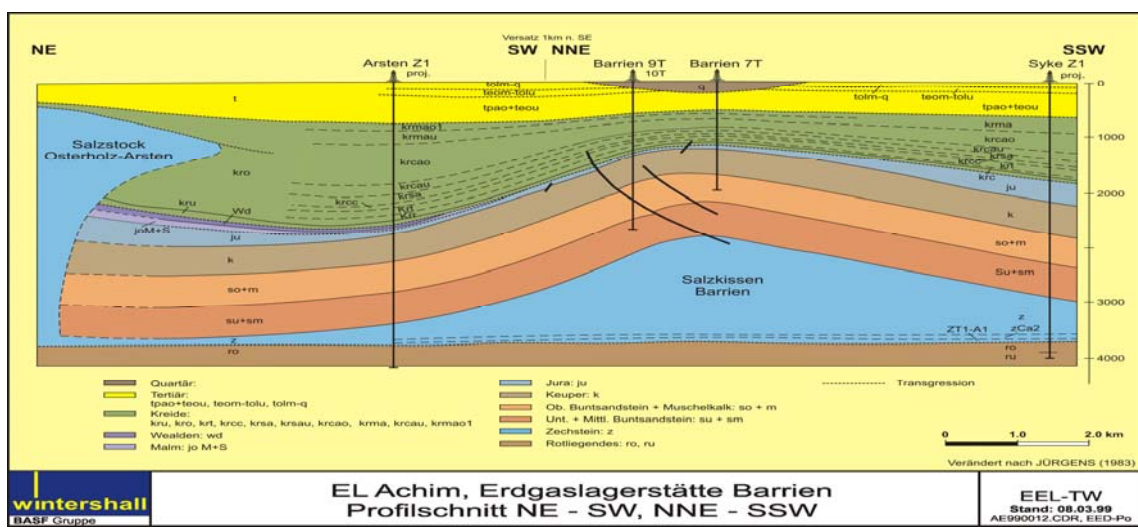


Fig. 3.3: NE – SW, NNE – SSW cross section of the Barrien gas field

Figure 3.4 shows an evaluation of gamma ray, resistivity, and acoustic impedance logs from well Barrien 11T. This evaluation provides the current stratigraphical division of the four formations, Solling, Hardegsen, Detfurth, and Volpriehausen.

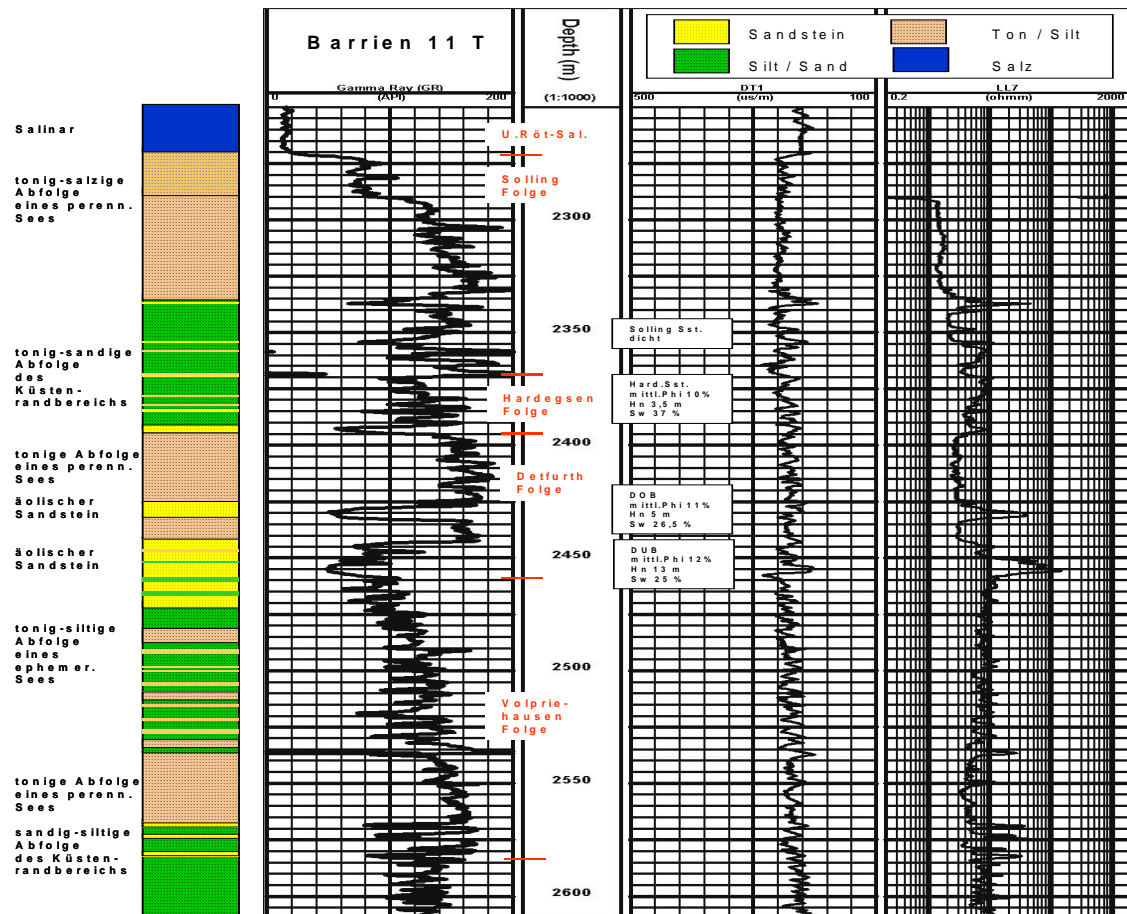


Fig. 3.4: Barien formations type log well BRIN11T

The average field porosity is 12%. Average field Permeability is 120 mD. Gas Water Contact is located initially at depth of 2980 m. Because of the gas production in the depletion stage, the gas water contact moved up to 2935 m.

Barien Production History.

Barien gas reservoir was discovered in 1964 and the production began in 1965. The initial gas in place in Barien gas field is $16.6 \times 10^9 \text{ Sm}^3$, 73 % of the natural gas has already been produced until October 2003, $12.1 \times 10^9 \text{ Sm}^3$. From 1981 to 1998 this field was a swing producer. Since 1989 the reservoir manifests a clear decline in the gas production rate (Figure 3.5). The initial reservoir pressure and temperature were approximately 408 bars and 121°C. Figure 3.6 shows the decline of the pressure in Barien, presently (end 2003) the pressure of the reservoir decreased to 66 bar.

The pilot area of this work will be on the south part of the field comprising in the blocks 1 and 2. The initial gas in place in these blocks is estimated to be up to $7.12 \times 10^9 \text{ Sm}^3$. Recovery factor of this area until 2003 is 82 %. Four production wells will be used in the study area, three producers in block 2 (Ba5, Ba8T, Ba11T) and one producer in region 1 (Ba5T), see also Figure 3.2 for details.

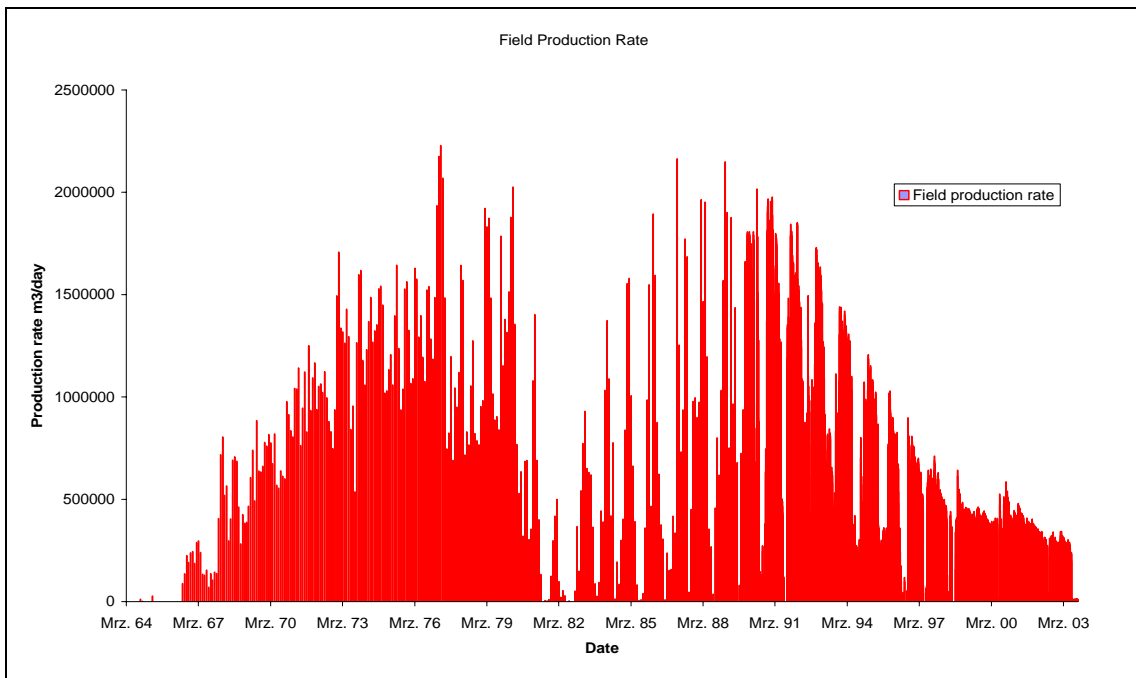


Fig. 3.5: Historical production rate from Barrien reservoir (1964 - 2003)

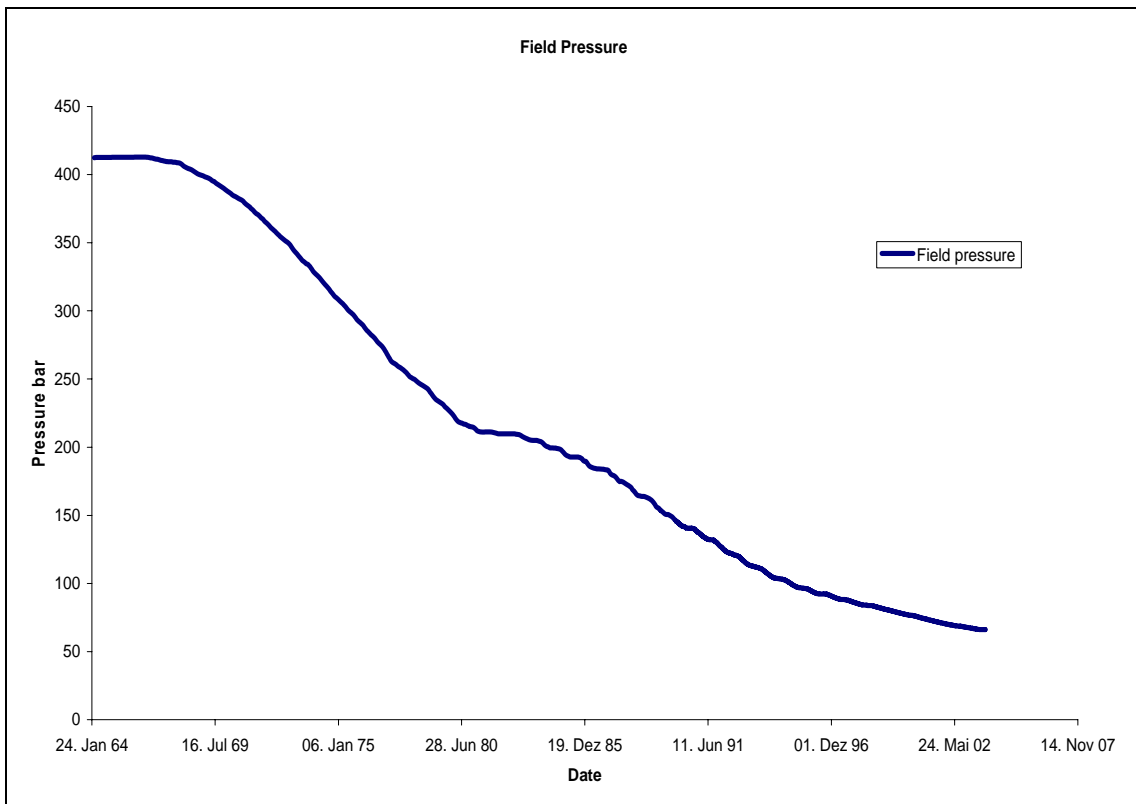


Fig. 3.6: Field pressure of Barrien gas field vs. time (1964 - 2003)

3.2 Altmark Reservoir Modeling

Kurzfassung

Das Projekt CSEGR (Carbon Dioxide Storage and Enhanced Gas Recovery) als Teil des vom BMBF und der DFG geförderten F&E-Programmes Geotechnologien beinhaltet unter anderem das Arbeitspaket Reservoir Modellierung (WP3). Darin wurden für weiterführende Untersuchungen zwei Testkandidaten ausgewählt, das Gasfeld Barrien bei Bremen (Wintershall) und Teile des Gasfeldes Altmark (EEG). Die im Rahmen des CSEGR-Projektes für den Bereich Altmark durchgeführten Modellierungsarbeiten werden im Folgenden kurz zusammengefasst.

Nach Auswahl geeigneter Teilgebiete innerhalb des Altmarkfeldes wurden zunächst alle notwendigen Bohrungsdaten in einer Digitalisierungskampagne in eine digitale Form überführt. Diese Daten sowie alle Informationen aus der Seismik (z.B. Störungspolygone und Top Rotliegendes Fläche) wurden mittels der verwendeten Modellierungssoftware PETREL¹ in einem zentralen Projekt zusammengestellt, um eine digitale Datenbasis zu erhalten. Daraufhin wurden die eingearbeiteten Bohrungsmarker unter Zuhilfenahme der digitalisierten Bohrlochmessungen (i.e.L. GR, DT, LL) und der vorhandenen Kerndaten überprüft und korreliert. Eingearbeitet wurden sowohl stratigraphische als auch reservoirspezifische Bohrungsmarker. Die vorhandenen Kernmessungen und weitere Informationen wie Kern- und Perforationstrecken oder lithologische Säulenprofile wurden ebenfalls integriert. Über mehrere Korrelationsketten wurden unterschiedliche Datentypen einer Qualitätskontrolle unterzogen.

Darauf aufbauend wurde mit der eigentlichen Modellierung begonnen. Für das ausgewählte Teilgebiet wurde auf Basis der Seismik eine Störungsmodellierung durchgeführt, so dass ein Störungsmodell vorlag, welches für die Konstruktion des 3D-Grids benötigt wurde. Das resultierende 3D-Grid enthält insgesamt 15 Reservoirzonen entsprechend der einzelnen Reservoirlagen. Dazwischen befinden sich die so genannten Nicht-Speicher-Bereiche und bilden so das Multilayer- oder Vielschicht-Modell der Altmarklagerstätte ab. Oberhalb des Top Rotliegendes wurde noch eine Caprock-Zone integriert. Als Ergebnis lag an dieser Stelle nach Durchführung einer vertikalen Feingliederung (Layering) ein in mehrere Segmente oder Blöcke unterteilbares 3D geologisches Modell vor, welches im Anschluss mit petrophysikalischen Eigenschaften versehen wurde. Dafür wurden die in den Bohrungen vorliegenden Daten zur Porosität und Permeabilität verwendet. Nach Erstellen eines kontinuierlichen Porositäts-Logs und der Auswertung der Kerndaten mit Erstellen eines Phi/k-Plots wurden die Daten zunächst innerhalb der Bohrungen einem Upscaling-Prozess unterzogen und anschließend auf das 3D-Grid verteilt.

Mit der Fertigstellung des geologischen Modells wurden verschiedene Simulationsmodelle erstellt und je nach Bedarf exportiert. Die ausgeladenen Daten (3D-Grid, Bohrlokationen und Bohrpfade, die petrophysikalischen Daten und ein Rescue-Modell) wurden übergeben und für erste Simulationen in ECLIPSE wieder eingeladen. Im Verlauf der folgenden Arbeiten wurden individuell kleinere Rechenschritte durchgeführt und je nach Bedarf weitere Daten überliefert.

3.2.1 Introduction and Project Summary

GEOTECHNOLOGIEN

In the research and development program named GEOTECHNOLOGIEN (www.geotechnologien.de), which was originated by the Federal Ministry for education and research (BMBF) and the German research council (DFG), lasting concepts for the use of the earth and to the protection on their living humans are to be developed. Universities, non-university research establishments and industrial partners work closely with one another within thirteen different focal points.

Focal point: Investigation, use and protection of the underground area

One of these focal points was named „Investigation, use and protection of the underground area.” and it contains again ten research projects.

CSEGR

This report deals with the modeling work on the project „CSEGR“ (Carbon Dioxide Storage and Enhanced Gas Recovery). The project has the title “Lagerung von CO₂ in tiefliegenden Erdgaslagerstätten und die Möglichkeit einer zusätzlichen Erdgasgewinnung (Enhanced Gas Recovery) – Eine Machbarkeitsstudie” and contains an investigation program about the storage potential of CO₂ in mature german gas reservoirs for enhanced gas recovery. The aim is to create a feasibility study.

Project partners

The leading partner within the project is the Technical University of Clausthal. Other supporting partners in this research group are the Federal Institution for Geoscience and Raw Materials (BGR) in Hanover as well as the industry partners E.ON-Ruhrgas, Vattenfall Europe, Wintershall (Kassel) and Erdgas Erdöl GmbH (EEG).

Work Packages

Several interconnected work packages, linking different subtasks and disciplines, are forming the complete project. This work focuses on the **WP3** – Reservoir Modeling.

3.2.2 Setting of Tasks

The aim of work package number three is to deliver two 3D reservoir models for further investigations within the project. Two different candidates, which are representative for german natural gas fields, were selected for the reservoir modeling [Figure 3.7]: the gas field Barrien south of Bremen (Wintershall) as well as the gas field Altmark in the area of Salzwedel and Peckensen (EEG Erdgas Erdöl GmbH). In this report the creation of the reservoir model for a part of the Altmark gas field is documented.

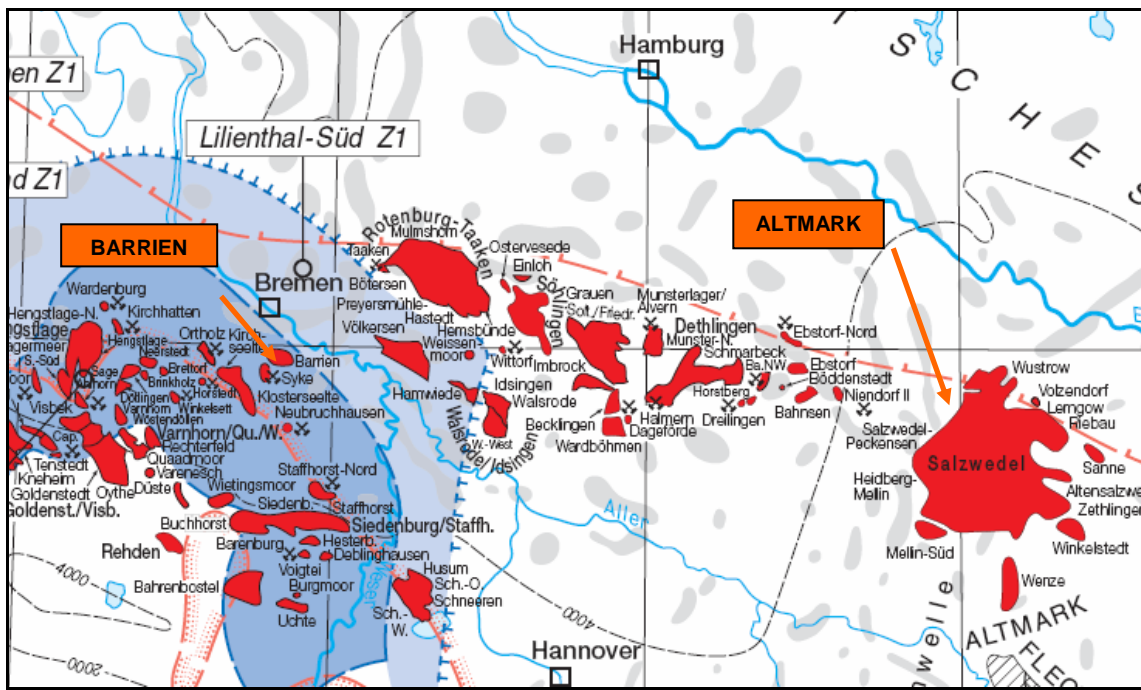


Fig. 3.7: Location of the two investigation areas (Source: BGR)

For the construction of this reservoir model, which divides the Altmark deposit and its most important petrophysical properties (i.e. porosity and permeability) into a three-dimensional cell grid, EEG delivers the available seismic data and all drilling information. These data have to be preprocessed and then to be implemented in a PETREL project file. Before the real modeling takes place a digital database has to be built, but not before an extensive quality control has been performed. The resulting static reservoir model will be used for a dynamic reservoir simulation using the ECLIPSE software.

3.2.3 Sphere of Activity: Altmark Gas Field

From the large number of subareas (blocks) of the gas field five were selected for the modeling process [Figure 3.8]: blocks 1e, 10, 12, 14 and 17. In order to be able to model a coherent area and to use model boundaries beyond the actual block borders, new boundaries were drawn. For distinction purpose these were called sectors. Thus some wells close to the block borders and between the individual blocks were added to the whole model.

Altogether 105 wells were included in the project, covering an area of 15 x 15 km. They were assigned to the individual sectors/blocks as follows [Tab. 1]:

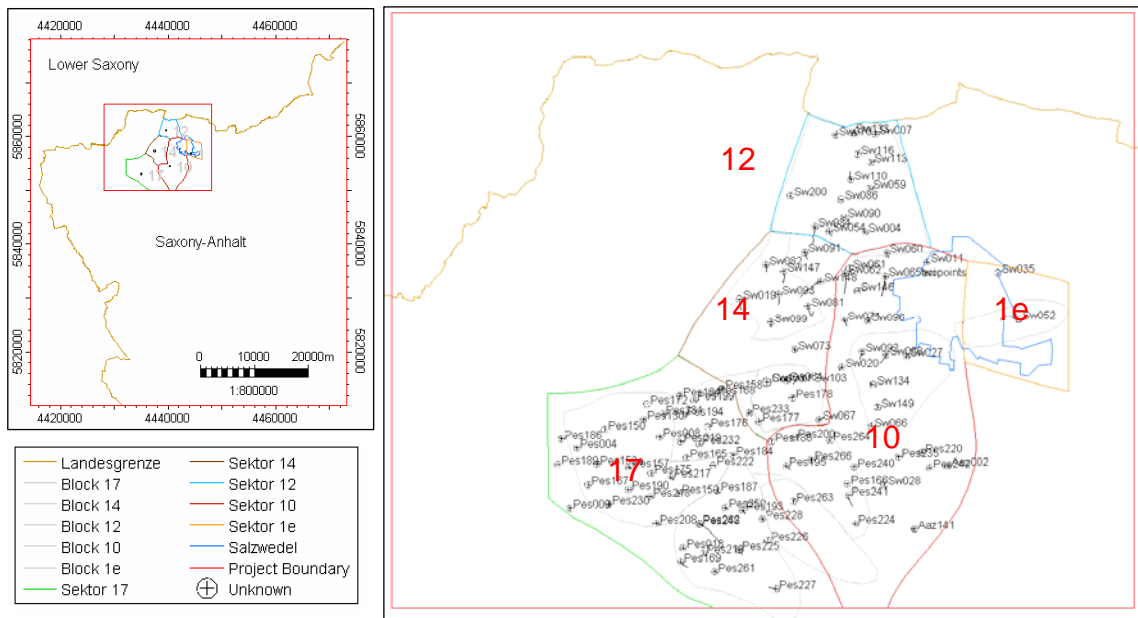


Fig. 3.8: Organisation of blocks and sectors

Tab. 3.1: Wells within the project (Sw = Salzwedel; Pes = Peckensen; Aaz = Altensalzwedel).

| Bohrungen und Blöcke in Petrel | | | | | |
|--------------------------------|----------------|------------------|--|---|--|
| Struktur | Altmark-NW | | | | |
| Block | 1e | 10 | 12 | 14 | 17 |
| Bohrungen | Sw035 Sw052 | Aaz002 Aaz141 | Sw004 Sw007 Pes166 Pes188 Pes195 Pes200 Pes220 Pes224 Pes235 Pes240 Pes241 Pes242 Pes263 Pes264 Pes266 Sw011 Sw020 Sw027 Sw028 Sw060 Sw061 Sw062 Sw065 Sw066 Sw068 Sw074 Sw092 Sw096 Sw134 Sw146 Sw149 | Sw004 Pes177 Pes178 Pes233 Pes019 Sw064 Sw067 Sw073 Sw090 Sw082 Sw091 Sw093 Sw099 Sw200 Sw103 Sw147 Sw148 Pes177 Pes184 Pes186 Pes187 Pes189 Pes190 Pes193 Pes194 Pes199 Pes208 Pes213 Pes217 Pes218 Pes219 Pes222 Pes225 Pes226 Pes227 Pes228 Pes230 Pes231 Pes232 Pes248 Pes250 Pes261 Pes262 | Pes004 Pes008 Pes009 Pes018 Pes150 Pes153A Pes153A Pes157 Pes158 Pes159 Pes160 Pes164 Pes165 Pes167 Pes168 Pes169 Pes172 Pes175 Pes176 Pes184 Pes186 Pes187 Pes189 Pes190 Pes193 Pes194 Pes199 Pes208 Pes213 Pes217 Pes218 Pes219 Pes222 Pes225 Pes226 Pes227 Pes228 Pes230 Pes231 Pes232 Pes248 Pes250 Pes261 Pes262 |
| Anzahl | 2 | 31 | 13 | 15 | 44 |
| Altmark-NW | | | | | |
| Gesamt | | | | | 105 |

3.2.4 Work Steps (General Workflow)

- Making of a schedule for the coordination of the work
- Selection of blocks and wells to work on as well as defining boundaries
- Acquisition of the desired data (from archive)
 - o Well data for all drillings concerned
 - o Information from seismics
 - o Additional information (e.g. production data)
- Digitisation of all not digitally available data (e.g. deviation data, log data etc.)
- Implementation of the data into the Petrel project (after preprocessing)
- Integration und revision of all drilling markers (*Well Tops*^{*}) and their correlation (*Make/Edit Well Tops* and *Well Correlation*)
- Fault Modeling (*Fault Modeling*)
- Producing surfaces on the basis of seismic grids (*Make Surface*)
- Providing correlation panels (*Well Sections*) of different contents
- Quality control of input data by simultaneous visualisation of different kinds of information (using well sections and the 3D view)
- Producing the 3D grid (*Pillar Gridding*) as well as defining horizons (*Make Horizons*), zones (*Make Zones*) and the vertical cell arrangement (*Layering*)
- Quality control of the 3D grid and if necessary the revision of the results
- Upscaling of some well properties / well logs (*Upscaling*)
- Distributing the information from the wells to the entire reservoir model (*Petrophysical Modeling*)
- Export of those data relevant for the following reservoir simulation (i.e. 3D grids, well locations and well paths as well as the petrophysical data for each 3D cell)

* *in italics: software specific terms or names of processes as used in PETREL (3D modeling software of Schlumberger Information Systems)*

3.2.5 Input Data

For the preparation of the not available digital database the following kinds of data were collected, preprocessed and implemented in the Petrel project, named „Altmark_CO2_final.pet“.

3.2.5.1 Used Data / Data Quality

These data types were in the end available for the digital database:

- Well locations (i.e. well header as x,y,z-point data)
- Deviation data (deviation files, usually as azimuth and inclination values)
- Termination points (TD) from an internal drilling database (BDB = Bohrdatenbank) to check the integrated deviation data
- Borehole measurements (primarily GR-, sonic- and resistivity log) as “LAS” files
- Drilling markers (well tops) concerning stratigraphy, taken from the database (BDB)
- Drilling markers concerning reservoir sections, taken from older tabs (paper)
- Information about cored sections
- Core plug measurements (porosity, permeability, density)
- Data about lithology in the wells
- Information about perforated sections (current status)
- 2D seismic lines (121 profiles in SEGY format)
- Fault polygons from seismics (vertical faults)
- Three marker horizons from seismics (Top Rotliegendes, Top and Base Wustrow)
- Upper horizons; interpreted in time
- Results from well tests

3.2.5.2 Data Preparations

Most data could not be loaded directly into the Petrel project. Here are the two main reasons:

1. Data were NOT present in digital form and had to be digitized before use.
2. Data were present in digital form, but not reduced to the sphere of activity and not in a format readable of the software Petrel.

Parallel to the time-intensive digitization, primarily deviation and log data of the more than 100 wells, all other information from different sources had to be selected, adjusted with one another and compiled in clearly arranged data sheets or in files readable of the program.

The data from seismics could be implemented without further preparation.

3.2.5.3 Data Types and Sources

Well Data

Well Locations

The well locations (well header) originate from the BDB and/or from older record sheets and were implemented as x,y,z-point data (Rechtswert, Hochwert, Rasensohle).

Borehole Deviation

In the Altmark gas field all wells are more or less deviated, some wells with a total deviation of more than 500 m referring to the vertical direction. Therefore it is necessary to implement the correct well path instead of using a simplified linear connection between the first and the last point of the well. Since most of the depth information refer to the well path (i.e. depth information is given in measured depth – MD), the inaccuracies would have been too large otherwise. For all drillings deviation measurements were accomplished, so that, after the digitisation, they were read into Petrel without greater problem [Figure 3.9]. There are different forms of deviation data available, but the form of azimuth and inclination was, being the most original type, preferred. Two other given data types are: changes in x- and y-direction (sometimes interchanged in the lists!) as well as changes in the local position (Rechts- und Hochwert). The data of the drilling deviation originate from tables in the drilling reports (“Bohrakten”), whereby the available GON values (complete circle = 400°) had to be converted (complete circle = 360°).

Termination Points of the Wells (TD – Total Depth)

As a check of the modeled borehole the total depth point coordinates as documented in the BDB were arranged and implemented in Petrel as well tops named TD. These TD well tops should meet with the end of the well paths [Figure 3.9].

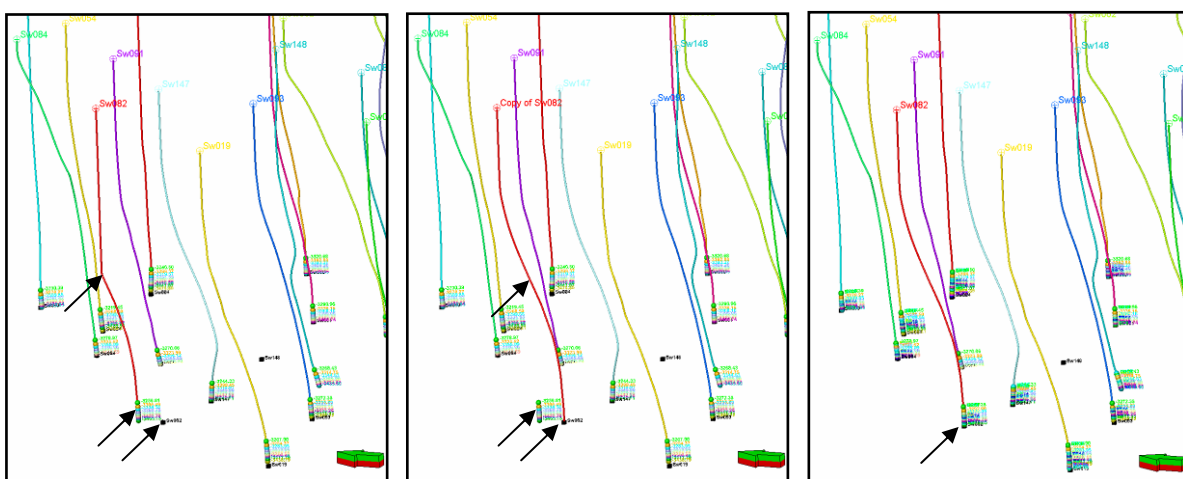


Fig. 3.9: Effects of an incomplete drilling path on the position of the drilling markers and its correction by means of TD point control.

Well Logging

Different types of well logs have been measured in different runs resulting in a huge amount of available paper logs in the archive. After looking through all the paper logs they have been digitised so far, that at least the following three types could be implemented in the project for each well: gamma ray, sonic and resistivity log (i.e. laterolog if available, otherwise ILD). Only this small step means to digitize more than 300 logs. Therefore the digitized section was limited to the lower and more interesting part, i.e. from near above Top Rotliegendes down to total depth. As a result now LAS-files are available for all the wells within the project area.

Furthermore three other log types (originating from the file Geo.xls) were integrated in Petrel: a porosity log named PKI (porosity after complex interpretation), a water saturation log (S_w) and a clay content log TKI (clay content after complex interpretation). These logs have been measured in an irregular interval and are, except the porosity log, not available for all the wells.

Well Tops

As well tops two groups of well tops were implemented besides the TD points mentioned above: the stratigraphic well tops [Figure 3.10] and the well tops of the reservoirs [Figure 3.11], i.e. the reservoir units within the stratigraphic sections. As visible in the figures fifteen reservoir units, distributed in ten stratigraphic sections, are worked on [Figure 3.11].

Well Tops: Stratigraphy

The depth values of the stratigraphic horizons have been compiled from different sources (BDB and older record sheets) and then compared. Figure 3.10 gives an overview about names and abbreviations of the stratigraphy used in the project. They refer to the eastern germany system and were not transferred, because all data refer to the eastern germany system. The orange points in the figure reflect all possible markers in this section. An example shall explain this: the Mellin 17 unit is limited by Top PMIn17 and Top PMIn16 (red circle). Some of the well tops can be on the same depth level: e.g. (see green box) PMIn17 is the same as PMIn (Perm Mellin), which is the same as PEb (Perm Elbe), PS (Perm Saxon) and PU (Unter-Perm).

The twelve markers listed on the right side of the figure are of greater importance for the project. An additionally used marker within the project (not shown in the figure) is the PWra (Top Werraanhhydrit), which was used as the top marker of the upper sealing unit. Therefore this cap rock ranges from Top Rotliegendes to Top Werraanhhydrit (PWra-PMIn17) and has an average thickness of 50 m.

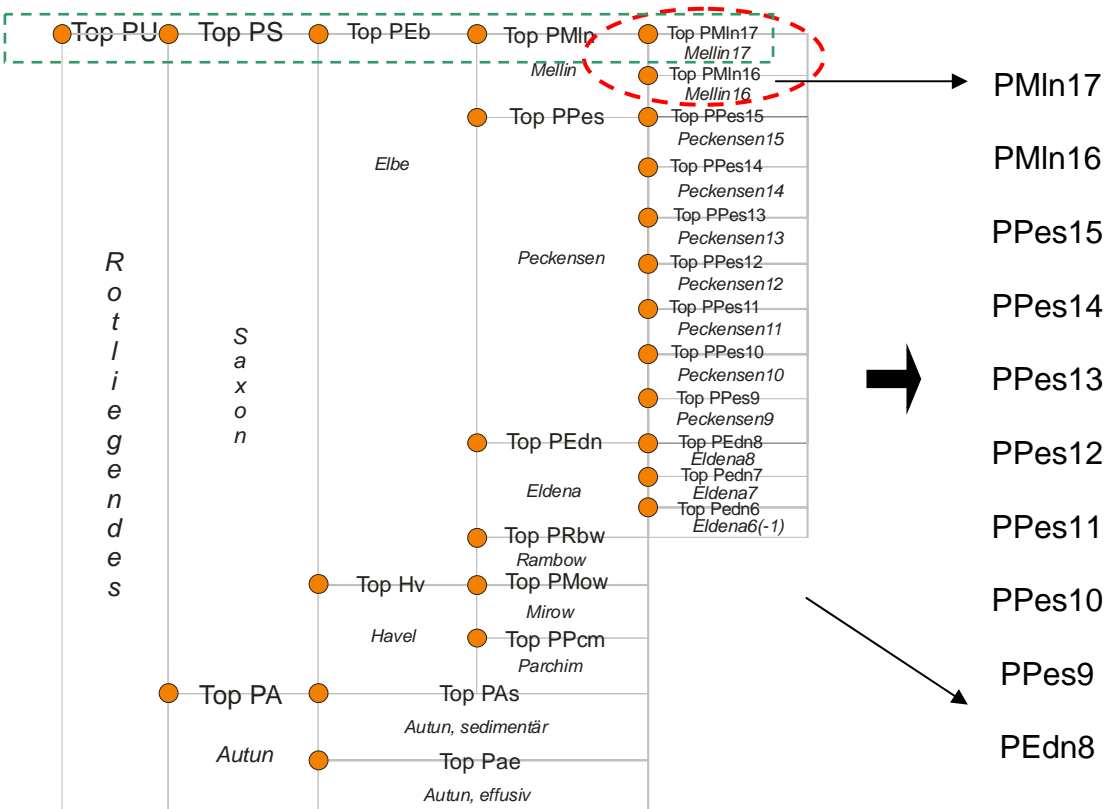


Fig. 3.10: Overview of the used stratigraphic well tops

Well Tops: Reservoirs

Taken from the record sheets and the file „Geo.xls“ the reservoir units were compiled and the collected data compared. An intensive revision has been made, which is described in chapter six.

Core Measurements

For only some wells inside the modelled area cores were drilled and core measurements accomplished. There are no core photos available unfortunately, apart from those of well Pes004. The parameters porosity, permeability and density were determined for the plugs. The regional distribution of the measurements is very heterogeneous. While in block 17 in eight wells measurements were accomplished, there are only two wells in block 10 with measurements [Figure 3.12]. Inside the other three blocks no core measurements are present or within the interesting interval. Thus measurements are available only for less than 10 % of all drillings. Sometimes only smaller sections or less interesting ranges were measured. The measurements were accomplished not continuously and not with a regular sampling interval (e.g. every 10 cm). The number of porosity measurements is often (as usually) larger than those of permeability measurements. The questions are: will it be possible to supply reliable phi-k relationships (phi-k plots) and can they be transferred to the entire area?

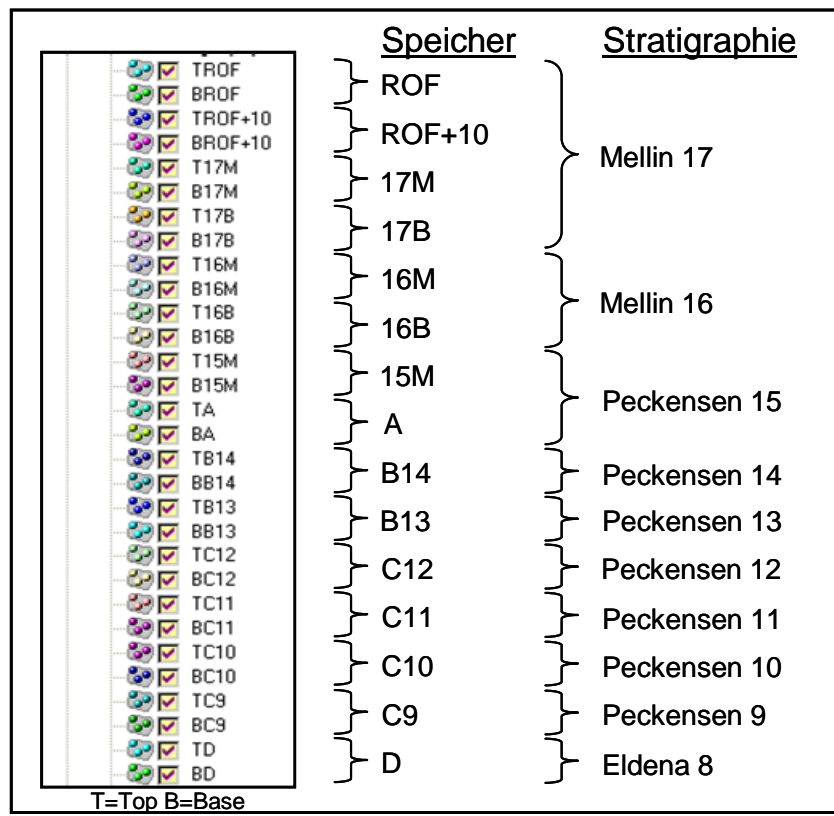


Fig. 3.11: Overview of the used reservoir well tops.

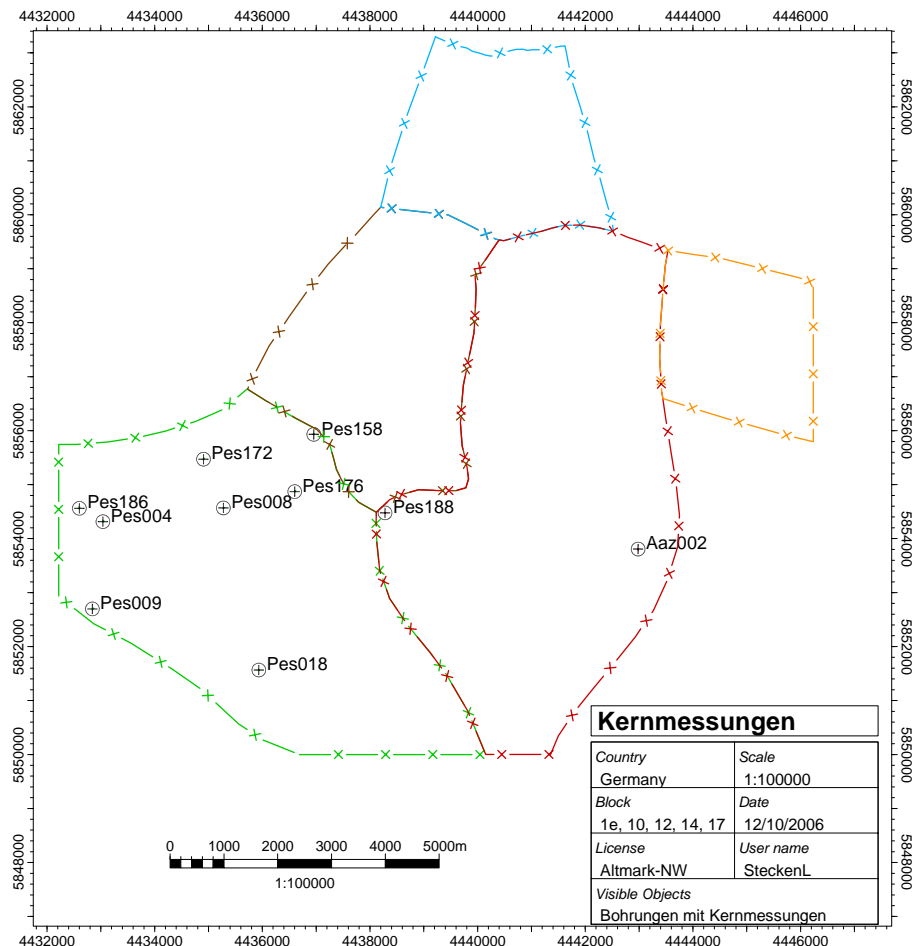


Fig. 3.12: Core measurements within the sphere of activity.

Cored Sections

For all wells discrete logs were produced, which make a fast distinction possible between cored and non cored sections. In addition these logs are useful for quality control purpose. For example: the available core measurements (their position) should lie within the cored sections. The cored sections can be visualised in the 3D window as well as in geological profiles [Figure 3.13].

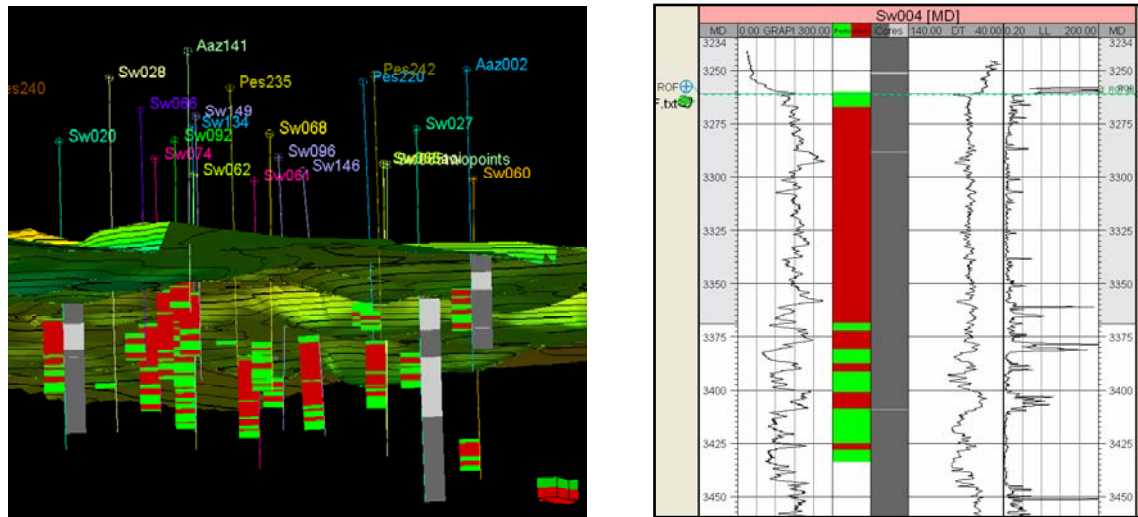


Fig. 3.13: Cored section (grey) and perforated sections (red/green) in 3D and 2D view.

Core Porosity Measurements

The values of the core porosity measurements originate from the file 'Perm-core.xls'. The related depths were converted and the measured values were implemented in the Petrel project as point data [Figure 3.14].

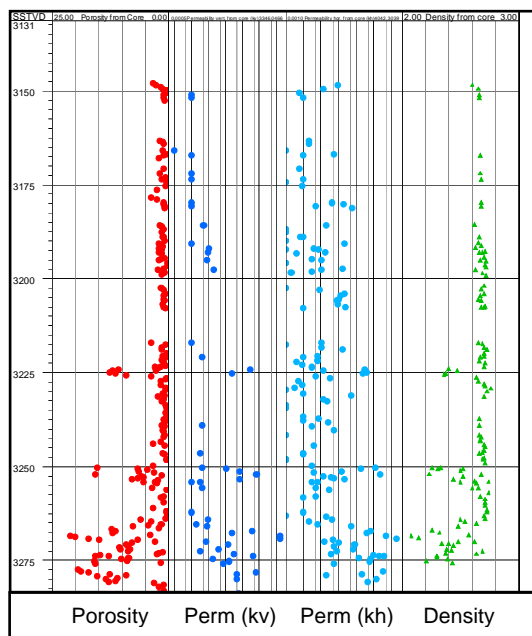


Fig. 3.14: Core measurements – porosity, vertical permeability (kv), horizontal permeability (kh) and density.

Core Permeability Measurements

The values of the core permeability measurements originate from the file 'Perm-core.xls'. The related depths were converted and the measured values were implemented in the Petrel project as point data [Figure 3.14]. Sometimes it was differentiated between horizontal (k_h) and vertical (k_v) permeability within the measurements.

Core Density Measurements

The values of the core density measurements originate from the file 'Perm-core.xls'. The related depths were converted and the measured values were implemented in the Petrel project as point data [Figure 3.14].

Lithology

Information about the lithology within the wells was listed in the file 'Geo.xls'. Thereby sand (S), silt (SI) and clay (T) has been differentiated. These data has been transferred into a lithology log [Figure 3.15], which has been build for each well and then imported into the Petrel project. The discrete lithology logs were used to control the log curves GR, DT and resistivity as well as a hint for the correctness of the porosity log (PKI).

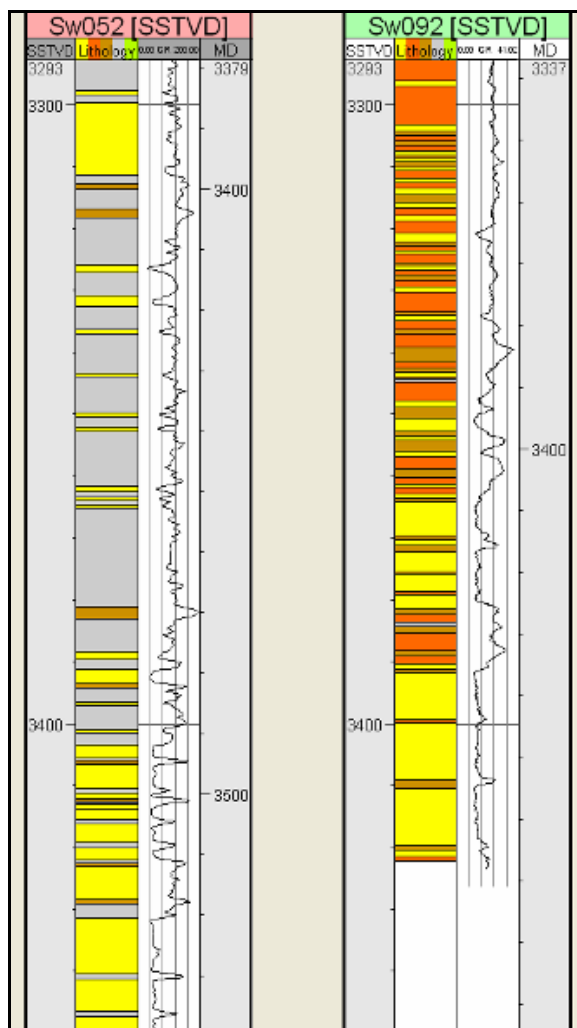


Fig. 3.15: Lithology log.

Perforations (Perforated Sections)

For all drillings discrete logs were produced, which make a fast distinction possible between the (up-to-date) perforated statuses (green) and not perforated or closed sections in the wells. These logs are useful for quality control purpose. For example: the opened sections should usually lie in those areas, where a good reservoir (e.g. higher porosity) is present. The perforated sections can be visualised in the 3D window as well as in geological profiles [Figure 3.13] as like as the cored sections.

Seismic Data

Four data sets were supplied by seismics: 2D seismic lines, fault polygons, three marker horizons and some of the overlying horizons.

The boundary used for seismics is more sparsely than the block boundaries in order to use information of the nearer environment. This serves primarily the avoidance of unacceptable edge effects / outliers (in the gridding process).

2D Seismic Lines

Within the sphere of activity no 3D seismics is available, but 2D seismics could be used. About 121 profiles are crossing the sphere of activity in a more or less regular way as it is visible in Figure 3.16.

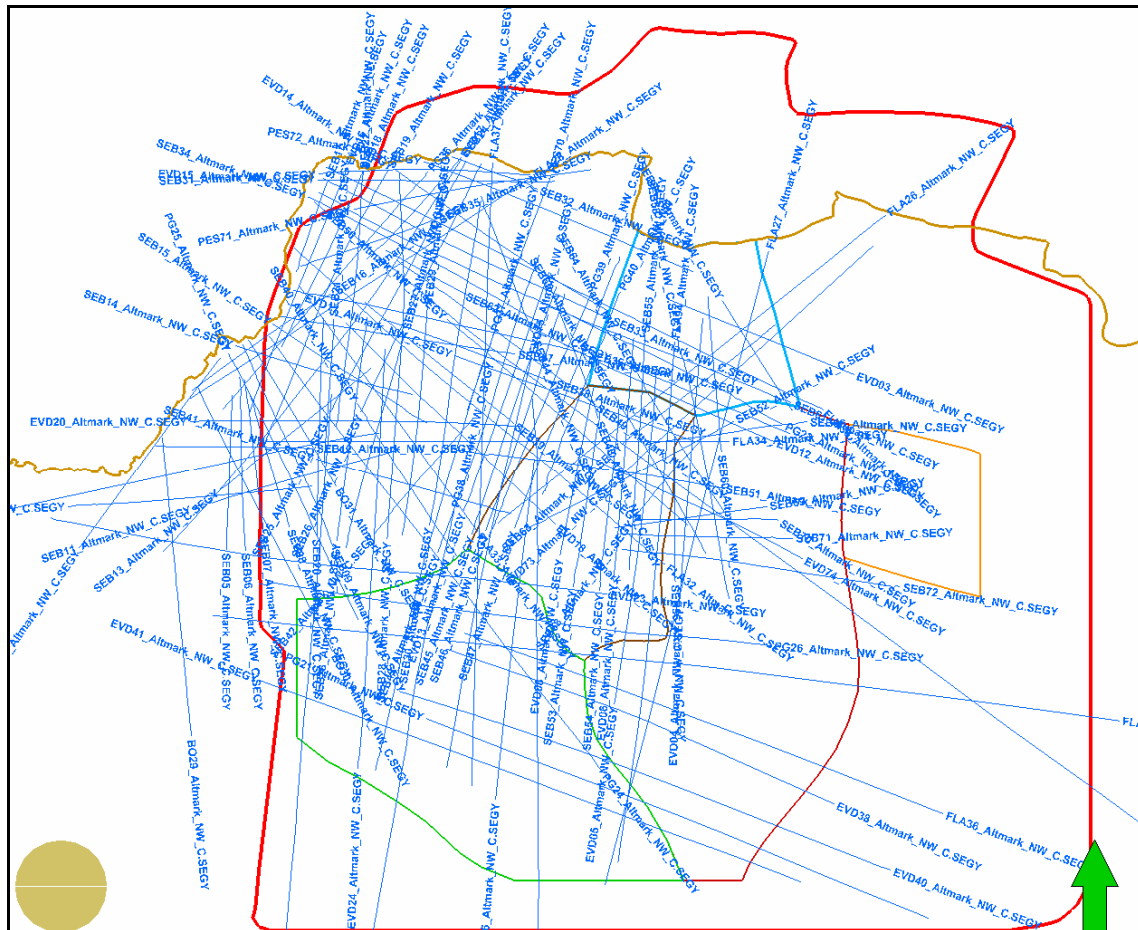


Fig. 3.16: Location of the profile lines (blue) of the 2D seismics (top view).

Faults

The area of the Altmark is tectonically strongly stressed. Numerous fault polygons were taken from seismics, interpreted on the basis of three marker horizons (see 5.3.2.3). Some points are to be considered thereby. For the sake of simplicity the faults were interpreted as vertical faults, which was judged to be sufficient for the modeling process. Then it should be clear that only the main faults, which are interpretable in the seismics, have been taken into account. It is obvious that there are a lot of smaller faults. The density/ distribution of the faults stands in a strong context to the density/ distribution of the profiles, i.e. there are more faults/ seismic profiles in the north-western area than e.g. at the southern edge [Figures. 3.16 3.17]. Generally an extensional tectonic system is present, therefore normal faults dominate. Figure 3.17 shows more than 300 of the interpreted faults within the sphere of activity.

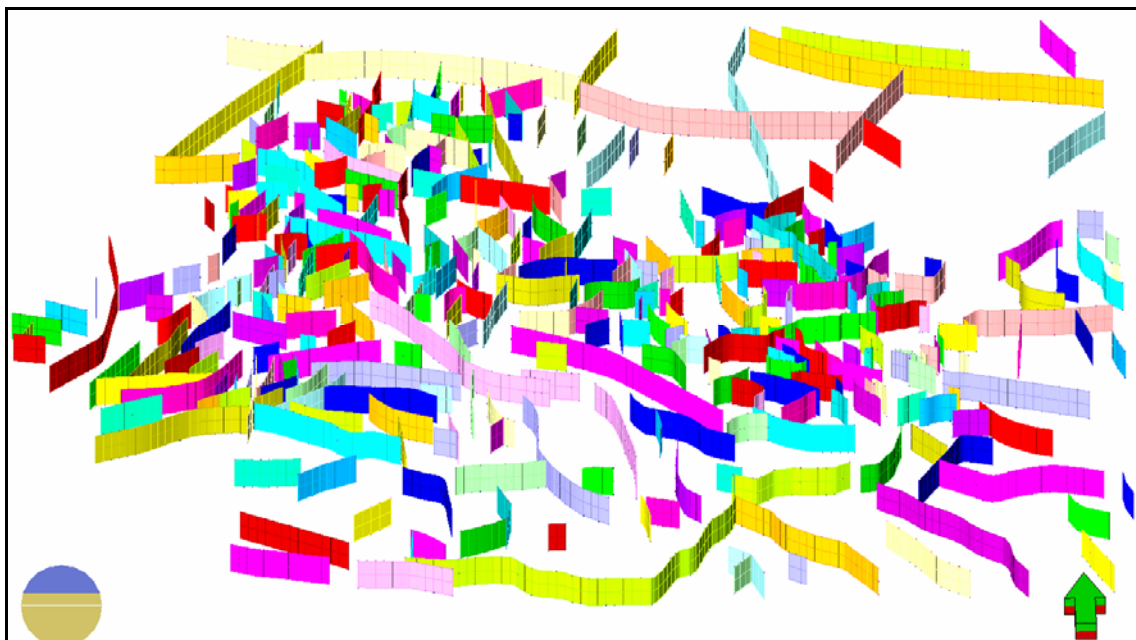


Fig. 3.17: Fault pattern.

Seismic Marker Horizons

Several marker horizons are available and usually used in eastern Germany. Three of them as listed below are important for and were used in the modeling process:

- Top Rotliegendes Z3 (Base Zechstein)
- Top Wustrow TC12
- Base Wustrow Rh9

The Top Rotliegendes horizon [Figure 3.18] can be correlated very easily because of a clearly visible change or peak in the log curves, especially in the GR log.

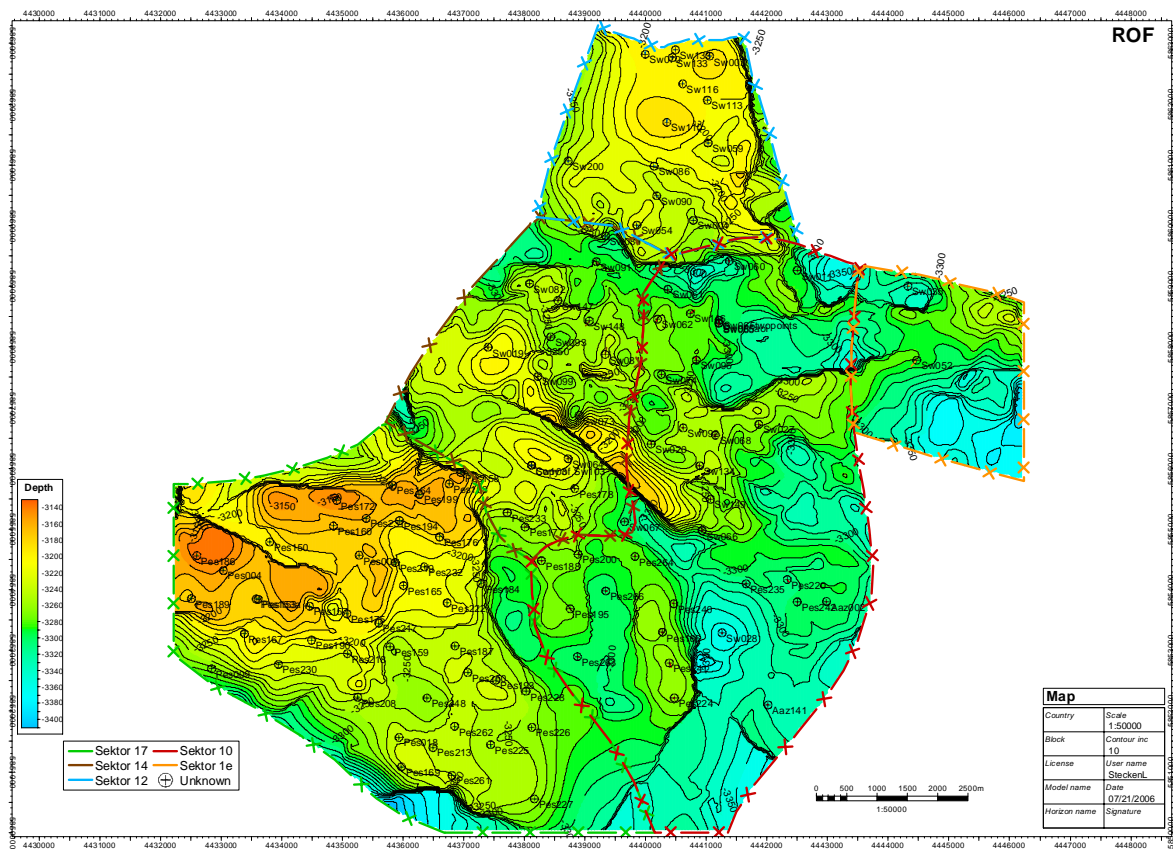


Fig. 3.18: Top Rotliegendes grid from the seismics (ROF) as surface in Petrel

Upper Horizons

Several other horizons above the Top Rotliegendes horizon were interpreted in the seismic profiles. Some of them were implemented in the Petrel project as point data and then surfaces were generated [Figure 3.19]. They were interpreted in time and are not relevant for the modeling, but were integrated for visualisation purpose. The horizons transferred to the Petrel project are from top to bottom:

- T1 Transgressionsfläche Känozoikum (unconformity Cenozoic/Mesozoic)
 - B1 (ungefähre) Grenze Turon und Coniac (boundary Turonian to Coniacian)
 - B2 Basis Oberkreide bzw. Cenoman-Basis (Base Upper Cretaceous)
 - M3 Basis Unterer Muschelkalk (Base Lower Middle Triassic)
 - X1 Oberfläche Zechstein (Top Zechstein)
 - Z1 Oberfläche Basalanhydrit (Top Base Anhydrite)

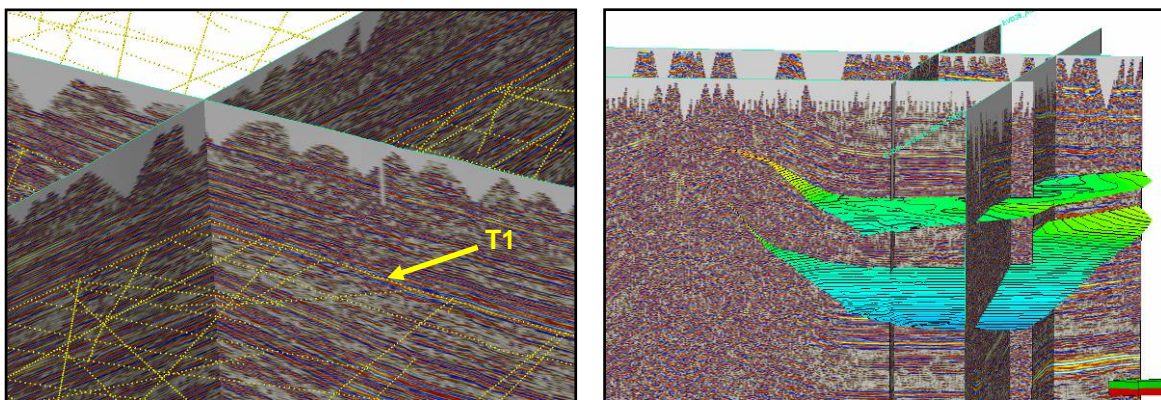


Fig. 3.19: Reflection seismic horizons above Top Rotliegendes (interpreted in time).

3.2.6 Modeling in PETREL

3.2.6.1 Defining Boundaries

The actual sphere of activity (all five blocks) covers an area of approximately 15×15 km in its longest expansions, whereby the total area amounts to about 100 km^2 . The total volume of the whole model amounts to about 25.6 km^3 including the modeled cap rocks (PWra-PEdn7) and 20.2 km^3 without (PMIn17-PEdn7). For this it follows that the volume of the cap rock in the model is roundabout 5 km^3 . These volumes were calculated with the assumption of a total thickness of 250 m respectively 200 m.

In the model the following boundaries were used:

- Block boundaries (multiple boundaries)
- Sector boundaries (five boundaries)
- Boundary whole model (one boundary for all sectors)
- Seismic boundary (larger than the boundary of the whole model)
- Combined sector boundaries (sectors 12+14 and 10+17)

The boundaries were digitized as polygons directly in the 2D window (*Make/Edit polygons*) or were imported.

3.2.6.2 Cultural Data

For a better orientation some geographical information [Figure 3.20] were implemented as polygons after a conversion of the coordinates, i.e. from geographical coordinates to UTM coordinates. There are political boundaries (e.g. frontier Lower Saxony/ Saxony Anhalt), rivers, towns (e.g. Salzwedel) etc.

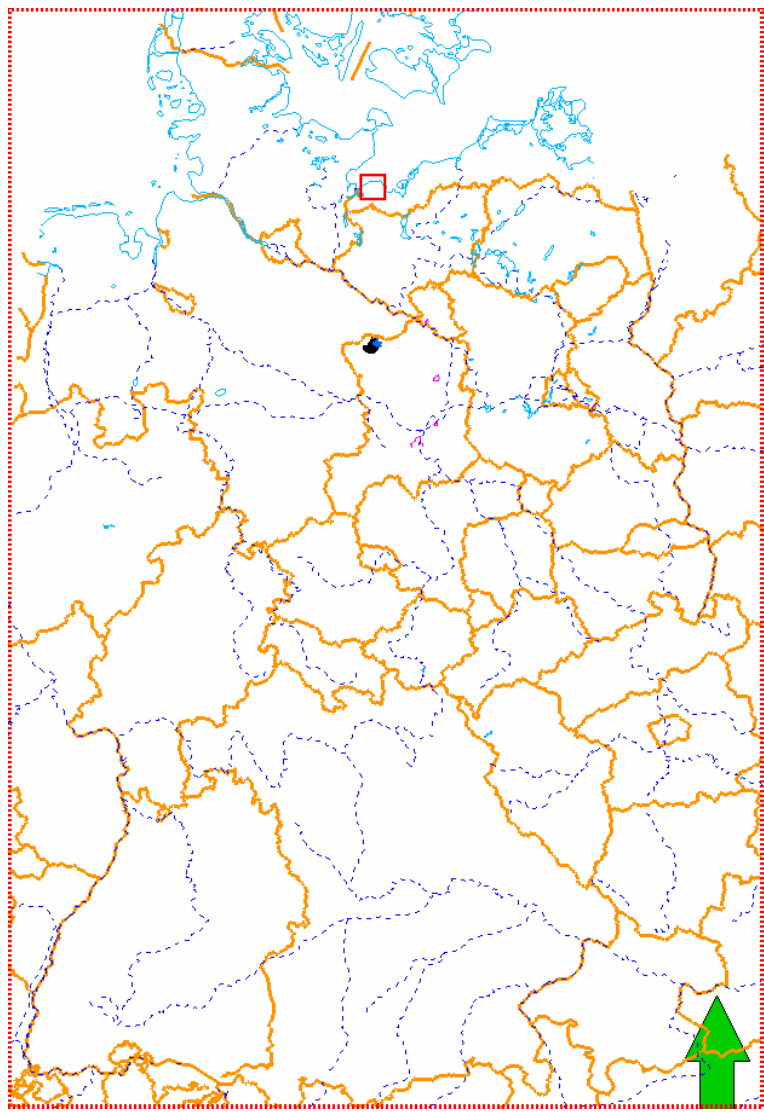


Fig. 3.20: Cultural data.

3.2.6.3 Data Import

All different available data types as described in chapter 4.3 were implemented in the Petrel project and if possible arranged block by block to get a clearly structured digital database.

3.2.6.4 Generating Surfaces from Seismic Grids (*Make Surface*)

From the three seismic marker horizons, which were imported as point data, surfaces were generated by using the *Make Surface* process and by including the revised fault pattern. In the next step it was controlled if the new surfaces are consistent with the well tops, i.e. if the depths of the well tops coincide with those points where the well paths are crossing the three surfaces. Later, after this first quality control, the seismic surfaces were adapted to the well markers by a process named well adjustment. If the differences were too large (e.g. more than 5 m) the markers and the seismic data had to be checked again.

3.2.6.5 Stratigraphic Modeling

During the stratigraphic modelling process the main well logs and especially the well tops, i.e. the stratigraphic well tops and the well tops of the reservoir units, will be brought together and be correlated. Several other types of information were used and visualised additionally in order to detect errors in the implemented input data and to eliminate them. An extensive quality control has been done and is important at this step because for the following step, the construction of the 3D grid, the correct position of the well tops is essential.

Revision of the Well Tops (*Edit Well Tops*)

For the quality control process the well tops were imported in Petrel and visualised in 2D-windows as well as in 3D-windows. If necessary they were revised.

Correlation of Well Data and Data QC (*Well Correlation*)

For both types of well tops, the stratigraphic and the reservoir related ones, thickness maps were generated in order to analyse and to judge the regional thickness distribution, especially between neighboured wells. By this method outliers, as a result of wrong input data, type errors or different interpretation, could be detected and if necessary corrected [Figure 3.21 showing four thickness anomalies before their correction].

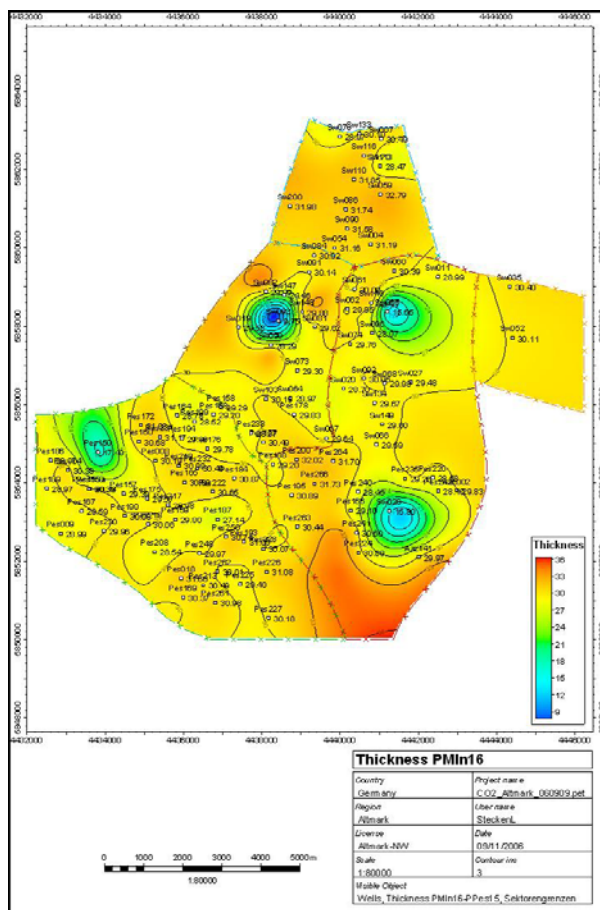


Fig. 3.21: Thickness map of PMIn16.

Furthermore several well correlation panels were created showing different types of data [Figure 3.22]. The lithology log, the geophysical logs (GR, DT and LL), the perforations, the cored sections, the well tops and all other data were visualised for cross checking.

Within the Petrel project it is at this step possible to combine diverse information in a relative fast way in order to control the consistence of the database. To give an example of the QC process: it was checked if all positions of the certain reservoir units as being interpreted in former times are not outside their belonging stratigraphic unit.

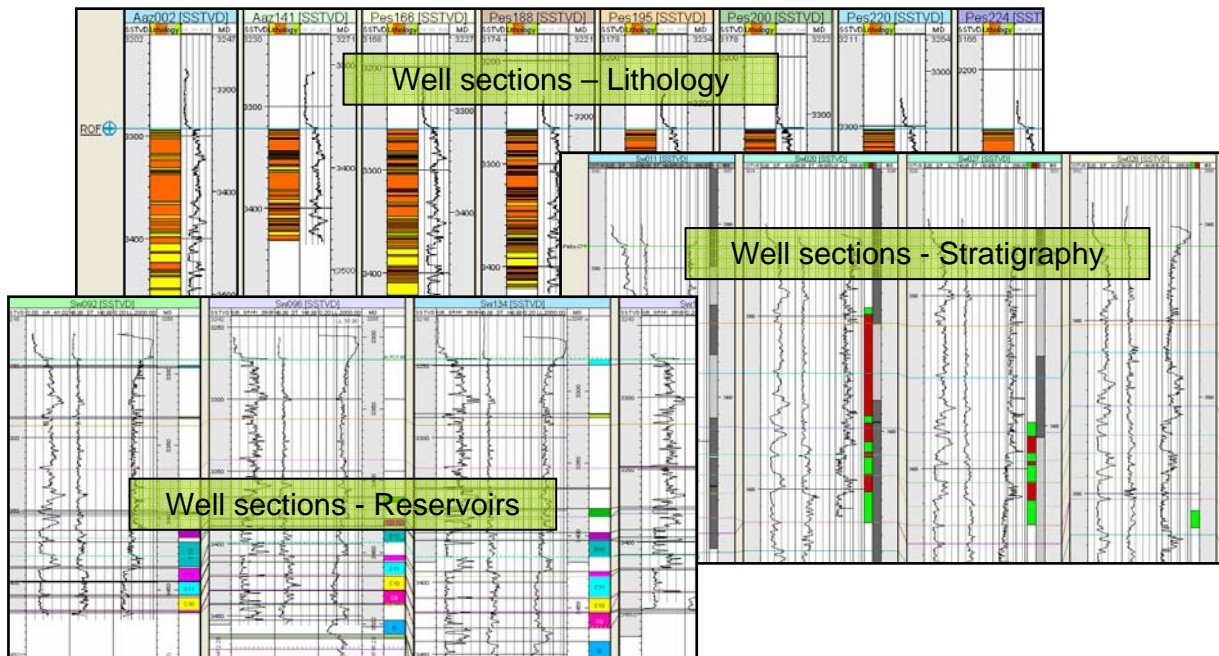


Fig. 3.22: Examples for well correlation panels as being used for QC.

3.2.6.6 Fault Modeling (*Fault Modeling*)

Due to the numerous faults within the sphere of activity an intensive work over of the fault pattern is necessary. The aim of this process (*Fault Modeling*) is to get a good 3D grid. To give an example: crossing faults which were not connected in an accurate way are leading to an irregular deformation of the grid within the gridding process. Moreover it is better to connect two faults which are close enough together in a geological meaningful way. Figure 3.23 shows some results of the gridding process before (above) and after (below) the fault modeling process. As mentioned above the faults were modeled as vertical faults. That is good enough, because a (time-intensive) reinterpretation of all the faults to detect the real dip and to model them as normal faults would not have a relevant result. The other way round it would complicate the modeling process in an unmanageable way.

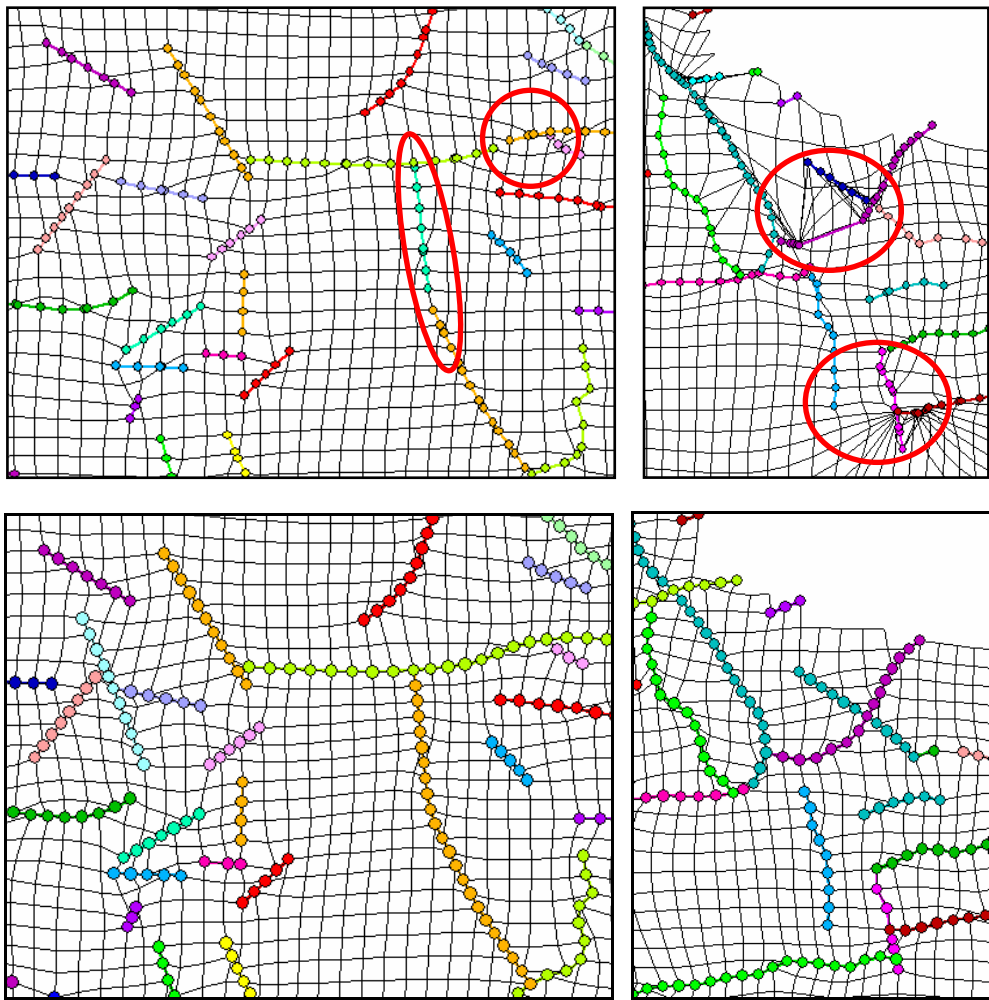


Fig. 3.23: Results of the fault modeling (above: before – below: after).

3.2.6.7 Building the 3D Grid (*Pillar Gridding*)

In order to be able to handle the model in the simulation process it was decided to create a complete model plus several sub-models. The reason is that the number of cells should not be too high for a simulation model. Therefore a coarse complete model (blocks 1e, 10, 12, 14 and 17), a finer sub-model for block 12 and two models with combined sectors will be applied [tab. 2].

Resizing the grid from 100 m x 100 m in x- and y-direction to 200 m x 200 m reduces the number of cells to 25 %.

Table 3.2: List of supplied reservoir models.

| Name | Classifica-tion | Blocks/Sector-s | x,y grid size |
|----------------|-----------------|--------------------|---------------|
| Complete Model | Coarse | 1e, 10, 12, 14, 17 | 200 x 200 |
| Model 10+12 | Fine | 10, 12 | 100 x 100 |
| Model 14+17 | Fine | 14, 17 | 100 x 100 |
| Block 12 | Fine | 12 | 100 x 100 |

3.2.6.8 Defining Horizons (*Make Horizons*)

or the construction of the 3D grids the three surfaces from seismics, Top ROF, Top Wustrow and Base Wustrow, were used as guiding surfaces, i.e. as second input. The main input was delivered by the revised well tops. All in all thirty horizons were built forming fifteen reservoir units in each well, if present [Figure 3.11]. Additionally two horizons were created for the so called cap rock, PWra (i.e. Top Werra-Anhydrit) and PMIn17 (i.e. Top Rotliegend-Oberfläche) [Figure 3.24].

3.2.6.9 Defining Zones (*Make Zones*)

The horizons chosen as described above were distributed into four zones [Figure 3.19]. The uppermost zone contains the “Abdeckgestein” (PWra-PMIn17), followed by the next zone from PMIn17 to PPes12 (representing the Top Wustrow seismic layer). The next zone begins with this PPes12 and ends at PEdn8, which represents the Base Wustrow layer. Below this third zone the last zone reaches from PEdn8 to BD (i.e. the Base of Reservoir D). Within the zones reservoir zones and intermediate zones coexist.

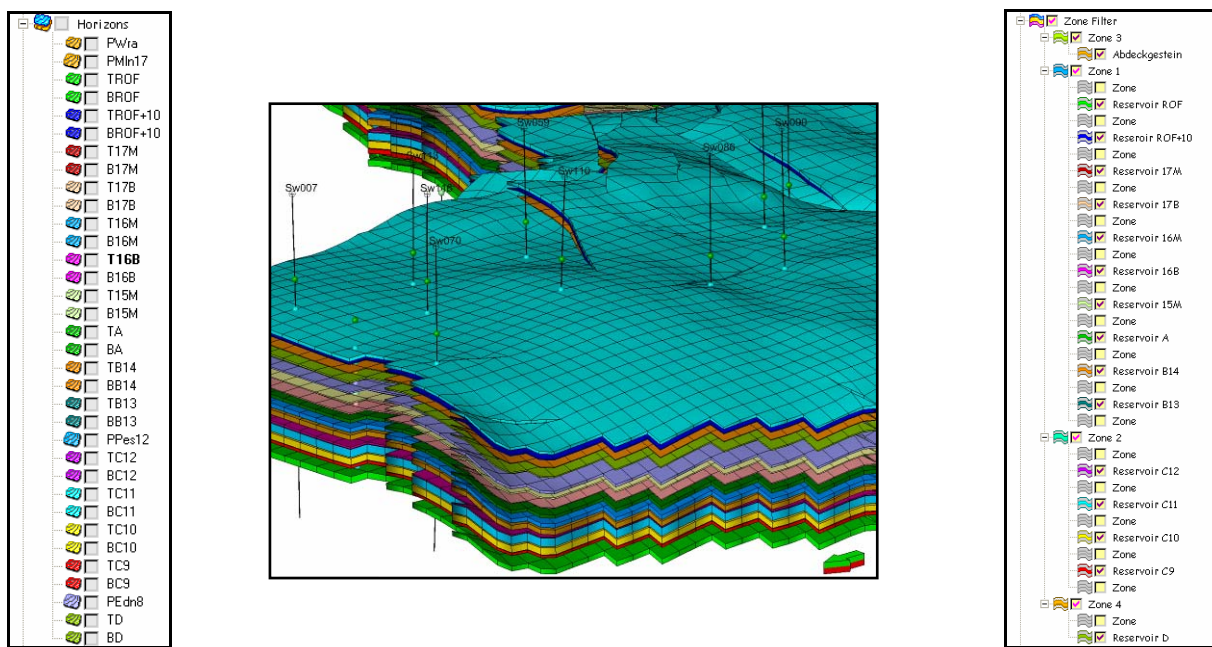


Fig. 3.24: Overview of the modeled horizons (left) and zones (right) and the resulting fifteen reservoir zones (middle). The cap rock (zone Abdeckgestein) and the intermediate zones are not visible.

3.2.6.10 Defining the Number of Vertical Cells (*Layering*)

The size of the cells in x- and y-direction is given by the pillar gridding process (100 x 100 and 200 x 200 m) [table 2]. Within the layering process the number of the z-component will be defined. For the non-reservoir zones it is enough to define one vertical layer, i.e. one cell in z-direction for each intermediate zone. Only the cap rock will be divided into more than one sub-layer for simulation purpose. An increasing thickness towards the top is possible, which means *fractional layering* [Figure 25 –

see uppermost (orange) zone]. All other zones will be subdivided by a *proportional layering* [Figure 3.25], whereby the number of layers is individually adapted to the average thickness of each reservoir zone.

The layering will affect the upscaling of the log data and should therefore be chosen carefully, e.g. characteristic peaks in a porosity log should be considered if possible.

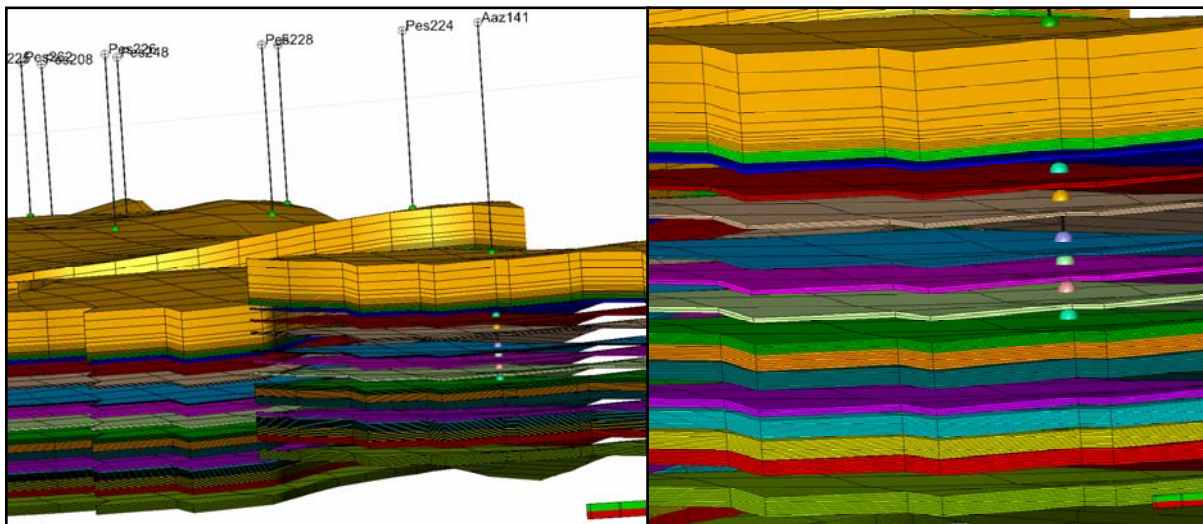


Fig. 3.25: Example for the vertical layering in the models.

3.2.6.11 QC of the 3D Grids

After the construction of the 3D grids well correlation panels were created again to control the grids in 2D. Above all in a 3D window the cell geometry has been checked as far as possible.

3.2.6.12 Upscaling of the Logs (*Upscaling*)

A permeability log was not available and therefore it was created for each well by means of a phi-k plot [Figure 3.26]. Core measurement data has been plotted and the resulting equation was used for the calculation of a permeability log for each well.

Due to the lack of high quality porosity logs the following method was used to calculate a porosity log. In a well section the porosity data from complex interpretation, named PKI (not continuous and, being point data, leading to wrong results if directly used for the calculation of the permeability), the core measurements (very low density) and some average values for the formerly interpreted reservoir zones were plotted together with the new calculated porosity log [Figure 3.27 see arrow]. This new porosity log, named “Gamma_Poro_Kalibrator”, is resulting from a mathematical equation, which uses the GR and the Sonic-Log for its calculation. It is continuous (step 0.1 m) and should fit with the other data described above. In a first step the log was calculated automatically and then adjusted individually for each single well. This was done by changing some parameters within the equation and calculating the log again in order to reach the best possible result (i.e. the best fit).

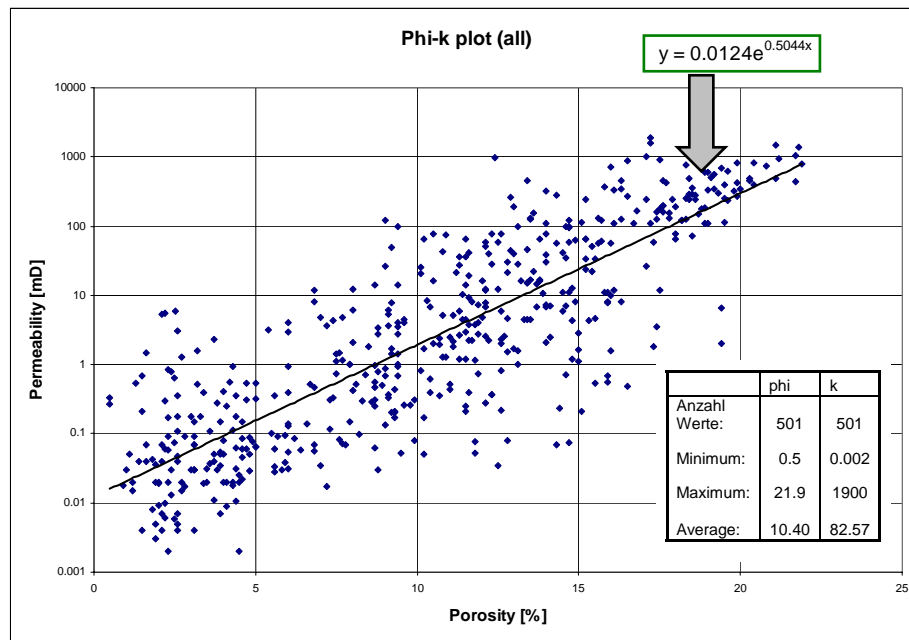


Fig. 3.26: Porosity and permeability cross plot (phi-k plot).

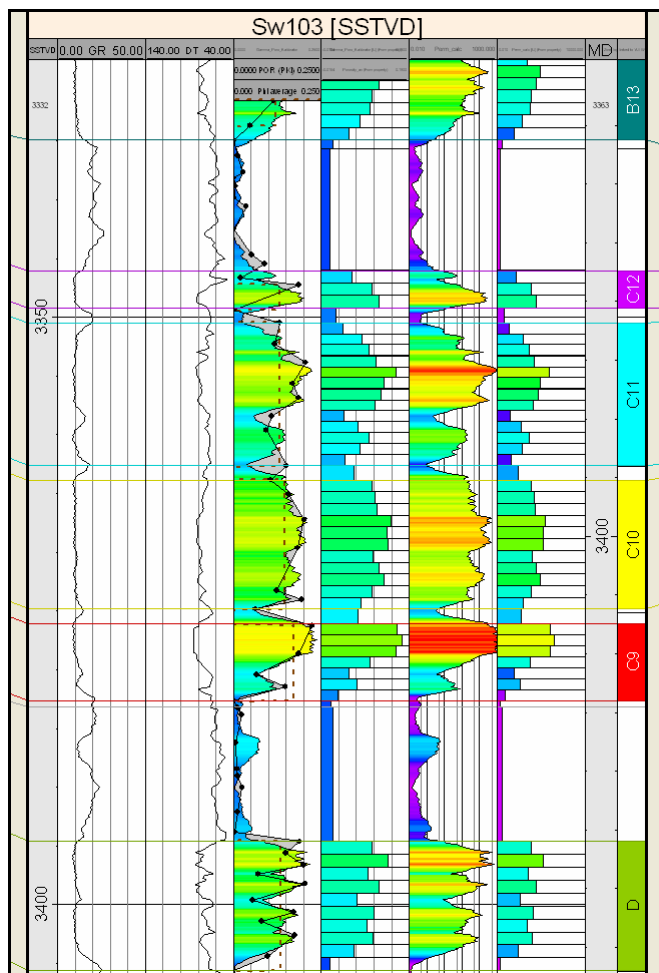


Fig. 3.27: Part of a well section showing from left to right: SSTVD, GR, DT, [Phi average (dotted) + PKI (log points) + Gamma_Poro_Kalibrator (coloured log)], upscaled phi (Gamma_Poro_Kalibrator [U]), Perm_calc, upscaled Perm_calc, MD, zone log.

Using this new porosity log and the equation from the phi-k plot [Figure 3.26] the permeability logs [Figure 3.27] were created. The calculated porosity logs and the calculated permeability logs were then upscaled in order to get one value for each cell [Figure 3.27]. For the porosity an arithmetic upscaling method was chosen and for the permeability a geometric one.

In Figure 3.28 the upscaled porosity cells are shown as well as E-W and N-S bearing well sections. The lower reservoirs are of better quality, i.e. the porosity values are generally higher there.

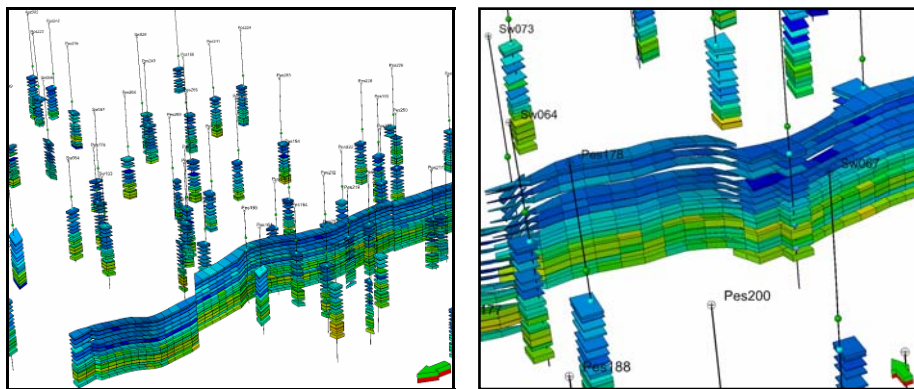


Fig. 3.28: Upscaled porosity values within the wells and N-S/E-W cross sections (see arrow).

3.2.6.13 Petrophysical Modeling

In the petrophysical modeling process the upscaled values within the wells were distributed allover the 3D grid [Figure 3.29] by using the stochastical method SGS (Sequential Gaussian Simulation). For each zone the minimum and maximum values were included in order to limit the output data range for both, the porosity and the permeability model.

For the uppermost zone, the cap rock zone, it was necessary to assign values, because no usable data were available and the calculated logs were useless there.

In order to get a representative porosity model several realizations (i.e. five) were calculated and averaged.

The permeability model was created under consideration of the property's logarithmic behavior.

For each model a porosity and permeability model was built (i.e. eight property models).

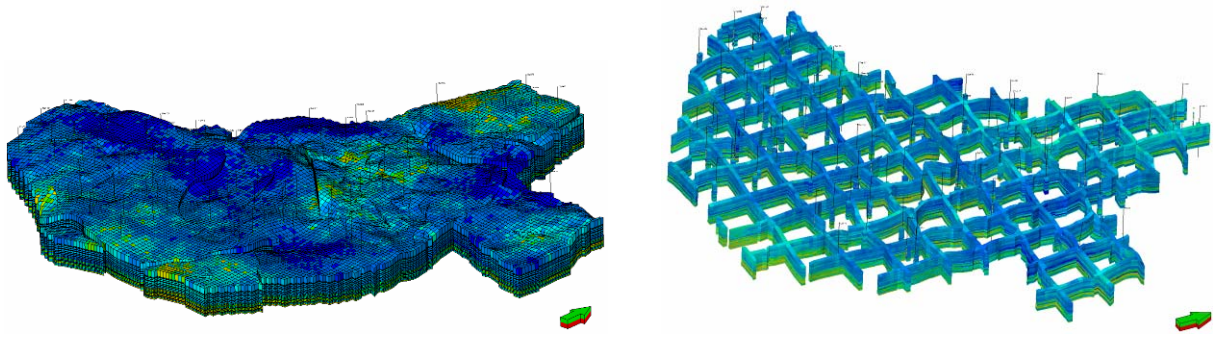


Fig. 3.29: Porosity model for the whole 3D model (left: with grid lines; right: using a filter).

3.2.6.14 Exporting Data and Results

In the end the Petrel project forms a local database, which can deliver different types of output data according to requirements. For the present task the 3D grids, the well locations and paths (well connection data) as well as the files with cell values for the desired petrophysical properties (property files) were exported. Additionally a rescue model was delivered.

The static models will then be imported in ECLIPSE for dynamic simulation purpose.

Work Package 4

Process Modelling

Issues:

- CH₄ and CO₂ composition, phase behaviour & properties PVTi-ECLIPSE 300
- Hydrodynamic dispersion effects
- Simulation of gas-mixing: Impact of grade of CO₂ purity
- Physical rock alteration

Authors:

G. Pusch, R. Meyn, G.F. Ionescu, K.N. Awemo ITE TU-Clausthal

F. May BGR Hannover

| | |
|--|-----|
| Kurzfassung..... | 137 |
| 4.1 Phase Behaviour and Properties CO ₂ –A-Gas : Benchmarking | 138 |
| 4.1.1 Density | 140 |
| 4.1.2 Viscosity..... | 141 |
| 4.1.3 Compressibility..... | 142 |
| 4.1.4 Solubility in brine | 142 |
| 4.1.5 Effects of impurities on the properties of CO ₂ -dominated gas mixtures (F.May) . | 145 |
| 4.2 Hydrodynamic Dispersion Effects..... | 147 |
| 4.2.1 Introduction | 147 |
| 4.2.2 Parameters of Dispersion..... | 148 |
| 4.2.3 Calculation of Effective CO ₂ Diffusion Coefficient | 149 |
| 4.2.4 Reservoir Simulation Model | 150 |
| 4.2.5 Results of Sensitivity Analysis..... | 152 |
| 4.2.5.1 Hydrodynamic and Numerical Dispersion..... | 152 |
| 4.2.5.2 Gravity Effects with Cross Flow between Layers..... | 155 |
| 4.2.5.3 Rate Effects – Injection/Production Profiles..... | 155 |
| 4.3 Physical Rock Alteration-Impact on Flow Processes..... | 156 |
| Conclusions | 172 |
| References: | 173 |

Kurzfassung

Hauptaufgabenstellung der physikalischen Prozessmodellierung mit Hilfe eines kommerziellen Simulators ECLIPSE 300 war die Überprüfung der Funktionalitäten der Programmoptionen für die Berechnung der Gaseigenschaften, der Schichtwassereigenschaften im Kontakt mit dem reaktiven Gas CO₂, der Vermischung der beiden Gase CO₂ und Erdgas, die Wechselwirkung des kohlensauren Schichtwassers mit dem Gestein und ihre Auswirkungen auf den Fließprozess. Die Untersuchung der Auswirkung einer Porendruckänderung beim Speichern von CO₂ auf die Fließeigenschaften konnte wegen der Defizite in der am ITE verfügbaren „Rock Mechanic Option“ von ECLIPSE nicht realisiert werden.

ECLIPSE ist ein Erdöl-/Erdgaslagerstättensimulator mit weltweiter Verbreitung und hoher Akzeptanz bei der Simulation von Produktionsvorhersagen für Erdöl- und von Erdgaslagerstätten bzw. Erdgasspeichern in der globalen Öl-/und Gasindustrie. Spezielle Erweiterungen des Programm Codes für die Simulation von gekoppelten Prozessen wie bei Einbeziehung von mechanischen Spannungszuständen, thermischen Transportvorgängen und/oder chemischen Reaktionen der am Fluss beteiligten Phasen /Komponenten existieren nur sektorenweise und in vereinfachter Form. ECLIPSE ist daher nicht als multi-funktionaler Prozesssimulator zu verwenden.

Das Speichern einer Gasphase wie CO₂ in natürlichen Gaslagerstätten ist aber zumindest in der Betriebsphase primär ein „Speicherraumbeschreibungsproblem“ und weniger ein „Prozessbeschreibungsproblem“ wie man aus der langen Erfahrung mit Erdgasspeichern weiß. Anders kann die Situation für Aquiferspeicher und für die Langzeiteffekte der Wechselwirkung des gespeicherten CO₂ mit dem Gestein beurteilt werden.

Der „Compositional Simulator“ ECLIPSE 300 (E 300) beschreibt das Phasenverhalten und die Phaseneigenschaften von Erdgaskomponenten und von CO₂, sowie ihren Mischungen auf der Basis von Zustandsgleichungen (Peng-Robinson III) hinreichend genau und darüberhinaus auch die Eigenschaften von CO₂- Wasser Mischungen nach Redlich-Kwong erweitert durch die Spycher/Pruess Modifikation. Die Notwendigkeit zur Erweiterung der Phaseneigenschaften auf seltene Komponenten wie Argon, Wasserstoff oder Sauerstoff besteht nicht, wenn man davon ausgehen kann, dass diese nur in Spuren vorhanden sind.

Die Einflüsse der hydrodynamischen Dispersion für CO₂ und Erdgas auf den Vermischungsprozess wurden mit der in E 300 integrierten Diffusionsoption in Verbindung mit einem Anpassungskoeffizienten modelliert. Die Auswirkung der Dispersion auf den Prozess wird erst bei einem Multiplikator des effektiven Diffusionskoeffizienten von mindestens 1000 deutlich bemerkbar. Die Ausschaltung von numerischen Fehlern erfordert eine sorgfältige Anpassung der räumlichen und zeitlichen Diskretisierung in den numerischen Lösungsverfahren der Differenzialgleichungen.

Die Diffusionswirkung von CO₂ im Schichtwasser in E 300 beruht auf Sättigungsgleichgewichtseinstellungen (CO₂-STORE), die keine zeitabhängigen Änderungen erlauben und daher den langsamen Prozess der Diffusion in der Wasserphase überzeichnen.

Der wichtigste Vorgang bei den Wechselwirkungen zwischen dem injizierten CO₂ und dem Haftwasser ist die Verdampfung des Wassers und die damit verbundene Injektivitätserhöhung. Dieser Prozess ist mit E 300 (GASWAT und CO2-STORE, realitätsnah zu modellieren. Treten dabei aber Übersättigungen der Haftwasserphase ein, so kann die nachfolgende Ausfällung von Haliten nicht mit E 300 modelliert werden. Lösungsprozesse von Zementanteilen des Lagerstättengesteins lassen sich nicht mit E 300 simulieren, wohl aber die Auswirkung auf die Permeabilität, wenn eine vom Porendruck und damit pH-Wert abhängige Funktion in E 300 installiert wird. Das bedeutet wiederum den Verzicht auf die Modellierung zeitabhängiger Veränderungen. Der Einfluss auf die Porosität ist vernachlässigbar.

Als Fazit der Untersuchungen kann E 300 als bewährter Lagerstättensimulator bis zum Vorliegen eines im Leistungsumfang vergleichbaren, besseren Produkts verwendet werden, um Speicherkapazitäten von CO₂ und Produktionsraten von Erdgas in ausgeförderten Erdgaslagerstätten hinreichend zuverlässig vorherzusagen.

4.1 Phase Behaviour and Properties CO₂ –A-Gas¹ : Benchmarking

In this sub-chapter the principal properties of CO₂ calculated with ECLIPSE are validated: density, viscosity, compressibility, brine solubility and surface tension in the water-CO₂ system. A benchmarking is done vs. measured properties existing in literature in order to confirm the use of the ECLIPSE PVTi package used in simulation runs. ECLIPSE 300 incorporates four equations of state and two additional variations to the Peng-Robinson equation (ECLIPSE Manual).

When an equation of state is selected, it is used to obtain z-factors and phase fugacities. These properties are handled to define inter-phase equilibrium and fluid densities.

The equations of state are:

- PR: Peng-Robinson
- RK: Redlich-Kwong
- SRK: Soave-Redlich-Kwong
- ZJ: Zudkevitch-Joffe-Redlich-Kwong.

These equations of state are implemented in generalized form using Martin's equation.

The generalized form of such an equation of state is:

$$Z^3 + E_2 Z^2 + E_1 Z + E_0 = 0$$

with:

¹ A-Gas = Altmark Gas: 65% N₂ + 35% CH₄

$$E_2 = (m_1 + m_2 - 1)B - 1$$

$$E_1 = A - (m_1 + m_2 - m_1 m_2)B^2 - (m_1 + m_2)B$$

$$E_0 = -[AB + m_1 m_2 B^2(B+1)]$$

The coefficients m_1 and m_2 depend upon the equation used, see table 4.1.

Table 4.1. The coefficients, and m_2 , variation wit the equation of state.

| Equation of State | m_1 | m_2 |
|---------------------|----------------|----------------|
| Redlich-Kwong | 0 | 1 |
| Soave-Redlich-Kwong | 0 | 1 |
| Zudkevitch-Joffe | 0 | 1 |
| Peng-Robinson | $1 + \sqrt{2}$ | $1 - \sqrt{2}$ |

The cubic equation for the Z-factor may be solved to obtain Z-factors for the liquid and vapour phases. Generally three solutions are obtained. The distinction between the liquid and the vapour phase is then made by choosing the smallest root as Z-factor for the liquid phase and the largest root as Z-factor for the vapour phase. A and B are calculated using the fugacities and the binary interaction coefficients.

In this study a modified three parameter Peng Robinson EOS was used. The traditional weakness of the two-parameter equations of state (EOS), such as the Peng-Robinson, Redlich-Kwong, etc. is their poor prediction of liquid properties, especially liquid densities and saturations. Peneloux *et al.* proposed a molar volume correction, referred to as volume shift, which adds a third parameter to the EOS, and, in turn, greatly improves liquid property estimation.

For a mixture of N components, the phase molar volume $V_{mol, p}$ is given by:

$$V_{mol, p} = V_{mol, p}^{EOS} - \sum_{i=1}^N z_i c_i$$

where

p represents the phase of the system

$V_{mol, p}^{EOS}$ is the molar volume of the phase predicted by the traditional 2-parameter EOS

$z_i = (x_i, y_i)$ are the liquid and vapour mole compositions

c_i constitute a set of volume corrections.

The component corrections are usually related to set of dimensionless shift parameters s_i , by:

$$s_i = \frac{c_i}{b_i}$$

where:

$$b_i = \frac{\Omega_{b,i} R T_{ci}}{p_{ci}}$$

For more details please refer to the ECLIPSE Technical Description.

In the subchapter 4.1.5 GERC 2004 Wide-Range Reference Equation of State for Natural Gases (Kunz et al. 2005) was used in order to calculate the properties of CO₂-dominated gases from oxy-fuel plants.

4.1.1 Density

CO₂ has a larger density as natural gases (methane) or inert gases (N₂) that can be usually found in natural gas reservoirs. A comparison between the densities of carbon dioxide, methane and nitrogen (Figure 4.1) at temperatures characteristic for the chosen reservoirs (Altmark and Barrien) 120°C shows that the CO₂ density is about 3 times bigger as CH₄ density and 2 times bigger as N₂ density at 50 bar (pressure of the depleted gas reservoir) whereas at 400 bar (initial reservoir conditions) the CO₂ density will be almost 4 times larger than CH₄ and 3 times larger than N₂ density.

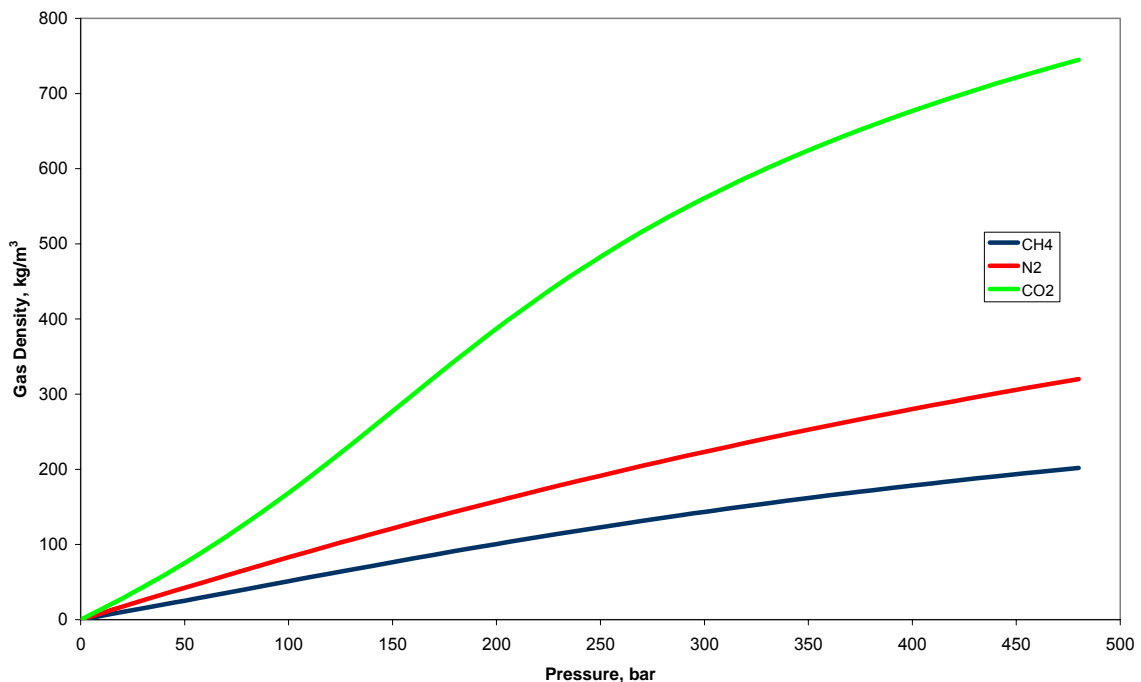


Fig. 4.1 Comparison between CO₂, CH₄, and N₂ densities at 120°C calculated with ECLIPSE PVTi

When comparing the CO₂ density, calculated using ECLIPSE PVTi and the measured values (Gmelin Handbuch der Physik), Figure 4.2., one can observe a very good agreement between the data points. We can conclude that ECLIPSE will be able to adequately calculate the CO₂ density in the simulation runs.

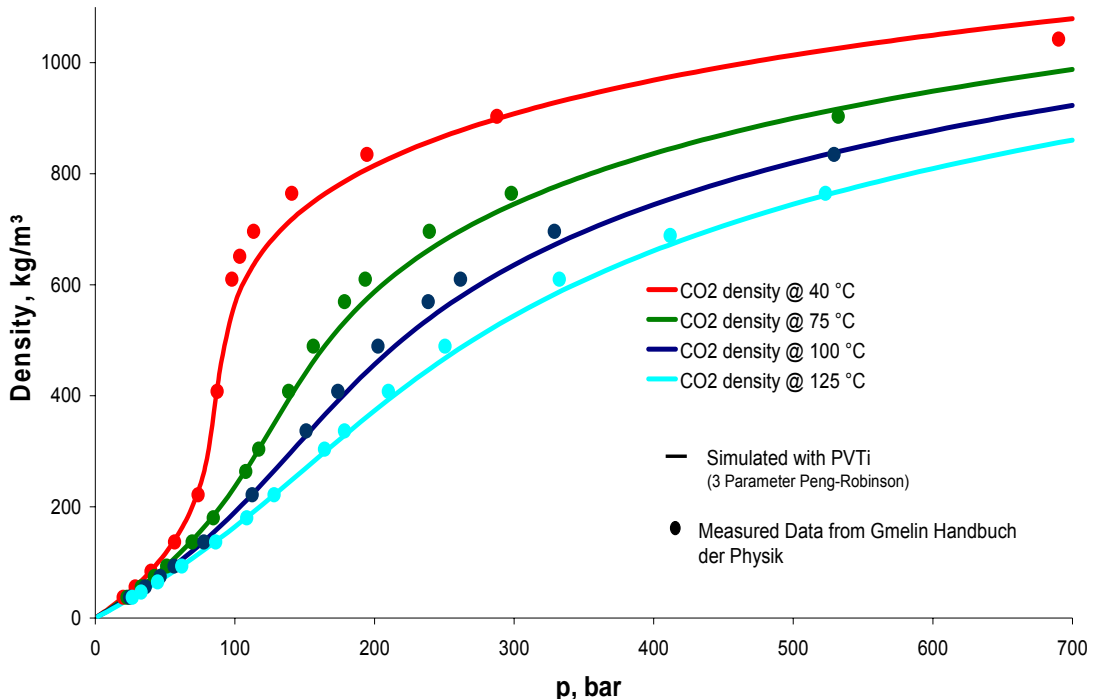


Fig. 4.2 CO₂ Density- Comparison between measured and PVTi calculated Data

4.1.2 Viscosity

The viscosity of CO₂ at reservoir temperatures (Figure 4.3) is close to the ones of methane and nitrogen until approx. 100 bar. Above this pressure the viscosity difference enlarges so that at 400 bar (initial reservoir pressure) it will be about 3 times larger than CH₄ and 2 times larger than N₂ viscosity respectively. Taking in account measured data (A. Fenghour) the viscosity of CO₂ calculated by ECLIPSE is in good agreement.

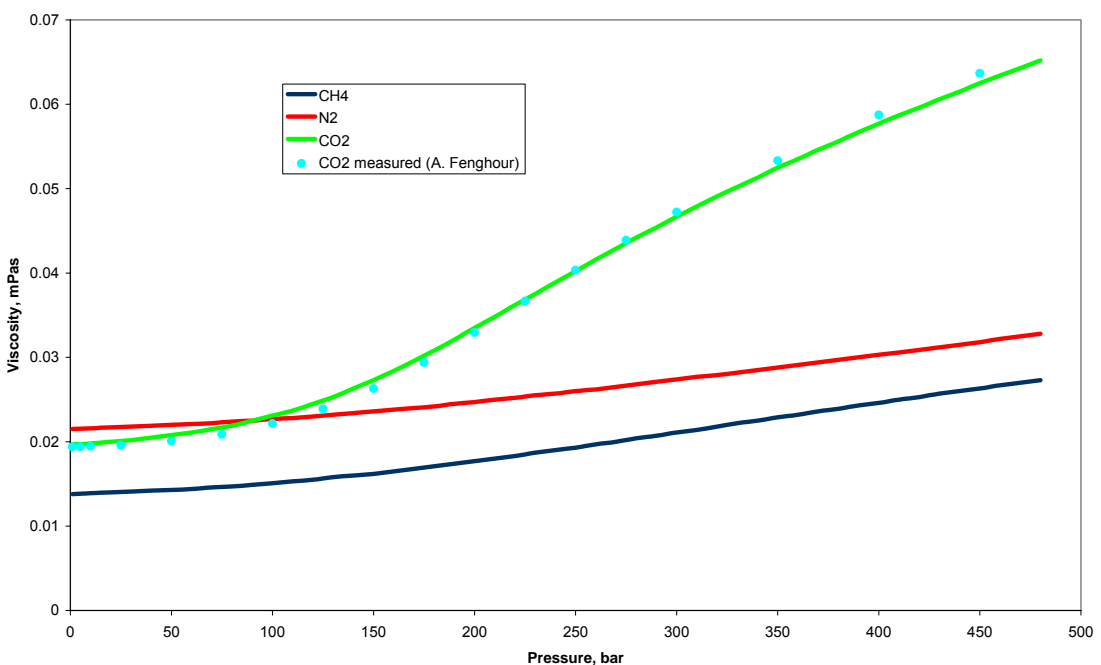


Fig. 4.3 Comparison between CO₂, CH₄, and N₂ viscosities calculated with ECLIPSE PVTi and measured CO₂ viscosity

4.1.3 Compressibility

The compressibility of the CO₂ (at 120°C) is larger than the one of CH₄ and N₂ until approx. 250 bars; above this value the CO₂ compressibility approaches the lower values (Figure 4.4).

For obtaining an average value the compressibility curve must be integrated over the defined pressure range, which finally yields a larger overall compressibility for CO₂ compared to the other gas components.

When speaking about the z- factor some comparisons were made at smaller temperatures (40°C), which are more typical for aquifer storages (B. Ülker). In Figure 4.5 there is a good agreement between the ECLIPSE calculated and measured data.

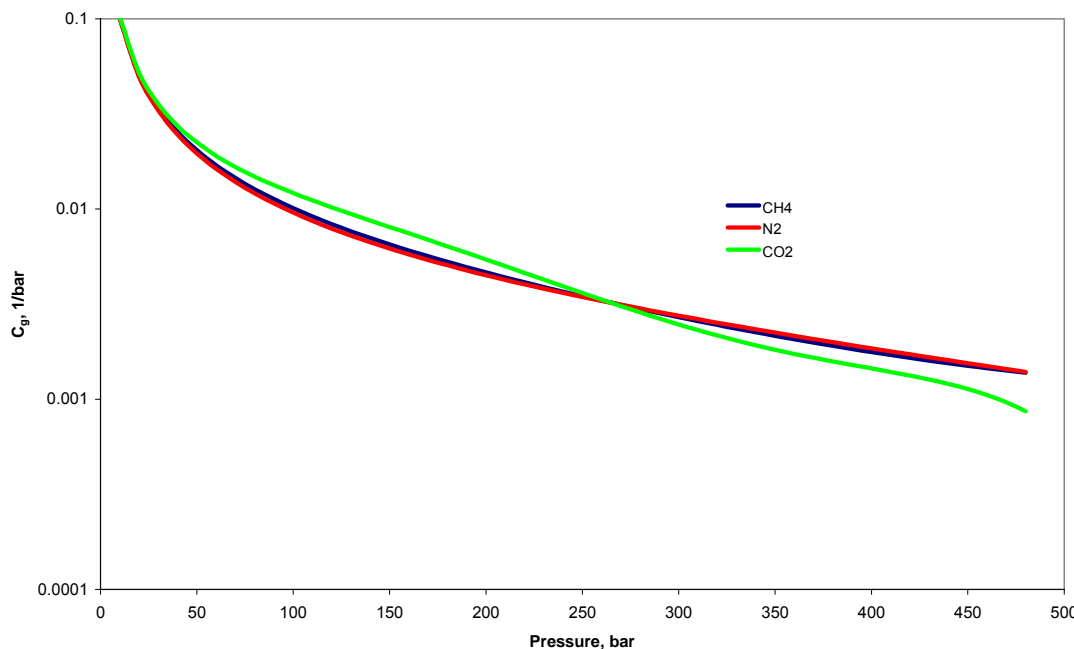


Fig. 4.4 Comparison between CO₂, CH₄ and N₂ compressibilities (PVTi).

4.1.4 Solubility in brine

Solubility functions are treated in more detail in Chapter 4.3.

The solubility of CO₂ in brine is larger than the one of CH₄. Figure 4.6 presents the solubility of methane and carbon dioxide in pure water and a 4m NaCl solution at 60°C calculated with Redlich-Kwong modified by Spycher-Pruess.

The solubility of CO₂ in an aqueous solution is a function of the pressure and temperature but also of salt components present in water. Figure 4.7 depicts the dependence of CO₂ solubility on the brine composition.

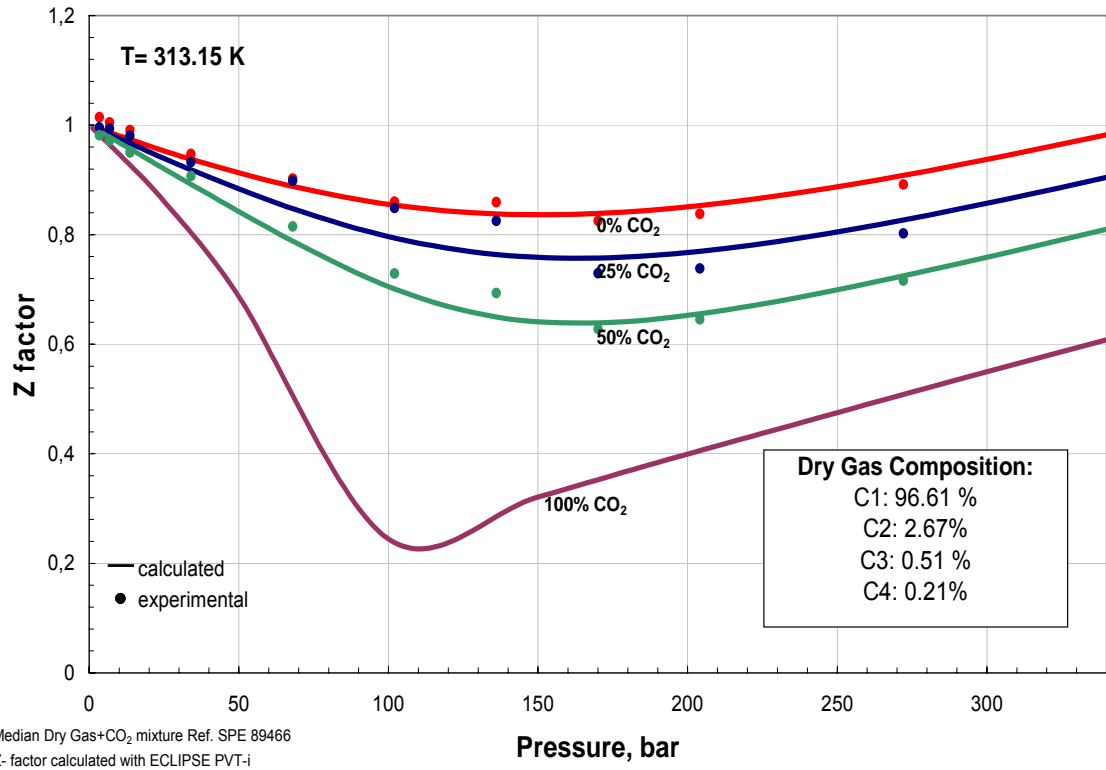


Fig. 4.5: Comparison between z- factor measured and calculated data (SPE 89466)

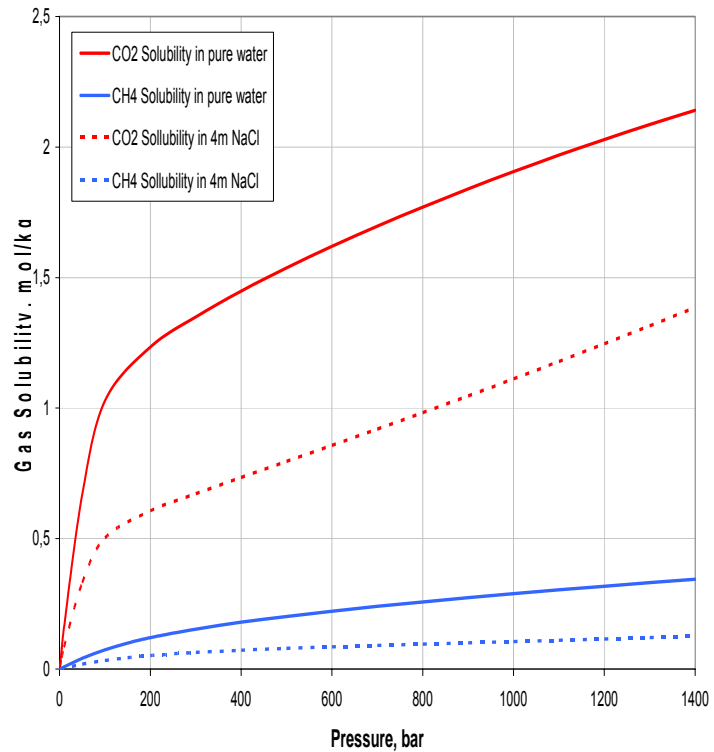


Fig. 4.6: Methane and CO₂ solubility in pure water and brine (B.Ülker).

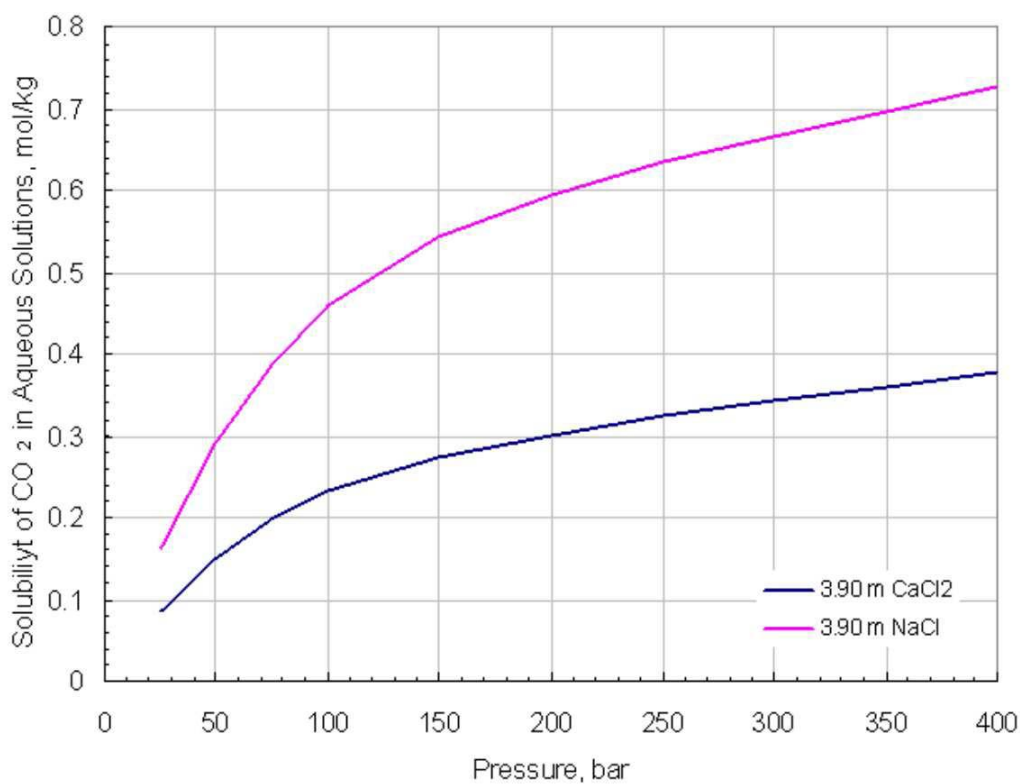


Fig. 4.7 CO₂ solubility in aqueous solutions of NaCl and CaCl₂ at 60°C (B.Ülker)

It is also known that when CO₂ is dissolving into water, the water density increases, unlike in the case of other gases, see Figure 4.8.

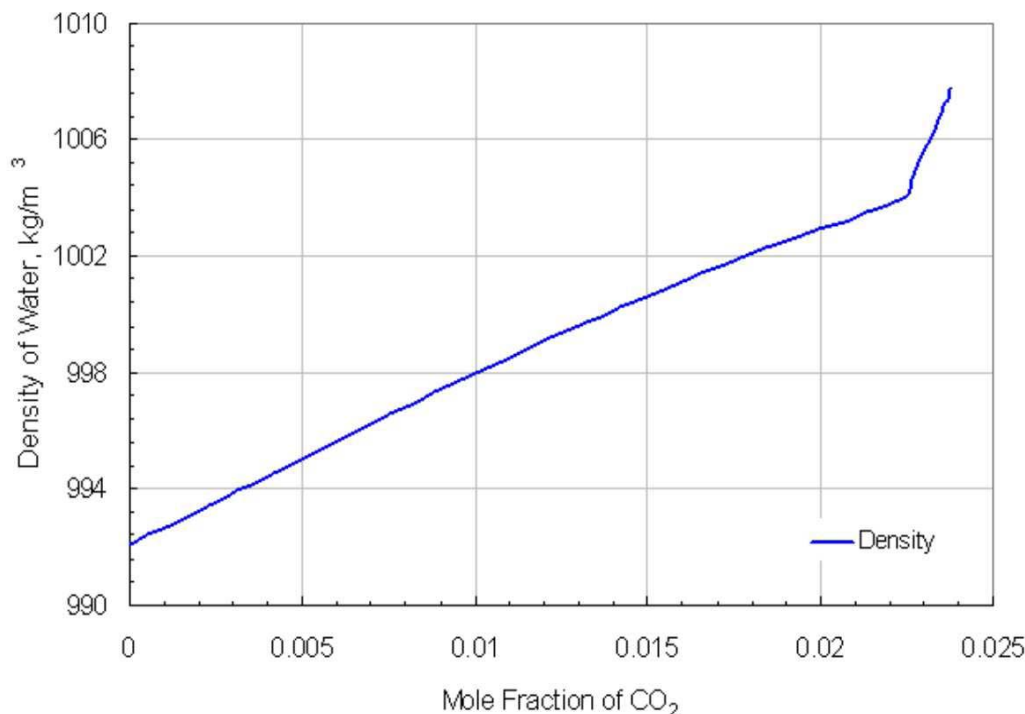


Fig. 4.8 Simulated Density of water with dissolved CO₂ at 60°C and 200 bar (B.Ülker).

4.1.5 Effects of impurities on the properties of CO₂-dominated gas mixtures (F.May)

CO₂ separated from a full-scale oxy-fuel power plant may contain impurities from air entering into the boiler and excess oxygen. A purity of about 96.4 mol-% of CO₂ is expected with O₂, Ar, and N₂ as the main impurities. The amount of impurities is expected to increase as the boiler ages. Schöneich et al. (2007) have used the GERG 2004 Wide-Range Reference Equation of State for Natural Gases (Kunz et al. 2005) to calculate the properties of CO₂-dominated gases from oxy-fuel plants.

The three air components, mentioned above cause similar reductions of the density of pure CO₂, so that their actual partial pressures can be neglected a sum of about 4 mol-% N₂, as the main air constituent is taken as representative impurity in figure 4.9. The density of the two gases is calculated for average geothermal gradients and hydrostatic conditions. The pure CO₂ density curve passes through a two-phase state, (vapour-liquid equilibrium, VLE) at about 600 m depth. At initial reservoir conditions in about 3500 m depth, as in the Altmark Rotliegend reservoir, the effect of impurities is low. Larger deviations are expected during filling of the pressure depleted reservoir, especially in the probably narrow zone of mixing with residual natural gas and during shut-in of wells. Concentrations of impurities exceeding 5 mol-% will reduce the storage capacity of the reservoir significantly. In order to fill the available pore volume, efficiently with impure CO₂, the final reservoir pressure should exceed 50 % of the initial reservoir pressure.

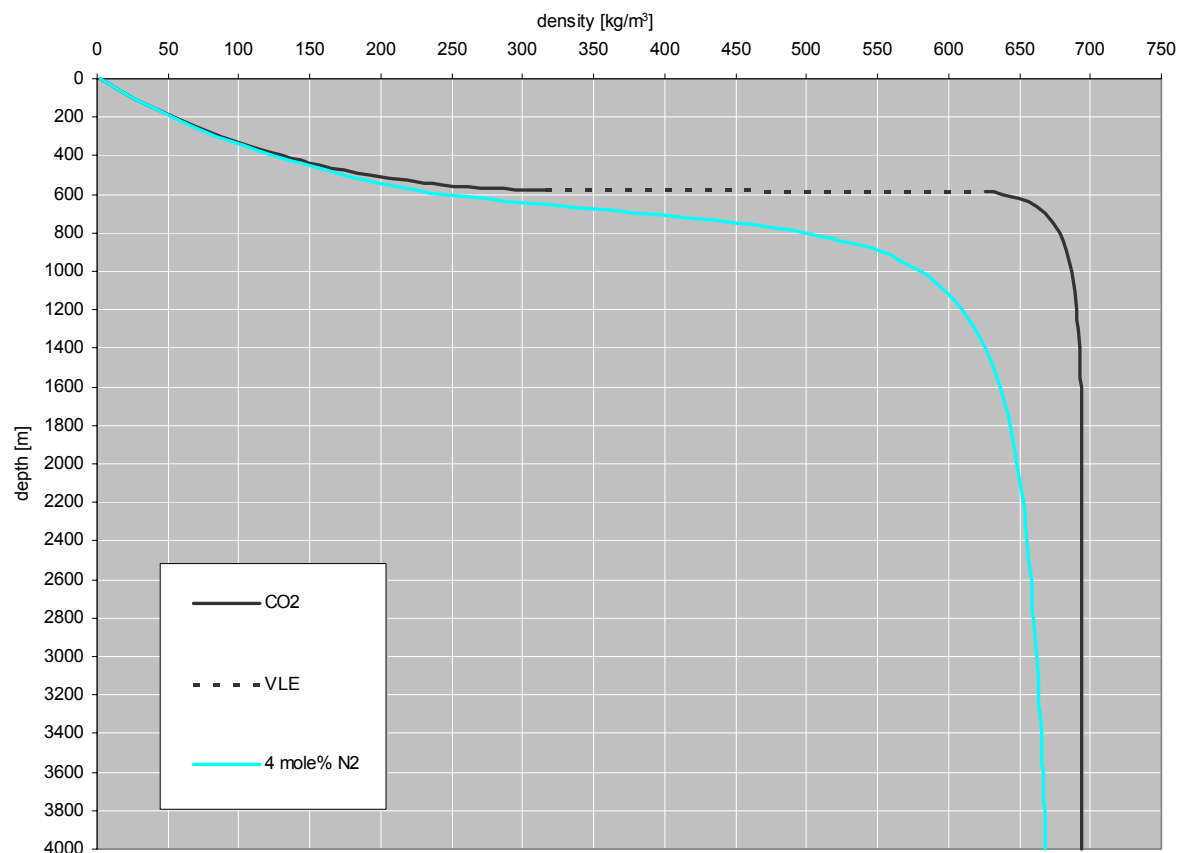


Figure 4.9: Density of pure CO₂ and CO₂ containing 4 mol-% of N₂, as function of depth (pressure and temperature).

The U.S. National Institute of Standard and Technology's Reference Fluid Thermodynamic and Transport Properties Database (REFPROP) software has been used to calculate gas densities. Nitrogen reduces the gas viscosity, while argon and oxygen admixtures only slightly impact the viscosity of the CO₂ rich mixtures. Thus, N₂ will affect the displacement of natural gas in the reservoir and EGR performance.

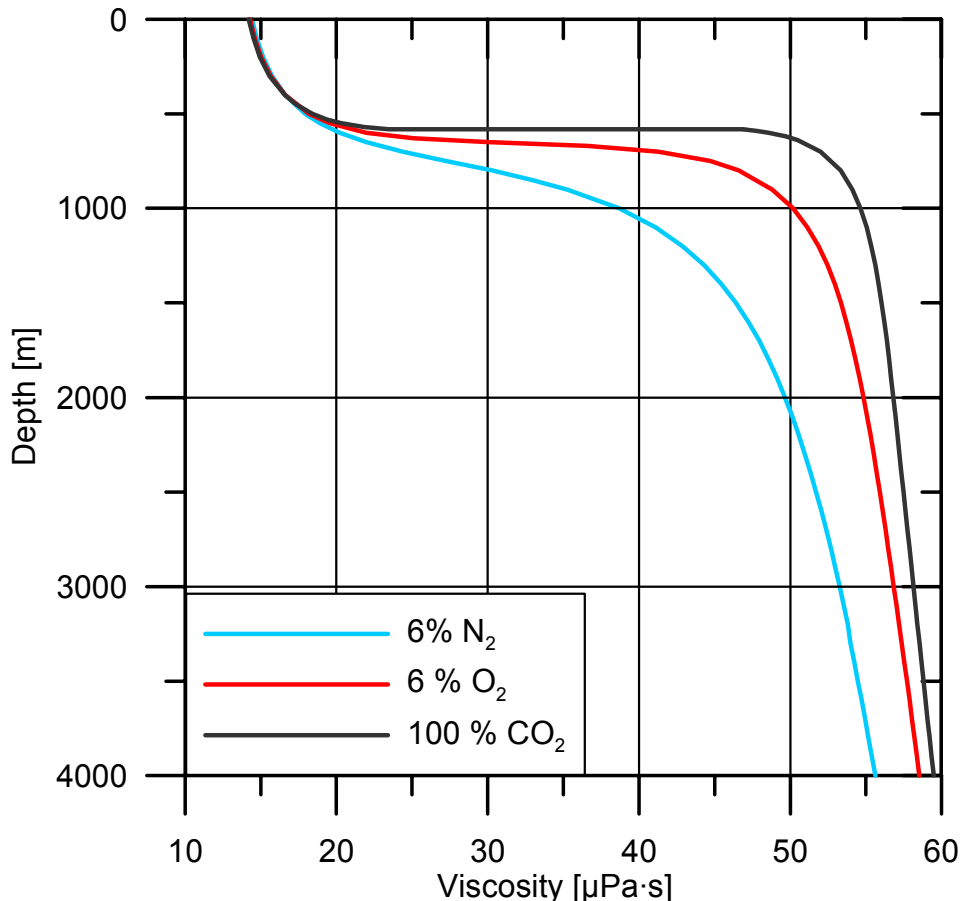


Figure 4.10: Density of pure CO₂ and CO₂ containing 6 mol-% of N₂ or O₂ as function of depth (hydrostatic pressure, temperature gradient of 33K/km).

At low pressures below the critical pressure and low temperatures, which could result from large injection rates and decompression of the gas within the reservoir, two phase conditions can occur, which would affect the relative permeability and reduce hinder spreading of CO₂ in the reservoir. Pressure-temperature conditions in the two-phase region shall be avoided. The two-phase region for CO₂ containing 6 mol-% of N₂ is indicated in figure 4.11. Under conditions enclosed by the blue curve two fluid phases can coexist in equilibrium, a high density CO₂ rich phase and a low density N₂-rich phase.

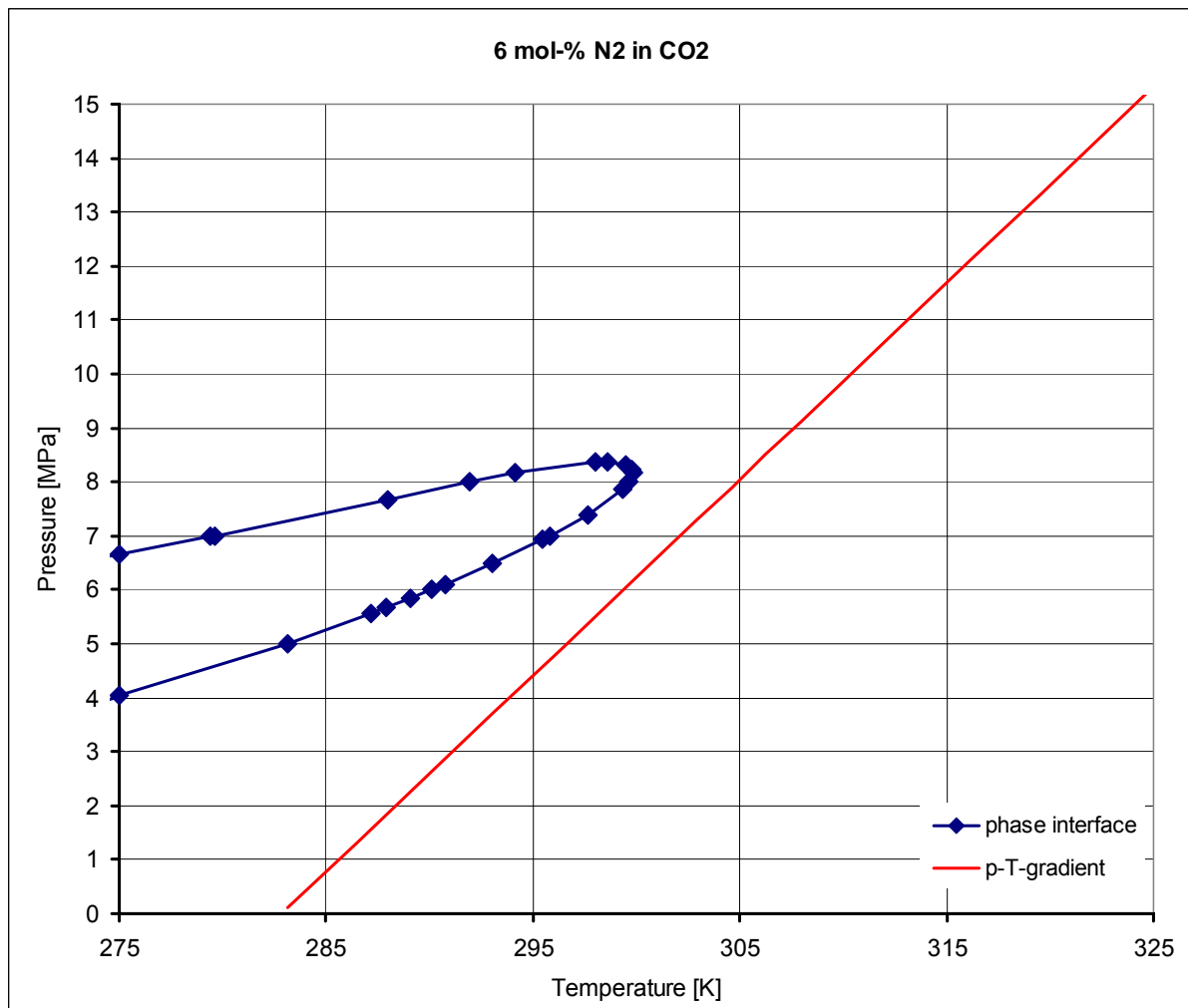


Figure 4.11: Phase envelope for CO₂ containing 6 mol-% of N₂ and p-T function of depth (hydrostatic pressure, temperature gradient of 33K/km).

4.2 Hydrodynamic Dispersion Effects

4.2.1 Introduction

The displacement of methane by CO₂ involves advective and diffusive transport mechanisms. Darcy's law well describes the advective flow, while the diffusion flow is controlled by Fick's law. If diffusion is combined with advection dispersive flow is created, which increases mixing of the injected CO₂ with methane. During CO₂ flooding of a depleted gas reservoir, CO₂ will undergo a spreading process beyond expected front position, following displacement flow principles in stratified layers. That is penetrating the higher permeability strata preferentially. This phenomenon whereby CO₂ concentration varies from strata to strata builds up a mixing zone and is generally termed **hydrodynamic dispersion**.

Hydrodynamic dispersion includes two basic transport phenomena; mechanical dispersion and molecular diffusion (Jacob Bear 1967). Mechanical dispersion describes mass transfer due to fluctuation of local velocity and molecular diffusion is caused by Brownian molecular flux due to concentration gradient. Actually, hydrodynamic dispersion should be incorporated in any model, defining gas mixing processes. In this chapter, effects of gas mixing,

CO_2 diffusion with its influencing parameters on CO_2 injection and mixing were investigated based on the dispersive flow model found in the ECLIPSE 300 code.

4.2.2 Parameters of Dispersion

Hydrodynamic dispersion coefficients elucidate dispersion processes in porous media by taking the bi-modal velocity dependent character of mechanical dispersion and molecular diffusion into account. The impact by diffusion during fluid flow in porous media is indeed small, especially at high velocities, but nevertheless is not to be neglected. According to Scheidegger (1961) the two physical processes (mechanical dispersion and molecular diffusion) can be combined into a coefficient of dispersion $D_{\text{disp.}}$, also called coefficient of hydrodynamic dispersion represented thus;

$$D_{\text{disp.}} = \underbrace{\alpha \bar{v}_f}_{\substack{\text{Dispersivity} \\ D=\text{Coefficient} \\ \text{Mechanical} \\ \text{dispersion}}} + \underbrace{D'_{o_{\text{eff}}}}_{\substack{\text{Molecular} \\ \text{Diffusion} \\ \text{coefficient}}}$$

The coefficient of mechanical dispersion D is defined as a function of the dispersivity α and the local velocity \bar{v}_f . The coefficient of hydrodynamic dispersion $D_{\text{disp.}} = D + D'_{o_{\text{eff}}}$ depends generally on velocity, molecular diffusion, and medium characteristic and includes both effects of mechanical dispersion and molecular diffusion as mentioned above.

Molecular diffusion, often called simply diffusion, is typically described mathematically using Fick's laws which relates the diffusive flux to the concentration field, by postulating that the net transport of molecules occurs from regions of high concentration to regions of low concentration, as a function of the concentration gradient by random molecular motion leading to a gradual mixing of material. In ECLIPSE simulator, the diffusion coefficients are input directly defined by conditions after Prausnitz *et al.* following Fick's law;

$$J_i = -c D_i \frac{\partial y_i}{\partial d}$$

c = total molar concentration, J_i = flux of component i per unit area

D_i and $\frac{\partial y_i}{\partial d}$ are the diffusion coefficient and molar concentration gradient of the component i .

These diffusion coefficients are used in ECLIPSE 300 to obtain gas inter-blocks diffusive flows in the form:

$$F_{ig}^{\text{diff}} = T_D D_{ig} (S_g b_g^m) \Delta y_i$$

Here,

T_D = Diffusivity (transmissibility for diffusive flow but porosity replaces permeability)

y_i = Vapour mole fractions, D_{ig} = Gas diffusion coefficient, S_g = Gas saturation

4.2.3 Calculation of Effective CO₂ Diffusion Coefficient

As mentioned above, molecular diffusion can be modelled in ECLIPSE simulator by solving diffusivity equations with diffusivities calculated from grid data. The simulation model requires a single explicit input for CO₂ diffusion coefficient at reservoir conditions. However, there is no reliable data available in open literature. Oldenburg *et al.* (2002) have suggested values in the range of 10⁻⁵ m²/s for CO₂ diffusion in natural gas. Nevertheless, Prausnitz *et al.* (1987) described several approaches to estimate diffusion coefficient at standard conditions. For a CO₂/CH₄ system estimation can be made after the Chapman and Enskog working equation:

$$D_{CO_2/CH_4} = \frac{1.86 \cdot 10^{-3} \cdot T^{1.5} \cdot \sqrt{M_{CO_2}^{-1} + M_{CH_4}^{-1}}}{p \cdot \sigma_{CO_2/CH_4}^2 \cdot \Omega}$$

D_{CO_2/CH_4} =Diffusion coefficient of CO₂/CH₄ system
 T =Temperature, K p =pressure, bar
 σ_{CO_2/CH_4} =Characteristic length, Å
 Ω =Collision integral, - M =Molecular weight
 $T^*=kT/\varepsilon_{CO_2/CH_4}$; A=1.06036; B=0.15610
C=0.19300; D=0.47635; E=1.03587
F=1.52996;
G=1.76474; H=3.89411

$$\sigma_{CO_2/CH_4} = \frac{\sigma_{CO_2} + \sigma_{CH_4}}{2}$$

$$\Omega = \frac{A}{(T^*)^B} + \frac{C}{\exp(DT^*)} + \frac{E}{\exp(FT^*)} + \frac{G}{\exp(HT^*)}$$

$$\varepsilon_{CO_2/CH_4} = (\varepsilon_{CO_2} \cdot \varepsilon_{CH_4})^{0.5}$$

For a CO₂/CH₄ system at standard conditions ($p_o = 1$ bar and $T_o = 273$ K) the diffusion coefficient, D_o , can be estimated with the above equation using values of needed parameter as obtained from Prausnitz *et. al.*.

$$\sigma_{CO_2} = 3.941 \text{ Å} \quad \text{and} \quad \sigma_{CH_4} = 3.758 \text{ Å} \quad \rightarrow \quad \sigma_{CO_2/CH_4} = 3.8495$$

$$\varepsilon_{CO_2}/K = 195.2 \text{ K} \quad \text{and} \quad \varepsilon_{CH_4}/K = 148.6 \text{ K} \quad \rightarrow \quad \varepsilon_{CO_2/CH_4}/K = 170 \text{ K}$$

Giving $\Omega = 1.169$ with $M_{CO_2} = 44$ g/mol and $M_{CH_4} = 16$ g/mol

$$D_o = 0.142 \text{ cm}^2/\text{s} \approx 1.4 \times 10^{-5} \text{ m}^2/\text{s}$$

Using Altmark Block 12 average data of 11 % porosity, we get an effective diffusion coefficient of;

$$D_{o_{eff}} = \frac{\phi\delta}{\tau} D_o = \tau\phi S_g D_o \approx \phi D_o \quad \rightarrow \quad D_{o_{eff}} = 1.5 \times 10^{-6} \text{ m}^2/\text{s}$$

where; ϕ = Porosity τ = Tortuosity δ = Medium characteristic

For known reservoir conditions the diffusion coefficient is computed as a function of pressure and temperature from standard conditions $D_o(p_o, T_o)$ (Vargaftik, 1975).

$$D_o(p, T) = D_o \frac{p_o}{p} \left(\frac{T}{T_o} \right)^n \quad D_{o_{eff}} = \phi D_o$$

Thus, assuming $n = 1.8$ and Altmark reservoir conditions of $p = 30$ bar, $T = 130$ °C;

$$D_o' = 10^{-7} \text{ m}^2/\text{s}$$

Hydrodynamic dispersion is considered and checked using a multiplying factor thus:

$$D_{disp} = M \cdot D_{o_{eff}}$$

M = Multiplier (in this study 0, 100, 1000)

4.2.4 Reservoir Simulation Model

The aims of the simulations are to investigate the effect of CO₂ diffusion and the relevant parameters of hydrodynamic dispersion on CO₂ drainage profiles. The base reservoir model is a layered 15 reservoir zones radial prototype Altmark block 12 model. The injected gas stream is pure CO₂. The reservoir top has a depth of 3050 m, with radius of 1000 m and a thickness of 212 m. Neglecting the non-reservoir interlayers the effective thickness is 77 m. The radial gridding is shown in Table 1.

Due to the lateral homogeneity of the reservoir, the formation properties in each model layer which are averaged and modified from properties of the block 12 Altmark model (Table 4.3) are assumed to be constant over the entire grid layer. The porosity/permeability distributions of the model follow a layered model (Figure 4.12). An injector and producer well is placed at the centre of the reservoir. The injection control is based on constant gas rate of 70000 m³/d, whereas for the production phase the production control is by a constant well head pressure of 15 bar using vertical flow performance table generated by VFP*i* software for a wide range of flow rates. The well is perforated in all reservoir layers. The k_v/k_h is set to 1. The formation properties distributions can be seen in Figure 2 as well as the relative permeability curves. The PVT*i* software is used to generate the necessary PVT data with 4 components Altmark B12 gas for the simulation (CH₄, N₂, CO₂, H₂O).

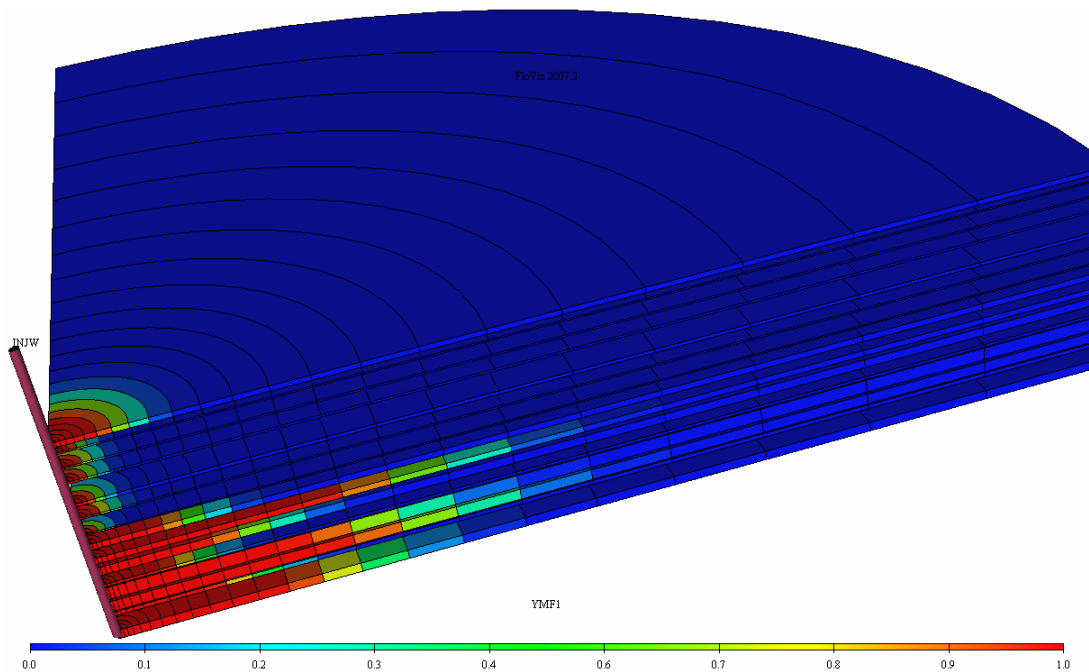


Fig. 4.12: Quarter of prototype Altmark block 12 radial model with CO₂ layer distribution.

Table 4.2: Radial grid dimensions; inner wellbore radius is 0.09 m and r = outer block radius.

| Block | 1 | 2 | 3 | 4 | 5 | 6 | 7 | 8 | 9 | 10 | 11 | 12 | 13 | 14 | 15 | 16 | 17 | 18 | 19 | 20 | 21 | 22 | 23 | 24 | 25 | 26 | 27 |
|---------|-----|---|---|---|---|----|----|----|----|----|----|----|-----|-----|-----|-----|-----|-----|-----|-----|-----|-----|-----|-----|-----|-----|------|
| r , m | 0.1 | 1 | 3 | 6 | 9 | 14 | 20 | 29 | 39 | 52 | 67 | 84 | 104 | 128 | 156 | 188 | 224 | 268 | 320 | 380 | 448 | 524 | 614 | 718 | 836 | 968 | 1114 |

Table 4.3: Formation properties and injection potential correlated with layer capacity after one year injection (approx. 26 Mm³ CO₂).

| Layer | ϕ | h_i , m | Base Case | | | |
|-------|--------|-----------|------------|------------|--------------|----------------------------|
| | | | k_i , mD | k_i/ϕ | kh_i , mDm | % Injected CO ₂ |
| R1 | 0.07 | 5.14 | 2.07 | 30 | 10.64 | 0.34 |
| I 1 | 0.05 | 5.40 | 0.16 | 3 | 0.86 | 0 |
| R2 | 0.05 | 1.51 | 0.23 | 5 | 0.35 | 0.01 |
| I 2 | 0.04 | 13.67 | 0.13 | 3 | 1.78 | 0 |
| R3 | 0.06 | 1.69 | 0.30 | 5 | 0.51 | 0.02 |
| I 3 | 0.03 | 13.24 | 0.05 | 2 | 0.66 | 0 |
| R4 | 0.05 | 2.09 | 0.24 | 5 | 0.50 | 0.02 |
| I 4 | 0.05 | 20.78 | 0.24 | 5 | 4.99 | 0 |
| R5 | 0.04 | 3.30 | 0.16 | 4 | 0.53 | 0.02 |
| I 5 | 0.03 | 11.71 | 0.07 | 2 | 0.82 | 0 |
| R6 | 0.07 | 1.68 | 0.39 | 6 | 0.66 | 0.02 |
| I 6 | 0.04 | 15.39 | 0.12 | 3 | 1.85 | 0 |
| R7 | 0.03 | 1.38 | 0.05 | 2 | 0.07 | 0.01 |
| I 7 | 0.03 | 9.91 | 0.07 | 2 | 0.69 | 0 |
| R8 | 0.07 | 6.24 | 4.63 | 66 | 28.89 | 0.96 |
| I 8 | 0.03 | 9.34 | 0.05 | 2 | 0.47 | 0 |
| R9 | 0.11 | 6.00 | 77.36 | 703 | 464.16 | 14.37 |
| I 9 | 0.03 | 4.15 | 0.07 | 2 | 0.29 | 0 |
| R10 | 0.09 | 8.52 | 14.63 | 163 | 124.65 | 4.08 |
| I 10 | 0.03 | 10.05 | 0.07 | 2 | 0.70 | 0 |
| R11 | 0.10 | 2.82 | 5.56 | 56 | 15.68 | 0.54 |
| I 11 | 0.11 | 1.07 | 11.31 | 103 | 12.10 | 0 |
| R12 | 0.14 | 12.78 | 70.44 | 503 | 900.22 | 28.84 |
| I 12 | 0.03 | 2.54 | 0.08 | 3 | 0.20 | 0 |
| R13 | 0.15 | 10.67 | 105.08 | 701 | 1121.20 | 35.78 |
| I 13 | 0.05 | 1.28 | 0.16 | 3 | 0.20 | 0 |
| R14 | 0.12 | 4.16 | 14.98 | 125 | 62.32 | 2.11 |
| I 14 | 0.03 | 15.90 | 0.06 | 2 | 0.95 | 0 |
| R15 | 0.12 | 9.18 | 42.25 | 352 | 387.86 | 12.88 |

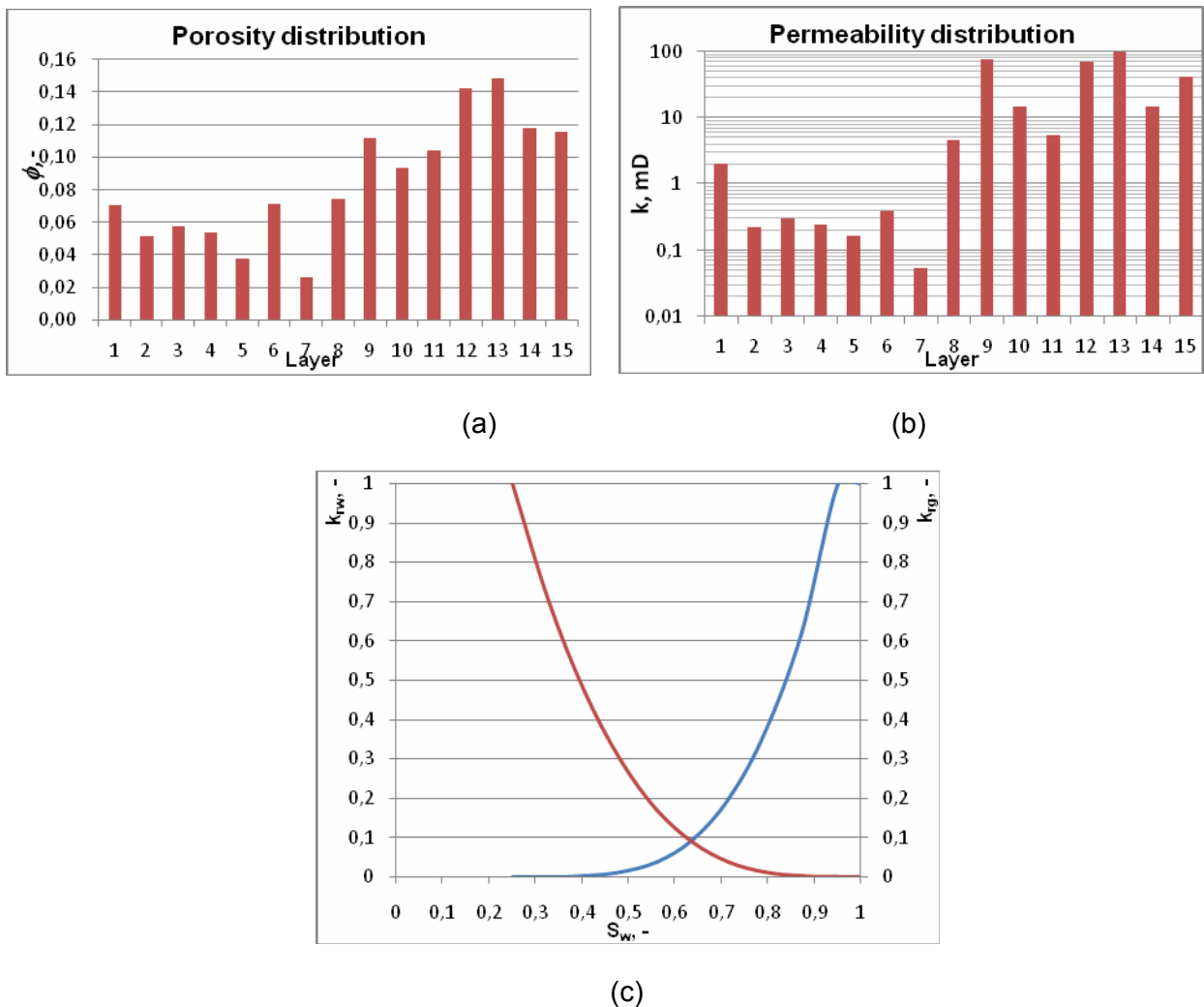


Fig. 4.13: Flow and storage properties of the Altmark block 12 prototype model: (a) porosity, (b) permeability distributions and relative (c) permeabilities.

4.2.5 Results of Sensitivity Analysis

4.2.5.1 Hydrodynamic and Numerical Dispersion

Figure 4.14 shows the simulation results of CO₂ front advancement and the mixing zone after 1 year of CO₂ injection in all 15 layers of the prototype model, where mixing is due to molecular diffusion, mechanical and numerical dispersion. Using a $D_{o\text{eff}} = 1.5 \times 10^{-7} \text{ m}^2/\text{s}$ a base for CO₂ diffusion, two cases are run with multipliers of M=100 and M=1000 using $D_{\text{disp.}} = M \cdot D_{o\text{eff}}$. It can be noticed that the front propagation is a function of the k/ϕ value and also a considerable dispersion effect can be noticed in case b, where the dispersion coefficient is taken very high.

Numerical dispersion is an artificial effect from finite difference approximations of differential equations for two-phase flow front advancement in Cartesian grid systems. The displacing phase does not enter the grid block frontally, but fills up the block from bottom or top, depending on density differences. Thereby the displacing phase reaches the end of the block simultaneously when it enters. This phenomenon causes an early break-through of the displacing phase, depending on the grid length. Numerical dispersion disappears

when grid size becomes very small. CO_2 injection into a gas reservoir and mixing is a one-phase flow phenomenon, but suffers also from numerical error of grid size effects.

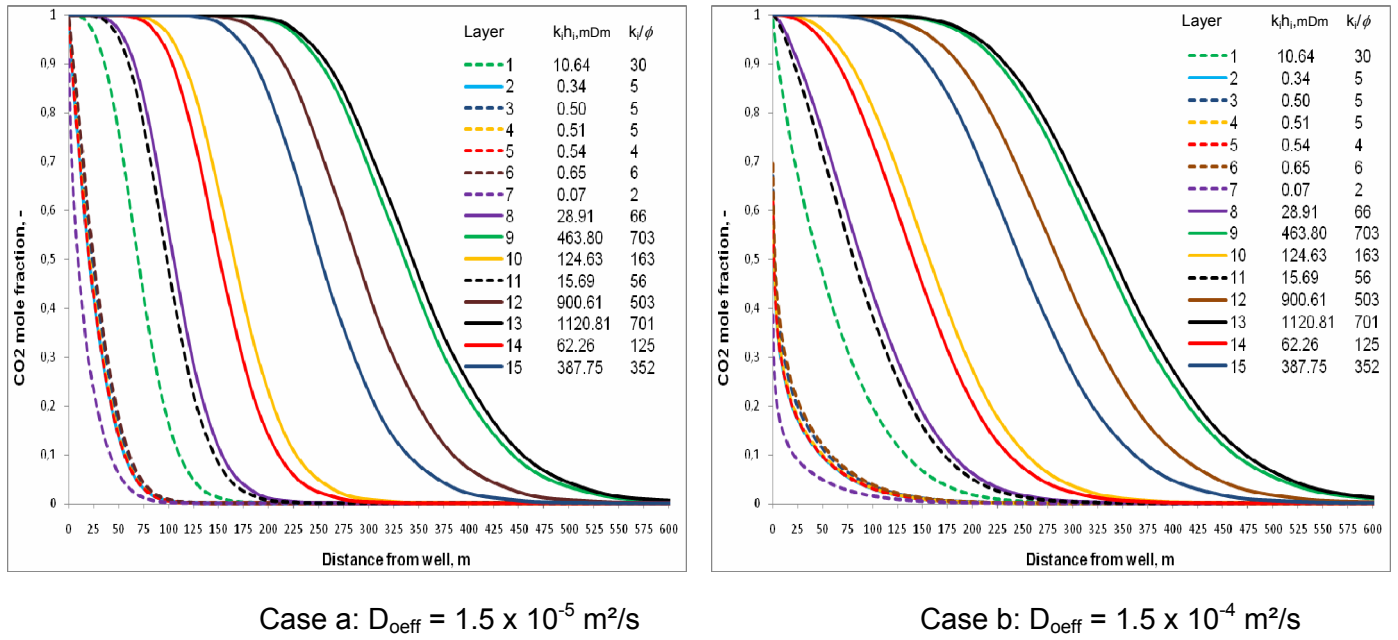


Fig. 4.14: CO_2 mole fraction profiles for all 15 layers at time of 1 year for case a $M=100$ and case b $M=1000$

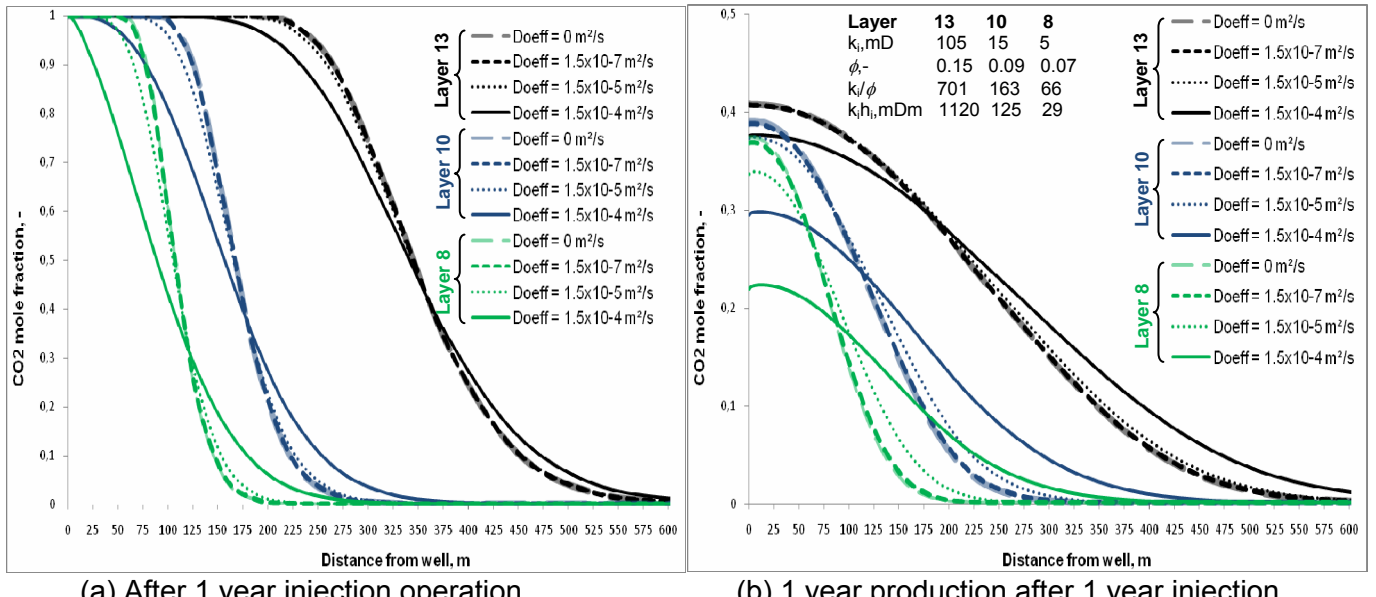


Fig. 4.15: CO_2 mole fraction profile showing different diffusion coefficient effects with multipliers of $M = 0, 1, 100$ and 1000 . Injection rates are $70,000 \text{ m}^3/\text{d}$, production is controlled by constant well head pressure of 15 bar.

The Figure 4.15 illustrates both the front propagation as a function of k_i / ϕ and in more detail the CO_2 dispersion effect during injection and reproduction from the same well in the form of CO_2 mole fraction. Several runs were performed with different dispersion coefficients; $0, 10^{-7}, 10^{-5}$ and $10^{-4} \text{ m}^2/\text{s}$. A noticeable CO_2 dispersion effect is seen in the situation with a multiplier $M=1000$, i.e. $1.5 \times 10^{-4} \text{ m}^2/\text{s}$, and as the multiplier reduces, the rate of

mixing by hydrodynamic dispersion also reduces. Values of $D_{\text{eff}} < 10^{-6}$ show no significant change on the profiles. It can thus be concluded that diffusion is negligible and mixing is purely due to mechanical dispersion depending on reservoir heterogeneity (permeability variation).

The mixing zone extension (distance between 0.1 to 0.9 CO₂ mole fraction positions) for some chosen layers is shown in Table 3 after one year of injection (25.5 Mm³). Numerical dispersion in this case has partially been accounted for by subtracting read-off dispersion values from base case with $D_{\text{eff}}=0$ m²/s and by using a grid refinement factor 10. It can be noticed that the effective mixing zone length calculated by a diffusion multiplier $M=1000$ and corrected partially for the influence of numerical dispersion follows inversely the k/ϕ trend.

Table 4.4: Mixing zones for 2 cases with different CO₂ diffusion coefficients showing incremental dispersion effect. Numerical dispersion is corrected by subtracting read-off dispersions from base run (no diffusion) using grid refinement of a factor 10.

| Layer | 8 | 9 | 10 | 11 | 12 | 13 | 14 | 15 |
|-------------------------|-------------------------------------|-----|-----|----|-----|-----|-----|-----|
| k_i , mD | 66 | 703 | 163 | 56 | 503 | 701 | 125 | 352 |
| Mixing Zone, m | $D_{\text{eff}}=1.5 \times 10^{-5}$ | 21 | 10 | 15 | 25 | 10 | 9 | 15 |
| | $D_{\text{eff}}=1.5 \times 10^{-4}$ | 88 | 54 | 81 | 92 | 62 | 56 | 83 |
| Eff. Mix Zone Length, m | 67 | 44 | 66 | 67 | 52 | 47 | 68 | 55 |

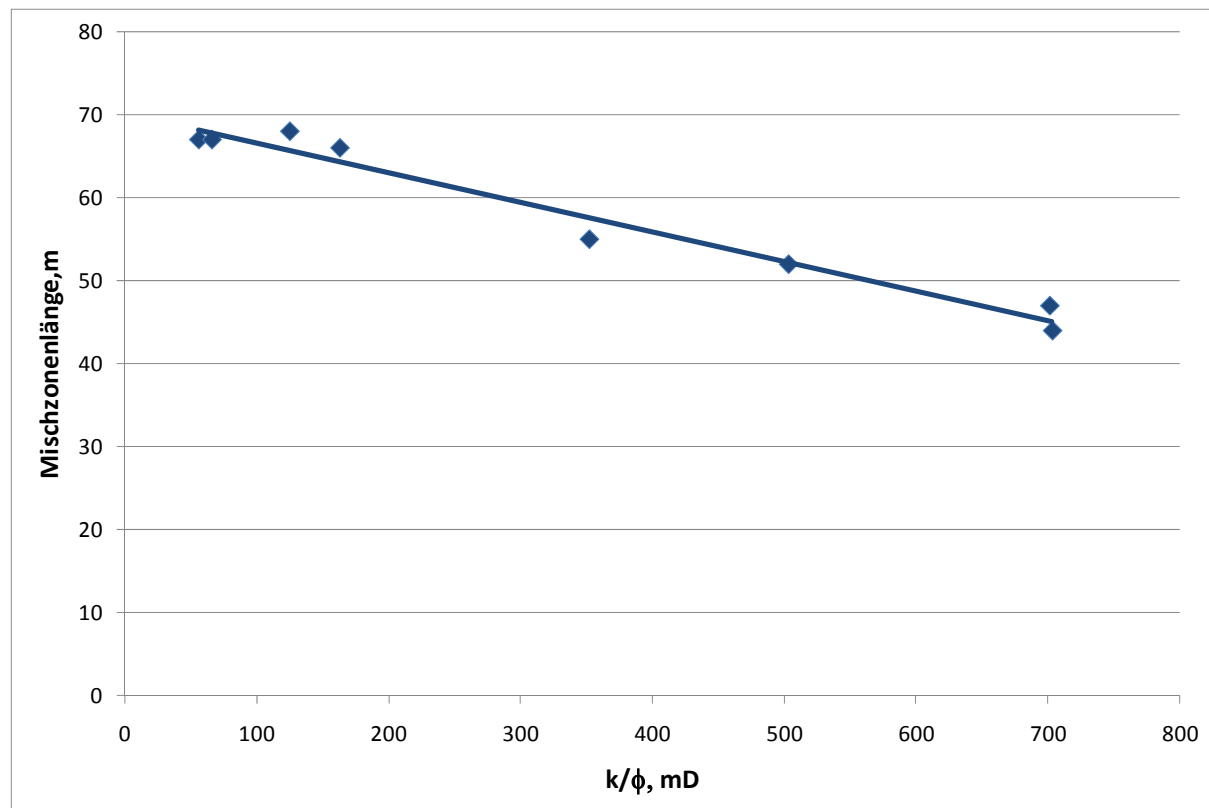


Fig. 4.16: Mixing Zone length after injection of 5 % pore volume CO₂

4.2.5.2 Gravity Effects with Cross Flow between Layers

Open literature shows that gravity is a dominant factor which will cause the less dense phase to migrate to the top of the reservoir. CO₂ which is generally more dense and viscous than CH₄ at reservoir conditions, will move downwards and therefore will influence the mixing process especially in the presence of cross flow. The radial grid model was modified to allow cross flow which was achieved by activating the non-pay inter-layers. In order to keep consistency, adjustments were made such that the non-pay zones contributed while increasing the gas-in-place by just 1.4 %. Figure 4.17 illustrates CO₂ mole fraction of two vertically overlying layers (13 and 14) at different diffusion coefficients to elucidate gravity effects. There is a clear downward shift of the profiles in the layer 13 (upper) and an upward shift in layer 14 (lower) which clearly indicates a CO₂ feeding of layer 14 by layer 13. This can be explained by gravity segregation of denser CO₂ and the existence of cross flow. The magnitude of downward and upward profile shifts for layer 13 and 14 respectively indicates once more the CO₂ dispersion and mixing with CH₄. The higher the diffusion coefficient, the larger the mixing zone and vice versa. The effect is much pronounced in 14 because its thickness is almost half that of 13 corresponding also with the smaller values of kh and k/φ.

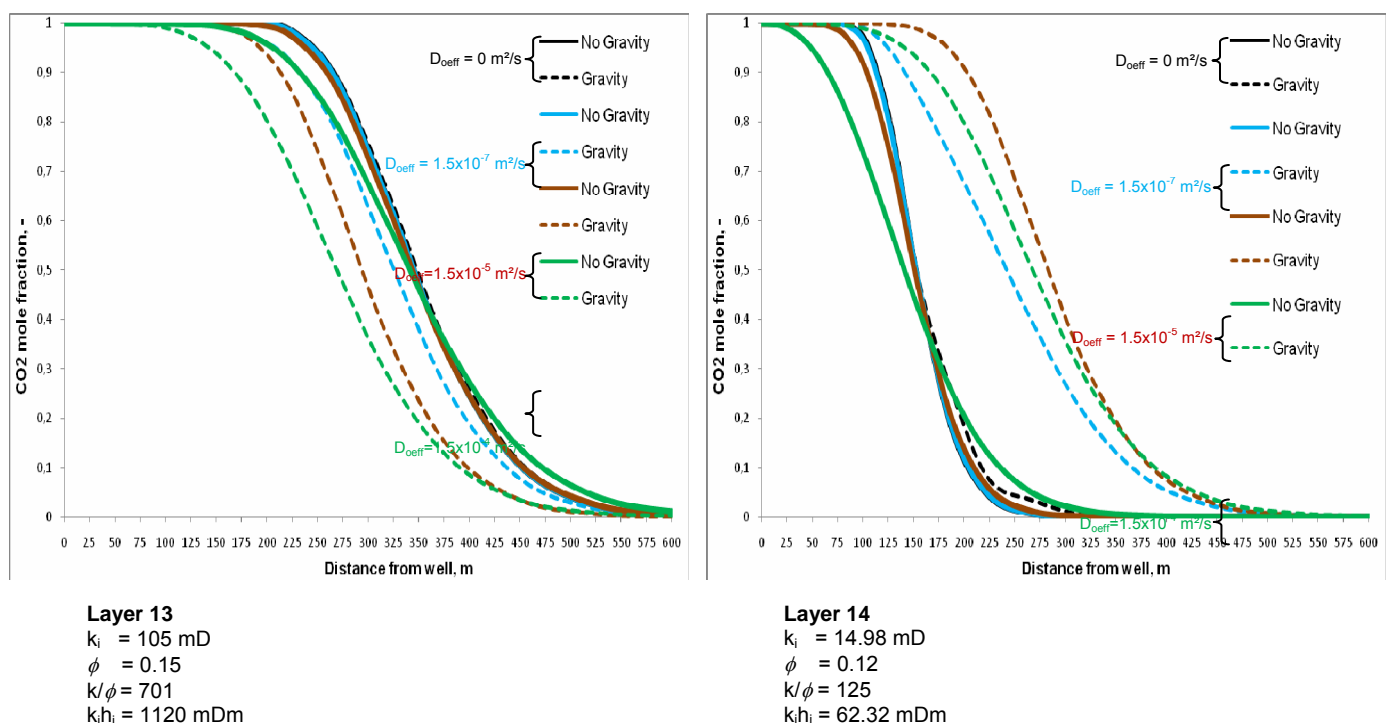


Fig. 4.17: Gravity Effects showing cross flow between layers 13 and 14 after 1 year CO₂ injection

4.2.5.3 Rate Effects – Injection/Production Profiles

As already mentioned by Fick's law, molecular diffusion is a function of the local concentration gradient. Thus, changes in concentration lead to changes in density which affects the flow regime and thence the flow velocity. This process is time dependent and hence the overall influence on hydrodynamic dispersion will be more significant at low flow velocities when advective transport is negligible. Actually, even at zero velocity molecular diffusion does take place. Figure 4.18 shows the effect of flow velocity from simulation runs

with different injection and production rates. From Figure 4.18a it follows that at any point the mixing zone, i.e. 90 % to 10 % of total CO₂ mole fraction concentration change, is directly proportional to the flow velocity (injection rate). This is illustrated in the CO₂ mole fraction profile as it steepens with reduction of rate.

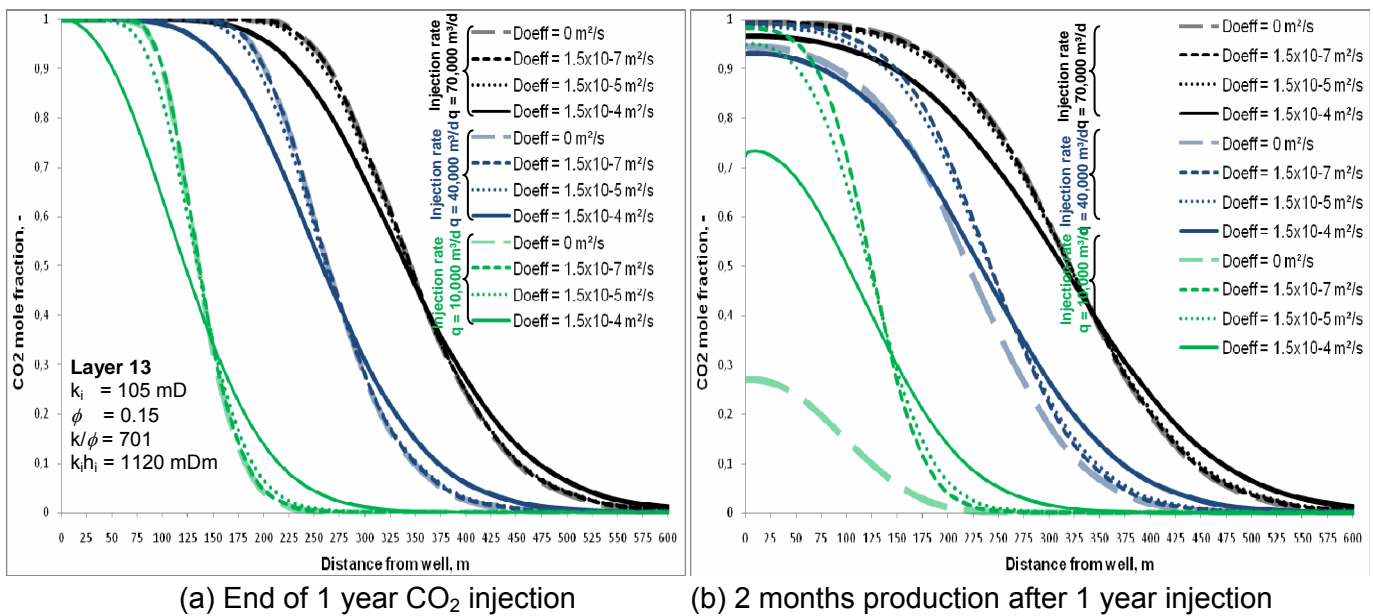


Fig. 4.18: CO₂ mole fraction at various injection and production rates.

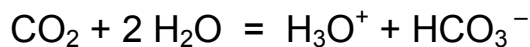
4.3 Physical Rock Alteration-Impact on Flow Processes

The Buntsandstein and Rotliegend rock type in Germany is characterized as siliciclastic, with individual grain size distribution, depending on the depositional environment, containing various cement minerals. Typical cement representatives are quartz, feldspar, calcite, dolomite, kaolinite, muscovite-illite, chlorite, and anhydrite.

Examples of mineralogical analyses are given in the Annexes to chapter 5. Especially for the Rotliegend formation diagenetic alterations of the compounds play an important role.

The cement quality is also responsible for the type of rock deformation as elastic or inelastic mode.

If carbon dioxide dissolves into the formation water, a weak acid is formed:



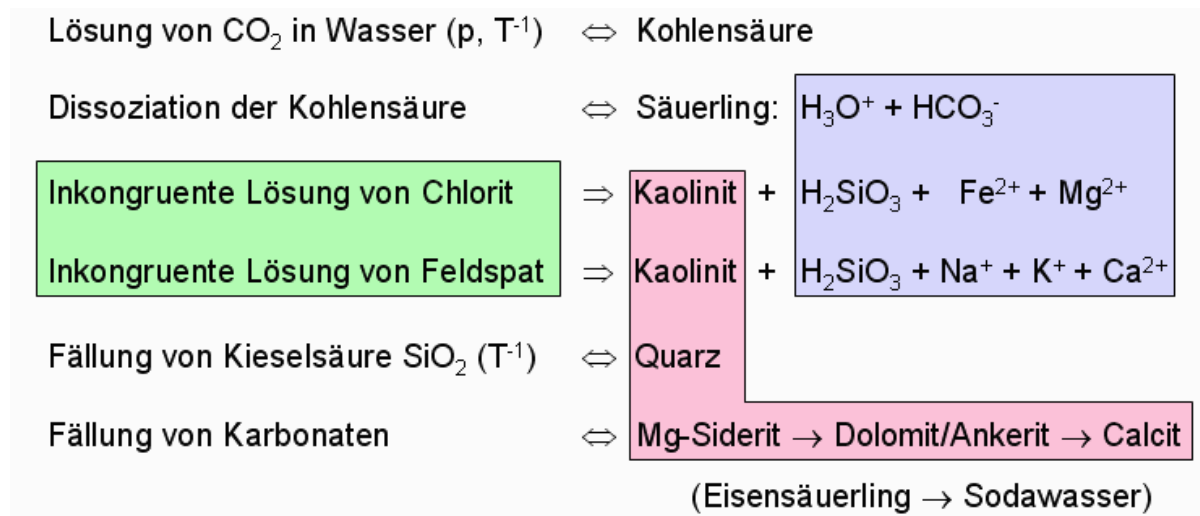
If the reaction occurs at normal temperatures, the pH-value yields 3,88. The acidic strength of the carbonic acid is comparable with formic acid and acetic acid.

The reactivity of this weak acid with the rock compounds depends strongly on the temperature, salt composition and concentration of the interstitial water and on the carbon dioxide pressure.

The quartz matrix of the siliciclastic rock is almost stable against carbonic acid, whereas other cement compounds behave more or less reactive.

The following table shows the most relevant chemical reactions of carbonic acid with types of cement minerals.

Table 4.5: Principle Reactions involved in alteration of siliciclastic rocks in CO₂-rich waters in the Rhenish Massif. Green: instable primary minerals, pink: secondary minerals, blue: dissolved species. After F. May



Another relevant physical interaction of the injected CO₂ on the connate water saturation is the “drying effect” observed in the previous field tests by vaporization of connate water into the gas phase. This phenomenon increases the concentration of the minerals in the brine and may cause super-saturation of mineral species with the lowest solubility according to the temperature dependent solubility product. As a follow-up of super-saturation mineral precipitation may occur, which can lead to pore plugging and reduced flow capacities.

In order to study these phenomena a fine gridding pattern is used to cope with the microscopic dimensions of the capillary phenomena. The compositional simulator ECLIPSE 300 is able to model the vaporization; however it cannot predict the mineral precipitation.

A synthetic model was prepared in order to be able to study the phenomenon of near well-bore connate water vaporization; this model is a radial one with the well in the centre, the basic permeability and porosity data are taken from the Altmark Block 12 Model as well as the number of layers (15). The radial grid used had an exponential increase in the radius of the cells from the centre to the outer boundary of the model as one can see in Figure 4.19. The ECLIPSE GASWAT option was used, which accounts for the presence of the water vapor in the gas phase as well as for the dissolution of different gases into the water. Presently the salt precipitation effects have not been included. In future this constraint has to be incorporated. The injection rate used in this study was 70000 m³/d (at standard conditions). The vaporization is instantaneous and the CO₂ flowing out of a reservoir element is considered to be water saturated until the whole quantity of water in the block is vaporized. The main parameters that control the vaporization effect are the pressure

(see Figure 4.20) and temperature (100°C constant) at which the injection begins. The reason lowering temperature compared to the real Altmark case is the fact that GASWAT option will be compared with CO₂ STORE option and the later is supposed to work only until 100°C . One can clearly see that, as the pressure at the initiation of the process is low (end of depletion) the vaporization is faster and more pronounced. This vaporization effect will provide higher injectivity for the gas (CO₂), when salt precipitation does not occur.

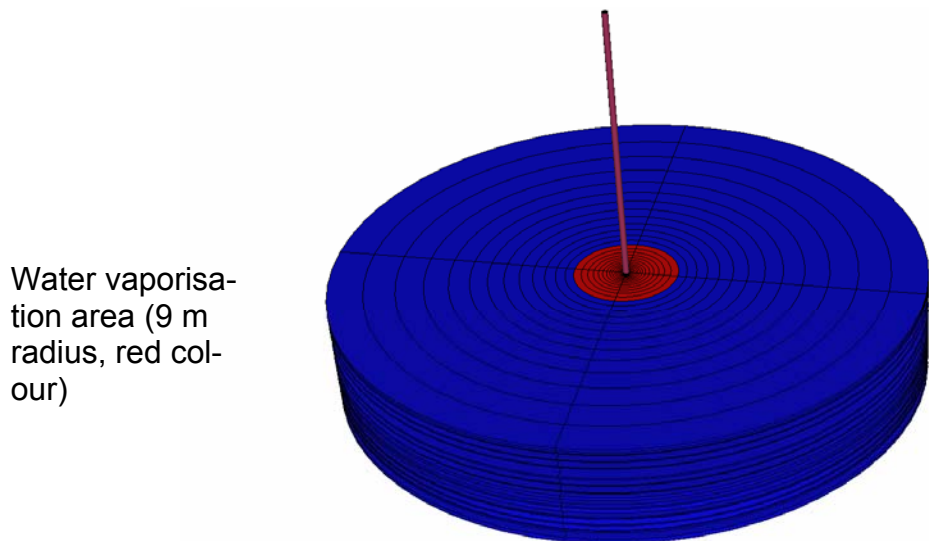


Fig. 4.19: Radial model for the study of connate water vaporization effects (gridding identical with Table 4.2).

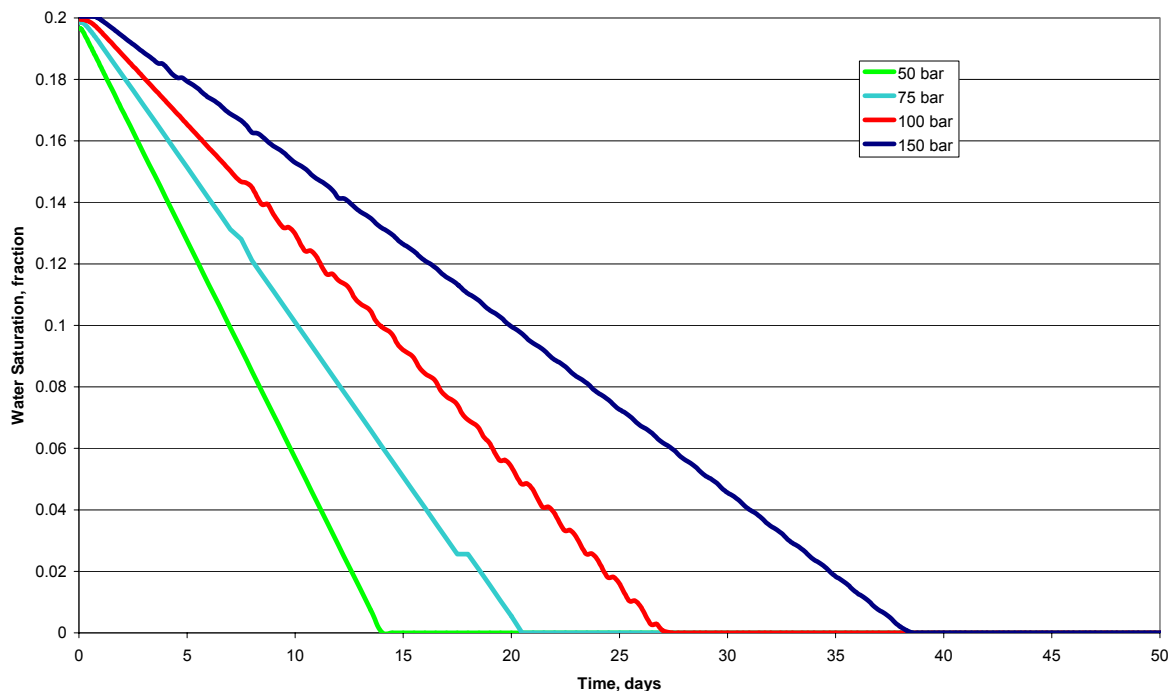


Fig. 4.20: Influence of initial pressure on the water vaporization near a CO₂ injection well

A coarse grid size will tend to underestimate the vaporization process as can be seen in Figure 4.21. So in general in order to better describe the process a relatively fine grid in

the vicinity of the injection well should be introduced. In case of large models this can be achieved by using local grid refinement (LGR) that also combines the radial flow in the block where the well is located permitting a better pressure distribution in this case.

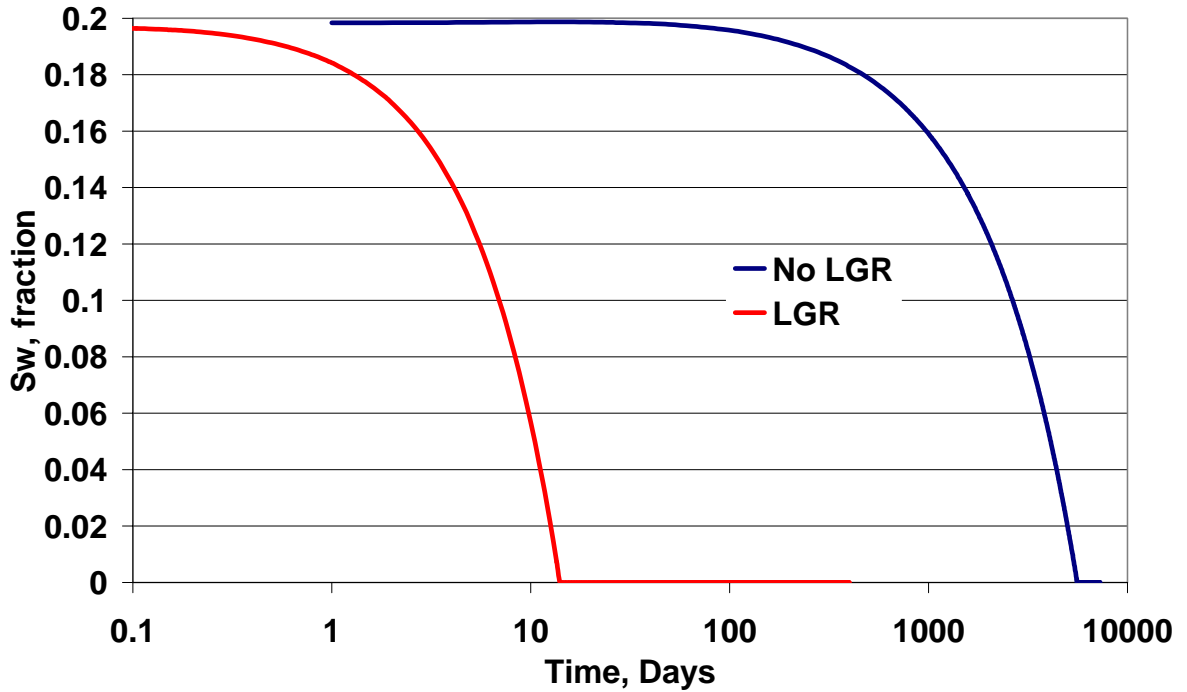


Fig. 4.21: Influence of grid block size on vaporization

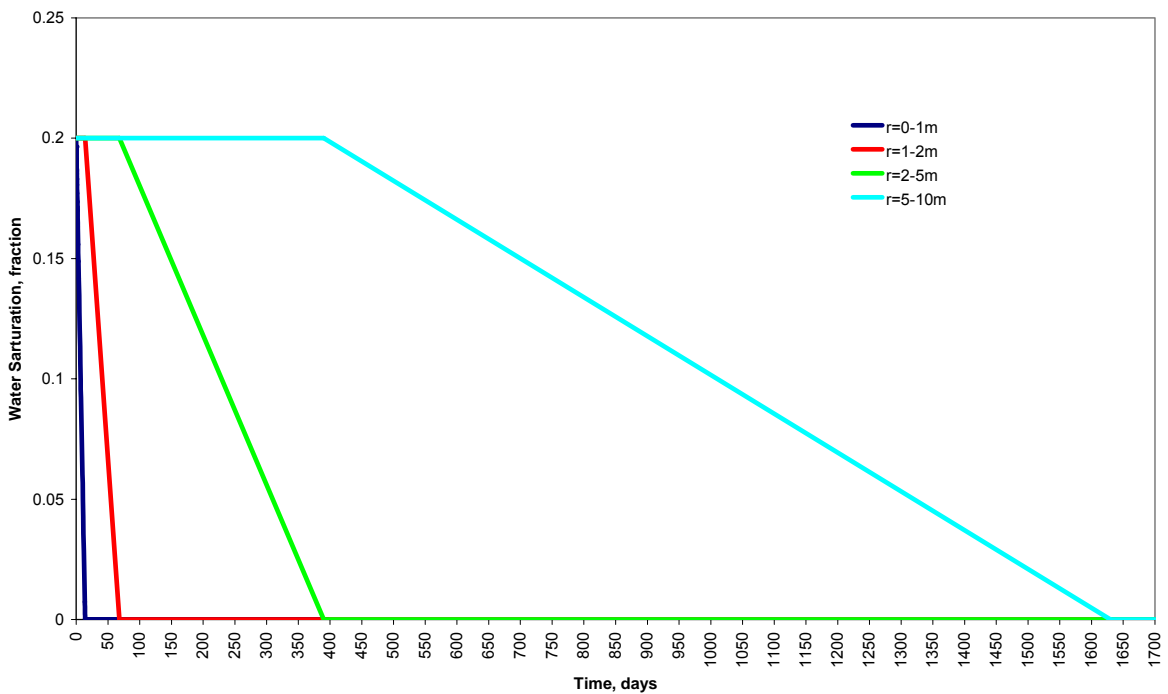


Fig. 4.22: Water vaporization at different distance from the wellbore

The saturation profiles in the Figure 4.22 demonstrate how the process of water vaporization is treated in ECLIPSE. One can observe that practically the process affects only one block at a time and only after the saturation in that block is zero the evaporation will start in

the next block. In Figure 4.20 the reservoir was not in communication with any external source of water, while for Figure 4.23 a weak aquifer was attached to the reservoir. The small difference in water saturation at the beginning of the injection can be explained due to the fact that in the no aquifer case the capillary pressure was neglected, whereas in the case with aquifer a capillary pressure curve is given, that causes a small (1%) difference in the initialization process of saturation. It can be seen by the comparison that even though initially the vaporization is not varying, the capillary forces will produce a re-saturation of water in the nearby well region. In this case the mineral concentration in the connate water will rise until the conditions of precipitating salts (super-saturation) are achieved and plugging may occur, thus reducing the permeability in the nearby region of the well.

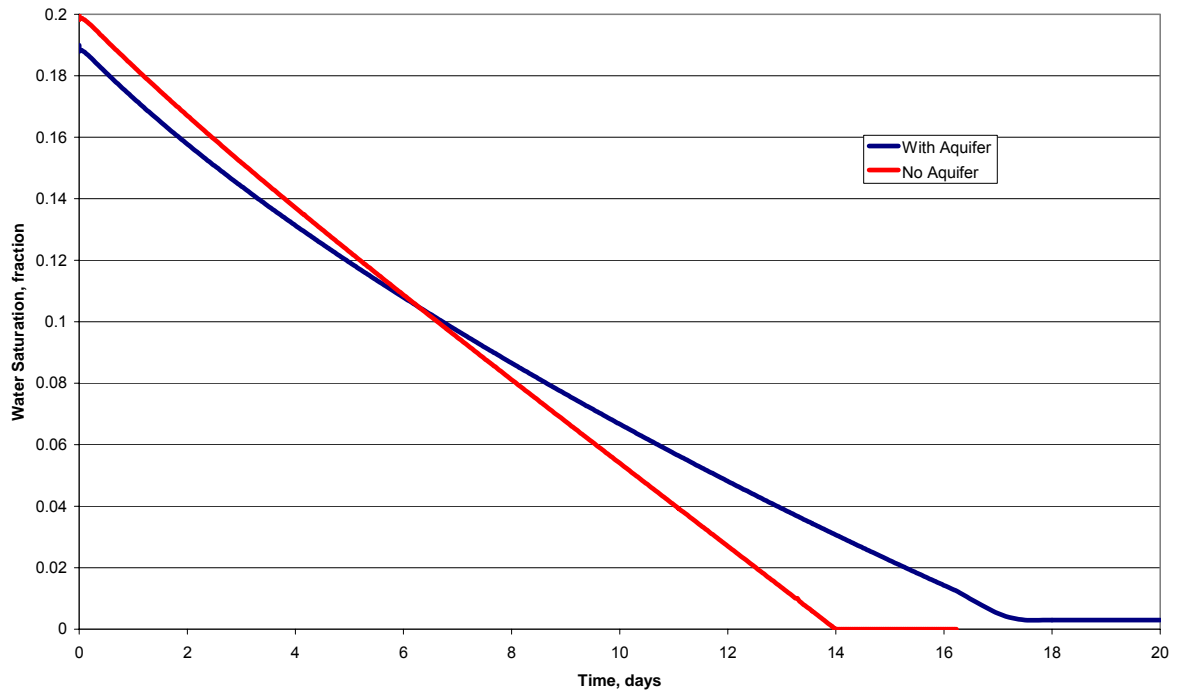


Fig. 4.23: Effect of the presence of an aquifer with capillary contact on the water vaporization.

Finally, a comparison between the vaporization effects of CO₂ and methane was performed. From Figure 4.24, it is clear that CO₂ has a larger potential of vaporizing the connate water. The theory supports these findings.

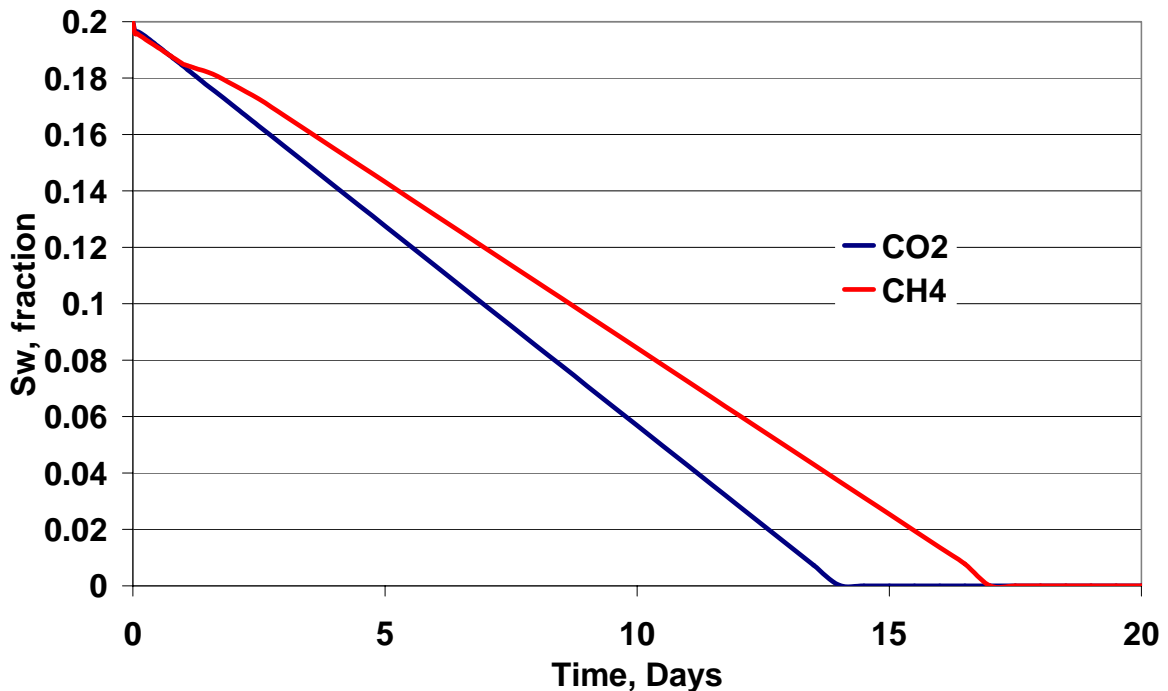


Fig. 4.24: Comparison of vaporization effects using 2 different gases

A comparison was made also with the new ECLIPSE option CO2 STORE (Figure 4.25).

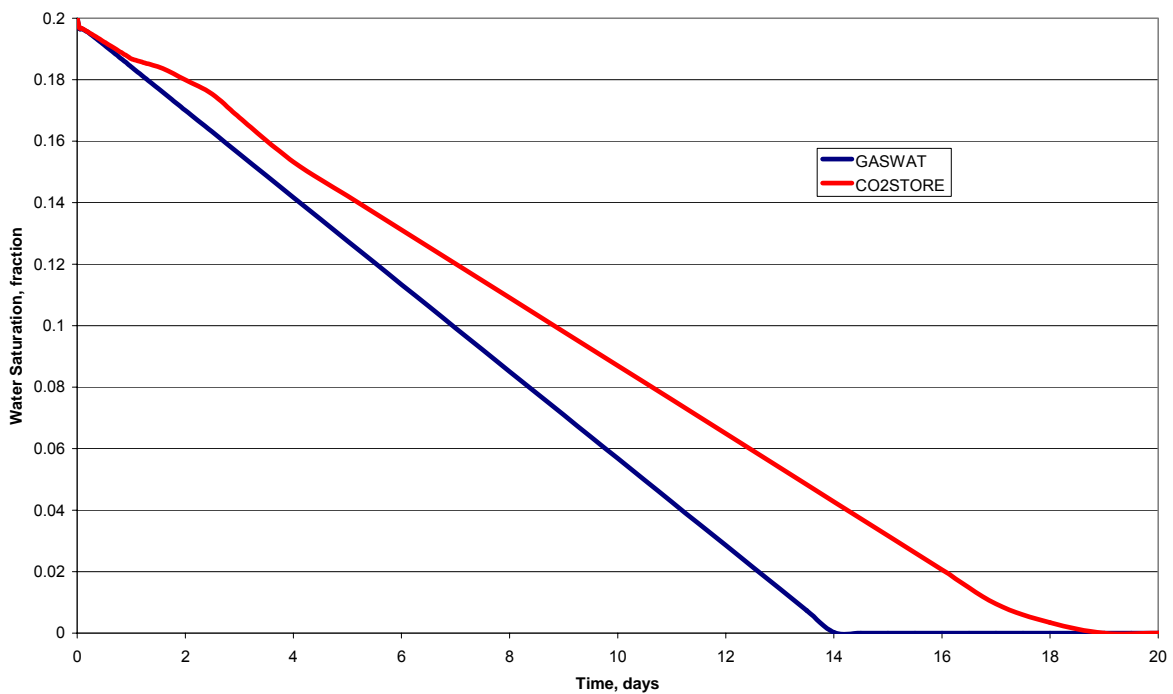


Fig. 4.25: Comparison between GASWAT and CO2 STORE, observation segment 0.09 -1 m

One can observe that in the CO2 STORE option the vaporisation process is slower. However this option uses only CO₂ and Water as phases, one cannot use any gas components (e.g. A-gas) and also the maximum temperature covered is only 100°C so it cannot be used in Altmark case where the temperatures are in range of 120 to 140°C.

The dissolution of CO₂ into the formation water can be modelled by the simulation program ECLIPSE using the embedded option CO₂ Store based on Redlich-Kwong equation of state and extended by the modification of Spycher and Pruess. The impact of salt concentration and mono- and divalent ionic composition is considered via the expression of ionic strength.

$$y_{H_2O} = \frac{K_{H_2O}^0 a_{H_2O}}{\Phi_{H_2O} P_{tot}} \exp\left(\frac{(p_{H_2O} - p^0) \bar{V}_{H_2O}}{RT}\right)$$

$$x_{CO_2} = \frac{\Phi_{CO_2}(1 - y_{H_2O}) p_{tot}}{55.508 \gamma_x' K_{CO_2(g)}^0} \exp\left(\frac{(p_{CO_2} - p^0) \bar{V}_{CO_2}}{RT}\right)$$

In these equations, y_i is the mole fraction of the component i in the gas phase, x_i is the mole fraction of i in the liquid phase, K^0 is the thermodynamic equilibrium constant for each component at temperature T and reference pressure $p_0 = 1$ bar, for respective reactions H₂O_(l) ↔ H₂O_(g) and CO_{2(aq)} ↔ CO_{2(g or l)}. p_{tot} is total pressure, p_i is the partial pressure of component i , \bar{V} is the average partial molar volume of each pure condensed phase over the pressure range $p_i - p_0$, Φ is the fugacity coefficient of each component in the CO₂-rich (compressed gas) phase, and R is the gas constant. The effect of dissolved salts is expressed through a_{H_2O} , the activity of liquid water up to a ionic strength of 6 molal, and $\gamma'x$, an activity coefficient for aqueous CO₂. For consistency $\gamma'x$ is on a mole fraction scale and is unity when no salts are present (i.e., $\gamma'x \rightarrow 1$ as $x_{salt} \rightarrow 0$).

In ECLIPSE 300 the PVT option which is applicable not only to gas-gas and gas-oil systems, but also to gas-water systems has been termed as PVTi, which means that additionally to the equations of state represented in this mode, the input (i) of modifying tables or correlations is possible. The graphic presentations of these relationships are shown in the following figures.

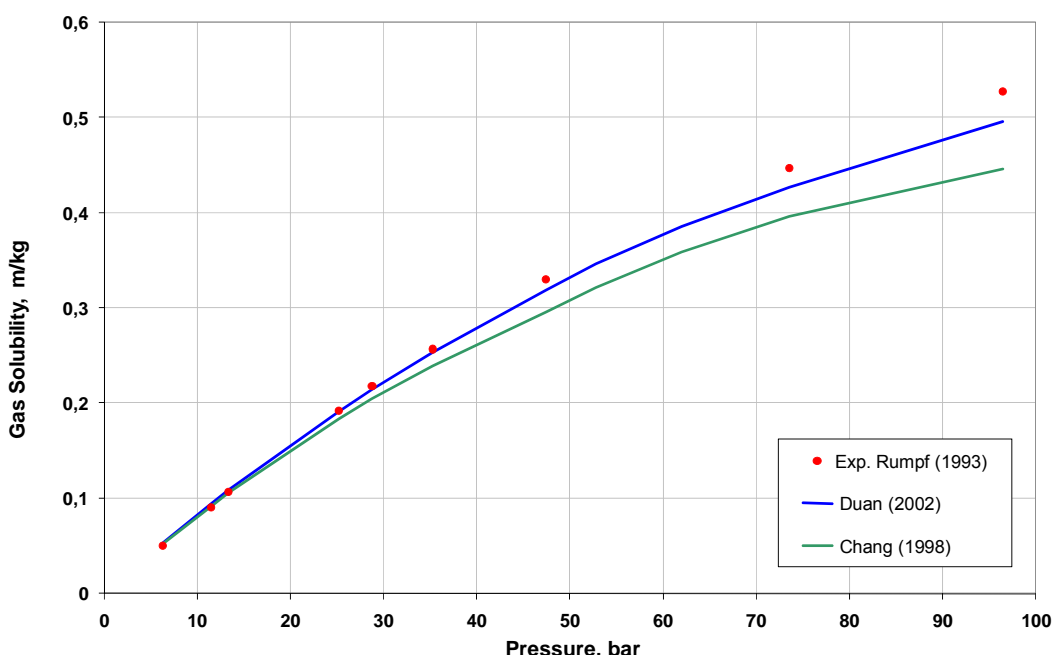


Figure 4.26: Calibration of CO₂ solubility in pure water calculated with ECLIPSE PVTi after published data by Rumpf, and correlations after Duan and Chang

Rumpf has published measured data of CO₂ solubility in pure water in 1993, which fit nearly perfectly to the correlation of Duan, almost identical with the Spycher correlation used in the ECLIPSE dissolution model. The Chang correlation however is somewhat more inaccurate. Based on this quality check the solubility of CO₂ is compared with the solubility of methane in pure water and in NaCl brine in the Figure 4.27.

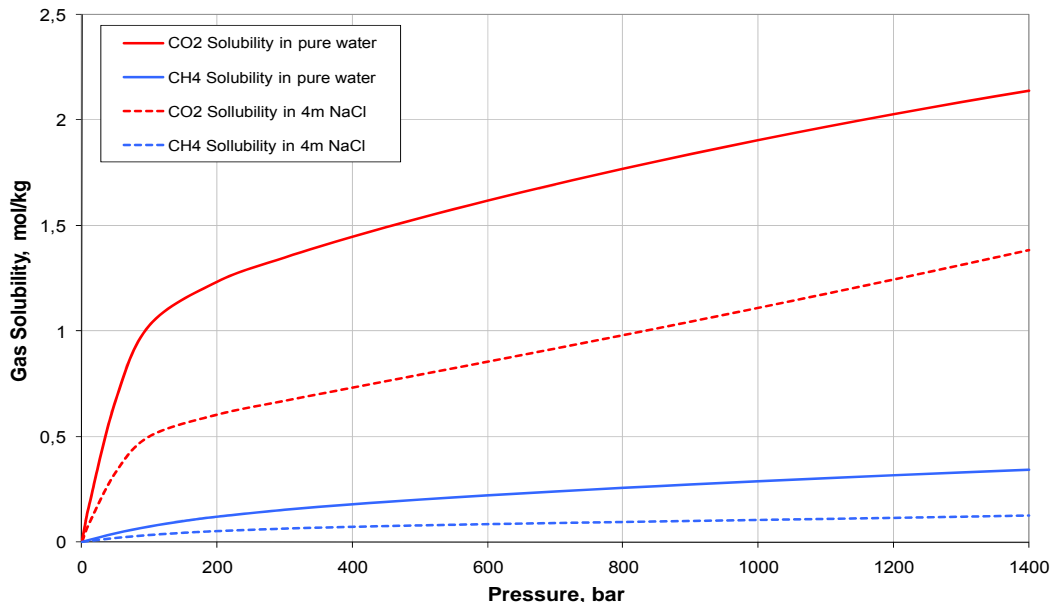


Figure 4.27: Comparison of CO₂ and CH₄ solubility in pure and mineralized water- calculations with ECLIPSE PVTi .

The solubility of CO₂ in water increases with pressure and is approximately 6 times larger than the solubility of CH₄. The salt concentration competes with the gas solubility and reduces the capacity by a factor 2. The solution of the gas into the brine changes its density. Depending on the CO₂ concentration the brine density is exceeding the pure water density in a saturated mode.

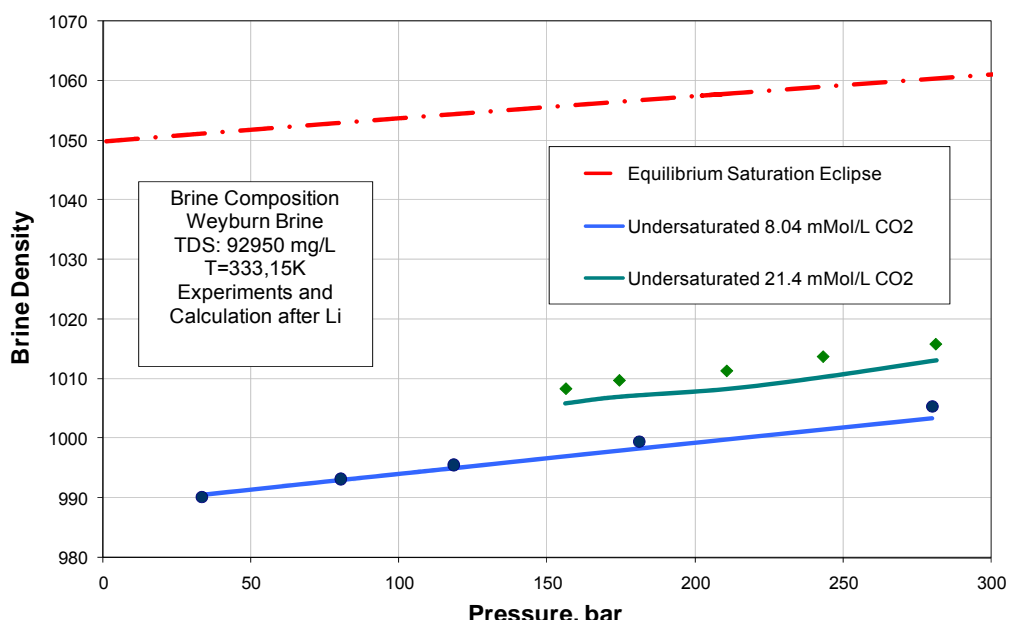


Figure 4.28: Calculated (solid line) and measured (symbols) brine densities for partially and fully gas saturated (carbon dioxide), mineralized, aqueous solutions (Thesis B. Ülker).

The salt concentration is not the only factor defining the level of CO₂ dissolution. The composition of the dissolute is of even bigger importance, as the following Figure 4.29 demonstrates. The calcium chloride and sodium chloride solutions show the same molality, but due to the higher ionic strength of the divalent calcium the solubility of CO₂ is only one half of the solubility in sodium chloride. The calculation by the ECLIPSE PVTi dissolution option gives reasonable results.

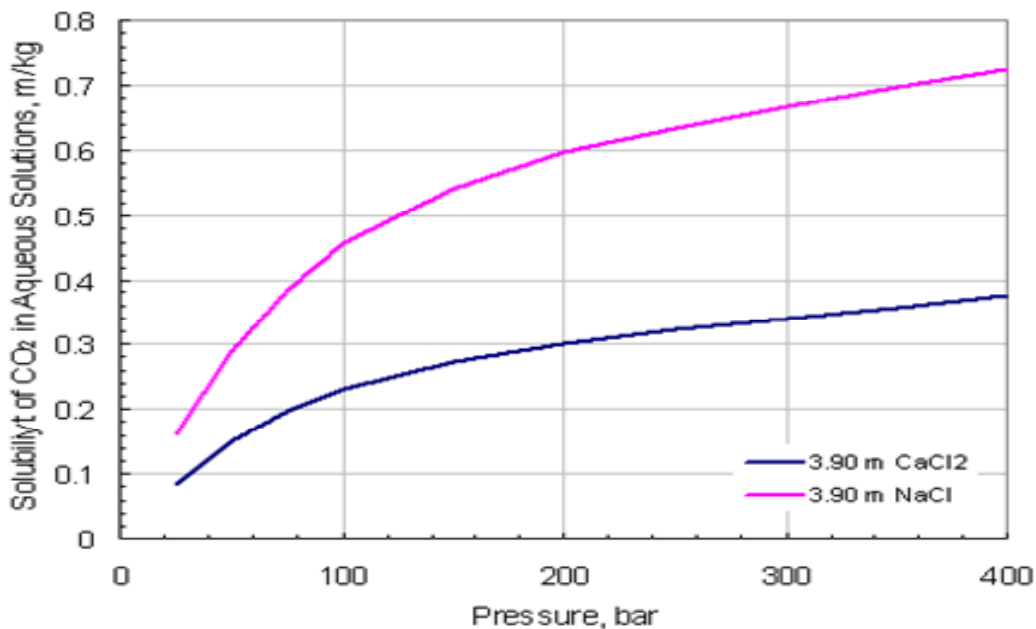


Figure 4.29: Carbon dioxide solubility in mono- and divalent ionic solutions, calculated with ECLIPSE PVTi (Thesis B. Ülker)

In the reservoir the temperature is almost constant, neglecting the near wellbore region. Therefore the pH value of the under-saturated brine, depending on the gas partial pressure, could be taken as a measure of the aggressivity of the brine, controlling the chemical reactions at equilibrium conditions. In ECLIPSE the pH-relationship with pressure and a pressure dependent poro-perm function could be implemented, to consider the changes of hydraulic parameters. The problem of discerning between different reactions, taking place simultaneously and time dependent (reaction kinetics), cannot be treated in ECLIPSE without a chemical reaction model. Such chemical reaction models of multi-component systems must be coupled with transport models, which do not exist so far.

The experimental basis to measure these effects in the pore space is heavily restricted by the scale dimension. The only integral method which allows estimating the combined mineral and pore reaction of the carbonic acid with real reservoir rock is the NMR relaxometry. This method takes into account the specific surface relaxivity of mineral compounds for water, the surface area and the relaxation time as a measure for pore dimensions.

In the rock tomography laboratory of the ITE at TU Clausthal, a series of cores from the 2 prototype gas reservoirs Buntsandstein and Rotliegend, provided by the field owners have been investigated by R. Meyn and interpreted with respect to their NMR spectra as well as to their hydraulic parameters. In the report the most specific results are shown for the carrier rock (sandstone/siltstone) as well as for the intercalated barrier rocks (clay-

stone/shale).

The sealing cap-rock was not investigated (WP 5) because it is composed of rock salt (Zechstein and Rötformation).

Figures 4.30 and 4.31 show the NMR spectra of Buntsandstein reservoir and clay interlayer rock and its derived capillary pressure spectra.

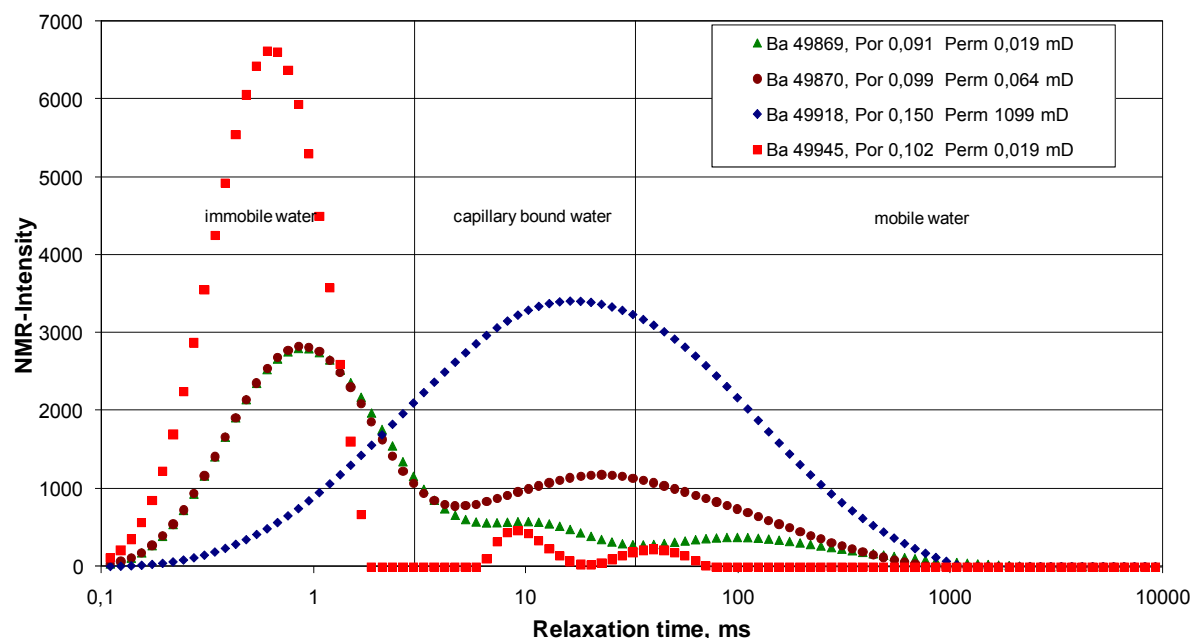


Fig. 4.30: NMR relaxation spectra for Buntsandstein reservoir rock and intercalations

It becomes obvious from this Figure 4.30 that cut-off values of the relaxation times distinguish between water in small, medium and large pores. This enables the expert, based on reliable measured capillary pressure curves, to define mobile and immobile water saturations and the water filled pore volume. The Buntsandstein samples with porosities below 10 % belong to the interlayer facies with small permeabilities, whereas the sample with 15 % represents a good quality reservoir facies. The attached corresponding capillary pressure curves (Figure 4.31) have been derived from the NMR spectra, based on master curve correlations of equal poro-perm classes

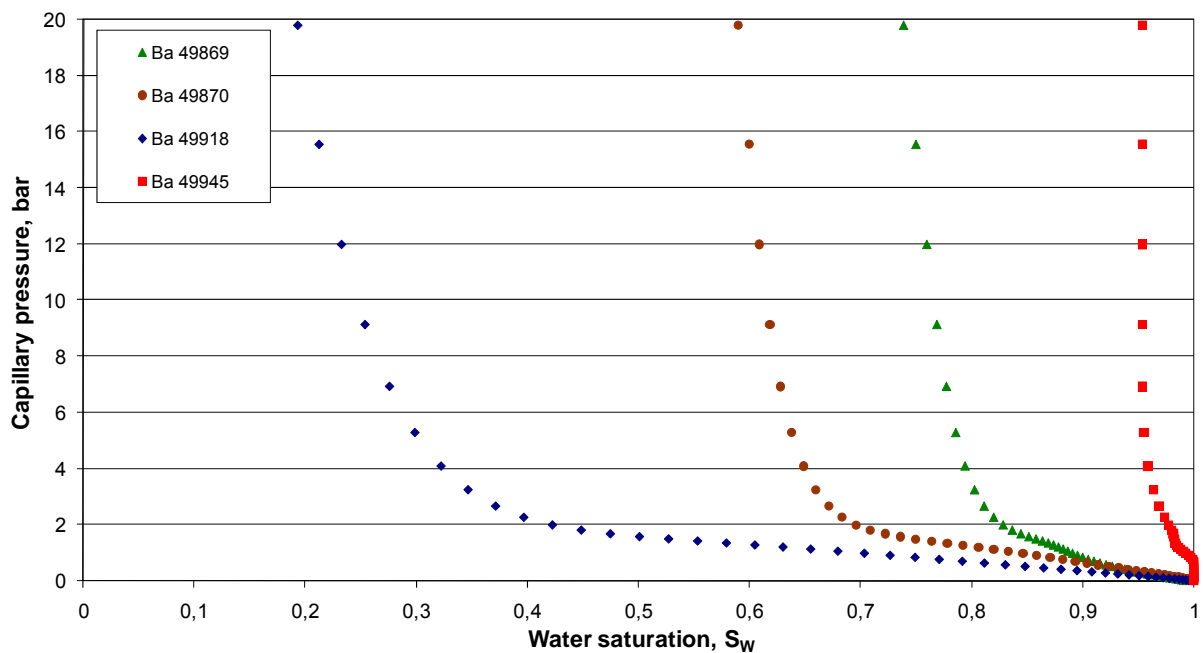


Figure 4.31: Capillary pressure curves for Buntsandstein core samples- derived from NMR measurements-legend for hydraulic core properties compare with Figure 4.30.

The NMR spectra from core samples of the Rotliegend reservoir prototype are presented in the Figure 4.32.

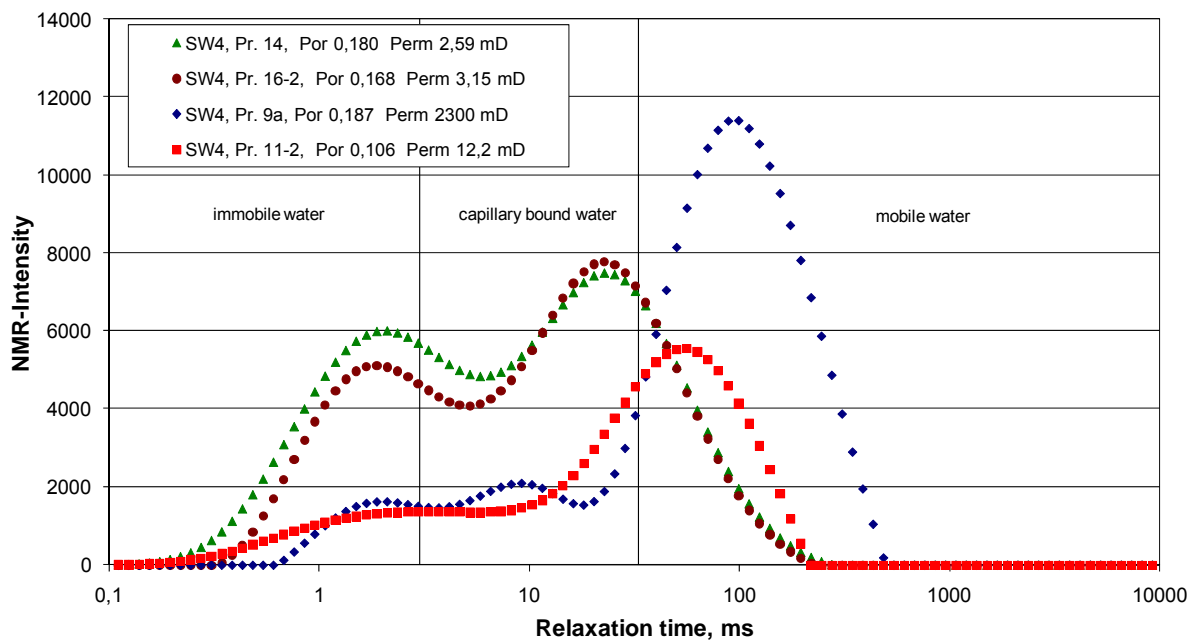


Figure 4.32: NMR spectra for Rotliegend sandstones-well Salzwedel 4

The NMR spectra of various cores include mainly good reservoir qualities. The typical interlayer facies is represented in Figure 4.33:

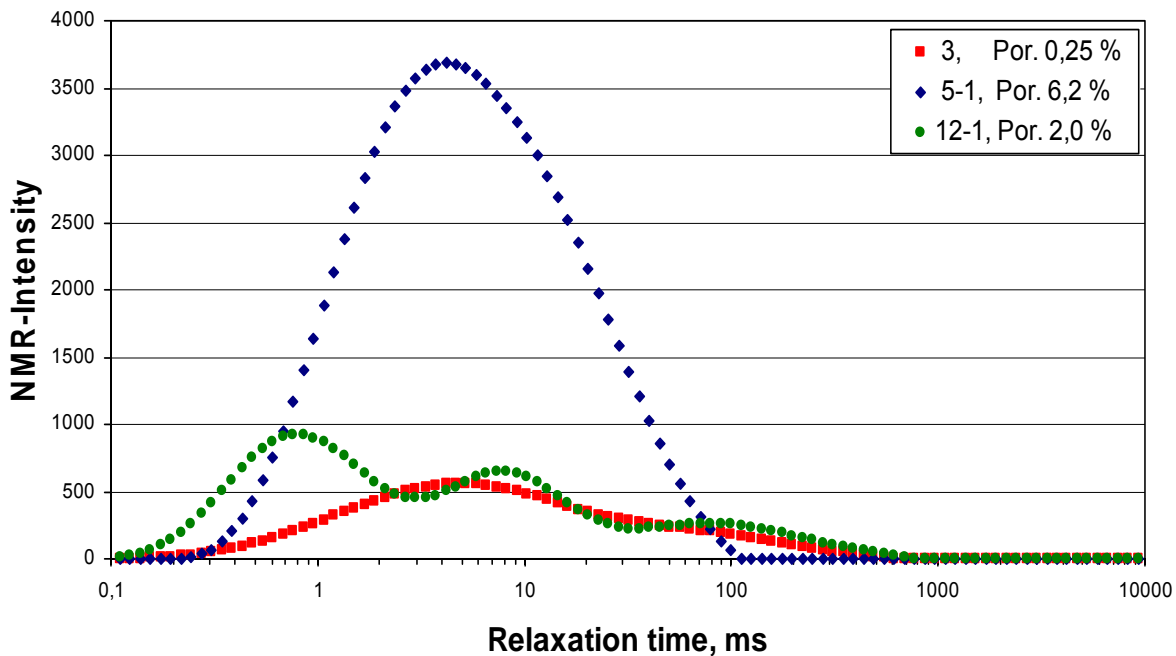


Figure 4.33: NMR spectra for a Rotliegend siltstone (interlayer facies)-well Salzwedel 4.

This interlayer rock has limited porosity and low permeability. Its lateral extension does not completely separate the productive sandstone layers; therefore these elements play an important role in cross flow. Derived capillary pressure curves are shown in the following Figure 4.34.

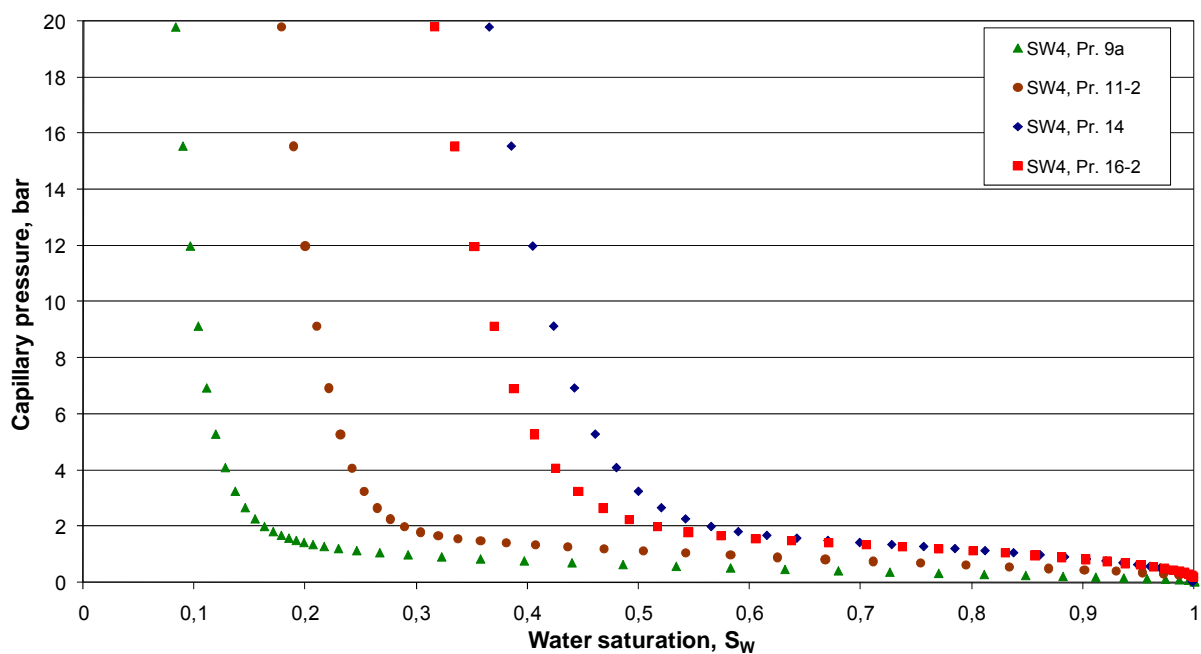


Figure 4.34: Capillary pressure curves for Rotliegend core samples, well Salzwedel 4, derived from NMR measurements- legend for hydraulic core properties compare with Figure 4.33.

The change of water saturation and mobility can be studied by long term alteration of the samples with weak acid, providing the same pH value as the carbonic acid ($pH=3$). This simplification of experimental design allows analogous process observations. In the follow-

up graphs the results of pre- and post imaging of the rock samples is presented and discussed.

Rock alterations by acid treatments:

The original samples have been measured in a saturated mode (synthetic Altmark brine 330 g/l NaCl). The re-saturation with acetic acid ($\text{pH} = 3$) was achieved by vacuum imbibition. The samples were stored at constant temperature and humidity. After 4 and 7 month reaction time, the samples were measured again in the NMR relaxometer. Figures 4.35 and 4.36 show the measured spectra of a typical carrier and interlayer rock.

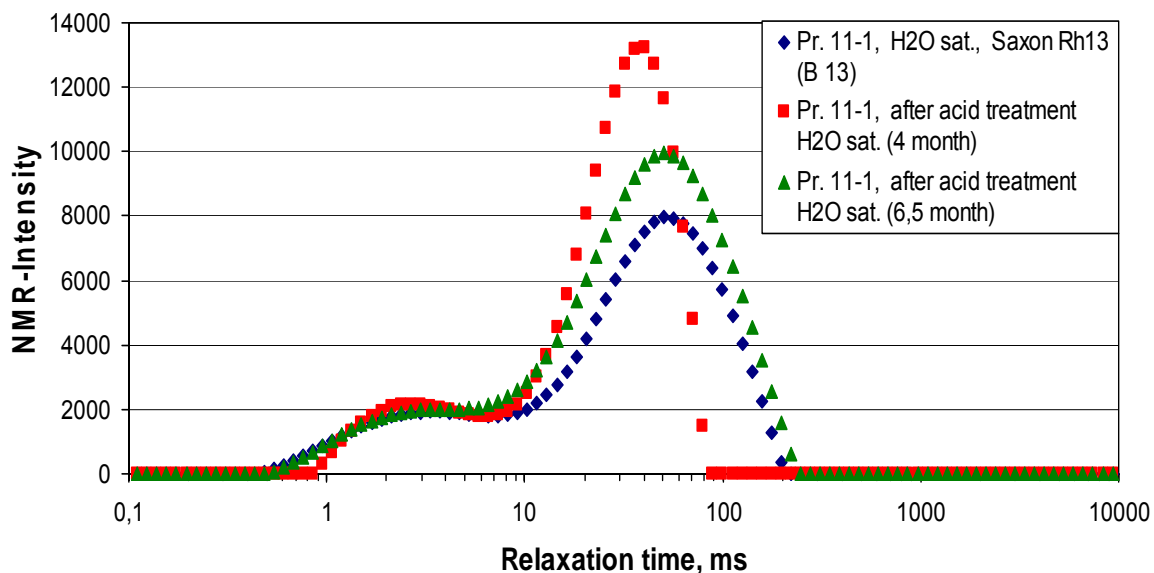


Figure 4.35: NMR spectra for a Rotliegend sandstone sample before and after acid treatment

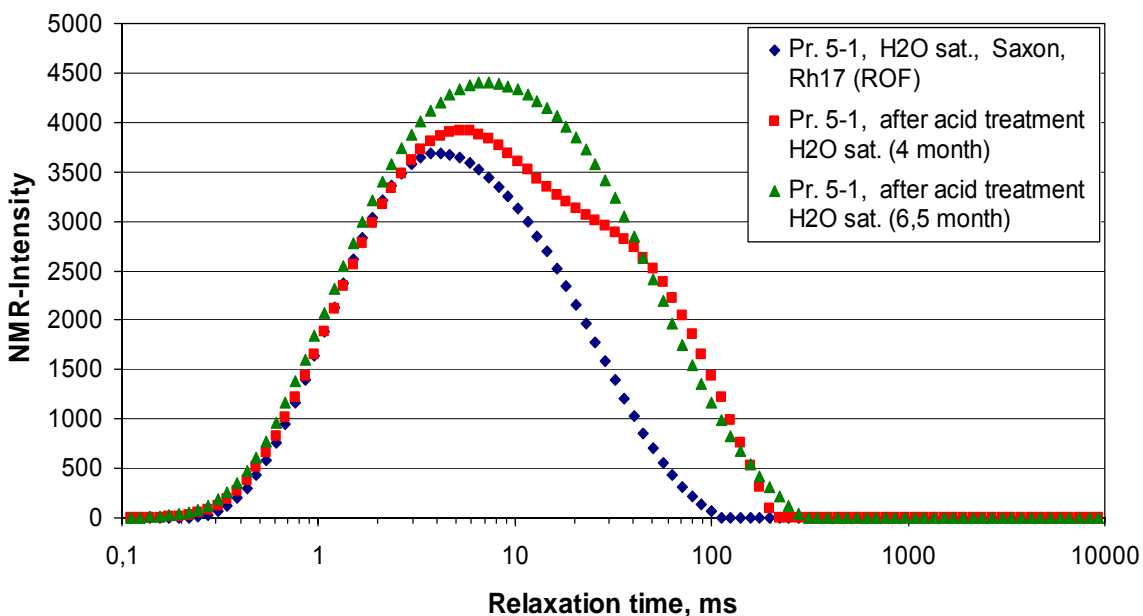


Figure 4.36: NMR relaxation spectra for a Rotliegend siltstone (interlayer facies) sample- before and after acid treatment.

The sandstone sample shows an increase in porosity after 4 month reaction time and a small reduction in water mobility. After 7 month the porosity increase becomes smaller, whereas the water mobility is shifted to the original spectrum. Reason for this phenomenon could be dissolution of carbonate cement or conversion of feldspar into chlorite, accompanied by volume shrinkage. In the siltstone interlayer sample the dissolution of carbonate cement is very probable, because gas bubbling was observed. The profile shift coincides with a potential increase in porosity and water mobility. Other reactions which could play a role are hydration or dehydration of clay minerals, which should be indicated by a left or right shift of the NMR spectrum. The hydraulic properties impact of these physical-chemical changes concern the irreducible phase saturations and the magnitude of the end points of the relative permeabilities. Lab data for the system CO_2 / water are rare in literature, because they are difficult to measure. An example from literature (Bennion SPE 106995) is shown in the following Figure 4.36. The consequences of rel-perm shifts with respect to specified chemical reactions, defining new hydraulic parameter sets, as for example porosity, irreducible water saturation and permeability, can be modelled in ECLIPSE using the Corey-Brooks end point correlation function. The Figure 4.38 shows an arbitrary range shift of end point positions for an original gas-water rel-perm function of a Rotliegend sandstone, caused by dehydration effects (left shift) and hydration effects (right shift).

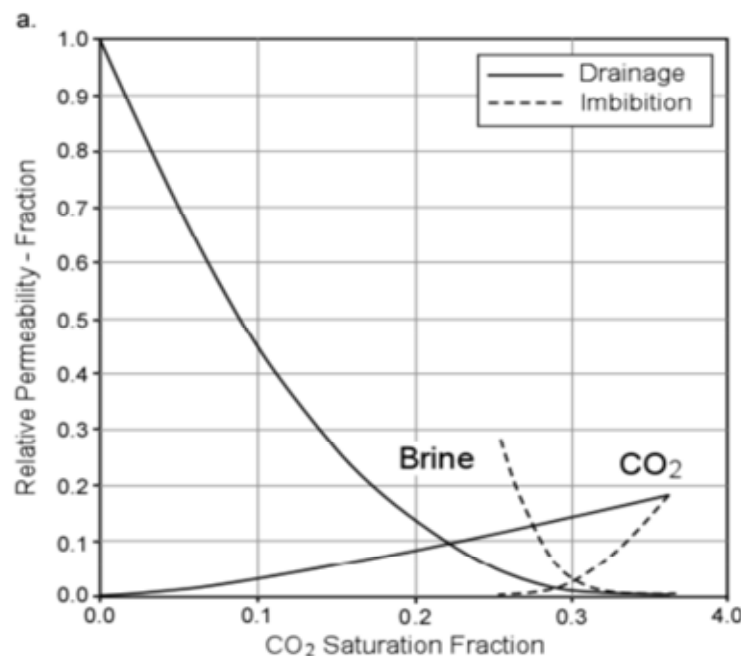


Figure 4.37: Relative gas-water permeabilities for a shaly rock after Bennion - hysteresis effects for drainage and imbibition

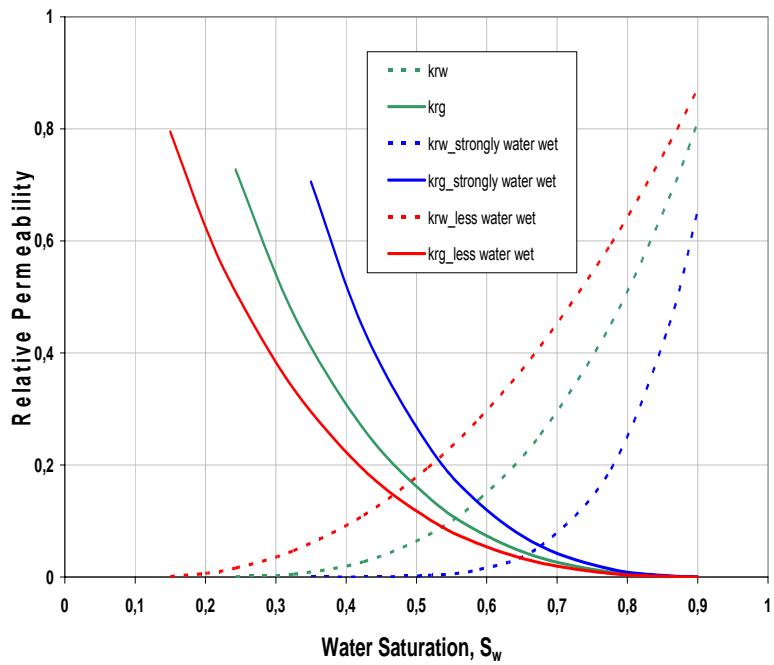


Fig. 4.38: Relative permeability curves gas-water for a Rotliegend sandstone-impact of end point shift by increased rock hydration or dehydration. The end points of the base curves have been measured as well as the capillary pressure functions and correlated by Corey-Brooks.

The effect of the shape of these curves on the CO₂ propagation into a layered reservoir was studied using a prototype model of the Rotliegend gas reservoir.

The main model parameters of this areal 3-D model and the injection data are described in table 4.3 on page 17.

For the sake of simplicity the interlayers have been set inactive in this model runs.

The reservoir parameters used in the input files are:

Reservoir Top: 3050 m, Total Thickness: 212 m, Effective Thickness: 77 m, Model Radius (closed system): 1000m, Gas Composition in Reservoir: 30 % Methane and 70 % Nitrogen, Injection Gas: 100 % Carbon Dioxide, Maximum Bottom Hole Injection Pressure: 1.5 Initial Reservoir Pressure, Reservoir Pressure at Start of Injection: 30 bar, Injection Rate: 70.000 m³/d, Initial Reservoir Pressure: 430 bar, Reservoir Temperature: 130° C, Physical Dispersion was neglected, however Numerical Dispersion covers the same range of mixing.

The impact of water binding to the rock surface, determined by the specific CO₂/ rock interactions, defines the form of relative permeability and capillary pressure curves and is therefore responsible for the distance of CO₂ propagation in the layer model of the reservoir, as it can be seen in the comparison of 2 cases: **weakly and strongly water wet conditions**

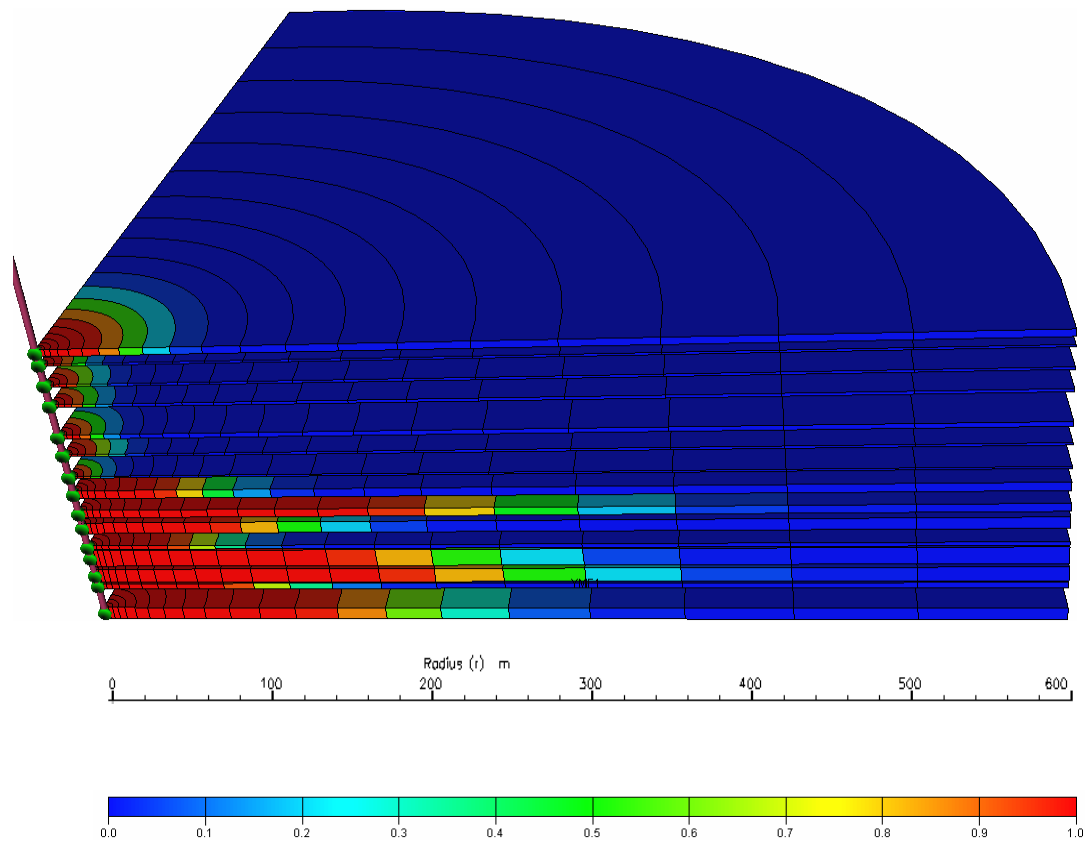


Fig. 4.39: CO₂ concentration profile for weakly water wet conditions after 1 year injection time- the colour spectrum defines the CO₂ concentration in the gas phase as molar fraction

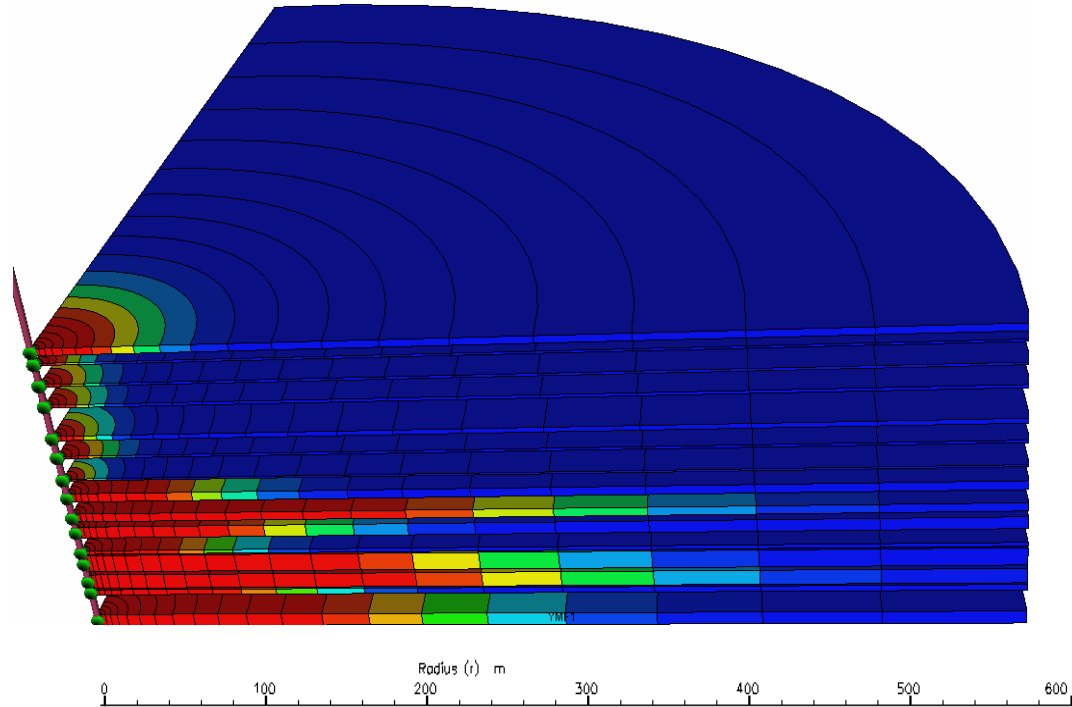


Fig. 4.40: CO₂ concentration profile for strongly water wet conditions after 1 year injection time- the colour spectrum defines the CO₂ concentration in the gas phase as molar fraction

Figure 4.39 compared with 4.40 clearly shows that the CO₂ has travelled more than 100 meters ahead if water is strongly bound to the rock surface and the effective pore space is reduced. However it must be considered that the gas injection was done in a constant rate mode, whereas in constant pressure mode this difference becomes smaller. But the simple example explains why the physical gas/water/rock interaction is so important for accurate modelling.

Conclusions

The ECLIPSE PVTi code can accurately predict the main properties of the CO₂ and the mixing of the CO₂ with different hydrocarbon gases. The benchmark of the PVTi calculated and the measured values for density, viscosity and compressibility of CO₂ and CO₂- natural gas mixtures show a good agreement. Adding other gases as impurities to the CO₂ will have an impact on the properties of injected gas, though this impact will occur only in the case of relatively large amounts of impurities.

Hydrodynamic dispersion may play a key role in the process performance of CO₂ storage and residual gas production. The extension of the mixing zone between the residual gas and the injected CO₂ determines the break-through of the storable gas and the EGR effect. The hydrodynamic dispersion consists of 2 parameters, the mechanical dispersion, responsible for the advective part of the mixing process and the effective diffusion coefficient, responsible for the molecular phenomenon. In the simulation programme ECLIPSE the diffusion effect is included and can be numerically converted into a adequate dispersion coefficient by using a multiplier. In order to avoid the influence of numerical dispersion, which has the same magnitude as the physical dispersion, one might be able to correct the total effect, based on experiments or by estimating the dispersion influence from grid refinements and by switching-off the diffusion option. Realistic dimensions of the mixing zone length require a multiplier in the range of 1000 to cope with the dimensions expected. A realistic determination of this parameter is only possible in field experiments, taking the heterogeneity of the rock into consideration. Another unknown factor is the impact of gravity on the hydrodynamic dispersion, which has to be investigated in detail.

Modelling of reactive fluid transport is no option in the existing ECLIPSE code, however the magnitude of such effects on the injection side are strongly overlaid by the vaporization effect of the dry gas on the connate water and mineral precipitation as a consequence of super-saturation of the residual brine. This phenomenon can be modelled with ECLIPSE 300 in a correct physical mode. Chemical effects as for example dissolution of carbonate cements, leading to porosity/permeability increase or changes of the water binding capacity by hydration or dehydration effects of low pH connate water on rock minerals can be modelled by shifts of endpoint values of relative permeabilities. In the programme code a correlation of these endpoint values with the pH of the reservoir brine must be implemented. This simplification of a reactive transport model does not account for time effects (kinetics) and pore size related transport phenomena.

References:

***** ECLIPSE Technical Description

Adisoemarta P.S. , S.M. Frailey, A.S. Lawal; Measured Z-Factor of CO₂--Dry Gas/Wet Gas/Gas Condensates for CO₂ Storage in Depleted Gas Reservoirs, SPE 89466, 2004

Al-Hashami A., Ren S. R., Tohidi B., 'CO₂ Injection for Enhanced Gas Recovery and Geo-Storage : Reservoir Simulation and Economics', SPE paper 94129 presented at the SPE Europec/EAGE Annual Conference, Madrid, Spain, June 2005

Bear Jacob, 'Dynamics of Fluids in Porous Media', American Elsevier Environmental Science Series, New York (1972)

Bennion, B.D.and Bachu, St.: Permeability and relative permeability measurements at reservoir conditions for CO₂ – H₂O systems in ultra-low permeability confining caprocks, SPE paper 106995, SPE Europec/EAGE Annual Conference and Exhibition. London, 11-14 June 2007.

Chang, Y. B. and Coats B. K.: A compositional model for CO₂ floods including CO₂ solubility in water. SPE Reservoir Evaluation and Engineering (1998), 155-160.

Duan, Z. et.al.: An equation of state for the CO₂-CH₄ H₂O system- 1. Pure systems from 0 to 1000° C and 0 to 8000 bar. Geochimica and Cosmochimica Acta 56 /1992), 2605-2617.

Duan,Z. and Sun, R.: An improved model calculating CO₂ solubility in pure water and aqueous NaCl solutions- from 273 to 533 K and 0- 2000 bar. Chemical Geology 193 (2003), 257-271.

Fenghour A. et all, The Viscosity of Carbon Dioxide, J. Phys. Chem Ref. Data, Vol 27, No. 1, 1998

Gmelin Handbuch der Physik Springer, Berlin, 1957

Kunz, O., Klimeck, R., Wagner, W., Jaeschke, M. (2005); The GERG-2004 wide-range reference equation of state for natural gases. To be published as GERG Technical Monograph. Fortschr.-Ber. VDI, VDI-Verlag, Düsseldorf (2005).

May, F. (2002) Quantifizierung des CO₂-Flusses zur Abbildung magmatischer Prozesse im Untergrund der Westeifel. Shaker Verlag, Aachen.

Pruess, K. Spycher, N.F.:CO₂-H₂O mixtures in the geological sequestration of CO₂ 1.assessment and calculation of mutual solubilities from 12 to 100° C and up to 600 bar. Geochimica and Cosmochimica Acta 67 (2003),3015-3031.

Oldenburg C. M., Benson S. M., 'CO₂ Injection for Enhanced Gas Production and Carbon Sequestration', SPE paper 74367 presented at SPE International Petroleum Conference and Exhibition, Mexico, Feb. 2002

Oldenburg C. M., Pruess K., Benson S. M., 'Process Modeling of CO₂ Injection into Natural Gas Reservoirs for Carbon Sequestration and Enhance Gas Recovery', Earth Science Division, Lawrence Berkeley National Laboratory, Berkeley California 94720, January 2001

Prausnitz J. M Reid, R. C.,, and Bruce E. P., 'The Properties of Gases and Liquids', 4th edition, McGraw Hill, New York (1987)

Rumpf, B. et.al.: Solubility of carbon dioxide in aqueous solutions of sodium chloride-experimental results and interpretations. Journal of Solution Chemistry 23 (1994). 432-448.

Scheidegger A. E., 'The Physics of Flow Through Porous Media', 3rd Edition, University of Toronto Press, Toronto and Buffalo (1974)

Schöneich S., F. May, H.-D. Vosteen (2007): Influence of Impurities in CO₂-rich Gas Mixtures on the Storage Capacity of Mature Natural Gas Fields. — DGMK-Tagungsbericht 2007-1, 6 S., ISBN 978-3-936418-65-1

Spycher, N. and Pruess,K. CO₂-H₂O mixtures in the geological sequestration of CO₂.II. Partitioning in chloride brines at 12-100 C and up to 600 bar Geochimica et Cosmochimica Acta, Vol. 69, No. 13, pp. 3309-3320, 22005

Ülker B. Implications of the Phase-Solubility Behaviour on the Performance Predictions of the CO₂ Trapping in Depleted Gas Reservoirs and Aquifers, EUROPEC/EAGE Conference and Exhibition, 11-14 June 2007, London, U.K

Ülker B.: Influence of structural heterogeneities on the carbon dioxide storage capacity of aquifer structures- CO₂ storage in a Buntsandstein prototype aquifer. PhD Thesis of TUC (Clausthal University of Technology), 2009.

Vargaftik, N.B. 'Tables on the Thermophysical Properties of Liquids and Gases', 2nd Edition, John Wiley & Sons, New York, NY, 1975

Work Package 5

Geochemical Risk Assessment

Issues:

- Reservoir Rocks And Natural Analogue
- Reactions Derived in Comparison with Analogue
- Verification of Alteration Reactions

Authors:

Franz May, Bundesanstalt für Geowissenschaften und Rohstoffe, Hannover

Hans-Dieter Vosteen, Landesamt für Bergbau Energie und Geologie, Hannover

| | |
|--|-----|
| Kurzfassung..... | 177 |
| Objective of WP5..... | 178 |
| 2.1 Review of Literature (State of the Art) | 179 |
| 2.2 Hydrostratigraphy of the Case Study Sites | 180 |
| 2.2.1 Altmark Case | 182 |
| 2.2.2 Barrien Case | 183 |
| 2.3 Sample Acquisition from Natural Analogues and from Wells in the Case Study Fields | 185 |
| 2.4 Water Analyses, basic Mineralogical and Geochemical Characterisation of Protoliths and Altered Rocks | 187 |
| 2.4.1 Altmark Formation Water | 187 |
| 2.4.2 Altmark Reservoir and Cap Rocks | 189 |
| 2.4.3 Barrien Rocks and Formation Water | 190 |
| 2.4.4 Bad Mergentheim Rocks..... | 191 |
| 2.4.5 Namedy Rocks..... | 194 |
| 2.4.6 Bad Oeynhausen | 195 |
| 2.5 Identification of Alteration Reactions involving CO ₂ | 196 |
| 2.6 Code Comparison and Numerical Simulation | 202 |
| 2.6.1 Code Comparison | 202 |
| 2.6.2 Numerical Simulation | 202 |
| 2.7 Interpretation of Geochemical Results..... | 204 |
| References | 205 |

Kurzfassung

Die Hydrostratigraphie der Fallstudien Altmark und Barrien zeigt, dass in beiden Gebieten zahlreiche (Reserve-)Aquitare und -aquitarde oberhalb des Caprocks existieren. Da keine ausreichende Zahl von Gesteinsproben der Deckschichten aus den beiden Erdgaslagerstätten vorhanden sind, stützen sich die geochemischen Interpretationen auf die Untersuchung auf analoger Gesteine aus anderen CO₂-führenden Bohrungen.

In den Arbeitsgebieten Altmark und Barrien treten in den Reservoirformationen hochmineralisierte Na-Ca-Cl-Solen auf. Aufgrund der hohen Stoffkonzentrationen können Änderungen der Fluid-Gesteinsgleichgewichte zu Ausfällung von Mineralen, wie beispielsweise Halit führen.

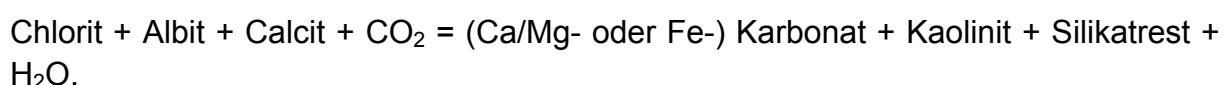
Untersuchungen an Gesteinen aus den Arbeitsgebieten zeigten, dass die Reservoirgesteine neben der Hauptkomponente Quarz bis zu 15 % aus Feldspat und als akzessorische Komponenten aus Karbonaten (Calcit, Dolomit, etwas Ankerit) und Schichtsilikaten (Muskowit-Illit, Chlorit) bestehen.

In der Altmark treten in der Reservoirformation gering- bis impermeable Siltstein-Lagen auf, die durch einen höheren Anhydrit- und Karbonatanteil von 5-10% gekennzeichnet sind. Vermutlich hat in diesen Lagen eine vollständige Anhydrit- oder Karbonatzementation stattgefunden.

Aus dem Arbeitsgebiet Barrien liegen aus der Reservoirformation nur sehr wenige Gesteinsproben vor. Diese zeigen eine ähnliche mineralogische Zusammensetzung mit etwas höheren Karbonatanteilen als in der Altmark.

Das Deckgebirge besteht in der Altmark aus Anhydrit und Zechsteinkalk. Die mächtigen Steinsalzschichten wurden in beiden Arbeitsgebieten nicht gekernt und konnten deshalb nicht beprobt und analysiert werden.

Um eine qualitative Aussage über die potentiellen geochemischen Reaktionen bei der CO₂-Injektion treffen zu können wurden ergänzende Untersuchungen an natürlichen Analoga vorgenommen. Aus gekernten Bohrungen von Bad Mergentheim, Namedy und Bad Oeynhausen, wurden CO₂-alterierte Vergleichsproben sowohl der Reservoirformationen (Rotliegend und Buntsandstein) als auch Analoga der Abdeckgesteine (Hunsrückshäfer) beprobt und analysiert. Die wesentlichen reaktiven Minerale sind neben den Karbonaten auch Feldspat und Chlorit. An den alterierten Gesteinsproben verschiedener Herkunft konnte die Korrosion von Feldspat und Chlorit sowie die Ausfällung von Ca/Mg-Karbonat oder Fe-Karbonat beobachtet werden. Anhand von vergleichenden Untersuchungen an den frischen und CO₂-alterierten Gesteinen konnte die generelle Alterationsreaktion ermittelt werden:



Da ein Simulatorvergleich ergab, dass zur Zeit keine geeignete reaktionskinetische Datenbank für die Berechnung CO₂-induzierter geochemischer Reaktionen unter Beteiligung hochsalinärer Fluide existiert, kann noch keine verlässliche Aussage über die Voraussetzungen zur Lösung oder Ausfällung von Fe- bzw. Ca/Mg-Karbonaten getroffen werden. Der Aufwand zur Anpassung der Datenbanken macht ein separates Forschungsprojekt erforderlich.

Objective of WP5

CO₂ can change rock properties due to chemical and physical processes in the reservoir, and in the case of leakage in the overburden. These reactions can either

- enhance porosity due to mineral dissolution, which might increase the storage capacity within a reservoir or else increase the risk of leakage in cap rocks, or
- reduce porosity and permeability due mineral precipitation which could result in long-term solid storage of CO₂ in the form of carbonates (in situ mineralisation). But precipitation also could reduce injectivity and thus storage capacity. Alteration reactions may also be a mechanism of self-sealing for fractures in the cap rock.

Reactions caused by leakage of reservoir fluids or CO₂ into shallow fresh water aquifers may liberate unwanted elements from the rock matrix.

The aim of this work package were to achieve the understanding of potential rock alteration and element mobilisation by CO₂ injection into the reservoir and in its overburden (plus impurities and residual reservoir fluids) in the case of leakage from wells and storage formations (accidents during injection, long-term loss). Physico-chemical conditions under which different geochemical reaction dominate should be quantification of their potential impact evaluated.

Method:

Geochemical and mineralogical investigations of fluids, reservoir and cap rocks from the case studiy sites and from natural analogue of the potential storage formations which are common and widely distributed in the southern Permian Basin: Rotliegend sandstones and the Buntsandstein (Bunter sandstone) and that have been affected by CO₂.

Work Package 5 included the following work tasks:

- Compilation of the hydro- and lithostratigraphy of two case study sites above and below Zechstein salt.
- Acquisition of information from natural analogues of relevant stratigraphic units, rock and fluid samples from wells in the case study fields, and in the wider region from wells that produce CO₂-rich thermal brines
- Detailed water analyses, basic mineralogical and geochemical characterisation of fresh and altered rocks

- Identification of alteration reactions involving CO₂, as necessary, supported by more detailed geochemical and mineralogical analyses (e.g. isotopes, fluid inclusions, single crystals).
- Comparison of codes, selection and installation of an appropriate geochemical simulation tools (e.g. TOUGHREACT, PHREEQC, SHEMAT, MUFTE_UG). Some of the codes are presently under development; routines relevant for CO₂ storage are being implemented. Thus the selection of the best code appropriate for the given task will take advantage from on-going developments.
- Numerical simulations of identified reactions were performed in order to validate selected software and thermodynamic data base.
- Predictive geochemical modelling applying reactive transport or reaction progress concepts to identify conditions sensitive for CO₂ storage including parameter variations. Additional simulations including likely minor components in the injected CO₂ phase or from reservoir fluids can be performed in case of unexpected fast project progress.
- Interpretation of geochemical results (natural analogues and simulation) concerning possible impact of leakage into aquifers and implications for injection and storage strategies in gas fields
- Inclusion of results into overall evaluation (WP 7)

2.1 Review of Literature (State of the Art)

Geochemical reactions of CO₂, formation fluids and adjacent rocks could lead to a change of reservoir- and cap rock characteristics. These changes (e.g., precipitation of carbonates within the pore space) could on the one hand lead to geotechnical problems during the injection phase but on the other hand to a long-term fixation of CO₂ in carbonates (May, 2004). Therefore the prediction of such processes and the development of methods to yield quantitative forecasts are topics of several international R&D-projects.

For this reason three different approaches can be utilized: the analysis of natural analogues, laboratory experiments and numerical simulation. Extensive experience with numerical simulation of potential geochemical reactions in the framework of CO₂-storage exists at the French geological survey BGRM (Czernichowski-Lauriol et al., 1996). Corresponding geochemical laboratory experiments were carried out at the British geological survey BGS (Bateman et al., 2005). Numerical simulation is very helpful to plan and to complement geochemical experiments. On the other hand, these experiments can yield the necessary input data for simulation of geochemical mineral- and rock reactions.

2.2 Hydrostratigraphy of the Case Study Sites

In a first step well bore logs were studied to yield the lithostratigraphy of the case study sites Altmark and Barrien. This information was further compared and fitted to the hydrostratigraphic structure of Lower Saxony (Reutter, 2005) (see Figure 5.1). This table is based upon former work of Manhenke et al. (2001) to yield a basic hydrostratigraphical structure of Northern Germany.

The hydrogeological units are numbered serially from top to bottom. In accordance with the legend of Reutter (2005), aquifers and aquitards are indicated by the letters L and H, respectively (Table 5.1).

Transmissivity classes and corresponding kf-values are based upon the hydrostratigraphic classification of Reutter (2005), too.

Hydraulic conductivity (m/s) is divided into different classes:

< 1E-9 extremely small

> 1E-9-1E-7 very small

> 1E-7-1E-5 small

> 1E-5-1E-4 moderate

> 1E-4-1E-3 medium

> 1E-3-1E-2 high

> 1E-2 very high

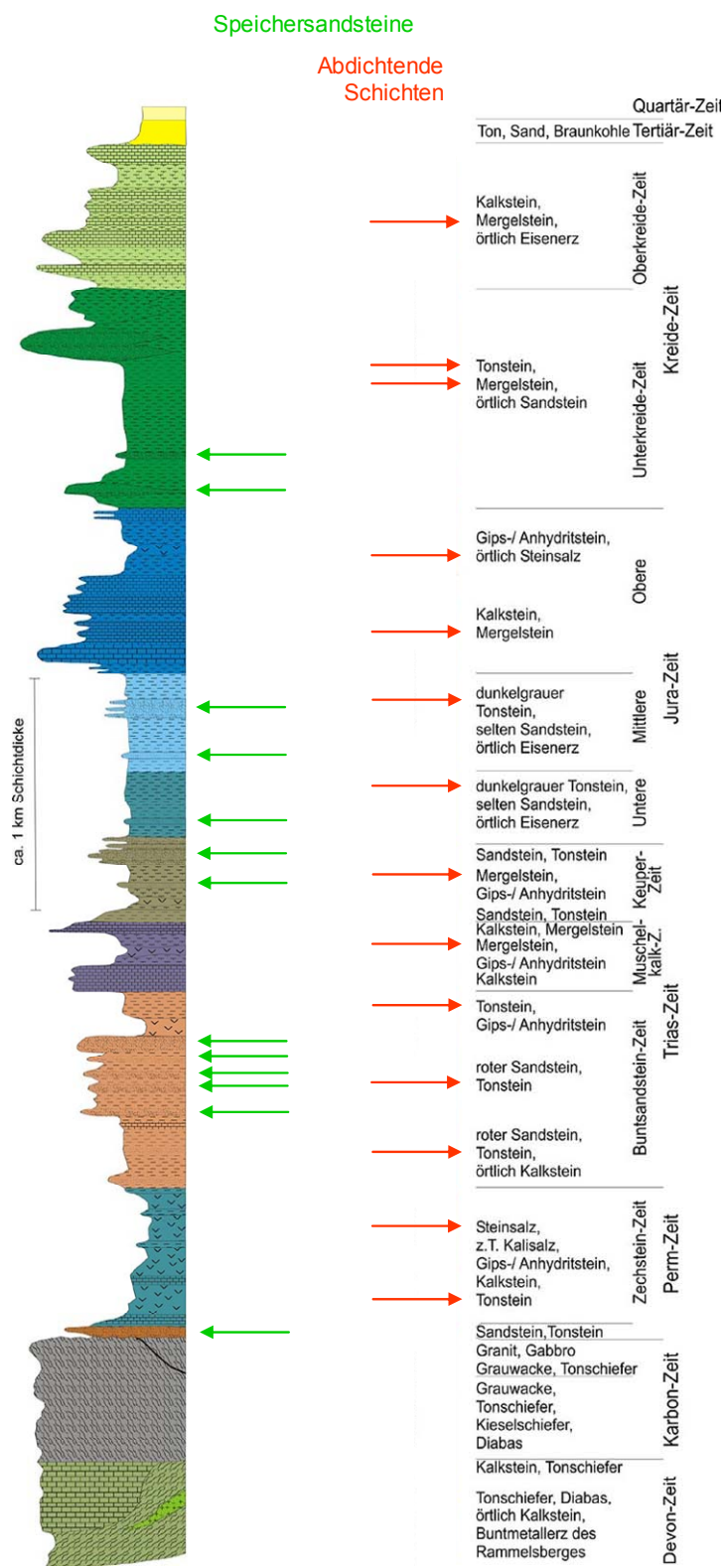


Figure 5.1: Comparison and fitting of lithostratigraphic information into the hydrostratigraphic structure of Lower Saxony, modified from Reutter (2005)

2.2.1 Altmark Case

Tab. 5.1: Hydrostratigraphy of Peckensen 4

| stratigraphy | depth [m] | thickness [m] | kf-value [m/s] | hydrostratigraphic unit |
|-------------------------------|-----------|---------------|----------------|-------------------------|
| Quaternary - Oligocene | -148,0 | 148,0 | 1E-4 - 1E-2 | L1-L6 |
| Oligocene - Miocene | -158,0 | 10,0 | < 1E-5 | H7 |
| Oligocene - Miocene | -162,0 | 4,0 | >1E-5 - 1E-3 | L7 |
| Oligocene | -331,0 | 169,0 | < 1E-5 | H8.1 |
| Oligocene | -343,5 | 12,5 | > 1E-4 - 1E-3 | L8 |
| Eocene | -367,0 | 23,5 | < 1E-5 | H9 |
| Eocene-Paleocene | -735,0 | 368,0 | >1E-5 - 1E-3 | L9 |
| Coniac - Campan | -1548,0 | 813,0 | 1E-7 - 1E-5 | H10 |
| Turon | -1708,0 | 160,0 | 1E-5 - 1E-4 | L10 |
| Turon | -1752,0 | 44,0 | < 1E-5 | H11 |
| Cenoman | -1805,0 | 53,0 | >1E-5 - 1E-3 | L11 |
| Alb | -1990,0 | 185,0 | 1E-9 - 1E-5 | H12 - H13 |
| Apt | -2002,0 | 12,0 | 1E-5 - 1E-4 | L13 |
| Apt | -2021,0 | 19,0 | 1E-9 - 1E-7 | H14 |
| Upper Muschelkalk - Barrême | -2190,0 | 169,0 | >1E-5 - 1E-3 | L14 - L20 |
| Middle Muschelkalk | -2264,0 | 74,0 | < 1E-5 | H23 |
| Lower Muschelkalk | -2374,0 | 110,0 | >1E-5 - 1E-3 | L21 |
| Upper Bunter (Röt) | -2609,0 | 235,0 | 1E-9 - 1E-7 | H24 |
| Lower- to Middle Bunter | -3091,0 | 482,0 | 1E-5 - 1E-3 | L23 - L22 |
| Zechstein | -3103,0 | 12,0 | < 1E-5 | H26 |
| Zechstein | -3122,0 | 19,0 | >1E-5 - 1E-3 | L24 |
| Zechstein | -3125,2 | 3,2 | < 1E-9 | H27 |
| Zechstein | -3132,7 | 7,5 | > 1E-4 - 1E-3 | L25 |
| Zechstein | -3181,0 | 48,3 | 1E-7 - 1E-5 | H28 |
| Red-Bed sediments - Zechstein | -3519,5 | 338,5 | 1E-5 - 1E-3 | L27 - L26 |

Summarized description of the hydrostratigraphic units:

- 70 m medium to high permeability: Quaternary sand and gravel with thin clay-layers
- 2070 m extremely small to medium permeability: Tertiary-Cretaceous clay to medium sand, sandstone, limestone and marley limestone
- Unconformity between lower Cretaceous and upper Muschelkalk
- 234 m extremely small to medium permeability: upper to lower Bunter siltstone and claystone, marlstone and limestone
- 235 m very small permeability: Röt anhydrite, claystone and rock salt
- 482 m moderate to medium permeability: middle to lower Bunter siltstone and fine- to medium sandstone
- 94.3 m extremely small to medium permeability: 31m Zechstein anhydrite with a 12m claystone and rock salt layer (H26 and L24), 3,2m Saßfurt rock salt (H27, extremely low permeability), 60,1m anhydrite with some several meters thick layers of limestone and claystone and 4.3m Zechstein bituminous Zechstein-limestone and carbonatic Kupferschiefer (L26, medium permeability).

- 338.5 m moderate permeability: Rotliegend silty fine- to medium sandstone with several, up to 4m thick claystone layers (L27).

2.2.2 Barrien Case

Tab. 5.2: Hydrostratigraphy of Barrien 2T

| stratigraphy | depth [m] | thickness [m] | kf-value [m/s] | hydrostratigraphic unit |
|---------------------------------|-----------|---------------|----------------|-------------------------|
| Pleistocene | -40 | 40 | >1E-3 - 1E-2 | L4 |
| Middle Oligocene-Miocene | -102 | 62 | <1E-5 | H5-H8 |
| Eocene+Paleocene | -567 | 465 | >1E-5 - 1E-3 | L9 |
| Maastricht - Coniac | -1085 | 518 | >1E-7 - 1E-5 | H10 |
| Cenoman-Turon | -1208 | 123 | >1E-5 - 1E-3 | L10-L11 |
| Lias alpha - Alb | -1329 | 119 | >1E-9 - 1E-5 | H12-H19 |
| Rhät | -1426 | 97 | >1E-5 - 1E-4 | L18 |
| Steinmergelkeuper | -1590 | 164 | >1E-9 - 1E-7 | H20 |
| region of Schilfsandstein | -1608 | 18 | >1E-5 - 1E-3 | L19 |
| Lower Keuper - Lower Gipskeuper | -1869 | 261 | >1E-7 - 1E-5 | H21 -H22 |
| Upper Muschelkalk | -1934 | 65 | >1E-5 - 1E-3 | L20 |
| Middle Muschelkalk | -2004 | 70 | <1E-5 | H23 |
| Lower Muschelkalk | -2118 | 114 | >1E-5 - 1E-3 | L21 |
| Upper Buntsandstein (Röt) | -2316 | 198 | >1E-9 - 1E-7 | H24 |
| Middle Buntsandstein | -2525 | 209 | >1E-5 - 1E-4 | L22 |

Summarized description of the hydrostratigraphic units:

The stratigraphic sequence includes several unconformities.

- 40 m high permeability: Quaternary coarse gravel-fine debris
- 527 m extremely small to medium permeability: Tertiary claystone, some marl with minor fine sand
- 641 m very small to medium permeability: Cretaceous to Jurassic limestone, marlstone and claystone
- 540 m very small to medium permeability: Keuper claystone, marlstone and silty sandstone with some anhydrite, lower Keuper with claystone, limy marlstone and limestone
- 249 m moderate to medium and extremely small to small permeability: Muschelkalk claystone, limy marlstone, limestone and anhydrite with up to 10 m thick rock salt layers
- 198 m very low permeability: upper Bunter (Röt) claystone, marly claystone with minor fine- to medium sand layers
- 209 m moderate permeability: middle Bunter fine- to medium sandstone with some clay layers

Tab. 5.3: Hydrostratigraphy of Barrien 3T

| stratigraphy | depth [m] | thickness [m] | kf-value [m/s] | hydrostratigraphic unit |
|---------------------------------|-----------|---------------|----------------|-------------------------|
| Paleocene - Pleistocene | -562 | 562 | >1E-5 - 1E-2 | L4.2 - L9 |
| Maastricht - Coniac | -1018 | 456 | >1E-7 - 1E-5 | H10 |
| Cenoman - Turon | -1164 | 146 | >1E-5 - 1E-3 | L10 - L11 |
| Lias alpha - upper Alb | -1336 | 172 | >1E-9 - 1E-5 | H12 - H19 |
| Rhät | -1445,5 | 109,5 | >1E-5 - 1E-4 | L18 |
| Steinmergelkeuper + Rote Wand | -1620 | 174,5 | >1E-9 - 1E-7 | H20 |
| region of Schilfsandstein | -1639 | 19 | >1E-5 - 1E-3 | L19 |
| Lower Gipskeuper - Lower Keuper | -1866 | 227 | >1E-7 - 1E-5 | H21 - H22 |
| Upper Muschelkalk | -1913 | 47 | >1E-5 - 1E-3 | L20 |
| Middle Muschelkalk | -2041 | 128 | <1E-5 | H23 |
| Lower Muschelkalk | -2160 | 119 | >1E-5 - 1E-3 | L21 |
| Upper Bunter (Röt) | -2384 | 224 | >1E-9 - 1E-7 | H24 |
| Middle Bunter | -2705,8 | 321,8 | >1E-5 - 1E-4 | L22 |
| Lower Bunter | -2743,4 | 37,6 | <1E-5 | H25 |

Summarized description of the hydrostratigraphic units:

- 527 m moderate to medium permeability: Tertiary sand to coarse gravel (160m) and claystone, marlstone and sandstone (367m)
- 774 m very small to medium permeability: Cretaceous to Jurassic limestone, marlstone and claystone
- 530 m very small to medium permeability: Keuper claystone, with some sandstone and anhydrite layers
- 294 m moderate to medium and extremely small to small permeability: Muschelkalk claystone and limestone and a 40 m thick rock salt layer
- 224 m very low permeability: upper Bunter (Röt) claystone, marly claystone with up to 76m thick rock salt layers with interneal anhydrite layers
- 321.8 m moderate permeability: middle Bunter sandstone with some claystone and marly claystone layers
- 37.6 m extremely small to small permeability: lower Bunter sandstone with siltstone and fine sandstone

At each of the case study sites, the storage formations are overlain by cap rocks of extremely small and very small hydraulic conductivities. A sequence of further aquifers and aquitards shall facilitate safe storage of CO₂ in the Rotliegend and Bunter sandstones at the two case study sites.

2.3 Sample Acquisition from Natural Analogues and from Wells in the Case Study Fields

The analysis of short- and long-term consequences of CO₂ storage on reservoir and cap rock will be carried out by means of natural analogue studies:

Most of the CO₂-induced mineral reactions are too slow to be detected in the laboratory. Therefore we are studying CO₂-rock reactions in regions where the natural CO₂ concentration is distinctly elevated.

Such natural analogues can be found in regions where we have got deep boreholes which were drilled to produce mineral water.

Geochemical and mineralogical studies on CO₂-altered and corresponding unaltered rocks can help to understand processes of mineral dissolution and mineral precipitation. This information can later on be compared to results of numerical simulation.

In Germany such wells can be found in several regions, for example near to the cities of Bad Oeynhausen and Bad Mergentheim.

Rock samples that were used as natural analogues were taken from deep wells which were exposed to large CO₂ concentrations over long time periods (CO₂ concentration of 1000 mg/l or more). In addition to that the chosen rock samples had to match those of the study areas regarding stratigraphy or petrography.

Based upon information from literature, internet and regional authorities the following locations were chosen:

| <u>Bad</u> | <u>Oeynhausen</u> |
|----------------------------------|----------------------------------|
| „Alexander | von Humboldt |
| Fe-silty | CO ₂ -bearing thermal |
| Cores: | claystone |
| free CO ₂ : 1452 mg/l | 1026-1027 |
| | m |
| | Sprudel“ brine (sm) |

Bad Mergentheim

| | |
|----------------------------------|-----------|
| „Paulsquelle“ | |
| CO ₂ -bearing | brine |
| claystone; | sandstone |
| (so, sm, su, z, r) | |
| Cores: | 34-548 |
| free CO ₂ : 2250 mg/l | m |

Namedy

"Inselsprudel"

periodically

Hunsrückshiefer

Cuttings: 0-336 m

erupting

soda

(Kaltwassergeysir)"

spring



Figure 5.2: Location of case study areas and wells sampled for natural analogue studies

Near to the city of Mad Mergentheim a 551 m deep well called "Paulsquelle" penetrates both Bunter sandstone and Rotliegend. It produces CO₂-rich mineral water. Well spring temperature is 16 °C. During drilling of the well all significant CO₂- fluxes were exactly documented. Drill cores of almost total depth range were carefully labeled and stored. This simplified a sampling of rocks that were exposed to CO₂-rich water.

Near to the city of Namedy there is an old well called geyser Andernach which can be regarded as a periodically erupting soda spring. It is located within the Hunsrück shists and cuttings were sampled down to a depth of 336 meters. These shists can be regarded as cap-rock analogs.

The geological survey North Rhine-Westfalia provided six Middle Bunter Sandstone samples of two different depth levels from the 1027 meters deep borehole "Alexander von Humboldt Sprudel".



Figure 5.3: Outburst of CO₂ and water from the intermittent degassing well at Nameda, near Andernach

Water analyses of representative wells in the Barrien case study area were provided by Wintershall. Complementary deep water samples were taken from three wells in the vicinity of the Altmark study area and analysed by BGR.

2.4 Water Analyses, basic Mineralogical and Geochemical Characterisation of Protoliths and Altered Rocks

2.4.1 Altmark Formation Water

Formation water samples of three wells in the study areas were obtained by down-hole samplers and analysed geochemically.

Formationwater in the studied formations is a Na-Ca-Cl-brine with in some cases quite high amounts of other alkali- and earthalkali elements and sulphate. The highly saline water contains approximately 1300 mg/l Ca²⁺, 800 mg/l Mg²⁺, and 3500 mg/l HCO₃⁻ (Henke et al., 2006; see Appendix A)

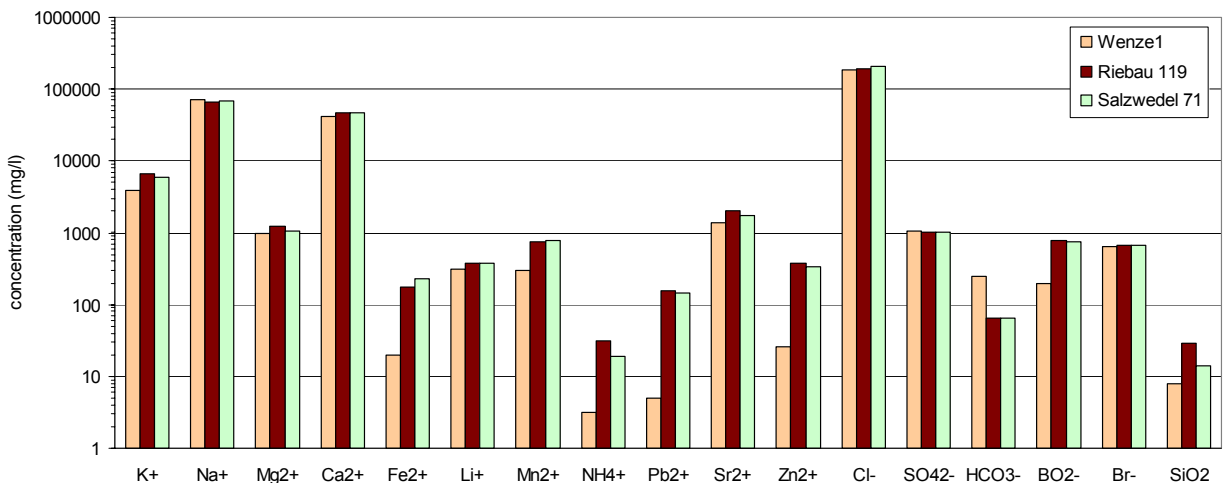


Figure 5.4: Chemical Composition of formation waters sampled from deep wells in the Altmark.



Figure 5.5: Precipitates obtained from the well Weenze 1

The fluid samples obtained from the wells Riebau and Salzwedel contained halite in the filtrate, which indicated the potential of salt precipitation from the high-concentrated fluids. The formation waters in the Altmark are also rich in heavy metals such as lead and mercury. From well Weenze1, which was out of production for a few months prior to sampling, precipitates rich in lead have been obtained. The precipitates are probably made up of (Na, Ca)-carbonates, halite and possibly CaSO_4 , covered by lead crystals.

The high concentrations of dissolved solids in the formation water could potentially cause geotechnical problems with CSEGR operations due to the precipitation of minerals:

- salt precipitation in the reservoir due to evaporation of water into dry injected gas (CO_2).
- precipitation of iron oxy-hydrates from oxygen contained as impurity in CO_2 from an oxy-fuel plant. H_2S , which could be an impurity from IGCC plants could cause the precipitation of lead sulfide.
- lead due to electrochemical reactions at production wells.

2.4.2 Altmark Reservoir and Cap Rocks

In collaboration with ITE (TU Clausthal) a sampling campaign was carried out at the core inventory of EEG in Steinitz. BGR obtained 13 rock samples.

Geochemical and mineralogical analyses were carried out on all rock samples (Figure 5.6, 5.8). Mineral abundance has been determined by semiquantitative XRF.

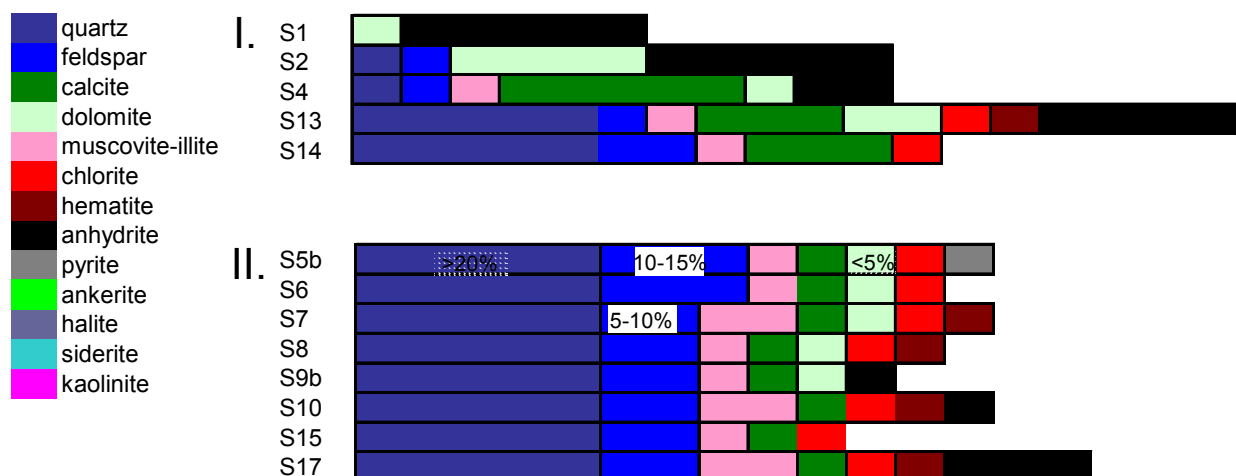


Figure 5.6: Altmark mineral composition for (I.) lowermost cap rocks and interbedding within reservoir and (II.) reservoir rocks

Figure 5.6 shows the composition of Altmark Zechstein rocks (S1-S4) and Rotliegend reservoir rocks (S5b-S17). Rock samples S13 and S14 represent low-permeability layers within the reservoir.

The lowermost Zechstein cap rocks mainly consist of carbonates (dolomite and calcite), anhydrite and contain less than 5 % of muscovite-illite, feldspar and quartz.

The Rotliegend reservoir rocks show the main minerals quartz and feldspar. Two samples contain 5-10 % of muscovite-illite and one sample contains 10-15 % of an-

hydrite. Besides to that the rocks contain minor amounts (<5%) of muscovite-illite, chlorite, hematite, anhydrite, pyrite, calcite and dolomite.

Regarding the mineral composition, the only difference between Rotliegend reservoir rocks and the interbedding layers is the higher amount of carbonates and anhydrite within the interbedding. Therefore it can be assumed that the permeability reduction within the interbedding layers is caused by an increased anhydrite or carbonate cementation.

2.4.3 Barrien Rocks and Formation Water

Mineralogical and geochemical analyses for the natural gas field Barrien were carried out for 4 rock samples from the reservoir and for 3 rock samples from the cap rock sequence (see Figure 5.8).

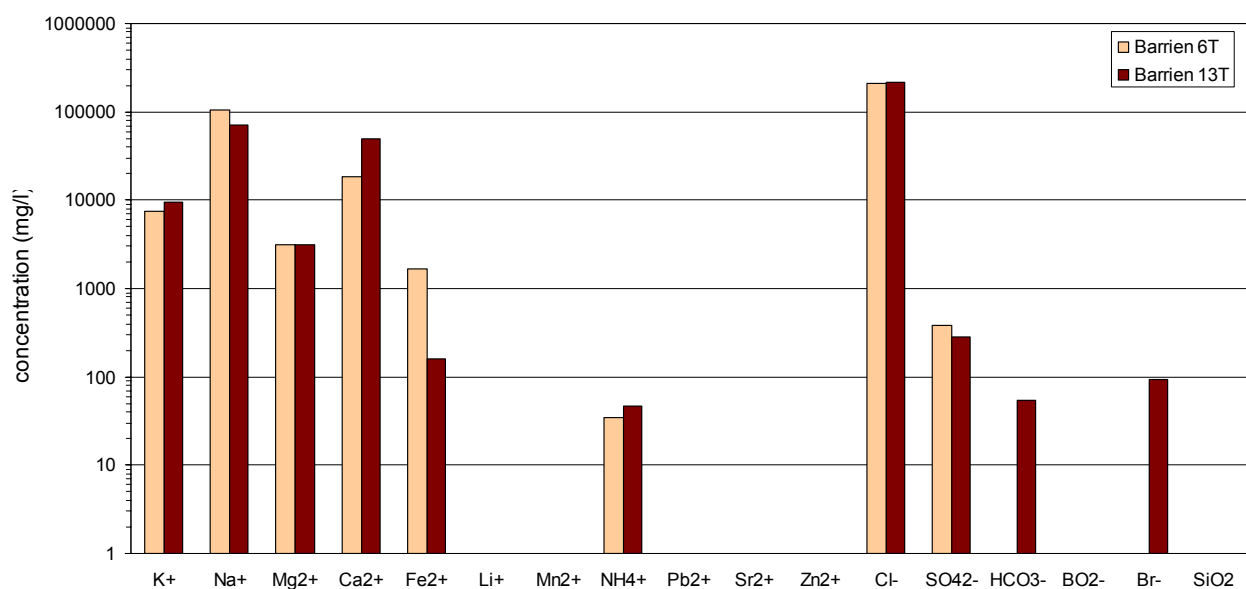


Figure 5.7: Hydrochemistry of Barrien formation water (provided by courtesy of Wintershall)

Barrien reservoir rocks are mainly composed of quartz, feldspar, muscovite-illite, carbonates (ankerite and calcite) and minor amounts of chlorite, and hematite. One rock sample contains 10-15 % of rock salt.

Figure 5.8 I. shows the composition of different rocks from the overburden. B3 is an upper Triassic (Keuper) sandstone, composed of quartz and minor amounts of feldspar, muscovite-illite, calcite and pyrite. B1 and B2 show the mineral composition of upper cretaceous and Lias α, respectively.

An appropriate means to yield an estimate of the qualitative reactions that are going to take place before executing numerical simulations is to study natural analogues. For the case of CO₂ injection, natural analogues can be found in regions with CO₂-rich water, e.g. in active volcanic regions. But also quite far away of volcanic regions, CO₂-rich waters can be found. CO₂-rich waters are preferentially occurring in regions

where anticlinal structures of Mesozoic cap rock lead to an accumulation of volcano-genic CO₂ underneath of low-permeable layers (e.g., Franconian shield; Bad Mergentheim, Ingelfingen (Larue et al., 2001)). The principal alteration reactions can be identified by geochemical studies of natural analogues. These examples can be used for the calibration of geochemical simulations.

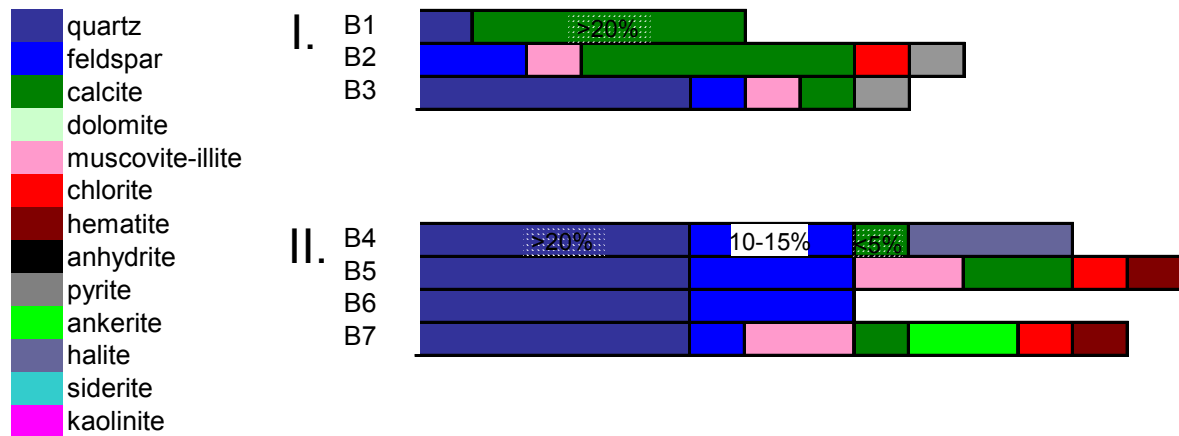


Figure 5.8: Barien mineral composition for different cap rocks (I.) and reservoir rocks (II.).

Besides to having a long-term circulation of CO₂-rich water the main problem and an important precondition is to find a natural analogue site that represents the study area as good as possible. In the present case we are studying two reservoir rock formations (Middle Bunter Sandstone and Rotliegend sandstone). Near to the city of Mad Mergentheim a 551 m deep well penetrates both Bunter Sandstone and Rotliegend sediments. It delivers CO₂-rich mineral water. Well-spring temperature is 16 °C. During the drilling campaign, all prominent CO₂ escape events were accurately documented. Drill-cores from all depth levels were thoroughly labelled and stored. This facilitated sampling rocks exposed to CO₂-rich water. A total of 49 samples from cores and 27 samples of cuttings were taken from different depth levels of the Rotliegend red bed sandstones, Zechstein and Bunter Sandstone. Complementary unaltered rock samples were collected from local Middle and Upper Bunter Sandstone quarries.

2.4.4 Bad Mergentheim Rocks

In the framework of a diploma mapping (Henke, 2007) mineralogical studies were carried out by means of thin section petrography, cathodoluminescence petrography and scanning electron microscopy. Porosity measurements were performed at four rock samples. In addition to that, 57 rock samples were analysed by means of XRF and XRD analyses.

Complementary mineralogical and geochemical studies were carried out on samples from core material of well “Alexander von Humboldt Sprudel” near to the city of Bad Oeynhausen.

During a sampling campaign in the core archives of the Baden Württembergisches Landesamts für Geologie, Rohstoffe und Bergbau in Freiburg i. Br., 551 m of rock samples from the well Paulsquelle in Bad Mergentheim have been inspected. 49 core samples and 27 samples of cuttings, from various depths, representing rocks from Rotliegend, Zechstein and Buntsandstein strata were selected for analyses. From Bad Mergentheim we took samples of clay and sandstones from the upper Bunter Sandstone to the Rotliegend Sandstone layers. Corresponding unaltered rocks from the Rotliegend and Bunter Sandstone were taken from active quarries at Brombach (Bunter, near Freiburg), and Schramberg (Rotliegend) as no Rotliegend quarries are in operation at Bad Mergentheim.

The mineralogical composition of the samples was obtained by means of thin sections and XRD-analyses. XRF-measurements yielded a geochemical analysis of all rock samples.

Bad Mergentheim Zechstein rocks mainly consist of quartz, dolomite and different amounts of feldspar, muscovite-illite, chlorite and hematite. Bad Mergentheim Rotliegend rocks are composed of quartz, feldspar and minor amounts of dolomite, muscovite-illite and chlorite.

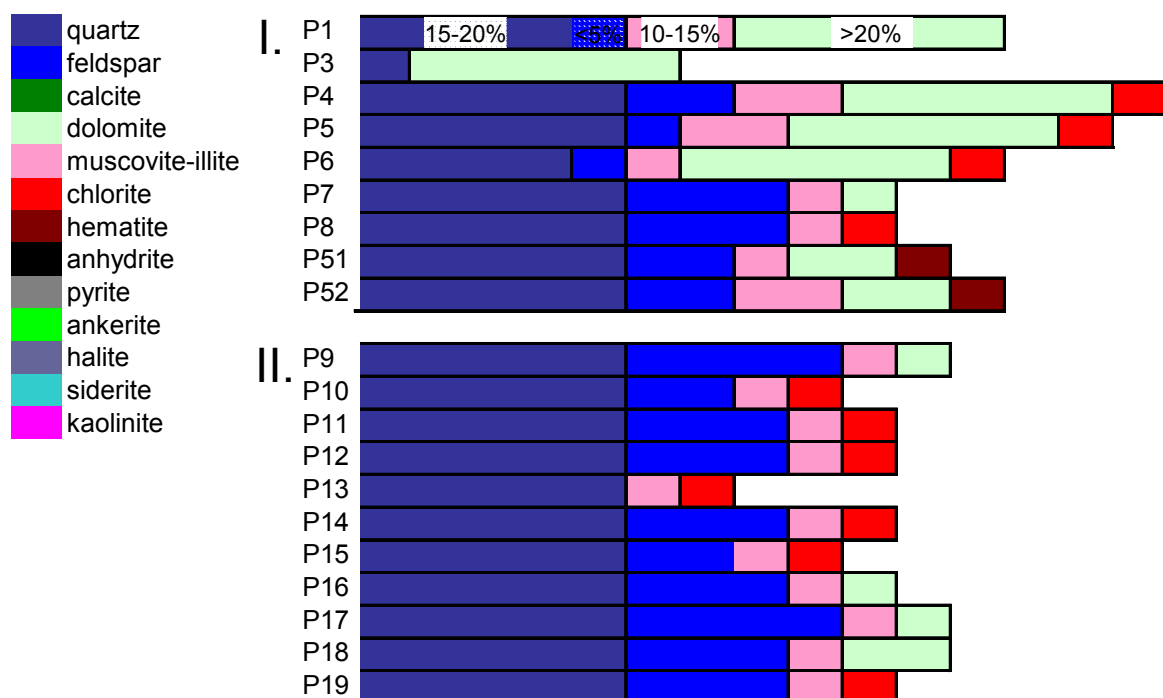


Figure 5.9: Bad Mergentheim CO₂-altered Zechstein rocks (I.) and Rotliegend rocks (II.)

Bad Mergentheim altered Upper Bunter (Röt) rocks consist of quartz, varying amounts of dolomite, muscovite-illite, feldspar, chlorite, hematite and anhydrite (Figure 5.10 I.b). The unaltered Upper Bunter rocks (Figure 5.10 I.a) is composed of quartz with minor amounts of feldspar, muscovite-illite, kaolinite and hematite.

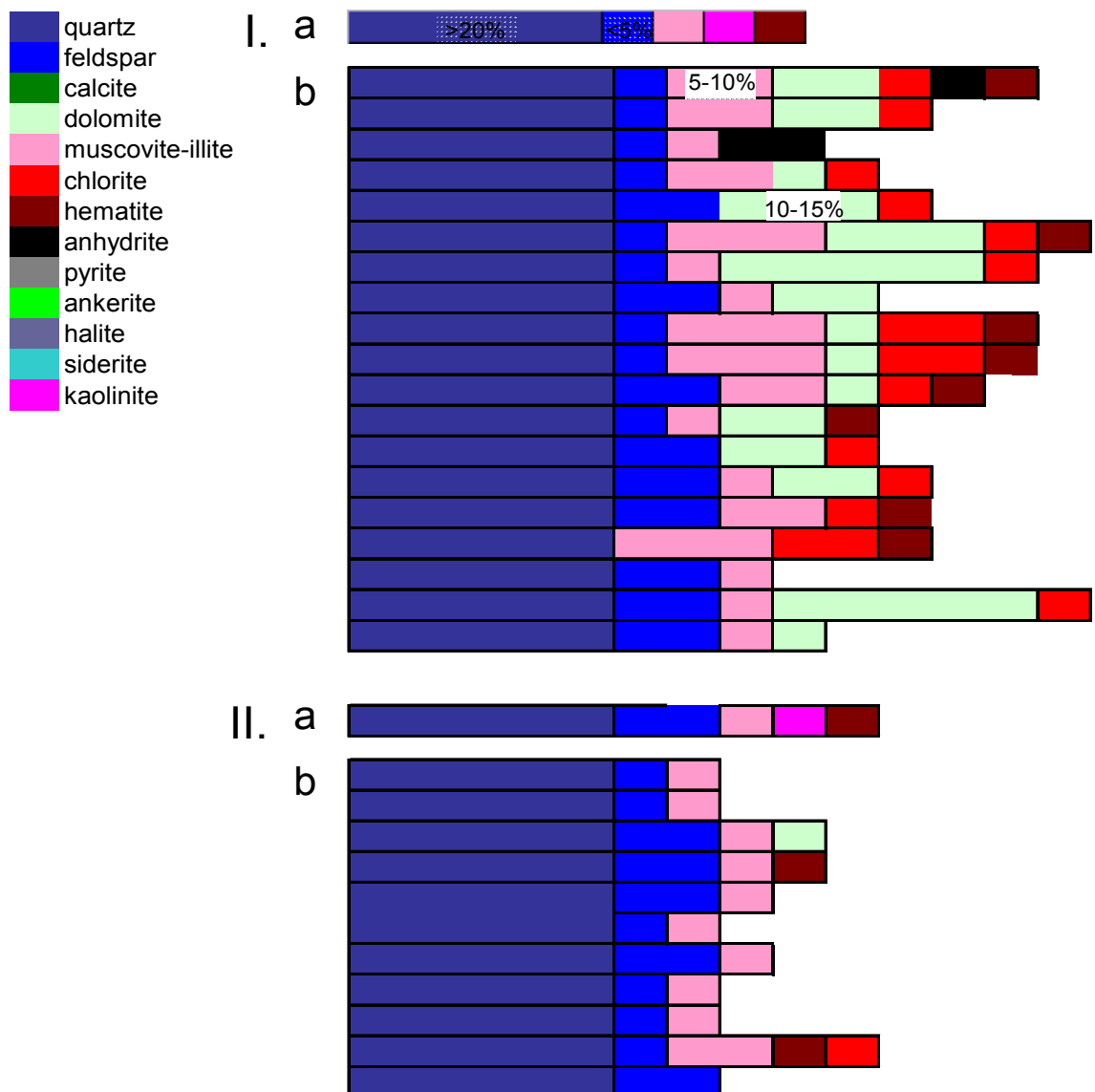


Figure 5.10: Bad Mergentheim CO₂-altered Upper Bunter (Röt) (I.) and Middle Bunter (II.); a shows unaltered rock from open quarries and b shows altered rocks.

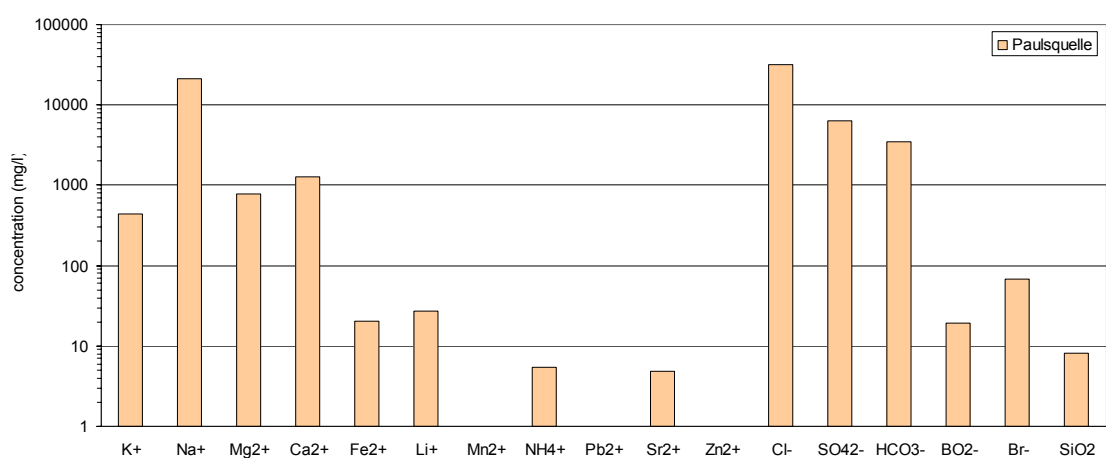


Figure 5.11: Concentrations of dissolved species in the Paulusquelle water from Bad Mergentheim

Detailed water analyses of mineral water spring “Paulsquelle” yielded a highly mineralised Na-Ca-Cl brine with an elevated amount of hydrogen carbonate, sulphate, Mg^{2+} , K^+ and Fe^{2+} . This water from the “Paulusquelle” is similar to the composition of highly mineralised brines of the study areas Altmark and Barrien, dominated by Na and Cl. The water contains 67,6 g of dissolved species. The content of free CO_2 is 2580 mg/l.

The water chemistry indicates equilibrium with quartz at temperatures of about 36 to 38 °C. This temperature would roughly correspond to a depth of 1 km, typical geothermal gradients provided. According to saturation indices calculated with the PHREEQC thermodynamic data base, dolomite precipitation could be expected at these temperatures at CO_2 partial pressures of less than 1 MPa. This would imply waters undersaturated with CO_2 at the depth of the Bunter and Rotliegend rocks containing dolomite.

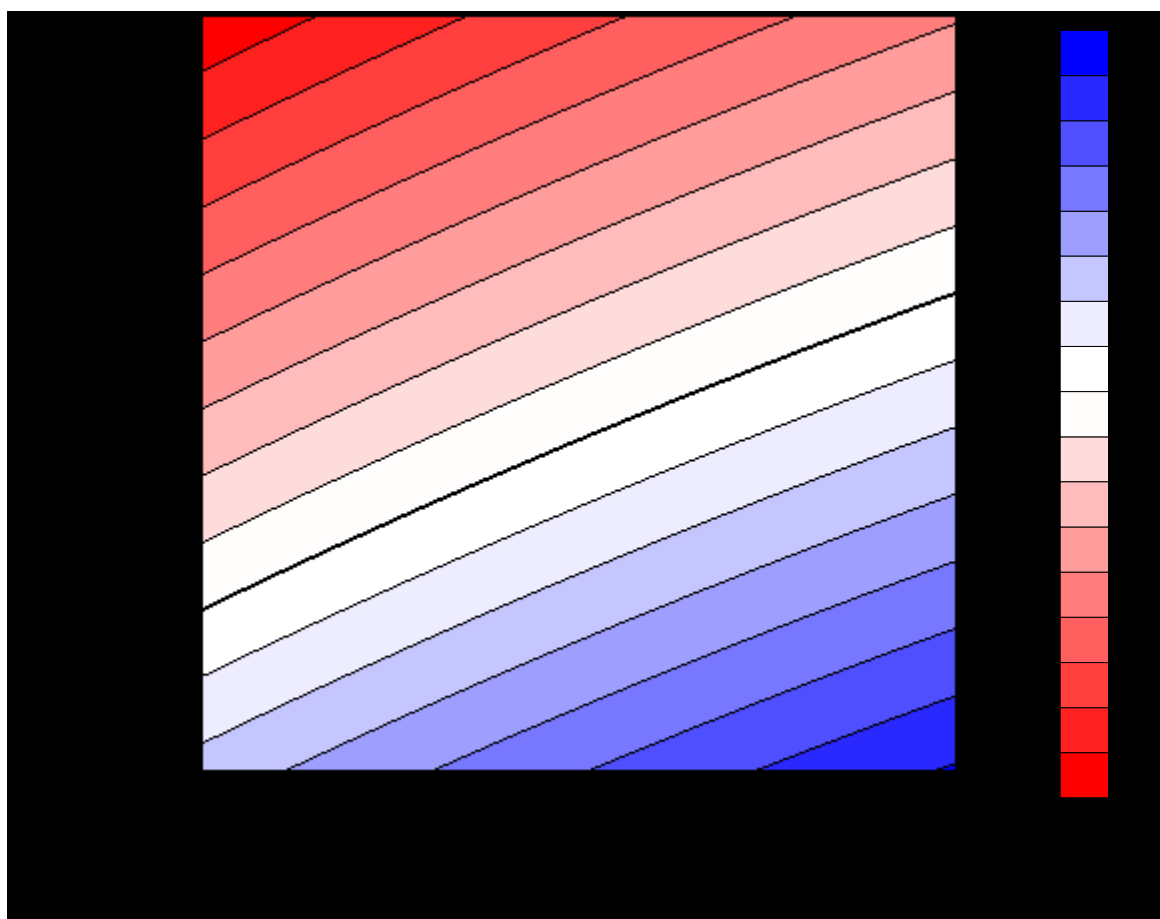


Figure 5.12: Saturation indices of dolomite calculated for water from the Paulusquelle, Bad Mergentheim.

2.4.5 Namedy Rocks

Altered Hunsrück shist from the “Inselsprudel” well in Namedy consists of quartz, muscovite-illite, siderite, kaolinite and minor amounts (<5%) of feldspar, ankerite and calcite. Chlorite and carbonates only occur in the upper part of the well. Literature data for unaltered Emsian silty shale (Flehmung, 1983, Figure 5.13 b.) yields large

amounts of quartz and muscovite-illite, 10-15 % of chlorite and minor amounts of siderite and kaolinite.

The well produces Na-HCO₃-Cl water, with 12 g/l of dissolved solids and 1.5 g/l of free CO₂ (Carlé, 1975). The gas phase is made up of 99,96 % of CO₂.

2.4.6 Bad Oyenhausen

The Alexander-von-Humbold-Sprudel has been described in detail by Geyh et al. (1977) beschrieben. Two pieces of core from 1025.8 and 1026.9 were available for analyses. The middle Bunter fine clastic rocks, silty claystone and anhydrite could be analogues for caprocks of the upper Bunter. The two samples contain reactive minerals in minor and trace amounts: feldspar, chlorite and calcite. Due to the limited number of samples, no further investigations were carried out for this analogue site.

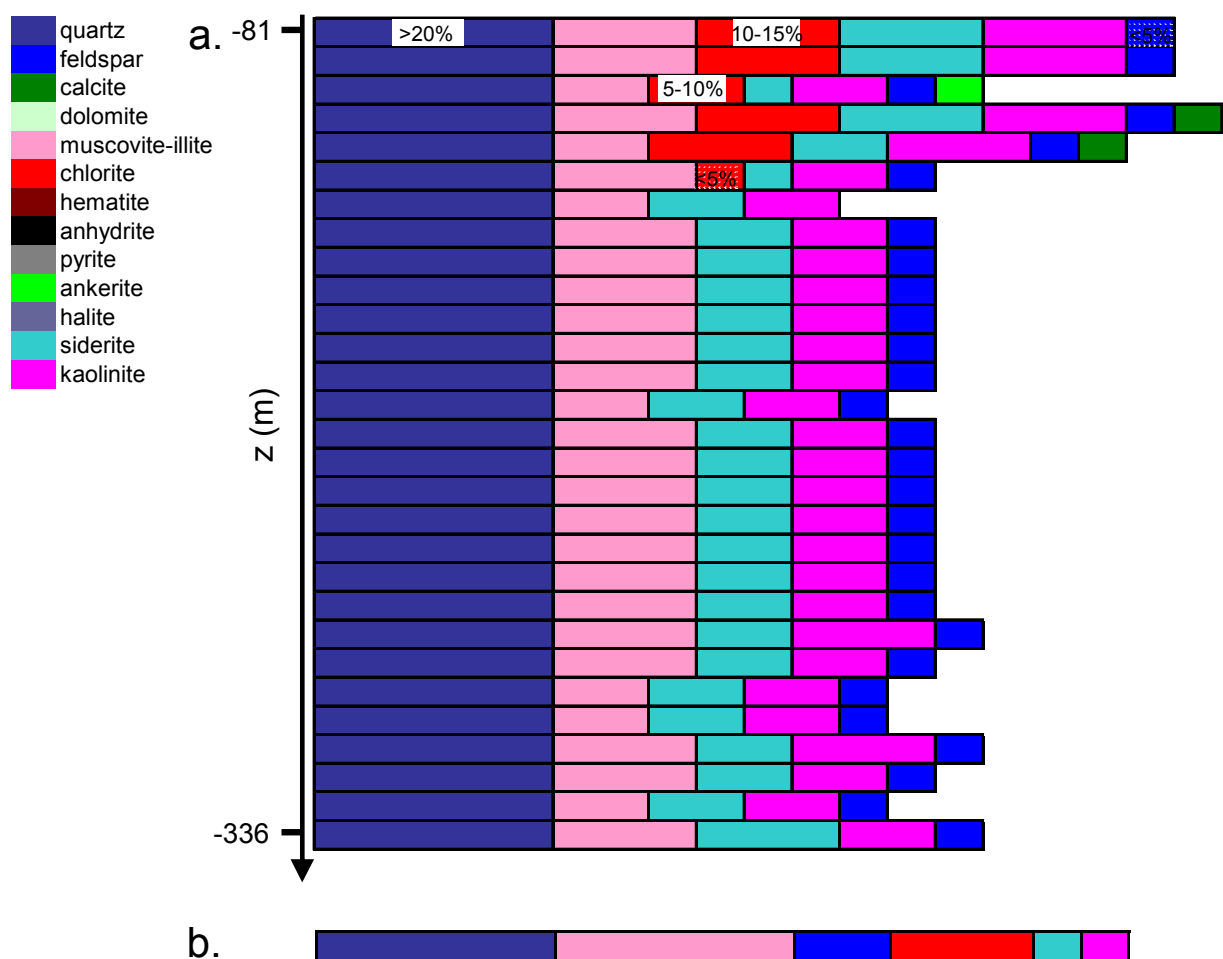


Figure 5.13: Namedy CO₂-altered Hunstrück shist (a.) and average Emsian silty shale (b.; Flehming, 1983)

2.5 Identification of Alteration Reactions involving CO₂

Comparing altered and unaltered Bunter sandstone from Barrien and Bad Mergentheim we can see that CO₂-rich water might have caused the dissolution of calcite and ankerite. Dissolution of alkali-feldspars by CO₂ is well known and could be indicated by the differences in relative abundance between Barrien and Bad Mergentheim samples. This could be the case for Chlorite as well. Illite and Hematite are less frequent in the Bad Mergentheim samples. As these minerals are rather stable, primary differences between the sandstones can not be ruled out without further investigations.

If we compare the altered - with unaltered Bunter sandstone samples from nearby quarries we can see that the “fresh” rock samples contain some kaolinite while the altered rocks do not show any kaolinite at all. The shallow samples from the quarries thus may be affected by Feldspar alteration by Mesozoic-tertiary saprolitic weathering. While dolomite is frequent in the upper Bunter, it has been detected in trace amounts only in one sample of the middle Bunter. This could be seen as an indication of dolomite dissolution, which is observed in experiments of Bunter sandstone alteration by Wiegand et al. (2008). However the ‘unaltered’ samples from the vicinity of Bad Mergentheim do not contain dolomite and hence the absence of dolomite may be a primary feature of the Middle Bunter near Bad Mergentheim.

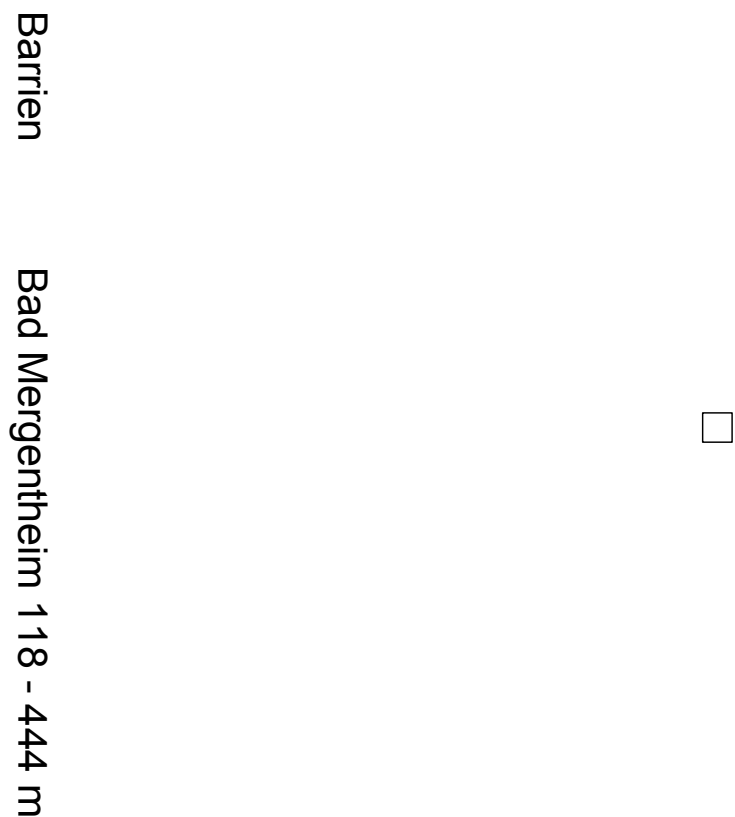


Figure 5.14: Relative mineral abundance of Middle Bunter sandstone samples from Barrien and Bad Mergentheim

In comparison to the Altmark rock samples the altered Rotliegend rocks from Bad Mergentheim do not contain any calcite at all. Therefore for the Rotliegend rocks from case study site Altmark we can assume that calcite will be dissolved by the CO₂-rich water.

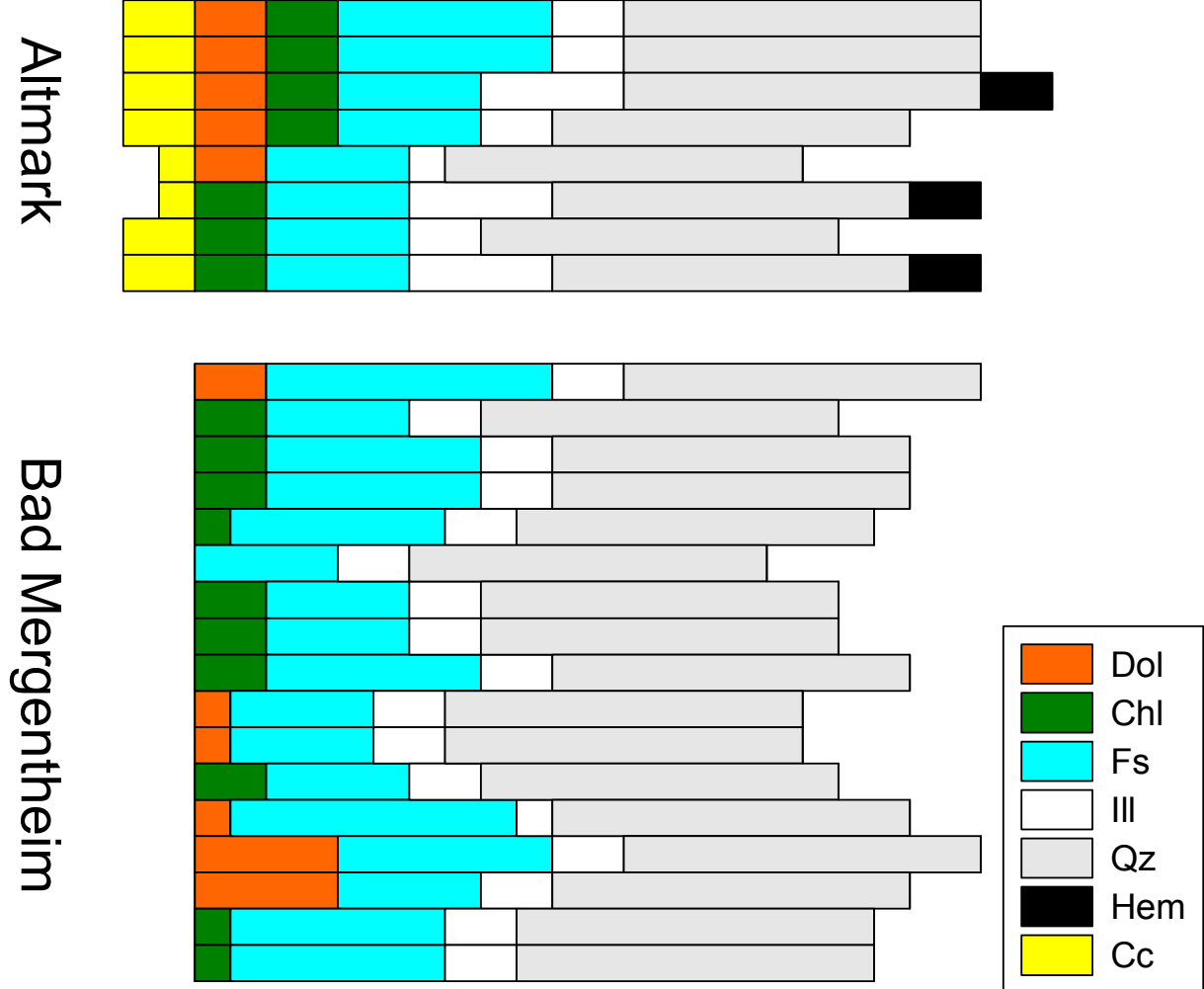


Figure 5.15: Relative mineral abundance of Rotliegend sandstone samples from the Altmark and Bad Mergentheim

The upper samples obtained from the Namedy well contain chlorite, a common primary mineral of Lower Devonian siliciclastic sediments. Chlorite has not been detected in the lower part of the samples. Compared to the unaltered Lower Devonian rocks, the samples from Namedy contain more siderite and kaolinite, which are products of chlorite alteration. This alteration of chlorite has been observed at other wells producing CO₂ rich water in the Rhenish Massif (May, 1994). Calcite and Ankerite occur in vicinity of a quartz veins with elevated concentrations of Cu, Pb, and As,

which indicate an epithermal mineralization, common in the region, not related to the recent mineral waters. The Namedy samples contain little illite and feldspar, but more kaolinite and siderite compared to the average Emsian silty shale (Flehmung 1983).

The geochemical composition of the shale samples from Namedy further indicates enrichment of Mg and a corresponding depletion of K compared to average Emsian clay stones (Redecke & Friedrich, 1991). This geochemical deviation could indicate incorporation of Mg into and release of K from illite during the alteration of chlorite.

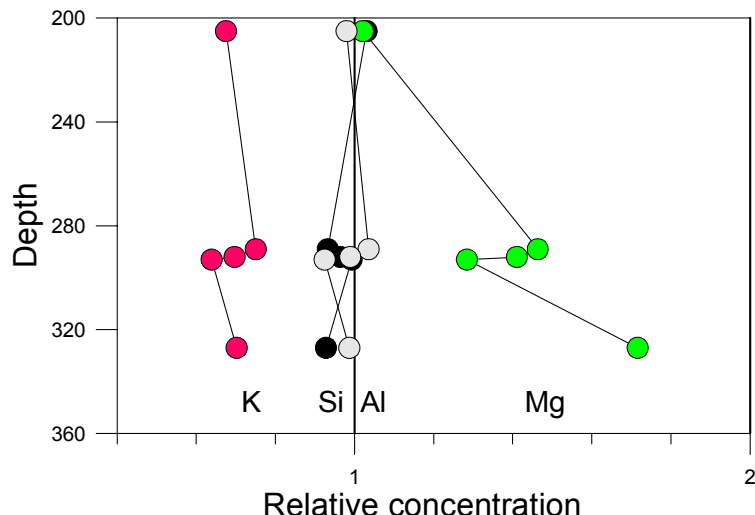


Figure 5.16: Geochemical composition of clay stones from Namedy, normalized to average Emsian shale composition.

Electron microscope images of altered rocks from a CO₂ exploration well in the East Eifel, 15 km from Namedy, reveal holes left from dissolved chlorite and adjacent patches of idiomorphic siderite crystals as well as idiomorphic kaolinite (Fig., 5.17, Niklas Mundhenk, BGR, pers. comm.)

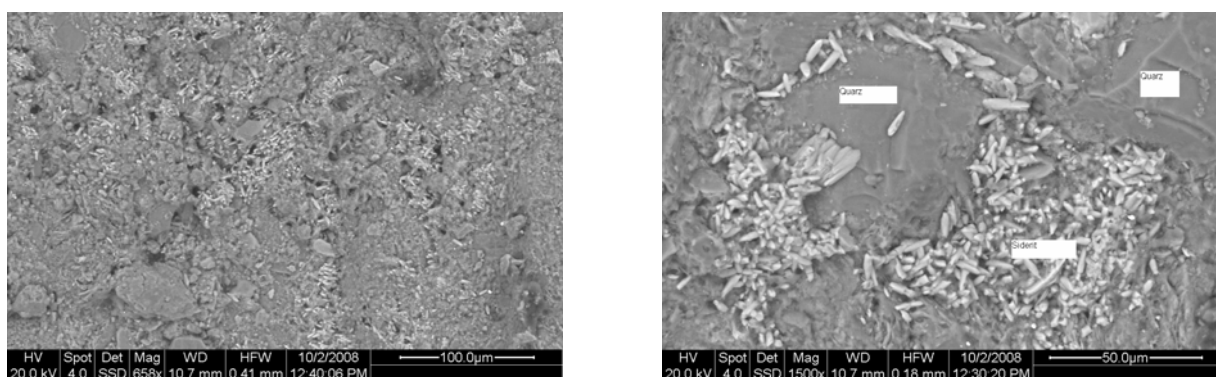
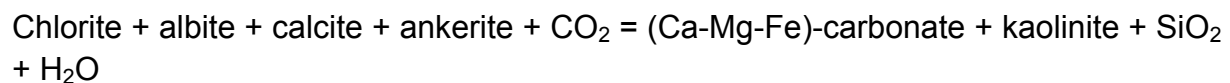


Figure 5.17: Korrosion of kaolinite (left) and idiomorphic siderite crystals (right) in Lower Devonian shale and sandstone from a CO₂ exploration well in the East Eifel; (pers. comm. Niklas Mindhenk, BGR).

Thin section microscopy at CO₂-altered rocks from Bad Mergentheim showed heavy corrosion of feldspar grains. This process can be interpreted as an onset of a slow CO₂-alteration reaction.

Summarizing these observations we can formulate the principal alteration reaction:



The reaction kinetics of reaction 1 is temperature dependent. Dolomite precipitation is also controlled by the salinity of the solution. High salinity reduces the solubility of dolomite and thus may lead to the precipitation of dolomite. Because of the dependence of temperature, CO₂-concentration and salinity on the respective alteration reaction, a decrease of CO₂-content or salinity or an increase of temperature yields dissolution of dolomite and a precipitation of chlorite. Carbonate precipitation and kaolinite dissolution might even support a locally increased pH value.

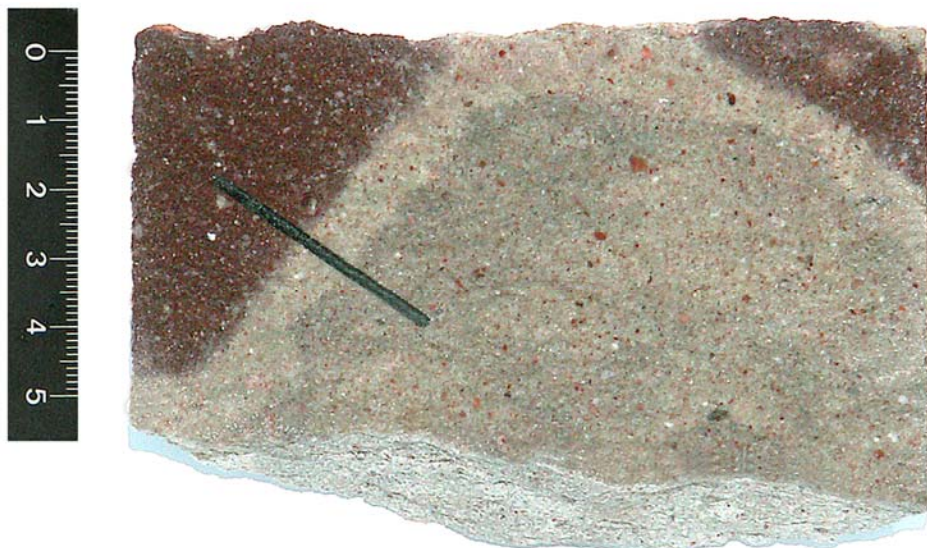


Figure 5.18: Altered Buntsandstein sample from core material of well Paulsquelle near Bad Mergentheim (depth 548.5 m) showing a colour-change induced by CO₂-rich water. Scale in cm. Detailed mineralogical and geochemical analyses were carried out along the black line.

One sample from Bad Mergentheim shows a distinct change of colours from red to grey, which represents a different level of alteration (see Figure 5.18).

Some samples from Bad Mergentheim were studied by means of cathodoluminescence petrography in order to detect alteration reactions and different carbonate generations. Different carbonate generations indicate a change of composition of mineral forming fluids.

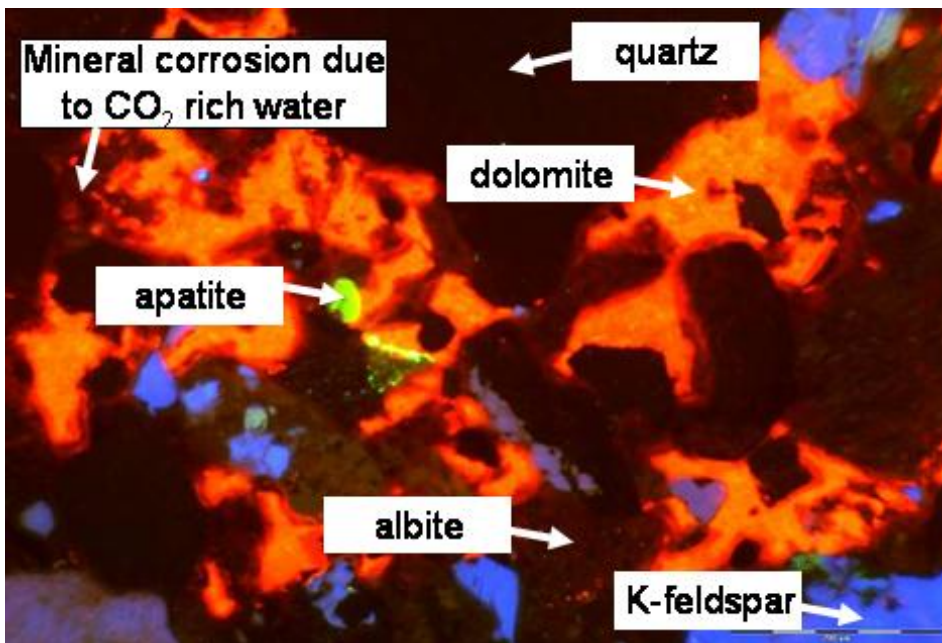


Figure 5.19: Chathodoluminescent thin section image of Rotliegend sandstone sample P11 from Bad Mergentheim, width of foto: 0.9 mm.

Figure 5.19 shows a cathodoluminescence picture of a CO₂-altered rock sample. The different rock forming minerals are luminescating in different colours. We can see blue luminescating potassium feldspar, dark Quartz and Albite and apple-green to yellow luminescating apatite. Raster-Electrone-Microscope analyses showed pure dolomite cement, luminescating. Besides to a distinct zonation of the dolomitic cement which is indicated by a colour change from red along the rim to orange in the core zones of the crystals we can see regions of heavy mineral corrosion, occurring around the dark grey to black albite grains. This corrosion might be due to the circulation of CO₂-rich water.

Drill core samples from Bad Mergentheim, macroscopically revealing an alteration zone (see Figure 5.18), were selected and studied with respect to chemical composition by EDX-mapping. Figure 5.20 shows the results of energy dispersive X-ray mapping within the altered rock along the sequence from red to grey. The intensity of the colours corresponds to the concentration of a certain element in this region.

The backscatter electron picture on the left hand side shows a porosity-decrease within the light grey transition zone (Figure 5.20, 1).

The porosity decrease in this region is also indicated by an increase of calcium, carbon and magnesium in the transition zone (Figure 5.20, 2-4). This confirms that dolomite was precipitated from the circulating water. The iron content is consistent except for enrichment near to the transition zone (5). Silicium does not show any changes.

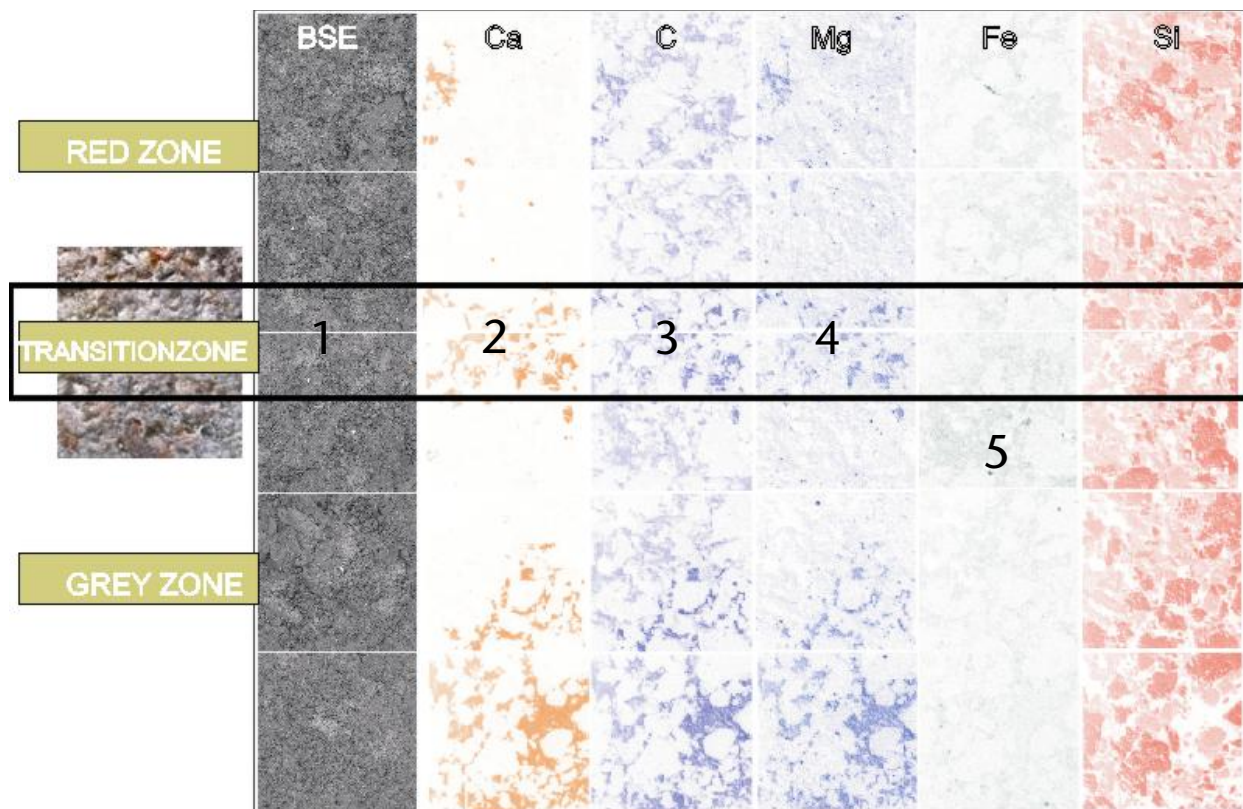


Figure 5.20: Supplementary geochemical and mineralogical analyses (EDX mapping)

XRF-analyses within the red, light grey and dark grey zones yielded chlorite in the dark grey zone while dolomite is completely absent. In the red part of the rock sample no chlorite but only dolomite was detected. Over all the dolomite content is decreasing from the red to the dark grey part, while the amount of chlorite is rising. As dolomite is the main cement within these rocks, porosity within the dark grey zone is distinctly higher than within the red zone. The reason for a precipitation of chlorite can be a rising temperature or a decrease of CO₂-content within the water. A dolomite precipitation also depends on the salinity of a fluid. A high salinity reduces dolomite solubility and thus can lead to a precipitation of dolomite. The depletion of Sr and Ba in the greenish Bunter sample from Bad Mergentheim (Bröckelschiefer) compared to the red surrounding rock (Henke, 2006) indicates liberation of these elements during Feldspar alteration.

A representative set of rock samples from Barrien, Salzwedel and Bad Mergentheim were studied with respect to the amount and estimated chemical composition of clay minerals as these minerals are supposed to be the key component regarding possible mineral reactions. Therefore, the < 2 µm fraction was separated by sedimentation (Atterberg principle) and investigated by XRD texture slides as well as infrared spectroscopy. XRD of the < 2 µm fraction of Salzwedel shows illite, quartz, and chlorite. The 001-reflexes of chlorite -compared with Moore & Reynolds (1997) - indicate the presence of Fe-rich chlorite with symmetric distribution of Fe (homogenous distribution over the two different octahedral layers). This result was confirmed by XRF yielding a Fe/Mg ratio of 2:1. Fe-dominated chlorites are less reactive than Mg-chlorites.

The applied analytical techniques were inapplicable in for the case study site Barrien due to the presence of kaolinite.

2.6 Code Comparison and Numerical Simulation

2.6.1 Code Comparison

As in the reservoir sequences of the study areas Barrien and Altmark highly saline brines are found, for numerical simulation the Pitzer model (Pitzer, 1991) has to be applied. To compare and to check software and available thermodynamic data bases, a code intercomparison study was carried out. The code comparison was performed together with TU Clausthal (Eclipse 300), RWTH Aachen (Shemat), Uni Stuttgart (Mufte UG) und IFP (SIMUSCOOP).

The results of the code intercomparison and further actions are:

For all existing geochemical simulation tools existing thermodynamic data bases are not applicable to the high salinity and mineralisation of the pore fluids in the Altmark and Barrien case study sites

BGR prepares for two projects to doubt these problems. Extensive laboratory measurements are planned to study the effect of pure and impure CO₂ on minerals and rocks

In addition to that a project will be carried out to improve existing reaction kinetic data bases, in collaboration with “Gesellschaft für Anlagen- und Reaktorsicherheit (GRS) mbH”.

Further necessary improvements of coupled T-H-M-C simulators necessary to simulate complex problems associated with the injection of CO₂ into subsurface reservoirs are planned in projects of the GEOTECHNOLOGIEN programme, site-specific for the Altmark CO₂ storage demonstration site in the CLEAN project (<http://www.fz-juelich.de/ptj/index.php?index=670>).

2.6.2 Numerical Simulation

In the beginning of the project the required hardware (computer and monitor) was acquired. Simultaneously the capability of different simulation software tools was evaluated. Special investigations and benchmark-tests were carried out by the University of Stuttgart in the framework of the GEOTECHNOLOGIEN research programme. After the evaluation of the available software tools, the simulation software TOUGHREACT which was developed at the Lawrence Berkeley National Laboratory, USA was chosen. In January 2006 the chosen simulation software was tested and some calculations of reactive transport combined with CO₂-storage were performed during a two days TOUGHREACT workshop in Berkeley, USA.

For model preparation and visualisation of results of TOUGHREACT simulations the pre- and post-processor PetraSim was purchased and installed. Some principal

TOUGHREACT simulations were carried out, where numerical model and input files were created with the PetraSim software.

There exist numerous experimental studies concerning geochemical reactions caused by CO₂ injection into reservoir sandstones (e.g., Pearce, et al., 2000, Shiraki & Dunn, 1998, Soong, et al., 2004). The test conditions were measurement intervals of few months to two years, pressures up to 20 MPa, temperatures up to 105 °C and different pore fluid compositions. Under these conditions in some cases distinct alteration reactions at primary calcites and dolomites was determined. For some experiments anhydrite was dissolved while calcite was simultaneously precipitated and incipient feldspar corrosion with formation of Na-Smektite or Kaolinite occurred. Further experiments were carried out to yield reactionkinetic and thermodynamic stability data for different minerals (e.g., Pokrowski & Schott, 1999, Gautelier et al., 1999, Cubillas et al., 2004).

On the other hand the currently existing mineral databases for a reliable simulation of long-term consequences of CO₂ storage in the deep subsurface still are very incomplete. This lack of information can not be eliminated by means of geochemical benchmark testing (Pruess et al., 2004).

Based upon available databases and for low salinity fluids numerous simulation calculations were already performed in order to yield fast and slow CO₂-induced mineral reactions. Fast mineral reactions, pH changes and CO₂-solubility in formation water that occur within a few years after injection were studied by Johnson (2004). Slow reactions and carbonate precipitation were recently studied by White et al., 2003, Xu et al., 2004, Knauss et al., 2005 and Hellevang, 2006, utilizing batch simulations and reactive transport simulation.

Geochemical simulation and first experiments of injection of a CO₂-rich solution in gypsum or anhydrite containing reservoir rocks with subsequent modification to calciumcarbonate is studied by Kühn et al. (2006) within the current GEOTECHNOLOGIEN programme. Accordingly, the basic Zechstein rocks, below the thick Salt cap rocks, would have potential for chemcal trapping of CO₂.

Though the quantitative interpretation of PHREEQC equilibrium simulation results is not possible for highly saline brines, the predicted alteration reactions coincide with the postulated reactions. The calculated pore volume changes resulting from chlorite dissolution and dolomitization of a calcite-bearing Rotliegend rock are little (<1 Vol.-%, May 2004). Though absolute porosity changes due to reactions are are little, permeability changes are possible (see chapter 4).

2.7 Interpretation of Geochemical Results

Geochemical transformation of potential reservoir rocks and cap rocks due to the effect of carbonic acid depends on the mineral composition.

Especially carbonates, feldspar and alumo-silicates will be dissolved or transformed by acid solutions. Other minerals, such as Quartz are quite stable regarding carbonic acid. On the other hand minerals can precipitate from acidic solution containing for example different alkaline earth metals or iron. These reactions are taking place in different velocities. Fast geochemical reactions can affect CO₂-injection; slow reactions will mainly influence long-term safety.

Regarding rock formations we can say that in pure sandstones dissolution reactions will be negligible, especially in combination with quartz cement. This also means that the potential of unwanted dissolution reactions essentially depends upon the amount of highly reactive minerals (e.g. carbonates, sulphates) within a rock formation. Mineral dissolution can either enhance injectivity or reduce long-term safety, depending on the position where it occurs, in the reservoir or cap rocks.

On the other hand there can also be mineral precipitation from the CO₂-rich and highly mineralized brines. In the investigated natural analogue sample from Bad Mergentheim the precipitation of carbonates (dolomite) in open pores could be proved unambiguously. Such mineral trapping will presumably occur in the long-term.

XRD analyses of rocks from the Altmark show that generally only small amounts of carbonates and clay minerals exist within the reservoir rocks. Both, Rotliegend sandstone and rocks of the middle Bunter sandstone mainly consist of quartz, feldspar and muscovite-illite. Larger amounts of 5-10 volume percent of calcite only occur within thin siltstone layers within the Rotliegend sandstone layers. In most of the rocks only traces of calcite and chlorite were detected. For this reason technically important fast alteration reactions near to the CO₂-injection wells which could lead to stability problems are not to be expected. Anyhow, a change of porosity and permeability, caused by dolomite precipitation, has to be considered. Especially for Rotliegend reservoir rocks where primary permeability already is quite low, dissolution of calcite or chlorite and a precipitation of dolomite could have geotechnically important effects.

A thick and laterally homogeneous rock salt layer most probably will be an ideal cap rock regarding potential fast and slow geochemical reactions. Generally, such thick rock salt layers can be found within the study areas.

A future task will be to determine, the conditions under which siderite, ankerite, or dolomite will be precipitated. Apart from the cationen-ratios of the source rocks, the carbonate composition depends on Temperature, CO₂ pressure and the reaction progress along the flow path of the waters (May 2005). Numerical simulation could also be used to obtain possible alteration reactions involving albite and microcline.

Simulations including reaction kinetics can distinguish fast and slow changes in mineral composition, porosity of reservoir and cap rocks due to injection of CO₂ in natural gas fields and thus help to quantify processes relevant to long-term safety and storage operation.

References

- Bateman, K., Turner, G., Pearce, J.M., Noy, D.J., Birchall, D. & Rochelle, C.A., 2005. Large-scale column experiment: Study of CO₂, porewater, rock reactions and model test case. *Oil and Gas Science and Technology* 60, (1), pp. 161-175.
- Carlé, W., 1975. Die Mineral- und Thermalwässer von Mitteleuropa. 643 p., Wissenschaftliche Verlagsgesellschaft, Stuttgart.
- Czernichowski-Lauriol, I., Sanjuan, B., Rochelle, C., Bateman, K., Pearce J. & Blackwell, P., 1996. Analysis of the geochemical aspects of the underground disposal of CO₂: scientific and engineering aspects. In: Apps, J.A. & Tsang, C. (eds.) *Deep Injection disposal of hazardous and industrial waste*. S. 565-583 (Academic Press).
- Cubillas, P., Köhler, P., Prieto, P., and Oelkers, E. H., 2004. Experimental determination of the dissolution rates of calcite, aragonite and bivalves. *Chem. Geol.*, 216, pp. 59-77.
- Gautier, M., Oelkers, E. H., and Schott, J., 1999. An experimental study of dolomite dissolution rates as a function of pH from -0.5 to 5 and temperature from 25 to 80°C. *Chem. Geol.*, 157, pp. 13-26.
- Geyh, M.A., Knauff, W., Langguth, H.R., Leichtle, Th, Michel, G., Nielsen, A., Scherp, A., Schwartz, U. (1977): Der Alexander-von-Humboldt-Sprudel in Bad Oeynhausen. *Fortschritte in der Geologie von Nordrhein-Westfalen* Band 26. Krefeld, 269 Seiten.
- Hellevang, H., 2006: Interactions between CO₂ saline water and minerals during geological storage of CO₂. PhD Thesis, Univ. of Bergen.
- Henke, C., 2006. Diplomkartierung, Charakterisierung potenzieller Rotliegend-Speichergesteine des Erdgas-Förderfeldes Altmark und Vergleich mit CO₂-beeinflußtem Rotliegend der Region Taubertal anhand von Dünnschliffen. 129 p. Hannover, unpubl.
- Henke, C., Hoth, P., May, F., 2006: Analyse von Tiefenwasserproben aus der Erdgaslagerstätte Altmark. Unveröffentl. Archivbericht, 36 Sp, BGR, Hannover.
- Johnson, J.W., Nitao, J.J., & Knauss, K.G., 2004: Reactive transport modeling of CO₂ storage in saline aquifers to elucidate fundamental processes, trapping mechanisms and sequestration partitioning. In: Baines, S.J., and Worden, R.H. (eds), *Geological Society, London, Special Publications*, 233, pp. 107-128.
- Knauss, K.G., Johnson, J.W., and Steefel, C.I., 2005: Evaluation of the impact of CO₂, co-contaminant gas, aqueous fluid and reservoir rock interactions on the geologic sequestration of CO₂. *Chem. Geol.*, 217, pp. 339-350.

Kühn, M., Clauser, C., Vosbeck, K., Stanjek, H., Back, M., Peiffer, S., 2006: Numerical simulation of CO₂ Storage by mineral trapping in geothermal reservoirs- SDGG, 50, 153.

Manhenke, V., Reutter, E., Hübschmann, M., Limberg, A., Lückstädt, M., Nommensen, B., Peters, A., Schlimm, W., Taugs, R., & Voigt, H.-J., 2001. Hydrostratigraphische Gliederung des norddeutschen und mitteldeutschen känozoischen Lockergesteinsgebietes. – Z. angew. Geol., 47/3-4 Hannover: pp. 146-152.

May, F., 1994: Zur Entstehung der Mineralwässer des Rheinischen Massivs. Dissertation Univ. Bonn, 136 p., unpubl.

May, F., 2004: Geochemical impact assessment of CO₂ storage in the North German Basin. — in: R. B. Wanty & R.R. Seal II: Water Rock Interaction. pp. 561–565 (Balkema).

Moore, D.M., Reynolds, R.C.Jr. (1997) X-ray diffraction and the identification and analysis of clay minerals, 2nd edition, Oxford University Press, Oxford

May, F., 2005: Alteration of wall rocks by CO₂-rich waters ascending in fault zones. – Oil & Gas Science and Technology – Rev. IFP, pp. 60,1:19-32.

Pearce, J.M., Czernichowski-Lauriol, I., Rochelle, C.A., Springer, N., Brosse, E., Sanjuan, B., Bateman, K., and Lanini, S., 2000. How will reservoir and caprock react with injected CO₂ at Sleipner? Preliminary evidence from experimental investigations. In: Williams et al. (eds.) Proceedings of the 5th International Conference on Greenhouse Gas Control Technologies. CSIRO, Cairns, Australia, p 355-359.

Pitzer, K.S., 1991. Ion interaction approach: theory and data correlation. In Activity coefficienc in electrolyte solutions, pp. 73-153. 2nd edn. CRC Press.

Pokrowski, O.S., and Schott, J., 1999: Processes at the magnesium-bearing carbonates / solution interface. II. kinetics and mechanism of magnesite dissolution. Geochim. et Cosmochim. Acta, Vol. 63, No. 6, pp. 881-897 (17).

Pruess K., Garcia J., Kovscek T., Oldenburg C., Rutqvist J., Steefel C. and Xu T., 2004: Code intercomparison builds confidence in numerical simulation models for geologic disposal of CO₂, Energy, Volume 29, Issues 9-10, 6th International Conference on Greenhouse Gas Control Technologies, pp. 1431-1444.

Redecke, P., Friedrich, G., 1991: Geochemische Charakterisierung paläozoischer Sedimente der Nordeifel mit Hilfe geostatistischer Methoden. Chemie der Erde 51: 115-130.

Reutter, E., 2005: Hydrostratigrafische Gliederung Niedersachsens, Geofakten, LBEG Hannover, 10 p.

Shiraki, R. und Dunn, T., 1998: Experimental study on water-rock interactions during CO₂ flooding in the Tensleep Formation, Wyoming, USA. Appl. Geochem. 15, pp. 265-279.

Soong, Y., Goodman, A.L., McCarthy-Jones, J.R. and Baltrus, J.P., 2004: Experimental and simulation studies on mineral trapping of CO₂ with brine. Energy Conversion and Management, 45 (11-12), pp. 1845-1859.

White, S.P., Allis, R.G., Moore, J., Chidsey, T., Morgan, C., Gwynn, W., and Adams, M., 2003. Injection of CO₂ into an unconfined aquifer located beneath the Colorado, Central Utah, USA. Proceeding, Annual Conference on Carbon Sequestration, Alexandria, VA. 15p.

Wigand, M., Carey, J.W. Schütt, H., Spangenberg, E., Erzinger, J., 2008: Geochemical effects of CO₂ sequestration in sandstones under simulated in-situ conditions of deep saline aquifers. Applied Geochemistry (in press).

Xu, T., Apps, J.A., and Pruess, K., 2004: Numerical simulation of CO₂ disposal by mineral trapping in deep aquifers. Appl. Geochem. 19, pp. 917-936.

Work Package 6

Simulation of CO₂ Sequestration and Natural Gas Production Enhancement

Issues:

- Upscaling geologic models to dynamic grid models
- History matching & production forecast until economic limits
- CO₂-injection & CH₄-production rates and pressures
- CSEGR injection/production scenarios & strategies
- Sensitivity study and evaluation
- Geological and reservoir-mechanic limits for CSEGR

Authors:

G.F. Ionescu, G. Pusch, ITE TU-Clausthal

| | |
|--|-----|
| Kurzfassung | 211 |
| 6.1 Introduction..... | 212 |
| 6.2 Prototype Case Barrien. | 212 |
| 6.2.1 Reservoir section Barrien Model. | 212 |
| 6.2.2 Model Validation: History Matching..... | 214 |
| 6.2.3 CO ₂ Injection Strategies..... | 219 |
| 6.3.4 Simulation results..... | 223 |
| 6.3 Simulation of Altmark Gas Field. CO ₂ - Disposal and its Effects on Gas Recovery | 232 |
| 6.3.1 Simulation of the sector model Altmark Block 12 | 232 |
| 6.3.1.1. Block 12 model description..... | 232 |
| 6.3.1.2 Injection strategy | 233 |
| 6.3.1.3 Simulation Results..... | 235 |
| 6.3.2. Simulation of the CO ₂ - disposal into a coupled sector model Altmark Block 12+14..... | 240 |
| 6.3.2.1 Model Description..... | 240 |
| 6.3.2.2 Injection strategies and sensitivities | 242 |
| 6.3.2.3 Simulation results. | 243 |
| 6.3.2.4 Simplified Generic - Two Regions Model..... | 245 |
| 6.4. Conclusions | 249 |

Kurzfassung

Eine Machbarkeitsstudie für neue Technologien der CO₂ Deponierung in erschöpften Erdgaslagerstätten bedarf einer soliden Programmunterstützung zur Modellierung des Speicherprozesses und der Auswirkung auf die Förderung des Restgases (EGR). Im WP 3 sind die beiden Kandidaten Barrien und Altmark als Prototypen für homogene Antiklinallagerstätten und stratifizierte Kompartimentlagerstätten geologisch beschrieben worden. Die Leistungsfähigkeit des Gasspeicher Simulators ECLIPSE 300 wird in WP 4 als gegenwärtig bester Kompromiss zwischen realer Lager-stättenmodellierung und Prozessmodellierung beschrieben. In WP 6 wurden die beiden Prototypen Barrien und Altmark an Hand von Sektormodellen auf die Auswirkung der CO₂ Injektion untersucht. Ein wichtiges Kriterium für die Festlegung der Zusatzförderung ist der tolerierbare CO₂ Gehalt im produzierten Gas. Eine Abtrennung und Re-injektion wurde dabei zunächst ausgeschlossen. Von der technischen Handhabung und dem Einfluss auf den Brennwert her gesehen erschien ein maximaler Wert von 10 % zulässig. Bei Überschreiten dieses Wertes wurden die Produktionssonden geschlossen. Verschiedene Szenarien mit simultaner Injektion/Produktion als auch verspäteter Produktionsaufnahme wurden untersucht. Nach dem Einschließen aller Produktionssonden endet die Phase der EGR und die Phase des ausschließlichen Deponierens von CO₂ beginnt. Dazu werden alle Sonden als Injektoren umgerüstet und die Injektion bis zum Erreichen des initialen Lagerstättendrucks fortgesetzt. Folgende wichtige Ergebnisse können aus diesen Simulationen abgeleitet werden:

- Die maximale Zusatzförderung durch CO₂ Injektion betrug im Falle Barrien bis zu 9 % des IGIP und im Falle Altmark bis zu 3 % des IGIP.
- Für EGR ist die simultane Injektions-/Produktionsstrategie die beste Variante. Für eine homogene Antikinalstruktur (Barrien) ist ein „overbalanced mode“, d.h. höhere Injektionsraten vorzuziehen, während bei stratifizierten Trägern der „underbalanced mode“ höhere EGR Ausbeuten verspricht.
- Im Block 12 der Altmark Gaslagerstätte können 45 Mt an CO₂ und in Verbindung mit der Nachbarscholle 14 sogar 112 Mt gespeichert werden. Das entspricht der Emission eines Großkraftwerks (1600 MW) über die Zeitdauer von 11 Jahren. Die ausgewählten Regionen der Buntsandsteinlagerstätte Barrien fassen ca. 17 Mt an CO₂.
- Die unterschiedlichen Lagerstättenformen- Antiklinale und stratifizierte Kompartimentlagerstätte -werden durch unterschiedliche Mechanismen der Speicherung geprägt. Bei Antikinalen dominieren die Dichteefekte, während bei stratifizierten Lagerstätten die Viskositätseffekte neben der Schwerkraft an Bedeutung gewinnen. In stratifizierten Speichern nimmt der Beschleunigungseffekt der Restgasgewinnung deutlich zu gegenüber homogenen Speichern.
- Fließbarrieren wie Störungen oder Faziesgrenzen sind für die CO₂ Ausbreitung und besonders für die Verzögerung des Durchbruchs von großer

Bedeutung und müssen daher möglichst realistisch modelliert werden, um glaubwürdige Aussagen zur EGR zu gewährleisten.

6.1. Introduction.

Depleted natural gas reservoirs are promising candidates in storing CO₂ while enhancing the recovery of natural gas. These reservoirs may be depleted but a certain amount of gas still existing in place, hence by injecting carbon dioxide part of the residual gas may be produced increasing thus the final recovery in the reservoir. CO₂ storage in a gas reservoir will be attractive for the operators if the process will provide economic benefits. There were two types of reservoirs chosen for this study: one is relatively homogenous with a large dip in order to make use of the large gravity of the CO₂ (Barrien), whereas the other one is flat and stratified with large vertical heterogeneity (Altmark).

In this chapter it will be evaluated the feasibility of storing and enhancing the recovery of two depleted German gas fields: Barrien and Altmark will be evaluated by means of numerical reservoir simulation.

6.2 Prototype Case Barrien.

6.2.1 Barrien Reservoir Sector Model.

A 3D reservoir-simulation model was build and validated in ECLIPSE 100 by WINTERSHALL AG for Barrien gas field comprising a total of 51 x 66 x 18 grid blocks on the basis of all available information, including reservoir characteristic data, aquifer data, fault data, and production data for the entire production period in the form of reports of daily gas production rates.

In this work, a sector model will be used, which will represent our study area (regions 1 and 2) with nearly half of the grid blocks in the original model. The study area in the Barrien gas field consists of two compartments; region 1 is located on the right side of the sector model and region 2 on the left side of the sector model, see Figure 6.1. It was mandatory to comprise region 12 in this sector model to obtain a pressure history match between actual and simulated data. Three production wells BRIN3T, BRIN8T, and BRIN11T exist in region 2 and one producer BRIN5T in region 1.

The compositional simulator ECLIPSE 300, with options for diffusion and gas dissolution in water, is used. The base reservoir model contains native gas, and the injected gas stream contains pure CO₂. The original model consists of 60588 grid blocks, with each cell having 150 m in X direction and 75 m in Y direction. Grid type is Cartesian while grid geometry is corner point. The simplified 3D model includes vertical zoning representing the compartments. The model is divided vertically into 18 grid blocks with different thicknesses.

The extension of both compartments is about 7000 m in X direction and 2500 in Y direction. The net thickness of gas column is about 20 - 45 m. The gas initially in place in Region 1 and Region 2 is $3.04 \times 10^9 \text{ sm}^3$ and $4.07 \times 10^9 \text{ sm}^3$ respectively. Two semi sealing faults, separate the two compartments, as present in Figure 6.7. A

cross-section of the model is presented in Figure 6.2. The Barrien gas composition comprises about 87% methane and 13% nitrogen.

Basics adaptation tests with E300 should be taken into account for matching the field data with the simulation results to ensure the reliability of the simulation model.

In this sector model, history matching is a must after the modifications done for the sector model, by taking out all unnecessary regions, wells, aquifers, production data, which were existing in the original model and the translation of the model in compositional simulation (ECLIPSE300).

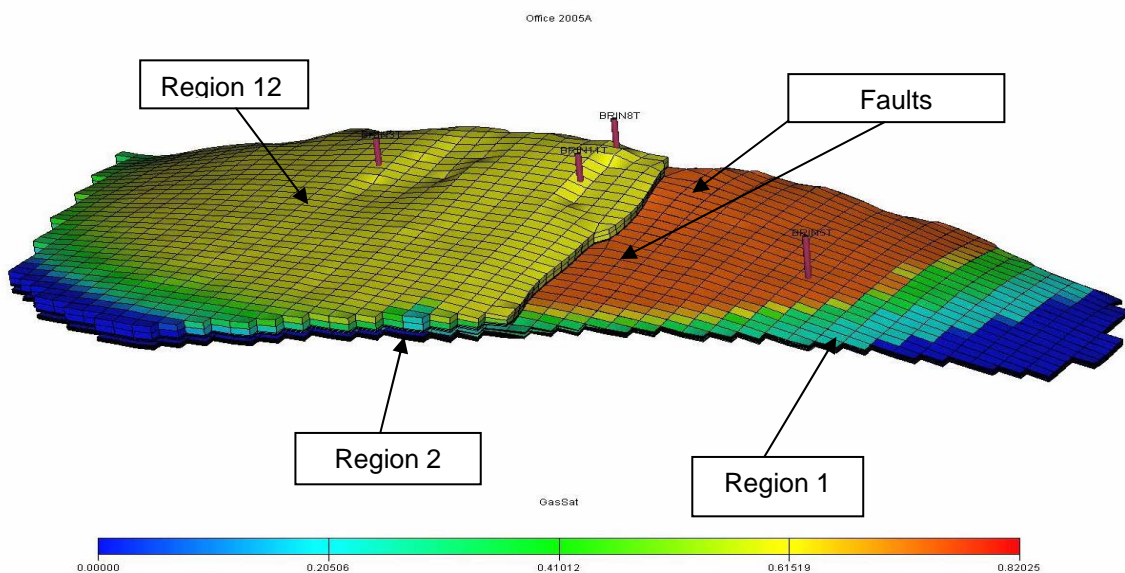


Fig. 6.1 - 3D view of the three regions model and existing production well locations.

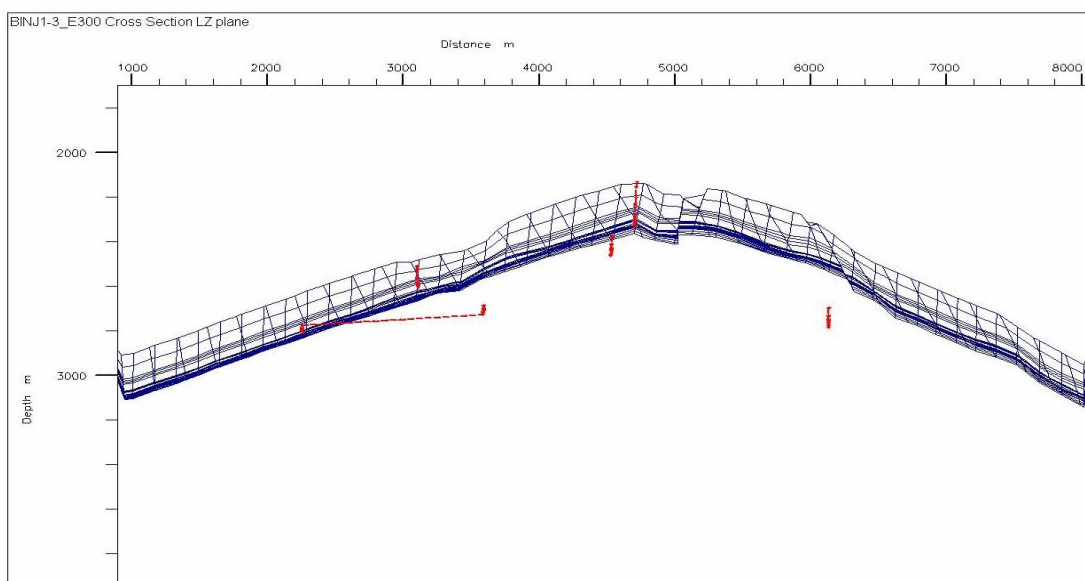


Figure 6.2 – E-W Cross-section of the Barrien Simulation Model

The validation of this sector model can be approached using bottomhole pressure matching. Simulated well bottomhole pressures (WBHP) are compared with the corresponding actual bottomhole pressures. The key parameters that effect the history match phase and grant good history match quality are:

1. Transmissibility of the semi sealing faults.
2. Energy supply from adjacent region 12.

6.2.2 Model Validation: History Matching

The sector model was run without any modification in the original form . Figures 6.3 – 6.6 show the initial results before history match presenting the observed and simulated data. No match was achieved between simulated bottomhole pressure and measured bottomhole pressure in the region 2, but there is an acceptable match in the region 1 with well BRIN5T. The original simulated WBHP without any adaptation are called “base case”

Several simulation runs with modified model properties were carried out to achieve a high-quality match. Four key wells BRIN3T, BRIN8T, BRIN11T, and BRIN5T were identified for the history match process. Aquifer data were not the key parameters to achieve a good match.

The transmissibility of all faults was adjusted to zero, except for the two faults which separate the two regions 1 and 2. For the aim of an acceptable history match, the original volume of gas in place was considered to be located in three compartments regions 1, 2, and 12 (termed as BARRIEN 1-5). A satisfactory match in both regions 1 and 2 was obtained. The following figures summarize the history match cases.

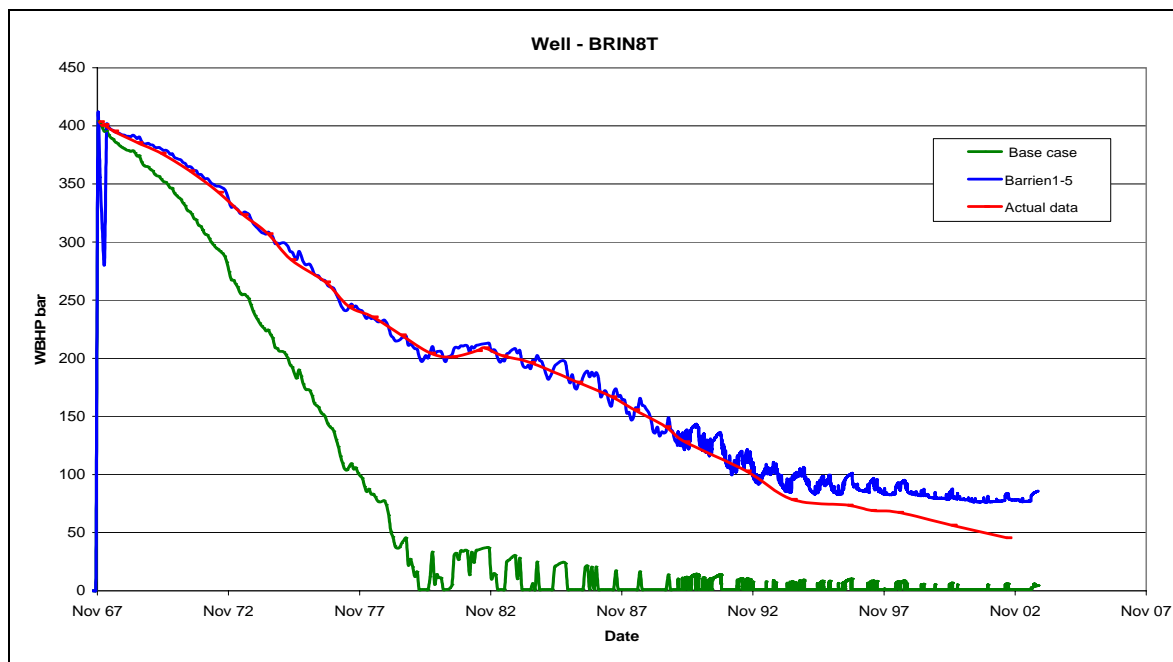


Figure 6.3 – BHP vs. time for well BRIN8T before History Matching

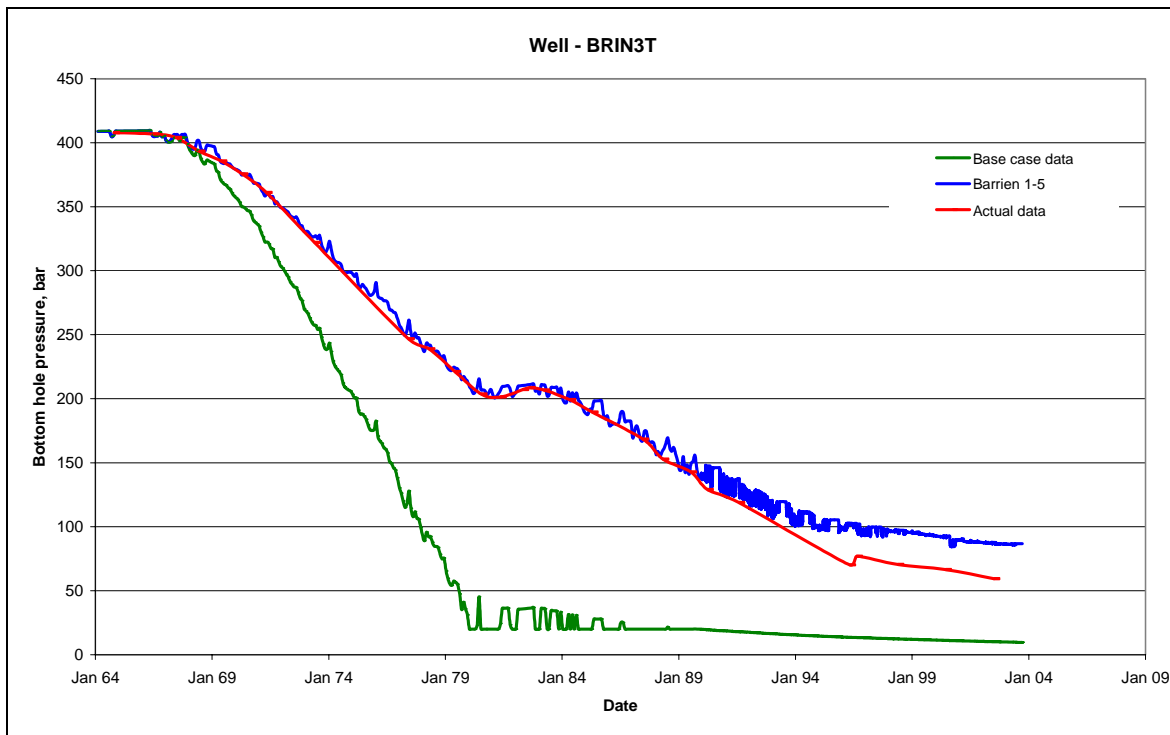


Figure 6.4 - Bottom BHP vs. time for well BRIN3T before History Matching

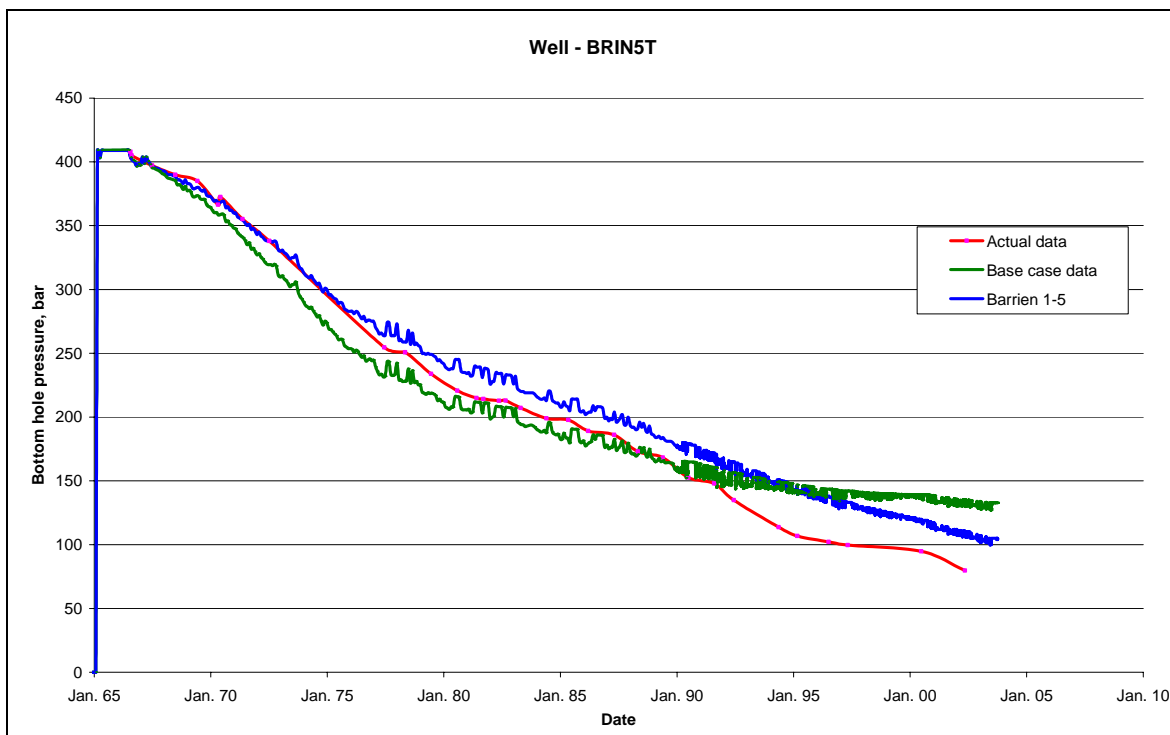


Figure 6.5 - BHP vs. time for well BRIN5T before History Matching

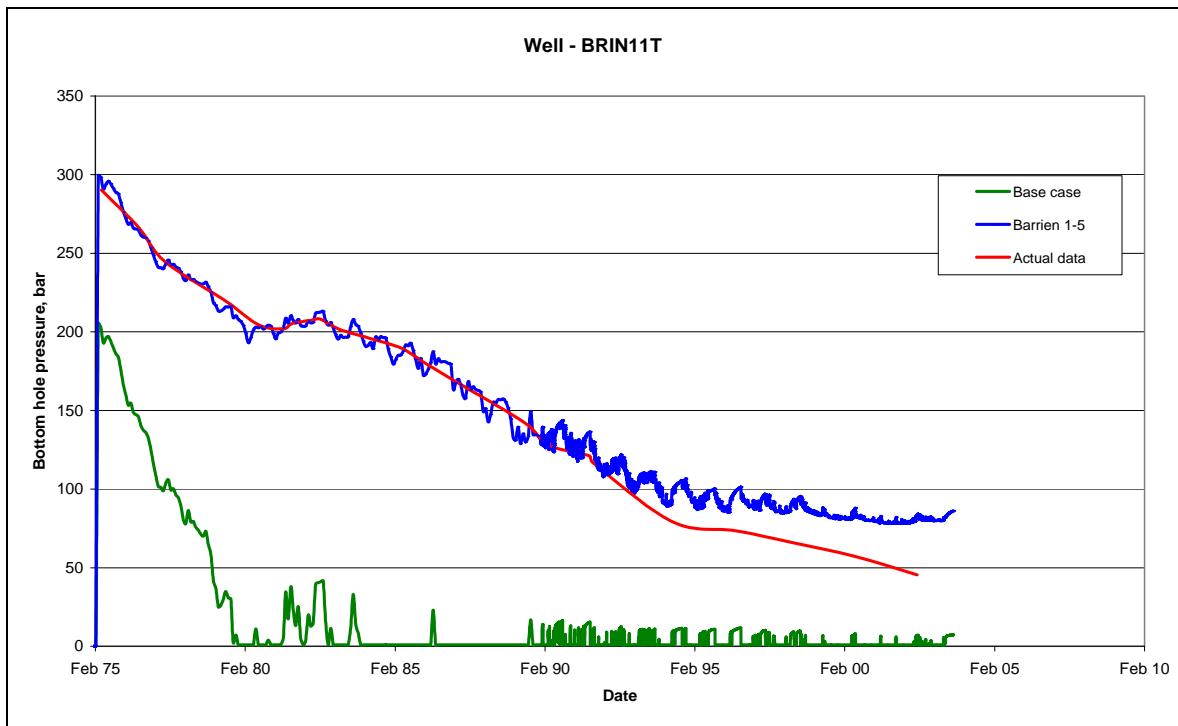


Figure 6.6 - BHP vs. time for well BRIN11T before History Matching

To obtain better history match, the transmissibilities of the faults (SUED21, SUED22) were modified as shown in Table 6.1. These faults are positioned between region 1 and region 2.

Table 6.1 - Transmissivity of the faults data

| Fault Name | Original Transmissivity | Altered Transmissivity |
|---------------|-------------------------|------------------------|
| SUED21 | 0.06 | 0.1 |
| SUED22 | 0.08 | 0.1 |

A good history match was achieved by altering the two faults transmissivities (Figures 6.7 -6.10). This modification yielded a good agreement between the measured and the simulated data and was taken as the “base case” for the definition of the “enhanced recovery” in the CO₂ injection study.

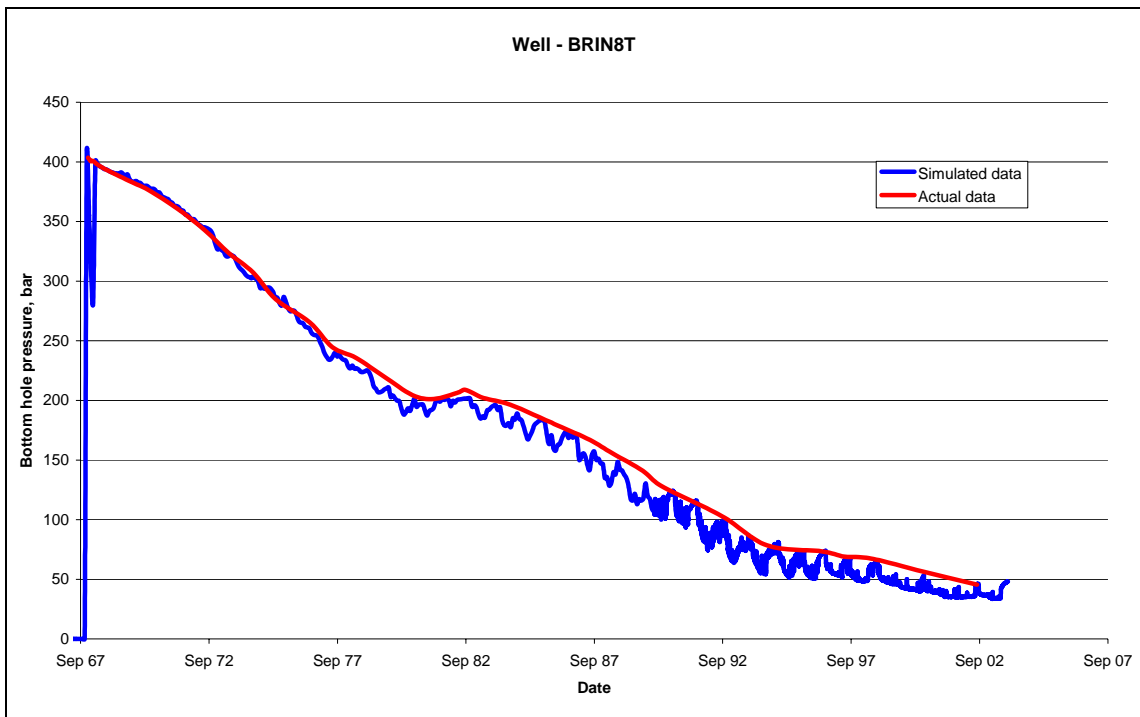


Figure 6.7 - History matching results, Actual vs. Simulated BHP Well BRIN8T

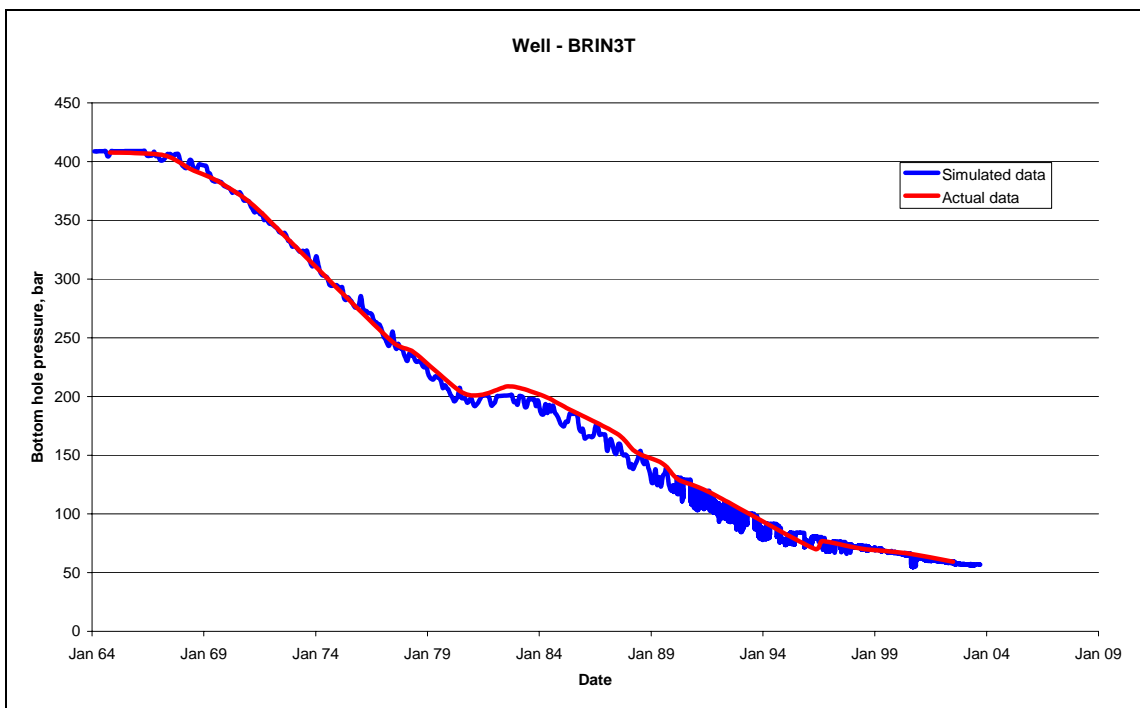


Fig. 6.8 History matching results, Actual vs. Simulated BHP Well BRIN3T

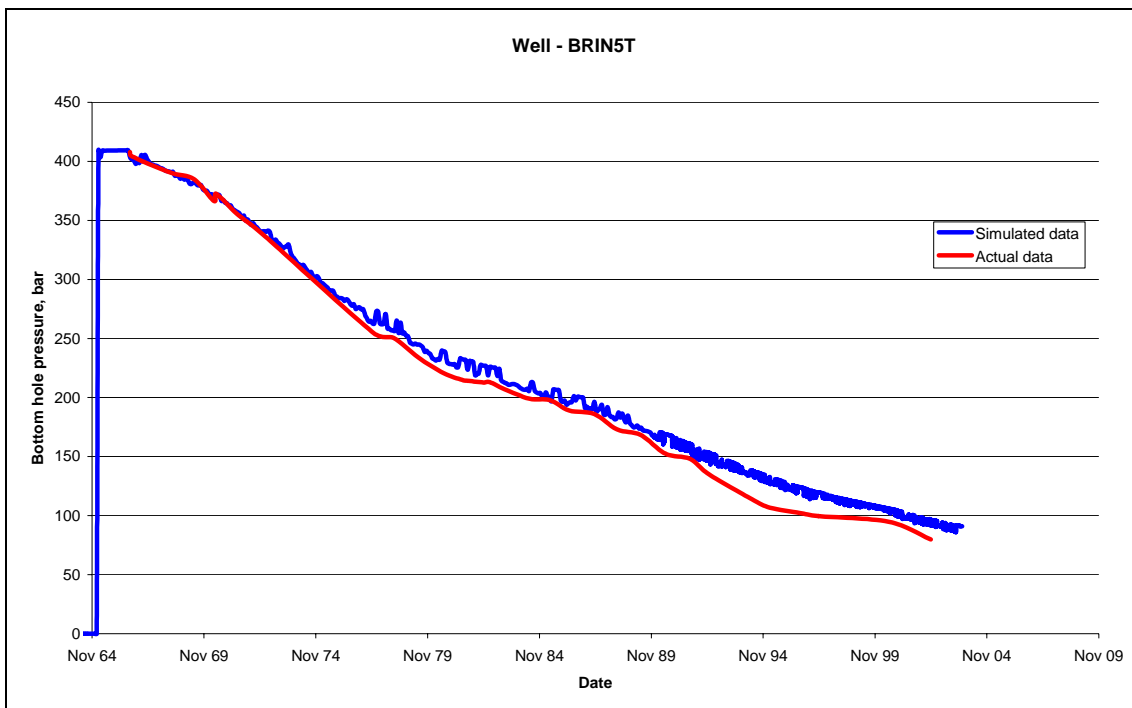


Fig. 6.9 History matching results, Actual vs. Simulated BHP Well BRIN5T

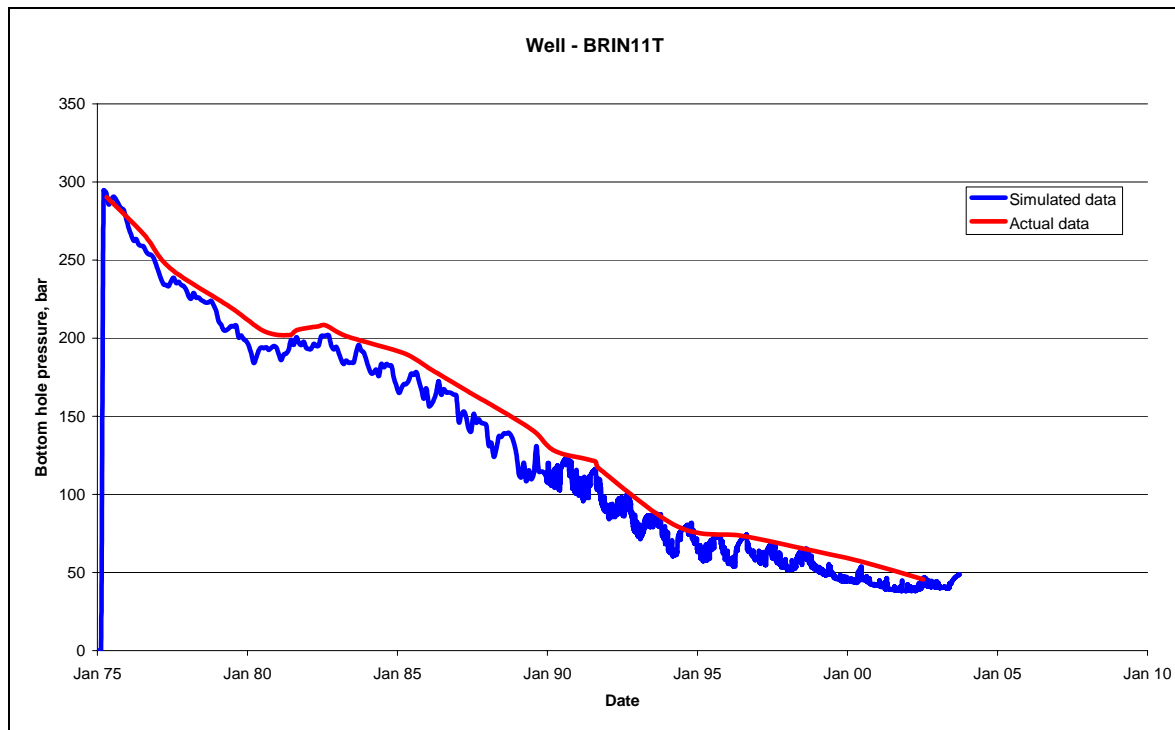


Figure 6.10 - History matching results, Actual vs. Simulated BHP Well BRIN11T

6.2.3. CO₂ Injection Strategies

To investigate the amount of carbon dioxide storable and the effect of carbon dioxide on gas recovery, different injection strategies were used. Two injection scenarios were studied:

- *Simultaneous CO₂ injection and gas recovery from the very beginning of the project,*
- *Primary injection of CO₂ to build up the reservoir pressure, followed by production of natural gas until the CO₂ content in the gas stream of the production wells reached 10%.*

Because the field has been already in the depletion stage, both injection strategies were studied in this simulation. The CO₂ injection started after the primary depletion of the gas reservoir (1964 – 2003). As the CO₂ content in the gas stream reached 10 %, the production wells must be shut-in because: the CO₂ concentration in the gas stream increases very fast from 10 to 60 % within few months (Figure 6.11). It is not intended to cycle or reinject CO₂ but to store it and the gas quality should not be poor. Therefore, after CO₂ breakthrough in production wells (10 % CO₂ in the gas stream) or if the tubing head pressure drops to 10 bar, the production wells were shut-in. Further on CO₂ is injected until a definite reservoir pressure of 400 bar (initial reservoir pressure) is achieved.

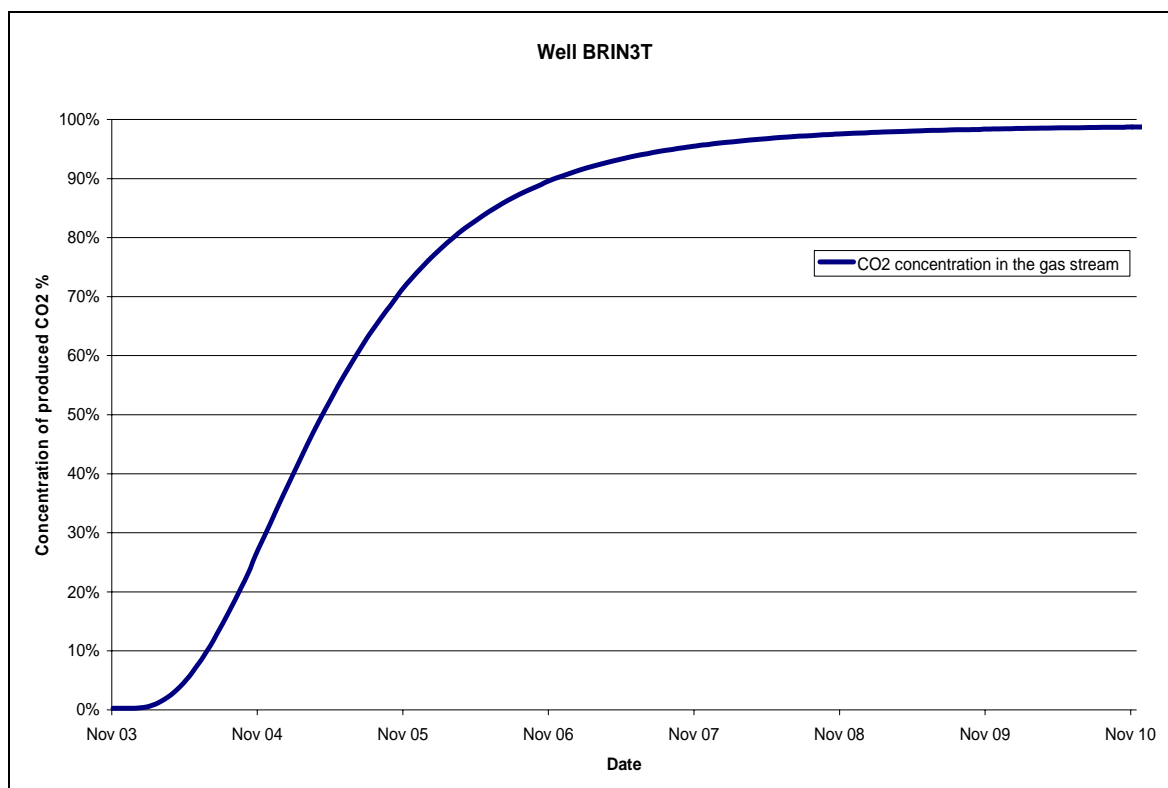


Figure 6.11 - CO₂ concentration in the produced gas stream

The tendency for CO₂ to segregate due to high density effects can be utilized in CSEGR by injecting CO₂ down-dip in the reservoir and producing native gas up-dip.

Since the amount of CO₂ provided from the source is not large enough, it is feasible to inject this amount in one injector, if the bottomhole pressure of the injector will not exceed the safety pressure limit of the formation. For the sensitivity tests, a higher injection rate was used. In this situation two injectors should be drilled.

The safety pressure limit = 1.3x initial pressure = 1.3x400 bar= 520bar

Taking into account the gas water contact depth in this location, a new CO₂ injection well was drilled and is located in almost all runs in the lower left of Region 2 at different locations and in the right side (Region 1) to investigate the sensitivity impact of injector placement on the gas recovery. The completion data of the injection well was chosen to fulfill the requirement of injection rates with a casing diameter of 177.8 mm (7 inch) and tubing diameter of 114.3 mm (4 ½ inch).

Base Case: Gas production without CO₂ injection

Gas production in Barrien field started in 1964. Gas production history was available from 1965 until 2003. The average reservoir pressure in 2003 was 75.15 bars in three regions. The field will continue gas production in the forecast from 2003 until 2033. The average production rate is 11000 m³/day. Increase of recovery factor obtained in the base case without CO₂ injection is 1.7 %. The average field pressure stayed constant at 75 bar due to the energy support from region 12.

A. Injection Strategy (1):

Simultaneously CO₂ injection and gas production from the very beginning of the process

The simulations listed in Table 6.2 were performed in order to investigate the influence of the operation parameters such as, injection rate, production rate, injector type by implementing the strategy (simultaneously CO₂ injection and gas production from the very beginning of the project).

Gas was produced until CO₂ concentration in the produced gas stream attained a value of 10%. The production wells were shut-in and CO₂ injection was continued up to the reservoir pressure (400 bar). In this strategy, both types of injectors vertical or horizontal were used for CO₂ injection. The CO₂ was injected at an injection pressure just below the safety limit of the formation pressure.

Table 6.2- Runs of three regions sector model (Injection strategy 1)

| | | | | |
|----------|--------|--------|-----------------------------|-------|
| A | 336000 | 52000 | Left side/vertical | - " - |
| B | 336000 | 160000 | Left side/vertical | - " - |
| C | 336000 | 336000 | Left side/ 2 vertical wells | - " - |
| D | 336000 | 336000 | Left side/vertical | - " - |
| E | 336000 | 300000 | Left side/vertical | - " - |

| | | | | |
|----------|---------|--------|----------------------|-----------------------|
| F | 336000 | 300000 | Left side/vertical | +Diffusion |
| G | 336000 | 300000 | Left side/vertical | +Solubility |
| H | 336000 | 300000 | Left side/vertical | +Solubility/Diffusion |
| I | 336000 | 300000 | Left side/horizontal | +Solubility/Diffusion |
| X | 720000 | 330000 | Left side/horizontal | Compositional |
| Y | 3600000 | 700000 | Left side/horizontal | - " - |

B. Injection Strategy (2)

Delayed gas production (primary CO₂ injection followed by gas production to the economic limit).

Table 6.3 – Runs of two regions sector model (Injection strategy 1 and 2)

| Case | Initial Injec-tion Rate, m ³ /day | Initial Pro-duction Rate, m ³ /day | CO ₂ Solubility Effects | Pressure build up |
|------------------|--|---|------------------------------------|-------------------|
| Base Case | - | 11000 | - | - |
| K | 336000 | 200000 | Solubility | 200 |
| L | 336000 | 200000 | Solubility | 150 |
| M | 336000 | 336000 | Solubility | 120 |
| N | 720000 | 200000 | - | 130 |
| P | 3,600000 Horizontal Injector | 300000 | - | 150 |

In order to optimize gas production and CO₂ injection, i.e., to pressurize the reservoir and to delay the CO₂ breakthrough at the production wells, all possible injection strategies must be investigated and controlled. A limited number of simulation runs were carried out using this strategy. Primary injection of CO₂ to build up the reservoir pressure to a certain value, followed by production of natural gas until the CO₂ content in the gas stream reached 10 % or the tubing head pressure of the production wells drop to 10 bar. After CO₂ breakthrough in the production wells (10 % CO₂ in the produced gas stream), the production wells were shut-in and CO₂ was injected up to a reservoir pressure of 400 bar. By varying the operation parameters, numbers of simulation runs have been carried out in order to demonstrate the influence of this strategy on the gas recovery (Table 6.3).

Simulations of Two Regions Sector Model (without natural energy support)

In this case, the effects of the gas transfer from Region 2 to 12 during the CSEGR process should be omitted, in order to compare the specific situation in Barrien with an undisturbed closed reservoir. Region 12 has been set inactive in the sector model. Both injection strategies were studied in this system to examine the different effects of CO₂ injection on gas recovery. Simulation run parameters are listed in Table 6.4. Figure 6.12 illustrates our study area Regions 1 and 2.

Table 6.4 – Runs of two regions sector model (closed system)

| Case | Injection strategy | Initial Injection Rate, m ³ /day | Initial Production Rate, m ³ /day | Injector location | Pressure build up, bar | Required time to build up the pressure, years |
|------------------|--------------------|---|--|-------------------|------------------------|---|
| Barrien R | 1 | 336000 | 330000 | Region 2 | - | - |
| Barrien S | 1 | 720000 | 600000 | Region 2 | - | - |
| Barrien T | 2 | 720000 | 400000 | Region 2 | 150 | 7 |
| Barrien U | 2 | 720000 | 400000 | Region 1 | 150 | 7 |
| Barrien V | 1 | 720000 | 500000 | Region 1 | - | - |

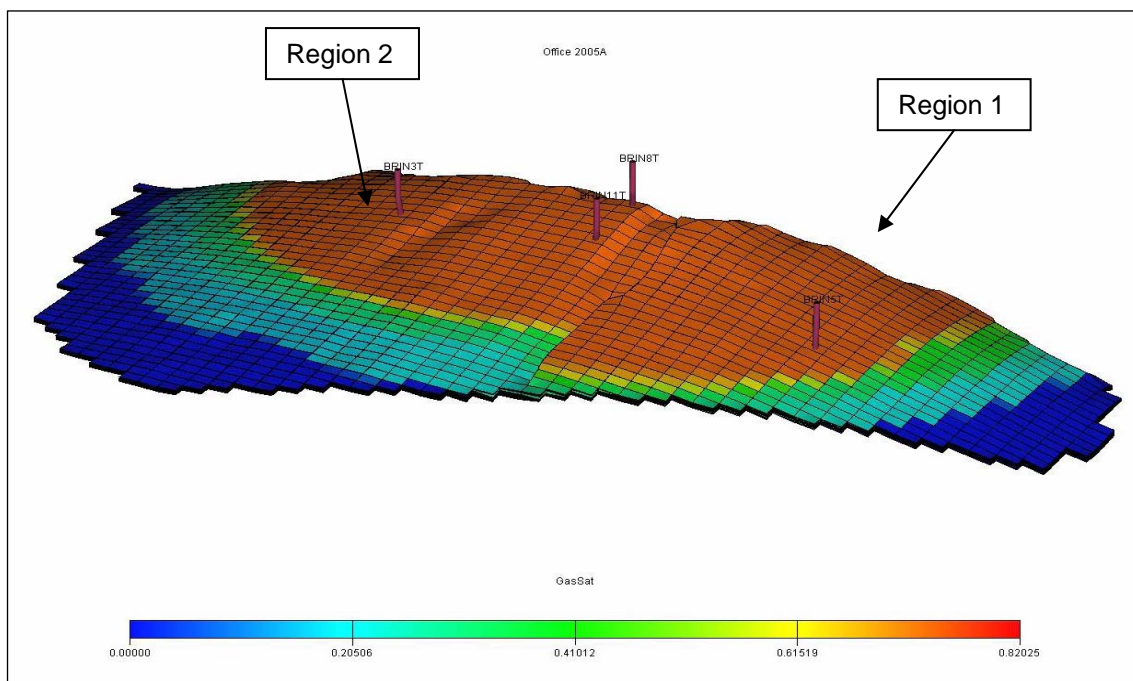


Figure 6.12 – 3D Display of the two regions sector model gas saturation

6.3.4. Simulation results

Three Regions Sector Model

The simulation results show that the highest additional gas recovery was obtained by simultaneous CO₂ injection and gas recovery from the beginning of the process. The maximum amount of incremental gas recovery was 6.78 % of the original gas in place in both regions 1 and 2. Lower recovery factors for gas were obtained in the case of production delay i.e., primary CO₂ injection to build up the reservoir pressure to a certain value, followed by gas production. The reason is that the pressure diffusivity is typically three to five orders of magnitude larger than molecular diffusivity, making repressurization occur much faster than mixing by molecular diffusion.

The calculated gas recovery of our study area regions 1 and 2 for depletion phase until 2003 was 82 %, while the CO₂ injection scheme using injection strategy 1 can achieve up to 89 % of IGIP, which is the maximum recovery by CO₂ injection. This means that gas recovery from both sides of the semi-sealing fault is maximized.

Figure 6.13 shows the effect of CO₂ injection on the additional gas recovery factor with different injection strategies used.

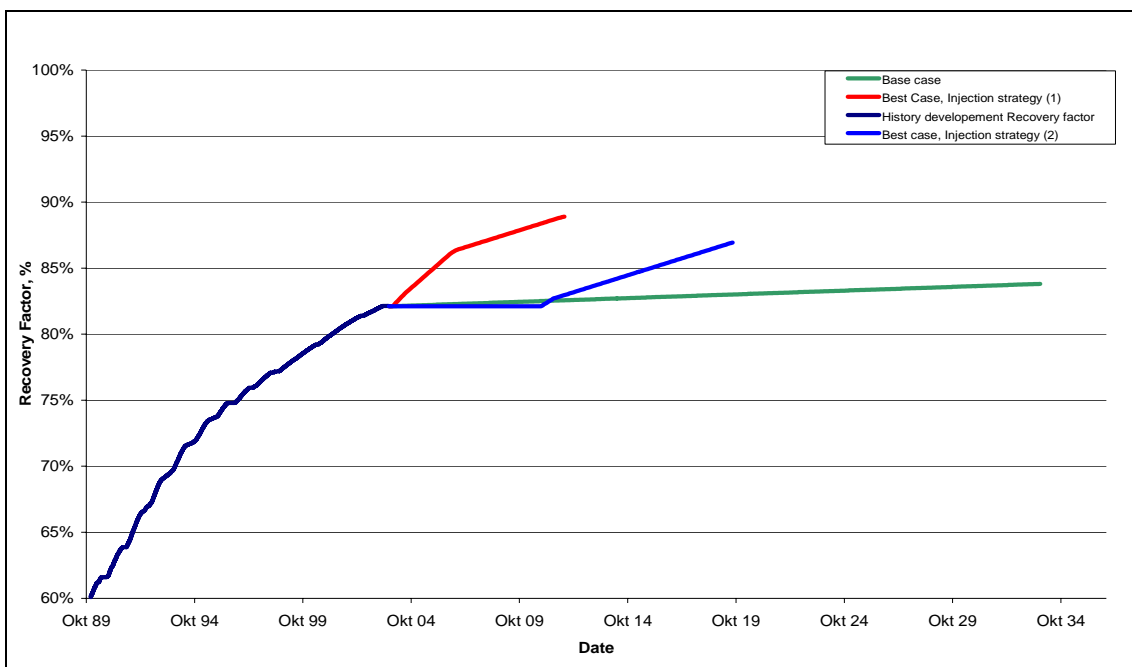


Figure 6.13 - Gas recovery factor of the three regions sector model for different injection strategies

Two Regions Sector Model

The simulation results show that, the incremental gas recovery is higher (9.78 %) in this case because region 12 has been removed, which means no gas escapes through the fault from region 2 to region 12 (Figure 6.14). The total gas recovery that can be achieved is up to 92 % IGIP. But the amount of CO₂ stored is slightly lower due to the smaller pore volume. The injected CO₂ was propagating by the effects of pressure gradient and the gravity.

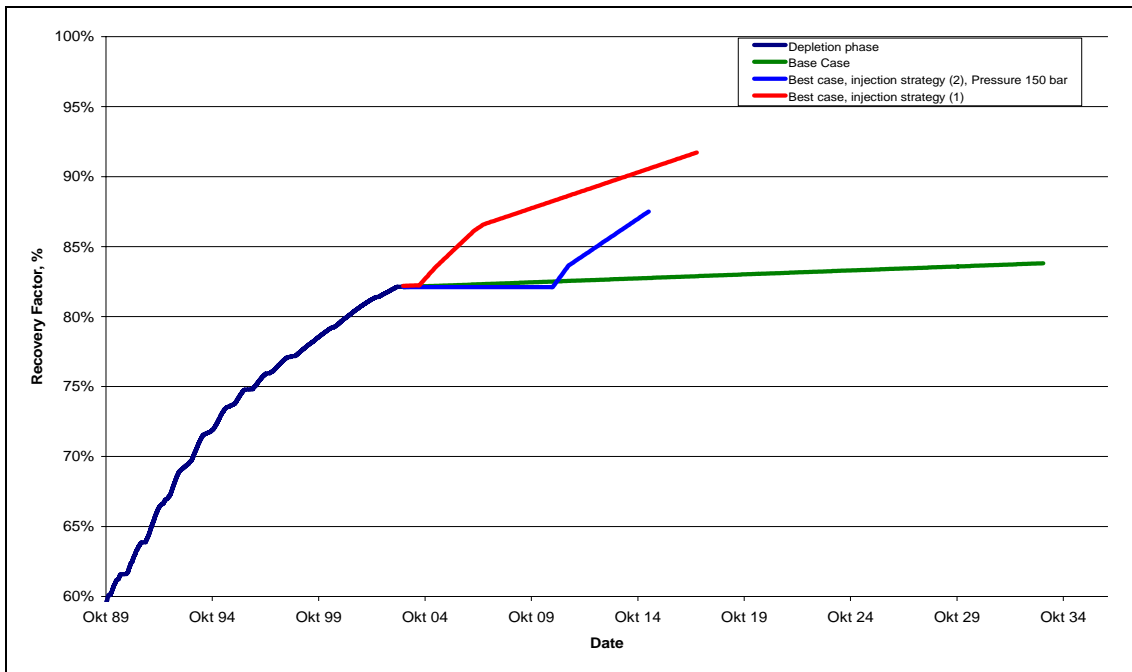


Figure 6.14 – Gas recovery factor of the two regions sector model for various injection strategies

Average Field Pressure

Figure 6.15 shows the average field pressure for the depletion phase and base case. It shows also how the pressure was developed using different injection strategies due to CO₂ injection. For simultaneous injection/production (strategy 1) the build-up is somewhat delayed compared to strategy 2(delayed production).

In the base case, the gas produced from region 2 was replaced by the gas transferred through the faults from region 12 to region 2; therefore, the pressure stays constant at 75.5 bar.

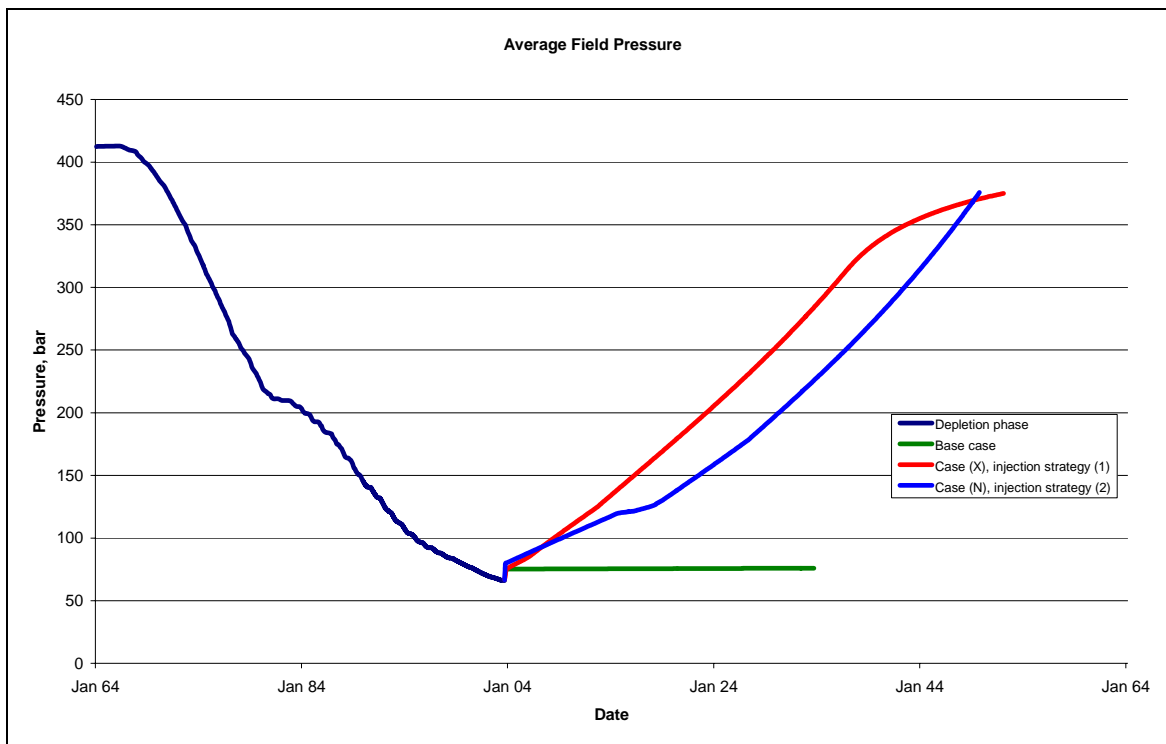


Figure 6.15 – Average field pressure vs. time in Barrien Sector Model

Gas Production Profiles

The produced gas composition profiles shown in Figures 6.16 - 6.17 for two producers (BRIN8T, BRIN3T) describe the formal extend of the mixing zone by numerical dispersion. The production was taken into account until 10% CO₂ content.

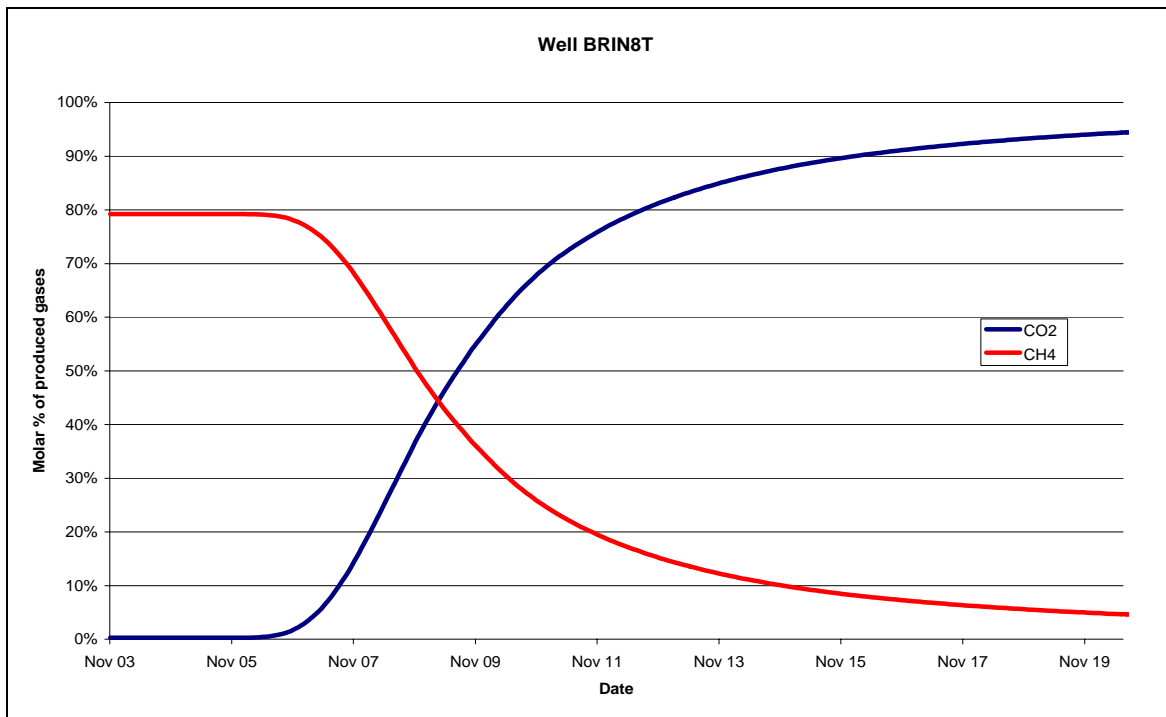


Figure 6.16 – Mole fraction of CH₄ and CO₂ in the produced gas for well BRIN8T

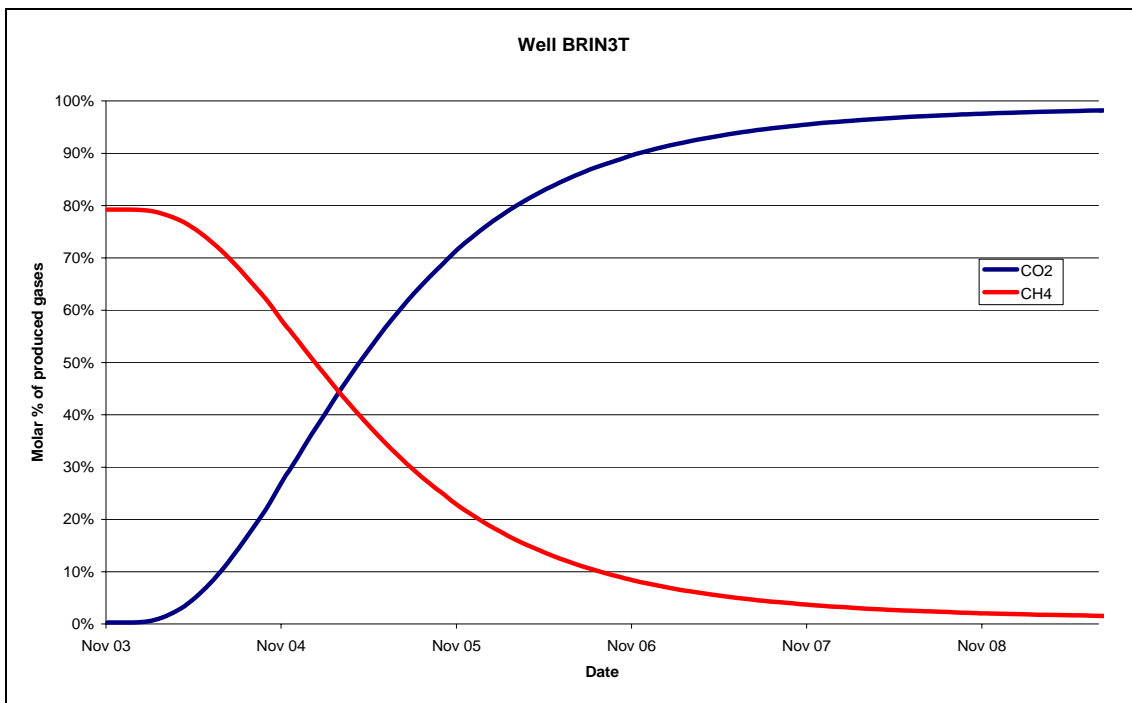


Figure 6.17 - Mole fraction of CH₄ and CO₂ in the produced gas for well BRIN3T

CO₂ Breakthrough Times

The appearance of the CO₂ in the production wells is of importance for the evaluation of enhanced gas recovery. Breakthrough was defined at 10% CO₂ content. The CO₂ breakthrough time varied because of different model assumptions by each run, such as CO₂ dissolution in formation water, injector type, production rate, injection rate, and distance between the injector and the producers. In the simulated cases the breakthrough occurs between one year and seven years (Figure 6.6). Figure 6.18 shows the breakthrough times of CO₂ (10 % of CO₂ in the gas stream) for well BRIN11T.

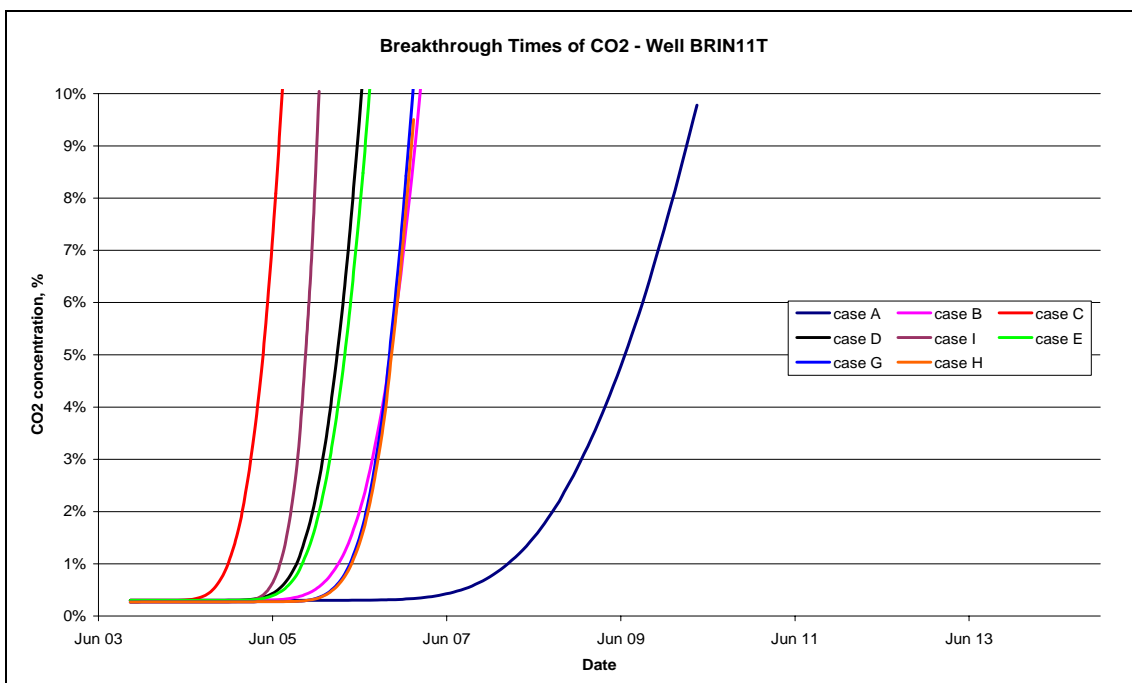


Figure 6.18 - CO₂ Breakthrough times Well BRIN11T

Effect of Horizontal Injectors

In the simulation case I a horizontal injector was used for the purpose of CO₂ injection. The additional gas recovery was 4.58 %. Simulations with a horizontal injector show a shorter breakthrough time than the vertical injectors as presented in Figure 6.19. Figure 6.20 illustrates the recovery obtained from different types of injectors with the same injection and production rate.

The CO₂ injection rate may depend on gas availability and injection facilities. In this study, different injection rates were used (14000, 30000, 750000 m³/d/well). Large CO₂ injection rates may accelerate gas production, but cause excessive mixing of the gases. It is important to understand how the CO₂ injection rate or the total amount of CO₂ injected affects the incremental gas recovery. Figure 6.20 shows the simulation results with different CO₂ injection rates 14000 and 30000 m³/d. In both cases of injection strategy 1, CO₂ injection started at the beginning of the process and the production rate was set to 14000 m³/d.

The additional gas recovery obtained from the balanced injection/production case (case D) is higher than that obtained from the overbalanced case (the injection rate higher than the production rate) case X. Lower additional recovery in case of overbalance is due to: s CO₂ injection started to displace the native gas in the direction of production wells, the displaced gas was transferred through the semi sealing fault from region 2 to region 12.

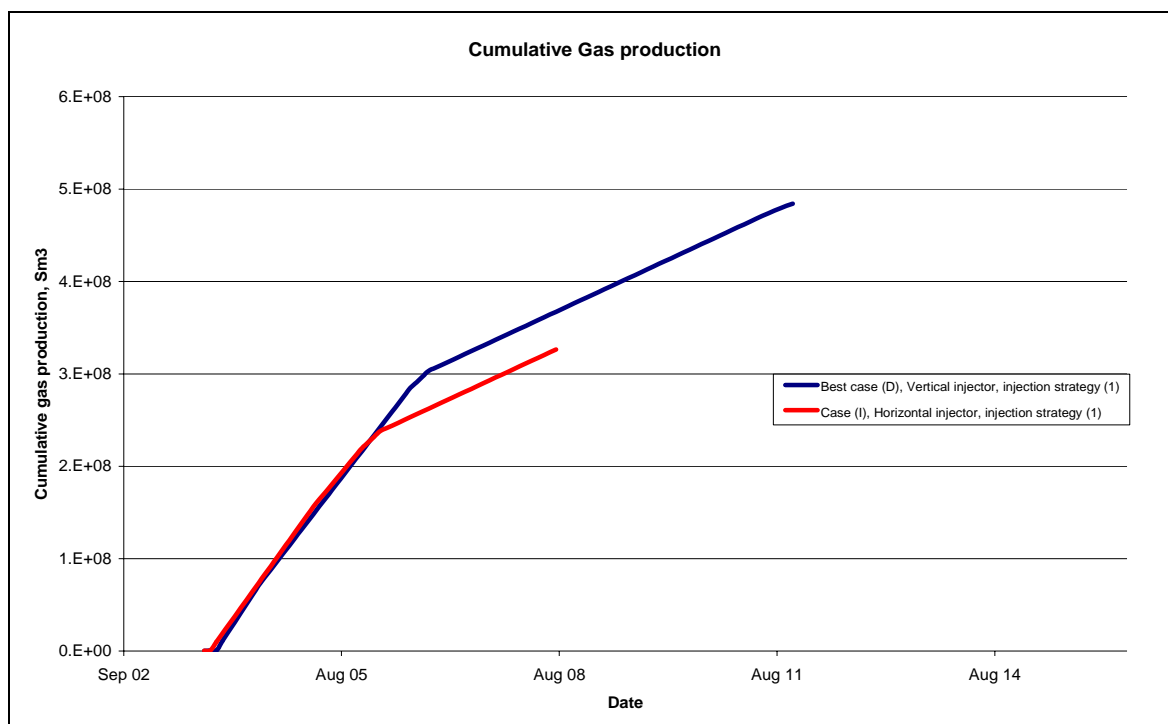


Figure 6.19 – Effect of horizontal injector on cumulative gas production

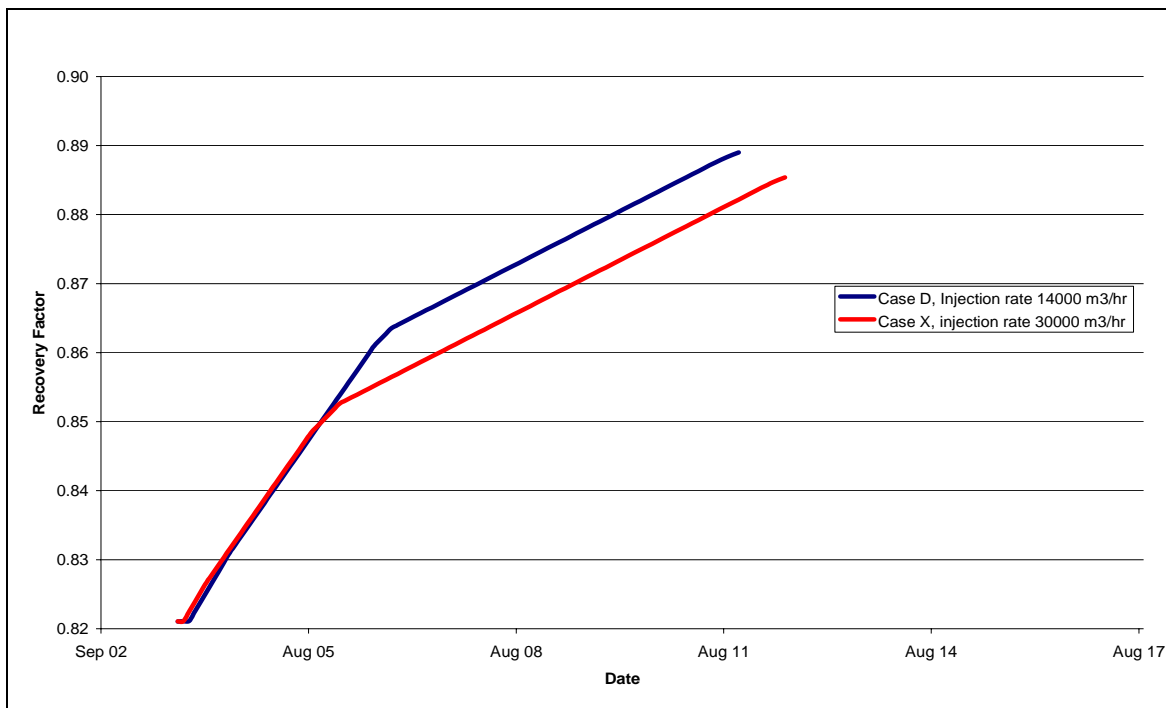


Figure 6.20 – Effect of injection rate on gas recovery

In the case of the two region sector model; the results are different as shown in Figure 6.21. It is interesting to note that low CO₂ injection rates (14000 m³/d) have a negative impact on gas recovery. Remarkably, when the injection rate was increased to 150000 m³/d, the incremental gas recovery reached 10.8 %.

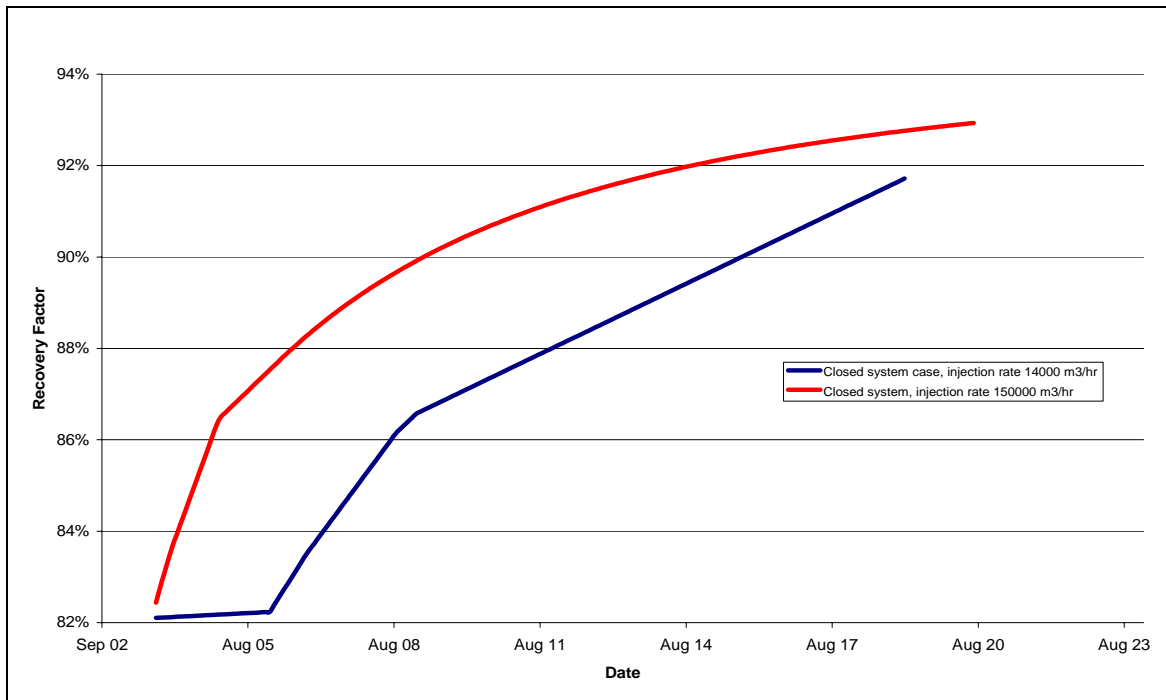


Figure 6.21 - Effect of injection rate variation on recovery

Effect of Production Rate

Additional gas recovery could be larger and associated CO₂ breakthrough faster if the production rates were larger. Also higher production rate means production acceleration as shown in Figure 6.22.

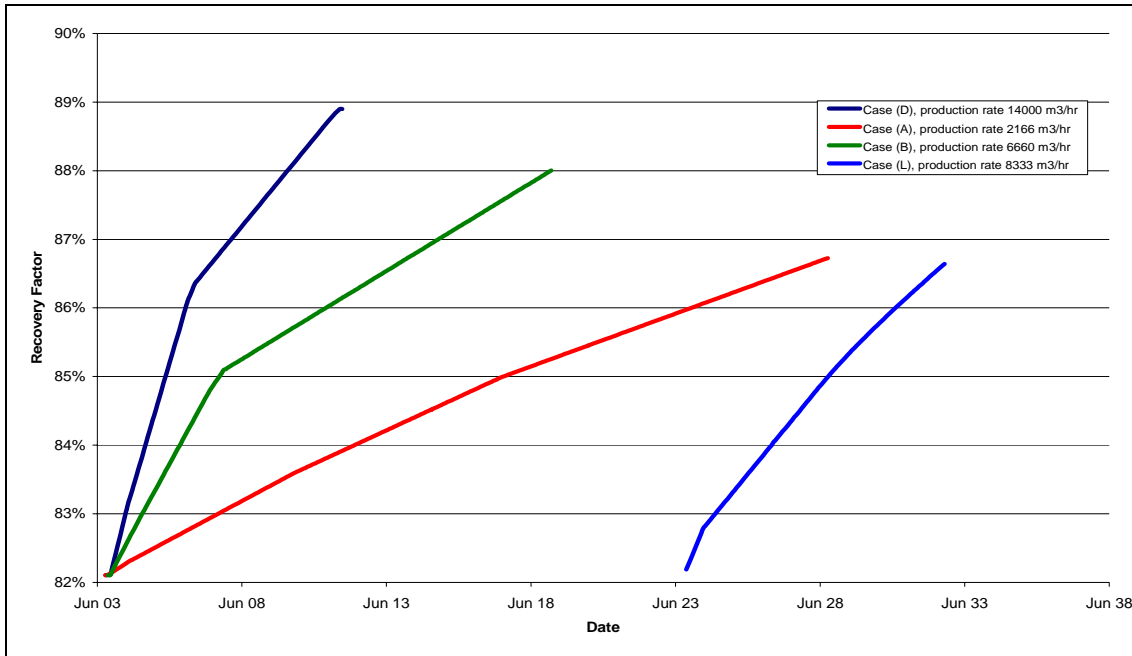


Figure 6.22 - Effect of production rate variation on gas recovery-cases A,B,D are in strategy 1 and case L in strategy 2 mode.

Sensitivity of injector location

Simulation results (Figure 6.23) show that, there is no significant effect of the injector position either in region 1 or region 2. Approximately the same additional gas recovery was obtained by implementing either well position in the left region or in the right.

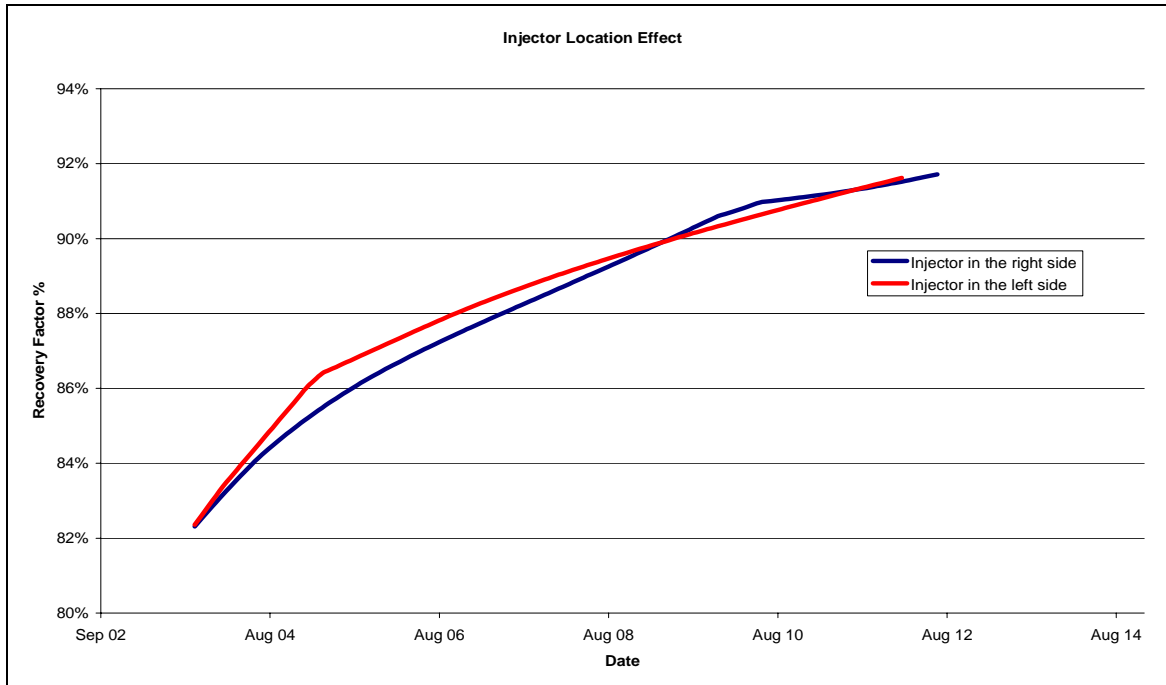


Figure 6.23 – Effect of injector position on recovery factor

Effect of CO₂ Solubility in Formation Water

Simulations with and without CO₂ dissolution in formation water were performed using the ECLIPSE model described above. In case G, the results indicate that, when CO₂ dissolution was taken into account in the simulation, CO₂ breakthrough time was delayed about 0.5 year compared to the case without considering CO₂ solubility in water. The dissolution of CO₂ in water has some positive effect on, which can delay CO₂ breakthrough. The additional gas recovery depends mostly on the gas produced from well BRIN5T in region 1 due to the fact that the production wells in region 2 are closer to the injector, which means early breakthrough of CO₂ in those wells, whereas the breakthrough of CO₂ in region 1 takes a longer time.

In this case G, the injected CO₂ is captured by the formation water in region 2, that means slightly lower pressure support affected region 1 (CO₂ front advanced slowly in the direction of region 1). Consequently, the pressure in well BRIN5T dropped very fast to a limiting tubing head pressure of 10 bars, which will cause early shut-in for well BRIN5T. Therefore, the incremental gas recovery in this case G is lower. See the summary Table 6.5. Also, the amount of CO₂ sequestered is less in the solubility case, because the total amount of gas produced by CO₂ injection is smaller compared with other cases. The maximum amount of CO₂ that can be stored in the subsurface is shown in Table 6.5 within different life spans of the storage site.

Table 6.5 – Summary of simulation results of the three regions sector model for both injection strategies (Strategy 1 grey shadow, Strategy 2 yellow shadow)

| Case | Total Time of injection | Time of Production | Incremental Recovery, % | Additional Gas Produced, millions sm ³ | Final Field pressure, bar | CO ₂ Storage capacity, 400 bar, million tons |
|------------------|-------------------------|--------------------|-------------------------|---|---------------------------|---|
| A | 2003 - 2081 | 2003 - 2028 | 4.62 | 327.5 | 400 | 17.5 |
| B | 2003 - 2081 | 2003 - 2019 | 5.9 | 420 | 400 | 17.65 |
| C | 2003 - 2082 | 2003 - 2023 | 6.16 | 438.6 | 400 | 17.7 |
| Best case | | | | | | |
| D | 2003 - 2083 | 2003 - 2011 | 6.78 | 482.7 | 400 | 17.78 |
| E | 2003 - 2083 | 2003- 2011 | 6.64 | 472.7 | 400 | 17.78 |
| F | 2003 - 2082 | 2003 -2011 | 6.63 | 470.6 | 400 | 17.74 |
| G | 2003 - 2083 | 2003- 2008 | 5.35 | 380.9 | 400 | 17.8 |
| H | 2003 - 2077 | 2003 -2008 | 5.39 | 383.7 | 400 | 16.3 |
| I | 2003 - 2075 | 2003 - 2008 | 4.58 | 326 | 400 | 16.2 |
| X | 2003 - 2052 | 2003 -2012 | 6.44 | 458.5 | 400 | 18.8 |
| Y | 2003 - 2011 | 2003 - 2009 | 6.34 | 450.6 | 400 | 18.8 |
| K | 2003 - 2074 | 2035 - 2040 | 2.74 | 195 | 400 | 15.94 |
| L | 2003 - 2075 | 2023 - 2032 | 4.54 | 323.2 | 400 | 16.27 |
| M | 2003 -2074 | 2014 - 2018 | 2.48 | 176.57 | 400 | 15.95 |
| N | 2003 - 2042 | 2010 - 2019 | 4.84 | 344.6 | 400 | 18.6 |
| Best case | | | | | | |
| P | 2003 - 2011 | 2006 - 2009 | 4.86 | 346 | 400 | 18.4 |

Table 6.6 – Summary of simulation results of the two regions sector model for both injection strategies (Strategy 1 grey shadow, Strategy 2 yellow shadow)

| Run | Time of injection | Time of Production | Additional Gas Recovery, % | CO ₂ Storage Capacity, 375 bar, Million tons. | Injection Strategy Definition |
|----------------------------|-------------------|--------------------|----------------------------|--|---|
| Best case Barrien R | 2003 - 2060 | 2003 - 2012 | 9.78 | 13.69 | strongly overbalanced injection/production |
| Barrien S | 2003 - 2078 | 2003 - 2016 | 9.62 | 13.7 | slightly overbalanced injection/production |
| Barrien T | 2003 - 2058 | 2011 - 2015 | 5.4 | 12.89 | delayed production – 150 bar |
| Barrien U | 2003 - 2044 | 2011 - 2019 | 5.22 | 13.34 | delayed production 150 bar |
| Barrien V | 2003 - 2029 | 2003 - 2012 | 9.54 | 12.26 | slightly over balanced injection/production |

6.3. Simulation of Altmark Gas Field. CO₂- Disposal and its Effects on Gas Recovery

6.3.1. Simulation of the sector model Altmark Block 12

A sector model was chosen since it was not possible to study the full field with the resources available in the project.

6.3.1.1. Block 12 model description.

The sector simulation model for Altmark Block 12 was selected and generated from the geological model of the reservoir Salzwedel- Peckensen presented in WP3. The model has as boundary conditions closed boundaries.

The simulation model has 44x38 blocks with lateral resolution of 100m in both X and Y direction, whereas in vertical direction 29 strata (38 blocks) with different thicknesses were simulated. The sealing interlayers between the strata were considered as inactive so that they behave as no flow barriers for the vertical migration of CO₂. This model is presented in Figure 6.24.

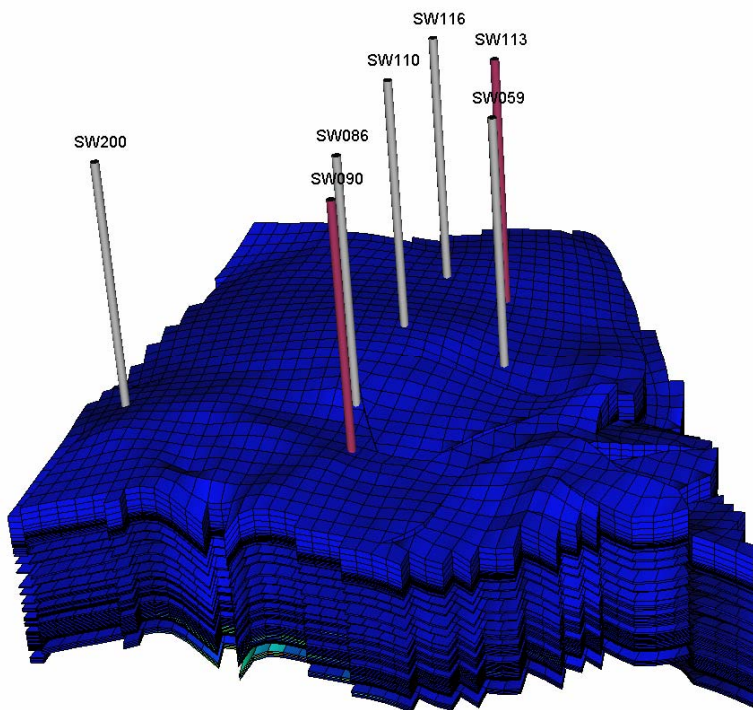


Fig. 6.24: Altmark Block 12 Simulation Model.

The pay zone average parameters (porosity, permeability and net thickness) and that of the silt intercalations are presented in Table 6.7. Note that the denomination of the strata is in coincidence with the geological description in WP3 whereas the silt intercalations were noted from I1 to I14 from top to bottom.

In this block 12 wells were drilled, 7 are still in production in the year 2007 with different production rates tallying around 204000 sm³/d. All wells were modeled as fully

perforated in all layers in order to study the distribution of the CO₂ into different layers (generic character).

The initialization of the model was made in depleted state the initial pressure being 50 bar, an average value of the existing pressure in this block at the start of this study.

Table 6.7 Average strata parameters for the Block 12 Simulation Model

| Layer | f_i , - | h_i , m | k_i , mD |
|--------|-----------|-----------|------------|
| ROF | 0.07 | 5.14 | 2.07 |
| I 1 | 0.05 | 5.4 | 0.16 |
| ROF+10 | 0.05 | 1.51 | 0.23 |
| I 2 | 0.04 | 13.67 | 0.13 |
| 17M | 0.06 | 1.69 | 0.3 |
| I 3 | 0.03 | 13.24 | 0.05 |
| 12B | 0.05 | 2.09 | 0.24 |
| I 4 | 0.05 | 20.78 | 0.24 |
| 16M | 0.04 | 3.3 | 0.16 |
| I 5 | 0.03 | 11.71 | 0.07 |
| 16B | 0.07 | 1.68 | 0.39 |
| I 6 | 0.04 | 15.39 | 0.12 |
| 15M | 0.03 | 1.38 | 0.05 |
| I 7 | 0.03 | 9.91 | 0.07 |
| A | 0.07 | 6.24 | 4.63 |
| I 8 | 0.03 | 9.34 | 0.05 |
| B14 | 0.11 | 6 | 77.36 |
| I 9 | 0.03 | 4.15 | 0.07 |
| B13 | 0.09 | 8.52 | 14.63 |
| I 10 | 0.03 | 10.05 | 0.07 |
| C12 | 0.1 | 2.82 | 5.56 |
| I 11 | 0.11 | 1.07 | 11.31 |
| C11 | 0.14 | 12.78 | 70.44 |
| I 12 | 0.03 | 2.54 | 0.08 |
| C10 | 0.15 | 10.67 | 105.08 |
| I 13 | 0.05 | 1.28 | 0.16 |
| C9 | 0.12 | 4.16 | 14.98 |
| I 14 | 0.03 | 15.9 | 0.06 |
| D | 0.12 | 9.18 | 42.25 |

6.3.1.2 Injection strategy

In order to be able to calculate the Tubing Head Pressures (THP) Vertical Flow Performance Curves were generated using ECLIPSE VFPI program. A constant temperature profile was used from 40°C at the surface increasing with depth to 120°C at the perforation level of the well. Such a profile for injection well SW 90 is presented in Figure 6.25. This figure shows the dependency of the BHP on the Gas Rate for different THP's ranging from 50 to 170 bar.

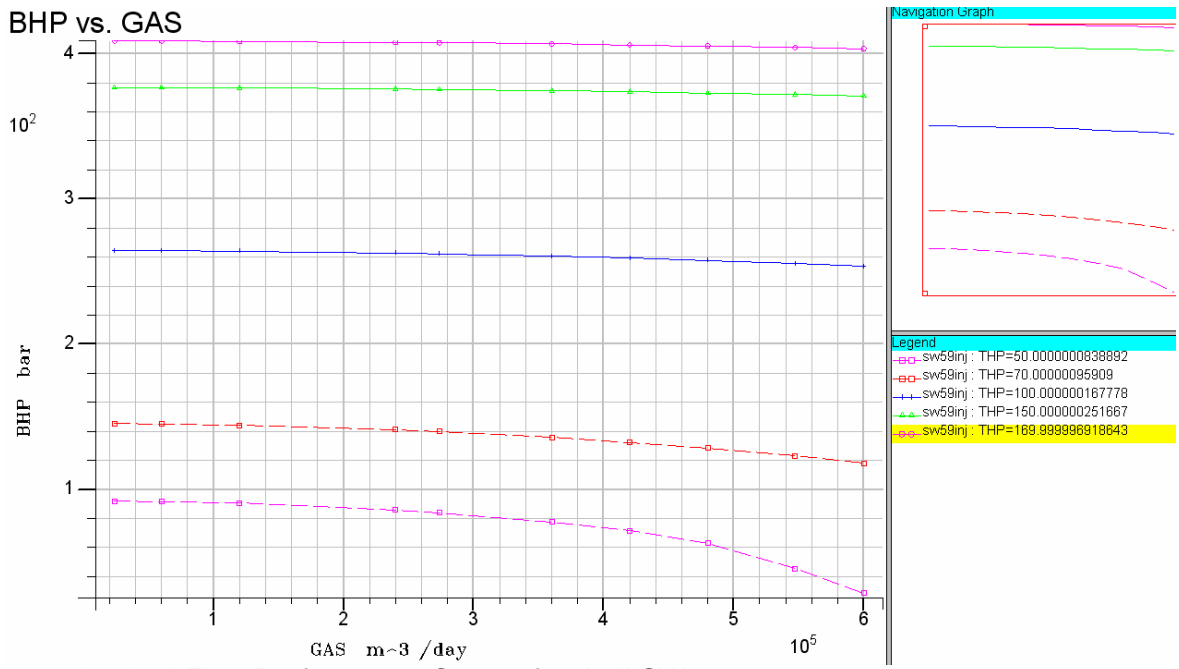


Fig. 6.25 Vertical Flow Performance Curves for Well SW 90

For the CO₂ injection simulation in this block two main injection strategies were considered (see a more detailed description in 6.2.3):

Injection Strategy (1): simultaneous CO₂ injection and gas recovery from the very beginning of the project until the CO₂ content in the gas stream reached 10 %.

Injection Strategy (2): primary injection of CO₂ to build up the reservoir pressure to 150 bar, followed by production of natural gas until the CO₂ content in the gas stream reached 10 %.

The injection was done through one well. For this purpose well SW 90 was chosen, since this well lies at the deepest location in the structure, which has a general dipping tendency from NE to SW direction, see Figure 6.26.

The injection and production constraints are:

Injection strategy 1:

- Injection well: SW 90
- Injection flow rates:
 - Case 1: 100000 m^3/day Underbalanced
 - Case 2: 204000 m^3/day Balanced
 - Case 3: 300000 m^3/day Overbalanced
- Production through 7 wells : 204000 m^3/day
- After all wells reached 10 % CO₂, inject through all wells 300000 $\text{m}^3/\text{day}/\text{well}$.

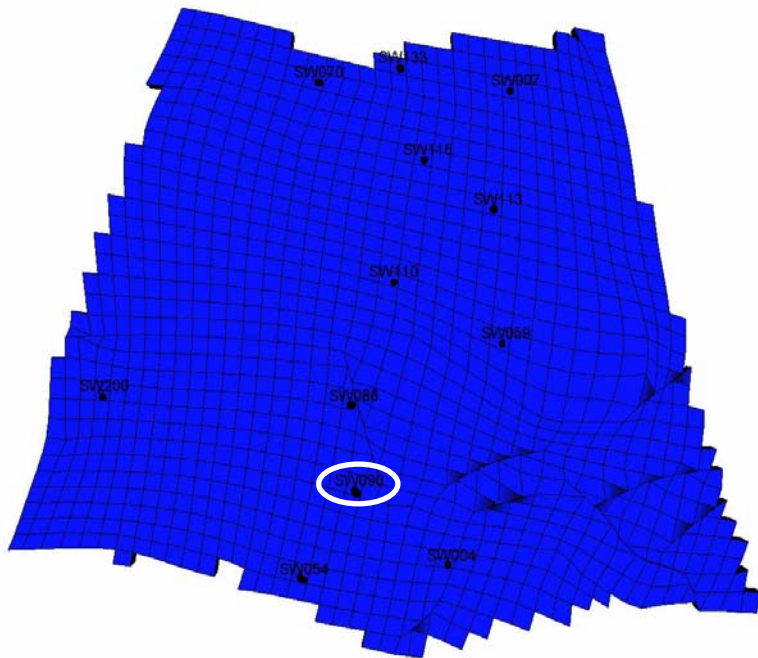


Figure 6.26 Injection well placement in Altmark Block 12

Injection strategy 2:

- Injection well: SW 90
- Injection flow rates: $300.00 \text{ m}^3/\text{day}$
- Production : $0 \text{ m}^3/\text{day}$
- All wells have reached more than 10% CO₂, when field pressure was build-up to 150 bar.

In all cases a limit to the injection bottomhole pressure was set to 520 bar, about 1.3 times the initial pressure conditions in this block.

6.3.1.3 Simulation Results

The breakthrough times of 10% CO₂ in the production stream for the injection strategy 1 is presented in Table 6.8 as well as graphically, for Case 2, in Figure 6.27.

Table 6.8 Breakthrough times in Strategy 1

| Well No. | Breakthrough Time (days) | | |
|----------|--------------------------|--------------------|------------------------|
| | Case 1 Underbalanced | Case 2 Balanced | Case 3 Overbalanced |
| SW086 | 115 | 65 | 50 |
| SW110 | 595 | 345 | 260 |
| SW200 | 865 | 485 | 360 |
| SW059 | 1600 | 1065 | 845 |
| SW116 | 1985 | 1225 | 930 |
| SW113 | 2650 | 1815 | 1450 |

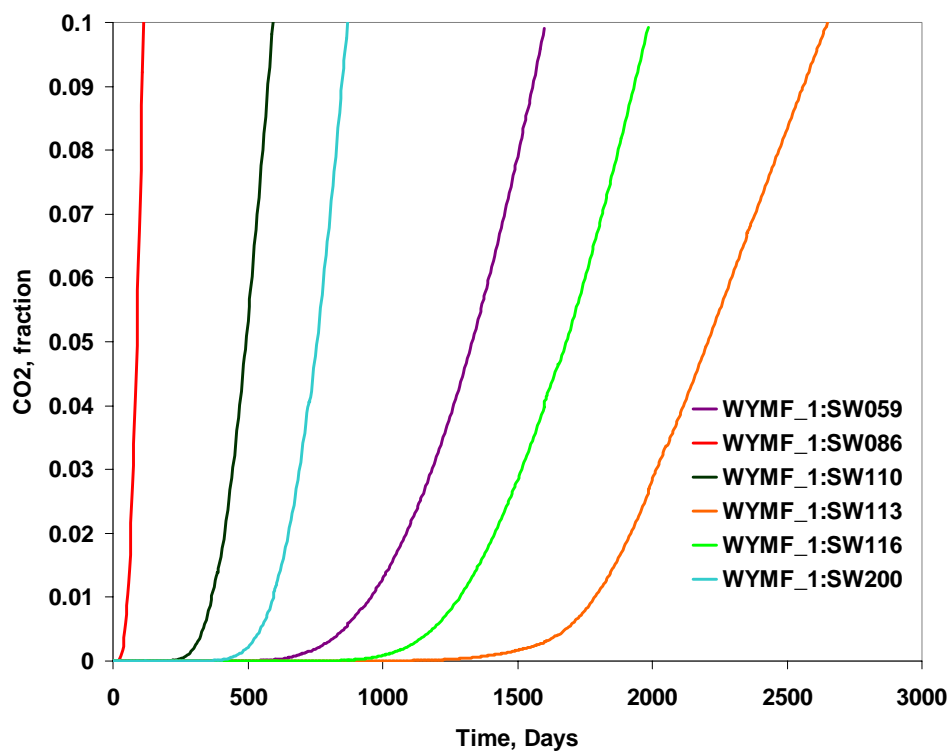


Fig. 6.27: Breakthrough times in Case 2.

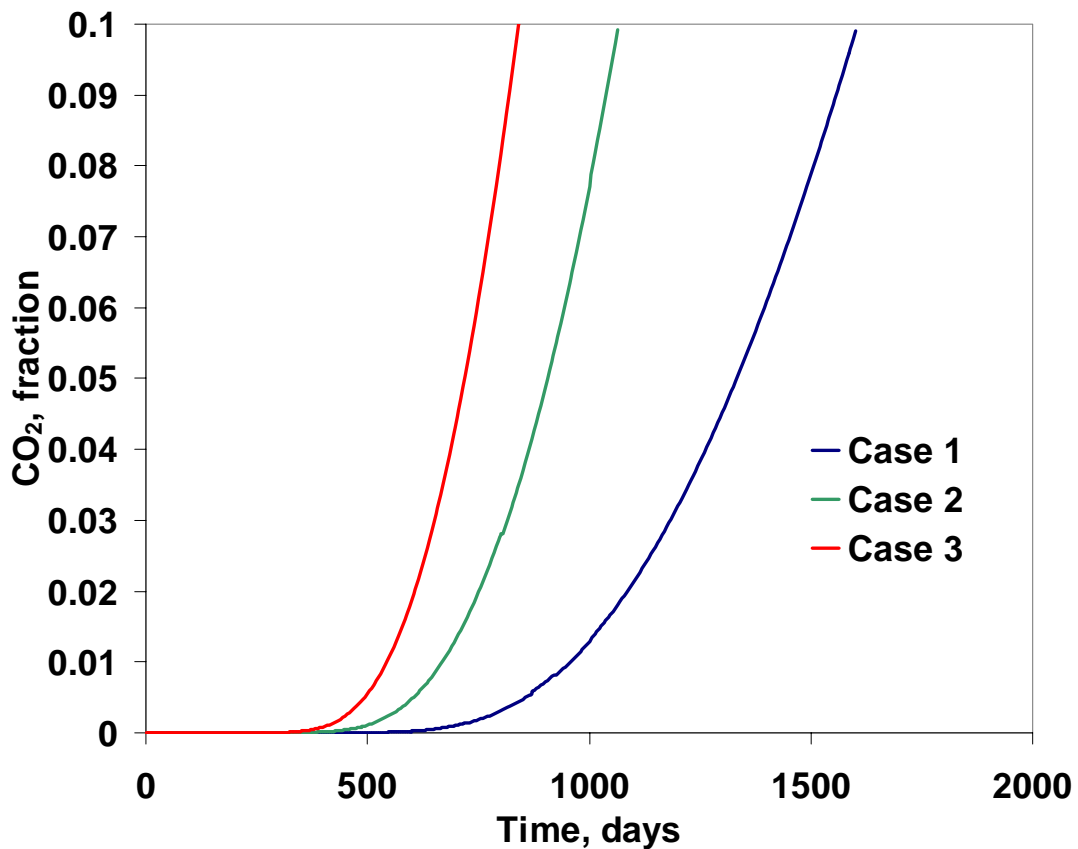


Figure 6.28: CO₂ fraction in gas production of well SW 59

As observed in Table 6.8 the sequence in which the CO₂ reaches the production wells is the same regardless of the injection/production constraints and as expected, higher production rates (Case 3) will have faster breakthrough (Case 2 and 1). This can be observed also from Figure 6.28 that presents the fraction of CO₂ produced in well SW59. For the field handling this means that CO₂ separation/processing has to be considered.

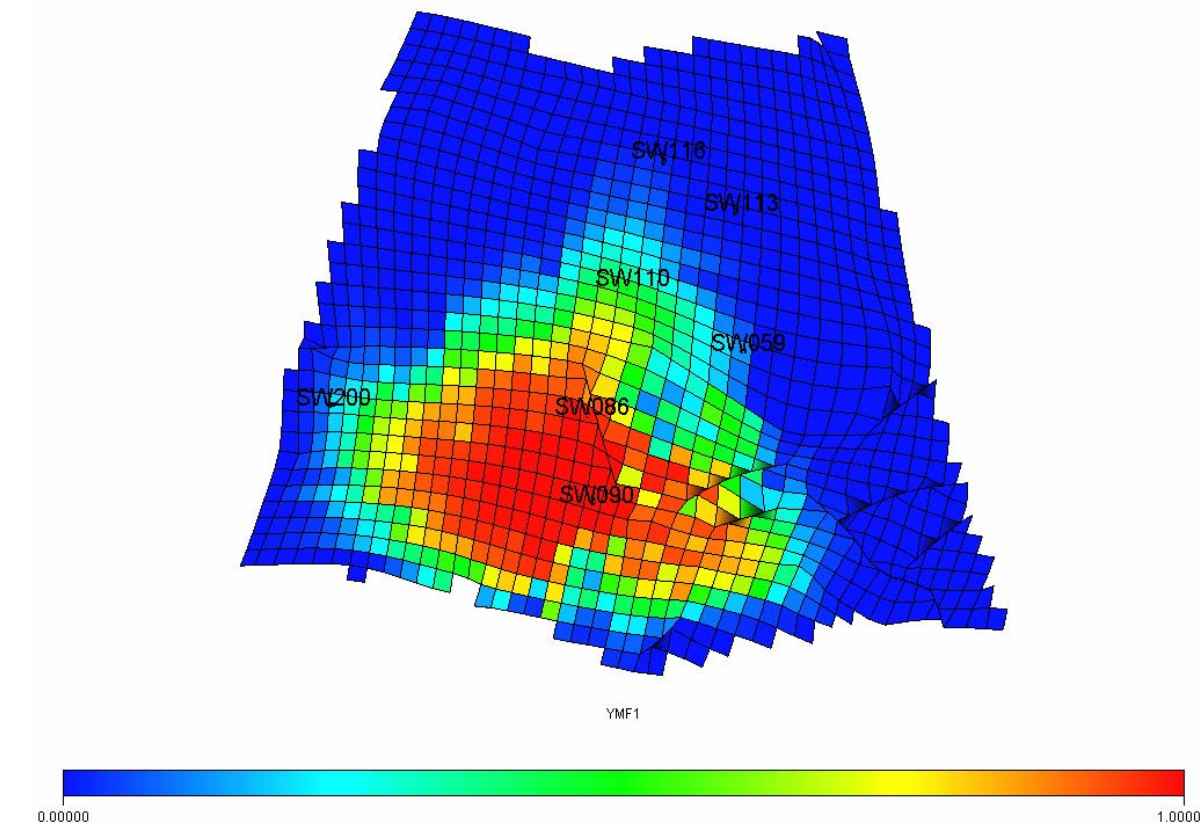


Fig. 6.29: Top View Breakthrough Time, well SW 59 Case 2

The lateral distribution of CO₂ in the reservoir is presented in Figure 6.29 for the layer C with the largest flow capacity. This view shows that the CO₂ distribution is in accordance with geological anomalies and position of the wells. Note the influence of faults, present in the model for the areal distribution of the CO₂. In this case the fault near the wells SW90 and SW86 is preventing the flow of CO₂ towards well SW 59 so that well SW110 although further away and located higher on the structure, shows faster CO₂ breakthrough compared to well SW59.

In Figure 6.30 one can view a vertical section through the reservoir in S-N direction in the vicinity of the injection well (SW 90). As expected the CO₂ will channel through the high permeability strata favored also by gravity segregated distribution.

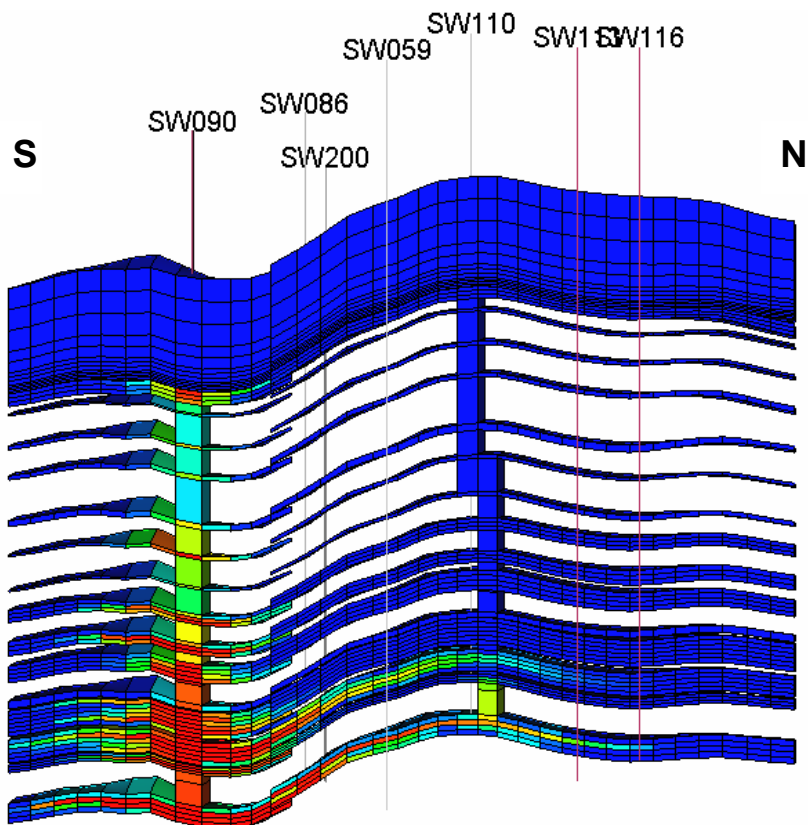


Fig. 6.30: Cross Section: Breakthrough Time, well SW 59 Case 2

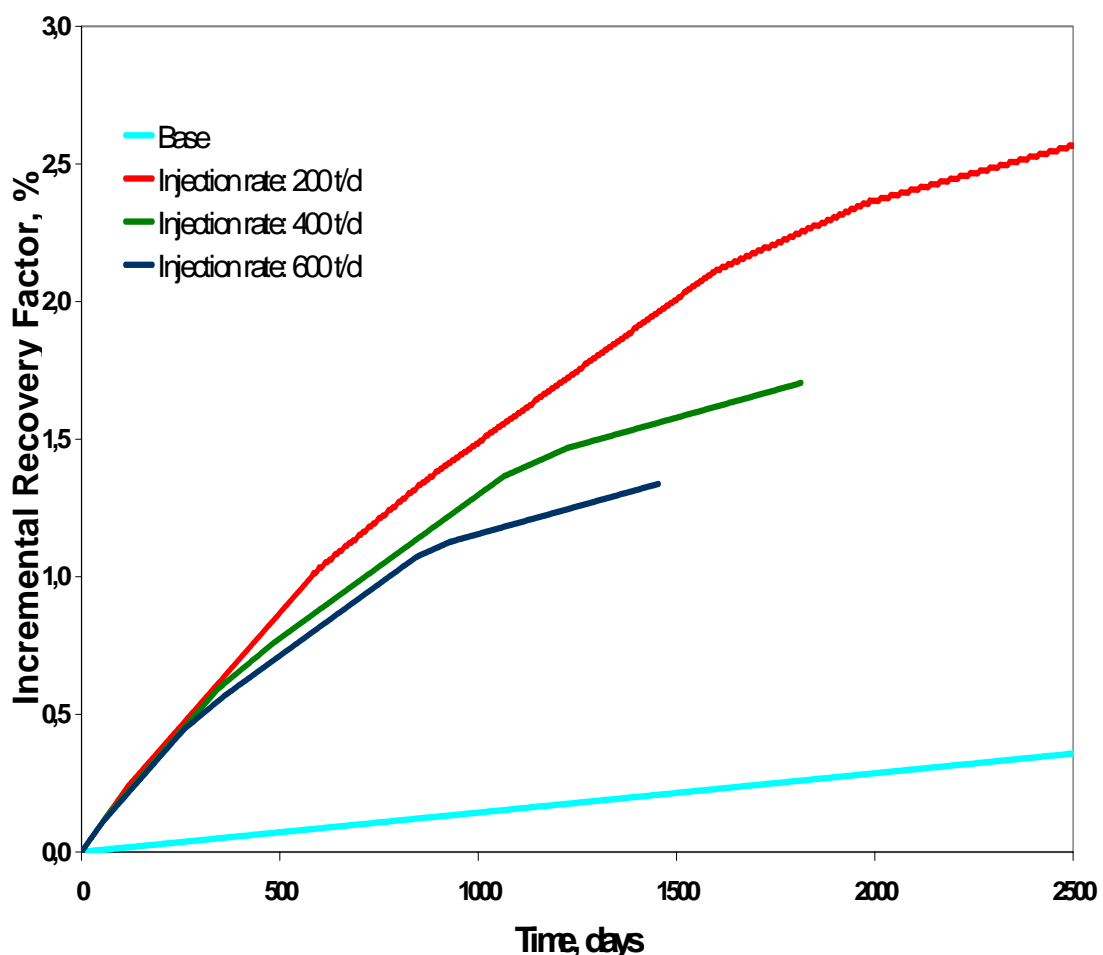


Fig. 6.31: Incremental recovery factor in Strategy 1

FiFig.

The main simulation results regarding the recovery and CO₂ storage capacity are summarized in Table 6.9.

Table 6.9 Simulation Results Altmark Block 12

| Case | Injection Strategy | Injection Time (years) | Production Time (years) | Incremental Recovery, % | Additional Gas Produced, 10 ⁶ . sm ³ | CO ₂ Storage Capacity, 400 bar, mil. tons |
|------|--------------------|------------------------|-------------------------|-------------------------|--|--|
| 1 | 1 | 38.6 | 7,3 | 2.63 | 262 | 45.46 |
| 2 | 1 | 36.3 | 5 | 1.71 | 170 | 44.96 |
| 3 | 1 | 35.3 | 4 | 1.34 | 133 | 44.78 |
| 4 | 2 | 81 | 0 | 0 | 0 | 46.25 |

The enhancement of the gas recovery based on the almost depleted stage of the gas reservoir is about 2.6 % of the OGIP (see also Figure 6.31) for the underbalanced mode of injection, but due to the fact that the gas resource is relatively large, the amounts recovered through CO₂ injection can be important. The CO₂ injection capacity is adequate, about 45 millions tons CO₂, which can be injected in this Block 12 of the Altmark field. Comparing the 2 injection strategies proposed, one can see that in the case of delayed production no incremental gas can be produced due to the fact that in all wells, when they are reopened, the CO₂ fraction is already larger than 10%.

The pressure performance of the field and of the injection well for the Block 12 sector model (injection strategy 1) is presented in Figure 6.32. It can be observed the bottom hole pressure (BHP) limit set for the injection is 520 bar. The tubing head pressure necessary to inject the CO₂ at the beginning of the injection period is just about 2 bar larger than the reservoir pressure due to the effect of the high density of CO₂ in the injection string.

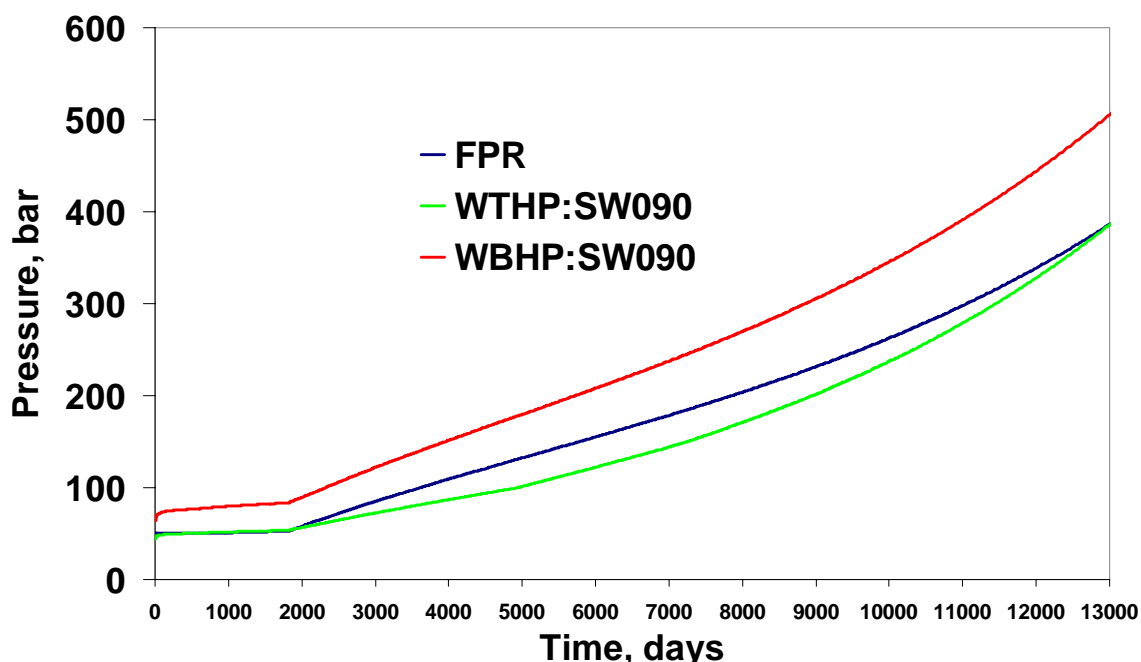


Figure 6.32 Pressure performance in Altmark Block 12

6.3.2. Simulation of the CO₂- disposal into a coupled sector model Altmark Block 12+14

The compartmentalization of the Altmark Gasfield does not allow to analyse the storage and recovery performance without taking interference with neighboring blocks into account. Therefore the model had to be extended with respect to the neighbor block 14.

6.3.2.1 Model Description

The sector model comprising the blocks 12 and 14 from the Altmark field was generated from the geo-models proposed in section WP3.

The simulation model has 62 blocks in X direction and 89 in Y direction having a resolution of 100x100 m whereas in Z direction from 67 grid blocks only 38 were active, corresponding to 15 pay zones. The total number of active cells in the model was 100588. The interlayers between these strata were considered inactive, acting as no flow barriers for the vertical migration of the CO₂. As in the case of simulation model of Block 12 all strata were perforated in all wells giving the model a generic character.

The model was divided into 2 regions corresponding to Altmark field Blocks 12, up-dip in the North (UDC), and 14 down-dip in the South (DDC), see Figure 6.33. Due to the fact that a half door fault is present in this model between the 2 regions and the generic character of the study the separation of the blocks was simulated by a imaginary fault, represented by the pink line in Figure 6.33, with variable transmissibilities. It was intended to study the effect of the fault transmissibility on the EGR process.

In this sector model 28 wells were drilled since the discovery of the field in 1969, 12 in UDC and 16 in DDC. At the start of this study 15 wells were producing about 300000 m³/d, 7 in the UDC and 8 in DDC. The initialization of the model was made in a depleted state with an initial pressure being 50 bars, as average value of the pressure existing in these blocks at the beginning of the CSEGR. In order to study the effect of the initial pressure on the EGR process some runs were done with a larger pressure (100 bars) initially in UDC or in DDC.

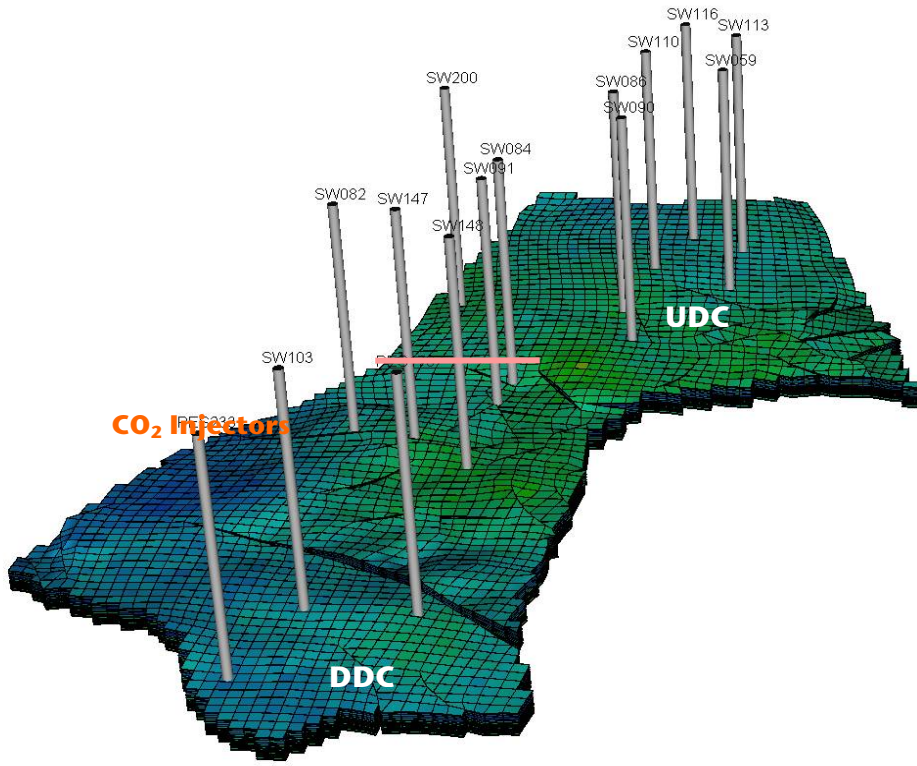


Fig. 6.33 Simulation Model Altmark blocks 12+14.

The pay zones average parameters (porosity, permeability and thickness) for each geological layer in both regions are presented in table 6.10. The denomination of the strata is in coincidence with the geological description that can be found in WP3, the interlayers are inactive and were not included in this table.

Table 6.10 Average strata parameters for UDC and DDC in simulation model Block 12 and 14

| Layer | UDC | | | DDC | | |
|---------------|--------------|-----------|------------|--------------|-----------|------------|
| | ϕ_i , - | h_i , m | k_i , mD | ϕ_i , - | h_i , m | k_i , mD |
| ROF | 0.07 | 5.14 | 2.07 | 0.06 | 5.79 | 0.63 |
| ROF+10 | 0.05 | 1.51 | 0.23 | 0.04 | 1.07 | 0.12 |
| 17M | 0.06 | 1.69 | 0.3 | 0.04 | 1.86 | 0.08 |
| 12B | 0.05 | 2.09 | 0.24 | 0.06 | 2.33 | 1.55 |
| 16M | 0.04 | 3.3 | 0.16 | 0.03 | 2.79 | 0.05 |
| 16B | 0.07 | 1.68 | 0.39 | 0.07 | 1.92 | 1.11 |
| 15M | 0.03 | 1.38 | 0.05 | 0.05 | 1.57 | 0.26 |
| A | 0.07 | 6.24 | 4.63 | 0.07 | 6.54 | 0.91 |
| B14 | 0.11 | 6 | 77.36 | 0.09 | 7.47 | 9.89 |
| B13 | 0.09 | 8.52 | 14.63 | 0.11 | 8.88 | 12.78 |
| C12 | 0.1 | 2.82 | 5.56 | 0.10 | 3.33 | 7.81 |
| C11 | 0.14 | 12.78 | 70.44 | 0.12 | 12.39 | 34.23 |
| C10 | 0.15 | 10.67 | 105.08 | 0.14 | 11.08 | 42.41 |
| C9 | 0.12 | 4.16 | 14.98 | 0.12 | 7.80 | 60.83 |
| D | 0.12 | 9.18 | 42.25 | 0.13 | 10.23 | 43.08 |

6.3.2.2. Injection strategies and sensitivities

The injection strategy chosen was to inject through 2 wells a quantity of CO₂ that is about double the production of the wells presently still active in the reservoir. The injection flow rate was 600000 m³/d CO₂ which was subdivided over 2 injection wells. The production was made through the rest of 13 active wells by evenly distributing 300000 m³/d which defines an overbalanced injection mode. Similar with the Block 12 Sector model VFP curves were generated in order to calculate THP condition in injectors.

Injection strategy 1: in this strategy CO₂ was injected in 2 down-dip located wells: SW103 and PES 233. From Figure 6.33 one can observe that these wells are located in the best possible location down-dip as the reservoir has a dip angle of about 4° from North to South. All other 13 wells were opened and producing until a value of 10% CO₂ in the gas stream, then the well was closed.

Injection Strategy 2: in this strategy the injection took place in 2 up-dip located wells SW113 and SW116 (see Figure 6.33) and the production wells were stopped in the same conditions, 10% CO₂ in the production stream, as in injection strategy 1.

Interference between the blocks was studied by using different fault transmissibility multipliers for the fault dividing the 2 regions having either fully communicating compartments (multiplier 1) or partly communicating compartments (multiplier<1). Another variable is coming from the initial pressure in the compartments either 50 bars in both or 100 bars in one and 50 bars in the other one, in order to study the effects of different GIP and pressures at the initialization of the EGR process. A detailed description of the injection strategies and sensitivities is presented in Table 6.11.

Table 6.11 Description of the Injection strategies and sensitivities used in simulation

| Case Description | Injection Rates, sm ³ /d | Production Rates, sm ³ /d | Fault Transmissibility Multiplier | Initial Reservoir Pressure, bar |
|--|--|--------------------------------------|-----------------------------------|---------------------------------|
| A: Down-dip Injection, Fully Communicating Compartments | SW103 +PES 233 600000 (1130 t/d) | 13 Wells 300000 | 1 | Block12: 50 |
| | | | | Block 14: 50 |
| B: Down-dip Injection, Partly Communicating Compartments | 600000 (1130 t/d) | 300000 | 0.01 | Block12: 50 |
| | | | | Block 14: 50 |
| C: Down-dip Injection, Fully Communicating Compartments | 600000 (1130 t/d) | 300000 | 1 | Block12: 50 |
| | | | | Block 14: 100 |
| D: Down-dip Injection, Partly Communicating Compartments | 600000 (1130 t/d) | 300000 | 0.01 | Block12: 50 |
| | | | | Block 14: 100 |
| E: Up-dip Injection, Fully Communicating Compartments | SW 113+116 600000 (1130 t/d) | 13 Wells 300000 | 1 | Block 12: 50 |
| | | | | Block 14: 50 |

6.3.2.3 Simulation results.

The breakthrough times for CO₂ 10% fraction in the production stream of 13 wells for the case A (see Table 6.11) are presented graphically in Figure 6.34.

The breakthrough times for the different injection cases are compiled in Table 6.12. One can observe from this table, that the sequence in which the CO₂ reaches the production wells depends on the propagation distance from the injector. Moreover the production period of the wells in DDC is the same in case A and B whereas the wells in the UDC can produce longer. This reflects also in the increased recoveries that can be achieved when the fault transmissibility multiplier is smaller, see Table 6.13 for details regarding the incremental recovery and storage capacity.

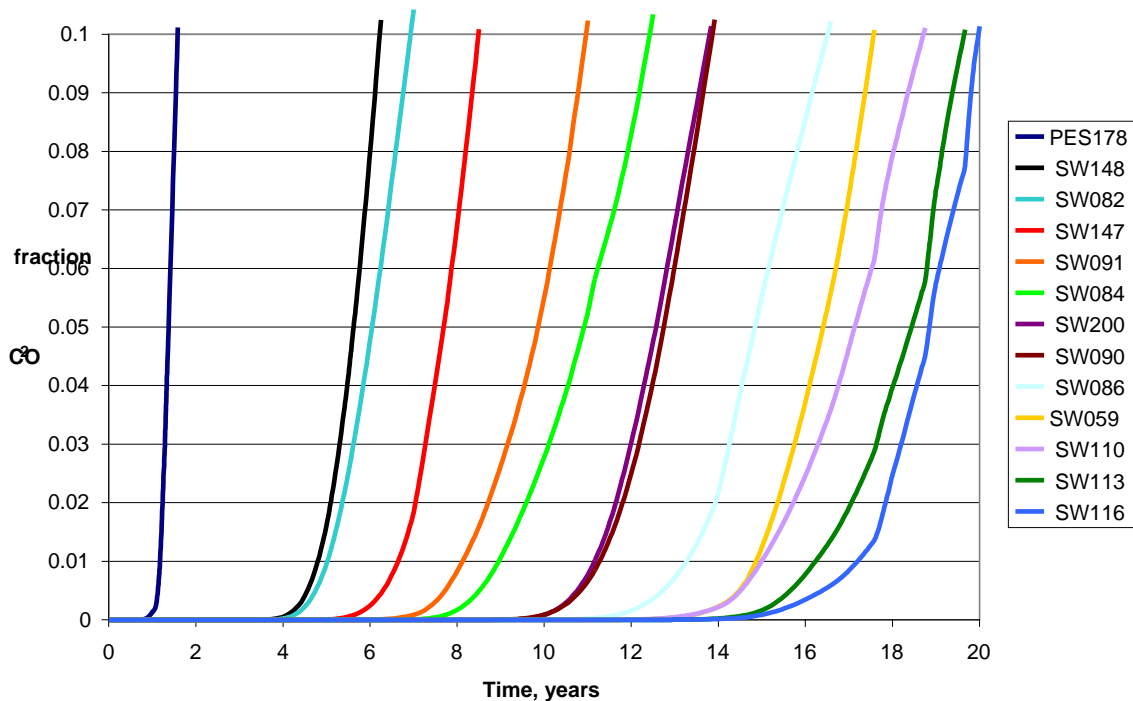


Figure 6.34 CO₂ breakthrough curves, Case A

Table 6.12 Breakthrough times for different injection strategies and sensitivities

| Well | Compartment | Breakthrough time (years) | | | | |
|--------|-------------|---------------------------|----------|----------|----------|----------|
| | | Case A | Case B | Case C | Case D | Case E |
| PES178 | DDC | 1.58 | 1.58 | 2.42 | 3.25 | 13.22 |
| SW148 | DDC | 6.24 | 6.24 | 7.08 | 7.91 | 12.83 |
| SW082 | DDC | 7.00 | 7.00 | 7.84 | 8.67 | 11.92 |
| SW147 | DDC | 8.50 | 8.50 | 9.34 | 10.17 | 10.16 |
| SW091 | DDC | 11.00 | 11.00 | 11.84 | 12.67 | 9.82 |
| SW084 | DDC | 12.50 | 12.50 | 13.34 | 14.17 | 9.32 |
| SW200 | UDC | 13.83 | 15.46 | 16.15 | 17.14 | 8.30 |
| SW090 | UDC | 13.91 | 15.54 | 16.23 | 17.22 | 7.92 |
| SW086 | UDC | 16.59 | 18.22 | 18.91 | 19.90 | 6.63 |
| SW059 | UDC | 17.58 | 19.21 | 19.90 | 20.89 | 4.43 |
| SW110 | UDC | 18.75 | 20.38 | 21.07 | 22.06 | 1.36 |
| SW113 | UDC | 19.67 | 21.30 | 21.99 | 22.98 | inj well |
| SW116 | UDC | 20.00 | 21.63 | 22.32 | 23.31 | inj well |
| SW103 | DDC | inj well | inj well | inj well | inj well | 14.12 |
| PES233 | DDC | inj well | inj well | inj well | inj well | 15.03 |

A top view of the CO₂ distribution in the layer C10 with the highest flow capacity at the moment of closing well SW116 (20 years) can be seen in Figure 6.35. A cross section of layer wise CO₂- fraction distribution is presented in Figure 6.36.

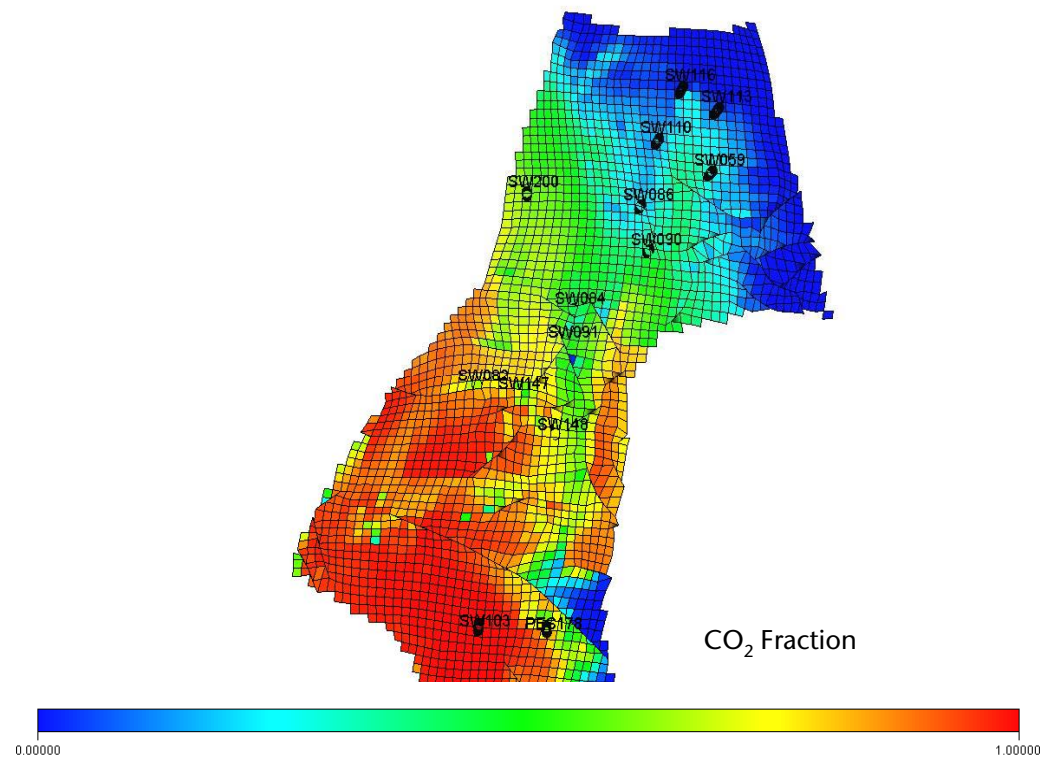


Fig. 6.35 Top View at Breakthrough - well SW116 (Case A)

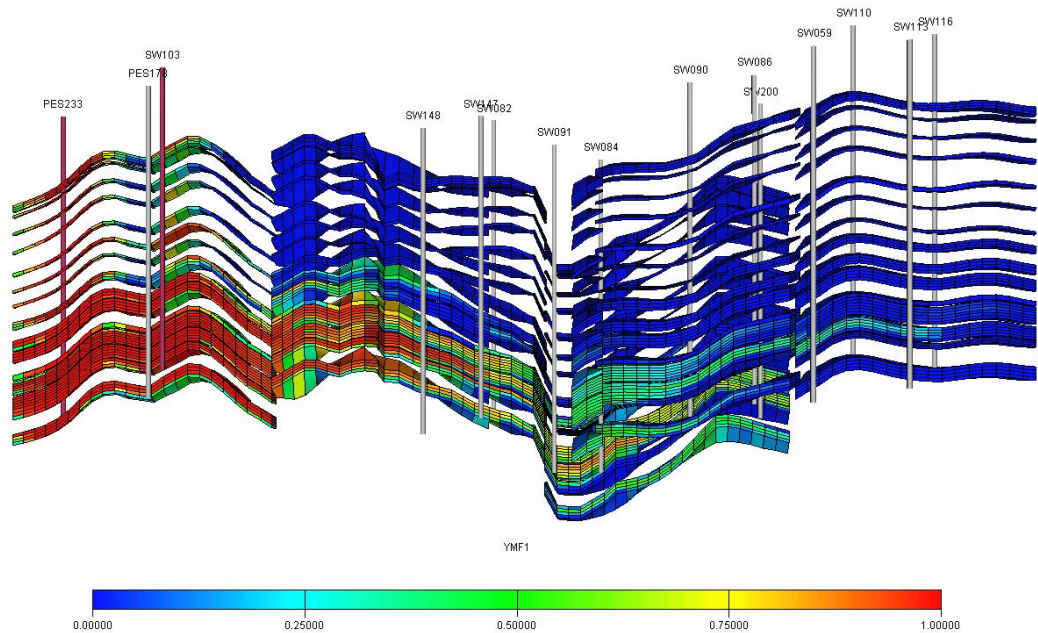


Fig. 6.36 Cross section of CO₂- Breakthrough in well SW116 for Case A

From Table 6.13 it can be seen that the cumulative recoveries for UDC (Block 12) + DDC (Block 14) are comparable with the results obtained in the Block 12, Section 6.3.1, whereas the recoveries in the UDC are somewhat larger than in the single compartment case.

Table 6.13 Simulation Results in Sector Simulation Model Altmark 12+14

| Case Description | Injection Time, years | Production Time, years | Incremental Recovery, % GIP | | CO ₂ Storage Capacity, Mt UDC+DDC UDC |
|---|-----------------------|------------------------|-----------------------------|------------|---|
| | | | UDC+DDC | UDC | |
| A: Down-dip Injection, Fully Communicating Compartments | 45 | 20.0 | 2.3 | 4 | 112.2 |
| | | | | | 45.9 |
| B: Down-dip Injection, Partly Communicating Compartments | 44 | 21.6 | 2.6 | 4.5 | 113.3 |
| | | | | | 46.3 |
| C: Down-dip Injection, Fully Communicating Compartments | 47 | 22.3 | 2.8 | 4.9 | 114 |
| | | | | | 46.6 |
| D: Down-dip Injection, Partly Communicating Compartments | 45 | 23.3 | 3 | 5.3 | 115.4 |
| | | | | | 47.2 |
| E: Up-dip Injection, Fully Communicating Compartments | 35 | 15 | 0.65 | 1.1 | 105.7 |
| | | | | | 43.2 |

The increase in recovery factor in the UDC is caused by the fact that part of the gas in DDC is flowing over the fault in UDC and the wells in this compartment can produce more. The fault acts as a barrier to the flow of CO₂ from one compartment to the other permitting a longer production time for the wells in UDC. In order to better understand this behavior a simplified model was created and will be presented in Section 6.3.2.4.

In case E the up-dip injection the wells are producing only briefly due to the fact that the CO₂ has a larger density than the Altmark gas and the CO₂ breakthrough in the producing stream of the wells is very fast. The last well PES 233, situated lowest on the structure, is closed after 15 years permitting a recovery factor of about only 1.1 % in UDC and 0.65% in UDC+DDC. So comparing the 2 injection strategies proposed, it is clear that the injection Strategy 1 (gravity stable) brings a larger recovery in all cases compared to injection Strategy 2.

The total CO₂ quantity that can be stored is quite high, about 114 millions tons of CO₂ in both compartments. This means that only these 2 blocks from the Altmark Field can accommodate about 11 years of CO₂ released into the atmosphere by a large coal fired power plant producing about 1600 MW (see WP2 Schwarze Pumpe).

6.3.2.4 Simplified Generic - Two Regions Model.

It was intended to analyze the mechanisms responsible for the enhancement of the recovery by the flow barrier.

The model is based on the average parameters presented in Table 6.10 and consists of 2 compartments. The orientation is flat so that gravity will not play an important role in the process and is divided in 2 regions by a fault with no displacement. The model is 1 km long and 500 m wide (Figure 6.37). Region 1 (left) covers 60% from OGIP and Region 2 (right), 40% of OGIP. One injection well and one production well (PROD1) were placed in Region 1, and one producer in Region 2 (PROD2). The injection rate was set to 60000 m³/day whereas the production wells are producing with 15000 m³/day/well. The production wells were closed when CO₂ fraction reached 10%. A second control for the wells was a minimum tubing head pressure of 20 bars.

A fault transmissibility multiplier was set at different values in this study: 1, 0.1, 0.01 and 0.001 respectively, in order to evaluate the breakthrough of CO₂, the recovery and the pressures in the two regions of the model. Base cases were run without injection in order to be able to calculate the incremental recovery factor obtained when injecting CO₂.

The main results of the simplified two region model simulations confirm the numerical results obtained in the simulation model of block 12+14 presented in the previous section of this study indicating that the fault acts as a protector of the wells in the Region 2 permitting them to produce for longer times and so achieve a larger recovery factor.

The well controls, the breakthrough times and the incremental recovery factors for different injection strategies and sensitivities are presented in Table 6.13. From this table it can be seen that the recovery factor in Region 2 will be larger if the fault transmissibility multiplier is smaller, this leads to the conclusion that in the event of applying the EGR process in a real reservoir the transmissibility of the faults between two compartments is a major control factor and it should be treated with great care in the history match process. Applying a tubing head pressure (THP) control instead of controlling the rate of the wells will result in an acceleration of the recovery process. The main reason for this behavior is the fact that the mass and the pressure transfer are different, even if less mass is transferred through the fault when the transmissibility is lower enough pressure support for production still exists in Region 2, thus the breakthrough of the CO₂ in the Region 2 is retarded permitting longer production and higher recovery factors to be achieved. Having a larger pressure in the production compartment and a lower in the injection compartment will also benefit the recovery process. Identifying such geological features, faults with relatively low transmissibilities, in a real reservoir will have an outmost importance in the process design.

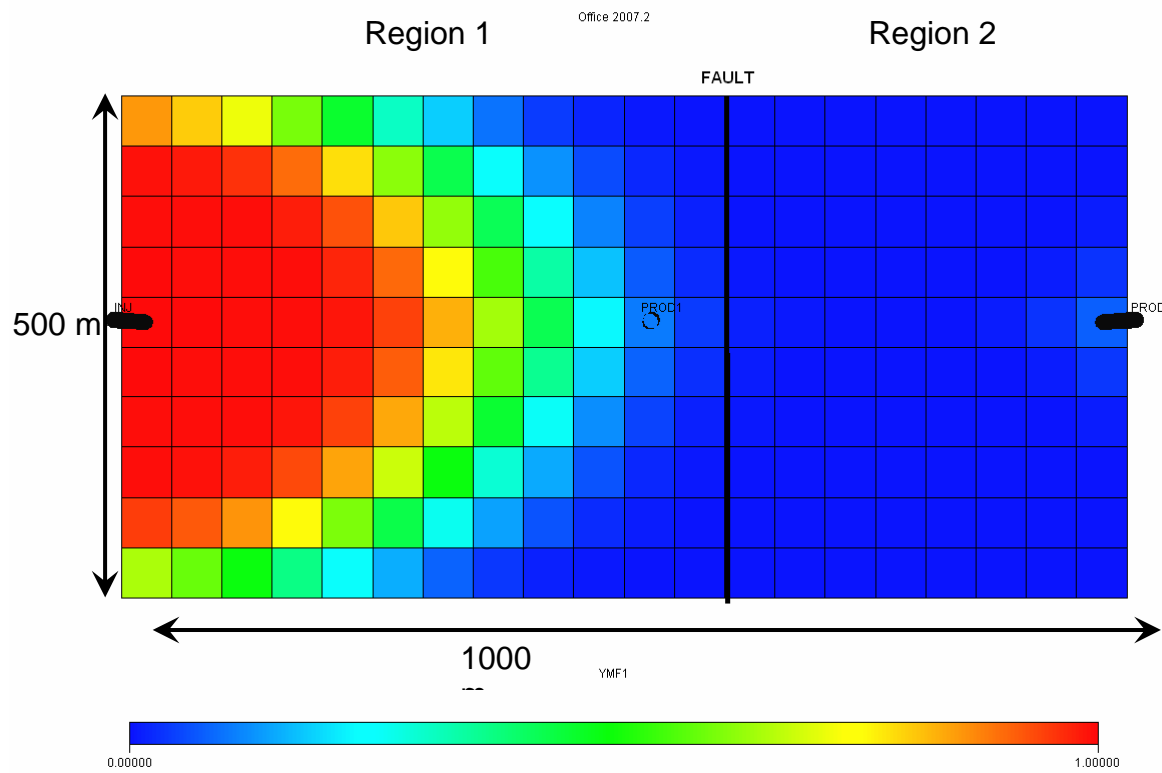


Figure 6.37 CO₂ distribution at 10% breakthrough in PROD1 strata 27 highest permeable

Table 6.13 Simulation Result for the simplified model

| MULTFLT | Well Control | Initial Pressure bar | Breakthrough, days | | Incremental Recovery at breakthrough, % | |
|---------|------------------|----------------------|--------------------|-------|---|----------|
| | | | PROD1 | PROD2 | Region 1 | Region 2 |
| 1 | Rate (15k sm3/d) | R1=50 R2=50 | 365 | 1400 | 0.912 | 3.62 |
| 0.01 | Rate (15k sm3/d) | R1=50 R2=50 | 396 | 1492 | 0.913 | 3.91 |
| 0.001 | Rate (15k sm3/d) | R1=50 R2=50 | 396 | 1733 | 0.914 | 5.1 |
| 1 | THP (20 bar) | R1=50 R2=50 | 197 | 410 | 0.921 | 3.68 |
| 0.01 | THP (20 bar) | R1=50 R2=50 | 212 | 578 | 0.925 | 4.12 |
| 0.001 | THP (20 bar) | R1=50 R2=50 | 227 | 1127 | 0.927 | 5.33 |
| 0.01 | THP (20 bar) | R1=100 R2=50 | 304 | 670 | 0.918 | 3.48 |
| 0.001 | THP (20 bar) | R1=100 R2=50 | 396 | 974 | 0.92 | 4.65 |
| 0.01 | THP (20 bar) | R1=50 R2=100 | 333 | 638 | 0.921 | 4.21 |
| 0.001 | THP (20 bar) | R1=50 R2=100 | 304 | 1154 | 0.922 | 5.48 |

In explaining these phenomena one must look into the pressure distribution in the 2 regions, presented here in Figure from 6.38.

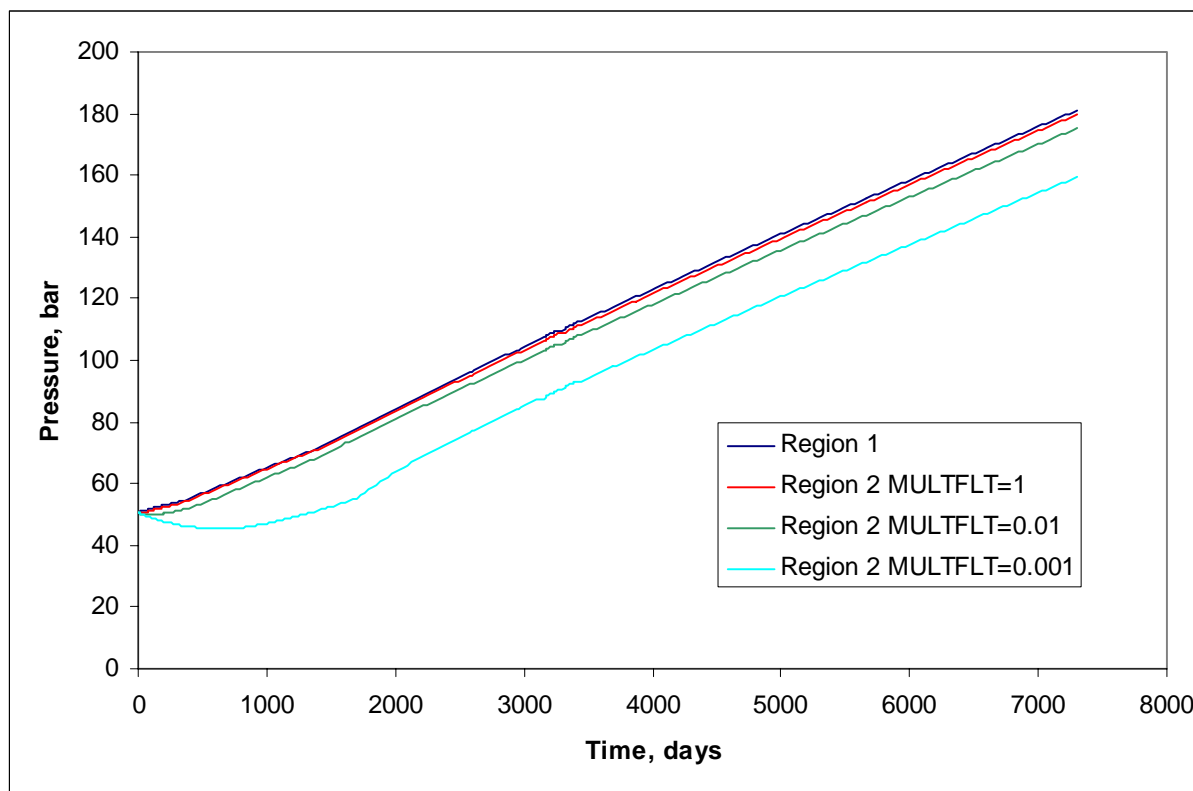


Figure 6.38 Region Pressure for different fault multipliers

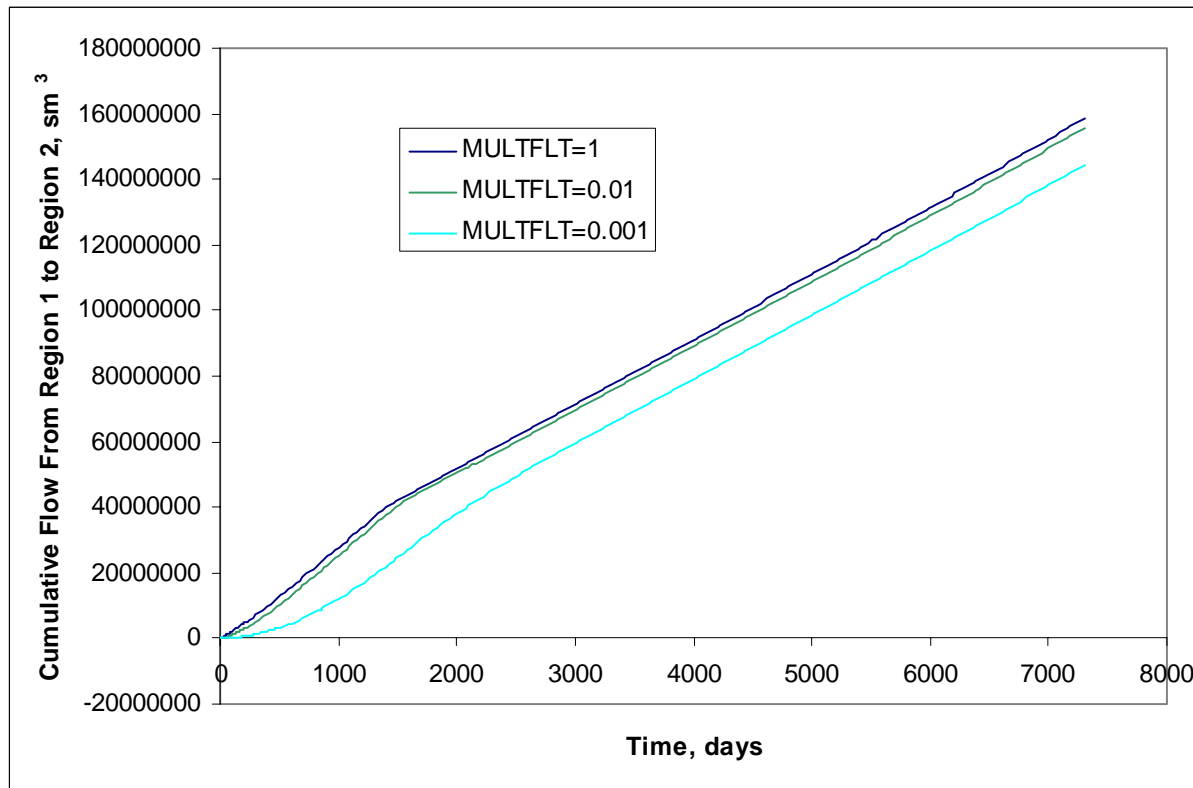


Fig. 6.39 Cumulative flow from Region 1 to Region 2 during the process

From these plots it can be observed that the pressure difference between the 2 regions is larger when the transmissibility of the fault is lower. But the fluid transfer between the regions is smaller as explained by the Figure 6.39. In other words the pressure in the right side of the model will stay at about the same level with a little increase whereas less CO₂ will flow from Region 1 into Region 2 thus the CO₂ breakthrough into the PROD2 well will be delayed permitting an increase in the recovery factors of this regions and of the model. The relative small differences in gas transfer are depending on the squared pressures of both sides of the fault.

6.4. Conclusions

1. The incremental recovery factors simulated in this study were as high as 10 % IGIP in Barrien gas field and approximately 3 % IGIP in the Altmark gas field.
2. From the injection strategies tested, the most promising is the simultaneous injection and production strategy, which gave better results in both reservoirs studied.
3. In the sector model study of the Barrien Gas Field, 17 million tons of CO₂ can be stored, after reaching the initial pressure of about 400 bar, providing sufficient capacity to inject the CO₂ amount coming from the separation of the North Sea Gas (see WP2).
4. The Block 12 from the Altmark Gas Field can store about 45 million tons of CO₂ whereas the Blocks 12 and 14 together can accommodate 112 million tones of CO₂. This represents 11 years of CO₂ emissions of a large coal fired power plant generating about 1600 MW (see WP2 Schwarze Pumpe).
5. The influence of structural types of gas traps on the EGR effects has been simulated and it could be proved that gravity effects are more beneficial in anticline structures with steep flanks (Barrien type reservoirs) and viscous/gravity displacement forces control the fill up of stratified reservoir types (Altmark type reservoirs).
6. In segregated flow patterns of multi-layer reservoirs the acceleration of residual gas recovery is the most important aspect.
7. The transmissibility of the faults between two compartments is a major control factor and it should be treated with great care in the history match process. Identifying such geological features in a real reservoir will have an outmost importance in the recovery process.
8. The simulator ECLIPSE can be used in simulating EGR processes in depleted gas reservoirs.

Work Package 7:

Technical, Economical and Environmental Analyses-Feasibility Report

Author: G. Pusch, F. May

| | |
|--|-----|
| Kurzfassung..... | 253 |
| Introduction..... | 254 |
| Main issues for the technical and economical realization of geologic storage | 255 |
| Technical issues | 255 |
| Simulation Tools and Models | 260 |
| Geochemical Risks of Failure | 261 |
| Description of potential health, safety and environmental hazards of geological CO ₂ storage (May)..... | 263 |
| Hazard Scenario | 266 |
| References | 271 |
| Field Project Simulation of CO ₂ Storage and Enhanced Gas Recovery | 272 |

Kurzfassung

Eine wirtschaftlich belastbare Bewertung der beiden Prototypen CO₂ Entsorgungsfälle: **Kraftwerk (Schwarze Pumpe)/ Rotliegenderdgaslagerstätte (Altmark) und Nordseegas (Dornum)/ Buntsandsteinlagerstätte (Barrien)** kann durch diese Studie nicht erbracht werden, da derzeit kein Markt für CCS existiert. Der Transport von CO₂ von Dornum nach Barrien würde die Emissionszertifikatgutschriften für CO₂ überschreiten, da die anfallenden Mengen für den Bau einer Pipeline zu niedrig sind. Die Transport-, Konditionierungs- und Kompressionskosten für das im flüssigen Zustand von der Lausitz nach Steinitz transportierte CO₂ sind im Bereich der erwarteten Emissionshandels Gutschriften von 30 €/t, benötigen jedoch zusätzlich den Bonus der Steigerung der Restgasförderung.

Die Speicherung von CO₂, welches mit hoher Reinheit (>98%) von den umweltschädlichen Emissionen abgetrennt wurde, in weitgehend ausgeförderten Erdgaslagerstätten ist technisch machbar, wenn günstige geologische Speicherstrukturen in der Natur existieren. Solche sind dann gegeben, wenn die Separation zwischen dem Erdgas und dem schwereren CO₂ begünstigt wird (steiles Einfallen der Schichten, Stratifizierung der Lagerstätte). Trockene Gaslagerstätten sind vorteilhaft, weil die Materialprobleme in den Sonden und Übertage sowie die unerwünschten hydro-mechanischen Effekte durch den Einfluss der aus dem gelösten CO₂ entstehenden Kohlensäure, sowie die massiven Austrocknungsprobleme (Salzausfällungen und Verstopfung) weniger gravierend sind. Den größten Stellenwert haben Erdgaslagerstätten aber im Hinblick auf ihren Erkundungsstand gegenüber allen anderen geologischen CO₂-Speichertypen. Nur so kann eine einigermaßen sichere Prognose mit den erprobten Simulationstools für Erdgasspeicherberechnungen auch für den CSEGR Prozess mit CO₂ erstellt werden. Der Compositional Simulator ECLIPSE 300 hat sich dafür als geeignet herausgestellt, wenn man die Langzeiteffekte der chemischen Speicherung und der gesteinsmechanischen Effekte vernachlässigen kann. Rein rechnerisch können EGR Effekte eine Mehrförderung von 200 bis 400 m³ Erd-gas je Tonne injiziertes CO₂ bringen, vorausgesetzt dass die Injektions-/Produktionsstrategien an die Struktur der Lagerstätte angepasst werden (hohe Raten bei homogenen Trägern und kleine Raten bei stratifizierten Trägern, Ausnutzung von Barrieren gegen die rasche Ausbreitung von CO₂).

Eine weitere wichtige Voraussetzung für die technische und vielmehr wirtschaftliche Machbarkeit ist die vorhandene und intakte Infrastruktur des Erdgasfeldes, damit die Kosten für eine Rekomplettierung vorhandener Sonden und die Verfüllungskosten der zu schließenden Sonden nicht ausufern. Neubohrungen mit CO₂ beständiger Untertageausrüstung und Bohrlochsabschlüssen kosten für Teufen bis zu 4000m in der Größenordnung von 8-12 Millionen Euro. Zu den Materialfragen und CO₂ dichten Bohrungskomplettierungen sind derzeit eine Reihe von Forschungsvorhaben initiiert worden, deren Ergebnisse von großer Bedeutung für die Sicherheit der CO₂ Speicherung in ausgeförderten Erdgaslagerstätten sind. Die konventionellen

Komplettierungsschemata von Erdgasspeicherbohrungen können auf CO₂ Speicherbohrungen übertragen werden, vorausgesetzt die richtigen hoch legierten (Nickel-Chrom reichen) Werkstoffe für Rohre und Kohlensäure resistenten Zemente stehen zur Verfügung. Zur Prozesskontrolle muss die CO₂ Ausbreitung in der Lagerstätte überwacht werden und ein Langzeit - Monitoring der geologischen Barrieren (Caprock), Zwischenspeichern in grundwasserführenden Schichten und an der Tagesoberfläche in Gang gehalten werden, dessen Kosten bisher noch nicht abgeschätzt werden konnten. Im Feldbetrieb stellt die Handhabung von CO₂ keine, über die Grenzen des Erd-gasförderbetriebes (z. B. von Sauergasfeldern) hinaus reichende Sicherheitsanforderung an den Umweltschutz dar. CSEGR ist eine Chance für die Erdgasindustrie und eine Herausforderung für die Forschung den Treibhauseffekt durch gezielte geologische Speicherung der klimaschädlichen Emissionen von CO₂ in den Griff zu bekommen. Viele andere Optionen haben wir nicht.

Introduction

The reduction of green house gas emissions is an environmental prerequisite for the global climate control and anthropogenic carbon dioxide release control.

In this integrated study on technical feasibility and economic constraints of the geologic storage option in depleted natural gas reservoirs emphasis was laid on the screening of natural and controllable parameters in the CCS chain.

Therefore CO₂ capture, transport, field conditioning, injection, propagation and the integrity of the deposit became the main concerns of the feasibility. The legal situation for CCS at the beginning of the project was not clear, so the approach for realization was treated under the existing mining laws for producing gas fields and the effects on enhancement of residual gas production as well as for production acceleration had to be studied.

The objects for the engineering work had been selected from potential and representative cases of CCS- that is the source/sink combination "*Lignite Power Plant Schwarze Pumpe/Altmark Rotliegend Gas Field*" and "*North Sea Natural Gas Processing Station Dornum/Barrien Buntsandstein Gas Field*". The orientation on real process and field data enables the applicability of solutions and problems to the practice, but due to the complexity of the real cases, increases the time demand for studying the sensitivity of all possible parameters. That means findings from process simulations, technical solutions for the practicability and long term scale effects of the storage process have more or less an exemplary character.

I could not be our target to analyze economics of carbon dioxide sequestration in detail, since at present no real market for CO₂ storage business exists. The political, legal and technological conditions have not been developed far enough to build a sound framework for a detailed analysis. Focus was given to the key factors of an

economic data basis: transportation cost, CO₂-well expenditures, well repair cost, production enhancement, additional recovery, storable volumes.

The time frame of the three field project phases in a full field study-- ***multi-well injection front build-up, residual gas production enhancement phase and final storage fill-up phase***—have not been scaled in the simulations of the prototype reservoir sector models with single well injection pattern. Therefore actual duration of the 3 phases is influenced by the arbitrary well selection, injection/production rates and abandonment criteria (10 % CO₂ content) and cannot be considered as realistic. There is an obvious demand for optimization of the time framework by number and position of injectors and producers in the field, because production enhancement economics and yearly storage capacity development depends on this well portfolio selection. General conclusions taken from the results of this case related feasibility study must be handled with caution, since they have no claim of global validity. But trends observed and technical solutions proposed can be considered as a guide for CCS Geologic Storage.

Main issues for the technical and economical realization of geologic storage

Technical issues

The project partner Vattenfall has build-up a demonstration plant for the capture of CO₂ in a so called oxyfuel O₂/CO₂ recycle combustion in a lignite fired power plant. So technical feasibility is granted. The other project partner EON-Ruhrgas has a proven technological basis for CO₂ removal from natural gas either by absorption or membrane techniques in his numerous natural gas processing plants. Main unexplored cost factor is the transportation of CO₂ in liquid, gaseous or supercritical state. The easiest way is to transport the CO₂ as a liquid, since it minimizes material problems. Transport in a supercritical state requires heating (temperature beyond 32° C) and insulation, whereas gaseous transport increases material problems (traces of moisture may aggravate corrosion problems). The outlet pressure from the plant at Schwarze Pumpe was calculated with 110 bar safeguarding a well head delivery pressure of 85 bar

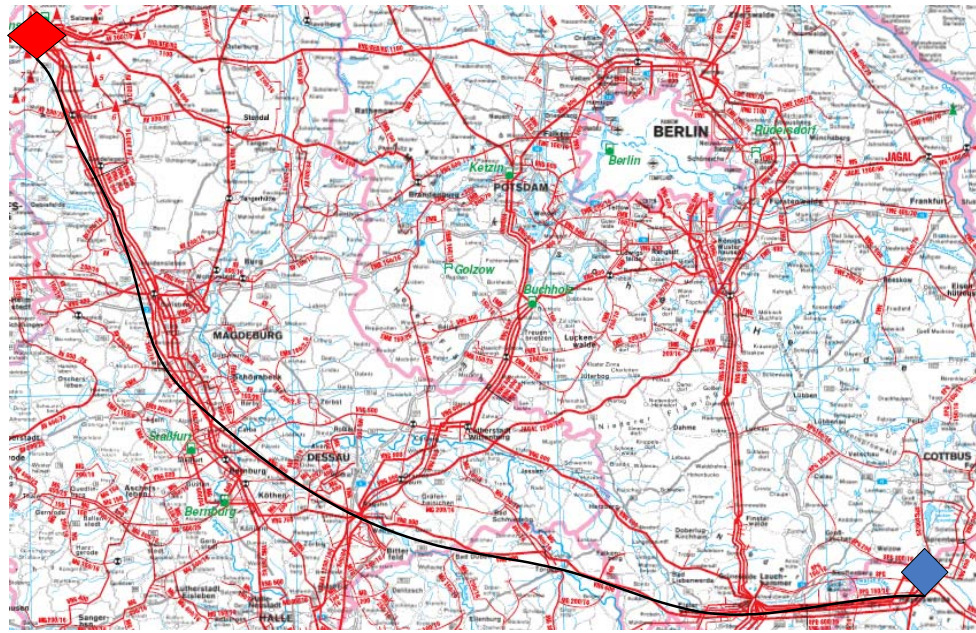


Figure 7.1: Pipeline route Schwarze Pumpe-Altmark, WP 1- Vattenfall

The pipeline route was designed comprising a total length of 330 km and diameters from 400 to 800 mm. Transport capacities for 5 Mt/y and maximum 10 Mt/y were used in a capital cost estimation software GESTCO-DSS and yielded a range of **190/380 M€ investment** volume for 400/800 mm pipeline diameters and specific cost of **4 to 6 €/t** presented in the following diagram. It must be pointed out that normal gas pipeline standards have been used and no concern was given to heating of gas to 40° C and insulation, if supercritical state transport is considered.

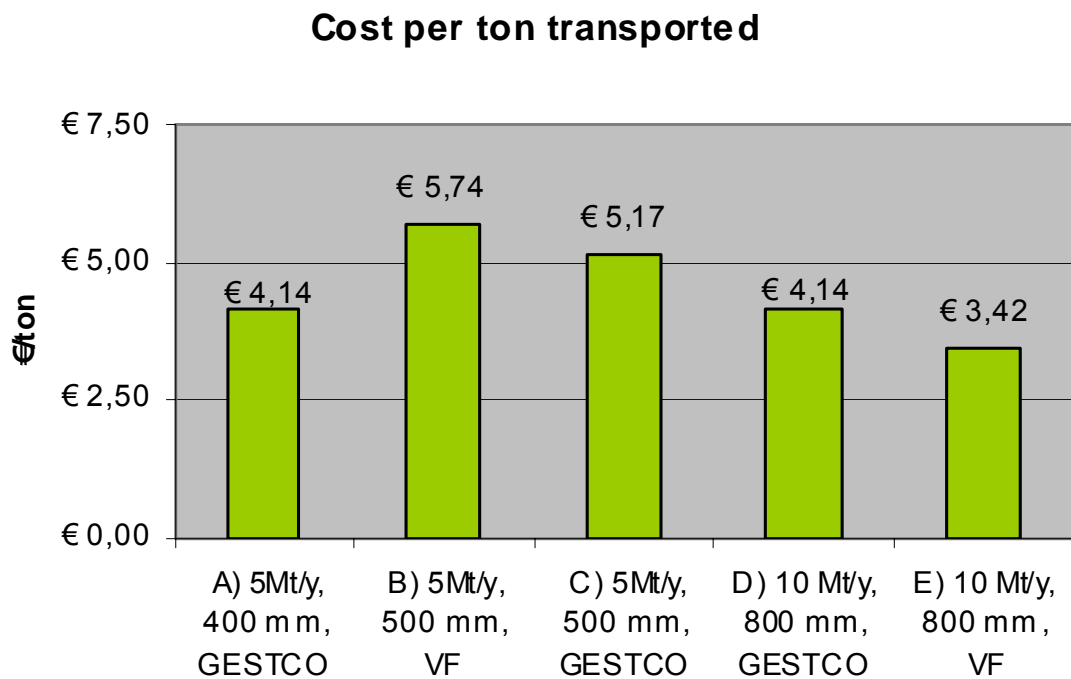


Figure 7.2: Specific CO₂ transportation cost, WP 1-Vattenfall

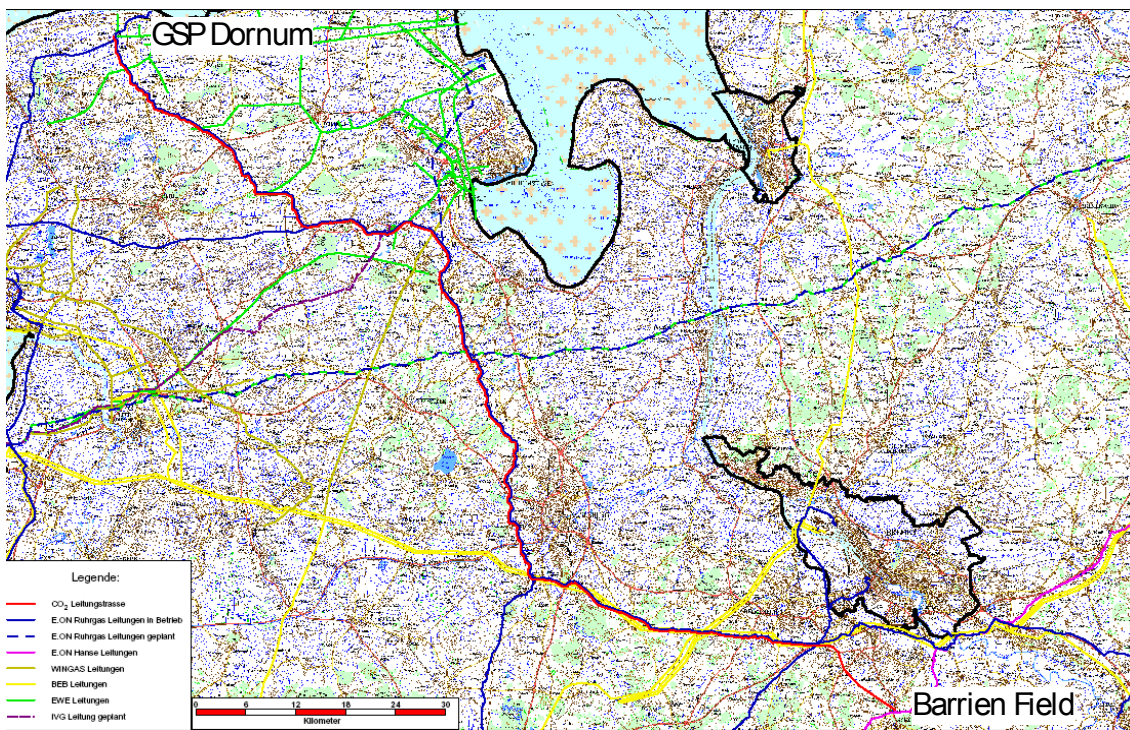


Figure 7.3: Pipeline route Dornum-Barrien, WP 1-Eon-Ruhrgas

In the case of Dornum-Barrien CO₂ transport system the length is reduced to 160 km and the transport capacity is calculated with 300000 t/y only. The pipeline diameter can be set to 300 mm with an operating pressure of 30 bar. In this case the GESTCO-DSS software calculates CAPEX of **80 M€** and specific cost of **30 €/t**, which does not include the extra cost for removal of the 200 ppm H₂S content of the North Sea Gas. This clearly shows that marginal amounts of CO₂ emissions must be locally deposited or admixed to other transport chains.

In depleted natural gas fields the infrastructure (transport lines, metering stations, gas-liquid separation, gas drying, gas-separation and compression) for the CO₂ distribution and natural gas production in the field is granted, if maintenance of the equipment was carefully executed. Material problems with dry and pure CO₂ are not critical. However in the case of liquid form transportation the vaporization of the liquid requires heating, either per well or at a central station. These extra costs have to be considered in the specific cost plan. In the framework of the CSEGR project careful inquiries have not been possible, therefore we have used best practice estimates (taking industry experience into account) giving a range of figures or average values.

Table 7.1: CAPEX and specific cost for CO₂ transport and distribution

| Measure | Technical Details | Capital Expenditures, Operating Expenditures |
|--|---|--|
| CO ₂ Transportation | Liquid state, 110 bar to 85 bar | Spec. Cost = 4-6 €/t |
| Field Infrastructure CO ₂ Adaptation | Cluster of 7 wells Flow Lines 6" V2A Processing Unit | Recompletion ¹ = 1000 k€/well Flow Lines ¹ = 370-450 k€/km Processing Unit ¹ = 5-8 M€ |
| CO ₂ Heating | T _{trans} = 10° C, T _{inj} = 40° C Spec. Heat CO ₂ = 0.85 kJ/kg K, Vapor-Enthalpy = 573 kJ/kg, Energy Cost = 3-5 ct/kWh, Process Efficiency = 70 % | Spec. Cost = 8-12 €/t |
| Compression Cost | P _{inlet} 50 bar P _{outlet} 150 bar, 280 t/d | Spec. Cost = 3 - 4,5 €/t ¹ |
| Operation Monitoring System | Injection Well | 50-100 k€ /yr-well ¹ |
| Operation Monitoring System | Production Well | 50-100 k€/yr-well ¹ |

For the injection of CO₂ new wells can be designed with materials that are capable to withstand CO₂ corrosion. From safe handling of CO₂ containing gas streams in the sour gas production and in the CO₂ Enhanced Oil Recovery materials are known, that can resist CO₂ attack for the operational phase of EGR. However we do not know the performance over hundreds of years. This is the task of new research projects with emphasis on chemical processes of material degradation, i.e. for steel, cement sealing materials and for the rock specimens. Operation expenditures of transporting, heating and compressing the CO₂ may easily exceed the 20 €/t margin for emission trading and may anticipate a bonus from enhanced residual gas recovery, to compensate the enhanced cost.

Well integrity of active and abandoned wells is a crucial issue in the long term capture concept of CCS by geological storage. The wellbore is the bottle neck where the existing geologic sealing is interrupted and provides the short circuit for gas escape to the atmosphere.

In our study practical solutions have been proposed for the recompletion of existing wells for injection and production, for the safe abandonment of wells and for the repair of leaking wells. Detailed cost estimations however depend on more insight into the technical applicability of the suggested solutions.

In the case of a rock salt cap rock, the natural sealing is proven and wells in this environment even with damaged cement annulus will have a potential sealing in the plastic salt trajectory or can be conditioned to become gas tight in the salt passage.

¹ Cost Estimates by GDF SUEZ E&P Deutschland GmbH

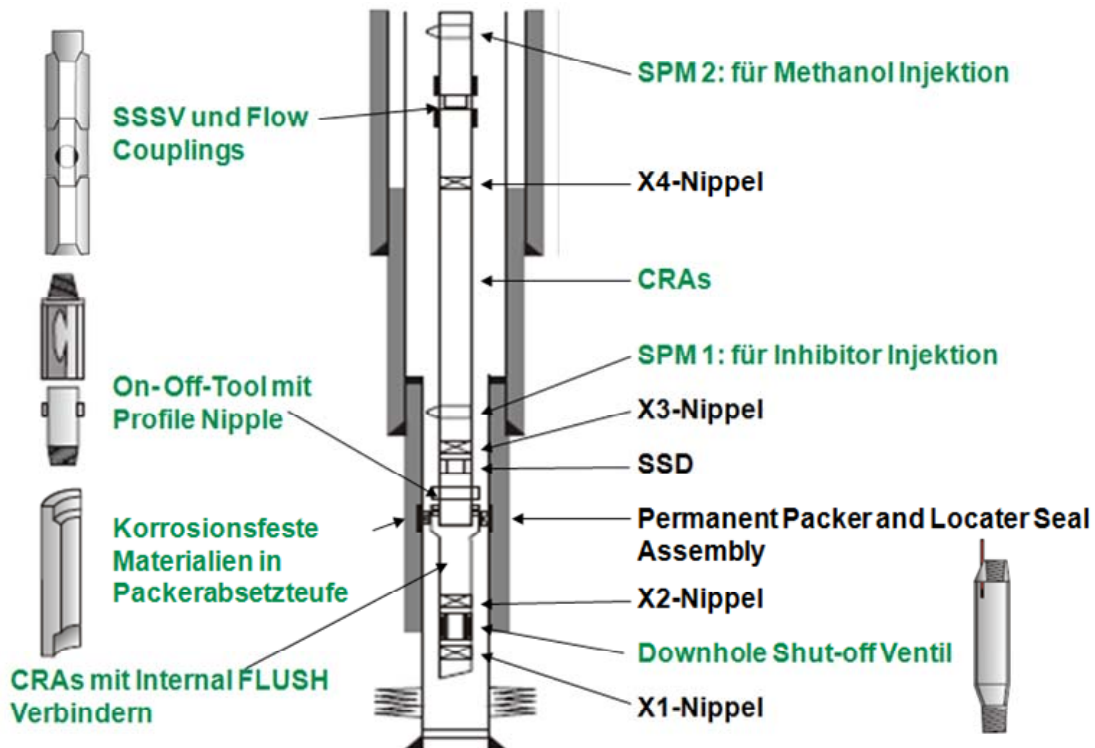


Figure 7.4: Design of a new Well for CSEGR, WP 2- K.M.Reinicke

Table 7.2: Economic parameters for well integrity

| Measure | Technical Details | Capital Expenditures, k € |
|--|---|---------------------------|
| Injection Well new ¹ | 3400 m, 7" Liner, 4½" Tubing, Rate 150 k m ³ /d | 8000-12000 k€ |
| Injection Well recompleted ¹ | 3400 m, 5 ½" Liner, 2 7/8" Tubing, Rate 150 k m ³ /d | 800-1200 k€ |
| Production Well new ¹ | 3400 m | 8000-10000 k€ |
| Production Well recompleted ¹ | 3400 m | 500 – 1000 k€ / well |
| Well Abandonment ¹ | 3400 m | 1500 k€ / well |
| Well Repair ¹ | 3400 m | 500-1000 k€ / well |

Investment cost for the implementation of new wells in the existing field structure is relatively high in the tail end phase of the field. A more feasible way is to recomplete old wells if they are mechanically stable. Another CAPEX issue is the abandonment of inactive wells, which will reach the same order of magnitude, if we consider the large ratio of existing gas field wells and required CO₂ injection wells in the final stage of sequestration

Technical issues play a vital role in the planning of CSEGR projects and are the key element for the economic realization of geologic CO₂ storage. The target value of a credit bonus / malus of 30 €/t is hardly compensating the rising cost of capture, transport, conditioning, distribution and compression without having an extra profit from EGR

Simulation Tools and Models

The build-up of geo-models based on the interpreted results of 3-D seismic, well logging, core and test analysis, geo-statistical interwell inter- and extrapolations, boundary conditions design and gridding structure is state of the art in petroleum geology/geophysics and reservoir engineering. Proven reservoir simulators are existing which have been certificated by benchmark testing and practical application. However even natural gas storage simulations are not directly applicable for CO₂ storage. The process performance is different because of different phase behavior, phase properties and CO₂- rock interactions. In this project the compositional simulator ECLIPSE 300 has been tested for CO₂ storage and EGR process performance description:

The ECLIPSE PVTi code can accurately calculate the main properties of the CO₂ and the mixing of the CO₂ with different gases. The benchmark of the PVTi calculated and the measured values for density, viscosity and compressibility of CO₂ and CO₂-natural gas mixtures is showing a good agreement. Adding different gases as impurities in the CO₂ will have an impact on the properties of injected gas though this impact will occur only in the eventuality of large amounts of impurities and that is not the case in the oxyfuel separation process.

Hydrodynamic dispersion may play a key role in the process performance of CO₂ storage and residual gas production. The extension of the mixing zone between the residual gas and the injected CO₂ determines the break-through of the storable gas and the EGR effect. The hydrodynamic dispersion consists of 2 parameters, the mechanical dispersion, responsible for the advective part of the mixing process and the effective diffusion coefficient, responsible for the molecular phenomenon. In the simulation programme ECLIPSE the diffusion effect is included and can be numerically converted into a adequate dispersion coefficient by using a multiplier. In order to avoid the influence of numerical dispersion, which has the same magnitude as the physical dispersion, one might be able to correct the total effect, based on experiments or by estimating the dispersion influence by switching-off the diffusion option. Realistic dimensions of the mixing zone length require a multiplier in the range of 1000 to cope with the dimensions expected. A realistic determination of this parameter is only possible in field experiments, taking the heterogeneity of the rock into consideration. Another unknown factor is the impact of gravity on the hydrodynamic dispersion, which has to be investigated in detail.

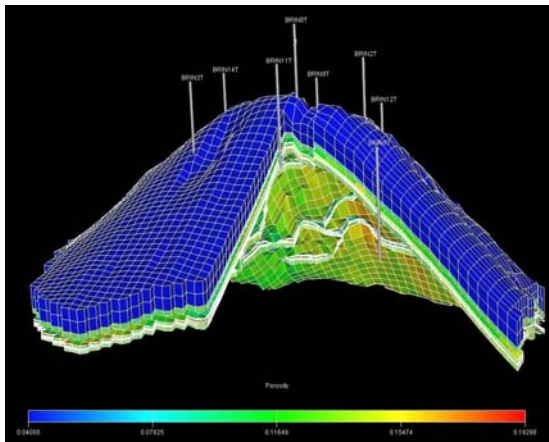


Figure 7.5.1: 3-D anticline structure
Barrien

WP 6- G.F. Ionescu

Modelling of reactive fluid transport is no option in the existing ECLIPSE code, however the magnitude of such effects on the injection side are strongly overlaid by the vaporization effect of the dry gas on the connate water and mineral precipitation as a consequence of super-saturation of the residual brine. This phenomenon can be modelled with ECLIPSE 300 in a correct physical mode. Chemical effects as for example dissolution of carbonate cements, leading to porosity/permeability increase or changes of the water binding capacity by hydration or dehydration effects of low pH connate water on rock minerals can be modelled by shifts of endpoint values of relative permeabilities. In the programme code a correlation of these endpoint values with the pH of the reservoir brine must be implemented. This simplification of a reactive transport model does not account for time effects (kinetics) and pore size related transport phenomena.

Consequently the field proven Compositional Simulator ECLIPSE 300 can be used for the prediction of CO₂ flow and mixing processes in gas reservoirs during the operational EGR phase with reasonable accuracy until we have a more precise instrument, which is capable of predicting long term chemical and rock mechanical effects.

Geochemical Risks of Failure

One concern in underground gas storage of aggressive gases as CO₂ is the failure of the storage sealing by leakage in the caprock, leakage through non sealing wells, geologic faults and other barriers. In the case of Zechstein and Rötsalt caprocks the problem of geologic sealing is relatively uncritical, since we can trust on the efficiency of these barriers over the geologic ages of conservation of natural gas deposits and from the extensive experimental evidence of salt seal tightness in underground natural gas storage (caverns) and nuclear waste remediation.

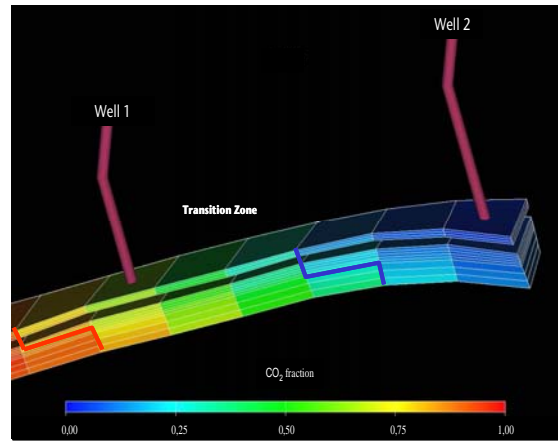


Figure 7.5.2: Simulated mixing zone extension

In the case of wet gas reservoirs, CO₂ dissolved in reservoir brines can react with the surrounding rocks. Rock samples from both reservoir formations investigated contain minerals that can be dissolved by carbonic acid: feldspar, chlorite and calcite. However, the most abundant mineral is quartz, which is practically inert against carbonic acid. The alteration of the silicate minerals is an incongruent reaction, involving the precipitation of secondary minerals. Depending on the water/rock ratios or the degree of alteration progress, the solid mineral volume might be reduced or increased. However, due to the limited amount of reactive minerals, dissolution will generally have little influence on the rock's porosity. The precipitation of dolomite, observed in some naturally altered samples could reduce permeability. The net effect of dissolution and precipitation reactions on permeability cannot be predicted without further geochemical experiments.

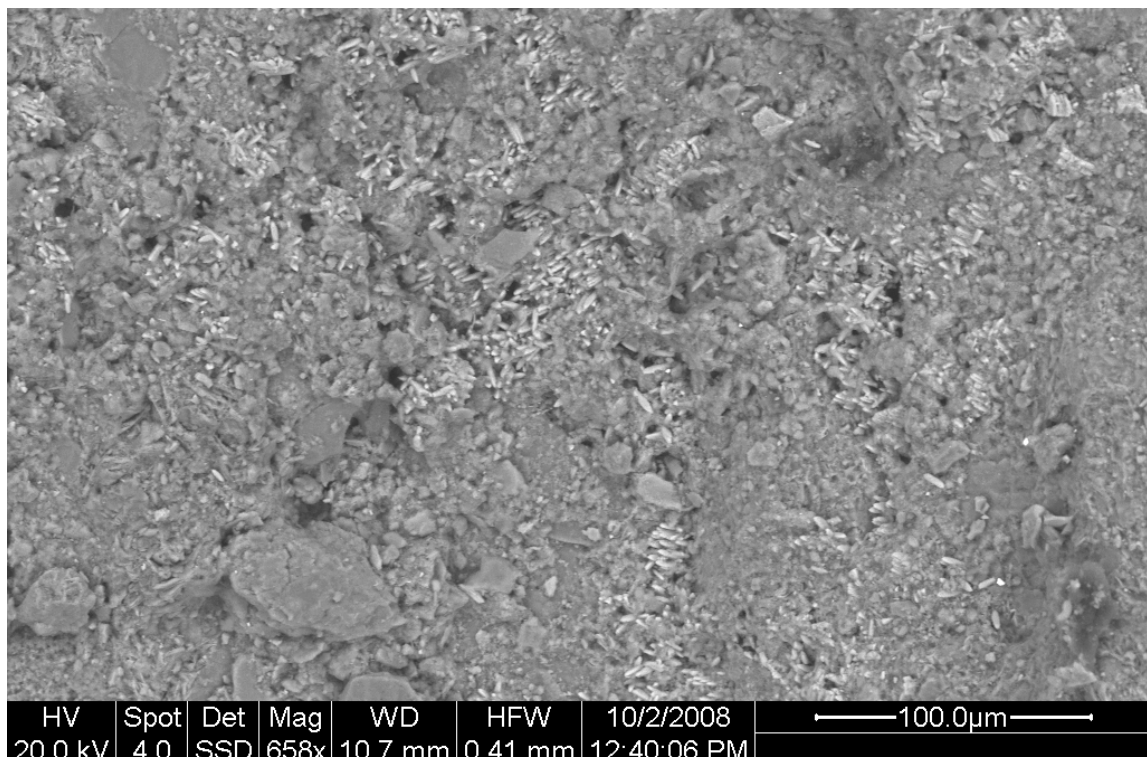


Figure 7.6: Corrosion of chlorite in Lower Devonian shale from a CO₂ exploration well in the East Eifel WP 5 F.May.

Reservoir compartments with elevated water saturation, e.g close to the gas-water contact may be affected by halite precipitation, due to the evaporation of brine in the dry CO₂ phase. Halite formation is expected to be a marginally relevant for CO₂ storage in dry gas reservoirs. It has to be studied in more detail in cases when CO₂ shall be injected below the gas-water contact of a reservoir. Injection of CO₂ containing oxygen as an impurity with higher concentration, e.g from oxy-fuel separation, will change the hydrochemical redox milieu, which could result in the precipitation of ore minerals from highly concentrated brines in the water bearing reservoir parts.

In summary, due to the dominance of quartz and the low water saturation in the natural gas reservoirs, we do not expect major geotechnical problems and chemical problems from chemical reactions within the reservoir. Further geochemical studies, ex-

periments and simulations with improved software and data bases are required for definitive answers though. As salt is the main non-reactive barrier for CO₂ in the Rotliegend and Bunter case study, we also do not expect safety relevant geochemical reactions that could trigger CO₂ leakage through intact cap-rocks. Slow alteration reactions, which convert free CO₂ into aqueous species and solid carbonates have a potential for binding CO₂ in the reservoir rocks and thus improving storage safety. These processes are subject of ongoing research.

Description of potential health, safety and environmental hazards of geological CO₂ storage (May)

In order to eliminate or reduce safety-, health- and environmental hazards of CO₂ injection and storage for yield increase, hazard analyses, accident precautions and corrective measures should be regarded in conjunction and site specifically. In the framework of this feasibility study, only a somewhat general assessment is possible. The hazards discussed here comply with those described in the "IPCC Special Report on Carbon Dioxide Capture and Storage" (IPCC 2005). More reliable hazard assessments require much more comprehensive data and detailed investigations.

When considering storage hazards, it is useful to distinguish between the actual operating site and the earth's surface above the storage area. The operating site is not publicly accessible. The persons who work there are, as a rule, trained in accident prevention and safety measures. The operating sites are subject to special monitoring. Emissions at the earth's surface above the stores, however, could affect unprepared persons at unexpected times at unknown places.

Operation sites

The technical handling of large gas volume flow rates contains, especially if the continuous injection is interrupted for maintenance or repair, the risk of technical or human failure which could cause CO₂ to leak at the operating site. A short-term leakage of gas at a well or a pipeline segment could release several tens of tons of CO₂. The worst case scenario would be a blowout as consequence of the destruction of a well-head.

Köckritz and Szary indicate for the case of a gas blowout leakage rates of 10,000 up to 500,000 m³/h. This volume would correspond to 20 – 1,000 tons of CO₂ per hour with the leakage rate of CO₂ being lower due to its comparably higher viscosity.

The use of modern blow-out preventers and underground safety valves allows minimizing the blowout hazard.

Leakiness and stealthy leakage of CO₂ can become a threat in unventilated well cellars. For the monitoring of probe sites, numerous measuring methods are available that were developed by the oil and gas industry for the monitoring of gas reservoirs or for ground water monitoring.

One part of the proposed monitoring programs of CO₂ stores is the direct measuring of CO₂ in the air, in the water or in the soil. The CO₂ concentration in the vicinity of injection wells should be recorded and monitored continually in order to guarantee well-timed repair and safety measurements for the protection of the personnel at the operating site and the surrounding area in the case of an unexpected leakage of CO₂.

Sensors for the monitoring of CO₂ concentrations have been used for several years in many areas like, for example, the monitoring of industrial production processes that might generate CO₂ (e. g. breweries). CO₂ sensors are also used for the measurement of greenhouse gases and combustion emissions. Small portable infrared gas detectors can be carried by persons. Depending on the operating conditions, there are different alarm programs, for example the activation of optical and acoustic alarm for excess of the maximum allowable concentration (MAC). In Germany, MACs of averaged 0.5 vol.-% per eight hours with maximum values of up to 1 %, up to a duration of 60 minutes are allowed up to three times a shift.

For a permanent monitoring of the CO₂ concentration gas analyzers are available that aspirate air samples from the ambient air automatically at regular time intervals and analyze them with the help of an integrated chromatograph. Measuring the CO₂ concentration with a mass spectrometer supplies additional results, especially on the origin of the gases. They can be used to clarify suspicion on subsoil CO₂ leakage, for example if increased CO₂ concentrations are found in the ground air.

Germany has decades of experience in the storage of natural gas, this is reflected in DIN 1918 which contains the standardized regulations on safe storage. These regulations can, in many cases, be used and adapted for CO₂ stores. The appendix of the EU guideline draft contains criteria for the setting-up of monitoring plans.

The operators of natural gas reservoirs in Germany are often also experienced in handling and extraction of acid gas, so that a safe state-of-the-art operation of CO₂ injection probes can be expected.

The methods usually applied for the measurement of injection rates in natural gas production and storage can also be used for the injection of CO₂. The measurement of the injection pressure at the wellhead as well as of the storage pressure at the bottom hole of injection and monitoring wells are standard measurements. A wide range of different sensors is suitable for the monitoring of the CO₂ injection pressure. In the last two decades, fibre optic pressure and temperature sensors have been developed, allowing a continuous, reliable and safe monitoring of the conditions in boreholes (BROWN & HARTOG 2002) and information on the dispersion of CO₂ in the reservoir. A comparison of these measurements with deposit simulations can supply first information on deviation of the planned infill of the reservoir and possible leakage.

Surface above the reservoir

CO₂ injected into geological reservoirs could reach the surface by different ways:

- through the covering strata if the capillary threshold pressure or the frac pressure of the covering strata is exceeded,
- by leaky backfilled abandoned wells,
- by permeable faults that were not detected during the reservoir's investigation or faults reactivated by CO₂ injection.

Covering strata:

For natural gas deposits it can be assumed, for the time being, that the quality of the covering strata is sufficient to offer good and adequate storing capacities for CO₂ as well, preventing the leakage of CO₂ quantities that could be hazardous for health and environment. In EGR activities, CO₂ is injected into deposits with a pressure significantly below the initial reservoir pressure. As long as it is not exceeded, there is hardly any risk of excessive capillary threshold or frac pressures.

Also locally, in the vicinity of the injection well, the pressure should be built up slowly in order to prevent a premature breakthrough of CO₂ into production wells (REBSCHER and OLDENBURG, 2004). Due to the fields' production history, the maximum pressures the covering strata can bear should be well known. Regulation of the injection rates and monitoring of the pressures will ensure a safe operation until the initial reservoir pressures are approximated.

Faults:

In compartmentalized deposits it is possible that extraction related pressure differences cause movements within faults of the covering strata and influence their quality. In the Altmark, however, the direct covering strata of the Rotliegend, consisting of Zechstein base layers, are covered by thick salt rocks that react plastically to the pressures that prevail in those depths, so that no extraction-related faults that would allow CO₂ to reach the surface must be expected. The same applies for the Roethian overlying the Barrien bunter deposit. The Roethian consists of low-permeable mudstone with embedded rock salt and has a thickness of some tens of meters.

The possibility that faults are generated and reactivated by seismotectonic movements is estimated as low in Northern Germany due to the low frequency and magnitude of earthquakes. It should, however, be quantified with regard to long term safety. During the extraction of natural gas from large deposits like in the vicinity of Groningen (Netherlands) or in the western Altmark, some smaller earthquakes occurred. According to van Eck (2006), small earthquakes (ML ≤ 3.6) are generally irrelevant in risk analysis. Occasionally, induced earthquakes up to ML = 3.5 have caused minor damage (such as cracks in buildings), more often the felt events are of general annoyance to the local population.

Boreholes:

Former production wells that were not designed for acid gas extraction or sealed pose a general problem for EGR projects. Therefore, a special work package has been dedicated to this problem. For leaky abandoned wells, only local effects close to the probe head are likely to occur. In the case of the damaged well of the Bad Lauchstädt cavern reservoir with high leakage rates (KATZUNG et al., 1996), the gas that leaked from the well could spread out widely in the surroundings of the well using temporary stores and faults situated further up. For pore-space stores, such high leakage rates through badly backfilled abandoned wells are not likely to occur, because the gas supply to the well will be slowed down by the reservoir rock. For abandoned wells that were not classified as risky and reconstructed there is a certain risk of leakage, therefore they should be monitored. In the Altmark, about 400 wells were constructed; many of them have been backfilled already. Here, careful assessment and risk analysis of the abandoned wells for every individual case is necessary.

Hazard Scenario

If CO₂ leaks from a reservoir formation, it moves upwards in the underground, together with formation waters, due to the lifting force. The increasing rise lessens the pressure in the surrounding medium, leading to expansion and dispersion of the gas.

Free or dissolved CO₂ can, penetrating the groundwater table, reach the overlying vadose zone, which is only periodically or episodically filled with water. The pore space not occupied by water is filled with soil gas. When CO₂ enters this region, it supersedes the ground air because it is heavier. This leads to an increased concentration of CO₂ in the vadose zone that can lead to a complete supersession of the ground air. Slightly increased CO₂ concentrations in the ground air of 0,3 – 0,5 Vol% still have an growth-accelerating influence on most plants, whereas concentrations higher than 5 Vol% have a harmful effect on the vegetation. Due to pressure related soil gas flows and diffusion, the gas finally reaches the surface and is discharged into the atmosphere. Generally, the velocity of the gas' ascent can be increased by coming out of solution and rapid expansion of the overcritical CO₂ into the gaseous state, which can, if leakage rates are especially high, lead to spontaneous eruptions of CO₂ (\pm groundwater, sediment and soil) at the earth's surface (RADGEN et al. 2006).

A leakage, caused for example by leaky abandoned wells, exposes human beings and animals at the surface to the discharged CO₂. Due to near-surface winds and turbulences the CO₂ concentration in the air decreases rapidly with increasing altitude as well as laterally. Animals and plants living close to the ground are more strongly affected by outpouring CO₂ than humans (OLDENBURG & UNGER 2004). Calms or topographic conditions (e. g. valleys or hollows) can slow down the mixing of the gas and the air. Since CO₂, with a density of 1.8 kg/m³ is heavier than air ($\rho = 1.2 \text{ kg/m}^3$), it can accumulate in the ground depressions.

During a leakage of about 50 tons of CO₂ from a fire fighting system in Mönchengladbach on 16th August 2008, several people lost consciousness due to the gas that hit them unexpectedly. The topography of the emersion point, inversion weather conditions and a chain of several malfunctions of the fire fighting system added to the extent of the effects.

In nature, however, these conditions are rather an exception. Natural CO₂ leakages like, for example, at the Laacher See or from a borehole near Niedermey (KRAUTHAUSEN, 2007) show that the gas intermixes rapidly and turbulently with the surrounding air and is diluted consequently so that no dangerous CO₂ concentrations develop in the surroundings (MAY, F. 2006; BENSON & COOK 2005). Nevertheless, a hazard analysis of potential storage locations must comprehend the risk of an accumulation of CO₂ on calm days, taking into account well locations, topography and population density.

In lower situated and poorly ventilated parts of buildings, like for example cellars, the leakage of CO₂ at the earth's surface poses a threat to humans. Already weak concentrations of CO₂ of 2 Vol% affect respiration, concentrations of 7 – 10 Vol% finally lead to unconsciousness, suffocation and death (BENSON & COOK 2005, IPCC 2005)

Examples for the effects of different CO₂ concentrations on other organisms are compiled in the following table (see also IPCC 2005).

| Ecosystem | no harmful effects | harmful effects | lethal effects |
|------------------------|--|--|---|
| groundwater | < 0,2 % CO ₂ , generally the normal groundwater concentration (Saripalli et al., 2003) | 0,2 – 2 % slightly enhances the acidity without significant effects | < 6 % CO ₂ , high acidity, borehole corrosion (Saripalli et al., 2003) |
| fresh water | The effects of a CO ₂ discharge into a freshwater reservoir depend on the solution rate, on the water's buffer properties and on the mixing | | |
| fish | < 1 % | 1 – 6 % CO ₂ : fish show signs of stress (Saripalli et al., 2003) | > 2 % CO ₂ : can have lethal effects (Saripalli et al., 2003) |
| terrestrial ecosystems | < 1 % | | |
| mammals | < 1 % | | |
| plants | slightly raised CO ₂ rates (500 – 800 ppm) enhance the growth of C3 plants. Minor effects on C4 and CAM plants. | > 5 % CO ₂ : harmful effects on growth and reduced crop yield. 5 – 30 % CO ₂ : serious damage (Saripalli et al., 2003) | > 20 % CO ₂ in the soil gas: macroscopic flora dies off (Benson et al., 2002). |

| | | | |
|--------------------|--|---|--|
| microbes and fungi | high CO ₂ concentrations over a short term are harmless | 5 – 60 % CO ₂ : decreasing growth, inline with increasing CO ₂ concentrations | 50 % CO ₂ generally has an inhibitory, if not lethal, effect on microbes and bacteria (Benson et al., 2002) |
| humans | < 1 % CO ₂ (Benson et al., 2002) MAC: 0.5 %/t > 1 % short term (15 min maximum) (Lindh, 2000) | 1 – 3 % CO ₂ : reduced respiration, headache and transpiration 3 – 5 % CO ₂ : significant effects on respiration, dropping blood pressure > 5 % CO ₂ : physical and mental abilities impaired, possibly loss of sense of direction (Benson et al., 2002; Hepple, 2004; Saripalli et al., 2003) | > 10 – 30 % CO ₂ : loss of sense of direction, apnoea, coma, death (Benson et al., 2002) |

Groundwater and soil water:

The dissolution of CO₂ generates carbonic acid whose dissociation leads to a decrease of the pH value. Depending on the mineral composition of the aquifer rocks the carbonate water can react with the rocks generating hydrogen carbonate and absorb the corresponding cations (e. g. Ca, Mg, Fe, Mn), possibly leading to a hardness increase of the groundwater. These alterations of the water's chemism depend on the composition of the aquifer rocks and also on the reaction times and on the water-rock-CO₂ rates. The slow alteration of silicates will, as a rule, have no significant effect because reaction products are dissipated in the groundwater stream. Carbonates are dissolved faster and can lead to hardness increase of the water. In some of the hydrogen carbonate waters generated by ascending natural CO₂ the limit values of the Drinking Water Ordinance are exceeded. The increased hardness does not prohibit the use of the water but it has negative effects of the groundwater's quality resp. on the effort necessary for its processing. Generally, the effect of natural CO₂ emissions ranges from slightly mineralized CO₂-containing acid waters to very hard, neutral hydrogen carbonate waters. Stronger effects are to be expected from possible contaminations of the CO₂ or from ascending saliniferous formation waters.

If saltwater is replaced by outpouring CO₂ and reaches the soil via faults it can have different effects: the formation of mycorrhizae (a fungus structure in the roots of a plant important for its nutrient uptake) decreases in alkalinized soils. A higher salt content of the soil can lead to washing-out of nutrients, deprivation of water in the rhizosphere and damaging of roots. At the same time, an increased salt content ob-

structs the plants' uptake of other important nutrient elements like for example nitrogen, phosphorus and also potassium.

Trees damaged by salt show some typical symptoms: they break into leaf later in spring, the leaves are smaller, often crinkly and show necroses (dying-off of parts of tissue) at the leaves' rims and points. Further consequences are early signs of age of the trees like discoloration of the leaves and premature fall of leaves, dying-off of parts or of the whole plant.

If reservoir waters from the Rotliegend in the Altmark should reach near-surface groundwater aquifers, also the high metal concentrations in these brines are environmentally problematic (see work package 5).

Natural CO₂ leakages are often connected with faults. The outlets have, as a rule, only a diameter of some meters up to some tens of meters (e. g. Jones et al. 2008) so that the described negative effects on the environment of theoretically possible CO₂ leakages can be rated as low, if no especially sensitive ecosystems are affected. In the Altmark and in the vicinity of Barrien, some smaller areas are accounted for as nature reserves (Fig. 7.7).

Potential leakage pathways for CO₂ and brine are to be identified within the scope of a risk analysis. In the vicinity of potential leakage pathways close to these reserves, a monitoring program should be established, provided that an adequate groundwater monitoring network does not already exist. With the help of multispectral remote sensing methods and mobile CO₂ monitoring instruments, it is possible to locate local CO₂ outlets at the earth's surface in a larger area over leakages in the surface rock (Jones et al. 2008).

If biotopes or farmland are affected by saltwater or CO₂ leakages, shallow boreholes can be used to collect these fluids. With the help of controlled drainage and disposal, as it is already done in natural gas production, it is possible to mitigate the local environmental effects.

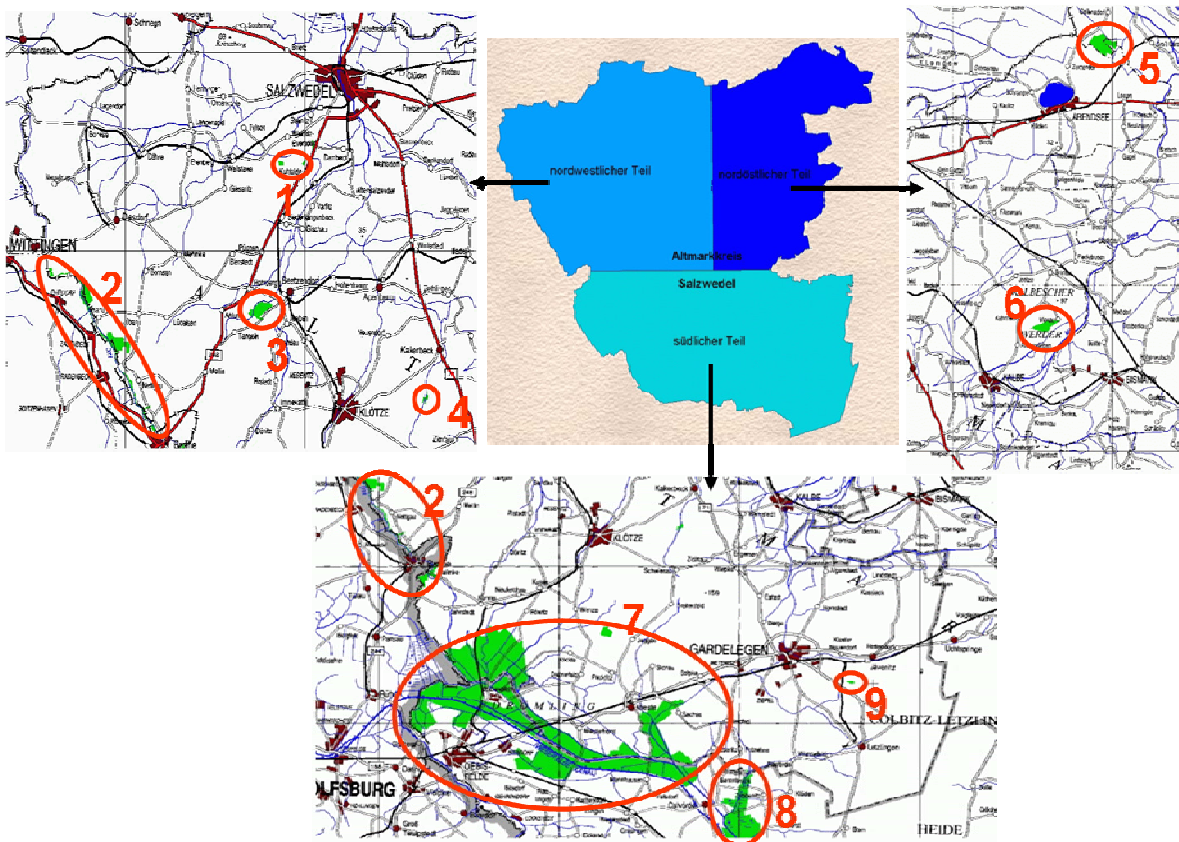


Fig. 7.7 Nature reserves in the Altmark (modified after: www.lvwa-natur.sachsen-anhalt.de): 1: Ferchauer Forst, 2: Ohreaue, 3: Beetzendorfer Bruchwald und Tangelscher Bach, 4: Jemmeritzer Moor, 5: Harper Moor, 6: Kalbescher Werder, 7: Ohre Drömling, 8: Klüdener Pax-Wanneweh, 9: Jävenitzer Moor.

Heavy metal mobilization:

In natural acid waters, depending on the surrounding rock, besides alkali and earth alkali elements also metals like for example nickel and arsenic occur, whose concentrations can, in particular cases, exceed drinking water thresholds. A prominent example of elevated Arsenic concentrations is the Kochbrunnen in Wiesbaden that has been used for spa treatments for a long time. On the basis of numerous groundwater analyses of the US Geological Survey, Birkholzer et al. (2008) could identify minerals that can be potential sources for heavy metals: amongst others ores like galena, arsenopyrite, sphalerite, barite. Their numerical simulations indicated that barium, cadmium, antimony and zinc are sensitive to changes in CO₂ partial pressure, but that only arsenic, and to a lesser extent lead and zinc, have the potential for exceeding their respective maximum contaminant levels (as defined by the U.S. Environmental Protection Agency).

Large-area soil damages are only to be expected if near-surface loose sediments allow a dispersion of groundwater oversaturated with CO₂ that release their CO₂ into the vadose zone or if brines from the cover strata leak at the surface and seep away in the surroundings.

An increasing acidification of the soil caused by CO₂ leaking from the reservoir provokes a mobilization of heavy metals in the soil. Increased mobilization of heavy metals and Al is accompanied by increasing dislocation and elution of these elements so that also groundwater and surface waters are subject to increasing contamination by heavy metals and Al (like for example in several bunter areas by atmospheric input of NO_x and SO_x). As a consequence of increased acidity of the forest soils, up to Al-toxicity and increased heavy metal availability, damage factors result like, for example, nutritional disturbances caused by trace element deficiencies (for example, deficiencies in boron or molybdenum) as well as the possibility of epidemics of pathogenic microorganisms.

Abandoned wells are most likely to offer pathways for leakage. They should, therefore be subject to thorough safety analyses. Possibly leakage areas, rates and environmental effects are supposedly unimportant. Heterogeneities, especially faults, in the near-surface cover strata determine the localization of the outlets. The existence of abandoned boreholes must not be regarded as a general knock-out criterion for the use of exhausted natural gas deposits for CSEGR measures because there are possibilities for monitoring and repair of leaky boreholes and methods for the localization of CO₂ and salt water leakages and for the mitigation of environmental effects.

References

- BENSON, S. & COOK, P. (2005): Underground geological storage. In: IPPC (Intergovernmental Panel on Climate Change) (Hrsg.) (2005): IPPC Special Report on Carbon dioxide Capture and Storage. Cambridge, United Kingdom and New York, S. 196 -276.
- BENSON, S.M., HEPPEL, R., APPS, J., TSANG, C.F. & LIPPmann, M. (2002): Lessons learned from natural and industrial analogues for storage of carbon dioxide in deep geological formations. Earth science division, E.O. Lawrence Berkley National laboratory, Berkeley, 135 S.
- BROWN, G.A. & HARTOG, A. (2002): Optical fiber sensors in upstream oil & gas. In: Journal of petroleum technology, Vol. 54, Nr. 11, S. 63-65.
- IPPC (Intergovernmental Panel on Climate Change) (Hrsg.) (2005): IPPC Special Report on Carbon dioxide Capture and Storage. Cambridge, United Kingdom and New York, 431 S.
- JONES, D.G., BARLOW, T., LISTER, T.R., SHAW, R.A., PEARCE, J.M., BEAUBIEN, S.E., LOMBARDI, S., MÖLLER, I., MAY, F., RANN, N., GAL, F., BRAIBANT, G. (2008): New and established techniques for surface gas monitoring at onshore CO₂ storage sites. Energy Procedia (in press).
- KATZUNG, G., KRULL, P., KÜHN, F. (1996): Die Havarie der UGS-Sonde Lauchstädt 5 im Jahre 1988 – Auswirkungen und geologische Bedingungen. — Zeitschrift für Angewandte Geologie 42: 19–26.
- KÖCKRITZ, V., SZARY, T. (2001): Untersuchungen zum Beanspruchungszustand von Steigrohrsträngen in eruptierenden Gasbohrungen. — DGMK Tagungsbericht 2001-2:317–329.

KRAUTHAUSEN, B. (2007): Neuerschließung eines Kaltwassergeysirs bei Andernach. GMIT 29: 17-18.

MAY, F. (2006): Sicherheit und Überwachung von CO₂-Speichern. Geotechnik 29 (2006) Nr. 4: 349-358. VGE-Verlag, Essen.

OLDENBURG, C.M. & UNGER, A.J.A. (2004): Coupled Vadose Zone and Atmospheric Surface-Layer Transport of Carbon Dioxide from Geological Carbon Sequestration Sites. In: Vadose Zone Journal 3, S. 848 – 857.

RADGEN, P., CREMER, C., WARKENTIN, S., GERLING, P., MAY, F. & KNOPF, S. (2006): Verfahren zur CO₂-Abscheidung und –Speicherung – Abschlussbericht. - UBA (Umweltbundesamt) (Hrsg.) (2006): Umweltforschungsplan des Bundesministeriums für Umwelt, Naturschutz und Reaktorsicherheit. Dessau, 163 S.

REBSCHER, D., OLDENBURG, C.M. (2004): Sequestration of Carbon Dioxide with Enhanced Gas Recovery. Case Study Altmark, North German Basin. Lawrence Berkeley National Laboratory Report 59033, 110 p.

SARIPALLI, K. P., MAHASENAN, N. M., and COOK, E. M.: (2003): Risk and hazard assessment for projects involving the geological sequestration of CO₂. In: GALE, J. & KAYA, Y. (Hrsg.): Sixth International Conference on Greenhouse Gas Control Technologies, Kyoto, Vol. I, Pergamon, Amsterdam, S. 511–516.

WRIGHT, G. & MAJEK, A. (1998): Chromatograph, RTU System Monitors CO₂ Injektion. In: Oil & Gas journal, Vol. 96, Nr.29, S. 75-77.

Field Project Simulation of CO₂ Storage and Enhanced Gas Recovery

The Buntsandstein and Rotliegend prototype gas reservoirs are suitable candidates for technical and economical CO₂ storage, if the process is tailored according to the geologic features of the reservoirs. Homogeneous anticline types of reservoirs will profit from the gravitational segregation of residual gas and heavier CO₂ in supercritical state. In this case overbalanced injection/production will yield a larger EGR. However the specific amount of incremental recovery per ton of injected CO₂ is decreasing due to the large areal distribution of the fill-up volume.

Stratified reservoirs are sensitive for early CO₂ break-through and give more positive results in underbalanced injection/production mode. Flow barriers as for example non sealing faults or permeability (facies) barriers may render the CO₂ break-through more positive and increase the EGR. The importance of restricted gas mixing has been identified, but realistic data have to be validated from field experiments. Field wide simulation of the interplay of reservoir compartments and their production enhancement and storability for CO₂ is essential for a realistic evaluation of the technical and economical feasibility. Key parameters from the simulation are reported in the following tables and figures.

Table 7.3: Incremental gas recovery, WP 6- G.F. Ionescu

| Injection Strategy | Incremental Recovery Factors, % IGIP | | Incremental Recovery/CO ₂ Injected, m ³ /t | |
|---------------------------------------|--------------------------------------|------------------|--|------------------|
| | Barrien 1+2+12 | Altmark Block 12 | Barrien 1+2+12 | Altmark Block 12 |
| Simultaneous Injection and Production | 6.78 | 2.63 | 226.10 | 491.00 |
| Delayed Production | 4.86 | 0.00 | 72.90 | 0.00 |

Table 7.4: Storage capacities, WP 6- G.F. Ionescu

| Pressure, bar | Storage Capacity, Mt | | |
|---------------|----------------------|------------------|---------------------|
| | Barrien | Altmark Block 12 | Altmark Block 12+14 |
| 250.00 | 12.29 | 31.37 | 79.10 |
| 300.00 | 14.38 | 36.93 | 94.51 |
| 350.00 | 16.37 | 41.58 | 106.08 |
| 400.00 | 17.78 | 45.46 | 115.40 |

The discrepancy of incremental recovery per ton of injected CO₂ between the Altmark and Barrien gas fields are explainable by the geologic differences in the layer structure of the stratified and the homogeneous carrier rock. In the homogeneous reservoir (Barrien), the CO₂ penetrates the rock in the outmost lower part of the perforated interval and breaks through without cross flow to the top of the layer. If the homogeneous reservoir is strongly dipping ($> 30^\circ$) the vertical extension is improved. High injection rates may render the vertical sweep more positive as it is represented in Figure 7.8.

However in a stratified reservoir many layers are penetrated simultaneously by the CO₂ and therefore provide a better structure for increasing vertical sweep efficiency.

Higher injection rates accelerate the pressure build-up, but they will force an early CO₂ break-through as it can be observed in Figure 7.5 Lower production rates are favourable because they may delay the CO₂ break-through.

EGR optimization measures in the field are the placement of wells and the magnitude of the injection/production rates.

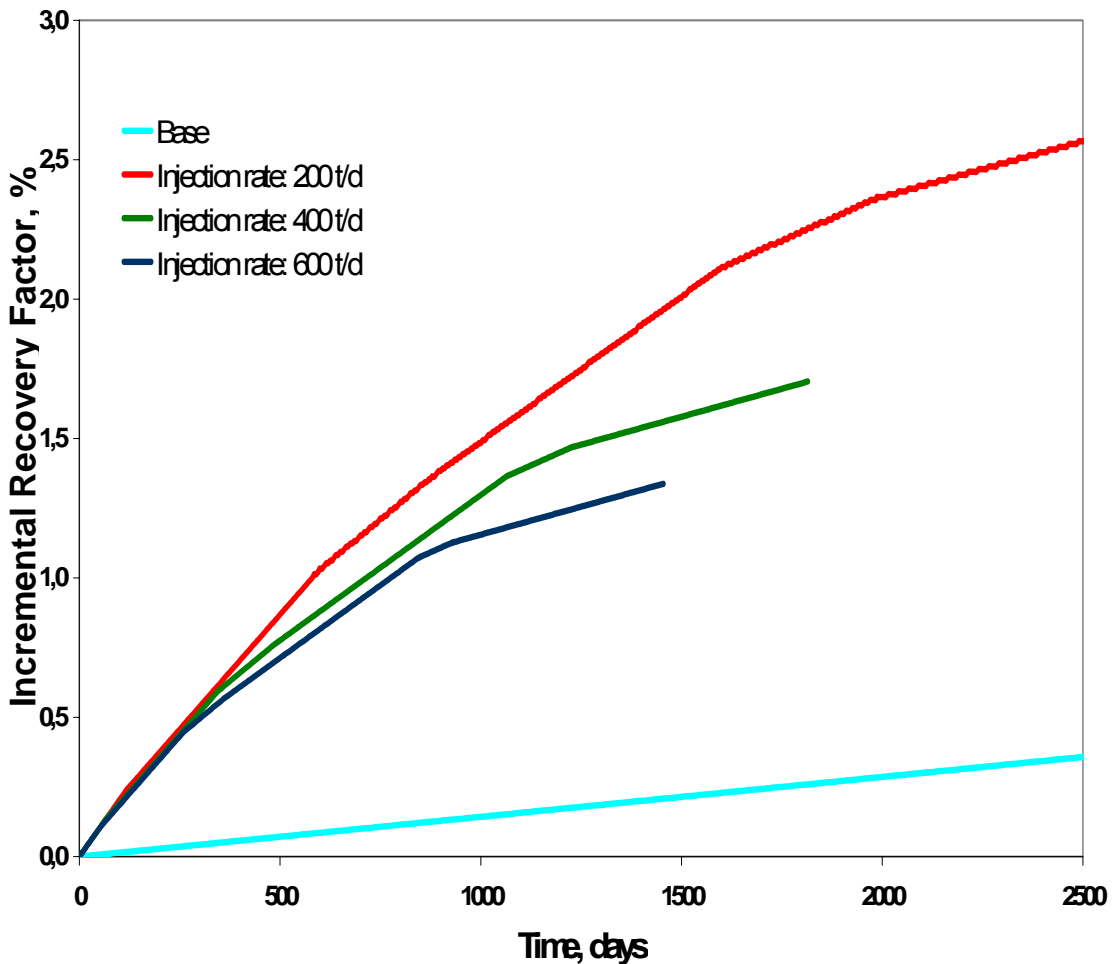


Figure 7.8: Dependence of the recovery factor on the injection rate, Altmark Block 12, G.F. Ionescu.

A final evaluation of the geotechnical and economic viability of CSEGR cannot be given for the two case study scenarios. The transport of CO₂ from Dornum to Barrien would exceed current values of emission certificates. CO₂ capture, transport and storage will not be economically viable for the small quantities to be transported, despite of the moderate distance to Barrien. The sequestration of carbon dioxide from coal fired power plants into depleted natural gas reservoirs is technically achievable if certain favourable geologic conditions exist, which can improve the segregation between the heavier CO₂ and the lighter residual gas. Dry gas reservoirs are more practical, because chemical interactions and material problems are less pronounced. The biggest advantage compared to other types of CO₂ geologic storages is the upgraded status of reservoir description from exploration and production, which provides an enormous economic value.

High injection rates improve the recovery in homogeneous reservoirs due to larger vertical sweep efficiencies, whereas in stratified reservoirs lower rates

and faults (CO_2 break-through barriers) may increase the recovery of residual gas.

Transport, compression and heating cost can render the economics of CCS to a negative balance if the credit note from emission trading (20-30 €/t) is too small. In this respect EGR with specific natural gas/ CO_2 ratios of 200 to 400 m^3/t is a must for CCS and economics depends strongly on the infra-structure of the gas field in operation, which is the cluster of active wells, network of transport lines, quality and condition of processing and metering stations, maintenance and inspection plans. Recompletion of wells and intelligent abandonment procedures for old wells can reduce the high investment for new wells and field equipment. Anyhow the final abandonment cost for all wells has to be budgeted in the finance programme.

Well integrity is a crucial decision point for the environmental and mining authorities in the approval phase of projects and requires high quality materials and technologies, which at the time being are not standard in the business. A comprehensive monitoring programme to safeguard the long term geologic capture is another cost factor in CSEGR, which was not calculated in our feasibility study. Therefore economical feasibility cannot be judged on the basis of the existing data base.

In the case of EGR driven implementation of CCS in a fully developed gas or oil field with an existing infrastructure the environmental impact of CSEGR is not exceeding the normal range of oil and gas field safety requirements and measures, which under the inspection of the mining authorities guarantee the safe operation of this process. CO_2 is not a poisonous material like H_2S or explosive like CH_4 and will not harm the field staff, provided that the atmosphere for breathing is not enriched over a critical concentration of CO_2 .

CSEGR is a chance for industry and challenge for research. The first step was done. It has not discouraged the expectations and needs therefore the continuation in pilot tests

Critical issues, not fully answered by this study are:

- **Wellbore flow characteristics**
- **Predictive numerical simulations of geochemical reactions, due to limitations of thermodynamic data and simulator capabilities**
- **Rock mechanic interactions on flow performance**
- **Mixing of gases in the reservoir (measured mixing parameters)**
- **Capillary threshold pressures of CO₂ for interlayers and overburden rocks**
- **Alternatives of CO₂ conditioning in the field (liquid transport and on site heating)**

Appendix of Analytical Data

Water Analyses

Altmark: Water analyses

The down-hole water sampling, and the hydrochemical analyses are described in a report by Henke et al. (2006).

| | | | | | | | | | |
|--|---------|---|-------------------------|-------------------------------|-----------|------------------------|-------------------------|-------------------------|------|
| BGR | | Bundesanstalt für Geowissenschaften und Rohstoffe | | | | | | | |
| | | Ref.: B 4.16 | | | | | | | |
| Hydrogeochemie | | | | | | | | | |
| Wasseranalyse Nr.: 0504600 | | | | | | | | | |
| Proben-ID | Wenze 1 | | | | | | | | |
| Leitfähigkeit | 230000 | µS/cm (25 °C) | | | Berechnet | 224680 | | | |
| pH-Wert | 7,00 | | | | | | | | |
| Gesamthärte | 073,99 | mmol/L | Karbonathärte | 2,01 | mmol/L | Σ gelöste Ionen (mg/L) | 09849 | | |
| Summenparameter (mg/L) | | | | | | | | | |
| NPOC | 19,8 | TIC | 5,5 | TNb | 0,9 | | | | |
| Kationen | | | | | | | | | |
| | mg/L | C _{eq} _mmol/L | %C _{eq} _mol/L | | | mg/L | C _{eq} _mmol/L | %C _{eq} _mol/L | |
| K ⁺ | 3820 | 97,7 | 1,8 | Cl ⁻ | 189000 | 5331,5 | 99,3 | | |
| Na ⁺ | 70400 | 3062,2 | 56,7 | SO ₄ ²⁻ | 1040 | 21,7 | 0,4 | | |
| Mg ⁺⁺ | 975 | 80,2 | 1,5 | HCO ₃ ⁻ | 246 | 4,0 | 0,1 | | |
| Ca ⁺⁺ | 41500 | 2070,9 | 38,4 | BO ₂ ⁻ | 198 | 4,6 | 0,1 | | |
| Fe ⁺⁺ | 20 | 0,7 | 0,0 | Br ⁻ | 650 | 8,1 | 0,2 | | |
| Li ⁺ | 306 | 44,1 | 0,8 | | | | | | |
| Mn ⁺⁺ | 300 | 10,9 | 0,2 | | | | | | |
| NH ₄ ⁺ | 3,2 | 0,2 | 0,0 | | | | | | |
| Pb ⁺⁺ | 5 | 0,0 | 0,0 | | | | | | |
| Sr ⁺⁺ | 1360 | 31,0 | 0,6 | | | | | | |
| Zn ⁺⁺ | 26 | 0,8 | 0,0 | | | | | | |
| | Summe | 5398,7 | | Fehler | 0,3% | Summe | 5369,9 | | |
| Nichtionogene Stoffe (mg/L) | | | | | | | | | |
| SiO ₂ | 8 | | | | | | | | |
| Anorganische Spuren (µg/L) | | | | | | | | | |
| Al | <50 | Co | <50 | Cu | 70 | Ni | <100 | As | <100 |
| Ba | 4400 | Be | <10 | Cd | 60 | Cr | 600 | Ti | 200 |
| Beurteilung | | | | | | | | | |
| Es handelt sich um eine sehr harte Na-Ca-Cl-Sole | | | | | | | | | |



Bundesanstalt für
Geowissenschaften
und Rohstoffe

Ref.: B 4.16
Hydrogeochemie

Wasseranalyse Nr.: 0504702

| | | | |
|---------------|------------|--|------------------|
| Proben-ID | Riebau 119 | | |
| Leitfähigkeit | 228000 | µS/cm (25 °C) | Berechnet 226298 |
| pH-Wert | 5,00 | | |
| Gesamthärte | 236,84 | mmol/L Karbonathärte 0,52 mmol/L Σ gelöste Ionen (mg/L) 19222 | |

Summenparameter (mg/L)

| | | | | | |
|------|------|-----|------|-----|-----|
| NPOC | 21,3 | TIC | 11,2 | TNb | 3,4 |
|------|------|-----|------|-----|-----|

| Kationen | | | Anionen | | | | |
|------------------------------|-------|-------------------------|-------------------------|-------------------------------|--------|-------------------------|-------------------------|
| | mg/L | C _{eq} _mmol/L | %C _{eq} _mol/L | | mg/L | C _{eq} _mmol/L | %C _{eq} _mol/L |
| K ⁺ | 6690 | 171,1 | 3,0 | Cl ⁻ | 192000 | 5416,1 | 99,1 |
| Na ⁺ | 65300 | 2840,4 | 50,4 | SO ₄ ²⁻ | 1020 | 21,2 | 0,4 |
| Mg ⁺⁺ | 1240 | 102,0 | 1,8 | HCO ₃ ⁻ | 64 | 1,0 | 0,0 |
| Ca ⁺⁺ | 47600 | 2375,2 | 42,1 | BO ₂ ⁻ | 770 | 18,0 | 0,3 |
| Fe ⁺⁺ | 175 | 6,3 | 0,1 | Br ⁻ | 660 | 8,3 | 0,2 |
| Li ⁺ | 375 | 54,0 | 1,0 | | | | |
| Mn ⁺⁺ | 760 | 27,7 | 0,5 | | | | |
| NH ₄ ⁺ | 31 | 1,7 | 0,0 | | | | |
| Pb ⁺⁺ | 157 | 1,5 | 0,0 | | | | |
| Sr ⁺⁺ | 2010 | 45,9 | 0,8 | | | | |
| Zn ⁺⁺ | 370 | 11,3 | 0,2 | | | | |
| | Summe | 5637,1 | | Fehler 1,6% | Summe | 5464,6 | |

Nichtionogene Stoffe (mg/L)

| | |
|------------------|----|
| SiO ₂ | 29 |
|------------------|----|

Anorganische Spuren (µg/L)

| | | | | | | | | | |
|----|------|----|----|----|------|----|-----|----|------|
| Al | 300 | Co | 50 | Cu | 50 | Ni | 00 | As | 1500 |
| Ba | 3000 | Be | 10 | Cd | 1000 | Cr | 600 | Ti | 200 |

Beurteilung

Es handelt sich um eine sehr harte Na-Ca-Cl-Sole

Wasseranalyse Nr.: 0504701

| | | | | | | | |
|---------------|---|--|--|-----------|--------|--|--|
| Proben-ID | Salzwedel 71 | | | | | | |
| Leitfähigkeit | 228000 µS/cm (25 °C) | | | Berechnet | 228764 | | |
| pH-Wert | 5,20 | | | | | | |
| Gesamthärte | 231,12 mmol/L Karbonathärte 0,53 mmol/L Σ gelöste Ionen (mg/L) 34540 | | | | | | |

Summenparameter (mg/L)

| | | | | | | | |
|------|------|-----|------|-----|-----|--|--|
| NPOC | 17,4 | TIC | 13,1 | TNb | 2,8 | | |
|------|------|-----|------|-----|-----|--|--|

| | Kationen | | | Anionen | | | |
|------------------------------|----------|-------------------------|-------------------------|-------------------------------|-------------------------|-------------------------|--------|
| | mg/L | C _{eq} _mmol/L | %C _{eq} _mol/L | mg/L | C _{eq} _mmol/L | %C _{eq} _mol/L | |
| K ⁺ | 5950 | 152,2 | 2,7 | Cl ⁻ | 206000 | 5811,0 | 99,2 |
| Na ⁺ | 67700 | 2944,8 | 51,6 | SO ₄ ²⁻ | 1010 | 21,0 | 0,4 |
| Mg ⁺⁺ | 1040 | 85,5 | 1,5 | HCO ₃ ⁻ | 65 | 1,1 | 0,0 |
| Ca ⁺⁺ | 47700 | 2380,2 | 41,7 | BO ₂ ⁻ | 760 | 17,8 | 0,3 |
| Fe ⁺⁺ | 230 | 8,2 | 0,1 | Br ⁻ | 680 | 8,5 | 0,1 |
| Li ⁺ | 375 | 54,0 | 0,9 | | | | |
| Mn ⁺⁺ | 788 | 28,7 | 0,5 | | | | |
| NH ₄ ⁺ | 19 | 1,0 | 0,0 | | | | |
| Pb ⁺⁺ | 143 | 1,4 | 0,0 | | | | |
| Sr ⁺⁺ | 1750 | 39,9 | 0,7 | | | | |
| Zn ⁺⁺ | 330 | 10,1 | 0,2 | | | | |
| | Summe | 5706,1 | | Fehler | -1,3% | Summe | 5859,4 |

Nichtionogene Stoffe (mg/L)

| | |
|------------------|----|
| SiO ₂ | 14 |
|------------------|----|

Anorganische Spuren (µg/L)

| | | | | | | | | | |
|----|------|----|----|----|-----|----|-----|----|------|
| Al | 300 | Co | 50 | Cu | 60 | Ni | 00 | As | 2700 |
| Ba | 4000 | Be | 10 | Cd | 900 | Cr | 500 | Ti | 200 |

Beurteilung

Es handelt sich um eine sehr harte Na-Ca-Cl-Sole

Barrien: Water analyses

| | Barrien 6T | |
|-------------------------------|---------------|---------|
| | mg/l | Gew.%/l |
| K ⁺ | 7435 | 2,1 |
| Na ⁺ | 104535 | 30,1 |
| Mg ²⁺ | 3103 | 0,9 |
| Ca ²⁺ | 18617 | 5,4 |
| Fe ²⁺ | 1664 | 0,5 |
| Li ⁺ | | 0,0 |
| Mn ²⁺ | | 0,0 |
| NH ⁴⁺ | 35 | 0,0 |
| Pb ²⁺ | 0,00001 | 0,0 |
| Sr ²⁺ | 0,00001 | 0,0 |
| Zn ²⁺ | 0,00001 | 0,0 |
| Cl ⁻ | 211324 | 60,9 |
| SO ₄ ²⁻ | 384 | 0,1 |
| HCO ₃ ⁻ | 0,00001 | 0,0 |
| BO ₂ ⁻ | 0,00001 | 0,0 |
| Br ⁻ | 0,00001 | 0,0 |
| SiO ₂ | 0,00001 | 0,0 |
| Summe Ionen | 347097 | |

| | Barrien 13T | |
|-------------------------------|----------------|---------|
| | mg/l | Gew.%/l |
| K ⁺ | 9643 | 2,7 |
| Na ⁺ | 72091 | 20,5 |
| Mg ²⁺ | 3160 | 0,9 |
| Ca ²⁺ | 49298 | 14,0 |
| Fe ²⁺ | 162 | 0,0 |
| Li ⁺ | | 0,0 |
| Mn ²⁺ | | 0,0 |
| NH ₄ ⁺ | 47 | 0,0 |
| Pb ²⁺ | | 0,0 |
| Sr ²⁺ | | 0,0 |
| Zn ²⁺ | | 0,0 |
| Cl ⁻ | 216263 | 61,6 |
| SO ₄ ²⁻ | 284 | 0,1 |
| HCO ₃ ⁻ | 55 | 0,0 |
| BO ₂ ⁻ | | 0,0 |
| Br ⁻ | 92 | 0,0 |
| Summe Ionen | 351095 | |

Bad Mergentheim: Water analyses

| Paulusquelle | (mg/L) | mmol(eq)/L |
|--|----------|------------|
| Kationen | | |
| Li+ | 27,5 | 3,96 |
| Na+ | 21320 | 927,37 |
| K+ | 443 | 11,33 |
| NH ₄ + | 5,4 | 0,3 |
| Mg++ | 790 | 64,99 |
| Ca++ | 1262 | 62,97 |
| Sr++ | 4,8 | 0,11 |
| Fe++/+++ | 20,3 | 0,73 |
| Mn++ | 0,6 | 0,02 |
| Kationensumme | 23873,6 | 1071,78 |
| | | |
| Anionen (mg/L) | | |
| F- | 0,06 | 0,003 |
| Cl- | 31270 | 882,01 |
| Br- | 67,9 | 0,85 |
| J- | 0,14 | 0,001 |
| NO ₂ - | <0,005 | 0 |
| NO ₃ - | <0,1 | 0 |
| SO ₄ -- | 6330 | 131,79 |
| HCO ₃ - | 3483 | 57,08 |
| HPO ₄ -- | 0,04 | 0,0008 |
| HS- | <0,005 | 0 |
| Anionensumme | 41151,14 | 1071,74 |
| | | |
| m-Kieselsäure (H ₂ SiO ₃) | 8,1 | |
| m-Borsäure (HBO ₂) | 19 | |
| Feststoffsumme | 65051,84 | |
| | | |
| O ₂ | 0,2 | |
| Freies CO ₂ | 2580 | |
| Lösungsinhalt | 67632,04 | |
| | | |
| Spurenelemente (µg/L) | (µg/L) | |
| Al | 160 | |
| As | 38 | |
| Be | 33 | |
| Cs | 50 | |
| Ni | 50 | |
| U | 14 | |
| V | 16 | |
| Zn | 6 | |

Basic mineralogical and geochemical data of fresh and altered rocks

Altmark

Stratigraphic correlation of rock samples:

| Altmark | | >20% | | 15-20% | | 10-15% | | 5-10% | | <5% | |
|---------|---------------------------------------|----------------|---------------------|------------------------|------------------------|--------|---|-------|----|-----|--|
| Probe | | HK | | HK | NK | NK | SP | NK | SP | | |
| S1 | Unterer Zechstein (Werra Anhydrit A1) | Abdecker | Anhydrite | | | | Dolomite | | | | |
| S2 | Unterer Zechstein (Zechsteinkalk Ca1) | Abdecker | Anhydrite, Dolomite | | | | Quartz, Feldspar | | | | |
| S4 | Unterer Zechstein (Zechsteinkalk Ca1) | Abdecker | Calcite | | | | Quartz, Feldspar, Dolomite, Musc.-Illite | | | | |
| S5b | Saxon, RH17 | Reservoir | Quartz | Feldspar | | | Calcite, Dolomite, Musc.-Illite, Chlorite, Pyrite | | | | |
| S6 | Saxon, RH18 | Reservoir | Quartz | Feldspar | | | Calcite, Dolomite, Musc.-Illite, Chlorite | | | | |
| S7 | Saxon, RH19 | Reservoir | Quartz | Feldspar, Musc.-Illite | | | Calcite, Dolomite, Chlorite, Hematite | | | | |
| S8 | Saxon, RH20 | Reservoir | Quartz | Feldspar | | | Calcite, Dolomite, Musc.-Illite, Chlorite, Hematite | | | | |
| S9b | Saxon RH14 | Reservoir | Quartz | Feldspar | | | Calcite, Dolomite, Musc.-Illite, Anhydrite | | | | |
| S10 | Saxon RH13 | Reservoir | Quartz | Feldspar, Musc.-Illite | | | Calcite, Anhydrite, Chlorite, Hematite | | | | |
| S13 | Saxon RH12 | Zwischenmittel | Quartz, Anhydrite | Calcite | Dolomite | | Chlorite, Hematite, Feldspar, Musc.-Illite | | | | |
| S14 | Saxon RH11 | Zwischenmittel | Quartz | Calcite | Feldspar | | Chlorite, Musc.-Illite | | | | |
| S15 | Saxon RH10 | Reservoir | Quartz | Feldspar | | | Calcite, Musc.-Illite, Chlorite | | | | |
| S17 | Saxon RH16 | Reservoir | Quartz | Anhydrite | Feldspar, Musc.-Illite | | Calcite, Chlorite, Hematite | | | | |

***** RF.- Analysen *****

Analyse von Haupt- und Spurenelementen im Silikatprogramm
 BGR - Hannover B4.15 RFA - Labor Tel.: 2761 (E31)
 () = Restkonzentration nach Glühen bei 1030°Celsius

Auftrag: 47269 / Einsender: Dr. Vosteen (3213)
 Probenart: Bohrkern / Salzwedel

| Probenidentifikation | | SiO2 | TiO2 | Al2O3 | Fe2O3 | MnO | MgO | CaO | Na2O | K2O | P2O5 | (SO3) | (Cl) | (F) | LOI | Sum | |
|----------------------|---------|------|-------|-------|-------|------|--------|-------|--------|-------|--------|-------|-------|--------|-------|-------|--------|
| | | % | % | % | % | % | % | % | % | % | % | % | % | % | % | % | |
| RF224601 | 0610885 | S 1 | <0.1 | 0.002 | <0.05 | 0.01 | <0.001 | 0.41 | 42.074 | <0.01 | <0.005 | 0.015 | 55.64 | <0.002 | 0.14 | 1.41 | 99.79 |
| RF224602 | 0610886 | S 2 | 2.67 | 0.037 | 0.53 | 0.38 | 0.092 | 11.02 | 36.360 | 0.11 | 0.045 | 0.016 | 23.99 | 0.004 | 0.21 | 24.09 | 99.55 |
| RF224603 | 0610887 | S 4 | 7.74 | 0.103 | 1.85 | 0.47 | 0.107 | 1.12 | 48.026 | 0.41 | 0.221 | 0.032 | 3.01 | 0.018 | 0.47 | 36.44 | 100.01 |
| RF224604 | 0610888 | S 5b | 66.49 | 0.589 | 9.97 | 3.03 | 0.123 | 1.95 | 4.830 | 2.72 | 2.082 | 0.123 | 0.80 | 0.009 | <0.05 | 6.96 | 99.69 |
| RF224605 | 0610889 | S 6 | 64.64 | 0.710 | 12.00 | 2.62 | 0.099 | 2.58 | 4.643 | 2.69 | 2.424 | 0.146 | 0.18 | 0.004 | 0.09 | 6.93 | 99.74 |
| RF224606 | 0610890 | S 7 | 60.70 | 0.760 | 13.51 | 5.75 | 0.090 | 2.76 | 3.968 | 2.16 | 3.062 | 0.156 | 0.07 | 0.003 | 0.05 | 6.64 | 99.69 |
| RF224607 | 0610891 | S 8 | 63.05 | 0.733 | 13.06 | 4.95 | 0.085 | 2.65 | 3.599 | 2.26 | 3.034 | 0.161 | 0.07 | 0.006 | <0.05 | 6.03 | 99.71 |
| RF224608 | 0610892 | S 9b | 86.20 | 0.136 | 4.98 | 0.78 | 0.052 | 0.42 | 1.643 | 1.34 | 1.720 | 0.047 | 0.70 | <0.002 | 0.08 | 1.74 | 99.83 |
| RF224609 | 0610893 | S 10 | 60.36 | 0.747 | 15.52 | 6.46 | 0.075 | 2.62 | 2.182 | 1.44 | 4.290 | 0.153 | 0.67 | <0.002 | <0.05 | 5.15 | 99.68 |
| RF224610 | 0610894 | S 13 | 34.89 | 0.437 | 8.65 | 4.08 | 0.464 | 5.30 | 18.671 | 0.75 | 1.905 | 0.104 | 9.92 | 0.003 | 0.06 | 14.45 | 99.69 |
| RF224611 | 0610895 | S 14 | 72.72 | 0.188 | 5.76 | 1.48 | 0.266 | 0.63 | 8.152 | 0.81 | 1.984 | 0.062 | 0.26 | 0.003 | 0.08 | 7.41 | 99.80 |
| RF224612 | 0610896 | S 15 | 83.76 | 0.130 | 5.08 | 1.19 | 0.152 | 0.54 | 2.695 | 1.00 | 1.862 | 0.058 | 0.33 | <0.002 | 0.09 | 2.91 | 99.78 |
| RF224613 | 0610897 | S 17 | 55.18 | 0.679 | 13.45 | 5.59 | 0.079 | 2.65 | 5.808 | 1.34 | 3.501 | 0.147 | 0.33 | <0.002 | 0.11 | 10.76 | 99.62 |

***** RF.- Analysen *****

Analyse von Haupt- und Spurenelementen im Silikatprogramm

BGR - Hannover B4.15 RFA - Labor Tel.: 2761 (E31)

() = Restkonzentration nach Glühen bei 1030°Celsius

Auftrag: 47269 / Einsender: Dr. Vosteen (3213)
Probenart: Bohrkern / Salzwedel

| Probenidentifikation | | (As) | Ba | Bi | Ce | Co | Cr | Cs | Cu | Ga | Hf | La | Mo | Nb | Nd | Ni | | |
|----------------------|---------|-------|-------|-------|-------|-------|-------|-------|-------|-------|-------|-------|-------|-------|-------|-------|-----|----|
| | | mg/kg | | |
| RF224601 | 0610885 | S 1 | | <2 | 4 | <20 | <3 | <5 | 13 | <3 | <5 | <20 | <2 | 2 | <50 | <3 | | |
| RF224602 | 0610886 | S 2 | | 4 | 197 | <3 | <20 | 4 | <3 | <5 | 55 | <3 | <5 | <20 | <2 | <50 | <3 | |
| RF224603 | 0610887 | S 4 | | 6 | 47 | 4 | 39 | <3 | 8 | <5 | 40 | <3 | <5 | <20 | <2 | <50 | 5 | |
| RF224604 | 0610888 | S 5b | | 80 | 380 | <3 | 46 | 42 | 74 | <5 | 237 | 14 | <5 | 29 | 9 | 13 | <50 | 29 |
| RF224605 | 0610889 | S 6 | | 16 | 372 | <3 | 55 | 6 | 88 | 8 | 29 | 16 | <5 | 41 | 9 | 19 | <50 | 27 |
| RF224606 | 0610890 | S 7 | | 10 | 445 | <3 | 68 | 11 | 90 | 11 | 28 | 19 | 8 | 40 | <2 | 19 | <50 | 41 |
| RF224607 | 0610891 | S 8 | | 10 | 454 | <3 | 72 | 14 | 86 | 11 | 29 | 19 | 15 | 27 | <2 | 15 | <50 | 39 |
| RF224608 | 0610892 | S 9b | | <2 | 470 | <3 | 22 | <3 | 15 | <5 | 26 | 5 | <5 | 20 | <2 | 3 | <50 | <3 |
| RF224609 | 0610893 | S 10 | | 42 | 426 | <3 | 104 | 17 | 98 | 25 | 25 | 22 | <5 | 49 | <2 | 16 | <50 | 57 |
| RF224610 | 0610894 | S 13 | | 17 | 387 | <3 | 77 | 11 | 56 | 13 | 66 | 11 | <5 | 27 | <2 | 8 | <50 | 29 |
| RF224611 | 0610895 | S 14 | | 8 | 288 | <3 | 27 | 6 | 22 | 6 | 34 | 8 | <5 | <20 | <2 | 6 | <50 | 10 |
| RF224612 | 0610896 | S 15 | | <2 | 899 | <3 | <20 | 9 | 10 | <5 | 26 | 5 | <5 | <20 | 3 | 8 | <50 | 11 |
| RF224613 | 0610897 | S 17 | | 29 | 436 | 13 | 65 | 8 | 91 | 25 | 127 | 22 | 8 | 58 | <2 | 20 | <50 | 24 |

***** RF.- Analysen *****
 Analyse von Haupt- und Spurenelementen im Silikatprogramm
 BGR - Hannover B4.15 RFA - Labor Tel.: 2761 (E31)
 () = Restkonzentration nach Glühen bei 1030°Celsius

Auftrag: 47269 / Einsender: Dr. Vosteen (3213)
 Probenart: Bohrkern / Salzwedel

| Probenidentifikation | | Pb | Rb | Sb | Sc | Sm | Sn | Sr | Ta | Th | U | V | W | Y | Zn | Zr | | |
|----------------------|---------|-------|-------|-------|-------|-------|-------|-------|-------|-------|-------|-------|-------|-------|-------|----|-----|-----|
| | | mg/kg | | | |
| RF224601 | 0610885 | S 1 | | <4 | 5 | <5 | 3 | <50 | <2 | 1338 | <5 | 12 | <3 | <5 | <3 | 9 | <3 | |
| RF224602 | 0610886 | S 2 | | 30 | 5 | <5 | <2 | <50 | <2 | 3450 | <5 | 11 | <3 | 16 | <5 | <3 | 204 | 8 |
| RF224603 | 0610887 | S 4 | | 40 | 7 | 5 | <2 | <50 | <2 | 518 | <5 | 9 | <3 | 10 | <5 | 6 | 147 | 30 |
| RF224604 | 0610888 | S 5b | | 19 | 60 | <5 | 8 | <50 | <2 | 95 | <5 | 13 | 4 | 72 | <5 | 17 | 25 | 241 |
| RF224605 | 0610889 | S 6 | | 7 | 84 | <5 | 12 | <50 | <2 | 110 | <5 | 12 | <3 | 78 | <5 | 24 | 39 | 298 |
| RF224606 | 0610890 | S 7 | | 14 | 117 | <5 | 13 | <50 | <2 | 133 | <5 | 18 | <3 | 89 | 6 | 30 | 50 | 228 |
| RF224607 | 0610891 | S 8 | | 12 | 121 | <5 | 12 | <50 | <2 | 137 | <5 | 18 | <3 | 82 | <5 | 30 | 47 | 267 |
| RF224608 | 0610892 | S 9b | | 8 | 54 | <5 | 3 | <50 | <2 | 83 | <5 | 7 | <3 | 15 | <5 | 3 | 10 | 118 |
| RF224609 | 0610893 | S 10 | | 18 | 200 | <5 | 14 | <50 | 4 | 137 | <5 | 19 | 4 | 102 | <5 | 23 | 65 | 249 |
| RF224610 | 0610894 | S 13 | | 6 | 99 | <5 | 11 | <50 | <2 | 547 | <5 | 12 | 6 | 74 | <5 | 24 | 63 | 114 |
| RF224611 | 0610895 | S 14 | | 7 | 93 | <5 | 6 | <50 | <2 | 70 | <5 | 8 | <3 | 26 | <5 | 13 | 21 | 93 |
| RF224612 | 0610896 | S 15 | | 11 | 76 | 7 | 3 | <50 | <2 | 97 | <5 | 5 | <3 | 18 | <5 | 6 | 22 | 98 |
| RF224613 | 0610897 | S 17 | | 51 | 147 | <5 | 15 | <50 | <2 | 243 | 19 | 39 | <3 | 81 | <5 | 28 | 106 | 212 |

Barrien

Stratigraphic correlation of rock samples

| Sample | Stratigraphy | Depth |
|---------|--------------|---------|
| B1 | kro | |
| B2 | Liasa | |
| | Keuper (Ob. | |
| B3 | Rhät) | |
| B4 | sm | |
| | Hardegsen- | |
| 49870 | Folge | 2389,6 |
| | Detfurth | |
| 54183 | Unterbank | 2894,15 |
| Barrien | 2T Detfurth | |
| 23095 | Oberbank | 2469,5 |

***** RF.- Analysen *****

Analyse von Haupt- und Spurenelementen im Silikatprogramm
 BGR – Hannover B4.15 RFA – Labor Tel.: 2761 (E31)
 () = Restkonzentration nach Glühen bei 1030 °Celsius

Auftrag: 47180 / Einsender: Dr. Vossteen (3153)

Probenart: Bohrkern / Barrien, Deutschland

| Probenidentifikation | SiO ₂ | TiO ₂ | Al ₂ O ₃ | Fe ₂ O ₃ | MnO | MgO | CaO | Na ₂ O | K ₂ O | P ₂ O ₅ | (SO ₃) | (Cl) | (F) | LOI | Sum |
|----------------------|------------------|------------------|--------------------------------|--------------------------------|------|-------|------|-------------------|------------------|-------------------------------|--------------------|------|-------|-------|-------|
| | % | % | % | % | % | % | % | % | % | % | % | % | % | % | % |
| RF223203 0604658 | 49870 | 71.58 | 0.376 | 10.02 | 2.08 | 0.045 | 0.95 | 4.151 | 2.24 | 2.531 | 0.133 | 0.12 | 0.017 | <0.05 | 5.00 |
| RF223204 0604659 | 54183 | 83.62 | 0.052 | 7.62 | 0.31 | 0.004 | 0.21 | 0.542 | 1.99 | 2.897 | 0.091 | 0.35 | 0.016 | <0.05 | 1.22 |
| RF223205 0604660 | Ba ST 2395 | 53.03 | 0.566 | 13.60 | 5.45 | 0.095 | 4.50 | 5.549 | 1.10 | 3.646 | 0.152 | 0.05 | 0.002 | <0.05 | 11.84 |
| Probenidentifikation | (As) | Ba | Bi | Ce | Co | Cr | Cs | Cu | Ga | Hf | Ia | Mo | Nb | Nd | Ni |
| RF223203 0604658 | 49870 | 8 | 4996 | <3 | 59 | 10 | 36 | 7 | 24 | 10 | 6 | <20 | <2 | 8 | <50 |
| RF223204 0604659 | 54183 | 5 | 7470 | <3 | 2.3 | <3 | 1.2 | <5 | 24 | 4 | <5 | <20 | <2 | 3 | <50 |
| RF223205 0604660 | Ba ST 2395 | 18 | 1888 | <3 | 64 | 16 | 75 | 9 | 20 | 18 | 8 | <20 | <2 | 13 | <50 |
| Probenidentifikation | Pb | Rb | Sb | Sc | Sm | Sn | Sr | Ta | Th | U | V | W | Y | Zn | Zr |
| RF223203 0604658 | 49870 | 33 | 80 | <5 | 6 | <50 | <2 | 194 | <5 | 12 | 4 | 47 | 37 | 18 | 95 |
| RF223204 0604659 | 54183 | 35 | 86 | <2 | <50 | <2 | 952 | <5 | 3 | 3 | 8 | 6 | 43 | 261 | |
| RF223205 0604660 | Ba ST 2395 | 19 | 123 | <5 | 14 | <50 | <2 | 289 | <5 | 17 | 5 | 109 | 19 | 23 | 309 |

08/11/2006 11:53

EXCEL-Datei: http://ginoapp/app/Linesuche_B4/linesuche_start.html

***** RF.- Analysen *****
 Analyse von Haupt- und Spurenelementen im Silikatprogramm
 BGR - Hannover B4, 15 RFA - Labor Tel.: 2761 (E31)
 () = Restkonzentration nach Glühen bei 1030 °Celsius

Ruftrag: 47270 / Einsender: Dr. Vosteen (3214)
 Probenart: Bohrkern / Barrien

| Probenidentifikation | Probenart: Bohrkern / Barrien | | | | | | | | | | | | | | | |
|-----------------------------|-------------------------------|-----------------------|-------------------------------------|-------------------------------------|----------|----------|----------|------------------------|-----------------------|------------------------------------|-------------------------|-----------|----------|----------|----------|-------|
| | SiO ₂ % | TiO ₂ % | Al ₂ O ₃ % | Fe ₂ O ₃ % | MnO % | MgO % | CaO % | Na ₂ O % | K ₂ O % | P ₂ O ₅ % | (SO ₃) % | (Cl) % | (F) % | LiO % | Sum % | |
| RF224614 0610898 | B 1 | 3.15 | 0.030 | 0.53 | 0.31 | 0.030 | 0.41 | 52.695 | <0.01 | <0.005 | 0.044 | 0.14 | 0.006 | 0.14 | 42.33 | 99.83 |
| RF224615 0610899 | B 2 | 23.54 | 0.388 | 8.50 | 6.61 | 0.202 | 1.32 | 28.955 | 0.48 | 0.923 | 0.121 | 4.24 | <0.002 | <0.05 | 24.45 | 99.75 |
| RF224616 0610900 | B 3 | 70.06 | 1.235 | 10.60 | 4.15 | 0.026 | 1.25 | 0.300 | 1.42 | 2.127 | 0.066 | 0.45 | <0.002 | <0.05 | 8.00 | 99.71 |
| RF224617 0610901 | B 4 | 80.25 | 0.028 | 5.38 | 0.21 | 0.011 | 0.08 | 1.212 | 3.37 | 2.417 | 0.062 | 0.44 | <0.05 | 5.32 | 99.66 | |
| probenidentifikation | | | | | | | | | | | | | | | | |
| RF224614 0610898 | B 1 | <2 | 30 | 4 | <20 | <3 | <3 | <5 | 46 | <3 | <5 | <20 | <2 | 3 | <50 | <3 |
| RF224615 0610899 | B 2 | 2.1 | 149 | <3 | 6.8 | 16 | 66 | <5 | 7.6 | 12 | 8 | 4.7 | 29 | 3 | <50 | 5.0 |
| RF224616 0610900 | B 3 | 17 | 305 | <3 | 11.8 | 14 | 75 | 6 | 30 | 13 | 10 | 6.7 | <2 | 22 | <50 | 3.8 |
| RF224617 0610901 | B 4 | <2 | 3611 | <3 | <20 | <3 | 82 | <5 | 35 | 4 | <5 | <20 | 15 | <2 | <50 | 4.9 |
| probenidentifikation | | | | | | | | | | | | | | | | |
| RF224614 0610898 | B 1 | <4 | 5 | <5 | <2 | <50 | <2 | 8.28 | <5 | 6 | <3 | 9 | <5 | 3 | 11 | 1.0 |
| RF224615 0610899 | B 2 | 35 | 46 | <5 | 11 | <50 | 3 | 288 | <5 | 11 | 3 | 11.8 | <5 | 28 | 12.1 | 7.6 |
| RF224616 0610900 | B 3 | 37 | 70 | <5 | 10 | <50 | 2 | 97 | <5 | 18 | <3 | 7.6 | <5 | 43 | 4.0 | 36.3 |
| RF224617 0610901 | B 4 | 13 | 63 | <5 | <2 | <50 | 2 | 177 | <5 | 6 | <3 | <5 | <5 | <3 | 18 | 4.6 |

Bad Mergentheim

Stratigraphic correlation of rock samples

| | | | |
|-----|-------|----------------------|-------------------------------|
| P1 | z | Handstück (Bohrkern) | Oberer Zechstein |
| P3 | z | Handstück (Bohrkern) | Oberer Zechstein |
| P4 | z | Handstück (Bohrkern) | Oberer Zechstein |
| P5 | z | Handstück (Bohrkern) | Oberer Zechstein |
| P6 | z | Handstück (Bohrkern) | Zechstein |
| P7 | z | Handstück (Bohrkern) | Zechstein |
| P8 | z | Handstück (Bohrkern) | Zechstein |
| P9 | r | Handstück (Bohrkern) | Rotliegendes |
| P10 | r | Handstück (Bohrkern) | Rotliegendes |
| P11 | r | Handstück (Bohrkern) | Rotliegendes |
| P12 | r | Handstück (Bohrkern) | Rotliegendes |
| P13 | r | Handstück (Bohrkern) | Rotliegendes |
| P14 | r | Handstück (Bohrkern) | Rotliegendes |
| P15 | r | Handstück (Bohrkern) | Rotliegendes |
| P16 | r | Handstück (Bohrkern) | Rotliegendes |
| P17 | r | Handstück (Bohrkern) | Rotliegendes |
| P18 | r | Handstück (Bohrkern) | Rotliegendes |
| P19 | r | Handstück (Bohrkern) | Rotliegendes |
| P20 | r | Handstück (Bohrkern) | Rotliegendes |
| P21 | so2 | Bohrklein | obere Röttone |
| P22 | so2 | Bohrklein | obere Röttone |
| P23 | so2 | Bohrklein | obere Röttone |
| P24 | so2 | Bohrklein | untere Röttone |
| P25 | so2 | Bohrklein | untere Röttone |
| P26 | so2 | Bohrklein | untere Röttone |
| P27 | so2 | Bohrklein | untere Röttone |
| P28 | so2 | Bohrklein | untere Röttone |
| P29 | so1 | Bohrklein | Plattensandstein |
| P30 | so1 | Bohrklein | Plattensandstein |
| P31 | so1 | Bohrklein | Plattensandstein |
| P32 | so1 | Bohrklein | Plattensandstein |
| P33 | so1 | Bohrklein | Plattensandstein |
| P34 | so1 | Bohrklein | Plattensandstein |
| P35 | so1 | Bohrklein | Plattensandstein |
| P36 | so1 | Bohrklein | Plattensandstein |
| P37 | so1 | Bohrklein | Plattensandstein |
| P38 | so-sm | Bohrklein | Obere Hardegsen-Folge |
| P39 | so-sm | Bohrklein | Obere Hardegsen-Folge |
| P40 | smc2 | Bohrklein | Untere Hardegsen-Folge |
| P41 | smc2 | Bohrklein | Untere Hardegsen-Folge |
| P42 | smc2 | Bohrklein | Untere Hardegsen-Folge |
| P43 | sm | Bohrklein | Dethfurt-/Volpriehausen-Folge |
| P44 | sm | Bohrklein | Dethfurt-/Volpriehausen-Folge |
| P45 | sm | Bohrklein | Dethfurt-/Volpriehausen-Folge |
| P46 | sm | Bohrklein | Dethfurt-/Volpriehausen-Folge |
| P47 | sm | Bohrklein | Dethfurt-/Volpriehausen-Folge |
| P48 | sm | Bohrklein | Dethfurt-/Volpriehausen-Folge |
| P49 | sm | Bohrklein | Salmünster-/Gelnhausen-Folge |
| P50 | sm | Bohrklein | Salmünster-/Gelnhausen-Folge |
| P51 | zT | Bohrklein | Oberer Zechstein |
| P52 | zT | Bohrklein | Oberer Zechstein |

Bad Mergentheim: XRF

20/03/200

6 14:40

***** RF.- Analysen *****

Analyse von Haupt-und Spurenelementen im
Silikatprogramm

BGR -Hannover B4.15 RFA - Labor Tel.:
2761(E31)

() =Restkonzentration nach Glühen bei 1000 °Celsius

Einsender: Dr.H.-D.Vosteen (3124)

Probenart:Bohrkerne / Bad Mergentheim

| Probenidentifikation | | SiO ₂ _SI | TiO ₂ _SI | Al ₂ O ₃ _SI | Fe ₂ O ₃ _SI | MnO_SI |
|----------------------------|------------|--------------------------|----------------------|------------------------------------|------------------------------------|--------|
| | | % | % | % | % | % |
| RF222622 47106\0601156TP01 | P1a grau | 29,71 | 0,316 | 8,53 | 2,03 | 0,237 |
| RF222623 47106\0601156TP02 | P1b rot | 33,86 | 0,345 | 9,41 | 2,91 | 0,224 |
| RF222624 47106\0601158TP01 | P3 | 1,13 | 0,016 | 0,41 | 0,13 | 0,553 |
| RF222625 47106\0601159TP01 | P4a grün | 48,09 | 0,361 | 10,81 | 1,61 | 0,155 |
| RF222626 47106\0601159TP02 | P4b rot | 62,1 | 0,3 | 11,91 | 1,69 | 0,077 |
| RF222627 47106\0601160TP01 | P5 | 48,86 | 0,626 | 8,23 | 2,64 | 0,189 |
| RF222628 47106\0601161TP01 | P6 | 22,09 | 0,133 | 4,65 | 1,32 | 0,222 |
| RF222629 47106\0601162TP01 | P7/1 | 75,75 | 0,11 | 10,61 | 1,05 | 0,025 |
| RF222630 47106\0601163TP01 | P8 | 80,64 | 0,128 | 9,67 | 0,63 | 0,005 |
| RF222631 47106\0601164TP01 | P9 | 80,08 | 0,046 | 8,6 | 0,43 | 0,023 |
| RF222632 47106\0601165TP01 | P10 | 77,97 | 0,172 | 11,22 | 0,89 | 0,005 |
| RF222633 47106\0601166TP01 | P11 | 77,58 | 0,172 | 10,89 | 1,01 | 0,013 |
| RF222634 47106\0601167TP01 | P12 | 77,14 | 0,168 | 10,89 | 0,9 | 0,016 |
| RF222635 47106\0601169TP01 | P14 | 77,83 | 0,082 | 10,77 | 0,61 | 0,013 |
| RF222636 47106\0601170TP01 | P15a grün | 76,87 | 0,206 | 11,78 | 1,05 | 0,007 |
| RF222637 47106\0601170TP02 | P15b rot | 75,51 | 0,197 | 12,26 | 1,6 | 0,008 |
| RF222638 47106\0601171TP01 | P16/1a rot | 83,35 | 0,055 | 7,63 | 0,41 | 0,014 |
| RF222639 47106\0601171TP02 | P16/1bweiß | 82,13 | 0,058 | 7,91 | 0,41 | 0,018 |
| RF222640 47106\0601172TP01 | P17 | 82,97 | 0,084 | 7,43 | 0,49 | 0,019 |
| RF222641 47106\0601173TP01 | P18a rot | 73,2 | 0,121 | 9,94 | 1,02 | 0,046 |
| RF222642 47106\0601173TP02 | P18b grau | 73,81 | 0,133 | 10,12 | 0,65 | 0,043 |
| RF222643 47106\0601173TP03 | P18c grau | 78,4 | 0,146 | 10,57 | 0,59 | 0,013 |
| RF222644 47106\0601174TP01 | P19 | 82,87 | 0,047 | 7,56 | 0,57 | 0,018 |
| RF222645 47106\0601175TP01 | P20 | 81 | 0,081 | 9,66 | 0,73 | 0,005 |
| RF222646 47106\0601241TP01 | P7 | 74,26 | 0,171 | 12,58 | 0,84 | 0,014 |
| RF222647 47106\0601242TP01 | P16/2 | 80,61 | 0,086 | 9,16 | 0,69 | 0,012 |
| RF222648 47106\0601243TP01 | B1 | 93,61 | 0,065 | 3,05 | 0,68 | 0,016 |
| RF222649 47106\0601244TP01 | VH1 | 85,36 | 0,381 | 6,88 | 1,94 | 0,008 |
| RF222650 47106\0601812TP01 | P2A grau | 35,41 | 0,389 | 11,2 | 2,16 | 0,252 |
| RF222651 47106\0601812TP02 | P2A rot | 52,82 | 0,547 | 16,22 | 4,21 | 0,076 |
| RF222652 47106\0601814TP01 | P13A weiß | 78,31 | 0,129 | 10,94 | 0,54 | 0,007 |
| RF222653 47106\0601814TP02 | P13A rot | 78,27 | 0,145 | 10,95 | 0,76 | 0,007 |
| | | | | | | |
| | | CO ₂ vermutet | | | | |

| | MgO_SI | CaO_SI | Na ₂ O_SI | K ₂ O_SI | P2O ₅ _SI | (SO ₃)_SI | (Cl)_SI | (F)_SI | LOI_SI | Sum_RF | (As)_SI |
|----------|--------|--------|----------------------|---------------------|----------------------|-----------------------|---------|--------|--------|--------|---------|
| | % | % | % | % | % | % | % | % | % | % | mg/kg |
| P1a grau | 12,29 | 16,08 | 0,25 | 3,262 | 0,675 | 0,19 | 0,01 | 0,16 | 25,86 | 99,59 | 9 |
| P1b rot | 11,22 | 13,944 | 0,29 | 3,603 | 0,364 | 0,17 | 0,017 | 0,06 | 23,14 | 99,56 | 8 |
| P3 | 21,05 | 29,591 | <0,01 | 0,053 | 0,05 | 0,18 | 0,022 | <0,05 | 46,52 | 99,75 | 11 |
| P4a grün | 8,43 | 8,977 | 0,52 | 3,762 | 0,136 | 0,06 | 0,034 | 0,09 | 16,61 | 99,65 | 8 |
| P4b rot | 5,11 | 3,929 | 0,49 | 4,518 | 0,129 | 0,22 | 0,035 | 0,06 | 8,83 | 99,41 | 5 |
| P5 | 8,38 | 10,068 | 0,67 | 2,322 | 0,162 | 0,04 | 0,025 | 0,07 | 17,25 | 99,54 | <2 |
| P6 | 14,86 | 21,007 | 0,66 | 1,35 | 0,072 | 0,25 | 0,018 | <0,05 | 33,13 | 99,74 | 11 |
| P7/1 | 1,82 | 1,239 | 1,7 | 3,884 | 0,089 | 0,01 | 0,039 | <0,05 | 3,34 | 99,69 | <2 |
| P8 | 0,97 | 0,226 | 1,62 | 3,919 | 0,088 | 0,08 | 0,019 | <0,05 | 1,51 | 99,52 | <2 |
| P9 | 1,22 | 0,963 | 1,31 | 3,833 | 0,077 | 0,23 | 0,042 | <0,05 | 2,43 | 99,32 | <2 |
| P10 | 1,39 | 0,244 | 1,77 | 3,814 | 0,104 | <0,01 | 0,043 | <0,05 | 2,04 | 99,68 | <2 |

| | | | | | | | | | | | |
|------------|-------|--------|------|-------|-------|-------|-------|-------|-------|-------|----|
| P11 | 1,31 | 0,566 | 1,83 | 3,896 | 0,099 | <0.01 | 0,039 | 0,05 | 2,25 | 99,71 | <2 |
| P12 | 1,43 | 0,701 | 1,85 | 3,942 | 0,099 | <0.01 | 0,038 | <0.05 | 2,48 | 99,68 | <2 |
| P14 | 1,56 | 0,652 | 1,54 | 3,981 | 0,077 | <0.01 | 0,04 | <0.05 | 2,57 | 99,69 | <2 |
| P15a grün | 1,36 | 0,236 | 1,66 | 4,289 | 0,102 | <0.01 | 0,041 | <0.05 | 2,09 | 99,74 | <2 |
| P15b rot | 1,45 | 0,236 | 1,77 | 4,293 | 0,103 | <0.01 | 0,023 | 0,05 | 2,21 | 99,72 | <2 |
| P16/1a rot | 0,93 | 0,676 | 1,08 | 3,566 | 0,056 | <0.01 | 0,026 | 0,06 | 1,86 | 99,73 | <2 |
| P16/1bweiß | 1,16 | 0,882 | 1,11 | 3,618 | 0,059 | <0.01 | 0,034 | 0,08 | 2,26 | 99,74 | <2 |
| P17 | 1,16 | 0,854 | 1,03 | 3,293 | 0,062 | <0.01 | 0,031 | 0,08 | 2,2 | 99,71 | <2 |
| P18a rot | 2,46 | 2,353 | 1,57 | 3,79 | 0,108 | <0.01 | 0,033 | 0,07 | 4,98 | 99,7 | <2 |
| P18b grau | 2,44 | 2,195 | 1,56 | 3,706 | 0,112 | <0.01 | 0,036 | <0.05 | 4,85 | 99,69 | <2 |
| P18c grau | 1,37 | 0,566 | 1,53 | 3,928 | 0,126 | <0.01 | 0,035 | <0.05 | 2,39 | 99,71 | <2 |
| P19 | 1,15 | 0,802 | 0,9 | 3,451 | 0,053 | 0,03 | 0,037 | <0.05 | 2,17 | 99,64 | <2 |
| P20 | 0,96 | 0,211 | 1,29 | 3,963 | 0,069 | <0.01 | 0,022 | <0.05 | 1,71 | 99,75 | <2 |
| P7 | 1,87 | 0,658 | 1,95 | 4,077 | 0,126 | <0.01 | 0,028 | 0,06 | 3,05 | 99,69 | <2 |
| P16/2 | 1,41 | 0,568 | 1,18 | 3,601 | 0,068 | <0.01 | 0,049 | <0.05 | 2,3 | 99,74 | <2 |
| B1 | 0,1 | 0,047 | 0,05 | 1,062 | 0,062 | 0,03 | 0,027 | 0,08 | 0,8 | 99,68 | 22 |
| VH1 | 0,28 | 0,133 | 0,29 | 3,108 | 0,1 | <0.01 | 0,018 | <0.05 | 1,21 | 99,68 | 4 |
| P2A grau | 10,71 | 12,393 | 0,27 | 3,82 | 0,109 | 0,06 | 0,032 | 0,1 | 22,73 | 99,64 | 30 |
| P2A rot | 5,4 | 3,615 | 0,39 | 5,949 | 0,158 | 0,03 | 0,029 | 0,13 | 10,13 | 99,7 | 8 |
| P13A weiß | 1,3 | 0,377 | 1,88 | 4,003 | 0,089 | <0.01 | 0,035 | <0.05 | 2,07 | 99,73 | <2 |
| P13A rot | 1,32 | 0,321 | 1,8 | 3,929 | 0,084 | <0.01 | 0,022 | <0.05 | 2,07 | 99,68 | <2 |

| | Ba_SI | Bi_SI | Ce_SI | Co_SI | Cr_SI | Cs_SI | Cu_SI | Ga_SI | Hf_SI | La_SI | Mo_SI |
|------------|-------|-------|-------|-------|-------|-------|-------|-------|-------|-------|-------|
| | mg/kg |
| P1a grau | 374 | 7 | 58 | 8 | 36 | 15 | 19 | 14 | <5 | 32 | <2 |
| P1b rot | 378 | 7 | 71 | 9 | 38 | 18 | 37 | 16 | <5 | 21 | <2 |
| P3 | 54 | 6 | <20 | <3 | <3 | <5 | 23 | <3 | <5 | <20 | <2 |
| P4a grün | 634 | <3 | 41 | 7 | 24 | 16 | <10 | 13 | 5 | 31 | <2 |
| P4b rot | 2954 | 5 | <20 | 9 | 19 | 16 | <10 | 14 | <5 | 21 | <2 |
| P5 | 290 | 4 | 81 | 8 | 45 | 13 | 16 | 11 | 9 | 37 | <2 |
| P6 | 172 | 7 | <20 | <3 | 7 | <5 | 35 | 5 | 13 | <20 | <2 |
| P7/1 | 731 | 4 | 39 | 4 | 12 | 9 | <10 | 11 | 9 | <20 | <2 |
| P8 | 1879 | 4 | 25 | <3 | 14 | <5 | 385 | 13 | <5 | <20 | <2 |
| P9 | 4525 | 4 | <20 | 4 | 4 | 7 | <10 | 6 | <5 | <20 | <2 |
| P10 | 744 | <3 | 34 | <3 | 12 | 7 | <10 | 9 | 9 | 27 | <2 |
| P11 | 765 | 4 | 43 | <3 | 11 | 11 | <10 | 12 | <5 | <20 | <2 |
| P12 | 751 | 4 | 51 | <3 | 14 | 8 | <10 | 10 | <5 | 20 | <2 |
| P14 | 766 | 4 | 20 | 4 | 10 | 10 | <10 | 12 | <5 | 35 | <2 |
| P15a grün | 708 | 5 | 41 | <3 | 17 | 16 | <10 | 16 | <5 | <20 | <2 |
| P15b rot | 708 | <3 | <20 | <3 | 18 | 20 | <10 | 14 | <5 | <20 | <2 |
| P16/1a rot | 907 | <3 | 27 | 5 | 7 | 8 | <10 | 8 | <5 | <20 | <2 |
| P16/1bweiß | 962 | 5 | <20 | 4 | 5 | 7 | <10 | 9 | <5 | <20 | <2 |
| P17 | 918 | 5 | <20 | <3 | 7 | <5 | <10 | 7 | <5 | <20 | <2 |
| P18a rot | 712 | 7 | 33 | <3 | 6 | 10 | <10 | 11 | 6 | <20 | <2 |
| P18b grau | 689 | 5 | 36 | <3 | 8 | 11 | <10 | 12 | <5 | 25 | 3 |
| P18c grau | 741 | 4 | 40 | <3 | 15 | 13 | <10 | 13 | 8 | <20 | <2 |
| P19 | 1316 | <3 | <20 | <3 | 11 | 7 | <10 | 7 | <5 | <20 | <2 |
| P20 | 789 | 6 | 22 | <3 | 10 | 9 | <10 | 10 | <5 | <20 | <2 |
| P7 | 643 | <3 | 46 | <3 | 23 | 13 | <10 | 15 | 5 | <20 | <2 |
| P16/2 | 704 | <3 | 42 | 6 | 9 | 7 | <10 | 8 | <5 | 27 | <2 |

| | | | | | | | | | | | |
|-----------|------|----|-----|----|----|----|-----|----|----|-----|----|
| B1 | 1288 | <3 | <20 | <3 | 11 | 6 | <10 | 4 | <5 | <20 | <2 |
| VH1 | 486 | <3 | 63 | <3 | 12 | 14 | <10 | 7 | 13 | 45 | <2 |
| P2A grau | 282 | 9 | 50 | 10 | 51 | 19 | <10 | 15 | <5 | 32 | <2 |
| P2A rot | 454 | 7 | 62 | 12 | 64 | 30 | 16 | 22 | <5 | 29 | <2 |
| P13A weiß | 777 | <3 | <20 | <3 | 18 | 9 | <10 | 11 | <5 | <20 | <2 |
| P13A rot | 781 | <3 | 31 | <3 | 15 | 11 | <10 | 10 | 8 | 49 | <2 |

| | Nb_SI | Nd_SI | Ni_SI | Pb_SI | Pr_SI | Rb_SI | Sb_SI | Sc_SI | Sm_SI | Sn_SI | Sr_SI |
|------------|-------|-------|-------|-------|-------|-------|-------|-------|-------|-------|-------|
| | mg/kg |
| P1a grau | 8 | <50 | 13 | 22 | <50 | 115 | <5 | 12 | <50 | 2 | 274 |
| P1b rot | 7 | <50 | 15 | 18 | <50 | 131 | 9 | 14 | <50 | 2 | 171 |
| P3 | 2 | <50 | <3 | 7 | <50 | 6 | <5 | <2 | <50 | <2 | 76 |
| P4a grün | 10 | <50 | 16 | 11 | <50 | 112 | <5 | 10 | <50 | <2 | 71 |
| P4b rot | 6 | <50 | 15 | 19 | <50 | 125 | <5 | 7 | <50 | <2 | 203 |
| P5 | 13 | 70 | 17 | 14 | <50 | 83 | <5 | 10 | <50 | <2 | 56 |
| P6 | 3 | <50 | <3 | 15 | <50 | 53 | <5 | <2 | <50 | <2 | 38 |
| P7/1 | <2 | <50 | 3 | 22 | <50 | 124 | <5 | <2 | <50 | <2 | 96 |
| P8 | 3 | <50 | 5 | 23 | <50 | 123 | <5 | 3 | <50 | <2 | 137 |
| P9 | <2 | <50 | <3 | 20 | <50 | 118 | <5 | <2 | <50 | <2 | 243 |
| P10 | 2 | <50 | <3 | 17 | <50 | 122 | <5 | <2 | <50 | 2 | 98 |
| P11 | 4 | <50 | 3 | 19 | <50 | 125 | <5 | 3 | <50 | <2 | 101 |
| P12 | 3 | <50 | 4 | 20 | <50 | 129 | <5 | <2 | <50 | <2 | 107 |
| P14 | 2 | <50 | 3 | 23 | <50 | 123 | <5 | <2 | <50 | <2 | 96 |
| P15a grün | 4 | <50 | 5 | 21 | <50 | 144 | <5 | 3 | <50 | <2 | 93 |
| P15b rot | 3 | <50 | 5 | 18 | <50 | 140 | <5 | <2 | <50 | <2 | 96 |
| P16/1a rot | 3 | <50 | <3 | 28 | <50 | 110 | <5 | <2 | <50 | <2 | 101 |
| P16/1bweiß | <2 | <50 | <3 | 18 | <50 | 113 | <5 | <2 | <50 | <2 | 105 |
| P17 | <2 | <50 | <3 | 21 | <50 | 101 | <5 | <2 | <50 | <2 | 93 |
| P18a rot | 2 | <50 | <3 | 19 | <50 | 123 | <5 | <2 | <50 | <2 | 96 |
| P18b grau | <2 | <50 | <3 | 19 | <50 | 123 | <5 | 3 | <50 | <2 | 96 |
| P18c grau | 2 | <50 | 6 | 19 | <50 | 129 | <5 | <2 | <50 | <2 | 105 |
| P19 | <2 | <50 | <3 | 18 | <50 | 108 | <5 | <2 | <50 | <2 | 112 |
| P20 | 3 | <50 | 5 | 20 | <50 | 125 | <5 | <2 | <50 | 2 | 107 |
| P7 | 4 | <50 | 6 | 19 | <50 | 133 | <5 | <2 | <50 | <2 | 94 |
| P16/2 | <2 | <50 | <3 | 14 | <50 | 120 | <5 | <2 | <50 | <2 | 85 |
| B1 | 3 | <50 | <3 | 18 | <50 | 42 | 5 | <2 | <50 | 2 | 424 |
| VH1 | 5 | <50 | 4 | 13 | <50 | 112 | <5 | 3 | <50 | 2 | 94 |
| P2A grau | 10 | <50 | 24 | 10 | <50 | 129 | 5 | 12 | <50 | <2 | 76 |
| P2A rot | 10 | <50 | 33 | 20 | <50 | 198 | <5 | 14 | <50 | 4 | 68 |
| P13A weiß | 3 | <50 | 6 | 19 | <50 | 129 | <5 | <2 | <50 | <2 | 102 |
| P13A rot | 3 | <50 | 3 | 23 | <50 | 124 | <5 | <2 | <50 | <2 | 99 |

| | Ta_SI | Th_SI | U_SI | V_SI | W_SI | Y_SI | Zn_SI | Zr_SI |
|-------------|-------|-------|-------|-------|-------|-------|-------|-------|
| | mg/kg |
| P1a grau | <5 | 14 | <3 | 40 | 8 | 24 | 847 | 66 |
| P1b rot | <5 | 15 | <3 | 32 | 8 | 20 | 909 | 75 |
| P3 | <5 | 10 | 4 | 14 | <5 | <3 | 235 | 4 |
| P4a grün | <5 | 25 | <3 | 46 | 7 | 26 | 223 | 198 |
| P4b rot | <5 | 23 | <3 | 40 | 8 | 13 | 127 | 183 |
| P5 | <5 | 25 | <3 | 30 | <5 | 47 | 149 | 364 |
| P6 | <5 | 12 | <3 | 8 | 6 | 7 | 91 | 118 |
| P7/1 | <5 | 18 | <3 | 8 | <5 | 6 | 46 | 101 |
| P8 | <5 | 21 | <3 | <5 | 8 | 5 | 32 | 212 |
| P9 | <5 | 13 | <3 | 6 | <5 | <3 | 20 | 56 |
| P10 | <5 | 25 | 5 | 21 | 6 | 9 | 35 | 233 |
| P11 | <5 | 19 | <3 | 18 | <5 | 9 | 30 | 193 |
| P12 | <5 | 21 | <3 | 5 | <5 | 8 | 25 | 181 |
| P14 | 9 | 18 | <3 | 12 | <5 | <3 | 28 | 79 |
| P15a grün | <5 | 23 | <3 | 5 | <5 | 7 | 33 | 158 |
| P15b rot | <5 | 19 | <3 | 13 | <5 | 6 | 35 | 158 |
| P16/1a rot | <5 | 18 | <3 | <5 | <5 | <3 | 14 | 55 |
| P16/1b weiß | <5 | 13 | <3 | 10 | <5 | <3 | 22 | 53 |
| P17 | <5 | 17 | <3 | <5 | <5 | 4 | 28 | 110 |
| P18a rot | <5 | 18 | 4 | 9 | <5 | 7 | 22 | 134 |
| P18b grau | <5 | 20 | <3 | 8 | <5 | 6 | 25 | 152 |
| P18c grau | <5 | 18 | <3 | 11 | 6 | 8 | 31 | 164 |
| P19 | <5 | 19 | <3 | <5 | 6 | <3 | 14 | 45 |
| P20 | <5 | 18 | <3 | 10 | 6 | <3 | 22 | 83 |
| P7 | <5 | 23 | <3 | 18 | 6 | 10 | 27 | 192 |
| P16/2 | <5 | 19 | <3 | 13 | 7 | <3 | 15 | 101 |
| B1 | <5 | 16 | <3 | <5 | <5 | 5 | 30 | 44 |
| VH1 | 9 | 25 | <3 | 40 | 10 | 13 | 26 | 259 |
| P2A grau | <5 | 13 | 11 | 62 | 6 | 13 | 69 | 72 |
| P2A rot | <5 | 23 | <3 | 78 | 7 | 16 | 80 | 127 |
| P13A weiß | <5 | 23 | <3 | 19 | 6 | 4 | 22 | 167 |
| P13A rot | <5 | 25 | <3 | 8 | 8 | 6 | 26 | 201 |

18/07/2006

11:18

***** RF.- Analysen *****

Analyse von Haupt-und Spurenelementen im Silikatprogramm

BGR -Hannover B4.15 RFA - Labor Tel.: 2761(E31)

() =Restkonzentration nach Glühen bei 1000 °Celsius

Einsender: Dr. H-D.Vosteen (3143)

Probenart:Bohrkern / BadMergentheim

| Probenidentifikation | | | SiO ₂ _SI | TiO ₂ _SI | Al ₂ O ₃ _SI | Fe ₂ O ₃ _SI | MnO_SI | MgO_SI |
|---------------------------------|---------------|--------|----------------------|----------------------|------------------------------------|------------------------------------|--------|--------|
| | | % | % | % | % | % | % | % |
| RF223125 | 47106\0603541 | P 22 | 68,41 | 0,412 | 11,21 | 2,82 | 0,059 | 3,42 |
| RF223126 | 47106\0603542 | P 23 | 77,78 | 0,115 | 2,92 | 0,46 | 0,006 | 0,48 |
| RF223127 | 47106\0603543 | P 24 | 72,79 | 0,857 | 10,75 | 3,32 | 0,042 | 2,22 |
| RF223128 | 47106\0603544 | P 37 | 91 | 0,262 | 4,25 | 0,34 | 0,002 | 0,21 |
| RF223129 | 47106\0603545 | P 44 | 91,05 | 0,063 | 4,06 | 0,39 | 0,004 | 0,26 |
| RF223130 | 47106\0603546 | P 52 | 59,48 | 0,45 | 14,51 | 5 | 0,059 | 4,17 |
| RF223131 | 47106\0603547 | P 21 | 51,47 | 0,601 | 15,83 | 6,34 | 0,075 | 5,52 |
| RF223132 | 47106\0603548 | P 24/2 | 70,76 | 0,35 | 8,16 | 2,05 | 0,096 | 3,42 |
| RF223133 | 47106\0603549 | P 25 | 53,06 | 0,653 | 15,75 | 4,64 | 0,072 | 5,41 |
| RF223134 | 47106\0603550 | P 26 | 52,8 | 0,64 | 15,81 | 5,93 | 0,105 | 5,05 |
| RF223135 | 47106\0603551 | P 27 | 38,49 | 0,342 | 8,01 | 3,14 | 0,234 | 10,4 |
| RF223136 | 47106\0603552 | P 28 | 74,74 | 0,289 | 6,65 | 3,9 | 0,116 | 2,56 |
| RF223137 | 47106\0603553 | P 29 | 64,98 | 0,763 | 15,65 | 4,94 | 0,032 | 2,47 |
| RF223138 | 47106\0603554 | P 30 | 63,41 | 0,776 | 16,12 | 5,57 | 0,034 | 2,52 |
| RF223139 | 47106\0603555 | P 31 | 80,64 | 0,386 | 7,55 | 2,35 | 0,034 | 1,36 |
| RF223140 | 47106\0603556 | P 32 | 79,26 | 0,348 | 4,96 | 2,01 | 0,075 | 2,36 |
| RF223141 | 47106\0603557 | P 33 | 77,56 | 0,412 | 7,47 | 1,89 | 0,059 | 2,08 |
| RF223142 | 47106\0603558 | P 34 | 82,4 | 0,262 | 5,49 | 1,3 | 0,05 | 1,68 |
| RF223143 | 47106\0603559 | P 35 | 73,36 | 0,896 | 12,44 | 2,87 | 0,016 | 1,38 |
| RF223144 | 47106\0603560 | P 36 | 52,02 | 0,811 | 20,74 | 9,59 | 0,035 | 2,97 |
| RF223145 | 47106\0603561 | P 38 | 61,58 | 0,43 | 6,84 | 1,04 | 0,246 | 5,66 |
| RF223146 | 47106\0603562 | P 39 | 87,1 | 0,208 | 4,27 | 0,94 | 0,032 | 1 |
| RF223147 | 47106\0603563 | P 40 | 92,97 | 0,096 | 3,11 | 0,75 | 0,006 | 0,29 |
| RF223148 | 47106\0603564 | P 41 | 93,02 | 0,056 | 3,33 | 0,38 | 0,006 | 0,19 |
| RF223149 | 47106\0603565 | P 42 | 90,71 | 0,094 | 3,33 | 1,15 | 0,013 | 0,51 |
| RF223150 | 47106\0603566 | P 43 | 85,76 | 0,105 | 7,14 | 0,74 | 0,006 | 0,42 |
| RF223151 | 47106\0603567 | P 45 | 91,66 | 0,086 | 3,77 | 0,39 | 0,005 | 0,26 |
| RF223152 | 47106\0603568 | P 46 | 89,84 | 0,076 | 4,45 | 0,53 | 0,006 | 0,3 |
| RF223153 | 47106\0603569 | P 47 | 94,56 | 0,057 | 2,4 | 0,42 | 0,005 | 0,19 |
| RF223154 | 47106\0603570 | P 48 | 93,67 | 0,039 | 3,09 | 0,19 | 0,002 | 0,13 |
| RF223155 | 47106\0603571 | P 49 | 71,17 | 0,545 | 13,2 | 4,19 | 0,028 | 1,85 |
| RF223156 | 47106\0603572 | P 50 | 90,15 | 0,054 | 4,3 | 0,87 | 0,006 | 0,48 |
| RF223157 | 47106\0603573 | P 51 | 68 | 0,286 | 9,72 | 3,01 | 0,065 | 3,55 |
| CO ₂ nachgewiesen | | | | | | | | |

| | SiO ₂ _SI | TiO ₂ _SI | Al ₂ O ₃ _SI | Fe ₂ O ₃ _SI | MnO_SI | MgO_SI | CaO_SI | Na ₂ O_SI | K ₂ O_SI |
|--------|----------------------|----------------------|------------------------------------|------------------------------------|--------|--------|--------|----------------------|---------------------|
| | % | % | % | % | % | % | % | % | % |
| P 22 | 68,41 | 0,412 | 11,21 | 2,82 | 0,059 | 3,42 | 2,257 | 0,17 | 3,676 |
| P 23 | 77,78 | 0,115 | 2,92 | 0,46 | 0,006 | 0,48 | 5,194 | 0,07 | 1,3 |
| P 24 | 72,79 | 0,857 | 10,75 | 3,32 | 0,042 | 2,22 | 1,013 | 0,25 | 3,873 |
| P 37 | 91 | 0,262 | 4,25 | 0,34 | 0,002 | 0,21 | 0,141 | 0,14 | 2,56 |
| P 44 | 91,05 | 0,063 | 4,06 | 0,39 | 0,004 | 0,26 | 0,375 | 0,17 | 2,312 |
| P 52 | 59,48 | 0,45 | 14,51 | 5 | 0,059 | 4,17 | 2,43 | 0,28 | 5,514 |
| P 21 | 51,47 | 0,601 | 15,83 | 6,34 | 0,075 | 5,52 | 3,647 | 0,2 | 4,778 |
| P 24/2 | 70,76 | 0,35 | 8,16 | 2,05 | 0,096 | 3,42 | 3,608 | 0,16 | 3,641 |
| P 25 | 53,06 | 0,653 | 15,75 | 4,64 | 0,072 | 5,41 | 3,702 | 0,34 | 5,019 |
| P 26 | 52,8 | 0,64 | 15,81 | 5,93 | 0,105 | 5,05 | 3,428 | 0,24 | 5,886 |
| P 27 | 38,49 | 0,342 | 8,01 | 3,14 | 0,234 | 10,4 | 13,152 | 0,2 | 2,571 |
| P 28 | 74,74 | 0,289 | 6,65 | 3,9 | 0,116 | 2,56 | 2,7 | 0,13 | 2,846 |

| | | | | | | | | | |
|------|-------|-------|-------|------|-------|------|-------|------|-------|
| P 29 | 64,98 | 0,763 | 15,65 | 4,94 | 0,032 | 2,47 | 0,53 | 0,35 | 4,912 |
| P 30 | 63,41 | 0,776 | 16,12 | 5,57 | 0,034 | 2,52 | 0,658 | 0,32 | 5,009 |
| P 31 | 80,64 | 0,386 | 7,55 | 2,35 | 0,034 | 1,36 | 0,964 | 0,13 | 3,26 |
| P 32 | 79,26 | 0,348 | 4,96 | 2,01 | 0,075 | 2,36 | 2,905 | 0,08 | 2,321 |
| P 33 | 77,56 | 0,412 | 7,47 | 1,89 | 0,059 | 2,08 | 2,09 | 0,1 | 3,229 |
| P 34 | 82,4 | 0,262 | 5,49 | 1,3 | 0,05 | 1,68 | 1,852 | 0,1 | 2,583 |
| P 35 | 73,36 | 0,896 | 12,44 | 2,87 | 0,016 | 1,38 | 0,338 | 0,21 | 5,071 |
| P 36 | 52,02 | 0,811 | 20,74 | 9,59 | 0,035 | 2,97 | 0,517 | 0,35 | 6,046 |
| P 38 | 61,58 | 0,43 | 6,84 | 1,04 | 0,246 | 5,66 | 7,57 | 0,15 | 3,107 |
| P 39 | 87,1 | 0,208 | 4,27 | 0,94 | 0,032 | 1 | 1,108 | 0,13 | 2,156 |
| P 40 | 92,97 | 0,096 | 3,11 | 0,75 | 0,006 | 0,29 | 0,165 | 0,07 | 1,478 |
| P 41 | 93,02 | 0,056 | 3,33 | 0,38 | 0,006 | 0,19 | 0,175 | 0,1 | 1,784 |
| P 42 | 90,71 | 0,094 | 3,33 | 1,15 | 0,013 | 0,51 | 0,566 | 0,09 | 1,592 |
| P 43 | 85,76 | 0,105 | 7,14 | 0,74 | 0,006 | 0,42 | 0,268 | 0,3 | 3,318 |
| P 45 | 91,66 | 0,086 | 3,77 | 0,39 | 0,005 | 0,26 | 0,306 | 0,17 | 2,055 |
| P 46 | 89,84 | 0,076 | 4,45 | 0,53 | 0,006 | 0,3 | 0,591 | 0,2 | 2,346 |
| P 47 | 94,56 | 0,057 | 2,4 | 0,42 | 0,005 | 0,19 | 0,176 | 0,08 | 1,249 |
| P 48 | 93,67 | 0,039 | 3,09 | 0,19 | 0,002 | 0,13 | 0,179 | 0,1 | 1,742 |
| P 49 | 71,17 | 0,545 | 13,2 | 4,19 | 0,028 | 1,85 | 0,326 | 0,18 | 4,596 |
| P 50 | 90,15 | 0,054 | 4,3 | 0,87 | 0,006 | 0,48 | 0,242 | 0,15 | 2,431 |
| P 51 | 68 | 0,286 | 9,72 | 3,01 | 0,065 | 3,55 | 3,295 | 0,22 | 4,164 |

| | P2O5_SI | (SO3)_SI | (Cl)_SI | (F)_SI | LOI_SI | Sum_RF | (As)_SI | Ba_SI | Bi_SI | Ce_SI | Co_SI | Cr_SI |
|--------|---------|----------|---------|--------|--------|--------|---------|-------|-------|-------|-------|-------|
| | % | % | % | % | % | % | mg/kg | mg/kg | mg/kg | mg/kg | mg/kg | mg/kg |
| P 22 | 0,118 | 0,12 | 0,005 | 0,05 | 7,1 | 99,84 | 8 | 347 | <3 | 82 | 11 | 47 |
| P 23 | 0,027 | 5,62 | 0,01 | 0,07 | 5,71 | 99,75 | <2 | 1372 | <3 | 25 | <3 | 9 |
| P 24 | 0,141 | 0,09 | 0,01 | <0,05 | 4,33 | 99,71 | 72 | 435 | <3 | 113 | 9 | 54 |
| P 37 | 0,07 | 0,02 | 0,013 | 0,1 | 0,78 | 99,88 | 8 | 585 | <3 | 42 | 6 | 9 |
| P 44 | 0,045 | 0,04 | 0,015 | 0,07 | 1,06 | 99,91 | 16 | 546 | <3 | <20 | 6 | 11 |
| P 52 | 0,185 | 0,05 | 0,016 | <0,05 | 7,65 | 99,78 | 23 | 555 | <3 | 111 | 9 | 100 |
| P 21 | 0,153 | 0,15 | 0,007 | <0,05 | 10,99 | 99,74 | 22 | 364 | <3 | 73 | 9 | 98 |
| P 24/2 | 0,098 | 0,12 | 0,015 | <0,05 | 7,3 | 99,8 | 12 | 436 | <3 | 36 | 8 | 47 |
| P 25 | 0,145 | 0,09 | 0,013 | <0,05 | 10,88 | 99,74 | 17 | 379 | <3 | 65 | 12 | 102 |
| P 26 | 0,154 | 0,05 | 0,014 | <0,05 | 9,65 | 99,78 | 50 | 511 | <3 | 59 | 17 | 166 |
| P 27 | 0,092 | 0,07 | 0,008 | <0,05 | 23,17 | 99,92 | 20 | 236 | <3 | 55 | 10 | 82 |
| P 28 | 0,086 | 0,05 | 0,013 | <0,05 | 5,73 | 99,8 | 23 | 580 | <3 | 50 | 7 | 49 |
| P 29 | 0,128 | 0,07 | 0,01 | <0,05 | 4,91 | 99,74 | 20 | 532 | <3 | 99 | 14 | 95 |
| P 30 | 0,15 | 0,06 | 0,012 | <0,05 | 5,11 | 99,68 | 27 | 528 | <3 | 111 | 12 | 150 |
| P 31 | 0,093 | 0,04 | 0,014 | <0,05 | 2,97 | 99,82 | 10 | 743 | <3 | 55 | 10 | 51 |
| P 32 | 0,118 | 0,04 | 0,013 | <0,05 | 5,3 | 99,82 | 9 | 498 | <3 | 56 | 6 | 49 |
| P 33 | 0,13 | 0,1 | 0,02 | 0,08 | 4,59 | 99,81 | 8 | 786 | <3 | 64 | 6 | 60 |
| P 34 | 0,1 | 0,11 | 0,017 | <0,05 | 3,78 | 99,77 | 10 | 1073 | <3 | 31 | 6 | 49 |
| P 35 | 0,164 | 0,04 | 0,019 | <0,05 | 2,83 | 99,68 | 12 | 786 | <3 | 104 | 11 | 90 |
| P 36 | 0,237 | 0,04 | 0,015 | <0,05 | 6,36 | 99,7 | 36 | 520 | <3 | 97 | 16 | 134 |
| P 38 | 0,098 | 0,06 | 0,011 | <0,05 | 13 | 99,84 | 14 | 453 | <3 | 61 | 7 | 49 |
| P 39 | 0,075 | 0,06 | 0,016 | <0,05 | 2,71 | 99,82 | 6 | 724 | <3 | 37 | <3 | 31 |
| P 40 | 0,046 | 0,02 | 0,016 | 0,05 | 0,84 | 99,92 | 7 | 396 | <3 | <20 | <3 | 14 |
| P 41 | 0,044 | 0,02 | 0,003 | <0,05 | 0,76 | 99,89 | 17 | 336 | <3 | <20 | 4 | 62 |
| P 42 | 0,054 | 0,06 | <0,002 | 0,06 | 1,66 | 99,89 | 26 | 328 | <3 | 20 | <3 | 23 |
| P 43 | 0,107 | 0,01 | 0,011 | <0,05 | 1,65 | 99,85 | 6 | 526 | <3 | 21 | <3 | 26 |

| | | | | | | | | | | | | |
|------|-------|------|--------|-------|------|-------|----|-----|----|-----|----|----|
| P 45 | 0,05 | 0,05 | 0,01 | <0,05 | 0,97 | 99,82 | 6 | 837 | <3 | <20 | <3 | 21 |
| P 46 | 0,058 | 0,05 | 0,009 | <0,05 | 1,39 | 99,85 | 5 | 524 | <3 | <20 | 4 | 51 |
| P 47 | 0,035 | 0,02 | 0,004 | 0,05 | 0,68 | 99,92 | 5 | 261 | <3 | <20 | <3 | 10 |
| P 48 | 0,05 | 0,02 | 0,011 | <0,05 | 0,66 | 99,9 | 2 | 340 | <3 | <20 | <3 | 17 |
| P 49 | 0,182 | 0,01 | 0,012 | <0,05 | 3,49 | 99,79 | 21 | 454 | <3 | 63 | 9 | 66 |
| P 50 | 0,04 | 0,02 | 0,015 | <0,05 | 1,08 | 99,86 | 8 | 485 | <3 | <20 | <3 | 46 |
| P 51 | 0,154 | 0,03 | <0,002 | <0,05 | 7,29 | 99,81 | 11 | 576 | <3 | 54 | 6 | 73 |

| | Cs_SI | Cu_SI | Ga_SI | Hf_SI | La_SI | Mo_SI | Nb_SI | Nd_SI | Ni_SI | Pb_SI | Rb_SI | Sb_SI |
|--------|-------|-------|-------|-------|-------|-------|-------|-------|-------|-------|-------|-------|
| | mg/kg |
| P 22 | 13 | 12 | 16 | <5 | <20 | <2 | 8 | <50 | 20 | 12 | 127 | <5 |
| P 23 | <5 | <10 | 4 | <5 | <20 | <2 | 5 | <50 | <3 | 19 | 38 | <5 |
| P 24 | 15 | 13 | 13 | 20 | <20 | <2 | 17 | 51 | 19 | 15 | 123 | <5 |
| P 37 | 6 | <10 | 4 | <5 | <20 | 3 | 5 | <50 | <3 | 13 | 62 | <5 |
| P 44 | <5 | 14 | 4 | <5 | <20 | <2 | 3 | <50 | <3 | 17 | 57 | <5 |
| P 52 | 23 | 11 | 19 | <5 | <20 | 7 | 10 | <50 | 50 | 37 | 186 | <5 |
| P 21 | 20 | 12 | 22 | <5 | <20 | <2 | 12 | <50 | 35 | 14 | 179 | <5 |
| P 24/2 | 8 | 12 | 10 | 5 | <20 | <2 | 8 | <50 | 9 | 14 | 99 | <5 |
| P 25 | 20 | 30 | 22 | <5 | <20 | <2 | 13 | <50 | 34 | 16 | 176 | 7 |
| P 26 | 20 | 26 | 21 | <5 | <20 | <2 | 15 | <50 | 39 | 20 | 190 | 5 |
| P 27 | 10 | 50 | 11 | <5 | <20 | <2 | 8 | <50 | 17 | 13 | 91 | <5 |
| P 28 | 7 | 38 | 9 | <5 | <20 | <2 | 6 | <50 | 19 | 15 | 83 | <5 |
| P 29 | 19 | 14 | 22 | 11 | <20 | <2 | 17 | <50 | 32 | 19 | 167 | <5 |
| P 30 | 22 | 18 | 21 | 12 | <20 | <2 | 15 | <50 | 35 | 16 | 171 | <5 |
| P 31 | 8 | 14 | 9 | 8 | <20 | <2 | 8 | <50 | 9 | 30 | 94 | <5 |
| P 32 | 6 | 13 | 4 | 7 | <20 | <2 | 8 | <50 | 3 | 13 | 60 | <5 |
| P 33 | 10 | <10 | 9 | 8 | <20 | 3 | 8 | <50 | 8 | 15 | 93 | <5 |
| P 34 | <5 | <10 | 6 | <5 | <20 | <2 | 6 | <50 | 4 | 13 | 69 | <5 |
| P 35 | 13 | 17 | 15 | 21 | <20 | <2 | 18 | 56 | 17 | 26 | 152 | <5 |
| P 36 | 26 | 15 | 30 | 7 | <20 | <2 | 15 | 57 | 41 | 27 | 209 | <5 |
| P 38 | <5 | 11 | 7 | 10 | <20 | <2 | 9 | <50 | 6 | 10 | 85 | <5 |
| P 39 | 6 | 14 | 4 | 7 | <20 | <2 | 3 | <50 | <3 | 17 | 59 | <5 |
| P 40 | <5 | <10 | 4 | <5 | <20 | <2 | 4 | <50 | <3 | 11 | 42 | <5 |
| P 41 | <5 | 11 | <3 | <5 | <20 | <2 | 2 | <50 | <3 | 11 | 43 | <5 |
| P 42 | <5 | <10 | <3 | <5 | <20 | <2 | 4 | <50 | 3 | 8 | 47 | <5 |
| P 43 | <5 | 14 | 7 | 5 | <20 | <2 | 2 | <50 | <3 | 19 | 81 | <5 |
| P 45 | <5 | 10 | <3 | 5 | <20 | <2 | 3 | <50 | <3 | 14 | 51 | <5 |
| P 46 | <5 | <10 | 4 | <5 | <20 | <2 | 4 | <50 | <3 | 18 | 58 | <5 |
| P 47 | <5 | <10 | <3 | <5 | <20 | <2 | 2 | <50 | <3 | 8 | 35 | <5 |
| P 48 | <5 | 13 | <3 | <5 | <20 | <2 | <2 | <50 | <3 | 13 | 45 | <5 |
| P 49 | 18 | 15 | 19 | <5 | <20 | <2 | 13 | <50 | 23 | 15 | 148 | <5 |
| P 50 | <5 | <10 | 4 | <5 | <20 | <2 | 3 | <50 | <3 | 15 | 62 | <5 |
| P 51 | 11 | 13 | 13 | <5 | <20 | <2 | 8 | <50 | 10 | 22 | 123 | <5 |

| | Sc_SI | Sm_SI | Sn_SI | Sr_SI | Ta_SI | Th_SI | U_SI | V_SI | W_SI | Y_SI | Zn_SI | Zr_SI |
|--|-------|-------|-------|-------|-------|-------|-------|-------|-------|-------|-------|-------|
| | mg/kg |

| | | | | | | | | | | | | |
|--------|----|-----|----|-----|----|----|----|-----|-----|----|-----|-----|
| P 22 | 10 | <50 | 5 | 108 | <5 | 15 | 5 | 83 | 14 | 18 | 57 | 175 |
| P 23 | 3 | <50 | <2 | 558 | <5 | 8 | <3 | 12 | 20 | 7 | 15 | 104 |
| P 24 | 9 | <50 | 2 | 140 | <5 | 21 | 8 | 55 | 36 | 31 | 53 | 731 |
| P 37 | <2 | <50 | <2 | 59 | <5 | 8 | 4 | 10 | 40 | 9 | 12 | 189 |
| P 44 | <2 | <50 | <2 | 67 | <5 | 6 | <3 | <5 | 43 | 4 | 18 | 67 |
| P 52 | 12 | <50 | 3 | 87 | <5 | 18 | 6 | 63 | 16 | 21 | 67 | 131 |
| P 21 | 14 | <50 | 2 | 96 | <5 | 17 | 8 | 86 | 6 | 23 | 88 | 121 |
| P 24/2 | 6 | <50 | <2 | 108 | <5 | 14 | 4 | 39 | 29 | 21 | 39 | 224 |
| P 25 | 14 | <50 | <2 | 127 | <5 | 17 | 7 | 85 | 6 | 24 | 82 | 178 |
| P 26 | 13 | <50 | 5 | 107 | <5 | 16 | 15 | 82 | 42 | 28 | 106 | 148 |
| P 27 | 10 | <50 | <2 | 105 | <5 | 9 | 5 | 36 | 9 | 13 | 68 | 88 |
| P 28 | 5 | <50 | 3 | 81 | <5 | 11 | 5 | 30 | <5 | 17 | 34 | 135 |
| P 29 | 13 | <50 | 5 | 147 | <5 | 19 | 8 | 95 | 9 | 31 | 76 | 295 |
| P 30 | 13 | <50 | <2 | 162 | <5 | 19 | 6 | 94 | 20 | 33 | 80 | 309 |
| P 31 | 5 | <50 | 3 | 84 | <5 | 11 | 4 | 36 | 30 | 19 | 33 | 195 |
| P 32 | 4 | <50 | 2 | 63 | <5 | 16 | 8 | 29 | 35 | 22 | 28 | 276 |
| P 33 | 5 | <50 | 3 | 85 | <5 | 13 | <3 | 41 | 33 | 22 | 37 | 275 |
| P 34 | 3 | <50 | <2 | 74 | <5 | 9 | 5 | 26 | 40 | 13 | 25 | 150 |
| P 35 | 7 | <50 | 5 | 93 | <5 | 27 | 6 | 55 | 28 | 48 | 48 | 707 |
| P 36 | 18 | <50 | <2 | 226 | <5 | 19 | 7 | 138 | 9 | 34 | 100 | 203 |
| P 38 | 5 | <50 | <2 | 105 | <5 | 13 | <3 | 30 | 32 | 23 | 30 | 307 |
| P 39 | 3 | <50 | <2 | 64 | <5 | 9 | 4 | 15 | 13 | 13 | 27 | 230 |
| P 40 | <2 | <50 | <2 | 54 | <5 | 7 | <3 | 13 | <5 | 4 | 22 | 88 |
| P 41 | <2 | <50 | <2 | 44 | <5 | <5 | 4 | <5 | 46 | 6 | 14 | 59 |
| P 42 | <2 | <50 | 5 | 58 | <5 | 6 | 6 | 14 | <5 | 7 | 28 | 100 |
| P 43 | <2 | <50 | <2 | 69 | <5 | 7 | <3 | 6 | 24 | 12 | 13 | 131 |
| P 45 | <2 | <50 | <2 | 66 | <5 | 9 | 3 | <5 | 26 | 6 | 14 | 109 |
| P 46 | <2 | <50 | <2 | 74 | <5 | 9 | 4 | 12 | 21 | 7 | 17 | 110 |
| P 47 | <2 | <50 | <2 | 34 | <5 | 5 | 4 | <5 | <5 | 4 | 15 | 67 |
| P 48 | <2 | <50 | 2 | 42 | <5 | <5 | 4 | 7 | <5 | 4 | 11 | 80 |
| P 49 | 10 | <50 | 3 | 163 | <5 | 18 | <3 | 52 | 17 | 24 | 62 | 182 |
| P 50 | <2 | <50 | <2 | 59 | <5 | 6 | 4 | <5 | 141 | 8 | 11 | 96 |
| P 51 | 8 | <50 | 2 | 101 | <5 | 13 | 4 | 34 | 56 | 18 | 45 | 144 |

Namedy (Andernach, Hunsrück shale)

Stratigraphic correlation of rock samples

| CO2-alterierte Proben (Andernach) | | | | |
|-----------------------------------|--------|--------|---|----------------------------------|
| Probennummer entspricht Teufe (m) | | | | |
| | >20% | 15-20% | 10-15% | 5-10% |
| | HK | HK-NK | NK | NK-SP |
| P81 | Quartz | | Musk-Illite, Chlorite/Kaolinite, Siderite | Feldspar |
| P82 | Quartz | | Musk-Illite, Chlorite/Kaolinite, Siderite | Feldspar |
| P83 | Quartz | | | Musk-Illite, Chlorite/Kaolinite |
| P84 | Quartz | | Musk-Illite, Chlorite/Kaolinite, Siderite | Siderite, Ankerite, Feldspar |
| P85 | Quartz | | Chlorite/Kaolinite | Calcite, Feldspar |
| P205 | Quartz | | Musk-Illite | Calcite, Feldspar |
| P206 | Quartz | | | Siderite, Feldspar, Chlorite |
| P207 | Quartz | | Musk-Illite | Musk-Illite, Kaolinite, Siderite |
| P289 | Quartz | | Musk-Illite | Kaolinite, Siderite |
| P290 | Quartz | | Musk-Illite | Kaolinite, Siderite |
| P291 | Quartz | | Musk-Illite | Kaolinite, Siderite |
| P292 | Quartz | | Musk-Illite | Kaolinite, Siderite |
| P293 | Quartz | | Musk-Illite | Kaolinite, Siderite |
| P317 | Quartz | | | Musk-Illite, Kaolinite, Siderite |
| P318 | Quartz | | Musk-Illite | Kaolinite, Siderite |
| P319 | Quartz | | Musk-Illite | Kaolinite, Siderite |
| P320 | Quartz | | Musk-Illite | Kaolinite, Siderite |
| P324 | Quartz | | Musk-Illite | Kaolinite, Siderite |
| P325 | Quartz | | Musk-Illite | Kaolinite, Siderite |
| P326 | Quartz | | Musk-Illite | Kaolinite, Siderite |
| P327 | Quartz | | Musk-Illite | Kaolinite, Siderite |
| P328 | Quartz | | Musk-Illite, Kaolinite | Kaolinite, Siderite |
| P329 | Quartz | | Musk-Illite | Kaolinite, Siderite |
| P331 | Quartz | | | Musk-Illite, Kaolinite, Siderite |
| P332 | Quartz | | | Musk-Illite, Kaolinite, Siderite |
| P333 | Quartz | | Musk-Illite, Kaolinite | Siderite |
| P334 | Quartz | | Musk-Illite | Kaolinite, Siderite |
| P335 | Quartz | | | Musk-Illite, Kaolinite, Siderite |
| P336 | Quartz | | Musk-Illite, Siderite | Kaolinite |

CO₂-alterierte Proben (Andernach)

Probennummer entspricht Teufe (m)

| | >20% | 15-20% | 10-15% | 5-10% | <5% |
|------|--------|--------|--|-------------------------------------|------------------------------------|
| | HK | HK-NK | NK | NK-SP | SP |
| P81 | Quartz | | Musk-Illite, Chlorite/Kaolinite, Siderite | | Feldspar |
| P82 | Quartz | | Musk-Illite, Chlorite/Kaolinite, Siderite | | Feldspar |
| P83 | Quartz | | | Musk-Illite, Chlorite/Kaolinite | Siderite, Ankerite, Feldspar |
| P84 | Quartz | | Musk-Illite, Chlorite/Kaolinite, Siderite | | Calcite, Feldspar |
| P85 | Quartz | | Chlorite/Kaolinite | Musk-Illite, Siderite | Calcite, Feldspar |
| P205 | Quartz | | Musk-Illite | Kaolinite | Siderite, Feldspar, Chlorite |
| P206 | Quartz | | | Musk-Illite, Kaolinite, Siderite | Feldspar |
| P207 | Quartz | | Musk-Illite | Kaolinite, Siderite | Feldspar |
| P289 | Quartz | | Musk-Illite | Kaolinite, Siderite | Feldspar |
| P290 | Quartz | | Musk-Illite | Kaolinite, Siderite | Feldspar |
| P291 | Quartz | | Musk-Illite | Kaolinite, Siderite | Feldspar |
| P292 | Quartz | | Musk-Illite | Kaolinite, Siderite | Feldspar |
| P293 | Quartz | | Musk-Illite | Kaolinite, Siderite | Feldspar |
| P317 | Quartz | | | Musk-Illite, Kaolinite, Siderite | Feldspar |
| P318 | Quartz | | Musk-Illite | Kaolinite, Siderite | Feldspar |
| P319 | Quartz | | Musk-Illite | Kaolinite, Siderite | Feldspar |
| P320 | Quartz | | Musk-Illite | Kaolinite, Siderite | Feldspar |
| P324 | Quartz | | Musk-Illite | Kaolinite, Siderite | Feldspar |
| P325 | Quartz | | Musk-Illite | Kaolinite, Siderite | Feldspar |
| P326 | Quartz | | Musk-Illite | Kaolinite, Siderite | Feldspar |
| P327 | Quartz | | Musk-Illite | Kaolinite, Siderite | Feldspar |
| P328 | Quartz | | Musk-Illite, Kaolinite | Kaolinite, Siderite | Feldspar |
| P329 | Quartz | | Musk-Illite | Kaolinite, Siderite | Feldspar |
| P331 | Quartz | | | Musk-Illite, Kaolinite, Siderite | Feldspar |
| P332 | Quartz | | | Musk-Illite, Kaolinite, Siderite | Feldspar |
| P333 | Quartz | | Musk-Illite, Kaolinite | Siderite | Feldspar |
| P334 | Quartz | | Musk-Illite | Kaolinite, Siderite | Feldspar |
| P335 | Quartz | | | Musk-Illite, Kaolinite, Siderite | Feldspar |
| P336 | Quartz | | Musk-Illite, Siderite | Kaolinite | Feldspar |

***** RF.- Analysen *****
 Analyse von Haupt- und Spurenelementen im Silikatprogramm
 BGR - Hannover B4.15 RFA - Labor Tel.: 2761 (E31)
 () = Restkonzentration nach Glühen bei 1030°Celsius

Auftrag: 47323 / Einsender: Dr. Vosteen (3217)
 Probenart: Bohrklein / Andernach

| Probenidentifikation | | SiO2 | TiO2 | Al2O3 | Fe2O3 | MnO | MgO | CaO | Na2O | K2O | P2O5 | (SO3) | (Cl) | (F) | LOI | Sum | |
|----------------------|---------|------|-------|-------|-------|-------|-------|------|-------|------|-------|-------|------|-------|-------|-------|-------|
| | | % | % | % | % | % | % | % | % | % | % | % | % | % | % | % | |
| RF224667 | 0612785 | 81 | 64.89 | 0.817 | 15.70 | 6.65 | 0.137 | 1.70 | 0.390 | 0.18 | 2.553 | 0.106 | 0.04 | 0.007 | <0.05 | 6.52 | 99.70 |
| RF224668 | 0612786 | 82 | 60.22 | 0.834 | 17.77 | 8.13 | 0.150 | 1.92 | 0.449 | 0.22 | 2.888 | 0.211 | 0.12 | 0.027 | <0.05 | 6.52 | 99.47 |
| RF224669 | 0612787 | 83 | 80.80 | 0.400 | 7.92 | 3.58 | 0.084 | 1.02 | 0.383 | 0.14 | 1.496 | 0.041 | 0.05 | 0.033 | 0.06 | 3.83 | 99.83 |
| RF224670 | 0612788 | 84 | 53.84 | 0.882 | 17.30 | 9.82 | 0.131 | 2.55 | 1.753 | 0.37 | 2.605 | 0.084 | 0.13 | 0.028 | <0.05 | 10.18 | 99.68 |
| RF224671 | 0612789 | 85 | 51.66 | 0.827 | 15.97 | 9.68 | 0.136 | 2.59 | 4.140 | 0.34 | 2.400 | 0.091 | 0.29 | 0.028 | <0.05 | 11.53 | 99.69 |
| RF224672 | 0612790 | 205 | 65.32 | 0.910 | 17.11 | 4.74 | 0.095 | 0.97 | 0.351 | 0.29 | 2.855 | 0.135 | 0.01 | 0.028 | <0.05 | 6.87 | 99.70 |
| RF224673 | 0612791 | 206 | 71.63 | 0.610 | 11.91 | 5.50 | 0.123 | 1.02 | 0.296 | 0.17 | 2.087 | 0.073 | 0.03 | 0.018 | 0.07 | 6.24 | 99.78 |
| RF224674 | 0612792 | 207 | 65.40 | 0.889 | 16.12 | 5.33 | 0.119 | 1.06 | 0.374 | 0.32 | 3.110 | 0.128 | 0.04 | 0.014 | <0.05 | 6.77 | 99.70 |
| RF224675 | 0612793 | 289 | 59.10 | 0.890 | 18.08 | 7.47 | 0.174 | 1.39 | 0.357 | 0.28 | 3.174 | 0.137 | 0.02 | 0.010 | <0.05 | 8.59 | 99.69 |
| RF224676 | 0612794 | 290 | 64.86 | 0.838 | 15.57 | 6.15 | 0.127 | 1.16 | 0.463 | 0.24 | 2.674 | 0.101 | 0.07 | 0.015 | <0.05 | 7.44 | 99.70 |
| RF224677 | 0612795 | 291 | 60.37 | 0.885 | 17.30 | 7.35 | 0.171 | 1.39 | 0.395 | 0.24 | 2.907 | 0.150 | 0.02 | 0.017 | <0.05 | 8.49 | 99.68 |
| RF224678 | 0612796 | 292 | 61.12 | 0.874 | 17.27 | 6.86 | 0.155 | 1.34 | 0.456 | 0.25 | 2.947 | 0.139 | 0.03 | 0.014 | <0.05 | 8.26 | 99.71 |
| RF224679 | 0612797 | 293 | 62.92 | 0.838 | 16.14 | 6.93 | 0.147 | 1.22 | 0.405 | 0.24 | 2.701 | 0.123 | 0.02 | 0.013 | <0.05 | 7.98 | 99.70 |
| RF224680 | 0612798 | 317 | 65.77 | 0.729 | 14.24 | 6.74 | 0.146 | 1.35 | 0.385 | 0.21 | 2.475 | 0.116 | 0.05 | 0.015 | <0.05 | 7.52 | 99.72 |
| RF224681 | 0612799 | 318 | 65.12 | 0.694 | 13.40 | 7.66 | 0.164 | 1.54 | 0.390 | 0.19 | 2.273 | 0.118 | 0.06 | 0.015 | <0.05 | 8.11 | 99.74 |
| RF224682 | 0612800 | 319 | 62.03 | 0.763 | 14.91 | 8.12 | 0.178 | 1.66 | 0.426 | 0.22 | 2.504 | 0.144 | 0.04 | 0.008 | <0.05 | 8.70 | 99.73 |
| RF224683 | 0612801 | 320 | 59.35 | 0.820 | 16.55 | 8.26 | 0.177 | 1.72 | 0.390 | 0.22 | 2.734 | 0.139 | 0.02 | 0.010 | <0.05 | 9.34 | 99.70 |
| RF224684 | 0612802 | 324 | 58.19 | 0.871 | 17.05 | 8.16 | 0.176 | 1.81 | 0.434 | 0.27 | 2.894 | 0.133 | 0.02 | 0.021 | <0.05 | 9.65 | 99.71 |
| RF224685 | 0612803 | 325 | 61.32 | 0.820 | 16.14 | 7.21 | 0.158 | 1.60 | 0.430 | 0.35 | 2.674 | 0.134 | 0.02 | 0.017 | <0.05 | 8.84 | 99.71 |
| RF224686 | 0612804 | 326 | 62.26 | 0.852 | 16.56 | 6.39 | 0.133 | 1.50 | 0.470 | 0.36 | 2.724 | 0.142 | 0.03 | 0.020 | <0.05 | 8.22 | 99.71 |
| RF224687 | 0612805 | 327 | 58.81 | 0.820 | 17.23 | 7.59 | 0.142 | 1.63 | 0.397 | 0.32 | 2.969 | 0.123 | 0.02 | 0.016 | <0.05 | 9.62 | 99.70 |
| RF224688 | 0612806 | 328 | 60.04 | 0.954 | 18.53 | 6.53 | 0.126 | 1.31 | 0.345 | 0.27 | 3.056 | 0.123 | 0.02 | 0.017 | <0.05 | 8.36 | 99.69 |
| RF224689 | 0612807 | 329 | 61.69 | 0.897 | 17.45 | 6.43 | 0.124 | 1.31 | 0.348 | 0.30 | 2.754 | 0.122 | 0.03 | 0.010 | <0.05 | 8.16 | 99.67 |
| RF224690 | 0612808 | 331 | 70.73 | 0.677 | 12.79 | 5.40 | 0.143 | 0.87 | 0.284 | 0.22 | 2.122 | 0.095 | 0.03 | 0.017 | 0.07 | 6.33 | 99.78 |
| RF224691 | 0612809 | 332 | 70.22 | 0.690 | 12.96 | 5.61 | 0.150 | 0.88 | 0.285 | 0.22 | 2.182 | 0.094 | 0.03 | 0.012 | <0.05 | 6.41 | 99.74 |
| RF224692 | 0612810 | 333 | 65.98 | 0.758 | 14.59 | 5.76 | 0.133 | 1.12 | 0.350 | 0.24 | 2.443 | 0.150 | 0.02 | 0.016 | <0.05 | 8.14 | 99.72 |
| RF224693 | 0612811 | 334 | 59.82 | 0.775 | 14.84 | 8.40 | 0.182 | 1.90 | 0.336 | 0.23 | 2.478 | 0.098 | 0.02 | 0.014 | <0.05 | 10.61 | 99.72 |
| RF224694 | 0612812 | 335 | 67.78 | 0.684 | 13.17 | 6.21 | 0.130 | 1.40 | 0.310 | 0.25 | 2.251 | 0.092 | 0.03 | 0.012 | <0.05 | 7.43 | 99.75 |
| RF224695 | 0612813 | 336 | 54.31 | 0.794 | 16.46 | 10.13 | 0.229 | 2.76 | 0.402 | 0.27 | 2.820 | 0.120 | 0.04 | 0.010 | <0.05 | 11.36 | 99.68 |

***** RF.- Analysen *****
 Analyse von Haupt- und Spurenelementen im Silikatprogramm
 BGR - Hannover B4.15 RFA - Labor Tel.: 2761 (E31)
 () = Restkonzentration nach Glühen bei 1030°Celsius

Auftrag: 47323 / Einsender: Dr. Vosteen (3217)
 Probenart: Bohrklein / Andernach

| Probenidentifikation | | (As) | Ba | Bi | Ce | Co | Cr | Cs | Cu | Ga | Hf | La | Mo | Nb | Nd | Ni |
|----------------------|---------|-------|-------|-------|-------|-------|-------|-------|-------|-------|-------|-------|-------|-------|-------|------------|
| | | mg/kg | |
| RF224667 | 0612785 | 81 | | 18 | 510 | <3 | 58 | 19 | 143 | <5 | 31 | 21 | <5 | 33 | <2 | 15 <50 72 |
| RF224668 | 0612786 | 82 | | 37 | 597 | <3 | 90 | 28 | 139 | 8 | 102 | 25 | <5 | 53 | <2 | 15 <50 89 |
| RF224669 | 0612787 | 83 | | 11 | 288 | <3 | 42 | 10 | 79 | <5 | 25 | 10 | <5 | <20 | <2 | 8 <50 42 |
| RF224670 | 0612788 | 84 | | 34 | 514 | <3 | 81 | 27 | 190 | 8 | 34 | 24 | 5 | 32 | <2 | 17 <50 115 |
| RF224671 | 0612789 | 85 | | 27 | 477 | <3 | 77 | 22 | 154 | 8 | 33 | 22 | <5 | 43 | <2 | 12 <50 97 |
| RF224672 | 0612790 | 205 | | 19 | 546 | <3 | 100 | 21 | 147 | 8 | 12 | 23 | 8 | 40 | <2 | 14 <50 61 |
| RF224673 | 0612791 | 206 | | 14 | 384 | <3 | 68 | 19 | 119 | <5 | 52 | 16 | <5 | 22 | <2 | 10 <50 68 |
| RF224674 | 0612792 | 207 | | 20 | 603 | <3 | 90 | 21 | 182 | <5 | 28 | 22 | 5 | 36 | <2 | 16 <50 64 |
| RF224675 | 0612793 | 289 | | 18 | 605 | <3 | 83 | 21 | 140 | 8 | 37 | 25 | <5 | 40 | <2 | 17 56 71 |
| RF224676 | 0612794 | 290 | | 16 | 483 | <3 | 81 | 17 | 148 | 6 | 61 | 20 | <5 | 47 | <2 | 16 <50 61 |
| RF224677 | 0612795 | 291 | | 20 | 568 | <3 | 83 | 21 | 145 | 8 | 30 | 24 | <5 | 42 | <2 | 16 <50 75 |
| RF224678 | 0612796 | 292 | | 19 | 566 | <3 | 91 | 23 | 145 | 8 | 31 | 23 | <5 | 40 | <2 | 15 <50 74 |
| RF224679 | 0612797 | 293 | | 20 | 520 | <3 | 74 | 21 | 147 | 8 | 31 | 22 | <5 | 44 | 4 | 13 <50 71 |
| RF224680 | 0612798 | 317 | | 11 | 443 | <3 | 60 | 18 | 135 | 6 | 37 | 21 | <5 | 34 | <2 | 12 <50 71 |
| RF224681 | 0612799 | 318 | | 13 | 404 | <3 | 76 | 21 | 123 | <5 | 29 | 16 | <5 | 41 | <2 | 12 <50 76 |
| RF224682 | 0612800 | 319 | | 16 | 459 | <3 | 62 | 20 | 138 | 6 | 31 | 20 | <5 | 36 | <2 | 12 <50 80 |
| RF224683 | 0612801 | 320 | | 12 | 500 | <3 | 98 | 23 | 138 | 7 | 30 | 21 | <5 | 51 | <2 | 17 <50 86 |
| RF224684 | 0612802 | 324 | | 15 | 524 | <3 | 92 | 23 | 139 | 7 | 40 | 25 | 6 | 42 | <2 | 15 <50 86 |
| RF224685 | 0612803 | 325 | | 16 | 481 | <3 | 76 | 19 | 133 | <5 | 27 | 21 | 5 | 58 | <2 | 14 <50 78 |
| RF224686 | 0612804 | 326 | | 14 | 477 | <3 | 92 | 22 | 140 | 8 | 30 | 22 | <5 | 49 | <2 | 15 <50 67 |
| RF224687 | 0612805 | 327 | | 16 | 506 | <3 | 64 | 23 | 143 | 8 | 42 | 23 | <5 | 50 | <2 | 15 <50 84 |
| RF224688 | 0612806 | 328 | | 15 | 580 | <3 | 101 | 21 | 154 | 9 | 23 | 24 | <5 | 56 | <2 | 17 <50 66 |
| RF224689 | 0612807 | 329 | | 14 | 542 | <3 | 77 | 23 | 169 | 7 | 84 | 24 | 8 | 38 | 5 | 16 51 83 |
| RF224690 | 0612808 | 331 | | 14 | 390 | <3 | 67 | 16 | 130 | 7 | 18 | 16 | <5 | 38 | <2 | 13 <50 53 |
| RF224691 | 0612809 | 332 | | 12 | 390 | <3 | 56 | 18 | 135 | <5 | 18 | 17 | 9 | 31 | <2 | 13 <50 53 |
| RF224692 | 0612810 | 333 | | 14 | 442 | <3 | 68 | 21 | 147 | <5 | 22 | 19 | 7 | 33 | 4 | 12 <50 63 |
| RF224693 | 0612811 | 334 | | 12 | 449 | <3 | 70 | 21 | 134 | 7 | 23 | 19 | <5 | 42 | <2 | 13 <50 87 |
| RF224694 | 0612812 | 335 | | 13 | 396 | <3 | 68 | 17 | 124 | 6 | 18 | 17 | <5 | 26 | <2 | 10 <50 64 |
| RF224695 | 0612813 | 336 | | 15 | 505 | <3 | 76 | 25 | 124 | <5 | 22 | 23 | 8 | 58 | <2 | 14 <50 116 |

***** RF.- Analysen *****
 Analyse von Haupt- und Spurenelementen im Silikatprogramm
 BGR - Hannover B4.15 RFA - Labor Tel.: 2761 (E31)
 () = Restkonzentration nach Glühen bei 1030°Celsius

Auftrag: 47323 / Einsender: Dr. Vosteen (3217)
 Probenart: Bohrklein / Andernach

| Probenidentifikation | | Pb | Rb | Sb | Sc | Sm | Sn | Sr | Ta | Th | U | V | W | Y | Zn | Zr | | |
|----------------------|---------|-------|-------|-------|-------|-------|-------|-------|-------|-------|-------|-------|-------|-------|-------|----|-----|-----|
| | | mg/kg | | | |
| RF224667 | 0612785 | 81 | | 12 | 110 | 10 | 15 | <50 | 5 | 78 | <5 | 17 | <3 | 107 | <5 | 33 | 87 | 227 |
| RF224668 | 0612786 | 82 | | 1482 | 123 | 5 | 17 | <50 | 5 | 220 | <5 | 18 | 3 | 124 | <5 | 30 | 110 | 162 |
| RF224669 | 0612787 | 83 | | 25 | 62 | <5 | 8 | <50 | <2 | 46 | <5 | 11 | <3 | 61 | <5 | 13 | 95 | 115 |
| RF224670 | 0612788 | 84 | | 19 | 107 | <5 | 18 | <50 | <2 | 80 | <5 | 18 | <3 | 123 | <5 | 33 | 130 | 195 |
| RF224671 | 0612789 | 85 | | 23 | 99 | <5 | 18 | <50 | <2 | 115 | <5 | 17 | <3 | 118 | <5 | 32 | 133 | 184 |
| RF224672 | 0612790 | 205 | | 6 | 121 | <5 | 16 | <50 | <2 | 87 | <5 | 16 | 5 | 110 | <5 | 32 | 84 | 237 |
| RF224673 | 0612791 | 206 | | 7 | 88 | <5 | 12 | <50 | 2 | 63 | <5 | 16 | <3 | 83 | 10 | 23 | 88 | 187 |
| RF224674 | 0612792 | 207 | | 23 | 131 | <5 | 16 | <50 | 6 | 97 | <5 | 17 | <3 | 108 | <5 | 33 | 79 | 327 |
| RF224675 | 0612793 | 289 | | 7 | 138 | <5 | 17 | <50 | <2 | 129 | <5 | 18 | 3 | 118 | <5 | 31 | 103 | 192 |
| RF224676 | 0612794 | 290 | | 10 | 116 | 7 | 14 | <50 | <2 | 96 | <5 | 17 | <3 | 106 | <5 | 29 | 94 | 255 |
| RF224677 | 0612795 | 291 | | 5 | 123 | 6 | 16 | <50 | <2 | 137 | <5 | 17 | 3 | 111 | <5 | 31 | 100 | 204 |
| RF224678 | 0612796 | 292 | | 7 | 130 | <5 | 17 | <50 | 4 | 123 | <5 | 18 | <3 | 109 | <5 | 31 | 93 | 203 |
| RF224679 | 0612797 | 293 | | 9 | 118 | <5 | 16 | <50 | <2 | 95 | <5 | 18 | <3 | 113 | 6 | 31 | 102 | 227 |
| RF224680 | 0612798 | 317 | | 14 | 107 | <5 | 14 | <50 | <2 | 99 | <5 | 12 | <3 | 90 | 9 | 28 | 100 | 213 |
| RF224681 | 0612799 | 318 | | 10 | 99 | <5 | 14 | <50 | <2 | 96 | <5 | 18 | <3 | 92 | <5 | 25 | 105 | 197 |
| RF224682 | 0612800 | 319 | | 6 | 113 | <5 | 14 | <50 | <2 | 118 | <5 | 18 | <3 | 95 | <5 | 25 | 111 | 216 |
| RF224683 | 0612801 | 320 | | 7 | 121 | <5 | 16 | <50 | <2 | 116 | <5 | 16 | <3 | 111 | <5 | 31 | 114 | 194 |
| RF224684 | 0612802 | 324 | | 9 | 127 | <5 | 17 | <50 | <2 | 98 | <5 | 17 | <3 | 103 | 17 | 31 | 115 | 206 |
| RF224685 | 0612803 | 325 | | 5 | 119 | <5 | 15 | <50 | 2 | 90 | <5 | 18 | <3 | 106 | 7 | 28 | 102 | 201 |
| RF224686 | 0612804 | 326 | | 11 | 114 | <5 | 16 | <50 | 4 | 97 | <5 | 17 | 6 | 115 | <5 | 31 | 91 | 218 |
| RF224687 | 0612805 | 327 | | 5 | 128 | <5 | 17 | <50 | 9 | 86 | <5 | 18 | 3 | 116 | <5 | 31 | 104 | 204 |
| RF224688 | 0612806 | 328 | | 10 | 133 | <5 | 17 | <50 | <2 | 86 | <5 | 19 | 4 | 118 | 11 | 32 | 87 | 246 |
| RF224689 | 0612807 | 329 | | 13 | 114 | <5 | 16 | <50 | 3 | 81 | <5 | 19 | <3 | 110 | 6 | 33 | 85 | 224 |
| RF224690 | 0612808 | 331 | | 14 | 92 | <5 | 12 | <50 | <2 | 58 | <5 | 16 | <3 | 80 | 13 | 26 | 73 | 229 |
| RF224691 | 0612809 | 332 | | 6 | 98 | <5 | 12 | <50 | <2 | 61 | <5 | 15 | 3 | 85 | 9 | 26 | 75 | 229 |
| RF224692 | 0612810 | 333 | | 10 | 103 | <5 | 14 | <50 | <2 | 89 | <5 | 16 | <3 | 95 | 63 | 28 | 73 | 222 |
| RF224693 | 0612811 | 334 | | 5 | 109 | <5 | 14 | <50 | <2 | 96 | <5 | 15 | <3 | 105 | 7 | 27 | 113 | 216 |
| RF224694 | 0612812 | 335 | | 9 | 97 | <5 | 12 | <50 | <2 | 85 | <5 | 15 | <3 | 86 | <5 | 27 | 96 | 204 |
| RF224695 | 0612813 | 336 | | <4 | 121 | <5 | 16 | <50 | 3 | 140 | <5 | 18 | <3 | 108 | 6 | 30 | 149 | 183 |

Bad Oeynhausen

Kernproben, Entnahmedatum 1974

P1 Siltiger Tonstein, Buntsandstein, 1025,8 m Tiefe

P2 Siltiger Tonstein, Buntsandstein, 1026,9 m Tiefe

**** RF - Analysen ****
 Analyse von Haupt- und Spurenelementen im Silikatprogramm
 BGR - Hannover B4.15 RFA - Labor Tel.: 2761 (E31)
 () = Restkonzentration nach Glühen bei 1030 °Celsius

Auftrag: 47168 / Einsender: Dr. Vosteen (3147)
 Probenart: Bohrkern / Bad Oeynhausen

| Probenidentifikation | SiO ₂ % | TiO ₂ % | Al ₂ O ₃ % | Fe ₂ O ₃ % | MnO % | MgO % | CaO % | Na ₂ O % | K ₂ O % | P ₂ O ₅ (SO ₃) % | (Cl) % | (F) % | LiO I % | Sum % | | | |
|----------------------|--------------------------------------|-----------------------|-------------------------------------|-------------------------------------|---------------|--------------|----------------|------------------------|-----------------------|--|----------------|----------------|---------------|-----------------|---------------|--------------|----------------|
| | RF223173 0603855 RF223174 0603856 | P 1 P 2 | 54.27 29.25 | 0.707 0.390 | 15.33 8.51 | 6.20 3.81 | 0.093 0.050 | 3.30 1.76 | 5.508 21.865 | 2.06 1.55 | 3.460 1.702 | 0.141 0.075 | 0.34 24.56 | <0.002 0.005 | <0.05 0.05 | 8.29 6.01 | 99.68 99.60 |
| Probenidentifikation | (HS) mg/kg | Ba mg/kg | Bi mg/kg | Ce mg/kg | Co mg/kg | Cr mg/kg | Cs mg/kg | Cu mg/kg | Ga mg/kg | Hf mg/kg | La mg/kg | Mo mg/kg | Rb mg/kg | Nd mg/kg | Ni mg/kg | | |
| | | P 1 P 2 | 14 26 | 575 434 | <3 <3 | 68 59 | 15 7 | 81 49 | 8 <5 | 32 36 | 22 12 | 5 <5 | <20 <20 | <2 <2 | 15 10 | <50 <50 | 43 17 |
| Probenidentifikation | Pb mg/kg | Rb mg/kg | Sb mg/kg | Sc mg/kg | Sn mg/kg | Sn mg/kg | Sr mg/kg | Ta mg/kg | Th mg/kg | U mg/kg | V mg/kg | W mg/kg | X mg/kg | Zn mg/kg | Zr mg/kg | | |
| | | P 1 P 2 | 17 10 | 133 63 | <5 <5 | 15 10 | <30 <30 | 3 <2 | 4.93 19.98 | <5 <5 | 17 12 | 11 4 | 9.5 5.5 | 17 19 | 25 13 | 5.7 3.3 | 16.7 9.8 |

Röntgenbeugungsanalysen

Bezug: Abt.-Nr.: 47168 LIMS-Nr.: 0603855 - 856
R 60873 - R 60874

Einsender: Dr. H.-D. Vosteen

Projekt: 05-0075-01-0812-01

Probenart: Bohrkerne

Herkunft: Bad Oeynhausen

Probenzahl: 2

Die eingesandten Proben wurden auf die Mineralzusammensetzung untersucht. In der nachfolgenden Tabelle sind die Ergebnisse aufgelistet.

Bemerkungen:

Eine genauere Charakterisierung der nachgewiesenen Tonminerale ist erst nach erneuter Diffraktometrie-Analyse an abgetrennten <2µm-Faktionen möglich.

Tabelle:

| Einsender-Nr. | Lims-Nr. | Hauptkomp. | Haupt-Nebenk. | Nebenkomp. | Nebenk.-Spuren | Spuren |
|---------------|----------|------------|---------------|------------|--|--|
| P1 | 0603855 | Quarz | | | Feldspat, Musk-Illit, Chlorit, Calcit | |
| P2 | 0603856 | Anhydrit | Quarz | Feldspat | Musk-Illit | Chlorit, Calcit, Dolomit, Hämatit |

Sachbearbeiter
Analytiker

Weck
(Dr. S. R. Dohrmann)

D.

Röntgenbeugungsanalysen

Bezug: Abt.- 47667 RD- 63780 bi 63790
Nr.: Nr: s

Einsende H.-D. Vosteen

r:

Projekt: 05-0075-01-0812-01

Probenart Gesteinsbohrungen

:

Herkunft: Altmark

Probenzahl: 11

Die eingesandten Proben wurden auf die Mineralzusammensetzung untersucht. In der nachfolgenden Tabelle sind die Ergebnisse aufgelistet.

Bemerkungen:

Eine genauere Charakterisierung der nachgewiesenen Tonminerale ist erst nach erneuter Diffraktometrie-Analyse an abgetrennten <2µm-Faktionen möglich.

Sachbearbeiter
Analytiker

D. Weck
(Dr. R. Dohrmann)

Tabelle:

| Einsender-Nr. | Lims-Nr. | RD-Nr. | Hauptkom.p. | Hauptkom.p.-Nebenkom.p. | Nebenko mp. | Nebenko mp.-Spuren | Spuren |
|---------------|----------|--------|----------------------|-------------------------------|------------------------|--------------------|---|
| 3 | 0801916 | 63780 | Anhydrit, Dolomit | | Calcit | | Quarz, Feldspat |
| 5a (dunkel) | 0801917 | 63781 | Quarz, Feldspat | | Dolomit, Calcit | | Muskovit- Illit, Chlorit, Pyrit, Anhydrit, ±Smektit oder Mixed Layer |
| 5b (hell) | 0801918 | 63782 | Quarz | Feldspat | Dolomit | Calcit | Muskovit- Illit, Chlorit, Pyrit, Anhydrit |
| 9a (dunkel) | 0801919 | 63783 | Quarz | | Feldspat | | Dolomit, Calcit, Anhydrit, ±Muskovit- Illit |
| 9b (hell) | 0801920 | 63784 | Quarz | | Feldspat | | Dolomit, Anhydrit, Calcit, Chlorit, ±Muskovit- Illit |
| 11 | 0801921 | 63785 | Quarz | Anhydrit | Feldspat | Calcit | Dolomit, Hämatit, Muskovit- Illit |
| 12a | 0801922 | 63786 | Quarz | Muskovit- Illit, Calcit | Chlorit | Feldspat | Hämatit |
| 12b | 0801923 | 63787 | Quarz | Calcit, Feldspat | Anhydrit, Muskovit- | Chlorit | Hämatit |

| | | | | | |
|----|-------------|-----------|-------|-----------------------|---|
| | | | | | Illit |
| 14 | 080192 4 | 6378 8 | Quarz | Feldspat | Calcit, Chlorit, Muskovit- Illit |
| 16 | 080192 5 | 6378 9 | Quarz | Feldspat | Calcit, Chlorit, Muskovit- Illit |
| 18 | 080192 6 | 6379 0 | Quarz | Anhydrit, Feldspat | Calcit, Dolomit (oder Ankerit), ±Muskovit- Illit |

***** RF.- Analysen *****
 Analyse von Haupt- und Spurenelementen im Silikatprogramm
 BGR - Hannover B4.15 RFA - Labor Tel.: 2761 (E31)
 () = Restkonzentration nach Glühen bei 1030°Celsius

Auftrag: 47667 / Einsender: Dr. Vosteen (3390)
 Probenart: Gesteinsbohrung / Altmark

| Probenidentifikation | | | SiO ₂ % | TiO ₂ % | Al ₂ O ₃ % | Fe ₂ O ₃ % | MnO % | MgO % | CaO % | Na ₂ O % | K ₂ O % | P ₂ O ₅ % | (SO ₃) % | (Cl) % | (F) % | LOI % | Sum % |
|----------------------|---------|-----|-----------------------|-----------------------|-------------------------------------|-------------------------------------|----------|----------|----------|------------------------|-----------------------|------------------------------------|-------------------------|-----------|----------|----------|----------|
| RF228916 | 0801916 | 3 | 2.82 | 0.042 | 0.70 | 0.31 | 0.065 | 7.53 | 36.728 | 0.16 | 0.086 | 0.010 | 25.39 | 0.006 | 0.07 | 22.34 | 96.25 |
| RF228917 | 0801917 | 5a | 69.20 | 0.447 | 8.57 | 2.45 | 0.138 | 1.73 | 5.168 | 2.72 | 1.644 | 0.099 | 1.12 | 0.028 | <0.05 | 6.39 | 99.72 |
| RF228918 | 0801918 | 5b | 73.27 | 0.348 | 5.99 | 2.00 | 0.154 | 1.88 | 5.006 | 2.23 | 1.176 | 0.078 | 0.78 | 0.023 | <0.05 | 6.65 | 99.57 |
| RF228919 | 0801919 | 9a | 85.13 | 0.110 | 4.83 | 0.70 | 0.094 | 0.52 | 2.142 | 1.33 | 1.697 | 0.048 | 0.75 | 0.024 | <0.05 | 2.39 | 99.78 |
| RF228920 | 0801920 | 9b | 85.10 | 0.118 | 5.09 | 0.81 | 0.079 | 0.45 | 1.856 | 1.41 | 1.761 | 0.049 | 0.59 | 0.019 | <0.05 | 2.34 | 99.69 |
| RF228921 | 0801921 | 11 | 75.70 | 0.119 | 4.64 | 1.04 | 0.119 | 0.34 | 6.277 | 1.22 | 1.769 | 0.045 | 5.11 | 0.019 | <0.05 | 3.30 | 99.73 |
| RF228922 | 0801922 | 12a | 46.03 | 0.761 | 15.62 | 5.95 | 0.220 | 3.90 | 9.661 | 1.11 | 4.158 | 0.157 | 0.07 | 0.012 | <0.05 | 11.99 | 99.67 |
| RF228923 | 0801923 | 12b | 56.70 | 0.515 | 10.44 | 4.69 | 0.162 | 2.41 | 9.202 | 1.44 | 2.488 | 0.121 | 3.55 | 0.013 | <0.05 | 7.90 | 99.65 |
| RF228924 | 0801924 | 14 | 86.65 | 0.136 | 5.56 | 1.29 | 0.032 | 0.45 | 0.845 | 1.08 | 1.982 | 0.061 | 0.10 | 0.016 | <0.05 | 1.51 | 99.76 |
| RF228925 | 0801925 | 16 | 86.58 | 0.138 | 4.57 | 1.14 | 0.059 | 0.29 | 1.477 | 1.00 | 1.717 | 0.043 | 0.40 | 0.018 | <0.05 | 1.87 | 99.32 |
| RF228926 | 0801926 | 18 | 74.45 | 0.086 | 4.53 | 0.37 | 0.110 | 0.60 | 6.955 | 1.19 | 1.507 | 0.039 | 5.88 | 0.019 | <0.05 | 3.84 | 99.58 |

***** RF.- Analysen *****
 Analyse von Haupt- und Spurenelementen im Silikatprogramm
 BGR - Hannover B4.15 RFA - Labor Tel.: 2761 (E31)
 () = Restkonzentration nach Glühen bei 1030°Celsius

Auftrag: 47667 / Einsender: Dr. Vosteen (3390)
 Probenart: Gesteinsbohrung / Altmark

| Probenidentifikation | | (As) | Ba | Bi | Ce | Co | Cr | Cs | Cu | Ga | Hf | La | Mo | Nb | Nd | Ni | |
|----------------------|---------|-------|-------|-------|-------|-------|-------|-------|-------|-------|-------|-------|-------|-------|-------|-------|----|
| | | mg/kg | |
| RF228916 | 0801916 | 3 | <2 | 35 | <4 | <20 | <3 | <5 | <4 | 27 | <2 | <6 | <16 | <3 | 3 | <14 | <2 |
| RF228917 | 0801917 | 5a | 45 | 384 | <4 | 45 | 23 | 51 | <3 | 236 | 10 | <6 | 14 | <3 | 8 | 33 | 17 |
| RF228918 | 0801918 | 5b | 51 | 977 | <4 | <18 | 26 | 43 | <3 | 245 | 5 | 7 | 15 | <3 | 10 | 16 | 10 |
| RF228919 | 0801919 | 9a | 5 | 691 | <4 | 22 | 4 | 8 | <3 | 27 | 5 | <6 | <14 | <2 | <13 | <2 | |
| RF228920 | 0801920 | 9b | 3 | 1801 | <4 | 22 | 4 | 10 | <3 | 18 | 5 | 8 | 15 | <2 | 4 | <13 | 2 |
| RF228921 | 0801921 | 11 | 7 | 605 | <4 | 30 | 3 | 5 | <3 | 26 | 4 | <6 | <15 | <3 | 4 | <13 | <2 |
| RF228922 | 0801922 | 12a | 20 | 328 | <4 | 81 | 23 | 111 | 35 | 14 | 22 | 7 | 38 | <3 | 17 | 44 | 53 |
| RF228923 | 0801923 | 12b | 22 | 517 | <4 | 54 | 18 | 56 | 14 | 21 | 15 | 13 | 24 | <3 | 12 | 35 | 34 |
| RF228924 | 0801924 | 14 | 2 | 1124 | <4 | <18 | 7 | 12 | <3 | 10 | 5 | <6 | <14 | <3 | 6 | <13 | 14 |
| RF228925 | 0801925 | 16 | <2 | 5172 | <4 | <18 | 8 | 23 | <3 | 12 | 3 | <6 | <14 | <2 | 5 | 14 | 10 |
| RF228926 | 0801926 | 18 | <2 | 1674 | <4 | <18 | <3 | <4 | <3 | 15 | 4 | <6 | <15 | <3 | 4 | 15 | 2 |

***** RF.- Analysen *****

Analyse von Haupt- und Spurenelementen im Silikatprogramm
BGR - Hannover B4.15 RFA - Labor Tel.: 2761 (E31)
() = Restkonzentration nach Glühen bei 1030°Celsius

Auftrag: 47667 / Einsender: Dr. Vosteen (3390)
Probenart: Gesteinsbohrung / Altmark

| Probenidentifikation | | Pb | Rb | Sb | Sc | Sm | Sn | Sr | Ta | Th | U | V | W | Y | Zn | Zr | |
|----------------------|---------|-------|-------|-------|-------|-------|-------|-------|-------|-------|-------|-------|-------|-------|-------|-------|-----|
| | | mg/kg | |
| RF228916 | 0801916 | 3 | 9 | 6 | <12 | <2 | <15 | <5 | 1641 | <5 | 7 | 6 | 7 | <4 | <3 | 87 | 18 |
| RF228917 | 0801917 | 5a | 20 | 51 | <7 | 7 | 17 | 9 | 85 | <4 | 11 | <3 | 49 | <4 | 20 | 18 | 213 |
| RF228918 | 0801918 | 5b | 346 | 35 | 8 | 5 | <14 | 14 | 129 | <4 | 12 | <3 | 27 | <4 | 16 | 22 | 235 |
| RF228919 | 0801919 | 9a | 8 | 58 | <7 | 3 | <13 | 21 | 76 | <4 | 5 | <3 | 12 | 7 | 8 | 14 | 92 |
| RF228920 | 0801920 | 9b | 9 | 59 | <6 | 3 | <13 | 53 | 103 | <4 | 7 | <3 | 8 | <4 | 8 | 12 | 106 |
| RF228921 | 0801921 | 11 | 10 | 57 | <7 | 3 | <14 | 4 | 216 | <4 | 4 | <3 | 15 | <4 | 8 | 10 | 133 |
| RF228922 | 0801922 | 12a | 10 | 239 | <8 | 17 | 20 | <4 | 130 | <5 | 22 | 4 | 124 | <4 | 30 | 87 | 176 |
| RF228923 | 0801923 | 12b | 16 | 132 | <8 | 10 | <15 | 13 | 314 | <5 | 18 | <3 | 67 | <4 | 20 | 63 | 201 |
| RF228924 | 0801924 | 14 | 9 | 83 | <6 | 2 | <14 | 9 | 67 | <4 | 7 | <3 | 11 | <4 | 8 | 22 | 118 |
| RF228925 | 0801925 | 16 | 10 | 64 | <6 | 2 | <14 | 6 | 164 | <4 | 7 | <3 | 15 | <4 | 9 | 15 | 138 |
| RF228926 | 0801926 | 18 | 6 | 50 | <8 | 3 | <14 | 15 | 522 | <4 | 7 | <3 | 11 | <4 | 6 | 6 | 78 |